Mengjun Hu · Chris Cornelis ·
Yan Zhang · Pawan Lingras ·
Dominik Ślęzak · JingTao Yao (Eds.)

LNAI 14840

Rough Sets

International Joint Conference, IJCRS 2024
Halifax, NS, Canada, May 17–20, 2024
Proceedings, Part II

Springer

Lecture Notes in Computer Science

Lecture Notes in Artificial Intelligence 14840

Founding Editor

Jörg Siekmann

Series Editors

The series Lecture Notes in Artificial Intelligence (LNAI) was established in 1988 as a topical subseries of LNCS devoted to artificial intelligence.

The series publishes state-of-the-art research results at a high level. As with the LNCS mother series, the mission of the series is to serve the international R & D community by providing an invaluable service, mainly focused on the publication of conference and workshop proceedings and postproceedings.

Mengjun Hu · Chris Cornelis · Yan Zhang ·
Pawan Lingras · Dominik Ślęzak · JingTao Yao
Editors

Rough Sets

International Joint Conference, IJCRS 2024
Halifax, NS, Canada, May 17–20, 2024
Proceedings, Part II

Springer

Editors
Mengjun Hu
Saint Mary's University
halifax, NS, Canada

Chris Cornelis
Ghent University
Ghent, Belgium

Yan Zhang
California State University
San Bernardino, CA, USA

Pawan Lingras
Saint Mary's University
Halifax, NS, Canada

Dominik Ślęzak
University of Warsaw
Warsaw, Poland

JingTao Yao
University of Regina
Regina, SK, Canada

ISSN 0302-9743 ISSN 1611-3349 (electronic)
Lecture Notes in Artificial Intelligence
ISBN 978-3-031-65667-5 ISBN 978-3-031-65668-2 (eBook)
https://doi.org/10.1007/978-3-031-65668-2

LNCS Sublibrary: SL7 – Artificial Intelligence

This Springer imprint is published by the registered company Springer Nature Switzerland AG
The registered company address is: Gewerbestrasse 11, 6330 Cham, Switzerland

Preface

This volume comprises the papers selected for presentation at IJCRS 2024, the 2024 International Joint Conference on Rough Sets, held at Saint Mary's University in Halifax, Canada, on May 17–20, 2024. The annual IJCRS series conferences combine four distinct conferences linking rough sets to various paradigms: RSCTC (data analysis), RSFDGrC (granular computing), RSKT (knowledge technology), and RSEISP (intelligent systems). The first Joint Rough Set Symposium took place in Toronto, Canada, in 2007; followed by Symposiums in Chengdu, China (2012); Halifax, Canada (2013); Granada and Madrid, Spain (2014); Tianjin, China (2015), where the acronym IJCRS was proposed; and subsequent conferences IJCRS 2016 in Santiago, Chile; IJCRS 2017 in Olsztyn, Poland; IJCRS 2018 in Quy Nhon, Vietnam; IJCRS 2019 in Debrecen, Hungary; IJCRS 2020 in La Habana, Cuba (online); IJCRS 2021 in Bratislava, Slovakia (hybrid); IJCRS 2022 in Suzhou, China (hybrid); and IJCRS 2023 in Kraków, Poland (hybrid).

IJCRS 2024 continued to receive significant attention from researchers in the rough sets community. We received 56 full-length paper submissions, which went through a rigorous single-blind reviewing process. Each submission was reviewed by at least three domain experts. Some authors were requested to make revisions, which were further reviewed before the final decision was made. As a result, 43 top-quality submissions were accepted as full-length papers. The camera-ready versions underwent further review by the Program Committee Chairs and General Conference Chairs. The scientific discourse at IJCRS 2024 was complemented by ten extended abstracts, describing ongoing work or research published elsewhere in the past year. These extended abstracts were rigorously reviewed by the Program Committee Chairs and compiled into a Book of Abstracts edited by the Publication Chair, Xiaodong Yue, and his PhD student Zihao Li. The success of the conference owes much to the contributions of the authors, reviewers, and Program Committee Members.

The IJCRS 2024 program featured eight invited talks, including two presentations by former presidents of the International Rough Set Society, Duoqian Miao and Wojciech Ziarko, and six keynote talks by renowned researchers in the field, Lipika Dey, Jimmy X. Huang, Ryszard Janicki, Eric T. Matson, Jesús Medina, and Jarosław Wąs. We are grateful to all the invited speakers for their visionary talks on research related to rough sets. IJRCS 2024 also hosted two workshops on "Uncertainty, Three-Way Decision, and Explainable Artificial Intelligence" and "Applications of Deep Learning and Soft Computing" and two special sessions on "General Rough Set Perspectives on Foundations of AI and Machine Learning" and "Formal Concept Analysis, General Operators and Related Topics". Our gratitude is extended to all the workshop and special session chairs, Duoqian Miao, Jianfeng Xu, Chuanlei Zhang, Ying Yu, Hong Yu, Raavee Kadam, A. Mani, Stefania Boffa, Davide Ciucci, Jesús Medina, M. Eugenia Cornejo, and Eloísa Ramírez-Poussa.

The IJCRS 2024 program was further augmented by a Rough Set School and Tutorials. We are grateful to the chairs, Piotr Artiemjew and Zaineb Chelly Dagdia, and the tutorial speakers, Stefania Boffa, James F. Peters, Usman Qamar, Andrzej Skowron, Dominik ŚlĘzak, Arkadiusz Wojna, and Yiyu Yao. IJCRS 2024 also hosted a Data Mining Competition, sponsored by Southwest Properties. We would like to extend our thanks to the chairs Yasushi Akiyama and Andrzej Janusz, the judges Chris Cornelis, Dun Liu, Kanngi Mahajan, Dan Penny, Jiju Poovvancheri, Sanjeevi Ramachandran, Trishla Shah, and Yiyu Yao, as well as the participants.

We appreciate the sponsorship from Springer for the two Best Student Paper Awards. The awards were assigned based on a competitive process, considering scientific excellence and clarity of both articles and presentations. With a competition among 29 eligible papers, the two awards were presented to Qiaoyi Li, from the University of Regina in Canada under the supervision of Yiyu Yao, for the paper entitled "Granular Approximations of Partially-Known Concepts", and Hajime Okawa, from the Muroran Institute of Technology in Japan under the supervision of Yasuo Kudo, for the paper entitled "A Vector Is a Granule: A Novel Extension of the Variable Precision Rough Set Model". We are also grateful to Jimmy X. Huang and IEEE for their sponsorship through the IEEE TCII Fund.

IJCRS 2024 would not have been successful without the support of many people and organizations. We are grateful to the Program Committee Members for their effort and engagement in providing a rich and rigorous scientific program. We greatly appreciate the cooperation, support, and sponsorship from the MSc in Computing and Data Analytics (MCDA) program at Saint Mary's University and the International Rough Set Society. We acknowledge the use of the EasyChair conference system for paper submission and review. We are also grateful to Springer for publishing the proceedings as two volumes of LNCS/LNAI.

Lastly, thanks are extended to Raavee Kadam, Neelam Pal, Vrushali Prajapati, and other members in the local organizational team for their logistical, technical, and administrative support, without which IJCRS 2024 would not have been possible.

May 2024

Mengjun Hu
Chris Cornelis
Yan Zhang
Pawan Lingras
Dominik Ślęzak
JingTao Yao

Organization

Honorary Chairs

James F. Peters	University of Manitoba, Canada
Andrzej Skowron	Systems Research Institute of the Polish Academy of Sciences, Poland
Yiyu Yao	University of Regina, Canada

General Conference Chairs

Pawan Lingras	Saint Mary's University, Canada
Dominik Ślęzak	University of Warsaw, Poland
JingTao Yao	University of Regina, Canada

Program Committee Chairs

Mengjun Hu	Saint Mary's University, Canada
Chris Cornelis	Ghent University, Belgium
Yan Zhang	California State University San Bernardino, USA

Steering Committee Chairs

Witold Pedrycz	University of Alberta, Canada
Roman Słowiński	Poznań University of Technology, Poland
Guoyin Wang	Chongqing University of Posts and Telecommunications, China

Data Mining Competition Chairs

Yasushi Akiyama	Saint Mary's University, Canada
Andrzej Janusz	Queensland University of Technology, Australia

Rough Set School and Tutorial Chairs

Piotr Artiemjew	University of Warmia and Mazury in Olsztyn, Poland
Zaineb Chelly Dagdia	Université Paris-Saclay, UVSQ, France

Special Session and Workshop Chairs

Eloísa Ramírez-Poussa	University of Cádiz, Spain
Hong Yu	Chongqing University of Posts and Telecommunications, China

Publicity Chairs

A. Mani	Indian Statistical Institute, Kolkata, India
Stefania Boffa	University of Milano-Bicocca, Italy

Publication Chair

Xiaodong Yue	Shanghai University, China

Local Organization Chair

Raavee Kadam	Saint Mary's University, Canada

Administrative Support

Neelam Pal	Saint Mary's University, Canada

Webmaster

Vrushali Prajapati	Saint Mary's University, Canada

Program Committee Members

A. Mani	Indian Statistical Institute, India
Lubomir Antoni	Jozef Šafárik University in Košice, Slovakia
Roberto G. Aragón	University of Cádiz, Spain
Piotr Artiemjew	University of Warmia and Mazury, Poland
Nouman Azam	National University of Computer and Emerging Sciences, Pakistan
Jaume Baixeries	Universitat Politècnica de Catalunya, Spain
María José Benítez Caballero	University of Cádiz, Spain
Stefania Boffa	Universitá degli Studi di Milano-Bicocca, Italy
Henri Bollaert	Ghent University, Belgium
Nizar Bouguila	Concordia University, Canada
Andrea Campagner	Universitá degli Studi di Milano-Bicocca, Italy
Mihir Chakraborty	Jadavpur University, India
Shradha Chavan	Symbiosis International Deemed University, India
Yingxiao Chen	Beijing University of Posts and Telecommunications, China
Yumin Chen	Xiamen University of Technology, China
Zehua Chen	Taiyuan University of Technology, China
Mu-Chen Chen	National Yang Ming Chiao Tung University, Taiwan
Zehua Chen	Taiyuan University of Technology, China
Yumin Chen	Xiamen University of Technology, China
Davide Ciucci	Universitá degli Studi di Milano-Bicocca, Italy
M. Eugenia Cornejo	University of Cádiz, Spain
Chris Cornelis	Ghent University, Belgium
Zoltán Ernő Csajbók	University of Debrecen, Hungary
Jianhua Dai	Hunan Normal University, China
Dayong Deng	Zhejiang Normal University, China
Tingquan Deng	Harbin Engineering University, China
Murat Diker	Hacettepe University, Turkey
Pawel Drozda	University of Warmia and Mazury, Poland
Soma Dutta	University of Warmia and Mazury, Poland
Zied Elouedi	Tunis Higher Institute of Management, Tunisia
Luis Farinas	Centre National de Recherche Scientifique, France
Andrew Fisher	Saint Mary's University, Canada
Hamido Fujita	Iwate Prefectural University, Japan
Can Gao	Shenzhen University, China
Anna Gomolinska	University of Białystok, Poland
Rafal Gruszczynski	Nicolaus Copernicus University, Poland

Shen-Ming Gu	Zhejiang Ocean University, China
Quang-Thuy Ha	VNU-University of Engineering and Technology, Vietnam
Christopher Hinde	Loughborough University, UK
Mengjun Hu	Saint Mary's University, Canada
Feng Hu	Chongqing University of Posts and Telecommunications, China
Qinghua Hu	Tianjin University, China
Ryszard Janicki	McMaster University, Canada
Jouni Jarvinen	University of Turku, Finland
Richard Jensen	Aberystwyth University, UK
Xiuyi Jia	Nanjing University of Science and Technology, China
Chunmao Jiang	Fujian University of Technology, China
Shi Jinyuan	Tianjin University, China
Raavee Kadam	Saint Mary's University, Canada
Ting Ke	Tianjin University of Science and Technology, China
Michal Kepski	University of Rzeszow, Poland
Md. Aquil Khan	Indian Institute of Technology Indore, India
Marzena Kryszkiewicz	Warsaw University of Technology, Poland
Yasuo Kudo	Muroran Institute of Technology, Japan
Sergei O. Kuznetsov	National Research University Higher School of Economics, Russia
Tamás Kádek	University of Debrecen, Hungary
Guangming Lang	Changsha University of Science and Technology, China
Dajiang Lei	Chongqing University, China
Oliver Urs Lenz	Leiden University, Netherlands
Tianrui Li	Southwest Jiaotong University, China
Min Li	Tianjin University of Science and Technology, China
Jinhai Li	Kunming University of Science and Technology, China
Huaxiong Li	Nanjing University, China
Jiye Liang	Shanxi University, China
Churn-Jung Liau	Academia Sinica, Taiwan
Pawan Lingras	Saint Mary's University, Canada
Caihui Liu	Gannan Normal University, China
Guilong Liu	Beijing Language and Culture University, China
Sujuan Liu	Tianjin University of Science and Technology, China

Jiangtao Liu	Tianjin University of Science and Technology, China
Junfang Luo	Southwestern University of Finance and Economics, China
Domingo López-Rodríguez	University of Málaga, Spain
Vijay Mago	York University, Canada
Jesús Medina	University of Cádiz, Spain
Ernestina Menasalvas	Universidad Politécnica de Madrid, Spain
Claudio Meneses	Universidad Católica del Norte, Chile
Duoqian Miao	Tongji University, China
Marcin Michalak	Silesian University of Technology, Poland
Tamás Mihálydeák	University of Debrecen, Hungary
Sonajharia Minz	Jawaharlal Nehru University, India
Mikhail Moshkov	King Abdullah University of Science and Technology, Saudi Arabia
Michinori Nakata	Josai International University, Japan
Amedeo Napoli	Université de Lorraine, France
Nikita Neveditsin	Saint Mary's University, Canada
Thuc Nguyen	University of Science-VNUHCM, Vietnam
Hoang Son Nguyen	Hue University, Vietnam
Khuong Nguyen-An	Bach Khoa University, Vietnam
Agnieszka Nowak-Brzezinska	University of Silesia, Poland
Manuel Ojeda-Aciego	University of Málaga, Spain
Vladimir Parkhomenko	Peter the Great St. Petersburg Polytechnic University, Russia
Andrei Paun	University of Bucharest, Romania
Daniel Peralta	Ghent University, Belgium
Alberto Pettorossi	Università di Roma Tor Vergata, Italy
Małgorzata Przybyła-Kasperek	Uniwersytet Śląski w Katowicach, Poland
Jianjun Qi	Xidian University, China
Jin Qian	East China Jiaotong University, China
Sheela Ramanna	University of Winnipeg, Canada
Eloísa Ramírez-Poussa	University of Cádiz, Spain
Marek Reformat	University of Alberta, Canada
Mauricio Restrepo	Universidad Militar Nueva Granada, Colombia
Sergio Ribeiro	Pontificia Universidade Católica do Paraná, Brazil
Henryk Rybiński	Warsaw University of Technology, Poland
Hiroshi Sakai	Kyushu Institute of Technology, Japan
Ambuja Salgaonkar	University of Mumbai, India
B. Uma Shankar	Indian Statistical Institute, India
Marek Sikora	Silesian University of Technology, Poland

Andrzej Skowron	Systems Research Institute of the Polish Academy of Sciences, Poland
Dominik Slezak	University of Warsaw, Poland
Roman Slowinski	Poznań University of Technology, Poland
Łukasz Sosnowski	Systems Research Institute of the Polish Academy of Sciences, Poland
Urszula Stańczyk	Silesian University of Technology, Poland
John Stell	University of Leeds, UK
Lin Sun	Tianjin University of Science and Technology, China
Langwangqing Suo	Shaanxi Normal University, China
Marcin Szczuka	University of Warsaw, Poland
Ryszard Tadeusiewicz	AGH University of Science and Technology, Poland
Adnan Theerens	Ghent University, Belgium
Dan Thu Tran	University of Management and Technology, Vietnam
Bala Krushna Tripathy	Vellore Institute of Technology, India
Li-Shiang Tsay	North Carolina Agricultural and Technical Sate University, USA
Bay Vo	Ho Chi Minh City University of Technology, Vietnam
Zhen Wang	Weihai Institute of Beijing Jiaotong University, China
Ye Wang	Texas A&M University, USA
Guoyin Wang	Chongqing University of Posts and Telecommunications, China
Wei Wei	Shanxi University, China
Jun Xie	Taiyuan University of Technology, China
Jianfeng Xu	Nanchang University, China
Xin Yang	Southwestern University of Finance and Economics, China
Hailong Yang	Shaanxi Normal University, China
Jilin Yang	Sichuan Normal University, China
Tian Yang	Hunan Normal University, China
Yiyu Yao	University of Regina, Canada
Ning Yao	Tongji University, China
Minda Yao	China University of Mining and Technology, China
JingTao Yao	University of Regina, Canada
Hong Yu	Chongqing University of Posts and Telecommunications, China
Ying Yu	East China Jiaotong University, China

Xiaodong Yue	Shanghai University, China
Yanhui Zhai	Shanxi University, China
Jianming Zhan	Hubei Institute for Nationalities, China
Chuanlei Zhang	Tianjin University of Science and Technology, China
Yuanjian Zhang	Shanghai University, China
Yan Zhang	Cal State University San Bernardino, USA
Qinghua Zhang	Chongqing University of Posts and Telecommunications, China
Li Zhang	Soochow University, China
Hongyun Zhang	Tongji University, China
Shu Zhao	Anhui University, China
Huilai Zhi	Shanghai University, China
Bing Zhou	Sam Houston State University, USA
Jie Zhou	Shenzhen University, China
Wojciech Ziarko	University of Regina, Canada
Beata Zielosko	University of Silesia, Poland
Jianhang Yu	Chongqing University of Posts and Telecommunications, China

Contents – Part II

Three-Way Decision in Broad Senses

Rental Market Data Mining

Applications of Deep Learning and Soft Computing

Contents – Part I

Three-Way Decision and Rough Sets

The Visual Analysis of Three-Way Decision Based on Decision-Theoretic Rough Set: A Perspective of Fusing Two-Way Decision Pair

Jing Tu[1,2], Hong Rao[1], Jianfeng Xu[1(✉)], Duoqian Miao[3(✉)], and Yuanjian Zhang[4]

[1] School of Software, Nanchang University, Nanchang 330047, Jiangxi, China
{raohong,jianfeng_x}@ncu.edu.cn
[2] School of Mathematics, Physics and Statistics, Shanghai University of Engineering Science, Songjiang, Shanghai 201620, China
[3] Department of Computer Science and Technology, Tongji University, Shanghai 201804, China
dqmiao@tongji.edu.cn
[4] China UnionPay Co., Ltd., Shanghai 201201, China
zhangyuanjian@unionpay.com

Abstract. Three-way decisions (3WDs) based on decision-theoretic rough set (DTRS), as a crucial theory in the field of granular computing, have received extensive attention. Meanwhile, visualization technologies have gained popularity, particularly for their intuitiveness and explainability. In order to understand the basic theory of 3WD more intuitively and enhance the interpretability analysis of threshold, this paper proposes the visual analysis of 3WD based on DTRS using the perspective of fusing two-way decision (2WD) pair. Firstly, the p-r space is defined via the geometric interpretations of the Bayesian decision procedure. Secondly, we propose a pair of 2WDs, i.e., the 2WD with acceptance and non-acceptance and the 2WD with rejection and non-rejection. And their geometrical interpretations are discussed in p-r space. Then, a fusing of the 2WD pair is proposed, and the geometric relations between its threshold and loss function are analyzed in p-r space. Finally, degeneration in the 2WD pair into the 3WD is obtained via the special loss function, which is employed to get the geometric interpretations for the threshold and loss function of single-evaluation-based 3WDs in p-r space. The method proposed in this paper uses the p-r space to obtain more intuitive explainability, which is more easily interpreted and reasoned of 3WD and has greater potential for generalization.

Keywords: Three-way decision · Decision-theoretic rough set · Geometric interpretation · Two-way decision pair

M. Hu et al. (Eds.): IJCRS 2024, LNAI 14840, pp. 3–13, 2024.
https://doi.org/10.1007/978-3-031-65668-2_1

1 Introduction

Rough sets, introduced by Pawlak, are an essential tool for processing uncertain and incomplete data in data mining [1–3]. The decision-theoretic rough set (DTRS), as an expansion of probabilistic in algebraic rough set theory, was proposed to address inadequate fault tolerances of classical rough set theory [4–6]. As the influential theory of studying knowledge discovery and addressing uncertain problems, three-way decisions (3WDs) based on DTRS have attracted widespread attention [7–10]. Thus far, research results of 3WD have been productive and further applied in many fields [11–17].

The determination of thresholds in the 3WD model with DTRS poses a challenge and has attracted significant attention from researchers. Specifically, as the positive, negative, and boundary rules generated by their respective regions are utilized for decision-making regarding acceptance, rejection, and deferred decisions, classification risk arises. Hence, the literature [18] proposed utilizing loss functions to assess risks from the perspective of loss. Following Bayesian decision rules, loss functions are utilized to infer thresholds in the 3WD model with DTRS. The threshold pair can be systematically computed by minimizing the overall ternary classification cost. Based on this theory, an algebraic method for solving thresholds in 3WD based on DTRS has been proposed by Yao [19]. This algebraic method has been widely studied and applied.

When researching and employing any theory, it is vital to pay attention to abstract theoretical representation and specific physical explanations [20–23]. Visual decision-making is a scientific tool that employs an interaction of visual interfaces to facilitate physical explanations and implement decisions [24–26]. It integrates data presentation and modeling analysis, interactivity, analytical tools, and visualization techniques to support decision-making and problem-solving. Currently, it is extensively applied in big data analysis, medical health care, bio-medicine, and other fields [27–29]. Excellent visual decision techniques not only visualize abstract data and theories but also enhance valid communication among decision-makers. In the field of 3WD research, many researchers have utilized visualization techniques to describe 3WD concepts and the analysis of experimental results [30,31].

In order to enhance the interpretability analysis of the threshold and more intuitively understand 3WD concepts, this paper proposes the visual analysis of 3WD based on DTRS employing the perspective of fusing a two-way decision (2WD) pair. Specifically, the definition of the p-r space is proposed. Then, in p-r space, the 2WD with acceptance and non-acceptance and the 2WD with rejection and non-rejection are proposed as a pair of 2WDs. Subsequently, the fusion of this pair of 2WDs is performed, and the geometric relations between its threshold and loss function are analyzed in p-r space. Finally, degeneration in the 2WD pair into the 3WD is obtained by a specific loss function and employed to visualize the relationship between the threshold and loss function in single-evaluation-based 3WD.

2 The Visual Bayesian Decision Procedure of Three-Way Decision Combing a Pair of Two-Way Decisions

2.1 The Geometric Interpretations for Bayesian Decision Procedure with Liner Cost Function

To unify symbols, let U be an object set, $C \in U$ be a target concept, $\overline{C}$ be the complement of C, $[x]$ be the equivalence class of object $x \in U$, and A be an action set. When the decision-maker takes an action $a \in A$, $\Pr(C|[x]) = \frac{|C \bigcap [x]|}{|[x]|}$ and $\Pr(\overline{C}|[x])$ are the probability of $[x] \in C$ and $[x] \in \overline{C}$, respectively; $\lambda(a|C)$ and $\lambda(a|\overline{C})$ are the corresponding action losses of $[x] \in C$ and $[x] \in \overline{C}$, respectively. In Bayes decision processor, the cost of taking action $a \in A$ via Bayes theory can be denoted as a cost function below:

$$R(a|[x]) \;=\; \lambda(a|C)\Pr(C|[x]) + \lambda(a|\overline{C})\Pr(\overline{C}|[x]). \tag{1}$$

Since $\Pr(\overline{C}|[x]) = 1 - \Pr(C|[x])$, substituting this into Eq. (1) results in the cost function $R(a|[x])$ can be expressed as follows.

$$R(a|[x]) \;=\; (\lambda(a|C) - \lambda(a|\overline{C}))\Pr(C|[x]) + \lambda(a|\overline{C}). \tag{2}$$

According to the linear function in Eq. (2) for $\Pr(C|[x])$, we display the relations between the cost and probability by a line R_a in the p-r space, depicted in Fig. 1.

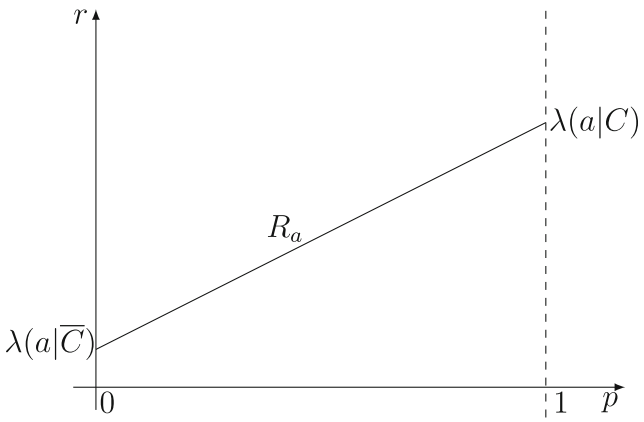

Fig. 1. Visualization of the liner cost function with action $a \in A$ based on Bayes theory

In Fig. 1, p-r space is a space defined by two independent coordinate axes, where the x-axis is the probability $p = \Pr(C|[x])$ and the y-axis is the corresponding costs of taking action $a \in A$, that is $r = R(a|[x])$. It can be seen that

when $\Pr(C|[x]) = 0$, $R(a|[x]) = \lambda(a|\overline{C})$; while $\Pr(C|[x]) = 1$, $R(a|[x]) = \lambda(a|C)$. $\lambda(a|C) - \lambda(a|\overline{C})$ is the slope of line R_a in p-r space. If $\lambda(a|C) < \lambda(a|\overline{C})$, $R(a|[x])$ decreases monotonically with $\Pr(C|[x])$; if $\lambda(a|C) > \lambda(a|\overline{C})$, $R(a|[x])$ increases monotonically with $\Pr(C|[x])$.

2.2 The Geometric Interpretations for Acceptance and Rejection Procedure

With regard to 2WD, we can use acceptance or rejection procedures to analyze its Bayesian decision procedure. Based on it, we can obtain a pair of 2WDs, i.e., the 2WD with acceptance and non-acceptance and the 2WD with rejection and non-rejection, which can be expressed as the following conceptual model, respectively.

(1) $(P, \neg P)$ model with liner cost functions represents the 2WD with acceptance and non-acceptance. It denotes that in the Bayes decision processor when the decision-maker takes actions of a_P and $a_{\bar{P}}$, if $[x] \in C$, the corresponding action losses are λ_{PP} and $\lambda_{\neg PP}$, respectively; if $[x] \in \overline{C}$, the corresponding action losses are λ_{PN} and $\lambda_{\neg PN}$, respectively. Hence, the corresponding costs of diverse actions can be respectively denoted as follows:

$$\begin{aligned} R(a_P|[x]) &= \lambda_{PP} \Pr(C|[x]) + \lambda_{PN} \Pr(\overline{C}|[x]) \\ &= (\lambda_{PP} - \lambda_{PN}) \Pr(C|[x]) + \lambda_{PN}, \\ R(a_{\bar{P}}|[x]) &= \lambda_{\neg PP} \Pr(C|[x]) + \lambda_{\neg PN} \Pr(\overline{C}|[x]) \\ &= (\lambda_{\neg PP} - \lambda_{\neg PN}) \Pr(C|[x]) + \lambda_{\neg PN}. \end{aligned} \tag{3}$$

According to the two linear functions in Eq. (3) for $\Pr(C|[x])$, when taking actions a_P and $a_{\bar{P}}$, we can display the relation between the corresponding costs and probability $\Pr(C|[x])$ using the lines R_P and $R_{\neg P}$ in p-r space, depicted in Fig. 2a.

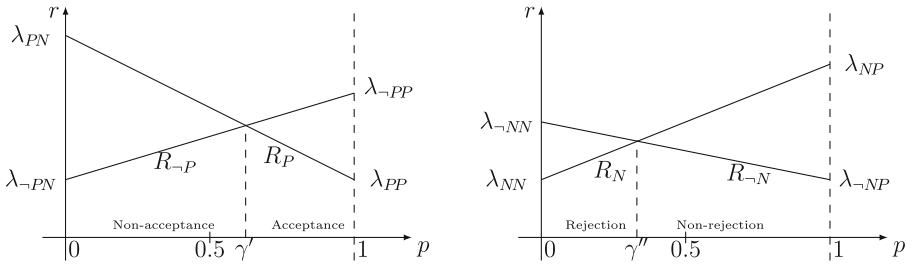

(a) 2WD with acceptance and non-acceptance

(b) 2WD with rejection and non-rejection

Fig. 2. Visualizations for 2WDs

As seen from Fig. 2a, in the p-r space, when $\Pr(C|[x]) = 1$, $R(a_P|[x]) = \lambda_{PP}$ and $R(a_{\bar{P}}|[x]) = \lambda_{\neg PP}$; when $\Pr(C|[x]) = 0$, $R(a_P|[x]) = \lambda_{PN}$ and $R(a_{\bar{P}}|[x]) =$

$\lambda_{\neg PN}$. The slopes of lines R_P and $R_{\neg P}$ are $\lambda_{PN} - \lambda_{PP}$ and $\lambda_{\neg PP} - \lambda_{\neg PN}$, respectively. When $\lambda_{PN} > \lambda_{PP}$, $R(a_P|[x])$ decreases monotonically with $\Pr(C|[x])$; when $\lambda_{PN} < \lambda_{PP}$, $R(a_P|[x])$ increases monotonically with $\Pr(C|[x])$. Similarly, when $\lambda_{\neg PP} > \lambda_{\neg PN}$, $R(a_{\bar{P}}|[x])$ increases monotonically with $\Pr(C|[x])$; when $\lambda_{\neg PP} < \lambda_{\neg PN}$, $R(a_{\bar{P}}|[x])$ decreases monotonically with $\Pr(C|[x])$.

To simply the discussion for $(P, \neg P)$ model, we have the below assumptions with respect to the loss function:

$$\begin{aligned} &(c1) \qquad \lambda_{PP} < \lambda_{\neg PP}, \lambda_{\neg PN} < \lambda_{PN}; \\ &(c2) \qquad \lambda_{PP} < \lambda_{PN}, \lambda_{\neg PN} < \lambda_{\neg PP}. \end{aligned}$$

The interpretations of the above assumptions are as follows: (c1) is consistent with the principle of the minimum loss of correct decisions; (c2) denotes there must be an intersection point between lines R_P and $R_{\neg P}$, whose abscissa is denoted as γ', it's formula can be obtained, as shown in Eq. (4):

$$\gamma' = \frac{\lambda_{PN} - \lambda_{\neg PN}}{(\lambda_{PN} - \lambda_{\neg PN}) + (\lambda_{\neg PP} - \lambda_{PP})}. \tag{4}$$

Hence, under assumptions (c1)-(c2), we can see from Fig. 2a that when $\Pr(C|[x]) > \gamma'$, we make a decision with acceptance; when $\Pr(C|[x]) < \gamma'$, we make a decision with non-acceptance.

(2) $(N, \neg N)$ model with liner cost functions denotes the 2WD with rejection and non-rejection. It represents that in the Bayes decision processor, when taking actions of a_N and $a_{\bar{N}}$, if $[x] \in C$, the corresponding action losses are λ_{NP} and $\lambda_{\neg NP}$, respectively; if $[x] \in \overline{C}$, the corresponding action losses are λ_{NN} and $\lambda_{\neg NN}$, respectively. Hence, the corresponding costs of diverse actions can be respectively denoted as follows:

$$\begin{aligned} R(a_N|[x]) &= \lambda_{NP} \Pr(C|[x]) + \lambda_{NN} \Pr(\overline{C}|[x]) \\ &= (\lambda_{NP} - \lambda_{NN}) \Pr(C|[x]) + \lambda_{NN}, \\ R(a_{\bar{N}}|[x]) &= \lambda_{\neg NP} \Pr(C|[x]) + \lambda_{\neg NN} \Pr(\overline{C}|[x]) \\ &= (\lambda_{\neg NP} - \lambda_{\neg NN}) \Pr(C|[x]) + \lambda_{\neg NN}. \end{aligned} \tag{5}$$

According to the two linear functions in Eq. (5) for $\Pr(C|[x])$, when taking actions a_N, and $a_{\bar{N}}$, we can display the relation between the corresponding costs and probability $\Pr(C|[x])$ using the lines R_N and $R_{\neg N}$ in p-r space, depicted in Fig. 2b.

As seen from Fig. 2b, in the p-r space, when $\Pr(C|[x]) = 1$, $R(a_N|[x]) = \lambda_{NP}$ and $R(a_{\bar{N}}|[x]) = \lambda_{\neg NP}$; when $\Pr(C|[x]) = 0$, $R(a_N|[x]) = \lambda_{NN}$ and $R(a_{\bar{N}}|[x]) = \lambda_{\neg NN}$. The slopes of lines R_N and $R_{\neg N}$ are $\lambda_{NP} - \lambda_{NN}$ and $\lambda_{\neg NN} - \lambda_{\neg NP}$, respectively. When $\lambda_{NP} > \lambda_{NN}$, $R(a_N|[x])$ increases monotonically with $\Pr(C|[x])$; when $\lambda_{NP} < \lambda_{NN}$, $R(a_N|[x])$ decreases monotonically with $\Pr(C|[x])$. Similarly, when $\lambda_{\neg NN} > \lambda_{\neg NP}$, $R(a_{\bar{N}}|[x])$ decreases monotonically with $\Pr(C|[x])$; when $\lambda_{\neg NN} < \lambda_{\neg NP}$, $R(a_{\bar{N}}|[x])$ increases monotonically with $\Pr(C|[x])$.

For $(N, \neg N)$ model, we also have the below assumptions to simplify discussion:

$$\begin{aligned} &\text{(c3)} \qquad \lambda_{NN} < \lambda_{\neg NN}, \lambda_{\neg NP} < \lambda_{NP}; \\ &\text{(c4)} \qquad \lambda_{NN} < \lambda_{NP}, \lambda_{\neg NP} < \lambda_{\neg NN}. \end{aligned}$$

The interpretation of (c3) is similar to that of (c1). (c4) denotes there must be an intersection point between lines R_N and $R_{\neg N}$, whose abscissa is denoted as γ''. Hence, the formula of γ'' can be obtained, as shown in Eq. (6):

$$\gamma'' = \frac{\lambda_{\neg NN} - \lambda_{NN}}{(\lambda_{\neg NN} - \lambda_{NN}) + (\lambda_{NP} - \lambda_{\neg NP})}. \tag{6}$$

Under assumptions (c3)–(c4), we can see from Fig. 2b that when $\Pr(C|[x]) < \gamma''$, we make a decision with rejection; when $\Pr(C|[x]) > \gamma''$, we make a decision with non-rejection.

2.3 The Geometric Interpretations for Three-Way Decision Combing a Pair of Two-Way Decisions

According to the geometric interpretations for a pair of 2WDs, we consider fusing a pair of 2WDs in p-r space. In a pair of two-way classifications, when the decision-maker takes actions a_P, $a_{\bar{P}}$, $a_{\bar{N}}$, and a_N, the corresponding costs can be denoted in Eq. (7):

$$\begin{aligned} R(a_P|[x]) &= (\lambda_{PP} - \lambda_{PN}) \Pr(C|[x]) + \lambda_{PN}, \\ R(a_{\bar{P}}|[x]) &= (\lambda_{\neg PP} - \lambda_{\neg PN}) \Pr(C|[x]) + \lambda_{\neg PN}, \\ R(a_{\bar{N}}|[x]) &= (\lambda_{\neg NP} - \lambda_{\neg NN}) \Pr(C|[x]) + \lambda_{\neg NN}, \\ R(a_N|[x]) &= (\lambda_{NP} - \lambda_{NN}) \Pr(C|[x]) + \lambda_{NN}. \end{aligned} \tag{7}$$

In p-r space, we can draw four lines via the four linear functions in Eq. (7) to display their relationship, as shown in Fig. 3.

In Fig. 3, the four lines have typical geometrical morphology in p-r space, which could be seen as a fusion of 2WD with acceptance and non-acceptance in Fig. 2a and 2WD with rejection and non-rejection in Fig. 2b. Therefore, the definitions of γ' and γ'' remain the same.

In combination with assumptions (c1)–(c4), we make the below assumption to simplify discussion:

$$\begin{aligned} &\text{(C1)} \qquad \lambda_{PP} < \lambda_{\neg NP} \leq \lambda_{\neg PP} < \lambda_{NP}, \\ &\qquad\qquad\ \ \lambda_{NN} < \lambda_{\neg PN} \leq \lambda_{\neg NN} < \lambda_{PN}. \end{aligned}$$

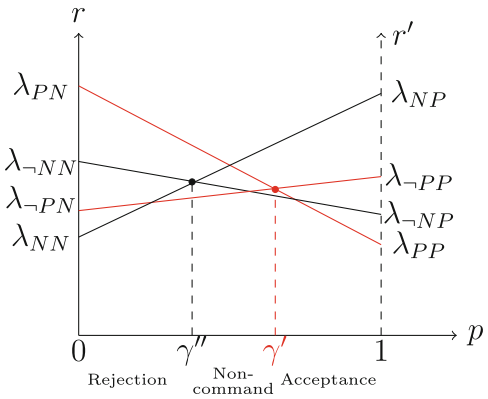

Fig. 3. The 3WD combing a pair of 2WDs

According to Fig. 3, assumption (C1) represents if $\Pr(C|[x]) = 1$ or 0, the corresponding costs of actions a_P, $a_{\bar{P}}$, $a_{\bar{N}}$, and a_N need to satisfy these conditions. It is consistent with the principle of the minimum loss of correct decisions and makes the four lines intersect in pairs.

Under the assumption (C1), we cannot infer the relation between γ' and γ''. To this end, we added an additional assumption:

$$\text{(C2)} \qquad \frac{\lambda_{\neg PP} - \lambda_{PP}}{\lambda_{PN} - \lambda_{\neg PN}} < \frac{\lambda_{NP} - \lambda_{\neg NP}}{\lambda_{\neg NN} - \lambda_{NN}}.$$

Under assumptions (C1) and (C2), the relation between γ' and γ'' can be given as $\gamma'' < \gamma'$. Based on it, we can see from Fig. 3 that when $\Pr(C|[x]) \leq \gamma''$, we decide with rejection; when $\gamma'' < \Pr(C|[x]) < \gamma'$, we decide with non-command; when $\Pr(C|[x]) \geq \gamma'$, we decide with acceptance. It is consistent with the idea of the 3WD.

3 The Geometric Interpretations of Degeneration in Two-Way Decision Pair into the Three-Way Decision

Based on a special loss function, i.e., $\lambda_{BN} = \lambda_{\neg PN} = \lambda_{\neg NN}$ and $\lambda_{BP} = \lambda_{\neg NP} = \lambda_{\neg PP}$, the line connecting $\lambda_{\neg PN}$ and $\lambda_{\neg PP}$ coincides with the line connecting $\lambda_{\neg NN}$ and $\lambda_{\neg NP}$. Hence, degeneration in a pair of 2WDs into the 3WD is obtained, which could be regarded as a single-evaluation-based 3WDs, as shown in Fig. 4.

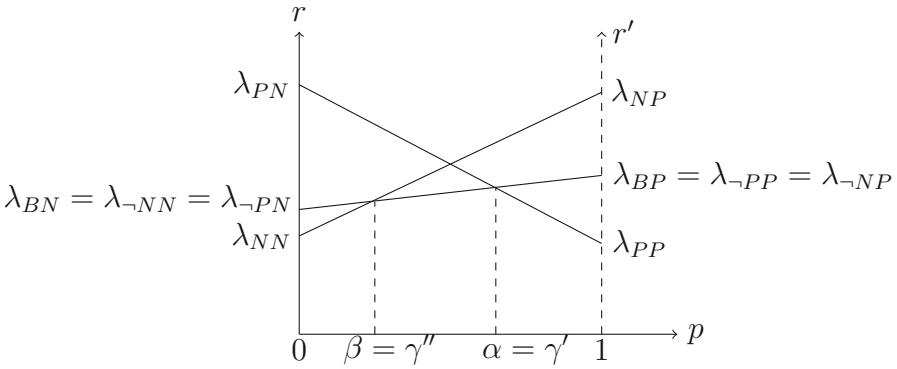

Fig. 4. The visualization of a single-evaluation-based 3WDs

In Fig. 4, we can get three linear functions in p-r space, as follows in Eq. (8):

$$\begin{aligned} R(a_P|[x]) &= (\lambda_{PP} - \lambda_{PN})\Pr(C|[x]) + \lambda_{PN}, \\ R(a_N|[x]) &= (\lambda_{NP} - \lambda_{NN})\Pr(C|[x]) + \lambda_{NN}, \\ R(a_B|[x]) &= (\lambda_{BP} - \lambda_{BN})\Pr(C|[x]) + \lambda_{BN}. \end{aligned} \tag{8}$$

Based on the Bayes decision processor, the above three linear functions can represent the costs of taking the corresponding actions of a_P, a_N, and a_B. Among them, when taking these actions, if $[x] \in C$, λ_{PP}, λ_{NP}, and λ_{BP} are respectively the corresponding losses; if $[x] \in \overline{C}$, λ_{PN}, λ_{NN}, and λ_{BN} are respectively the corresponding losses.

To make the three lines intersect in pairs, we make the below assumptions:

$$\begin{aligned} &\text{(C3)} \qquad \lambda_{PP} \leq \lambda_{BP} = \lambda_{\neg PP} = \lambda_{\neg NP} < \lambda_{NP}, \\ &\qquad\qquad\ \ \lambda_{NN} \leq \lambda_{BN} = \lambda_{\neg NN} = \lambda_{\neg PN} < \lambda_{PN}. \end{aligned}$$

For assumption (C3), its interpretation is similar to the case of assumption (C1). Based on Fig. 4, it can be seen that the abscissa of the intersection of the line connecting λ_{BP} and λ_{BN} with the line connecting λ_{PN} and λ_{PP} and the line connecting λ_{NN} and λ_{NP} are α and β, respectively. Hence, the formulas of α and β can be obtained, as shown in Eq. (9):

$$\begin{aligned} \alpha &= \frac{\lambda_{PN} - \lambda_{BN}}{(\lambda_{PN} - \lambda_{BN}) + (\lambda_{BP} - \lambda_{PP})}, \\ \beta &= \frac{\lambda_{BN} - \lambda_{NN}}{(\lambda_{BN} - \lambda_{NN}) + (\lambda_{NP} - \lambda_{BP})}. \end{aligned} \tag{9}$$

Compared with Fig. 3 and Eqs. (4, 6), it can be found $\beta = \gamma''$ and $\alpha = \gamma'$. To infer the relation between α and β, ensure that $\alpha > \beta$, we further add an assumption, which is similar to assumption (C2):

$$\text{(C4)} \qquad \frac{\lambda_{NP} - \lambda_{BP}}{\lambda_{BN} - \lambda_{NN}} > \frac{\lambda_{BP} - \lambda_{PP}}{\lambda_{PN} - \lambda_{BN}}.$$

Under assumptions (C3)-(C4), we can see from Fig. 4 that when $\Pr(C|[x]) \leq \beta = \gamma''$, we decide with rejection; when $\Pr(C|[x]) \geq \alpha = \gamma'$, we decide with acceptance; when $\beta < \Pr(C|[x]) < \alpha$, we decide with non-command.

In conclusion, we can use a pair of 2WDs to obtain the geometric explanation of 3WD based on DTRS, which is consistent with the concept of classical 3WD.

4 Conclusion and Prospect

3WD based on DTRS is a significant achievement in the field of granular computing, which can effectively deal with uncertain problems. Meanwhile, visualization technology has received extensive attention in various fields for its importance in solving problems and achieving explainability. From the novel perspective of fusing 2WD pair, this paper discusses the visualization analysis of 3WD based on DTRS. The study uses the p-r space to provide a visual and intuitive understanding of 3WD, which can help us better explain the loss function and threshold and understand the relationship between cost and probability. This method not only employs an interaction of visual interfaces to have better interpretability and facilitate decision-making, but also can effectively ease the difficulty of 3WD reasoning. Therefore, it has great potential for application in more complex studies of 3WD and can be widely promoted. However, this paper only discusses the monotonicity of the linear cost function. In real life, the non-monotonic cost situation exists in the delayed decision. The use of linear cost function has some limitations in delayed decision behavior. Therefore, nonlinear cost functions deserve a more in-depth study.

Acknowledgements. This work was supported in National Natural Science Foundations of China (Grant No. 62266032), Jiangxi Training Program for Academic and Technical Leaders in Major Disciplines-Leading Talents Project (Grant No. 20225BCI22016).

References

1. Pawlak, Z.: Rough sets. Int. J. Comput. Inform. Sci. **11**, 341–356 (1982)
2. Pawlak, Z.: Some issues on rough sets. In: Peters, J.F., Skowron, A., Grzymała-Busse, J.W., Kostek, B., Świniarski, R.W., Szczuka, M.S. (eds.) Transactions on Rough Sets I. LNCS, vol. 3100, pp. 1–58. Springer, Heidelberg (2004). https://doi.org/10.1007/978-3-540-27794-1_1
3. Pawlak, Z.: Rough Sets: Theoretical Aspects of Reasoning About Data, vol. 9. Springer, Dordrecht (2012). https://doi.org/10.1007/978-94-011-3534-4
4. Yao, Y.Y., Wong, S.K.M.: A decision theoretic framework for approximating concepts. Int. J. Man Mach. Stud. **37**, 793–809 (1992)
5. Yao, Y.: Decision-theoretic rough set models. In: Yao, J.T., Lingras, P., Wu, W.-Z., Szczuka, M., Cercone, N.J., Ślęzak, D. (eds.) RSKT 2007. LNCS (LNAI), vol. 4481, pp. 1–12. Springer, Heidelberg (2007). https://doi.org/10.1007/978-3-540-72458-2_1
6. Yao, Y.Y.: The superiority of three-way decisions in probabilistic rough set models. Inf. Sci. **181**, 1080–1096 (2011)

7. Yao, Y.: Rough sets and three-way decisions. In: Ciucci, D., Wang, G., Mitra, S., Wu, W.-Z. (eds.) RSKT 2015. LNCS (LNAI), vol. 9436, pp. 62–73. Springer, Cham (2015). https://doi.org/10.1007/978-3-319-25754-9_6
8. Zou, D.D., Xu, Y.L., Li, L.Q., et al.: Novel variable precision fuzzy rough sets and three-way decision model with three strategies. Inf. Sci. **629**, 222–248 (2023)
9. Stepaniuk, J., Skowron, A.: Three-way approximation of decision granules based on the rough set approach. Int. J. Approximate Reasoning **155**, 1–16 (2023)
10. Zou, D., Xu, Y., Li, L., et al.: Novel variable precision fuzzy rough sets and three-way decision model with three strategies. Inf. Sci. **629**, 222–248 (2023)
11. Li, R., Yang, J., Zhang, X.: Optimal scale selection based on three-way decisions with decision-theoretic rough sets in multi-scale set-valued decision tables. Int. J. Mach. Learn. Cybern. **14**(11), 3719–3736 (2023)
12. Liu, F., Liu, Y., Abdullah, S.: Three-way decisions with decision-theoretic rough sets based on covering-based q-rung orthopair fuzzy rough set model. J. Intell. Fuzzy Syst. **40**(5), 9765–9785 (2021)
13. Wang, N., Zhu, P.: A three-way decision model associated with decision-theoretic rough fuzzy sets based on computing with words. J. Intell. Fuzzy Syst. **45**(1), 285–304 (2023)
14. Guo, C., Yu, Z.H., Wu, S.Y., et al.: A three-way decision approach combining probabilistic and decision-theoretic rough set. In: International Conference on Computer and Information Science, pp. 296–301 (2022)
15. Ali, Z., Mahmood, T., Khan, M.B.: Three-way decisions with complex q-rung orthopair 2-tuple linguistic decision-theoretic rough sets based on generalized Maclaurin symmetric mean operators. AIMS Math. **8**(8), 17943–17980 (2023)
16. Zhang, H.D., Ma, Q.: Three-way decisions with decision-theoretic rough sets based on Pythagorean fuzzy covering. Soft. Comput. **24**(24), 18671–18688 (2020)
17. Abdullah, S., Al-Shomrani, M.M., Liu, P., et al.: A new approach to three-way decisions making based on fractional fuzzy decision-theoretical rough set. Int. J. Intell. Syst. **37**(3), 2428–2457 (2022)
18. Yao, Y.Y.: Three-way decisions with probabilistic rough sets. Inf. Sci. **180**, 341–353 (2010)
19. Yao, Y.: An outline of a theory of three-way decisions. In: Yao, J.T., Yang, Y., Słowiński, R., Greco, S., Li, H., Mitra, S., Polkowski, L. (eds.) RSCTC 2012. LNCS (LNAI), vol. 7413, pp. 1–17. Springer, Heidelberg (2012). https://doi.org/10.1007/978-3-642-32115-3_1
20. Li, B., Tian, L.Y., Han, Y., et al.: Three-way decision of target threat decision making based on adaptive threshold algorithms. J. Eng. **2020**(13), 293–297 (2020)
21. Li, Y.S., Shao, X.Y.: Thresholds learning of three-way decisions in pairwise crime linkage. Appl. Soft Comput. **120**, 108638 (2022)
22. Yang, J., Zhang, G.M.: Dynamic dual-threshold virtual machine merging method based on three-way decision. Symmetry **14**(9), 1865 (2022)
23. Liu, J.B., Hu, S.L., Li, H.X., et al.: Achieving threshold consistency in three-way group decision using optimization methodology and expert-weight-updating-strategy. Int. J. Approximate Reasoning **158**, 108922 (2023)
24. Muntwiler, C., Eppler, M.J.: Improving decision making through visual knowledge calibration. Manag. Decis. **61**(8), 2374–2390 (2023)
25. Saito, T., Sudo, R., Takano, Y.: The gaze bias effect in toddlers: preliminary evidence for the developmental study of visual decision-making. Dev. Sci. **23**(6), e12969 (2020)

26. Xu, J.F., Miao, D.Q., Zhang, L., et al.: Algebraic formulations and geometric interpretations of decision-theoretic rough sets. In: Campagner, A., Urs Lenz, O., Xia, S., Ślęzak, D., Was, J., Yao, J. (eds.) IJCRS 2023. LNCS, vol. 14481, pp. 31–45. Springer, Cham (2023). https://doi.org/10.1007/978-3-031-50959-9_3
27. Germar, M., Duderstadt, V.H., Mojzisch, A.: Social norms shape visual appearance: taking a closer look at the link between social norm learning and perceptual decision-making. Cognition **241**, 105611 (2023)
28. Bleichman, I., Yadav, P., Ayali, A.: Visual processing and collective motion-related decision-making in desert locusts. Proc. R. Soc. B **290**, 20221862 (2023)
29. Widyatama, A., Narsa, I.M.: The use of visual presentations for integrated reports in the investment decision-making process. J. Appl. Acc. Res. **24**(1), 106–133 (2023)
30. Hu, M.: Three-way data analytics: preparing and analyzing data in threes. Inf. Sci. **573**, 412–432 (2021)
31. Xu, J.F., Zhang, Y.J., Miao, D.Q.: Three-way confusion matrix for classification: a measure driven view. Inf. Sci. **507**, 772–794 (2020)

Triangular Fuzzy Number Intuitionistic Fuzzy Covering Rough Sets and Applications to Decision Making

Zhongling Bai[1,3], Jiang Chen[1,2(✉)], and Xianyong Zhang[1,3]

[1] School of Mathematical Sciences, Sichuan Normal University, Chengdu 610066, China
cjiangwork@163.com
[2] College of Mathematics and Statistics, Sichuan University of Science and Engineering, Zigong 643000, China
[3] Visual Computing and Virtual Reality Key Laboratory of Sichuan Province, Sichuan Normal University, Chengdu 610066, China

Abstract. The triangular fuzzy number intuitionistic fuzzy set, as an extension and generalization of intuitionistic fuzzy set, has more advantages than the single value representation of membership degree and non-membership degree and interval number representation of intuitionistic fuzzy set. In this paper, the triangular fuzzy number intuitionistic fuzzy set and rough set are fused, and the triangular fuzzy number intuitionistic fuzzy rough set model is constructed based on the intuitionistic fuzzy approximation relation of triangle fuzzy number. Firstly, the approximate operators, correlation properties and three-way regions are discussed and verified by numerical examples. Furthermore, combined with the covering rough set, the triangular fuzzy number intuitionistic covering rough set is constructed, which can be used for multi-attribute decision making. Then, combined with the covering rough set, the triangular fuzzy number intuitionistic fuzzy covering rough set is constructed, which can be used for multi-attribute decision making. Finally, the multi-attribute decision making is carried out with an example considering the expert weight. The results show that the triangular fuzzy number intuitionistic fuzzy covering rough set become novel and effective for multi-attribute decision making. This study provides an in-depth insight into decision making from model and method.

Keywords: Triangular fuzzy number intuitionistic fuzzy set · Triangular fuzzy number intuitionistic fuzzy rough set · Three-way decision · Covering rough set · Multi-attribute decision making

1 Introduction

Rough set (RS) is a mathematical method introduced by Pawlak [15] to handle imprecision, uncertainty, and fuzziness in data analysis. It has been widely applied in many research fields such as pattern recognition [20,29], data mining

M. Hu et al. (Eds.): IJCRS 2024, LNAI 14840, pp. 14–28, 2024.
https://doi.org/10.1007/978-3-031-65668-2_2

[5,28], and machine learning [9,18]. The Pawlak rough set model is designed to deal with qualitative data, but it is not effective for real value data. To solve this problem, a large number of researchers strive to generalize and improve classical fuzzy sets to compensate for the rigidity of Pawlak rough set conditions. Among them, the fuzzy set (FS) theory proposed by Zadeh [26] is one of the methods to solve such problems and has been widely applied. Dubois and Prade [8] combined fuzzy set models with rough set models to generate fuzzy rough sets and rough fuzzy sets. By establishing equivalent knowledge and different frameworks of fuzzy knowledge, they can effectively solve knowledge reasoning and decision-making problems for fuzzy data.

The intuitionistic fuzzy set (IFS) proposed by Atanassov [3] is also an extension of Zadeh's fuzzy set theory. Compared with classical fuzzy sets, IFS comprehensively considers the information of membership, non-membership, and hesitancy, and can describe and characterize the essence of fuzziness in the objective world in detail. Therefore, it has been favored and further studied by many scholars. Singh and Som [16] further proposed the basic concepts, properties, topological structure, logical operators, approximation operators, and similarity relationships of intuitionistic fuzzy rough sets (IFRSs), and conducted in-depth research on several extensions of IFRSs and their integration with other extended RS theories. Liu et al. [12] used the idea of intuitionistic fuzzy similarity to define conflict distance, and combined it with variable precision rough sets (VPRSs) to establish a variable precision intuitionistic fuzzy rough sets (VPIFRSs) model. And studied the properties of VPIFRS and proposed an attribute reduction algorithm based on VPIFRSs. Zhang [30] combines the classic Pawlak RS theory with interval valued intuitionistic fuzzy sets (IVIFSs) theory to propose an interval valued intuitionistic fuzzy rough sets (IVIFRSs) model, and studies in detail the relevant properties of interval valued intuitionistic fuzzy rough approximation operators. Sun et al. [17] proposed interval valued information system as an extension of classical real valued information system, defining interval dominance relationships of conditional attributes on interval valued information systems, and further establishing rough set models and attribute reductions. By introducing IVIFSs into three-way decisions, Ye et al. [25] provide a new description of the loss function, and further propose a model of interval-valued intuitionistic fuzzy decision-theoretic rough set (IVIFDTRS). In addition, there is a large amount of research and application based on the background of IFSs, mainly involving model expansion [2,4], measurement construction [6,10], and corresponding attribute reduction [1,14].

The three-way decision (3WD) theory was originally proposed by Yao [23,24], which means that we divide a whole into three parts, and take actions according to the three parts to achieve the desired result. The three options of accepting, rejecting and delaying in the decision-making process correspond to the three parts, respectively. In recent years, as uncertainty and complexity have increased, the 3WD theory has been applied in many fields, among which the fusion research of the 3WD theory and IFSs have also received widespread attention [7,21]. Furthermore, some scholars have extended the membership values of

FSs to triangular fuzzy numbers and trapezoidal fuzzy numbers based on FSs, IFSs, and IVIFSs. Zhang et al. [27] introduced triangular fuzzy numbers into IFSs, proposed triangular fuzzy number intuitionistic fuzzy sets (TFNIFSs), and studied their system stability. Xu [22] defines some basic operations of TFNIFSs and obtains some very important properties, laying a solid foundation for the aggregation of intuitionistic fuzzy information and decision-making applications of triangular fuzzy numbers.

Based on the above discussions, there still a lack of further research and discussion on the fusion and expansion construction of TFNIFSs and RSs. Therefore, we consider integrating TFNIFSs and RSs to construct a triangular fuzzy number intuitionistic fuzzy rough set (TFNIFRS), and then further generalize the fuzzy covering to establish a triangular fuzzy number intuitionistic fuzzy β-covering rough set. The contributions are briefly summarized as follows:

(1) From the perspective of model construction, the membership degree and non-membership degree in TFNIFSs were respectively modified into triangular fuzzy numbers, and then RS was fused to construct a TFNIFRS, and the relevant properties on it were discussed. Moreover, we further constructed a triangular fuzzy number intuitionistic fuzzy β-covering rough set by introducing β-covering [13] into TFNIFRS.
(2) From the perspective of model application, triangular fuzzy number intuitionistic fuzzy β-covering rough set model can be well applied to multi-attribute group decision-making. For this purpose, we verified through examples and also considered expert weights, and the results showed the effectiveness of the model.

The remainder of this paper is structured as follows. In Sect. 2, some preliminary definitions are introduced. In Sect. 3, we constructed TFNIFRS model and discussed its related properties. By introducing β-covering into TFNIFRS, a triangular fuzzy number intuitionistic fuzzy β-covering rough set model is constructed, and the application of the established model in multi-attribute group decision-making was validated in Sect. 4. We conclude the paper in Sect. 5.

2 Preliminaries

In this section, we review some basic concepts related to triangular fuzzy number, IFS, TFNIFS, score function, and exact function, which will be needed in the following analysis.

Definition 1 ([19]). *Let $I = [0, 1]$, $\tilde{a} = [a^-, a, a^+] \in F(I)$ is called a triangular fuzzy number, where $a^-, a, a^+ \in I$ and $0 \leq a^- \leq a \leq a^+ \leq 1$.*

Definition 2 ([11]). *Suppose $\tilde{a} = [a^-, a, a^+], \tilde{b} = [b^-, b, b^+] \in F(I)$ be any two triangular fuzzy numbers, the following ordinal relations and basic operations for two triangular fuzzy numbers can derive:*

(1) $\tilde{a} \subseteq \tilde{b} \Leftrightarrow a^- \leq b^- \wedge a \leq b \wedge a^+ \leq b^+$;
(2) $\tilde{a} = \tilde{b} \Leftrightarrow a^- = b^- \wedge a = b \wedge a^+ = b^+$;
(3) $\tilde{a} \cap \tilde{b} \Leftrightarrow a^- < b^- \wedge a < b \wedge a^+ < b^+$, *therefore* $\tilde{a} \supseteq \tilde{a} \cap \tilde{b}$, $\tilde{b} \supseteq \tilde{a} \cap \tilde{b}$;
(4) $\tilde{a} \cup \tilde{b} \Leftrightarrow a^- > b^- \wedge a > b \wedge a^+ > b^+$, *therefore* $\tilde{a} \subseteq \tilde{a} \cup \tilde{b}$, $\tilde{b} \subseteq \tilde{a} \cup \tilde{b}$.

Definition 3 ([3]). *Let U be a nonempty finite universe, an intuitionistic fuzzy set (IFS) A on U is defined as:*

$$A = \{\langle x, \mu_A(x), \nu_A(x)\rangle | x \in U\}, \tag{1}$$

where $\mu_A : U \to [0,1]$, $\nu_A : U \to [0,1]$ are two functions on A, respectively, and $\mu_A(x)$, $\nu_A(x)$ are called membership degree and non-membership degree of x belonging to A, respectively. Moreover, $\mu_A(x)$, $\nu_A(x)$ satisfy the follow relation:

$$0 \leq \mu_A(x) + \nu_A(x) \leq 1, \forall x \in U, \tag{2}$$

and we call $A(x) = \langle \mu_A(x), \nu_A(x)\rangle$ an intuitive fuzzy number.

Definition 4 ([11]). *Let U be a nonempty finite universe, then the triangular fuzzy number intuitionistic fuzzy set (TFNIFS) M is defined as:*

$$M = \{\langle x, \tilde{\mu}_M(x), \tilde{\nu}_M(x)\rangle | x \in U\}, \tag{3}$$

where,

$$\tilde{\mu}_M(x) = [\mu_M^-(x), \mu_M(x), \mu_M^+(x)],$$
$$\tilde{\nu}_M(x) = [\nu_M^-(x), \nu_M(x), \nu_M^+(x)],$$

and we call $M(x) = \langle \tilde{\mu}_M(x), \tilde{\nu}_M(x)\rangle$ $(\mu_M^+(x) + \nu_M^+(x) \leq 1)$ a triangular fuzzy number intuitionistic fuzzy number. For any α_1, α_2 is a triangular fuzzy number intuitionistic fuzzy number, i.e.,

$$\alpha_1 = \langle \tilde{\mu}_1, \tilde{\nu}_1\rangle = \langle [\mu_1^-, \mu_1, \mu_1^+], [\nu_1^-, \nu_1, \nu_1^+]\rangle,$$
$$\alpha_2 = \langle \tilde{\mu}_2, \tilde{\nu}_2\rangle = \langle [\mu_2^-, \mu_2, \mu_2^+], [\nu_2^-, \nu_2, \nu_2^+]\rangle,$$

then we can get:

(1) if $\alpha_1 \preceq \alpha_2$ then $\tilde{\mu}_1 \subseteq \tilde{\mu}_2 \wedge \tilde{\nu}_1 \supseteq \tilde{\nu}_2$;
(2) if $\alpha_1 \succeq \alpha_2$ then $\tilde{\mu}_1 \supseteq \tilde{\mu}_2 \wedge \tilde{\nu}_1 \subseteq \tilde{\nu}_2$.

Furthermore, for $\forall M, N \in \Omega$ (Ω is the set of all TFNIFSs), then the normalized Hamming distance between M and N is defined as:

$$\begin{aligned} D(M,N) = \tfrac{1}{8}[&|\mu_M^-(x) - \mu_N^-(x)| + 2|\mu_M(x) - \mu_N(x)| + |\mu_M^+(x) - \mu_N^+(x)| \\ &+ |\nu_M^-(x) - \nu_N^-(x)| + 2|\nu_M(x) - \nu_N(x)| + |\nu_M^+(x) - \nu_N^+(x)|]. \end{aligned}$$

Definition 5 ([11]). *For any $M, N \in \Omega$, i.e.,*

$$M = \{\langle x, [\mu_M^-(x), \mu_M(x), \mu_M^+(x)], [\nu_M^-(x), \nu_M(x), \nu_M^+(x)]\rangle | x \in U\},$$
$$N = \{\langle x, [\mu_N^-(x), \mu_N(x), \mu_N^+(x)], [\nu_N^-(x), \nu_N(x), \nu_N^+(x)]\rangle | x \in U\},$$

then it has the following basic operations:

(1) $M \subseteq N \Leftrightarrow \tilde{\mu}_M(x) \subseteq \tilde{\mu}_N(x) \wedge \tilde{\nu}_M(x) \supseteq \tilde{\nu}_N(x), \forall x \in U$;
(2) $M = N \Leftrightarrow \tilde{\mu}_M(x) = \tilde{\mu}_N(x) \wedge \tilde{\nu}_M(x) = \tilde{\nu}_N(x), \forall x \in U$;
(3) $\sim M = \{\langle x, \tilde{\nu}_M(x), \tilde{\mu}_M(x)\rangle | x \in U\}$;
(4) $M \cap N = \{\langle x, [\mu_M^-(x) \wedge \mu_N^-(x), \mu_M(x) \wedge \mu_N(x), \mu_M^+(x) \wedge \mu_N^+(x)], [\nu_M^-(x) \vee \nu_N^-(x), \nu_M(x) \vee \nu_N(x), \nu_M^+(x) \vee \nu_N^+(x)]\rangle | x \in U\}$;
(5) $M \cup N = \{\langle x, [\mu_M^-(x) \vee \mu_N^-(x), \mu_M(x) \vee \mu_N(x), \mu_M^+(x) \vee \mu_N^+(x)], [\nu_M^-(x) \wedge \nu_N^-(x), \nu_M(x) \wedge \nu_N(x), \nu_M^+(x) \wedge \nu_N^+(x)]\rangle | x \in U\}$;
(6) $M \bigoplus N =$
$\{\langle x, [\mu_M^-(x) + \mu_N^-(x) - \mu_M^-(x)\mu_N^-(x), \mu_M(x) + \mu_N(x) - \mu_M(x)\mu_N(x), \mu_M^+(x) + \mu_N^+(x) - \mu_M^+(x)\mu_N^+(x)], [\nu_M^-(x)\nu_N^-(x), \nu_M(x)\nu_N(x), \nu_M^+(x)\nu_N^+(x)]\rangle | x \in U\}$.

Definition 6 ([19]). *For a triangular fuzzy number intuitionistic fuzzy number $\alpha = \langle[\mu^-, \mu, \mu^+], [\nu^-, \nu, \nu^+]\rangle$, the score function S and the exact function H of α are defined as follows:*

$$S(\alpha) = \frac{1}{4}[(\mu^- - \nu^-) + 2(\mu - \nu) + (\mu^+ - \nu^+)], \tag{4}$$

$$H(\alpha) = \frac{\mu^- + 2\mu + \mu^+}{4} + \frac{\nu^- + 2\nu + \nu^+}{4}. \tag{5}$$

If $\alpha = \langle[1,1,1],[0,0,0]\rangle$, then $S(\alpha) = 1$; if $\alpha = \langle[0,0,0],[1,1,1]\rangle$, then $S(\alpha) = -1$, and hence $S(\alpha) \in [-1,1]$. Based on the above functions, the ordering law for two triangular fuzzy number intuitionistic fuzzy numbers α_1, α_2 are as follows:

(1) *If $S(\alpha_1) < S(\alpha_2)$, then $\alpha_1 < \alpha_2$;*
(2) *If $S(\alpha_1) < S(\alpha_2)$, when $H(\alpha_1) < H(\alpha_2)$, then $\alpha_1 < \alpha_2$; when $H(\alpha_1) = H(\alpha_2)$, then $\alpha_1 = \alpha_2$.*

3 TFNIFRSs Model and Related Properties

In this section, the TFNIFRSs model is constructed by fusing TFNIFSs and RSs. Firstly, we give the relevant definitions, operators, and three-way regions, and then relevant properties are investigated. Finally, relevant properties and conclusions are verified by an example.

3.1 TFNIFRSs

Definition 7. *Let U and V be two finite nonempty universes and $D = [0,1]$, the subset of triangular fuzzy number intuitionistic fuzzy defined on $U \times V$ is called the triangular fuzzy number intuitionistic fuzzy approximation relation between U and V. Denoted as:*

$$R = \{\langle (x,y), \tilde{\mu}_R(x,y), \tilde{\nu}_R(x,y)\rangle | (x,y) \in U \times V\}, \tag{6}$$

where $\tilde{\mu}_R : U \times V \to F(D)$ and $\tilde{\nu}_R : U \times V \to F(D)$. Meanwhile, we call the triplet (U, V, R) as a triangular fuzzy number intuitionistic fuzzy approximate space. In particular, when $U = V$, we abbreviate (U, V, R) as (U, R).

Definition 8. *Given a triangular fuzzy number intuitionistic fuzzy approximation space (U, V, R), R is a triangular fuzzy number intuitionistic fuzzy approximation relation on $U \times V$. For $A \in \Omega$, the lower and upper approximations of A about (U, V, R) are respectively*

$$\begin{aligned}
\underline{R}(A) &= \{\langle x, \tilde{\mu}_{\underline{R}(A)}(x), \tilde{\nu}_{\underline{R}(A)}(x)\rangle | x \in U\} \\
&= \{\langle x, \underset{y\in V}{inf}\{\tilde{\mu}_A(y) \vee \tilde{\nu}_R(x,y)\}, \underset{y\in V}{sup}\{\tilde{\nu}_A(y) \wedge \tilde{\mu}_R(x,y)\}\rangle | x \in U\}, \\
\overline{R}(A) &= \{\langle x, \tilde{\mu}_{\overline{R}(A)}(x), \tilde{\nu}_{\overline{R}(A)}(x)\rangle | x \in U\} \\
&= \{\langle x, \underset{y\in V}{sup}\{\tilde{\mu}_R(x,y) \wedge \tilde{\mu}_A(y)\}, \underset{y\in V}{inf}\{\tilde{\nu}_A(y) \vee \tilde{\nu}_R(x,y)\}\rangle | x \in U\}.
\end{aligned} \tag{7}$$

The sequential pair $(\overline{R}(A), \underline{R}(A))$ is called the TFNIFRS. Further, the corresponding three-way regions (i.e., positive, negative, and boundary regions) are: $POS_R(A) = \underline{R}(A), NEG_R(A) = U - \overline{R}(A), BND_R(A) = \overline{R}(A) - \underline{R}(A)$, where the three-way regions form a division of U corresponding to the implementation of acceptance, rejection, and delayed decisions.

Definition 9. *For a triangular fuzzy number intuitionistic fuzzy relation R on U and $\forall x \in U$, then we define*

(1) R is self-inverse, when $\tilde{\mu}_R(x,x) = [1,1,1] := \tilde{1}$ and $\tilde{\nu}_R(x,x) = [0,0,0] := \tilde{0}$;
(2) R is symmetrical, when $\tilde{\mu}_R(x,y) = \tilde{\mu}_R(y,x)$ and $\tilde{\nu}_R(x,y) = \tilde{\nu}_R(y,x)$.

Furthermore, when R is self-inverse, we call R a triangular fuzzy number intuitionistic fuzzy approximate relation; when R is self-inverse and symmetrical, we call R a triangular fuzzy number intuitionistic fuzzy similarity relation.

Theorem 1. *Let (U, R) be a triangular fuzzy number intuitionistic fuzzy approximation space, where R is an approximate relation, then the lower and upper approximation of A have the following properties:*

(1) (Pinchability) $\underline{R}(A) \subseteq A \subseteq \overline{R}(A)$;
(2) (Bipolarity) $\underline{R}(\emptyset) = \overline{R}(\emptyset) = \emptyset, \underline{R}(U) = \overline{R}(U) = U$;
(3) (Monotonicity) $A \subseteq B \Rightarrow \underline{R}(A) \subseteq \underline{R}(B), \overline{R}(A) \subseteq \overline{R}(B)$;
(4) $\overline{R}(A \cup B) = \overline{R}(A) \cup \overline{R}(B), \underline{R}(A \cap B) = \underline{R}(A) \cap \underline{R}(B)$;
(5) $\underline{R}(A) \cup \underline{R}(B) \subseteq \underline{R}(A \cup B), \overline{R}(A \cap B) \subseteq \overline{R}(A) \cap \overline{R}(B)$.

Proof. (1) For $\forall x \in U$ and self-inverse R, we have

$$\tilde{\mu}_R = [1,1,1] := \tilde{1}, \quad \tilde{\nu}_R(x,x) = [0,0,0] := \tilde{0},$$

thus, we an get

$$\tilde{\mu}_{\underline{R}(A)}(x) = \underset{y\in V}{inf}\{\tilde{\mu}_A(y) \vee \tilde{\nu}_R(x,y)\} \subseteq \tilde{\mu}_A(x) \vee \tilde{\nu}_R(x,x) = \tilde{\mu}_A(x) \vee \tilde{0} = \tilde{\mu}_A(x), \forall y \in U,$$

$$\tilde{\nu}_{\underline{R}(A)}(x) = \underset{y\in V}{sup}\{\tilde{\nu}_A(y) \wedge \tilde{\mu}_R(x,y)\} \supseteq \tilde{\nu}_A(x) \wedge \tilde{\mu}_R(x,x) = \tilde{1} \wedge \tilde{\nu}_A(x) = \tilde{\nu}_A(x), \forall y \in U,$$

i.e., $\underline{R}(A) \subseteq A$. $A \subseteq \overline{R}(A)$ similarly certifiable. Therefore $\underline{R} \subseteq A \subseteq \overline{R}$ is proved. Moreover, the proofs of Properties (2)–(5) are obvious by Definitions 5, 8 and 9.

3.2 TFNIFRSs Model Example

In this subsection, the above properties of the TFNIFRSs model (on the pinchability, monotonicity, and concurrency relations) are demonstrated by an example.

Example 1. Let $U = \{x_1, x_2, x_3, x_4\}$, the triangular fuzzy number intuitionistic fuzzy similarity relation R provided in Table 1. Take TFNIFSs $A \subseteq B$ as follows:

$$\begin{aligned} A = \{&\langle x_1, [0.2, 0.4, 0.5], [0.4, 0.45, 0.5]\rangle, \langle x_2 [0.3, 0.43, 0.5], [0.3, 0.37, 0.5]\rangle, \\ &\langle x_3, [0.4, 0.5, 0.6], [0.2, 0.25, 0.3]\rangle, \langle x_4, [0.4, 0.6, 0.7], [0.0, 0.1, 0.2]\rangle\}, \\ B = \{&\langle x_1, [0.3, 0.4, 0.6], [0.3, 0.4, 0.4]\rangle, \langle x_2 [0.55, 0.6, 0.7], [0.1, 0.2, 0.4]\rangle, \\ &\langle x_3, [0.6, 0.6, 0.7], [0.1, 0.2, 0.2]\rangle, \langle x_4, [0.5, 0.7, 0.8], [0.0, 0.1, 0.1]\rangle\}. \end{aligned}$$

Table 1. Triangular fuzzy number intuitionistic fuzzy relationship R

U/U	x_1	x_2	x_3	x_4
x_1	{[1.00, 1.00, 1.00], [0.00, 0.00, 0.00]}	{[0.56, 0.60, 0.70], [0.10, 0.20, 0.30]}	{[0.36, 0.40, 0.55], [0.20, 0.30, 0.40]}	{[0.28, 0.30, 0.55], [0.10, 0.30, 0.40]}
x_2	{[0.56, 0.60, 0.70], [0.10, 0.20, 0.30]}	{[1.00, 1.00, 1.00], [0.00, 0.00, 0.00]}	{[0.50, 0.60, 0.70], [0.20, 0.20, 0.30]}	{[0.30, 0.44, 0.50], [0.25, 0.30, 0.40]}
x_3	{[0.36, 0.40, 0.55], [0.20, 0.30, 0.40]}	{[0.50, 0.60, 0.70], [0.20, 0.20, 0.30]}	{[1.00, 1.00, 1.00], [0.00, 0.00, 0.00]}	{[0.70, 0.80, 0.80], [0.10, 0.15, 0.20]}
x_4	{[0.28, 0.30, 0.55], [0.10, 0.30, 0.40]}	{[0.30, 0.40, 0.50], [0.25, 0.30, 0.40]}	{[0.70, 0.80, 0.80], [0.10, 0.15, 0.20]}	{[1.00, 1.00, 1.00], [0.00, 0.00, 0.00]}

As an example, the computation of the sample x_1 is provided here. By Definition 8, we have:

$$\begin{aligned} \tilde{\mu}_{\underline{R}(A)}(x_1) &= \inf_{x_i \in U} [\tilde{\mu}_A(x_i) \vee \tilde{\nu}_R(x_1, x_i)] \\ &= inf\{[0.20, 0.40, 0.50] \vee [0.00, 0.00, 0.00], [0.30, 0.43, 0.50] \vee [0.10, 0.20, 0.30], \\ &\quad [0.40, 0.50, 0.60] \vee [0.20, 0.30, 0.40], [0.40, 0.60, 0.70] \vee [0.10, 0.30, 0.40]\} \\ &= inf\{[0.20, 0.40, 0.50], [0.30, 0.43, 0.50], [0.45, 0.50, 0.60], [0.40, 0.60, 0.70]\} \\ &= [0.20, 0.40, 0.50], \\ \tilde{\nu}_{\underline{R}(A)}(x_1) &= \sup_{x_i \in U} [\tilde{\mu}_R(x_1, x_i) \wedge \tilde{\nu}_A(x_i)] \\ &= sup\{[1.00, 1.00, 1.00] \wedge [0.40, 0.45, 0.50], [0.56, 0.60, 0.70] \wedge [0.30, 0.37, 0.50], \\ &\quad [0.36, 0.40, 0.55] \wedge [0.20, 0.25, 0.30], [0.28, 0.30, 0.55] \wedge [0.00, 0.10, 0.20]\} \\ &= sup\{[0.40, 0.45, 0.50], [0.30, 0.37, 0.50], [0.20, 0.25, 0.30], [0.00, 0.10, 0.20]\} \\ &= [0.40, 0.45, 0.50]. \end{aligned}$$

Therefore, the lower and upper approximation for x_1 can be obtained as:

$$\begin{aligned} \underline{R}(A)(x_1) &= \{\langle [0.20, 0.40, 0.50], [0.40, 0.45, 0.50]\rangle\}, \\ \overline{R}(A)(x_1) &= \{\langle [0.36, 0.43, 0.55], [0.10, 0.30, 0.40]\rangle\}. \end{aligned}$$

Similarly, it can be inferred that the upper and lower approximations of A and B by x_1 are respectively:

$$\begin{aligned}
\underline{R}(B)(x_1) &= \{\langle x_1, [0.30, 0.40, 0.60], [0.30, 0.40, 0.40]\rangle\},\\
\overline{R}(B)(x_1) &= \{\langle x_1, [0.50, 0.60, 0.70], [0.10, 0.20, 0.30]\rangle\},\\
\underline{R}(A) \cap \underline{R}(B)(x_1) &= \{\langle x_1, [0.20, 0.40, 0.50], [0.40, 0.45, 0.50]\rangle\},\\
\underline{R}(A \cap B)(x_1) &= \{\langle x_1, [0.20, 0.40, 0.50], [0.40, 0.45, 0.50]\rangle\},\\
\overline{R}(A) \cup \overline{R}(B)(x_1) &= \{\langle x_1, [0.50, 0.60, 0.70], [0.10, 0.20, 0.30]\rangle\},\\
\overline{R}(A \cup B)(x_1) &= \{\langle x_1, [0.50, 0.60, 0.70], [0.10, 0.20, 0.30]\rangle\}.
\end{aligned}$$

According to the result of Example 1, the approximation set of the TFNIFS is still an TFNIFS. From the subset relation of Definition 5, we can obtain $\underline{R}(A) \subseteq A \subseteq \overline{R}(A), \underline{R}(A) \subseteq \underline{R}(B), \overline{R}(A) \subseteq \overline{R}(B), \underline{R}(A \cap B) = \underline{R}(A) \cap \underline{R}(B), \overline{R}(A \cup B) = \overline{R}(A) \cup \overline{R}(B)$. The numerical results above can support and verify Theorem 1.

4 Triangular Fuzzy Number Intuitionistic Fuzzy β-Covering Rough Sets Model and Application

In this section, we give the definition of triangular fuzzy number intuitionistic fuzzy β-covering and the neighborhood system based on covering sets to build the rough sets model. Then we combine it with multi-attribute decision making to carry out practical examples in decision making under triangular fuzzy number intuitionistic fuzzy information system.

4.1 Triangular Fuzzy Number Intuitionistic Fuzzy β-Covering Rough Sets

Definition 10. *Let $C = \{C_1, \cdots, C_m\}$, where $C_i (i = 1, \cdots, m)$ is a triangular fuzzy number intuitionistic fuzzy number. $\beta = \langle \beta_1, \beta_2 \rangle$ is a triangular fuzzy number intuitionistic fuzzy number, and C is called a triangular fuzzy number intuitionistic fuzzy β-covering on U, if $(\bigcup_{i=1}^{m} C_i)(x_i) \succeq \beta$. Moreover, (U,C) is called the triangular fuzzy number intuitionistic fuzzy covering approximation space.*

Definition 11. *Let (U, C) be the triangular fuzzy number intuitionistic fuzzy covering approximation space, $\beta = \langle \beta_1, \beta_2 \rangle$ is a triangular fuzzy number intuitionistic fuzzy number, $C = \{C_1, \cdots, C_m\}$ is the triangular fuzzy number intuitionistic fuzzy β-covering. $\hat{N}_x^{\beta} = \cap\{C_j \in C | C_j \succeq \beta, j = 1, \cdots, m\}$ is the triangular fuzzy number intuitionistic fuzzy β-neighborhood of x, and $\tilde{N}_C^{\beta} = \{\langle y, \hat{N}_x^{\beta}(y)\rangle | y \in U\}$ is a triangular fuzzy number intuitionistic fuzzy β-neighborhood system induced by the triangular fuzzy number intuitionistic fuzzy β-covering.*

Definition 12. *Let (U, C) be the triangular fuzzy number intuitionistic fuzzy covering approximation space, $\beta = \langle \beta_1, \beta_2 \rangle$ is a triangular fuzzy number intuitionistic fuzzy number, $C = \{C_1, \cdots, C_m\}$ is the triangular fuzzy number intuitionistic fuzzy β-covering, for any A is a TFNIFS, the upper and lower approximations and of A under the triangular fuzzy number intuitionistic fuzzy β-neighborhood system $\tilde{N}_C^\beta$ are defined as follows:*

$$\begin{aligned}
\underline{\tilde{N}_C^\beta}(A) &= \{\langle x, \underline{\hat{N}_C^\beta}(A)(x)\rangle | x \in U\} \\
&= \{\langle x, \underset{y\in V}{inf}\{\tilde{\mu}_A(y) \vee \tilde{\nu}_{\hat{N}_x^\beta}(y)\}, \underset{y\in V}{sup}\{\tilde{\nu}_A(y) \wedge \tilde{\mu}_{\hat{N}_x^\beta}(y)\}\rangle | x \in U\}, \\
\overline{\tilde{N}_C^\beta}(A) &= \{\langle x, \overline{\hat{N}_C^\beta}(A)(x)\rangle | x \in U\} \\
&= \{\langle x, \underset{y\in V}{sup}\{\tilde{\mu}_{\hat{N}_x^\beta}(y) \wedge \tilde{\mu}_A(y)\}, \underset{y\in V}{inf}\{\tilde{\nu}_{\hat{N}_x^\beta}(y) \vee \tilde{\nu}_A(y)\}\rangle | x \in U\}.
\end{aligned} \tag{8}$$

Moreover, the sequential pair $(\underline{\tilde{N}_C^\beta}(A), \overline{\tilde{N}_C^\beta}(A))$ is called the triangular fuzzy number intuitionistic fuzzy β-covering rough sets, and the corresponding three-way regions (i.e., positive, negative, and boundary regions) are: $POS_{\tilde{N}_C^\beta}(A) = \underline{\tilde{N}_C^\beta}(A)$, $NEG_{\tilde{N}_C^\beta}(A) = U - \overline{\tilde{N}_C^\beta}(A)$, $BND_{\tilde{N}_C^\beta}(A) = \overline{\tilde{N}_C^\beta}(A) - \underline{\tilde{N}_C^\beta}(A)$, where the three-way regions form a division of U corresponding to the implementation of acceptance, rejection, and delayed decisions.

4.2 Model Application

Let $U = \{x_1, \cdots, x_n\}$ be the set of n recruitment objects, $C = \{C_1, \cdots, C_m\}$ be the description of evaluation criteria for each recruitment object, $d = \{d_1, \cdots, d_t\}$ be the t experts involved in the evaluation, and $\omega = \{\omega_1, \cdots, \omega_t\}$ be the weight of each expert, $\omega_k \geq 0$ and satisfies $\sum_{k=1}^t \omega_k = 1$. The steps for determining the expert weights are given below.

Definition 13. *The consistency measure of expert d_k on x_i is defined:*

$$CM_k(x_i) = \sum_{r\neq k} \sum_{j=1}^m D(C_j^r(x_i), C_j^k(x_i)), \tag{9}$$

and the consistency measure of expert d_k about triangular fuzzy number intuitionistic fuzzy decision matrix $M(K) = \{C_j^k(x_i)\}_{(n\times m)}$ is defined:

$$CM_k = \sum_{i=1}^n CM_k(x_i) = \sum_{r\neq k} \sum_{i=1}^n \sum_{j=1}^m D(C_j^r(x_i), C_j^k(x_i)). \tag{10}$$

Assuming that $\omega = \{\omega_1, \cdots, \omega_t\}$ is the experts' weight vector, we get:

$$\omega_k = \frac{CM_k}{\sum_{r=1}^t CM_r}. \tag{11}$$

Clearly, $0 \leq \omega_k \leq 1$ and $\sum_{k=1}^t \omega_k = 1$.

4.3 Multi-attribute Decision-Making Algorithm Based on Triangular Fuzzy Number Intuitionistic Fuzzy β-Covering Rough Sets

In this subsection, we propose a multi-attribute decision-making algorithm based on the triangular fuzzy number intuitionistic fuzzy β-covering rough sets, where $U = \{x_1, \cdots, x_n\}$, and there are m TFNIFSs on U constituting the triangular fuzzy number intuitionistic fuzzy decision matrix C.

Algorithm 1. The optimal object is selected by using triangular fuzzy number intuitionistic fuzzy β-covering rough sets

Input: Multi-attribute triangular fuzzy number intuitionistic fuzzy decision-making information system (U, C, A) and β.

Output: Sorting results for all objects in U.

1: Import experts' evaluation data;
2: Compute the β-neighborhood system $\tilde{N}_C^{\beta}$;
3: Compute the upper and lower approximations $\underline{\tilde{N}_C^{\beta}}(A)$ and $\overline{\tilde{N}_C^{\beta}}(A)$ of A;
4: Calculate the score function $S_i(\underline{\tilde{N}_C^{\beta}}(A) \bigoplus \overline{\tilde{N}_C^{\beta}}(A))(x)$ for each expert;
5: Calculate the total score function value $S_U(x_i)$ according to the experts' weights, sort by function value size.

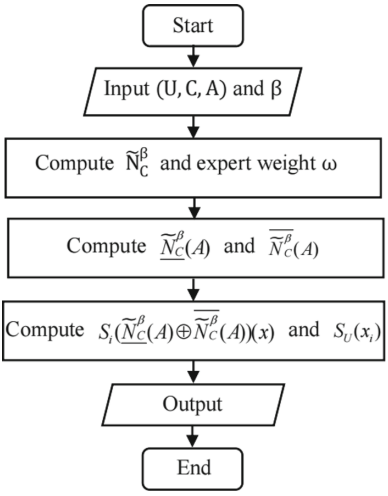

Fig. 1. Algorithm 1's flows chart on objects sorting

Algorithm 1 calculates and sorts for objects in U by using triangular fuzzy number intuitionistic fuzzy β covering rough set, which follows the follows the flow chart of Fig 1. The total time complexity of Algorithm 1 is $O(|U|^3 \times |V|)$.

4.4 Example Illustration

A company in September 2023 for the vacancy of a certain position to go to each high school to recruitment of talents, set $U = \{x_1, \cdots, x_5\}$ represents the demand collected by the initial review of the five project applications. The project applications are collected on demand, from which one or two outstanding recruits are selected. In order to ensure the scientific nature of the evaluation, denotes 3 experts in the field hired by the company to evaluate these 5 recruitment targets, $d = \{d_1, d_2, d_3\}$ denotes the weight of each expert and gives 6 job criteria $C = \{C_1, \cdots, C_6\}$, i.e., specialized knowledge ability (C_1), practicality of theories and applications (C_2), innovativeness (C_3), inquisitiveness (C_4), insightfulness (C_5), and foresight (C_6). The 3 experts give the value of 5 recruitment targets x_i under the job criteria C_j, denoted as $C_j(x_i) = \langle[\tilde{\mu_{ij}}, \tilde{\nu_{ij}}]\rangle$ respectively. Where $\tilde{\mu_{ij}}$ denotes the set of triangular fuzzy numbers for which x_i satisfies the job criterion C_j, and $\tilde{\nu_{ij}}$ denotes the set of triangular fuzzy numbers for which x_i does not satisfy the job criterion C_j. These values form the triangular fuzzy number intuitionistic fuzzy decision matrix as shown in Table 2 below. At the same time, the company according to its own preference to use the triangular intuitionistic fuzzy number to evaluate each recruitment target, denoted by A.

$$\begin{aligned} A = \{&\langle x_1, [0.3, 0.3, 0.4], [0.5, 0.55, 0.6]\rangle, \langle x_2, [0.6, 0.7, 0.8], [0.1, 0.1, 0.2]\rangle, \\ &\langle x_3, [0.5, 0.7, 0.8], [0.1, 0.2, 0.2]\rangle, \langle x_4, [0.65, 0.7, 0.8], [0.1, 0.2, 0.2]\rangle, \\ &\langle x_5, [0.4, 0.5, 0.6], [0.2, 0.3, 0.4]\rangle\}. \end{aligned}$$

Let $\beta = \langle[0.4, 0.44, 0.5], [0.2, 0.3, 0.55]\rangle$, from Definition 10, $C = \{C_1, \cdots, C_6\}$ constitutes a triangular fuzzy number intuitionistic fuzzy β-covering of U. Taking expert 1 as an example, we can get $\hat{H}^{\beta}_{x_1} = C_2 \cap C_3 \cap C_4 \cap C_5 \cap C_6, \hat{H}^{\beta}_{x_2} = C_2 \cap C_5 \cap C_6, \hat{H}^{\beta}_{x_3} = C_3 \cap C_4 \cap C_6, \hat{H}^{\beta}_{x_4} = C_1 \cap C_2 \cap C_6, \hat{H}^{\beta}_{x_5} = C_1 \cap C_2 \cap C_5 \cap C_6$ by Definition 11, and the results of β-neighbor systems are presented in Table 3.

To avoid tedious length, only the upper and lower approximation of $\tilde{N}^{\beta}_{1C}(A)$ are given below. By Definition 12, $\underline{\tilde{H}^{\beta}_{C}}(A)$ and $\overline{\tilde{H}^{\beta}_{C}}(A)$ are calculated as follows:

$$\begin{aligned} \underline{\tilde{N}^{\beta}_{1C}}(A) = \{&\langle x_1, [0.3, 0.3, 0.4], [0.5, 0.5, 0.6]\rangle, \langle x_2, [0.3, 0.3, 0.4], [0.5, 0.5, 0.6]\rangle, \\ &\langle x_3, [0.3, 0.3, 0.4], [0.5, 0.5, 0.6]\rangle, \langle x_4, [0.4, 0.5, 0.5], [0.3, 0.4, 0.5]\rangle, \\ &\langle x_5, [0.4, 0.5, 0.5], [0.3, 0.4, 0.5]\rangle\}, \\ \overline{\tilde{N}^{\beta}_{1C}}(A) = \{&\langle x_1, [0.4, 0.5, 0.6], [0.3, 0.3, 0.4]\rangle, \langle x_2, [0.5, 0.6, 0.7], [0.1, 0.2, 0.3]\rangle, \\ &\langle x_3, [0.4, 0.6, 0.7], [0.1, 0.2, 0.3]\rangle, \langle x_4, [0.5, 0.6, 0.7], [0.2, 0.2, 0.3]\rangle, \\ &\langle x_5, [0.5, 0.6, 0.6], [0.2, 0.3, 0.4]\rangle\}. \end{aligned}$$

Table 2. Evaluation values of the guidelines given by experts 1–3

U/C	C_1	C_2	C_3	C_4	C_5	C_6
x_1	$\{[0.3,0.4,0.5],$	$\{[0.6,0.7,0.8],$	$\{[0.6,0.6,0.7],$	$\{[0.5,0.6,0.7],$	$\{[0.6,0.6,0.7],$	$\{[0.5,0.5,0.6],$
	$[0.4,0.5,0.5]\}$	$[0.1,0.1,0.2]\}$	$[0.2,0.2,0.3]\}$	$[0.1,0.2,0.2]\}$	$[0.1,0.2,0.5]\}$	$[0.2,0.2,0.3]\}$
x_2	$\{[0.4,0.5,0.6],$	$\{[0.5,0.6,0.6],$	$\{[0.4,0.5,0.6],$	$\{[0.2,0.3,0.4],$	$\{[0.4,0.6,0.7],$	$\{[0.6,0.6,0.8],$
	$[0.2,0.3,0.4]\}$	$[0.1,0.2,0.3]\}$	$[0.2,0.3,0.4]\}$	$[0.4,0.5,0.6]\}$	$[0.1,0.2,0.2]\}$	$[0.1,0.1,0.2]\}$
x_3	$\{[0.2,0.3,0.4],$	$\{[0.4,0.5,0.6],$	$\{[0.7,0.8,0.9],$	$\{[0.5,0.6,0.8],$	$\{[0.5,0.5,0.6],$	$\{[0.4,0.6,0.7],$
	$[0.4,0.5,0.6]\}$	$[0.3,0.3,0.4]\}$	$[0.1,0.1,0.1]\}$	$[0.1,0.2,0.2]\}$	$[0.3,0.3,0.4]\}$	$[0.1,0.2,0.3]\}$
x_4	$\{[0.5,0.6,0.7],$	$\{[0.5,0.8,0.8],$	$\{[0.5,0.6,0.6],$	$\{[0.4,0.5,0.6],$	$\{[0.6,0.6,0.7],$	$\{[0.5,0.6,0.7],$
	$[0.1,0.2,0.2]\}$	$[0.1,0.1,0.2]\}$	$[0.2,0.3,0.4]\}$	$[0.3,0.4,0.4]\}$	$[0.1,0.3,0.4]\}$	$[0.2,0.2,0.3]\}$
x_5	$\{[0.7,0.7,0.8],$	$\{[0.5,0.5,0.5],$	$\{[0.7,0.7,0.7],$	$\{[0.4,0.5,0.6],$	$\{[0.5,0.5,0.7],$	$\{[0.4,0.6,0.6],$
	$[0.1,0.1,0.2]\}$	$[0.2,0.3,0.4]\}$	$[0.1,0.1,0.2]\}$	$[0.3,0.3,0.4]\}$	$[0.2,0.3,0.3]\}$	$[0.1,0.1,0.2]\}$
x_1	$\{[0.3,0.4,0.4],$	$\{[0.5,0.6,0.7],$	$\{[0.5,0.5,0.6],$	$\{[0.4,0.5,0.6],$	$\{[0.4,0.6,0.6],$	$\{[0.5,0.6,0.7],$
	$[0.2,0.3,0.4]\}$	$[0.1,0.1,0.1]\}$	$[0.1,0.1,0.2]\}$	$[0.1,0.2,0.4]\}$	$[0.2,0.2,0.2]\}$	$[0.1,0.2,0.3]\}$
x_2	$\{[0.4,0.5,0.5],$	$\{[0.5,0.5,0.6],$	$\{[0.4,0.5,0.5],$	$\{[0.6,0.7,0.7],$	$\{[0.5,0.6,0.7],$	$\{[0.4,0.5,0.5],$
	$[0.1,0.2,0.3]\}$	$[0.2,0.2,0.4]\}$	$[0.1,0.2,0.2]\}$	$[0.1,0.1,0.3]\}$	$[0.1,0.3,0.3]\}$	$[0.1,0.2,0.4]\}$
x_3	$\{[0.5,0.6,0.7],$	$\{[0.4,0.5,0.6],$	$\{[0.4,0.6,0.6],$	$\{[0.5,0.5,0.6],$	$\{[0.4,0.5,0.5],$	$\{[0.5,0.6,0.7],$
	$[0.1,0.1,0.3]\}$	$[0.2,0.2,0.3]\}$	$[0.2,0.2,0.4]\}$	$[0.2,0.3,0.3]\}$	$[0.3,0.3,0.4]\}$	$[0.1,0.1,0.2]\}$
x_4	$\{[0.4,0.5,0.7],$	$\{[0.5,0.6,0.6],$	$\{[0.5,0.6,0.6],$	$\{[0.6,0.6,0.7],$	$\{[0.6,0.6,0.6],$	$\{[0.5,0.6,0.6],$
	$[0.1,0.1,0.2]\}$	$[0.1,0.2,0.3]\}$	$[0.2,0.3,0.4]\}$	$[0.1,0.1,0.2]\}$	$[0.2,0.2,0.3]\}$	$[0.1,0.3,0.3]\}$
x_5	$\{[0.4,0.5,0.5],$	$\{[0.6,0.6,0.7],$	$\{[0.5,0.6,0.7],$	$\{[0.7,0.7,0.8],$	$\{[0.4,0.5,0.5],$	$\{[0.6,0.6,0.7],$
	$[0.2,0.3,0.5]\}$	$[0.1,0.3,0.3]\}$	$[0.2,0.3,0.3]\}$	$[0.1,0.1,0.1]\}$	$[0.2,0.3,0.4]\}$	$[0.1,0.2,0.2]\}$
x_1	$\{[0.4,0.5,0.6],$	$\{[0.6,0.7,0.7],$	$\{[0.4,0.5,0.6],$	$\{[0.6,0.6,0.7],$	$\{[0.5,0.5,0.6],$	$\{[0.5,0.5,0.7],$
	$[0.2,0.3,0.4]\}$	$[0.1,0.2,0.3]\}$	$[0.3,0.3,0.4]\}$	$[0.1,0.2,0.3]\}$	$[0.1,0.2,0.3]\}$	$[0.1,0.2,0.2]\}$
x_2	$\{[0.4,0.4,0.5],$	$\{[0.5,0.5,0.6],$	$\{[0.5,0.6,0.7],$	$\{[0.5,0.6,0.6],$	$\{[0.5,0.6,0.6],$	$\{[0.6,0.7,0.8],$
	$[0.2,0.3,0.3]\}$	$[0.1,0.3,0.3]\}$	$[0.2,0.2,0.3]\}$	$[0.1,0.2,0.2]\}$	$[0.2,0.2,0.3]\}$	$[0.1,0.2,0.2]\}$
x_3	$\{[0.5,0.5,0.6],$	$\{[0.5,0.6,0.7],$	$\{[0.5,0.5,0.6],$	$\{[0.6,0.6,0.8],$	$\{[0.6,0.6,0.7],$	$\{[0.4,0.5,0.6],$
	$[0.1,0.3,0.3]\}$	$[0.2,0.2,0.2]\}$	$[0.1,0.2,0.4]\}$	$[0.1,0.1,0.2]\}$	$[0.1,0.2,0.2]\}$	$[0.2,0.3,0.4]\}$
x_4	$\{[0.6,0.6,0.7],$	$\{[0.6,0.6,0.8],$	$\{[0.6,0.6,0.7],$	$\{[0.4,0.5,0.6],$	$\{[0.4,0.4,0.6],$	$\{[0.6,0.7,0.7],$
	$[0.2,0.3,0.3]\}$	$[0.1,0.1,0.1]\}$	$[0.1,0.1,0.2]\}$	$[0.1,0.2,0.3]\}$	$[0.2,0.3,0.4]\}$	$[0.1,0.1,0.2]\}$
x_5	$\{[0.5,0.5,0.6],$	$\{[0.5,0.5,0.5],$	$\{[0.4,0.4,0.5],$	$\{[0.6,0.7,0.8],$	$\{[0.5,0.6,0.6],$	$\{[0.4,0.5,0.6],$
	$[0.2,0.2,0.3]\}$	$[0.2,0.2,0.4]\}$	$[0.2,0.2,0.4]\}$	$[0.1,0.2,0.4]\}$	$[0.1,0.3,0.3]\}$	$[0.2,0.2,0.4]\}$

Moreover, according to Definition 6, the score functions for the three experts are calculated as follows:

$$S_1(\underline{\tilde{N}^{\beta}_{1C}}(A) \bigoplus \overline{\tilde{N}^{\beta}_{1C}}(A))(x) = \{\langle x_1, 0.4875\rangle, \langle x_2, 0.62\rangle, \langle x_3, 0.6025\rangle, \langle x_4, 0.695\rangle, \langle x_5, 0.65\rangle\},$$

$$S_2(\underline{\tilde{N}^{\beta}_{2C}}(A) \bigoplus \overline{\tilde{N}^{\beta}_{2C}}(A))(x) = \{\langle x_1, 0.5575\rangle, \langle x_2, 0.5625\rangle, \langle x_3, 0.5825\rangle, \langle x_4, 0.555\rangle, \langle x_5, 0.5825\rangle\},$$

$$S_3(\underline{\tilde{N}^{\beta}_{3C}}(A) \bigoplus \overline{\tilde{N}^{\beta}_{3C}}(A))(x) = \{\langle x_1, 0.5325\rangle, \langle x_2, 0.5375\rangle, \langle x_3, 0.5375\rangle, \langle x_4, 0.52\rangle, \langle x_5, 0.5475\rangle\}.$$

Then, the three experts' weights are calculated as: $\omega_1 = 0.3483, \omega_2 = 0.3327, \omega_3 = 0.3189$ by Definition 13, and the total score function values as follows:

Table 3. Triangular fuzzy number intuitionistic fuzzy β-neighborhood systems for experts 1–3

$\tilde{H}_C^\beta$	x_1	x_2	x_3	x_4	x_5
$\hat{H}_{x_1}^\beta$	$\{[0.5,0.5,0.6],$	$\{[0.2,0.3,0.4],$	$\{[0.4,0.5,0.6],$	$\{[0.4,0.5,0.6],$	$\{[0.4,0.5,0.5],$
	$[0.2,0.2,0.3]\}$	$[0.4,0.5,0.6]\}$	$[0.3,0.3,0.4]\}$	$[0.3,0.4,0.4]\}$	$[0.3,0.4,0.4]\}$
$\hat{H}_{x_2}^\beta$	$\{[0.5,0.5,0.6],$	$\{[0.4,0.6,0.6],$	$\{[0.4,0.5,0.6],$	$\{[0.5,0.6,0.7],$	$\{[0.4,0.5,0.5],$
	$[0.2,0.2,0.3]\}$	$[0.1,0.2,0.3]\}$	$[0.3,0.3,0.4]\}$	$[0.2,0.3,0.4]\}$	$[0.2,0.3,0.4]\}$
$\hat{H}_{x_3}^\beta$	$\{[0.5,0.5,0.6],$	$\{[0.2,0.3,0.4],$	$\{[0.4,0.6,0.7],$	$\{[0.4,0.5,0.6],$	$\{[0.4,0.5,0.6],$
	$[0.2,0.2,0.3]\}$	$[0.4,0.5,0.6]\}$	$[0.1,0.2,0.3]\}$	$[0.3,0.4,0.4]\}$	$[0.3,0.4,0.4]\}$
$\hat{H}_{x_4}^\beta$	$\{[0.3,0.4,0.5],$	$\{[0.4,0.5,0.6],$	$\{[0.2,0.3,0.4],$	$\{[0.5,0.6,0.7],$	$\{[0.4,0.5,0.5],$
	$[0.4,0.5,0.5]\}$	$[0.2,0.3,0.4]\}$	$[0.4,0.5,0.6]\}$	$[0.2,0.2,0.3]\}$	$[0.2,0.3,0.4]\}$
$\hat{H}_{x_5}^\beta$	$\{[0.3,0.4,0.5],$	$\{[0.4,0.5,0.6],$	$\{[0.2,0.3,0.4],$	$\{[0.5,0.6,0.6],$	$\{[0.4,0.5,0.6],$
	$[0.4,0.5,0.5]\}$	$[0.2,0.3,0.4]\}$	$[0.4,0.5,0.6]\}$	$[0.2,0.3,0.4]\}$	$[0.2,0.3,0.3]\}$
$\hat{H}_{x_1}^\beta$	$\{[0.4,0.5,0.6],$	$\{[0.4,0.5,0.5],$	$\{[0.4,0.5,0.5],$	$\{[0.5,0.6,0.6],$	$\{[0.4,0.5,0.5],$
	$[0.2,0.2,0.3]\}$	$[0.2,0.3,0.4]\}$	$[0.3,0.3,0.4]\}$	$[0.2,0.3,0.4]\}$	$[0.2,0.3,0.4]\}$
$\hat{H}_{x_2}^\beta$	$\{[0.3,0.4,0.4],$	$\{[0.4,0.5,0.5],$	$\{[0.4,0.5,0.5],$	$\{[0.4,0.5,0.6],$	$\{[0.4,0.5,0.5],$
	$[0.2,0.3,0.4]\}$	$[0.1,0.3,0.3]\}$	$[0.3,0.3,0.4]\}$	$[0.2,0.3,0.4]\}$	$[0.2,0.3,0.5]\}$
$\hat{H}_{x_3}^\beta$	$\{[0.3,0.4,0.4],$	$\{[0.4,0.5,0.5],$	$\{[0.4,0.5,0.6],$	$\{[0.4,0.5,0.6],$	$\{[0.4,0.5,0.6],$
	$[0.2,0.3,0.4]\}$	$[0.2,0.2,0.4]\}$	$[0.2,0.3,0.3]\}$	$[0.1,0.3,0.3]\}$	$[0.2,0.3,0.5]\}$
$\hat{H}_{x_4}^\beta$	$\{[0.3,0.4,0.4],$	$\{[0.4,0.5,0.5],$	$\{[0.4,0.5,0.5],$	$\{[0.4,0.5,0.6],$	$\{[0.4,0.5,0.5],$
	$[0.2,0.3,0.4]\}$	$[0.2,0.3,0.4]\}$	$[0.3,0.3,0.4]\}$	$[0.2,0.3,0.3]\}$	$[0.2,0.3,0.5]\}$
$\hat{H}_{x_5}^\beta$	$\{[0.4,0.5,0.6],$	$\{[0.4,0.5,0.5],$	$\{[0.4,0.5,0.6],$	$\{[0.4,0.5,0.6],$	$\{[0.5,0.6,0.7],$
	$[0.1,0.2,0.4]\}$	$[0.2,0.2,0.4]\}$	$[0.2,0.3,0.4]\}$	$[0.2,0.3,0.3]\}$	$[0.2,0.3,0.3]\}$
$\hat{H}_{x_1}^\beta$	$\{[0.5,0.5,0.6],$	$\{[0.5,0.5,0.6],$	$\{[0.4,0.5,0.6],$	$\{[0.4,0.4,0.6],$	$\{[0.4,0.5,0.5],$
	$[0.1,0.2,0.3]\}$	$[0.2,0.3,0.3]\}$	$[0.2,0.3,0.4]\}$	$[0.2,0.3,0.4]\}$	$[0.2,0.3,0.4]\}$
$\hat{H}_{x_2}^\beta$	$\{[0.4,0.5,0.6],$	$\{[0.5,0.5,0.6],$	$\{[0.4,0.5,0.6],$	$\{[0.4,0.4,0.6],$	$\{[0.4,0.4,0.5],$
	$[0.3,0.3,0.4]\}$	$[0.2,0.3,0.3]\}$	$[0.2,0.3,0.4]\}$	$[0.2,0.3,0.4]\}$	$[0.2,0.3,0.4]\}$
$\hat{H}_{x_3}^\beta$	$\{[0.4,0.5,0.6],$	$\{[0.4,0.4,0.5],$	$\{[0.5,0.5,0.6],$	$\{[0.4,0.4,0.6],$	$\{[0.5,0.5,0.5],$
	$[0.2,0.3,0.4]\}$	$[0.2,0.3,0.3]\}$	$[0.2,0.3,0.3]\}$	$[0.2,0.3,0.4]\}$	$[0.2,0.3,0.4]\}$
$\hat{H}_{x_4}^\beta$	$\{[0.4,0.5,0.6],$	$\{[0.4,0.4,0.5],$	$\{[0.4,0.5,0.6],$	$\{[0.4,0.5,0.6],$	$\{[0.4,0.4,0.5],$
	$[0.3,0.3,0.4]\}$	$[0.2,0.3,0.3]\}$	$[0.2,0.3,0.4]\}$	$[0.2,0.3,0.3]\}$	$[0.2,0.2,0.4]\}$
$\hat{H}_{x_5}^\beta$	$\{[0.4,0.5,0.6],$	$\{[0.4,0.4,0.5],$	$\{[0.5,0.5,0.6],$	$\{[0.4,0.4,0.6],$	$\{[0.5,0.5,0.6],$
	$[0.4,0.5,0.6]\}$	$[0.2,0.3,0.3]\}$	$[0.1,0.3,0.3]\}$	$[0.2,0.3,0.4]\}$	$[0.2,0.3,0.3]\}$

$$S_U = \{\langle x_1, 0.5251\rangle, \langle x_2, 0.5745\rangle, \langle x_3, 0.5751\rangle, \langle x_4, 0.5925\rangle, \langle x_5, 0.5948\rangle\}. \quad (12)$$

Based on the above calculations, the 5 recruitment targets were ranked by the comparison method of Definition 6. From Eq. (12), it can be seen that the score function values ranked in the first two recruitment targets are x_5, x_4. Therefore, the most suitable employees for the company are the 5th recruitment target and the 4th recruitment target, and the other cases can be analyzed in an analogous way. Similar analysis can be done for other cases.

5 Conclusion

In this paper, the TFNIFRS model is established by fusing the TFNIFS with RS, and using the intuitionistic fuzzy approximation relation of triangular fuzzy numbers. At the same time, the corresponding approximation operators, correlation properties, three-way regions, and the numerical calculation are studied and verified. Secondly, based on TFNIFS and covering rough set, the concepts of triangular fuzzy number intuitionistic fuzzy β-coverage and neighborhood are proposed, and the triangular fuzzy number intuitionistic fuzzy β-covering rough set is establish, which is applicable to multi-attribute decision-making and enhances the management of fuzzy information as well as the analysis of uncertainty. Finally, the feasibility and effectiveness of the triangular fuzzy number intuitionistic fuzzy β-covering rough set for multi-attribute decision making are verified by an example. Based on TFNIFRSs, related measurement construction, attribute reduction and rule extraction become our next research target. In addition, more multi-attribute decision making methods and their corresponding comparative analysis are worthy of further study.

Acknowledgements. The work was supported by National Natural Science Foundation of China (62206228), Natural Science Foundation of Sichuan Province of China (24NSFSC1487, 2022NSFSC0929), Sichuan Science and Technology Program of China (2022ZYD0001), and Humanities and Social Sciences Project of the Ministry of Education of China (23YJA630114).

Disclosure of Interests. The authors declare that they have no conflicts of interest to this work.

References

1. Anh, P.V., Thuy, N.N., Thi, V.D., Giang, N.L.: On distance-based attribute reduction with α, β-level intuitionistic fuzzy sets. IEEE Access **11**, 138095–138107 (2023)
2. Atanassov, K.T.: Circular intuitionistic fuzzy sets. J. Intell. Fuzzy. Syst. **39**(5), 5981–5986 (2022)
3. Atanassov, K.T.: Intuitionistic fuzzy sets. Fuzzy. Set. Syst. **20**(1), 87–96 (1986)
4. Atanassov, K., Vassilev, P.: Intuitionistic fuzzy sets and other fuzzy sets extensions representable by them. J. Intell. Fuzzy. Syst. **318**(1), 525–530 (2020)
5. Chen, H., Li, T., Luo, C., Horng, S.-J., Wang, G.: A decision-theoretic rough set approach for dynamic data mining. IEEE. Trans. Fuzzy Syst. **23**(6), 1958–1970 (2015)
6. Chen, Z.C., Liu, P.H.: Intuitionistic fuzzy value similarity measures for intuitionistic fuzzy sets. Comput. Appl. Math. **41**(1), 45 (2022)
7. Dai, J.H., Chen, T., Zhang, K.: The intuitionistic fuzzy concept-oriented three-way decision model. Inf. Sci. **619**, 52–83 (2023)
8. Dubois, D., Prade, H.: Rough fuzzy sets and fuzzy rough sets. Int. J. Gener. Syst. **17**(2), 191–209 (1990)
9. Gangadhari, R.K., Khanzode, V., Murthy, S.: Application of rough set theory and machine learning algorithms in predicting accident outcomes in the Indian petroleum industry. Concurr. Comput.-Pract. **34**(26), e7277 (2022)

10. He, X.X., Li, Y.F., Du, L.M., Qin, K.Y.: Two computational formulae for similarity measures on intuitionistic fuzzy sets based on intuitionistic fuzzy equivalencies. J. Intell. Fuzzy. Syst. **37**(5), 7073–7086 (2019)
11. Liu, F., Yuan, X.H.: Fuzzy number intuitionistic fuzzy set. Fuzzy Set. Syst. **21**(1), 88–91 (2007)
12. Liu, Y., Lin, Y., Zhao, H.H.: Variable precision intuitionistic fuzzy rough set model and applications based on conflict distance. Expert. Syst. **32**(2), 220–227 (2015)
13. Ma, L.W.: Two fuzzy covering rough set models and their generalizations over fuzzy lattices. Fuzzy Set. Syst. **294**, 1–17 (2016)
14. Ma, X.Q., Qin, H.W., Abawajy, J.H.: Interval-valued intuitionistic fuzzy soft sets based decision-making and parameter reduction. IEEE. Trans. Knowl. Data. Eng. **30**(2), 357–369 (2022)
15. Pawlak, Z.: Rough sets. Int. J. Comput. Inf. Sci. **11**, 341–356 (1982)
16. Singh, S., Som, T.: Intuitionistic fuzzy rough sets: theory to practice. Math. Comput. Sci. Eng. 91–133 (2022)
17. Sun, B.Z., Ma, W.M., Gong, Z.T.: Dominance-based rough set theory over interval-valued information systems. Expert. Syst. **31**(2), 185–197 (2014)
18. Tiew, S.T., et al.: A fragrance prediction model for molecules using rough set-based machine learning. Chem. Ing. Tech. **95**(3), 438–446 (2023)
19. Verma, R.: Generalized Bonferroni mean operator for fuzzy number intuitionistic fuzzy sets and its application to multiattribute decision making. Int. J. Intell. Syst. **30**(5), 499–519 (2015)
20. Xia, S.Y., et al.: GRRS: accurate and efficient neighborhood rough set for feature selection. IEEE Trans. Knowl. Data Eng. **35**(9), 9281–9294 (2022)
21. Xue, Z.A., Sun, B.X., Hou, H.D., Pang, W.L., Zhang, Y.N.: Three-way decision models based on multi-granulation rough intuitionistic hesitant fuzzy Sets. Cogn. Comput. **14**(6), 1859–1880 (2022)
22. Xu, Y.J.: Some new operations on triangular fuzzy number intuitionistic fuzzy set. In: 2019 Chinese Control and Decision Conference (CCDC), Nanchang, China, pp. 3760–3763 (2019)
23. Yao, Y.: Three-way decision: an interpretation of rules in rough set theory. In: Wen, P., Li, Y., Polkowski, L., Yao, Y., Tsumoto, S., Wang, G. (eds.) RSKT 2009. LNCS (LNAI), vol. 5589, pp. 642–649. Springer, Heidelberg (2009). https://doi.org/10.1007/978-3-642-02962-2_81
24. Yao, Y.Y.: Three-way decisions with probabilistic rough sets. Inf. Sci. **180**(3), 341–353 (2010)
25. Ye, D.Y., Liang, D.C., Hu, P.: Three-way decisions with interval-valued intuitionistic fuzzy decision-theoretic rough sets in group decision-making. Symmetry-Basel. **10**(7), 281 (2018)
26. Zadeh, L.A.: Fuzzy sets. Inf. Control **8**, 338–353 (1965)
27. Zhang, Q.L., Liu, F., Fan, C.Q., Xie, W.H.: Fuzzy numbers intuitionistic fuzzy descriptor systems. Inf. Sci. **469**, 44–59 (2018)
28. Zhang, X., He, Z.Q., Yang, Y.Y.: A fuzzy rough set-based undersampling approach for imbalanced data. Int. J. Mach. Learn. Cybern. 1–12 (2024)
29. Zhang, X.Y., Fan, Y.R., Yao, Y.S., Yang, J.L.: Class-specific attribute reducts based on neighborhood rough sets. J. Intell. Fuzzy. Syst. **43**(6), 7891–7910 (2022)
30. Zhang, Z.M.: An interval-valued intuitionistic fuzzy rough set model. Fund. Inform. **97**(4), 471–498 (2009)

Three-Way Decision of Granular-Ball Rough Sets Based on Fuzziness

Zhuangzhuang Liu[1], Taihua Xu[1(✉)], Jie Yang[2], and Shuyin Xia[3]

[1] School of Computer, Jiangsu University of Science and Technology, Zhenjiang 212100, Jiangsu, China
xth19890410@163.com

[2] School of Physics and Electronic Science, Zunyi Normal University, Zunyi 563002, China

[3] Chongqing Key Laboratory of Computational Intelligence, Chongqing University of Posts and Telecommunications, Chongqing 400065, China

Abstract. Granular-ball computing (GBC) proposed by Xia adaptively generates a different neighborhood for each object, resulting in greater generality and flexibility. Moreover, GBC greatly improves the efficiency by replacing point input with granular-ball. However, traditional granular-ball classifiers may lead to risky classification on uncertain cases. In this paper, we introduce three-way decision (3WD) into GBC to construct a novel three-way decision of granular-ball rough sets (3WD-GBRS) from the perspective of uncertainty. This helps to construct reasonable multi-granularity spaces for handling complex decision problems with uncertainty. 3WD-GBRS is constructed in a data-driven method based on fuzziness, which avoids the subjective definition of certain risk parameters when calculating the threshold pairs. We further analyze the fuzziness loss of multilevel decision result in 3WD-GBRS. Extensive comparative experiments are conducted with 3 state-of-the-art GB-based classifiers and 1 classical machine learning classifiers on 6 public benchmark datasets. The results show that 3WD-GBRS almost outperforms other comparison methods in term of effectiveness and efficiency.

Keywords: granular-ball rough sets · three-way decision · fuzziness

1 Introduction

Granular computing (GrC) [1–4] is about formation, processing and communicating information granules, which provides solutions to simulate the human cognitive thinking to solve complex problems. From diverse perspectives, rough sets [5], fuzzy sets [6], and quotient spaces [7] are three main models of GrC. Rough sets are widely used to measure the uncertainty and incompleteness of information systems. Classical rough sets exploit an equivalence relation to divide the universe, separating an information system into an upper approximation set

M. Hu et al. (Eds.): IJCRS 2024, LNAI 14840, pp. 29–43, 2024.
https://doi.org/10.1007/978-3-031-65668-2_3

and a lower approximation set. To process continuous data, neighborhood rough sets (NRS) [8] utilize the neighborhood granulation to convert the equivalence relation into the covering relation in neighborhood space. In addition, numerous extended GrC-based classifiers [9] are designed to employ the information granule as the fundamental computing unit, significantly enhancing the efficiency for knowledge discovery. Nevertheless, the majority of these classifiers treat the granules as a preliminary feature procession method, without modifying the mathematical model or enhancing the primary performance of the classifiers themselves.

Based on the idea of GrC, granular-ball computing (GBC) [10,11] proposed by Xia is a novel method to process data and represent knowledge by replacing traditional information granule input with granular-ball (GB), which follows the rule of 'global topology precedence' [12]. After several years of development, GBC is constantly being improved in terms of methods and applications. Chen [13] introduced a GB-based attribute selector, resulting in better classification performance based on the obtained reduction. Recently, granular-ball neighborhood rough sets (GBNRS), as a novel NRS model, is proposed by Xia et al. [14]. Compared with traditional NRS methods, GBNRS is a multi-granularity learning tool with greater robustness and efficiency by replacing neighborhood granule with granular-ball. However, current works of GBC focus on the traditional two-way classification, which may result in misclassification on uncertain cases. As well known, three-way decision (3WD) [15–17] theory proposed by Yao is an emerging approach to address the complex problem with uncertainty. The basic principle of 3WD refers to dividing a universe into three distinct regions and each region corresponds to a decision action. As a generalization of the traditional two-way decision model, 3WD further incorporates a third option, which provides a trisecting-and-acting way for decision-making. Currently, 3WD has been widely applied in different fields. Yao [18] further proposed the sequential three-way decisions (S3WD) by introducing the idea of GrC. In essence, S3WD is a progressive computing method with granularity being finer. This means that the same problem can be handled in a multi-granularity spaces. In term of the advantage of 3WD, we introduce 3WD into GBC to construct the three-way decision of granular-ball rough sets (3WD-GBRS). The delayed decision action reduces decision-making risk to a greater extent by considering the cost or uncertainty of problem-solving. This contributes to establish the reasonable multi-granularity structures to address the complex problem with uncertain and insufficient information. The most works of 3WD focuses on calculating thresholds by utilizing the given risk parameters from the perspective of misclassification cost. However, in real applications, it is difficult to accurately obtain the risk parameters based on the expert experience. To address the above issue, it is beneficial to introduce fuzziness into 3WD-GBRS, which provides an objective method to calculate the threshold pairs from perspective of uncertainty.

The following sections of this paper are structured with the subsequent manner. In Sect. 2 is a review of related preliminary definitions. In Sect. 3, a 3WD-GBRS is constructed by maintaining the fuzziness invariance. Then, the relevant

experiments for the verification of the viability and rationality of our models are shown in Sect. 4. Finally, Sect. 5 summarizes the conclusions.

2 Preliminaries

In this section, to facilitate the framework of this paper, we review some necessary definitions related to 3WD and granular-ball rough set.

Definition 1. *(Granular-ball [10]) Let $U = \{x_1, x_2, \ldots, x_n\}$ be a non-empty finite set. $\forall x \in U$, a granular ball gb_i is defined as:*

$$gb_i = \{x \in U \mid d(x, c_i) \leq r_i\} \tag{1}$$

Here, c_i and r_i represent the center and radius of gb_i respectively, and $d(x_i, c_i)$ represents the distance from x_i to c_i.

Definition 2. *(The Center and Radius of Granular-ball [10])*

Let gb be a Granular-ball from definition 1, which contains m objects $x_1, x_2, ..., x_m$, the center of gb, c, is the gravity of the m objects, where m is the size of gb. The radius of gb, r, is the average distance from all objects in GB to c. They are computed as (2) and (3), respectively:

$$c = \frac{1}{m} \sum_{i=1}^{m} x_i \tag{2}$$

$$r = \frac{1}{m} \sum_{i=1}^{m} \|x_i - c\| \tag{3}$$

where $\|x_i - c\|$ represents the distance from x_i to c.

Definition 3. *(Indiscernible granular-ball relation) Let $S = (U, AT \cup D, V, f)$ be a decision system, where U is a nonempty finite set, and an element $x \in U$ is called an object; AT is the set of conditional attributes, $a \in AT$ is an attribute, and D is the decision attribute; $V = V_{AT} \cup V_D$, where $V_{AT} = \bigcup_{a \in AT} V_a$ is the range of values for AT and V_a is the range of values for the conditional attribute a;$V_D = \{l_1, l_2, \ldots, l_z\}$ is the range of values for D or the label set; $f : U \times (AT \cup \{D\}) \rightarrow V$ is a mapping function such that $f(x, a) \in V_a$ and $f(x, D) \in V_D$. $\forall x_1, x_2 \in U$ and $B_1 \subseteq AT$, the indiscernible granular ball relation $INDGB(B_1)$ of the attribute subset B_1 is defined as:*

$$INDGB(B_1) = \{(x_1, x_2) \in U^2 | f(x_1, a) = f(x_2, a) = gb, \forall a \in B\} \tag{4}$$

If $(x_1, x_2) \in INDGB(B_1)$, the relationship between x_1 and x_2 is denoted as $x_1 : x_2$. In granular-ball rough set, $INDGB(B_1)$ denotes an equivalence relation

on U, which can create a granular-ball space of U, denoted as $U/GB(B_1)$, that is, $U/GB(B_1) = [x]_{GB_1} = \{gb_1^1, gb_2^1, \ldots, gb_m^1\}$.

Let $S = (U, AT \cup D, V, f)$ be a decision system, $B_1, B_2 \subseteq AT$. $[x]_{GB_1} = \{gb_1^1, gb_2^1, \ldots, gb_m^1\}$ and $[x]_{GB_2} = \{gb_1^2, gb_2^2, \ldots, gb_l^2\}$ denote two granular-ball spaces induced by $INDGB(B_1)$ and $INDGB(B_2)$, respectively.
If $\forall_{gb_i^2 \in U/GB(B_2)} (\exists_{gb_k^1 \in U/GB(B_1)} (gb_i^2 \subseteq gb_k^1))$ then $[x]_{GB_1}$ is finer than $[x]_{GB_2}$, denoted as $[x]_{GB_2} \preceq [x]_{GB_1}$. If $\forall_{gb_i^2 \in U/GB(B_2)} (\exists_{gb_k^1 \in U/GB(B_1)} (gb_i^2 \subset gb_k^1))$,then $[x]_{GB_1}$ is strictly finer than $[x]_{GB_2}$, denoted as $[x]_{GB_2} \prec [x]_{GB_1}$.

Definition 4. *(Granular-ball rough set [14]) Let $S = (U, AT \cup D, V, f)$ be a decision system, $B_1 \subseteq AT$.X denotes a target fuzzy subset on U, $[x]_{GB_1} = \{gb_1^1, gb_2^1, \ldots, gb_m^1\}$ is a granular-ball space on U. The definition of the upper and lower approximation sets of X based on B are represented by:*

$$\begin{aligned} \overline{GBR_{B_1}}(X) &= \bigcup \{gb_i^1 \in [x]_{GB_1} \mid gb_i^1 \cap X \neq \emptyset\} \\ \underline{GBR_{B_1}}(X) &= \bigcup \{gb_i^1 \in [x]_{GB_1} \mid gb_i^1 \subseteq X\} \end{aligned} \tag{5}$$

Definition 5. *(Step-fuzzy set) Let $U = \{x_1, x_2, \ldots, x_n\}$ be a non-empty finite set. $B_1 \subseteq AT$.X denotes a target fuzzy subset on U, $[x]_{GB_1} = \{gb_1^1, gb_2^1, \ldots, gb_m^1\}$ is a granular-ball space on U, where $gb_i^1 = \{x_{i1}, x_{i2}, \ldots, x_{i|gb_i^1|}\}$ $(i = 1, 2, \ldots, m)$. If $\mu_X(x_{i1}) = \mu_X(x_{i2}) = \ldots = \mu_X(x_{i|gb_i^1|}) = \varepsilon_i$ $(0 \leq \varepsilon_i \leq 1,\ i = 1, 2, \ldots, m)$, then X is a step-fuzzy set of granular-ball.*

Definition 6. *(Average granular-ball fuzzy sets) Let $U = \{x_1, x_2, \ldots, x_n\}$ be a non-empty finite set. GBR is a corresponding equivalence relation, X denotes a fuzzy set on U, $[x]_{GB_1} = \{gb_1^1, gb_2^1, \ldots, gb_m^1\}$ is a granular-ball space on U, where $gb_i^1 = \{x_{i1}, x_{i2}, \ldots, x_{i|gb_i^1|}\}$ $(i = 1, 2, \ldots, m)$. $\overline{\mu}(gb_i^1) = \frac{\sum_{x \in gb_i^1} \mu(x)}{|gb_i^1|}$ is called the average membership degree of granular-ball gb_i^1, $\mu(x)$ denotes the membership of an object x, where $x \in gb_i^1$, and $|gb_i^1|$ is the cardinality of the set gb_i^1. we refer to $X_{GB_1}^J$ as the average fuzzy set of X*

$$X_{GB_1}^J = \frac{\bar{\mu}\left(gb_1^1\right)}{gb_1^1} + \frac{\bar{\mu}\left(gb_2^1\right)}{gb_2^1} + \cdots + \frac{\bar{\mu}\left(gb_m^1\right)}{gb_m^1} \tag{6}$$

In Definition 5, $\overline{\mu}(gb_i^1)$ can be understood as the probability that granular-ball gb_i^1 belongs to the target concept X, which is more general than rough membership degree [19].

According to the formula of average fuzziness $F_X = \frac{4}{|U|} \sum_{x \in U} \mu(x)(1 - \mu(x))$ [20] where X denotes a target subset on U, we define the average granular-ball fuzziness as follows:

Definition 7. *(Average granular-ball fuzziness) Let $S = (U, AT \cup D, V, f)$ be a decision system, $B_1 \subseteq AT$.X denotes a target fuzzy subset on U, $[x]_{GB_1} =$*

$\{gb_1^1, gb_2^1, \ldots, gb_m^1\}$ is a granular-ball space on U. The average granular-ball fuzziness is defined as follows:

$$F_{X_{GB_1}^J} = \frac{4}{|U|} \sum_{i=1}^{m} h(gb_i^1) \tag{7}$$

where, $h(gb_i^1) = \overline{\mu}(gb_i^1)(1 - \overline{\mu}(gb_i^1))$.

The uncertainty of granular-ball rough set comes from three regions: positive region, negative region, and boundary region, that is to say,

$$\begin{aligned} F_{X_{GB_1}^J} &= \frac{4}{|U|} \sum_{gb \in POS(X_{GB_1}^J)} \overline{\mu}(gb)(1 - \overline{\mu}(gb)) \\ &+ \frac{4}{|U|} \sum_{gb \in BND(X_{GB_1}^J)} \overline{\mu}(gb)(1 - \overline{\mu}(gb)) \\ &+ \frac{4}{|U|} \sum_{gb \in NEG(X_{GB_1}^J)} \overline{\mu}(gb)(1 - \overline{\mu}(gb)) \\ &= F(POS(X_{GB_1}^J)) + F(BND(X_{GB_1}^J)) + F(NEG(X_{GB_1}^J)) \end{aligned}$$

3 Three-Way Decision of Granular-Ball Rough Sets Based on Fuzziness Loss

In the process of generating granular-balls, Algorithm 1 shows the detailed process of generating GBs, which utilizes the distributional characteristics. Whether the GB is further split is primarily influenced by the number of objects within it (i.e., the size of the GB). When the count of objects is sufficiently small, it can be ensured that the majority of objects encompassed belong to the same class.

Algorithm 1: Generate-GB_list [21]

Input: $\mathbb{D}$: the dataset
Output: GB_list:the set of granular balls
Initializing: $n = |\mathbb{D}|$, $gb = \mathbb{D}$, $GB\_list = \emptyset$; Add gb to an empty queue Q;
while Q *is not empty* **do**
  Get the first element gb from Q and delete it from Q; **if** *the size of* gb *is larger than* $\sqrt{n}$ **then**
    Employ 2-means algorithm to divide gb into two sub-balls $Sub1$ and $Sub2$;
    Add $Sub1$ and $Sub2$ to the tail of Q;
  end
  if *the size of* gb *is less than or equal to* $\sqrt{n}$ **then**
    Compute the center c and radius r of gb according to Eq. 2-3;
    $GB\_list = GB\_list \cup gb$;
  end
end
Return GB_list;

In the general 3WD framework [15], the current 3WD can be summarized into three aspects: minimum distance, minimum cost, and uncertainty invariance. Fuzziness, as an uncertainty measure, is able to describe the uncertain information of granular-ball space. Fuzziness loss is objectively to describe the variations of uncertain information. For example, the change from fuzzy sets to average granular-ball fuzzy sets may generate the fuzziness loss. Therefore, we introduce fuzziness into three-way decision of granular-ball rough sets (3WD-GBRS), which provides a new way for 3WD-GBRS from a different perspective. In this section, 3WD-GBRS is established based on fuzziness loss, and the relevant theories are presented. This paper proposes a 3WD-GBRS based on fuzziness loss by constructing the shadowed map. This is easy to obtain clearer decision rules and represent uncertain information, which avoids the need for priori expert knowledge. More specifically, the granular-ball with average membership degree below α and above β will be assigned to shadowed areas. That is, the range of average membership degree is extended to an uncertain area $[\beta, \alpha]$, which is defined as follows:

Definition 8. *(Shadowed map) Let* $S = (U, AT \cup D, V, f)$ *be a decision system,* $B_1 \subseteq AT$.X *denotes a target fuzzy subset on* U, $[x]_{GB_1} = \{gb_1^1, gb_2^1, \ldots, gb_m^1\}$.*Let a mapping* $M : X_{GB_1}^J \to \{0, [\beta, \alpha], 1\}$, *which is from* $X_{GB_1}^J$ *to the set* $\{0, [\beta, \alpha], 1\}$, *and* M *is denoted by:*

$$M(X_{GB_1}^J) = \begin{cases} 0 & \overline{\mu}(gb_i^1) \leq \beta \\ [\beta, \alpha] & \beta < \overline{\mu}(gb_i^1) < \alpha \\ 1 & \overline{\mu}(gb_i^1) \geq \alpha \end{cases} \tag{8}$$

where $(i = 1, 2, \ldots, m)$.

The three regions divided according to thresholds ensure the minimum fuzziness loss of 3WD-GBRS. Corresponding to any average membership degree of granular-ball, 3WD-GBRS is established to approximately characterize the fuzzy target concept as follows:

1. If the average membership degree $\bar{\mu}(gb_i^1)$ is below or equal to β, $\bar{\mu}(gb_i^1)$ is reduced to 0. This indicates that allocating granular-ball gb_i^1 to the negative region will minimize the fuzziness loss.
2. If the average membership degree $\bar{\mu}(gb_i^1)$ is above or equal to α, $\bar{\mu}(gb_i^1)$ is elevated to 1. This indicates that allocating granular-ball gb_i^1 to the positive region will minimize the fuzziness loss.
3. If the average membership degree $\bar{\mu}(gb_i^1)$ is below α and above β, $\bar{\mu}(gb_i^1)$ is transformed into $[\beta, \alpha]$. This indicates that allocating granular-ball gb_i^1 to the boundary region will minimize the fuzziness loss.

From Definition 8, $F(\mathrm{POS}(M(X_{GB_1}^J))) = F(\mathrm{NEG}(M(X_{GB_1}^J))) = 0$. Therefore, the total fuzziness can be calculated as follows:

$$\begin{aligned} & F_{M(X_{GB_1}^J)} \\ & = F_{M(X_{GB_1}^J)}(\mathrm{BND}(M(X_{GB_1}^J))) \\ & = \frac{4}{|U|} \sum_{i=1}^{m} \left| \{x \mid x \in gb_i^1 \wedge \beta < \bar{\mu}(gb_i^1) < \alpha\} \right| \frac{\int_\beta^\alpha t(1-t)\, dt}{\alpha - \beta} \end{aligned} \tag{9}$$

According to the shadowed map, the 3WD-GBRS presented can be defined as follows:

Definition 9. *(3WD-GBRS) Let $S = (U, AT \cup D, V, f)$ be a decision system, $B_1 \subseteq AT$. X denotes a target fuzzy subset on U, $[x]_{GB_1} = \{gb_1^1, gb_2^1, \ldots, gb_m^1\}$. α, β denotes a pair of thresholds. The positive region, negative region and boundary region are represented by:*

$$\begin{aligned} POS(X_{GB_1}^J) &= \{x \in U \mid \bar{\mu}(gb_i^1) \geq \alpha\}, \\ BND(X_{GB_1}^J) &= \{x \in U \mid \beta < \bar{\mu}(gb_i^1) < \alpha\}, \\ NEG(X_{GB_1}^J) &= \{x \in U \mid \bar{\mu}(gb_i^1) \leq \beta\}. \end{aligned} \tag{10}$$

where, $\bar{\mu}(gb_i^1)$ denotes the average membership degree of gb_i^1.

Fuzziness loss is able to objectively characterize the change of uncertain information without expert experience. To maintain the fuzziness invariance, the objective function is proposed to obtain the optimal threshold pair (β, α).

$$\underset{0 \leq \beta \leq \alpha \leq 1}{\operatorname{argmin}} \left| F_{M(X_{GB_1}^J)} - F_{X_{GB_1}^J} \right| \tag{11}$$

where

$$
\begin{aligned}
&F_{M(X^J_{GB_1})} - F_{X^J_{GB_1}} \\
&= \frac{4}{|U|}\sum_{i=1}^{m}\Bigg(\Big|\{x \,|\, x \in gb_i^1 \wedge \beta < \bar{\mu}(gb_i^1) < \alpha\}\Big| \\
&\quad \frac{\int_\beta^\alpha t(1-t)dt}{\alpha-\beta} - \bar{\mu}(gb_i^1)(1-\bar{\mu}(gb_i^1))\Bigg)
\end{aligned} \tag{12}
$$

Firstly, the optimal thresholds are acquired by minimizing the fuzziness loss between average granular-ball fuzzy sets $X^J_{GB_1}$ and its shadowed map $M(X^J_{GB_1})$ based on objective function. Then, the granular-balls in GBRS are divided to establish the three regions to make a decision according to the thresholds. The granular-balls with $\bar{\mu}(gb_i^1)$ greater than α are considered to belong to the positive region. The granular-balls with $\bar{\mu}(gb_i^1)$ less than β are considered to belong to the negative region. The granular-balls with $\bar{\mu}(gb_i^1)$ between β and α are considered to belong to the boundary region. The actual fuzziness of the granular-ball space is characterized by average granular-ball fuzzy sets, then a shadowed map is constructed to provide thresholds for 3WD-GBRS by minimizing the fuzziness loss.

For the 3WD-GBRS model, we perform fuzzy loss analysis on the average granular fuzzy set from the perspective of fuzzy loss. In 3WD-GBRS model, the uncertainty typically originates three regions at each granular-ball space, because the granular-balls of positive and negative region are uncertain; namely, the average membership degree of these granular-balls may be not completely equal to 0 or 1. With the finer granular-ball space, the granular-balls of positive and negative region may be reclassified and the three disjoint regions will change. As a result, the uncertainty loss at each granular-ball space in 3WD-GBRS model will be changed accordingly. In the next section, we continue our analysis of the changing patterns of uncertainty loss in 3WD-GBRS.

Theorem 1. *Let* $S = (U, AT \cup D, V, f)$ *be a decision system,* $Seq\_GBS = ([x]_{GB_1}, [x]_{GB_2}, \ldots, [x]_{GB_N})$ *and* X *be a target fuzzy subset on* U*. Then,* $F_{(X^J_{GB_{j+1}})} \leq F_{(X^J_{GB_j})}$ *holds.*

Proof. Suppose $[x]_{GB_j} = \{gb_1^j, gb_2^j, \ldots, gb_m^j\}$ *and* $[x]_{GB_{j+1}} = \{gb_1^{j+1}, gb_2^{j+1}, \ldots, gb_l^{j+1}\}$ *are two granular-ball spaces in* Seq_GBS*, respectively. Because* $[x]_{GB_{j+1}} \subseteq [x]_{GB_j}$*, to simplify the proof, suppose that only a granular ball* gb_1^j *is subdivided into* gb_1^{j+1} *and* gb_2^{j+1} *from* $[x]_{GB_j}$ *to* $[x]_{GB_{j+1}}$*, while no change in other granular balls (more complex situations can be translated into this case, so no more repeat here). Based on the above assumptions, we have* $gb_1^j = gb_1^{j+1} \cup gb_2^{j+1}, gb_2^j = gb_3^{j+1}, gb_3^j = gb_4^{j+1}, \ldots, gb_m^j = gb_l^{j+1} (l = m+1)$*. That is,* $[x]_{GB_j} = \{gb_1^{j+1}, gb_2^{j+1}, gb_2^j, gb_3^j, \ldots, gb_m^j\}$.

$$\begin{aligned} & F_{(X^J_{GB_{j+1}})} - F_{(X^J_{GB_j})} \\ &= \frac{4}{|U|}\left(h(gb_1^j) - h(gb_1^{j+1}) - h(gb_2^{j+1})\right) \\ &= \frac{4}{|U|}\left(\bar{\mu}(gb_1^j)(1-\bar{\mu}(gb_1^j)) - \bar{\mu}(gb_1^{j+1})(1-\bar{\mu}(gb_1^{j+1}))\right. \\ &\quad \left. - \bar{\mu}(gb_2^{j+1})(1-\bar{\mu}(gb_2^{j+1}))\right) \end{aligned} \tag{13}$$

Because $gb_1^j = gb_1^{j+1} \cup gb_2^{j+1}$, *then* $\bar{\mu}(gb_1^j) = \frac{|gb_1^{j+1}|}{|gb_1^j|}\bar{\mu}(gb_1^{j+1}) + \frac{|gb_2^{j+1}|}{|gb_1^j|}\bar{\mu}(gb_2^{j+1})$, *we have*

$$\begin{aligned} & F_{(X^J_{GB_{j+1}})} - F_{(X^J_{GB_j})} \\ &= 4\frac{|gb_1^{j+1}||gb_2^{j+1}|}{|U||gb_1^j|}(\bar{\mu}(gb_1^{j+1}) - \bar{\mu}(gb_2^{j+1}))^2 \geq 0 \end{aligned} \tag{14}$$

Therefore, $F_{(X^J_{GB_{j+1}})} \leq F_{(X^J_{GB_j})}$.

From Theorem 1, the fuzziness monotonically decreases with the granularity refinement in 3WD-GBRS. When $[x]_{GB_{j+1}}$ in Theorem 1 reaches the finest granular-ball space $[x]_{GB_N}$, Corollary 1 can be obtained:

Corollary 1. *Let* $S = (U, AT \cup D, V, f)$ *be a decision system,* $Seq\_GBS = ([x]_{GB_1}, [x]_{GB_2}, \ldots, [x]_{GB_N})$ *and* X *be a target fuzzy subset on* U. *Then,* $F_{(X^J_{GB_j})} \geq F_{(X^J_{GB_N})}$ *holds.*

Theorem 2. *Let* $S = (U, AT \cup D, V, f)$ *be a decision system,* $Seq\_GBS = ([x]_{GB_1}, [x]_{GB_2}, \ldots, [x]_{GB_N})$ *and* X *be a target fuzzy subset on* U. *Then,* $|F_{X^J_{GB_{j+1}}} - F_{X^J_{GB_N}}| \leq |F_{X^J_{GB_j}} - F_{X^J_{GB_N}}|$ *holds.*

Proof. From Corollary 1, $F_{X^J_{GB_j}} \geq F_{X^J_{GB_N}}$ *holds. Then, we have*

$$|F_{X^J_{GB_{j+1}}} - F_{X^J_{GB_N}}| - |F_{X^J_{GB_j}} - F_{X^J_{GB_N}}| = F_{X^J_{GB_{j+1}}} - F_{X^J_{GB_j}} \tag{15}$$

Obviously, according to Theorem 1, $|F_{X^J_{GB_{j+1}}} - F_{X^J_{GB_N}}| \leq |F_{X^J_{GB_j}} - F_{X^J_{GB_N}}|$ *holds.*

From Theorem 2, the fuzziness loss between the arbitrary granular-ball space and the finest granular-ball space $[x]_{GB_N}$ in 3WD-GBRS monotonically decreases with the granularity refinement in 3WD-GBRS.

It is well known that calculating the fuzziness of the three decision regions is important for decision making in the 3WD theory. However, the fuzziness of each decision region may not monotonically decrease as the granular-ball space is refined in 3WD-GBRS. For simplicity, we only analyze the three situations of fuzziness in the boundary region.

4 Experiment

In this section, we meticulously outline the experimental setup, encompassing validation procedures, evaluation metrics and comparison methods. Initially, we present the findings pertaining to the uncertainty exhibited by 3WD-GBRS. Subsequently, we conduct an ablation study to demonstrate the effectiveness of our proposed approach. Finally, we provide a comprehensive assessment of the performance of 3WD-GBRS in terms of effectiveness and efficiency.

Datasets: Experiments are performed based on six UCI datasets, which are shown in Table 1.

Table 1. The information of experimental datasets.

No.	Datasets	Characteristics	Instances	Attributes
1	Raisin	Integer, Real	900	7
2	Steel Plates Faults(SPF)	Integer, Real	1941	27
3	Wifi_Localization(Wifi_Loc)	Real	2000	7
4	Rice	Real	3810	7
5	Twonorm	Integer, Real	7400	20
6	Dry Bean	Integer, Real	13611	16

4.1 General Settings

Validation Procedures and Evaluation Metrics: To mitigate the potential false performance resulting from overfitting, we utilize the 10-fold cross-validation technique in each subsection of Sect. 4 to accurately assess the true generalizability of our proposed method.

For the experiment, the performance of 3WD-GBRS is validated, including accuracy, time cost. Furthermore, we employ the Wilcoxon rank-sum test to ascertain the presence of any substantial differences between the compared classifiers.

4.2 An Analysis of Uncertainty for 3WD-GBRS

As shown in Fig. 1, the x-coordinate represents four granularity levels, ranging from the coarsest (level-4) to the finest (level-1), while the y-coordinate focuses on individual values of fuzziness. We can note the following points:

- The uncertainty is mainly derived from boundary region at each granularity layer in 3WD-GBRS.
- From the coarser to finer levels in 3WD-GBRS, the total uncertainty $F_{X^J_{GB_1}}$ monotonously decrease, while the uncertainty with respect to three regions exhibit a non-monotonicity.
- The difference between $F_{M(X^J_{GB_1})}$ and $F_{X^J_{GB_1}}$ is very small on each granularity.

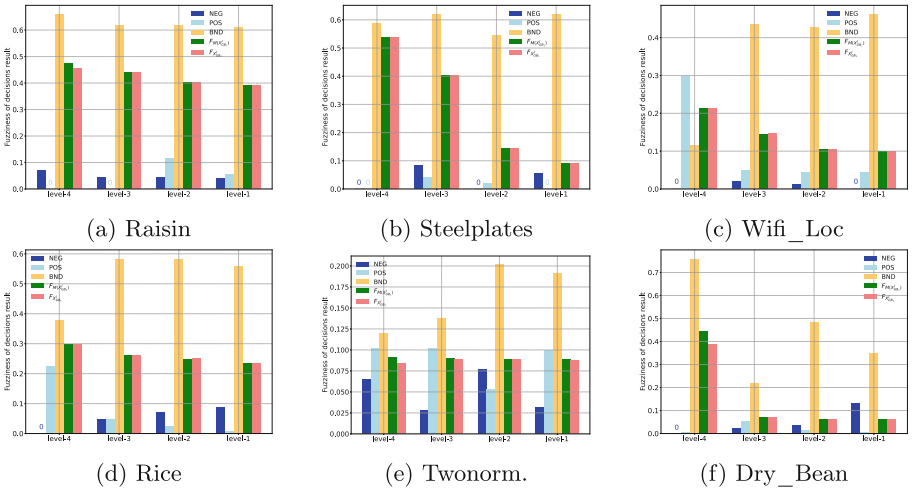

(a) Raisin (b) Steelplates (c) Wifi_Loc

(d) Rice (e) Twonorm. (f) Dry_Bean

Fig. 1. The change of uncertainty for 3WD-GBRS.

This is easily understood because several GBs containing in different regions are probably subdivided into numerous finer GBs with granularity being finer, leading to an increased or decreased uncertainty in the three regions simultaneously. Moreover, the total increment of decreased uncertainty is greater than or equal to the total increment of increased uncertainty, since the total uncertainty in the 3WD-GBRS decreases with granularity being finer, which is consistent with Theorem 1.

4.3 3WD-GBRS VS Other Classifiers

Effectiveness: The comparison experiment includes 4 different classification algorithms, including 3WD-NRS, GBKNN, GBKNN++ and ACC-GBKNN, etc. Table 2 presents four evaluation metrics, namely *Accuracy*, *Precision*, *Recall* and $F1$. *Accuracy* is determined by two variables, R_{test} and U_{test}, which represent the ratio of correctly predicted test samples to the total number of test samples. *Precision* quantifies the proportion of elements accurately predicted as positive. Specifically, let tp denote the total number of correctly predicted positive elements, fp the total number of false positives. The formulas for *Accuracy*,and *Precision*,are as follows:

$$Accuracy = \frac{R_{\text{test}}}{U_{\text{test}}} \tag{16}$$

$$Precision = \frac{tp}{tp + fp} \tag{17}$$

Subsequently, statistical analysis is performed on the results, including Friedman test, Wilcoxon rank-sum test, and mean ranking analysis. $Win/Loss$ represents the win-loss ratio following pairwise comparisons between 3WD-GBRS and the comparison algorithms. $p-value$ reflects the difference between 3WD-GBRS and the comparison algorithms. If $p-value < 0.05$, it indicates a significant difference between 3WD-GBRS and the comparison algorithms; otherwise, there is no statistical difference. Rank represents the average ranking. A higher rank value indicates a more effective algorithm. As shown in Table 2, in terms of $Win/Loss$, 3WD-GBRS wins 89 times out of 96 total comparison times against other algorithms. In terms of $p-value$, 3WD-GBRS shows significant differences with the comparison algorithms. Regarding $rank$, 3WD-GBRS obtains the highest overall score, followed by GBKNN and GBKNN++.

The superior performance of 3WD-GBRS in terms of effectiveness can be attributed to the following reasons: (1) Compared to the traditional classifiers including 3WD-NRS, 3WD-GBRS inherits the advantages of granular-balls-based classifiers. That is, on one hand, granular-balls are more suitable for describing datasets with spherical distributions and exhibit robustness to noisy data. (2) Compared to the GB-based classifiers including GBKNN, GBKNN++ and ACC-GBKNN, the idea of 3WD enhances uncertainty handling, which improves the classification performance to a great extent.

Efficiency: Figure 2 shows the time required for 3WD-GBRS and comparison methods on each dataset. For all classifiers, the average execution time of each classifier on each data is processed by taking the logarithm. With the increase in dataset size, the time required for classification by 3WD-NRS significantly increases. It is obviously that the time required for 3WD-GBRS is not significantly different from that of GBKNN++, GBKNN, ACC-GBKNN. This implies that the time required by 3WD-GBRS is not significantly different from that of other GB-based methods. Due to the acquirement of thresholds in 3WD introduced, 3WD-GBRS incurs slightly more time compared to the other GB-based methods. However, this increase of time cost is entirely acceptable. Overall, 3WD-GBRS provides a classification solution with relatively low time complexity.

5 Conclusion

Considering the shortcomings of the existing GB-based classifier, this paper introduce the three-way decision theory into GBC to construct a novel three-way decision of granular-ball rough sets (3WD-GBRS) from the perspective of uncertainty. According to the experiment, the performance of 3WD-GBRS is validated, that is, 3WD-GBRS almost outperforms other comparison methods in term of effectiveness, and efficiency. This comprehensive comparison encompassed 3 state-of-the-art GB-based classifiers and 1 classical machine learning classifiers, on 6 public benchmark datasets. Consequently, our work establishes a robust foundation for future endeavors in granular-ball computing, aiming for enhanced robustness and generality. Notably, our efforts are exploratory in nature and inevitably carry certain limitations.

Table 2. The statistical analysis of various algorithms.

No.	Metrics	GBKNN	GBKNN++	ACC-GBKNN	3WD-NRS	3WD-GBRS
1	*Accuracy*	0.8489	0.8522	0.8033	0.5114	0.8790
	*F*1	0.8438	0.8513	0.8025	0.6767	0.8693
	Recall	0.8659	0.8156	0.8333	1.0000	0.9048
	Precision	0.8267	0.8811	0.7889	0.5114	0.8406
2	*Accuracy*	0.9043	0.8643	0.8663	0.4818	0.9829
	*F*1	0.8458	0.8513	0.8524	0.6503	0.9859
	Recall	0.8048	0.9777	0.9677	1.0000	0.9863
	Precision	0.9455	0.7794	0.7797	0.4818	0.9871
3	*Accuracy*	0.9745	0.9660	0.9640	0.6408	0.9806
	*F*1	0.9743	0.9660	0.9639	0.7811	0.9791
	Recall	0.9769	0.9690	0.9670	1.0000	0.9853
	Precision	0.9730	0.9647	0.9631	0.6408	0.9744
4	*Accuracy*	0.9202	0.9050	0.8858	0.8040	0.9419
	*F*1	0.9061	0.9028	0.8838	0.8914	0.9314
	Recall	0.9092	0.8859	0.8840	1.0000	0.9344
	Precision	0.9043	0.8924	0.8557	0.8040	0.9293
5	*Accuracy*	0.9708	0.9561	0.9473	0.7857	0.9827
	*F*1	0.9708	0.9561	0.9473	0.8800	0.9825
	Recall	0.9709	0.9613	0.9527	1.0000	0.9862
	Precision	0.9708	0.9513	0.9426	0.7857	0.9789
6	*Accuracy*	0.9597	0.9439	0.9536	0.8446	0.9843
	*F*1	0.8749	0.9066	0.9168	0.9158	0.9324
	Recall	0.8612	0.9032	0.9096	1.0000	0.9717
	Precision	0.8958	0.8175	0.8284	0.8446	0.9077
Statistics	*win/loss*	24/0	23/1	24/0	18/6	89/7
	$p-vlaue$	0.0017	0.0010	0.0006	0.0069	
	rank	**3.2500(2)**	**2.6667(3)**	2.1667	2.2083	**4.7083(1)**

Acknowledgment. This work was supported by the National Science Foundation of China (Grant number 62066049).

References

1. Zadeh, L.A.: Toward a theory of fuzzy information granulation and its centrality in human reasoning and fuzzy logic. Fuzzy Sets Syst. **90**(2), 111–127 (1997)
2. Pedrycz, W., Homenda, W.: Building the fundamentals of granular computing: a principle of justifiable granularity. Appl. Soft Comput. **13**(10), 4209–4218 (2013)
3. Wang, G.Y., Yang, J., Xu, J.: Granular computing: from granularity optimization to multi-granularity joint problem solving. Granular Comput. **2**, 105–120 (2017)
4. Yao, Y.Y.: Three-way granular computing, rough sets, and formal concept analysis. Int. J. Approximate Reasoning **116**, 106–125 (2020)

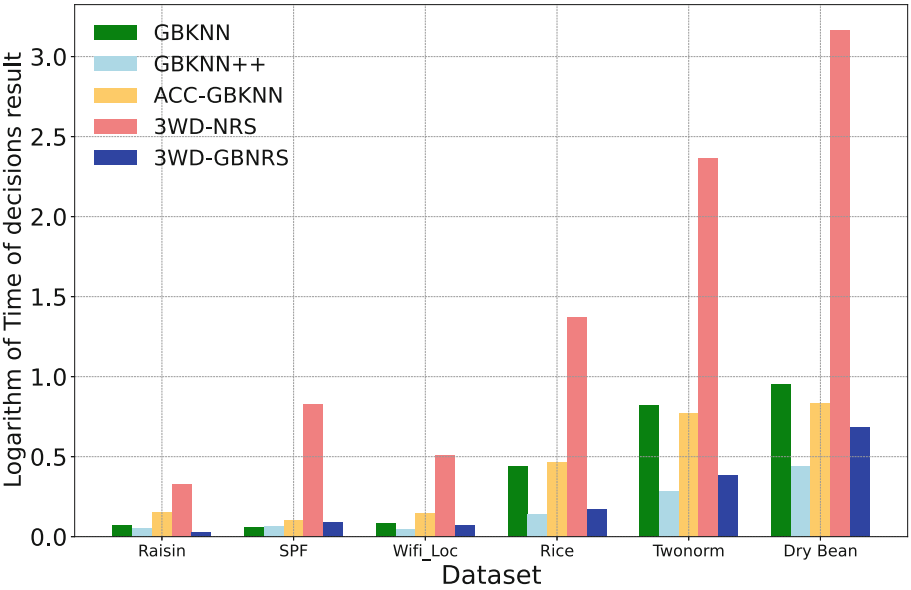

Fig. 2. Execution time on datasets.

5. Pawlak, Z.: Rough sets. Int. J. Comput. Inf. Sci. **11**, 341–356 (1982)
6. Zadeh, L.A.: Fuzzy sets. Inf. Control **8**(3), 338–353 (1965)
7. Zhang, L., Zhang, B.: The quotient space theory of problem solving. Fund. Inform. **59**(2–3), 287–298 (2004)
8. Hu, Q.H., Yu, D.R., Xie, Z.X.: Neighborhood classifiers. Expert Syst. Appl. **34**(2), 866–876 (2008)
9. Fu, C., Yang, J.H.: Granular classification for imbalanced datasets: a Minkowski distance-based method. Algorithms **14**(2), 54 (2021)
10. Xia, S.Y., Liu, Y.S., Ding, X., Wang, G.Y., Yu, H., Luo, Y.G.: Granular ball computing classifiers for efficient, scalable and robust learning. Inf. Sci. **483**, 136–152 (2019)
11. Xia, S.Y., et al.: An efficient and accurate rough set for feature selection, classification, and knowledge representation. IEEE Trans. Knowl. Data Eng. **35**(4), 5319–5331 (2024)
12. Xie, Q., et al.: GBG++: a fast and stable granular ball generation method for classification. IEEE Trans. Emerg. Top. Comput. Intell. **8**(2), 2022–2036 (2024)
13. Chen, Y., Wang, P.X., Yang, X.B., Mi, J.S., Liu, D.: Granular ball guided selector for attribute reduction. Knowl.-Based Syst. **229**, 107326 (2021)
14. Xia, S., Zhang, H., Li, W., Wang, G., Giem, E., Chen, Z.: GBNRS: a novel rough set algorithm for fast adaptive attribute reduction in classification. IEEE Trans. Knowl. Data Eng. **34**(3), 1231–1242 (2020)
15. Yao, Y.Y.: The superiority of three-way decisions in probabilistic rough set models. Inf. Sci. **181**(6), 1080–1096 (2011)
16. Yao, Y.Y.: Three-way decision and granular computing. Int. J. Approximate Reasoning **103**, 107–123 (2018)

17. Chen, J., Chen, Y., He, Y., Xu, Y., Zhao, S., Zhang, Y.: A classified feature representation three-way decision model for sentiment analysis. Appl. Intell. **52**, 7995–8007 (2021). https://doi.org/10.1007/s10489-021-02809-1
18. Yang, X., Li, T.R., Fujita, H., Liu, D., Yao, Y.Y.: A unified model of sequential three-way decisions and multilevel incremental processing. Knowl.-Based Syst. **134**, 172–188 (2017)
19. Zhang, Q.H., Wang, J., Wang, G.Y.: The approximate representation of rough-fuzzy sets. Chin. J. Comput. Jisuanji Xuebao **38**(7), 1484–1496 (2015)
20. Yang, J., Wang, X.Q., Wang, G.Y., Xia, D.Y.: Constructing three-way decision of rough fuzzy sets from the perspective of uncertainties. Cogn. Comput. 1–17 (2023)
21. Cheng, D.D., Li, Y., Xia, S.Y., Wang, G.Y., Huang, J.L., Zhang, S.L.: A fast granular-ball-based density peaks clustering algorithm for large-scale data. IEEE Trans. Neural Netw. Learn. Syst. (2023)

Three-Way Decision in Data Analytics

Three-Way Cost-Performance Approximate Attribute Reduction

Jialin Hou(✉) and Yiyu Yao

Department of Computer Science, University of Regina, Regina, SK S4S 0A2, Canada
{jhv842,Yiyu.Yao}@uregina.ca

Abstract. An attribute reduct is a minimum subset of attributes that satisfies certain requirements with respect to the entire set of attributes. We consider two basic properties of a reduct. One is the cost of the reduct (i.e., the cost of using the attributes in the reduct), and the other is the performance of the reduct. A cost-performance reduct is a reduct with a cost constraint and a performance requirement. An approximate reduct considers a trade-off or balance of cost and performance. In this paper, we propose a model of three-way cost-performance approximate attribute reduction. The model uses two pairs of (cost, performance) parameters to construct a pair of reducts with a low-error/high-performance and high-cost reduct and a high-error/low-performance and low-cost reduct. The trade-off between performance and cost gives users more flexibility in choosing different reducts in different situations.

Keywords: Three-way decision, attribute reduction · approximate reduction · cost-sensitive reduction · cost-performance approximate reduction

1 Introduction

An attribute reduct is a minimum subset of attributes that satisfies certain requirements of properties compared to the entire set of attributes [1]. The basic properties which have been studied most are performance and cost [2–7]. From the performance view, a reduct is a minimum subset of attributes that satisfies the performance requirement, in comparison with the entire set of attributes [1]. Cost can be interpreted by various units, such as time, money, volume, etc., and categories, such as computation cost, test cost, and so on [8,9]. Test cost, also known as attribute cost, is a measurement cost used to evaluate the cost of using an attribute [8,10]. Cost-sensitive reduction is to find a reduct with a cost constraint [5]. The classical way to get reducts from the performance perspective is based on Pawlak rough sets [11]. Yao and Zhao [3] consider the attribute reduction based on different classification measures in the decision-theoretic rough sets model. Zhang and Yao [4] proposed a tri-level reduction in

Y. Yao—This work was partially supported by a Discovery Grant from NSERC, Canada. The authors thank the reviewers for their constructive comments.

M. Hu et al. (Eds.): IJCRS 2024, LNAI 14840, pp. 47–58, 2024.
https://doi.org/10.1007/978-3-031-65668-2_4

rough set theory, which does the object-specific reduction from the micro-bottom level. Based on local attribute significance, Yu et al. [7] proposed a variable precision rough set attribute reduction algorithm. Min et al. [12] proposed a test-cost-sensitive reduction model, which can obtain a reduct with a minimum test cost. Liu [9] introduced a total-cost-sensitive model that considers both process cost and result cost.

However, all these studies only consider one type of the properties. Approximate attribute reduction, introduced by Slezak [13,14], can accommodate a certain level of error by relaxing the measure criterion [15]. By the idea of approximate attribute reduction, a concept of cost-performance approximate attribute reduction has been proposed in this paper. We consider the trade-off between error and cost in this approximate reduction. Three-way decision, proposed by Yao [16,17], gives us a novel view to look at the process of reduction. By the philosophy of thinking in three [16,18–23], we utilize two pairs of (cost, performance) parameters to construct different levels of cost-performance approximate reduction which can satisfy the users' needs in different situations.

More specifically, we propose a model of three-way cost-performance approximate attribute reduction, which can trisect the attribute set based on the different levels of performance with a cost constraint. Two pairs of parameters have been used to achieve a high-performance/low-error and high-cost (HPHC) reduct R_{hphc} and a low-performance/high-error and low-cost (LPLC) reduct R_{lplc}. The HPHC reduct R_{hphc} is an approximate reduct with high performance and high cost. In certain scenarios, users may prioritize cost considerations. In such cases, an LPLC reduct R_{lplc} can be attained by exploring within the HPHC reduct while imposing stricter constraints on both performance and cost. The trade-off between performance and cost gives users more flexibility in choosing reduct in different situations.

Other sections of this paper are structured as follows. Section 2 reviews attribute reduction in a decision table. Our model is presented in Sect. 3, and Sect. 4 gives the conclusion and the future work direction.

2 Attribute Reduction in a Decision Table

In this section, we will review some concepts of attribute reduction in a decision table [4]. A decision table is a tuple:

$$L = (OB, AT = C \cup D, \{V_a \mid a \in AT\}, \{I_a : OB \to V_a \mid a \in AT\}), \quad (1)$$

where OB is a finite set of objects organized as rows, AT is a finite set of attributes organized as columns, C is a set of condition attributes, D is a set of decision attributes, and $C \cap D = \emptyset$. V_a is a domain that defines the possible values for an attribute $a \in AT$, $I_a : OB \to V_A$ is an information function that assigns a value from V_a to each object of OB for the given attribute $a \in AT$. If no ambiguity arises, the decision table can be simplified as:

$$L = (OB, AT = C \cup D). \tag{2}$$

There are two kinds of equivalence relations in a decision table. One is based on the condition attributes, the other is based on the decision attributes. Theoretically, the objects in a decision table have been partitioned by these two types of equivalence relations. Let $L = (OB, AT = C \cup D)$ denotes a decision table, and A is a subset of condition attributes, the equivalence relation E_A on a decision table L can be defined as [4]:

$$E_A = \{(x, y) \in OB \times OB \mid \forall a \in A \ (I_a(x) = I_a(y))\}. \tag{3}$$

Based on the equivalence relation E_A defined in Eq. (3), the partition OB/E_A can be given as follows:

$$OB/E_A = \{[x]_{E_A} \mid x \in OB\}, \tag{4}$$

which can also be denoted as:

$$OB/E_A = \{X_1, X_2, ..., X_n\}, \tag{5}$$

where $n = |OB/E_A|$ is the set of partition' cardinality. Similarly, the equivalence relation based on the decision attributes can be defined as:

$$E_D = \{(x, y) \in OB \times OB \mid \forall d \in D \ (I_d(x) = I_d(y))\}. \tag{6}$$

The decision classification based on equivalence relation E_D can be defined as:

$$OB/E_D = \{[x]_{E_D} \mid x \in OB\}, \tag{7}$$

which can also be denoted as:

$$OB/E_D = \{Y_1, Y_2, ..., Y_m\}, \tag{8}$$

where $m = |OB/E_D|$ is the number of decision classes.

Consider the two types of classifications in Eq. (5) and (8), we have [2]: for $Y \in OB/E_D$

$$\begin{aligned} \underline{apr}(Y|A) &= \bigcup \{X \in OB/E_A \mid X \subseteq Y\} = POS(Y|A), \\ \overline{apr}(Y|A) &= \bigcup \{X \in OB/E_A \mid X \cap Y \neq \emptyset\}. \end{aligned} \tag{9}$$

Equation (9) presents the lower and upper approximations of a decision class Y based on the subset of attributes A. The lower approximation of Y given A is the partition of OB/E_A within Y. The upper approximation of Y given A is the partition of OB/E_A intersecting with Y, where the intersection part is not empty.

Accuracy, also known as the degree of partial dependency, is an important indicator to show the performance preserved by a subset of condition attributes.

Given a subset of condition attribute A, the positive region of a decision classification OB/E_D induced by A is given by:

$$\begin{aligned} POS(OB/E_D|A) &= \bigcup\{POS(Y|A) \mid Y \in U/E_D\} \\ &= POS(Y_1|A) \cup POS(Y_2|A) \cup ... \cup POS(Y_m|A). \end{aligned} \tag{10}$$

Then the accuracy can be defined as follows [9]:

$$\gamma(A \to D) = \frac{|POS(OB/E_D|A)|}{|OB|}. \tag{11}$$

Table 1. A Decision Table

Object	a_1	a_2	a_3	a_4	a_5	class
O_1	1	1	1	2	0	d_1
O_2	0	0	0	0	0	d_2
O_3	0	0	0	0	0	d_2
O_4	0	0	0	0	0	d_2
O_5	0	1	0	1	0	d_3
O_6	0	1	0	1	0	d_3
O_7	0	1	0	1	0	d_3
O_8	1	1	2	0	3	d_4
O_9	1	1	0	0	3	d_4
O_{10}	1	0	0	0	0	d_5

Example 1. *In Table 1, suppose* $A_1 = \{a_1, a_2, a_3, a_4, a_5\}$ *and* $D = \{class\}$, *we have* $OB/E_{A_1} = \{\{O_1\}, \{O_2, O_3, O_4\}, \{O_5, O_6, O_7\}, \{O_8\}, \{O_9\}, \{O_{10}\}\}$, *and* $OB/E_D = \{\{O_1\}, \{O_2, O_3, O_4\}, \{O_5, O_6, O_7\}, \{O_8, O_9\}, \{O_{10}\}\}$. *According to Eq. (9), the* $POS(d_1|A_1) = \{O_1\}$, $POS(d_2|A_1) = \{O_2, O_3, O_4\}$, $POS(d_3|A_1) = \{O_5, O_6, O_7\}$, $POS(d_4|A_1) = \{O_8, O_9\}$, $POS(d_5|A_1) = \{O_{10}\}$. *Finally, we have:*

$$\begin{aligned} \gamma(A_1 \to D) &= \frac{|POS(OB/E_D|A_1)|}{|OB|} \\ &= \frac{|POS(d_1|A_1) \cup POS(d_2|A_1) \cup POS(d_3|A_1) \cup POS(d_4|A_1) \cup POS(d_5|A_1)|}{|OB|} \\ &= \frac{|\{O_1\} \cup \{O_2, O_3, O_4\} \cup \{O_5, O_6, O_7\} \cup \{O_8, O_9\} \cup \{O_{10}\}|}{|\{O_1, O_2, O_3, O_4, O_5, O_6, O_7, O_8, O_9, O_{10}\}|} \\ &= \frac{10}{10} \\ &= 1. \end{aligned}$$

Example 2. *In Table 1, suppose* $A_2 = \{a_1, a_4\}$ *and* $D = \{class\}$, *we have* $OB/E_{A_2} = \{\{O_1\}, \{O_2, O_3, O_4\}, \{O_5, O_6, O_7\}, \{O_8, O_9, O_{10}\}\}$, *and* $OB/E_D =$

$\{\{O_1\},\{O_2,O_3,O_4\},\{O_5,O_6,O_7\},\{O_8,O_9\},\{O_{10}\}\}$. *According to Eq.* (9), *the* $POS(d_1|A_2) = \{O_1\}$, $POS(d_2|A_2) = \{O_2,O_3,O_4\}$, $POS(d_3|A_2) = \{O_5,O_6,O_7\}$, $POS(d_4|A_2) = \{\emptyset\}$, $POS(d_5|A_2) = \{\emptyset\}$. *Finally, we have:*

$$\begin{aligned}\gamma(A \to D) &= \frac{|POS(OB/E_D|A_2)|}{|OB|} \\ &= \frac{|POS(d_1|A_2) \cup POS(d_2|A_2) \cup POS(d_3|A_2) \cup POS(d_4|A_2) \cup POS(d_5|A_2)|}{|OB|} \\ &= \frac{|\{O_1\} \cup \{O_2,O_3,O_4\} \cup \{O_5,O_6,O_7\} \cup \{\emptyset\} \cup \{\emptyset\}|}{|\{O_1,O_2,O_3,O_4,O_5,O_6,O_7,O_8,O_9,O_{10}\}|} \\ &= \frac{7}{10} \\ &= 0.7.\end{aligned}$$

Example 1 shows the accuracy can be get up to 1 if all the condition attributes are used. In Example 2, the accuracy is 0.7 based on only a_1 and a_4 two attributes. Actually, the range of accuracy is $[0,1]$. The following monotonic property holds:

$$A \subseteq B \Longrightarrow \gamma(A \to D) \leq \gamma(B \to D). \tag{12}$$

That means if A is a subset of B, the accuracy induced by A is no more than B. If a subset of the condition attributes R can achieve the same accuracy as the entire condition attribute set C while keeping the minimum condition, then this subset R is a relative attribute reduct of C.

Definition 1. *Given a decision table* $L = (OB, AT = C \cup D)$, *let* γ *denote a measure of dependency. A subset* $R \subseteq C$ *is called a relative reduct of* C *with respect to* D, *if and only if the following conditions are satisfied:*

$$\begin{aligned}&(1) \quad \gamma(R \to D) = \gamma(C \to D), \\ &(2) \quad \forall R' \subset R, \neg(\gamma(R' \to D) = \gamma(C \to D)).\end{aligned} \tag{13}$$

The first condition in the Definition 1 maintains the sufficiency condition, which means the reduct R keeps the same accuracy as the entire condition attribute set. The second condition shows R is the minimum subset that can preserve the performance in condition 1.

Example 3. *In Table 1, suppose we have a subset of condition attribute* $R = \{a_1,a_2,a_4\}$ *and a decision class* $D = \{class\}$. *Then we have* $OB/E_R = \{\{O_1\},\{O_2,O_3,O_4\},\{O_5,O_6,O_7\},\{O_8,O_9\},\{O_{10}\}\}$, *and* $OB/E_D = \{\{O_1\},\{O_2,O_3,O_4\},\{O_5,O_6,O_7\},\{O_8,O_9\},\{O_{10}\}\}$. *According to Eq.* (9), *the* $POS(d_1|R) = \{O_1\}$, $POS(d_2|R) = \{O_2,O_3,O_4\}$, $POS(d_3|R) = \{O_5,O_6,O_7\}$, $POS(d_4|R) = \{O_8,O_9\}$, $POS(d_5|R) = \{O_{10}\}$. *Then, we have:*

$$\begin{aligned}\gamma(R \to D) &= \frac{|POS(OB/E_D|R)|}{|OB|} \\ &= \frac{|POS(d_1|R) \cup POS(d_2|R) \cup POS(d_3|R) \cup POS(d_4|R) \cup POS(d_5|R)|}{|OB|} \\ &= \frac{|\{O_1\} \cup \{O_2, O_3, O_4\} \cup \{O_5, O_6, O_7\} \cup \{O_8, O_9\} \cup \{O_{10}\}|}{|\{O_1, O_2, O_3, O_4, O_5, O_6, O_7, O_8, O_9, O_{10}\}|} \\ &= \frac{10}{10} \\ &= 1.\end{aligned}$$

From Example 1, we can get that the accuracy based on the entire condition attribute set is 1. It follows $\gamma(R \to D) = \gamma(C \to D)$. After exploring every subset $R' \subset R$, we couldn't find any R' that satisfies $\gamma(R' \to D) = \gamma(C \to D)$, demonstrating that R is the smallest. Another reduct $R'' = \{a_1, a_2, a_5\}$ can be found similarly.

3 Three-Way Cost-Performance Approximate Attribute Reduction

In Sect. 3.1, we introduce the cost-sensitive attribute reduction. In Sect. 3.2, we give a review of approximate attribute reduction. Then we present the cost-performance approximate attribute reduction in Sect. 3.3. Finally, in Sect. 3.4, we propose our model of three-way cost-performance approximate attribute reduction.

3.1 Cost-Sensitive Attribute Reduction

A cost-independent decision table is a decision table with a cost function c, which is used to measure the cost of condition attributes. Cost-independent means that the costs associated with different attributes have no relation to each other [12].

Definition 2. [12] *A cost-independent decision table is a six-tuple:*

$$LC = (OB, AT = (C \cup D), \{V_a \mid a \in AT\}, \{I_a : OB \to V_a \mid a \in AT\}, c), \quad (14)$$

where the meaning of $OB, AT, C, D, \{V_a\}, \{I_a\}$ are same as we defined in a decision table. $c : C \longrightarrow \Re^+ \cup \{0\}$ is an attribute cost function, where $\Re^+$ denotes the set of positive real numbers, and $\Re^+ \cup \{0\}$ means the cost of attribute is non-negative. For simplicity, the cost-independent decision table can be shortened as:

$$LC = (OB, AT = (C \cup D), c). \quad (15)$$

We can also straightforwardly represent the attribute cost by a vector:

$$c = (c(a_1), c(a_2), ..., c(a_{|C|})). \quad (16)$$

Table 2. A Cost Vector

Attribute	a_1	a_2	a_3	a_4	a_5
c	1	10	5	1	15

Example 4. *Table 2 denotes a cost vector. Table 1 and Table 2 together represent a cost-independent decision table.*

Then we discuss the computation of the cost of a subset of condition attributes. The cost function for a subset of the condition attributes is defined by:

$$c^* : 2^A \longrightarrow \Re^+ \cup \{0\}, \tag{17}$$

where c^* maps the subset of the condition attributes A to a non-negative real number. Similarly, c^* can be represented by a vector [12]:

$$c^* = (c^*(\emptyset), c^*(\{a_1\}), c^*(\{a_2\}), ..., c^*(\{a_1\}, \{a_2\}), ..., c^*(R)). \tag{18}$$

The length of c^* is $2^{|A|}$. If a subset is empty:

$$c^*(\emptyset) = 0. \tag{19}$$

For any individual attribute $a \in A$, we have:

$$c^*(\{a\}) = c(a). \tag{20}$$

Since the cost of each attribute is independent, the total cost of a subset of condition attributes can be given by [12]:

$$c^*(A) = \sum_{a \in R} c^*(\{a\}) = \sum_{a \in R} c(a), \tag{21}$$

where $A \subseteq C$ and $A \neq \emptyset$.

Given a cost-independent decision table, the cost-sensitive attribute reduction not only satisfies the sufficiency condition and minimum condition as shown in Definition 1 but also has to satisfy the cost constraint condition.

Definition 3. *Let $LC = (OB, (AT = C \cup D), c)$ denotes a cost-independent decision table, and γ denotes a measure of dependency. A subset $R \subseteq C$ is called an δ cost-sensitive relative attribute reduct, if and only if the following conditions hold:*

$$\begin{aligned} &(1) \quad \gamma(R \to D) = \gamma(C \to D), \\ &(2) \quad \forall R' \subset R, \neg(\gamma(R' \to D) = \gamma(C \to D)), \\ &(3) \quad c^*(R) \leq \delta \cdot c^*(C), \end{aligned} \tag{22}$$

where $c^*(R) = \sum_{a \in R} c(a)$ and $c^*(C) = \sum_{b \in C} c(b)$.

The third condition is the cost constraint condition. That means the maximum cost of the reduct R can not exceed the δ percentage of the cost of the entire conditional set C.

Example 5. *We continue the Example 3. Suppose we have a decision table as shown in Table 1 and a cost table as shown in Table 2. From the Example 3, we can get two reducts* $R = \{a_1, a_2, a_4\}$ *and* $R' = \{a_1, a_2, a_5\}$. *The cost of reduct* R *is* $c^*(R) = \sum_{a \in R} c(a) = 12$, *and the cost of reduct* R' *is* $c^*(R') = \sum_{a \in R'} c(a) = 26$. *The cost of the entire condition attributes is* $c^*(C) = \sum_{a \in C} c(a) = 32$. *Let's set* $\delta = 0.8$, *which means the cost of the reduct defined by Definition 3 should be no more than 80% of the cost of the entire condition attribute. But* $c^*(R') = 26 > c^*(C) \times 80\% = 32 \times 0.8 = 25.6$, *that means* R' *can not satisfy the cost constraint condition.* $c^*(R) = 12 < c^*(C) \times 80\% = 32 \times 0.8 = 25.6$, *which shows* R *satisfies the cost constraint condition. Finally, the* δ *cost-sensitive reduct with* $\delta = 0.8$ *is* $R = \{a_1, a_2, a_4\}$.

3.2 Approximate Attribute Reduction

In some situations, it is hard to preserve the same performance as the entire attribute set because of the efficiency or other constraints [1]. The users might be willing to tolerate some degree of error in the outcome [13–15]. An approximate reduct can be defined by Definition 4, in which we put a tolerance degree on the first condition.

Definition 4. *Given a decision table* $L = (OB, AT = C \cup D)$, *and* γ *denotes a measure of dependency. A subset* $R \subseteq C$ *is called an* α*-approximate relative attribute reduct, if and only if the following conditions hold:*

$$\begin{aligned} &(1) \quad \gamma(R \to D) \geq \alpha \cdot \gamma(C \to D), \\ &(2) \quad \forall R' \subset R, \neg(\gamma(R' \to D) \geq \alpha \cdot \gamma(C \to D)). \end{aligned} \tag{23}$$

The parameter α in Definition 4 is used to determine whether the performance of the approximate reduct is acceptable. The first condition is the sufficiency condition, which requires the accuracy of the result reduct at least to be kept at α percent accuracy of the entire attribute set. The second condition is the minimum condition, which makes sure that R is the minimum subset satisfying the first condition.

Example 6. *Given a decision table as shown in Table 1, and let* $\alpha = 0.9$. *Based on Example 3, we have two reducts that satisfy the Definition 4. One is* $R = \{a_1, a_2, a_4\}$, *the other one is* $R' = \{a_1, a_2, a_5\}$. *Both of these two reducts' accuracy is 1, which shows they satisfy the performance condition. After testing every possible subset of* R *and* R', *we can not find a subset that satisfies the performance condition, which shows they are the minimum subsets.*

Example 7. *Given a decision table as shown in Table 1, let's set* $\alpha = 0.8$. *Except for the two reducts we find in Example 6, another reduct* $R'' = \{a_1, a_3, a_4\}$ *can also satisfy the Definition 4. The accuracy of* R'' *is* $\gamma(R'' \longrightarrow D) = 0.8$, *and no subset in* R'' *can satisfy the performance condition after we test every possible subset of* R''. *Finally, we can get three reducts that satisfy the* α*-approximate relative attribute reduction with* $\alpha = 0.8$, *and they are* $R = \{a_1, a_2, a_4\}$, $R' = \{a_1, a_2, a_5\}$, *and* $R'' = \{a_1, a_3, a_4\}$.

3.3 Cost-Performance Approximate Attribute Reduction

In some situations, a certain level of performance is sufficient since the users may be more sensitive to the cost of the condition attributes. This entails the necessity of maintaining specific performance requirements within cost constraints, leading us to define the concept of cost-performance approximate attribute reduction.

Definition 5. *Given a cost-independent decision table* $LC = (OB, (AT = C \cup D), c)$*, and* γ *denotes a measure of dependency. A subset* $R \subseteq C$ *is called an* (δ, α)*-cost-performance approximate attribute reduct, if and only if the following conditions hold:*

$$\begin{aligned} &(1) \quad \gamma(R \to D) \geq \alpha \cdot \gamma(C \to D), \\ &(2) \quad \forall R' \subset R, \neg(\gamma(R' \to D) \geq \alpha \cdot \gamma(C \to D)), \\ &(3) \quad c(R) \leq \delta \cdot c(C). \end{aligned} \tag{24}$$

Definition 5 outlines the specific criteria for a (δ, α)-cost-performance approximate attribute reduct. The initial requirement is the sufficiency condition, which necessitates that the reduct R achieve at least α percent of the performance attained by the entire set of condition attributes. The second condition is the minimum condition, which means the reduct R is the minimum subset to maintain the first condition. Lastly, the cost constraint condition stipulates that the cost of the reduct R should not exceed δ percent of the cost of the entire set of condition attributes.

Example 8. *Given a decision table as shown in Table 1, let* $\delta = 0.8$ *and* $\alpha = 0.9$*. Based on Examples 5 and 6, we can observe that the reduct* $R = \{a_1, a_2, a_4\}$ *satisfies both the sufficiency and cost constraint conditions while also maintaining the minimum requirement. Then the result of* (δ, α)*-cost-performance approximate attribute reduct with* $\delta = 0.8$ *and* $\alpha = 0.9$ *is* $R = \{a_1, a_2, a_4\}$*.*

3.4 Three-Way Cost-Performance Approximate Attribute Reduction

The philosophy of thinking in three presents a novel view of cost-performance approximate attribute reduction. Instead of utilizing a single pair of parameters (δ, α), we introduce two pairs of parameters $[(\delta_l, \alpha_l), (\delta_h, \alpha_h)]$, where $\delta_l < \delta_h$ and $\alpha_l < \alpha_h$. This approach leads to a pair of cost-performance approximate attribute reducts (R_{lplc}, R_{hphc}). Two pairs of parameters represent two different levels of users' needs. A three-way cost-performance approximate attribute reduction is given by Definition 6.

Definition 6. *Given a cost-independent decision table* $LC = (OB, (AT = C \cup D), c)$*, and two pairs of parameters* $[(\delta_l, \alpha_l), (\delta_h, \alpha_h)]$ *with* $\delta_l < \delta_h$*, and* $\alpha_l < \alpha_h$*. A pair of subsets* (R_{lplc}, R_{hphc}) *is called a three-way cost-performance approximate attribute reducts if* $R_{lplc} \subseteq R_{hphc}$*, where* R_{lplc} *is a* (δ_l, α_l)*-cost-performance approximate attribute reduct, and* R_{hphc} *is a* (δ_h, α_h)*-cost-performance approximate attribute reduct.*

The output of our model is a pair of reducts (R_{lplc}, R_{hphc}) with $R_{lplc} \subseteq R_{hphc}$. R_{hphc} can be viewed as a high-performance-high-cost reduct obtained through a higher level of requirements, which is determined by a larger pair of parameters (δ_h, α_h). R_{lplc} can be viewed as a low-performance-low-cost reduct obtained through a lower level of requirements, which is determined by a smaller pair of parameters (δ_l, α_l). We can obtain R_{lplc} by searching inside of R_{hphc}. According to the Definition 5, the attributes in reduct R_{hphc} can preserve a better performance than R_{lplc} since the sufficiency parameter α_h is higher than α_l. Nevertheless, the cost produced by R_{lplc} is lower than R_{hphc} since it has fewer attributes and the cost constraint parameter δ_l is lower than δ_h. The entire condition attribute set can be tri-partitioned by the reduct pair (R_{lplc}, R_{hphc}) as shown below:

$$\begin{aligned} \text{NECE} &= R_{lplc}, \\ \text{IMPR} &= R_{hphc} - R_{lplc}, \\ \text{REDU} &= R^c_{hphc}, \end{aligned}$$

where NECE denotes the necessary attributes, IMPR denotes the performance-improved attributes, and REDU denotes the redundant attributes. The attributes in NECE are essential for the users to meet basic sufficiency requirements. Selecting both the NECE and IMPR attribute sets simultaneously will lead to an improvement in performance to a higher level. However, a higher level of performance will bring a higher cost. The user may make the trade-off between performance and cost. The attributes in REDU are redundant, which means the user can directly remove the superfluous attributes in REDU. Finally, the union of the three pair-wise disjoint subsets is composed of the entire condition attribute set C.

Example 9. *Given a decision table as shown in Table 1 and a cost table as shown in Table 2, let's set the two pair of parameters as* $[(\delta_l = 0.2,\ \alpha_l = 0.7), (\delta_h = 0.8,\ \alpha_h = 0.9)]$. *We first explore the subset of entire condition attributes to get the* $(\delta_h = 0.8, \alpha_h = 0.9)$*-cost-performance approximate attribute reduct. That is our HPHC reduct* R_{hphc}. *From the results in Example 8, we can directly get* $R_{hphc} = \{a_1, a_2, a_4\}$. *Then we explore all the subsets of* R_{hphc}, *we can have* $R' = \{a_1, a_4\}$ *and* $R'' = \{a_1, a_2\}$ *with the accuracy of 0.7, which satisfies the lower performance requirement. The cost for* R' *is* $c^*(R') = 2$, *and the cost for* R'' *is* $c^*(R'') = 11$. *The cost constraint is* $c^*(C) \times \delta_l = 32 \times 0.2 = 6.4$. *Obviously,* R' *satisfies the requirement of LPLC reduct, and* $R_{lplc} = R' = \{a_1, a_4\}$. *Finally, we have:*

$$R_{lplc} = \{a_1, a_4\} \subseteq R_{hphc} = \{a_1, a_2, a_4\}.$$

The tri-partition over OB is:

$$\begin{aligned} \text{NECE} &= R_{lplc} = \{a_1, a_4\}, \\ \text{IMPR} &= R_{hphc} - R_{lplc} = \{a_2\}, \\ \text{SUPF} &= R^c_{hphc} = \{a_3, a_5\}. \end{aligned}$$

4 Conclusion

Three-way decision provides a novel view to look at attribute reduction. In this research, a model of three-way cost-performance approximate attribute reduction is proposed. We utilize two pairs of parameters, $[(\delta_l, \alpha_l), (\delta_h, \alpha_h)]$, with $\delta_l < \delta_h$ and $\alpha_l < \alpha_h$ to obtain a pair of reducts, (R_{lplc}, R_{hphc}), where $R_{lplc} \subseteq R_{hphc}$. Here, R_{hphc} represents an HPHC reduct, while R_{lplc} signifies an LPLC reduct. We can first get the HPHC reduct R_{hphc} by the pair of constriction parameters (δ_h, α_h), then we search inside of the R_{hphc} to get the LPLC reduct R_{lplc} which satisfies lower constriction requirement (δ_l, α_l).

The proposed model aims to achieve a three-way cost-performance approximate attribute reduct by employing two pairs of parameters, $[(\delta_l, \alpha_l), (\delta_h, \alpha_h)]$. This process results in obtaining a pair of reducts, (R_{lplc}, R_{hphc}), where $R_{lplc} \subseteq R_{hphc}$. These reducts are designed to satisfy various levels of performance requirements while considering the corresponding costs. One future research direction is how to select the two pairs of parameters to get a pair of reducts which can mostly benefit the users. Another future work is to do some comparative analysis based on actual experiments. Since this paper primarily focuses on theoretical analyses, additional experiments should be done to compare theory and actuality. Finally, how to quickly search for a possible candidate is also important. In this research, we exhaustively test every subset to find the pair of reducts which is a time-consuming process. A more efficient algorithm should be designed in the future.

References

1. Shi, C., Wang, Z., Wei, L., Yao, Y.: Three-way approximate criterion reduction in multi-criteria decision analysis. In: Yao, J., Fujita, H., Yue, X., Miao, D., Grzymala-Busse, J., Li, F. (eds.) IJCRS 2022. LNCS, vol. 13633, pp. 289–303. Springer, Cham (2022). https://doi.org/10.1007/978-3-031-21244-4_22
2. Yao, Y.Y., Zhang, X.Y.: Class-specific attribute reducts in rough set theory. Inf. Sci. **418**, 601–618 (2017)
3. Yao, Y.Y., Zhao, Y.: Attribute reduction in decision-theoretic rough set models. Inf. Sci. **178**, 3356–3373 (2008)
4. Zhang, X.Y., Yao, Y.Y.: Tri-level attribute reduction in rough set theory. Expert Syst. Appl. **190**, 116187 (2022)
5. He, H.P., Min, F., Zhu, W.: Attribute reduction in test-cost-sensitive decision systems with common-test-costs. In: Proceedings of the 3rd International Conference on Machine Learning and Computing, pp. 432–436 (2011)
6. Bazan, J.G., Skowron, A., Synak, P.: Dynamic reducts as a tool for extracting laws from decisions tables. In: Raś, Z.W., Zemankova, M. (eds.) ISMIS 1994. LNCS, vol. 869, pp. 346–355. Springer, Heidelberg (1994). https://doi.org/10.1007/3-540-58495-1_35
7. Yu, B., Hu, Y., Kang, Y., Cai, M.J.: A novel variable precision rough set attribute reduction algorithm based on local attribute significance. Int. J. Approximate Reasoning **157**, 88–104 (2023)

8. Turney, P.D.: Types of cost in inductive concept learning. arXiv preprint arXiv:cs/0212034 (2002)
9. Liu, K.F.: A study of cost-sensitive attribute reducts. Master's thesis, University of Regina (2015)
10. Fang, Y., Gao, C., Yao, Y.Y.: Granularity-driven sequential three-way decisions: a cost-sensitive approach to classification. Inf. Sci. **507**, 644–664 (2020)
11. Pawlak, Z.: Rough sets. Int. J. Comput. Inf. Sci. **11**, 341–356 (1982)
12. Min, F., He, H.P., Qian, Y.H., Zhu, W.: Test-cost-sensitive attribute reduction. Inf. Sci. **181**, 4928–4942 (2011)
13. Ślęzak, D.: Approximate reducts in decision tables. In: Proceedings of the Sixth International Conference on Information Processing and Management of Uncertainty in Knowledge-Based Systems, pp. 1159–1164 (1996)
14. Ślęzak, D.: Approximate entropy reducts. Fund. Inform. **53**, 365–390 (2002)
15. Jiang, F., Yu, X., Du, J.W., Gong, D.W., Zhang, Y.Q., Peng, Y.J.: Ensemble learning based on approximate reducts and bootstrap sampling. Inf. Sci. **547**, 797–813 (2021)
16. Yao, Y.Y.: Three-way decisions with probabilistic rough sets. Inf. Sci. **180**, 341–353 (2010)
17. Yao, Y.: An outline of a theory of three-way decisions. In: Yao, J.T., et al. (eds.) RSCTC 2012. LNCS (LNAI), vol. 7413, pp. 1–17. Springer, Heidelberg (2012). https://doi.org/10.1007/978-3-642-32115-3_1
18. Yu, H.: A framework of three-way cluster analysis. In: Polkowski, L., Yao, Y., Artiemjew, P., Ciucci, D., Liu, D., Ślęzak, D., Zielosko, B. (eds.) IJCRS 2017. LNCS (LNAI), vol. 10314, pp. 300–312. Springer, Cham (2017). https://doi.org/10.1007/978-3-319-60840-2_22
19. Yu, H., Zhang, C., Wang, G.Y.: A tree-based incremental overlapping clustering method using the three-way decision theory. Knowl.-Based Syst. **91**, 189–203 (2016)
20. Li, H.X., Zhang, L.B., Hua, B., Zhou, X.Z.: Sequential three-way decision and granulation for cost-sensitive face recognition. Knowl.-Based Syst. **91**, 241–251 (2016)
21. Qi, J.J., Qian, T., Wei, L.: The connections between three-way and classical concept lattices. Knowl.-Based Syst. **91**, 143–151 (2016)
22. Li, J.H., Huang, C.C., Qi, J.J., Qian, Y.H., Liu, W.Q.: Three-way cognitive concept learning via multi-granularity. Inf. Sci. **378**, 244–263 (2017)
23. Li, M.Z., Wang, G.Y.: Approximate concept construction with three-way decisions and attribute reduction in incomplete contexts. Knowl.-Based Syst. **91**, 165–178 (2016)

Granular Approximations of Partially-Known Concepts

Qiaoyi Li[1(✉)], Chengjun Shi[1], Han Yang[1,2], and Yiyu Yao[1]

[1] Department of Computer Science, University of Regina, Regina, SK S4S 0A2, Canada
li992@uregina.ca

[2] School of Mathematics, Southwest Jiaotong University, Chengdu 611756, Sichuan, People's Republic of China

Abstract. The theory of rough sets concerns approximating a concept, represented by a set of objects as its instances, with a pair of lower and upper approximations. In some situations, we do not have complete knowledge of the set of instances of a concept, resulting in the need to study a partially-known concept. There are two ways to represent a partially-known concept. A triplet representation consists of a set of objects known to be instances, a set of objects known to be non-instances, and the rest objects of the concept. An interval set representation includes all possible sets that fall within a pair of a lower bound and an upper bound. In this paper, we systematically investigate rough set approximations of a partially-known concept under the two presentations. By approximating a partially-known concept, we can divide the universe into either seven or five regions. The analysis using seven regions or five regions can provide detailed analytics of a partially-known concept.

Keywords: Interval set · Rough set · Three-way decision · Granular computing · Partially-known concept

1 Introduction

A concept is typically understood as a pair of a set of objects and a set of attributes, known as the extension and intension of the concept respectively. In rough sets theory [19], given a concept, it is assumed that we know exactly its extension as a subset of objects. However, this subset may not necessarily be described by using available attributes. Such a concept is called an undefinable concept. The main task of rough sets theory is to approximate undefinable concepts by a pair of definable concepts called lower and upper approximations or

This work was partially supported by a Discovery Grant from NSERC, Canada, and a grant from the China Scholarship Council (Grant No. 202107000028). We are grateful to the reviewers for their constructive comments and to Dr. Mengjun Hu for her valuable suggestions. We thank Professor Jianfeng Xu, Professor Chuanlei Zhang, and Professor Ying Yu for organizing the workshop on Uncertainty, Three-way Decision, and Explainable Artificial Intelligence.

M. Hu et al. (Eds.): IJCRS 2024, LNAI 14840, pp. 59–73, 2024.
https://doi.org/10.1007/978-3-031-65668-2_5

by the positive, negative, and boundary regions [19]. The three-region formulation has led to the introduction of a theory of three-way decision that involves thinking, problem-solving, and information processing with triads [29]. Three-way decision has become an important theory covering many research topics and a wide range of applications [4,5,10–12,21,22,30,33].

In real-world scenarios, some concepts have only some objects whose belongings can be determined. Such concepts are referred to as partially-known concepts. Various studies exist in developing theories of partially-known concepts [9,15,20]. There are two ways to represent a partially-known concept: a triplet of sets and an interval set. A triplet representation is inherent in the nature of partially-known concepts. It contains three disjoint sets, respectively representing the set of objects that are known to be instances of the concept, the set of objects that are known to be non-instances of the concept, and the set of unknown objects. An interval set representation, introduced by Yao [23], consists of a family of subsets that fall within the range between a lower bound and an upper bound. Each of the subsets may be the actual extension of the concept, if the information was complete. Many existing studies use interval sets to represent incomplete information [14,16–18]. It may be commented that both the triplet and the interval set representations can be equivalently expressed in terms of the notion of an orthopair (i.e., a pair of disjoint sets) introduced by Ciucci [1,2].

The sets in the triplet representation and interval set representation of a partially-known concept may be undefinable. This motivates a study on the approximation of the partially-known concepts in light of Pawlak rough sets. Zhang et al. [31,32] investigated the approximation of an interval set within the Pawlak approximation space. They introduced the lower and upper approximations of an interval set and considered the optimal approximations of rough sets based on similarity measure [13] for finding the optimal approximations of the interval set. Greco and Słowiński [8] represented a partially-known concept by an orthopair and studied approximations of the orthopair. They showed that approximations of partially-known sets are related to the notion of a seven-valued logic within the Pawlak-Brouwer-Zadeh lattice, which offers a new methodology for the analysis of the approximations of partially-known concepts. In these studies, approximations of a partially-known concept are given in terms of sets of objects. On the other hand, combining rough sets with granular computing provides a new way to approximate concepts in terms of sets of granules [3,6,24]. Bryniarski [3] considered a representation of the lower and upper approximations by families of equivalence classes. Yao and Yang [27,28] interpreted equivalence classes as granular objects in the quotient space induced by an equivalence relation and introduced the notion of granular rough sets that approximate a concept by sets of granular objects. Granular approximation offers a more structured interpretation and enhances the semantic understanding of approximation.

Based on these studies, the main objective of this paper is to introduce the notion of granular approximation of partially-known concepts by comparing and integrating the two representations within the framework of granular approxima-

tion. Rough sets deal with a kind of uncertainty due to the inability to define a concept precisely by using a finite set of attributes, although we know exactly the extension of the concept. Partially-known concepts are caused by another type of uncertainty due to our partial knowledge of all instances of a concept, that is, we only know the instance/non-instance states of some, but not all objects. The notion of granular approximation of partially-known concepts can deal with the two types of uncertainty simultaneously.

The rest of the paper is organized as follows. The two representations of a partially-known concept are provided in Sect. 2 and the granular approximations of concepts under two representations are presented in Sect. 3. Section 4 offers two ways, respectively based on seven regions derived from a triplet representation and five regions derived from an orthopair representation, to analyze partially-known concepts and provide illustrative examples for these analyses. The last section summarizes the findings of this paper.

2 Partially-Known Concepts

A concept is a pair consisting of a set of objects and a set of attributes, where the set of objects is referred to as the extension of the concept, and the set of attributes is referred to as the intension of the concept. A concept is exactly known if, for any object in the universe, the object is known to be either an instance or not an instance of the concept; and a concept is partially-known if there exist some objects that cannot be determined whether they are or are not instances of the concept [25]. There are two forms to represent a partially-known concept, namely, the triplet representation and the interval set representation.

Definition 1. *Let U be a non-empty finite universe. A triplet representation of a partially-known concept is defined as follows.*

$$\mathbf{X} = \langle X^+, X^-, X^? \rangle,$$

where X^+ is the set of objects known to be instances, X^- is the set of objects known to be non-instances, and $X^?$ is the set of rest objects. The three sets $X^+, X^-, X^? \subseteq U$ are pairwise disjoint and their union is the universe U, i.e., $X^+ \cup X^- \cup X^? = U$.

The triplet representation may be simplified based on the notion of an orthopair consisting of two disjoint sets [1,7]. For example, a partially-known concept can be equivalently represented by one of the three orthorpairs $(X^+, X^?)$, (X^+, X^-), and $(X^-, X^?)$. We explicitly use three sets to show the connection between partially-known concepts and three-way decision [26]. In other words, the uncertainty represented by partially-known concepts naturally leads to three-way decision.

An interval set representation can be shown by a pair of sets, which respectively represent the lower bound and the upper bound, in a closed interval [25]. An intuitive way of interpreting the lower bound and upper bound is through the

possible-world semantics [16], where the lower bound is the set that includes all 'sure' instances and the upper bound is the set that includes all 'sure or possible' instances. Every set in between, including the two bounds, is one possibility of the partially-known concept.

Definition 2. [25] *Let U be a finite non-empty universe. An interval set representation of a partially-known concept is defined as follows:*

$$\mathbb{X} = [X_*, X^*] = \{X \subseteq U \mid X_* \subseteq X \subseteq X^*\},$$

where X_* represents the lower bound, X^* represents the upper bound, and $X_* \subseteq X^* \subseteq U$.

A close relationship exists between the triplet and the interval set representations of a partially-known concept:

$$\begin{aligned} &X_* = X^+, \quad X^* = X^+ \cup X^?; \\ &X^+ = X_*, \quad X^- = (X^*)^c, \quad X^? = X^* - X_*. \end{aligned} \tag{1}$$

This enables the transformation between the two representations of a partially-known concept. Both representations obtain a distinct view of the partially-known concept; we may selectively use them for different purposes.

3 Granular Approximations of Concepts and Partially-Known Concepts

Depending on the representations of a partially-known concept, a granular approximation provides information from different perspectives. In this section, the granular approximations of a partially-known concept under the triplet and the interval set representations are introduced.

3.1 Granular Approximations of Concepts

The granular approximation of concepts is built on top of partitions. A partition of a given universe splits the universe into several non-empty disjoint parts called blocks.

Definition 3. *Let U be a finite non-empty universe. A family of subsets of U, π, is a partition of U if it satisfies the following conditions:*

$$\begin{aligned} &(1) \quad \forall B \in \pi, B \neq \emptyset, \\ &(2) \quad \bigcup_{B \in \pi} B = U, \\ &(3) \quad \forall B, B' \in \pi, B \cap B' = \emptyset. \end{aligned}$$

In an approximation space $apr = (U, \pi)$, U is the universe set representing the ground space and π is a partition of universe representing the quotient space [27, 28]. Each individual in a ground space is an object, whereas in the quotient space is a granular object. A granular object B can be viewed as a block of a partition, i.e. $B \in \pi$, and also can be viewed as a set of elements, i.e. $B \subseteq U$. The granular lower and upper approximations of a concept describe the concept by a collection of granular objects.

Definition 4. [27] *In an approximation space $apr = (U, \pi)$, the granular lower and upper approximations of set $X \subseteq U$ are defined as follows:*

$$\begin{aligned} \underline{apr}(X|\pi) &= \{B \in \pi \mid B \subseteq X\}, \\ \overline{apr}(X|\pi) &= \{B \in \pi \mid B \cap X \neq \emptyset\}. \end{aligned}$$

The pair of sets:

$$apr(X|\pi) = \langle \underline{apr}(X|\pi), \overline{apr}(X|\pi) \rangle,$$

is called a granular approximation of X in the quotient space π.

Based on the definition, we can easily prove that rough set approximations have some interesting properties summarized in the next proposition.

Proposition 1. *The granular lower and upper approximations hold the following properties:*

$$\begin{aligned} &\text{(L0)} \quad \underline{apr}(U|\pi) = \pi, \\ &\text{(U0)} \quad \overline{apr}(U|\pi) = \pi, \\ &\text{(L1)} \quad \underline{apr}(\emptyset|\pi) = \emptyset, \\ &\text{(U1)} \quad \overline{apr}(\emptyset|\pi) = \emptyset, \\ &\text{(L2)} \quad (\underline{apr}(X|\pi))^c = \overline{apr}(X^c|\pi), \\ &\text{(U2)} \quad (\overline{apr}(X|\pi))^c = \underline{apr}(X^c|\pi), \\ &\text{(L3)} \quad X \subseteq X' \subseteq U \implies \underline{apr}(X|\pi) \subseteq \underline{apr}(X'|\pi), \\ &\text{(U3)} \quad X \subseteq X' \subseteq U \implies \overline{apr}(X|\pi) \subseteq \overline{apr}(X'|\pi), \\ &\text{(L4)} \quad \underline{apr}(X \cap X'|\pi) = \underline{apr}(X|\pi) \cap \underline{apr}(X'|\pi), \\ &\text{(U4)} \quad \overline{apr}(X \cup X'|\pi) = \overline{apr}(X|\pi) \cup \overline{apr}(X'|\pi). \end{aligned}$$

In (L2) and (U3), the complement of X is defined in the ground space, namely, $X^c = U - X$; the complements of the granular lower and upper approximations are defined in the quotient space, for example, $(\underline{apr}(X|\pi))^c = \pi - \underline{apr}(X|\pi)$. They state the duality of granular approximations with respect to two spaces U and π. The other properties correspond to Pawlak rough set approximations.

3.2 Granular Approximations of Partially-Known Concepts Under Triplet Representation

The granular approximation of a partially-known concept under triplet representation takes granular approximations of X^+, X^-, and $X^?$. By Definition 4, the granular approximations of three sets can be simply formed. Based on these granular approximations, we give the following definition.

Definition 5. *In an approximation space $apr = (U, \pi)$, the granular approximation of a partially-known concept under triplet representation $\mathbf{X} = \langle X^+, X^?, X^- \rangle$ is defined by:*

$$apr(\mathbf{X}|\pi) = \langle apr(X^+|\pi), apr(X^?|\pi), apr(X^-|\pi) \rangle.$$

We may also express the granular approximation by a pair of triplets of granular lower and upper approximations:

$$\begin{aligned} apr(\mathbf{X}|\pi) &= \langle \underline{apr}(\mathbf{X}|\pi), \overline{apr}(\mathbf{X}|\pi) \rangle \\ &= \langle \langle \underline{apr}(X^+|\pi), \underline{apr}(X^?|\pi), \underline{apr}(X^-|\pi) \rangle, \\ &\quad \langle \overline{apr}(X^+|\pi), \overline{apr}(X^?|\pi), \overline{apr}(X^-|\pi) \rangle \rangle. \end{aligned}$$

Although the two different representations are equivalent mathematically, they provide complementary views for interpreting granular approximations. Together, they provide a deeper understanding.

3.3 Granular Approximations of Partially-Known Concepts Under Interval Set Representation

An interval set representation of a partially-known concept includes all possible sets in between the lower and upper bounds. However, not every possible set can be presented by a set of granular objects. Therefore, a granular approximation of a partially-known concept under interval set representation should be approached by approximating each possible set within the interval set.

Definition 6. *In an approximation space $apr = (U, \pi)$, the granular approximation of a partially-known concept under interval set representation $\mathbb{X} = [X_*, X^*]$ is defined by:*

$$\begin{aligned} apr(\mathbb{X}|\pi) &= \{apr(X|\pi) \mid X_* \subseteq X \subseteq X^*\} \\ &= \{\langle \underline{apr}(X|\pi), \overline{apr}(X|\pi) \rangle \mid X_* \subseteq X \subseteq X^*\}. \end{aligned}$$

We may also represent the granular approximation as a pair of sets:

$$\begin{aligned} apr(\mathbb{X}|\pi) &= \langle \underline{apr}(\mathbb{X}|\pi), \overline{apr}(\mathbb{X}|\pi) \rangle \\ &= \langle \{\underline{apr}(X|\pi) \mid X_* \subseteq X \subseteq X^*\}, \{\overline{apr}(X|\pi) \mid X_* \subseteq X \subseteq X^*\} \rangle. \end{aligned}$$

These two representations of the granular approximation of an interval set are equivalent mathematically.

An interval set exhibits different properties in different spaces. In a ground space, an interval set collects sets of objects; whereas in a quotient space, an interval set collects sets of granular objects.

Definition 7. *In an approximation space $apr = (U, \pi)$, an interval set in a quotient space is defined as follows:*

$$\mathbb{Y} = [Y_*, Y^*]_\pi = \{S \subseteq \pi \mid Y_* \subseteq S \subseteq Y^*\},$$

where $Y_*, Y^* \subseteq \pi$ are respectively called the granular lower and upper bounds, and $Y_* \subseteq Y^*$.

To distinguish an interval set in different spaces, we use the footnote π to represent an interval set in the quotient space. For example, $[A_*, A^*]$ shows an interval set in the ground space, whereas $[B_*, B^*]_\pi$ shows an interval set in the quotient space. It is important to note that a partially-known concept under interval set representation is an interval set in the ground space.

Theorem 1. *In an approximation space $apr = (U, \pi)$, given a partially-known concept under interval set representation $\mathbb{X} = [X_*, X^*]$, the granular lower and upper approximations of the partially-known concept are two interval sets in the quotient space:*

$$(1)\ \underline{apr}(\mathbb{X}|\pi) = [\underline{apr}(X_*|\pi), \underline{apr}(X^*|\pi)]_\pi,$$
$$(2)\ \overline{apr}(\mathbb{X}|\pi) = [\overline{apr}(X_*|\pi), \overline{apr}(X^*|\pi)]_\pi.$$

Proof. (1) The inclusion $\underline{apr}(\mathbb{X}|\pi) \subseteq [\underline{apr}(X_*|\pi), \underline{apr}(X^*|\pi)]_\pi$ can be proved as follows. Assume $Y \in \underline{apr}(\mathbb{X}|\pi)$, by Definition 2, there must exist a $X \in [X_*, X^*]$ such that $Y = \underline{apr}(X|\pi)$. By Proposition 1(L3), we have $\underline{apr}(X_*|\pi) \subseteq \underline{apr}(X|\pi) \subseteq \underline{apr}(X^*|\pi)$. It follows that $Y = \underline{apr}(X|\pi) \in [\underline{apr}(X_*|\pi), \underline{apr}(X^*|\pi)]_\pi$.

The inclusion $[\underline{apr}(X_*|\pi), \underline{apr}(X^*|\pi)]_\pi \subseteq \underline{apr}(\mathbb{X}|\pi)$ is proved as follows. Suppose $S \in [\underline{apr}(X_*|\pi), \underline{apr}(X^*|\pi)]_\pi$. We construct $X = X_* \cup (\bigcup S) \subseteq U$. Obviously, $X \in [X_*, X^*]$. We show that $\underline{apr}(X|\pi) = S$, namely, $S \in \underline{apr}(\mathbb{X}|\pi)$.

The inclusion $S \subseteq \underline{apr}(X|\pi)$ easily follows the properties of approximation, that is, by $\bigcup S \subseteq X$, we can conclude $S = \underline{apr}(\bigcup S) \subseteq \underline{apr}(X|\pi)$. The other direction of inclusion can be shown as follows. Assume that $B \in \underline{apr}(X|\pi) = \underline{apr}(X_* \cup (\bigcup S))$. By definition, $B \subseteq X_* \cup (\bigcup S)$. We can show that $B \in S$ by contradiction. Assume that $B \notin S$. By the properties of the partition π and the structure of S, it follows that $B \cap (\bigcup S) = \emptyset$. From $B \subseteq X_* \cup (\bigcup S)$, we must have $B \subseteq X_*$. On the other hand, $B \subseteq X_*$ implies $B \in \underline{apr}(X_*|\pi) \subseteq S$, contradicting the assumption $B \notin S$. Therefore, we must have $B \in S$.

By summarizing the results, we have $\underline{apr}(X|\pi) = S$. We can prove (2) by following the same argument. □

Theorem 1 shows that the granular approximation of a partially-known concept results in two interval sets in the quotient space. The lower approximation shows the range of necessity as it takes the largest set of granular objects that

are contained by both bounds, and the upper approximation shows the range of possibility as it takes the smallest set of granular objects that intersects with both bounds. One may use them to extract information for different purposes.

3.4 Transformation Between Two Granular Approximations

Similar to the transformation between interval set and triplet representations of a partailly-known concept, there exists a transformation between the granular lower and upper approximations of it under two representations.

Proposition 2. *The following properties hold:*

$$
\begin{aligned}
&\text{(LL)} \quad \underline{apr}(X_*|\pi) = \underline{apr}(X^+|\pi),\\
&\text{(UL)} \quad \overline{apr}(X_*|\pi) = \overline{apr}(X^+|\pi),\\
&\text{(LU)} \quad \underline{apr}(X^*|\pi) = (\overline{apr}(X^-|\pi))^c,\\
&\text{(UU)} \quad \overline{apr}(X^*|\pi) = (\underline{apr}(X^-|\pi))^c,\\
&\text{(LN)} \quad \underline{apr}(X^-|\pi) = (\overline{apr}(X^*|\pi))^c,\\
&\text{(UN)} \quad \overline{apr}(X^-|\pi) = (\underline{apr}(X^*|\pi))^c,\\
&\text{(LB)} \quad \underline{apr}(X^?|\pi) = \underline{apr}(X^*|\pi) - \overline{apr}(X_*|\pi),\\
&\text{(UB)} \quad \overline{apr}(X^?|\pi) = \overline{apr}(X^*|\pi) - \underline{apr}(X_*|\pi).
\end{aligned}
$$

Proof. (LL) By definition, $X_* = X^+ \implies \underline{apr}(X_*|\pi) = \underline{apr}(X^+|\pi)$.

(UL) We can use a similar procedure as (LL) to prove (UL).

(LU) By Proposition 1 (L2) and (L3), $X^* = (X^-)^c \implies \underline{apr}(X^*|\pi) = \underline{apr}((X^-)^c|\pi) \implies \underline{apr}(X^*|\pi) = (\overline{apr}(X^-|\pi))^c$.

(UU) We can use a similar procedure as (LU) to prove (UU).

(LN) By taking the complement of both sides in (LU), we can get (LN).

(UN) By taking the complement of both sides in (UU), we can get (UN).

(LB) By the properties of the partition π and the structure of $\underline{apr}(X_*|\pi)$ and $\overline{apr}(X_*|\pi)$, $\forall B \in \overline{apr}(X_*|\pi)$, we have $B \subseteq X_*$ or $B \cap X_* = \emptyset$. According to definition and Eq. (1), $\underline{apr}(X^?|\pi) = \underline{apr}(X^* - X_*|\pi) = \{B \in \pi \mid B \subseteq X^* \wedge B \cap X_* = \emptyset\} = \underline{apr}(X^*|\pi) - \overline{apr}(X_*|\pi)$.

(UB) We can use a similar procedure as (LB) to prove (UB). □

Proposition 2 enables transformations between the granular approximations of a partially-known concept under two representations, meaning that there is no difference between acquiring the granular lower and upper approximations of X_*, X^* and $X^+, X^?, X^-$.

4 Analysis of the Granular Approximations of Partially-Known Concepts

Through the granular approximation of a partially-known concept, one may have two ways to analyze it, through either a 7-region analysis or a 5-region

analysis. As the granular approximation of a partially-known concept under two representations can be transformed into each other by Proposition 2, we uniformly use the triplet representation in this section for convenience.

Example 1. We use an example to illustrate the two analyses. Consider a partially-known concept as shown in Fig. 1a where the solid rectangle box represents the universe. The smaller peanut shape, which is surrounded by a solid line, represents the lower bound of an interval set representation of a partially-known concept; and the larger peanut shape, which is surrounded by a dashed line, represents the upper bound of it. As the partially-known concept under two representations can be transformed, we get that the region within the solid peanut shows X^+, the region between the solid peanut and the dashed peanut shows $X^?$, and the region in between the dashed peanut and the solid rectangle shows X^-. There are some shared lines at the left bottom of two peanut shapes.

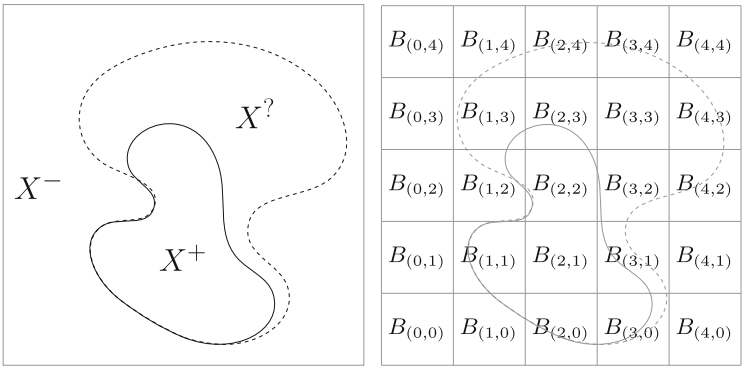

(a). Partially-Known Concept **(b).** A Partition of the Universe

Fig. 1. A Partially-Known Concept Example

The grid shown in Fig. 1b represents a partition of the universe, where each grid cell represents a block of the partition. To better distinguish among blocks, we use locations, i.e. (column, row), as the footnote of the block to identify them. The column number is in ascending order from left to right and the row number is in ascending order from bottom to top, both ranging from 0 to 4. For example, $B_{(2,3)}$ represents the block that is located in the third column and the fourth row.

4.1 The 7-Region Analysis

Greco and Słowiński [8] constructed seven disjoint regions based on rough set approximations of a partially-known concept within a Pawlak-Brouwer-Zadeh lattice. We here show the seven disjoint regions from the perspective of a granular approximation of a partially-known concept. In the triplet representation, the

upper approximations of X^+, X^-, and $X^?$ normally have non-empty overlaps, which allow us to use them to represent their lower approximations as follows:

$$\begin{aligned}
\underline{apr}(X^+|\pi) &= \overline{apr}(X^+|\pi) \cap (\overline{apr}(X^?|\pi))^c \cap (\overline{apr}(X^-|\pi))^c,\\
\underline{apr}(X^?|\pi) &= \overline{apr}(X^?|\pi) \cap (\overline{apr}(X^+|\pi))^c \cap (\overline{apr}(X^-|\pi))^c,\\
\underline{apr}(X^-|\pi) &= \overline{apr}(X^-|\pi) \cap (\overline{apr}(X^?|\pi))^c \cap (\overline{apr}(X^+|\pi))^c.
\end{aligned}$$

By using the three upper approximations, we can construct $2^3 = 8$ combinations as follows:

$$\begin{aligned}
\mathrm{Non}(X) &= (\overline{apr}(X^+|\pi))^c \cap (\overline{apr}(X^?|\pi))^c \cap (\overline{apr}(X^-|\pi))^c = \emptyset,\\
\mathrm{Uni}^{\mathrm{P}}(X) &= \overline{apr}(X^+|\pi) \cap (\overline{apr}(X^?|\pi))^c \cap (\overline{apr}(X^-|\pi))^c = \underline{apr}(X^+|\pi),\\
\mathrm{Uni}^{\mathrm{B}}(X) &= (\overline{apr}(X^+|\pi))^c \cap \overline{apr}(X^?|\pi) \cap (\overline{apr}(X^-|\pi))^c = \underline{apr}(X^?|\pi),\\
\mathrm{Uni}^{\mathrm{N}}(X) &= (\overline{apr}(X^+|\pi))^c \cap (\overline{apr}(X^?|\pi))^c \cap \overline{apr}(X^-|\pi) = \underline{apr}(X^-|\pi),\\
\mathrm{Bi}^{\mathrm{PN}}(X) &= \overline{apr}(X^+|\pi) \cap (\overline{apr}(X^?|\pi))^c \cap \overline{apr}(X^-|\pi),\\
\mathrm{Bi}^{\mathrm{BP}}(X) &= \overline{apr}(X^+|\pi) \cap \overline{apr}(X^?|\pi) \cap (\overline{apr}(X^-|\pi))^c,\\
\mathrm{Bi}^{\mathrm{BN}}(X) &= (\overline{apr}(X^+|\pi))^c \cap \overline{apr}(X^?|\pi) \cap \overline{apr}(X^-|\pi),\\
\mathrm{Tri}(X) &= \overline{apr}(X^+|\pi) \cap \overline{apr}(X^?|\pi) \cap \overline{apr}(X^-|\pi).
\end{aligned}$$

A block in π must be in at least one of the three upper approximations. This means that $\mathrm{Non}(X)$ is always the empty set. Therefore, we only have the 7 regions potentially non-empty and pairwise disjoint regions. Figure 2 visualizes these seven regions in a Venn diagram. The Venn diagram represents the intersections among three upper approximations, where the rectangle in the Venn diagram is the universe, the top-left circle shows the upper approximation of X^+, the top-right circle shows the upper approximation of X^-, and the bottom circle shows the upper approximation of $X^?$.

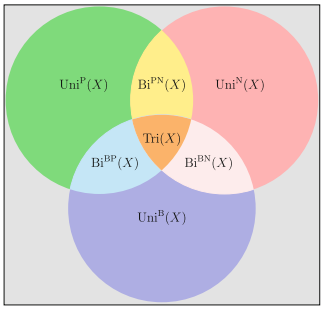

Fig. 2. Seven Regions of a Partially-Known Concept

These seven regions are formed by managing the blocks of the partition based on the number of upper approximations they intersect with. A block intersects

only with the upper approximation of X^+ should be in the region $\text{Uni}^{\text{P}}(X)$; a block intersects only with the upper approximation of $X^?$ should be in the region $\text{Uni}^{\text{B}}(X)$; a block intersects only with the upper approximation of X^- should be in the region $\text{Uni}^{\text{N}}(X)$; a block intersects with both upper approximations of X^+ and $X^?$ but not intersects with the upper approximation of X^- should be in the region $\text{Bi}^{\text{BP}}(X)$; a block intersects with both upper approximations of X^- and $X^?$ but not intersects with the upper approximation of X^+ should be in the region $\text{Bi}^{\text{BN}}(X)$; a block intersects with both upper approximations of X^+ and X^- but not intersects with the upper approximation of $X^?$ should be in the region $\text{Bi}^{\text{PN}}(X)$; and a block intersects with all upper approximations of X^+, $X^?$ and X^- should be in the region $\text{Tri}(X)$.

Example 2. Recall Example 1. By using the naming as given in Example 1, we give the seven regions as follows:

$$\begin{aligned}
\text{Uni}^{\text{N}}(X) &= \{B_{(0,0)}, B_{(0,1)}, B_{(0,2)}, B_{(0,3)}, B_{(0,4)}, B_{(4,0)}, B_{(4,1)}\},\\
\text{Uni}^{\text{P}}(X) &= \{B_{(2,1)}\},\\
\text{Uni}^{\text{B}}(X) &= \{B_{(3,3)}\},\\
\text{Uni}^{\text{PN}}(X) &= \{B_{(1,0)}, B_{(1,1)}, B_{(2,0)}\},\\
\text{Uni}^{\text{BN}}(X) &= \{B_{(1,4)}, B_{(2,4)}, B_{(3,4)}, B_{(4,2)}, B_{(4,3)}, B_{(4,4)}\},\\
\text{Uni}^{\text{BP}}(X) &= \{B_{(2,3)}\},\\
\text{Tri}(X) &= \{B_{(1,2)}, B_{(1,3)}, B_{(2,2)}, B_{(3,0)}, B_{(3,1)}, B_{(3,2)}\}.
\end{aligned}$$

4.2 The 5-region Analysis

In some situations, we may only focus on the sets X^+ and X^- as the set $X^?$ lacks information. The union of upper approximations of X^+ and X^- is a proper subset of the universe, i.e. $X^+ \cup X^- \subset U$, meaning that we cannot represent the lower approximations of X^+ and X^- by using their upper approximations. By having their granular lower and upper approximations, we can form the five regions as follows:

$$\begin{aligned}
\text{P}(X) &= \underline{apr}(X^+|\pi) = \text{Uni}^{\text{P}}(X),\\
\text{N}(X) &= \underline{apr}(X^-|\pi) = \text{Uni}^{\text{N}}(X),\\
\text{PN}(X) &= \overline{apr}(X^+|\pi) \cap \overline{apr}(X^-|\pi) = \text{Bi}^{\text{PN}}(X) \cup \text{Tri}(X),\\
\text{BP}(X) &= \overline{apr}(X^+|\pi) - (\text{PN}(X) \cup \text{P}(X)) = \text{Bi}^{\text{BP}}(X),\\
\text{BN}(X) &= \overline{apr}(X^-|\pi) - (\text{PN}(X) \cup \text{N}(X)) = \text{Bi}^{\text{BN}}(X).
\end{aligned}$$

Figure 3 shows the 5 regions formed from a granular approximation of a partially-known concept, where the rectangle is the universe, the left big circle shows the upper approximation of X^+, the left small circle shows the lower approximation of X^+, the right big circle shows the upper approximation of X^-, and the right small circle shows the lower approximation of X^-.

The five regions are formed by the intersections between the blocks of π and the four approximation sets. A block should be in the region $\mathrm{P}(X)$, if it is contained by the lower approximation of X^+; a block is in the region $\mathrm{N}(X)$, if it is contained by the lower approximation of X^-; a block is in the region $\mathrm{PN}(X)$, if it interacts with both the upper approximations of X^+ and X^-; a block is in the region $\mathrm{BP}(X)$, if it interacts with the upper approximations of X^+ but is not contained by the lower approximations of X^+ and not interacts with the upper approximation of X^-; and a block is in the region $\mathrm{BN}(X)$, if it interacts within the upper approximation of X^- but is not contained by the lower approximation of X^- and not interacts the upper approximation of X^+.

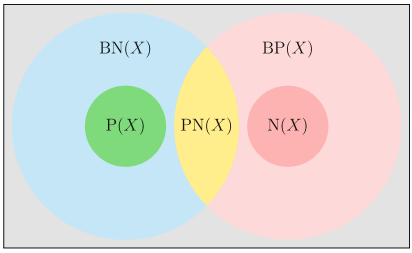

Fig. 3. Five Regions of a Partially-Known Concept

Example 3. Recall Example 1. By using the naming method as discussed in Example 1, we give the five regions as follows:

$$\begin{aligned}
\mathrm{N}(X) &= \{B_{(0,0)}, B_{(0,1)}, B_{(0,2)}, B_{(0,3)}, B_{(0,4)}, B_{(4,0)}, B_{(4,1)}\},\\
\mathrm{P}(X) &= \{B_{(2,1)}\},\\
\mathrm{PN}(X) &= \{B_{(1,0)}, B_{(1,1)}, B_{(1,2)}, B_{(1,3)}, B_{(2,0)}, B_{(2,2)}, B_{(3,0)}, B_{(3,1)}, B_{(3,2)}\},\\
\mathrm{BN}(X) &= \{B_{(1,4)}, B_{(2,4)}, B_{(3,4)}, B_{(4,2)}, B_{(4,3)}, B_{(4,4)}\},\\
\mathrm{BP}(X) &= \{B_{(2,3)}\}.
\end{aligned}$$

5 Conclusion

In this paper, we made an attempt to combine two kinds of uncertainty. The notion of a triplet of sets or an interval set (i.e., a family of sets) models a partially-known concept due to incomplete or partial information. That is, we represent a partially-known concept by three sets or an interval set. These two representations give two distinct semantics. A triplet represents the concept by three disjoint sets, and the interval set represents the concept by a family of possible concepts between a pair of lower and upper bounds. The notion of rough sets concerns approximations of a concept that cannot be precisely defined in terms of a set of finite attributes. In particular, the notion of granular approximations provides a better interpretation and semantic understanding of undefinable

concepts. By extending the idea of approximating a concept to approximating a partially-known concept, we introduced the notion of the granular approximation of partially-known concepts, which combines both types of uncertainty.

We have shown the granular approximations of a partially-known concept under both representations and also shown that a transformation exists between these granular approximations. The granular approximation of a partially-known concept provides two ways to analyze the concept, respectively named as, the 7-region analysis and the 5-region analysis. These analyses may serve as guidance for implementing varied strategies for processing partially-known concepts.

We have examined both the separation and integration of two kinds of uncertainty. Uncertainty due to incomplete information results in partially-known concepts, in comparison with concepts under complete information. Uncertainty due to the use of a finite number of attributes results in undefinable concepts and approximations of undefinable concepts by definable concepts. A clear separation of the two types of uncertainty enables us to see clearly the different semantics of various notions used. On the other hand, the integration gives us a common framework in which both kinds of uncertainty are used simultaneously. This separation-integration methodology may be applicable to study other types of uncertainty. Based on the results of the paper, it is possible to expand further explorations.

References

1. Ciucci, D.: Orthopairs: a simple and widely used way to model uncertainty. Fundam. Inform. **108**, 287–304 (2011). https://doi.org/10.3233/FI-2011-424
2. Boffa, S., Ciucci, D.: Orthopartitions and possibility distributions. Fuzzy Sets Syst. **455**, 53–76 (2023). https://doi.org/10.1016/j.fss.2022.04.022
3. Bryniarski, E.: A calculus of rough sets of the first order. Bull. Pol. Acad. Sci. Math. **37**, 71–78 (1989)
4. Campagner, A., Cabitza, F., Ciucci, D.: Three-way decision for handling uncertainty in machine learning: a narrative review. In: Bello, R., Miao, D., Falcon, R., Nakata, M., Rosete, A., Ciucci, D. (eds.) IJCRS 2020. LNCS (LNAI), vol. 12179, pp. 137–152. Springer, Cham (2020). https://doi.org/10.1007/978-3-030-52705-1_10
5. Chen, Y.X., Zhu, P., Yao, Y.Y.: An axiomatic framework for three-way clustering. Inf. Sci. **675**, 120761 (2024). https://doi.org/10.1016/j.ins.2024.120761
6. Ślezak, D., Wasilewski, P.: Granular sets – foundations and case study of tolerance spaces. In: An, A., Stefanowski, J., Ramanna, S., Butz, C.J., Pedrycz, W., Wang, G. (eds.) RSFDGrC 2007. LNCS (LNAI), vol. 4482, pp. 435–442. Springer, Heidelberg (2007). https://doi.org/10.1007/978-3-540-72530-5_52
7. Greco, S., Matarazzo, B., Słowiński, R.: Distinguishing vagueness from ambiguity in rough set approximations. Int. J. Uncertain. Fuzziness Knowl.-Based Syst. **26**, 89–125 (2018). https://doi.org/10.1142/S0218488518400135
8. Greco, S., Słowiński, R.: Pawlak, belnap and the magical number seven. In: Campagner, A., Urs Lenz, O., Xia, S., Ślęzak, D., Wąs, J., Yao, J. (eds.) Rough Sets. IJCRS 2023. LNCS, vol. 14481, pp. 216–228. Springer, Cham (2023). https://doi.org/10.1007/978-3-031-50959-9_15

9. Hao, F., Sun, Y.F., Lin, Y.G.: Rough maximal cliques enumeration in incomplete graphs based on partially-known concept learning. Neurocomputing **496**, 96–106 (2022). https://doi.org/10.1016/j.neucom.2021.08.160
10. Hu, B.Q.: Three-way decisions space and three-way decisions. Inf. Sci. **281**, 21–52 (2014). https://doi.org/10.1016/j.ins.2014.05.015
11. Hu, M.J.: Three-way Bayesian confirmation in classifications. Cogn. Comput. **14**, 2020–2039 (2022). https://doi.org/10.1007/s12559-021-09924-8
12. Hu, M.J.: Three-way data analytics: preparing and analyzing data in threes. Inf. Sci. **573**, 412–432 (2021). https://doi.org/10.1016/j.ins.2021.05.058
13. Janicki, R., Lenarčič, A.: Optimal approximations with rough sets and similarities in measure spaces. Int. J. Approx. Reason. **71**, 1–14 (2016). http://dx.doi.org/10.1016/j.ijar.2015.12.014
14. Li, H.X., Wang, M.H., Zhou, X.Z., Zhao, J.B.: An interval set for learning rules from incomplete information table. Int. J. Approx. Reason. **53**, 24–37 (2012). https://doi.org/10.1016/j.ijar.2011.09.002
15. Lingras, P., West, C.: Interval set clustering of web users with rough K-means. J. Intell. Inf. Syst. **23**, 5–16 (2004). https://doi.org/10.1023/B:JIIS.0000029668.88665.1a
16. Luo, J.F., Hu, M.J., Qin, K.Y.: Three-way decision with incomplete information based on similarity and satisfiability. Int. J. Approx. Reason. **120**, 151–183 (2020). https://doi.org/10.1016/j.ijar.2020.02.005
17. Luo, J.F., Hu, M.J.: A bipolar three-way decision notion and its application in analyzing incomplete data. Int. J. Approx. Reason. **152**, 94–123 (2023). https://doi.org/10.1016/j.ijar.2022.10.011
18. Ma, J.M., Hu, L.L., Qian, Y.H.: Object-oriented interval-set concept lattices. Int. J. Approx. Reason. **110**, 64–81 (2019). https://doi.org/10.1016/j.ijar.2019.03.012
19. Pawlak, Z.: Rough sets. Int. J. Comput. Inf. Sci. **11**, 341–356 (1982). https://doi.org/10.1007/BF01001956
20. Ren, R.S., Wei, L., Yao, Y.Y.: An analysis of three types of partially-known formal concepts. Int. J. Mach. Learn. Cybern. **9**, 1767–1783 (2018). https://doi.org/10.1007/s13042-017-0743-z
21. Yang, B., Li, J.H.: Complex network analysis of three-way decision researches. Int. J. Mach. Learn. Cybern. **11**, 973–987 (2020). https://doi.org/10.1007/s13042-020-01082-x
22. Yao, J.T., Medina, J., Zhang, Y., Ślęzak, D.: Formal concept analysis, rough sets, and three-way decisions. Int. J. Approx. Reason. **140**, 1–6 (2022). https://doi.org/10.1016/j.ijar.2021.09.011
23. Yao, Y.Y.: Interval-set algebra for qualitative knowledge representation. In: Proceedings of ICCI'93: 5th International Conference on Computing and Information, pp. 370–374. IEEE Press, New York (1993). https://doi.org/10.1109/ICCI.1993.315346
24. Yao, Y.Y.: A partition model of granular computing. In: Peters, J.F., Skowron, A., Grzymała-Busse, J.W., Kostek, B., Świniarski, R.W., Szczuka, M.S. (eds.) Transactions on Rough Sets I. LNCS, vol. 3100, pp. 232–253. Springer, Heidelberg (2004). https://doi.org/10.1007/978-3-540-27794-1_11
25. Yao, Y.Y.: Interval sets and three-way concept analysis in incomplete contexts. Int. J. Mach. Learn. Cybern. **8**, 3–20 (2017). https://doi.org/10.1007/s13042-016-0568-1
26. Yao, Y.Y.: Three-way decision and granular computing. Int. J. Approx. Reason. **103**, 107–123 (2018). https://doi.org/10.1016/j.ijar.2018.09.005

27. Yao, Y.Y., Yang J.L.: Granular rough sets and granular shadowed sets: three-way approximations in Pawlak approximation spaces. Int. J. Approx. Reason. **142**, 231–247 (2022). https://doi.org/10.1016/j.ijar.2021.11.012
28. Yao, Y.Y., Yang J.L.: Granular fuzzy sets and three-way approximations of fuzzy sets. Int. J. Approx. Reason. **161**, 109003 (2023). https://doi.org/10.1016/j.ijar.2023.109003
29. Yao, Y.Y.: The Dao of three-way decision and three-world thinking. Int. J. Approx. Reason. **162**, 109032 (2023). https://doi.org/10.1016/j.ijar.2023.109032
30. Yang, X., Li, Y.H., Li, T.R.: A review of sequential three-way decision and multi-granularity learning. Int. J. Approx. Reason. **152**, 414–433 (2023). https://doi.org/10.1016/j.ijar.2022.11.007
31. Zhang, Q.H., Wang, J., Wang, G.Y., Hu, F.: Approximation set of the interval set in Pawlak's space. Sci. World J. **2014**, 317387 (2014). https://doi.org/10.1155/2014/317387
32. Zhang, Q., Zhao, F., Yubin, X., Yang, J.: Constructing the optimal approximation sets of rough sets in multi-granularity spaces. In: Mihálydeák, T., et al. (eds.) IJCRS 2019. LNCS (LNAI), vol. 11499, pp. 341–355. Springer, Cham (2019). https://doi.org/10.1007/978-3-030-22815-6_27
33. Zhang, Y., Yao, J.T.: Game theoretic approach to shadowed sets: a three-way tradeoff perspective. Inf. Sci. **507**, 540–552 (2020). https://doi.org/10.1016/j.ins.2018.07.058

Robust Online Satellite Video Object Tracking with Self-adoption Uncertainty

Ziye Wang and Duoqian Miao(✉)

Department of Computer Science and Technology, Tongji University, No. 4800, Cao'an Highway, Jiading District, Shanghai 201804, People's Republic of China
{yeziwang,dqmiao}@tongji.edu.cn

Abstract. Tracking moving targets in satellite videos has lately gained popularity. However, the growth of target tracking in satellite videos is slower than in general videos due to the following factors. Satellite video tracking faces challenges stemming from low frame rates, causing significant object movement between frames and impacting prediction accuracy, while high-resolution footage exacerbates tracking difficulties by requiring extensive search regions for targets occupying a minimal percentage of the total pixel count. In overall, the level of uncertainty surrounding the target in the satellite footage is excessive. To address the above problems, we propose a novel DiMP-based tracker and introduce SES to stabilize the estimation of target motion in satellite videos. Furthermore, we introduce an uncertainty measure, which is included into network outputs and a loss function to remove unreliable samples from the training set. Extensive experiments have demonstrated that our technique can track targets with the highest precision score and success rate on both the SatSOT and SV248S datasets, achieving state-of-the-art status.

Keywords: Object Tracking · Satellite Videos · Uncertainty · Correlation Filters

1 Introduction

In computer vision and remote sensing, object tracking is a popular topic. Generally, it uses a bounding box that locks onto the region of interest (ROI) when the target's initial state (in a video frame) is all that is available [1,2]. Many satellites with sophisticated onboard cameras have been deployed to collect very high resolution (VHR) satellite movies for military and civilian applications, owing to the advancements in satellite imaging technology [3]. Satellite video object tracking (SVOT) is a growing topic in the remote sensing field, with applications ranging from traffic control to ocean monitoring [4] and smart city construction [5].

Traditional video-based target tracking has garnered more attention recently, as evidenced by the several algorithms that have been suggested for precise

M. Hu et al. (Eds.): IJCRS 2024, LNAI 14840, pp. 74–85, 2024.
https://doi.org/10.1007/978-3-031-65668-2_6

tracking in computer vision. There are two types of methods that make use of either discriminant models [6–9]or generative models [10–12]. Discriminant models view object tracking as a binary classification problem and have received a lot of attention for their efficiency and robustness [13,14]. In contrast, the generative model-based target tracking can be viewed as a search problem, in which the object area in the current frame is modeled and the most similar region is picked as the anticipated location in the next frame [15,16].

Object tracking tasks are usually divided into three components: feature extraction [17], target location, and target scale estimate [18]. Discriminative Correlation Filter (DCF) and Siamese tracking techniques are the dominant tracking pipelines for target localization solutions available today. Correlation filters are first introduced into tracking in 2010 [19], and correlation filter tracking methods remain popular to this day. Initially, researchers employed hand-crafted features such as color histogram [20], CN (Color Names) [21,22], gray [23], and HOG (Histogram of Oriented Gradient) [24] as target features. Since that a single feature is insufficient to address a wide range of complicated scene problems, some scholars attempted to combine many hand-crafted features to characterize the target [25,26]. With the rise of deep learning, a few researchers attempted to replace standard features with deep features [27,28], however the tracking results were not competitive when compared to popular correlation filter trackers that used traditional features. Some trackers [29,30] considered hand-crafted features (HOG and CN) to be shallow features, and used the deep convolutional neural networks such as ResNet [31] and VGG-Net [32] as deep feature extractor framework for adaptive weighted fusion. In 2016, SiamFC [33] suggested an accepted Siamese network architecture that only used the target template feature of the first frame and did not have an online updating mechanism. As a result, some Siamese network tracking methods based on SiamFC appeared one after another [16,34–36]. Though the tracking speed of the above-mentioned siamese tracking methods are quite rapid, the robustness and accuracy is still needed to be improved.

Given only the initial object location of a moving object in a satellite video sequence, SVOT algorithms attempt to automatically predict the trajectory of the target object throughout the sequence. Although generic object tracking technology has made significant development in recent years, the majority of available tracking frameworks are developed for traditional videos captured by fixed optical cameras. When compared to conventional object tracking jobs or aerial image tracking utilizing unmanned aerial vehicles (UAVs), satellite video tracking has encountered a number of challenges due to the distinct characteristics of remote sensing images. For instance, the frame rate of satellite video is usually low due to onboard hardware restrictions, which causes significant movement of the object targets between frames and further affects tracking prediction and model update. Current tracking systems are prone to missing targets that are suddenly stopped, concealed, or relocated. In addition, high-resolution satellite footage typically has widths and heights of more than 2000 pixels, yet the target of interest only occupies 0.01% or less of the total number of pixels in the

video frame. While diminishing tracking performance, the large-size background increases the searching region of traditional tracking algorithms. Trackers are more likely to be deceived and drift to the interfering objects when multiple highly SOs are packed surrounding the tracked target, as most moving objects in satellite films have the shape of points and lines.

Based on the above-mentioned reasons, it can be considered that the uncertainty of targets in satellite videos is stronger, creating more obstacles for tracking. We contend that uncertainty can also be used to direct the network's constituent parts. In order to tackle uncertainty and improve the robustness of object tracking in satellite videos, we propose an uncertainty-adjusted sampling strategy for the online learning of object trackers. Motivated by the characteristic of motion smoothness of the satellite targets, in this paper, we combine a spatial-temporal regularized correlation filter and motion smoothness requirement to build a high-efficiency SVOT technique. In order to properly screen out noisy samples and increase the robustness of the branch, our tracker models the uncertainty contained in frame samples that are sent to the classification branch of the model. To the best of our knowledge, this is the first instance of end-to-end training and uncertainty estimation being integrated into the sample selection process in the field of SVOT.

Our main contributions in this paper are summarized as follows:

(1) We propose a trajectory prediction technique based on SES method, which stabilizes the estimation of target motion in satellite videos, thereby enhancing target localization accuracy.
(2) We introduce a separate regression branch to handle target uncertainty more effectively. This branch assesses target shape and is trained to compute the Intersection Over Union (IOU) with proposed bounding boxes. Additionally, the paper introduces a measure of uncertainty, which is incorporated into network outputs and loss function to filter unreliable samples from the training set.
(3) We propose a novel DiMP-based satellite videos object tracking method. Numerous experiments have proven that our method can track targets with the best precision score and success rate on both the SatSOT and SV248S datasets, achieving the state-of-the-art level.

2 Related Work

2.1 CF-Based Object Tracking

Beginning with the Bolme et al. [19] minimum output sum of square error (MOSSE) algorithm, the CF paradigm has been successfully integrated into the field of visual object tracking. The kernelized CF (KCF) tracker gained a lot of traction because of how easily it could be expanded. CF-based tracking has been implemented extensively in recent years using deep features that are collected from convolutional neural networks (CNNs) [18,37]. Many CF-based

trackers currently in use [27,29,38,39] combine jointly created and deep features to provide strong feature representation.

By resolving ridge regression in the Fourier domain, the discriminative correlation filter (DCF) offers an attractively efficient solution to the visual tracking problem [25,28,40–43]. These techniques usually aim to develop a discriminative convolution kernel and then convolve with the search region in order to obtain a response map. ATOM [44] used an optimization approach based on Gauss-Newton and conjugate gradient to speed up the kernel learning rate, allowing for quick online training. The learnt convolution kernel in an end-to-end tracking architecture gained more discriminative strength as a result of the recent DiMP [45], which was further upgraded from the standpoint of probabilistic regression [46].

2.2 Object Tracking in Satellite Videos

In recent years, there has been a growing interest in moving object tracking in satellite videos. Du et al. [47] combined the previously mentioned KCF tracker with a three-frame-difference technique. Shao et al. [48] also used KCF as the foundation and two supplementary features, optical flow (OF) and HOG, to improve the filter's object representation capabilities. To address the target occlusion problem, Li et al. [49] integrated STRCF with an interacting multiple model (IMM). In order to achieve more accurate tracking, some research [50–52] have combined the Kalman filter (KF) with the CF framework, taking into account that motion limitations can assist reduce tracking failures. In order to monitor small objects more reliably, Yang et al. [53] most recently proposed a SiamMDM network that fuses several response maps and takes advantage of spatiotemporal restrictions. The tracking drift problem can also be partially addressed by the SiamMDM tracker with the use of a score-guided motion model.

2.3 Uncertainty Estimation

Errors could originate from a wide range of potential sources in complex situations containing a lot of data and variables, especially in the searching field of computer vision. For this reason, it's very important to quantify this uncertainty and appropriately weigh intermediate forecasts. The field of computer vision literature had a long association with uncertainty estimation. In the context of 3D target detection, MonoPair [54] suggested a prediction module for uncertainty perception. In pedestrian placement, Monoloco [55] assessed and illustrates the uncertainty of azimuth prediction. Gaussian-YOLO v3 [56] used loss function reconstruction and Gaussian modeling to determine the uncertainty of bounding box (bbox) prediction values.

3 Proposed Tracker

3.1 General Architecture

Since the majority of the traffic objects in the satellite videos are seen from above, most of them go along predetermined routes (such as cars on the road or trains on the rail), exhibiting clear regularity. As a result, the trajectory of a moving object in frames that follow an initial one frequently exhibits a certain regularity, and the motion data from those frames can be regarded as an essential cue to help with target localization. In our investigation, the motion trajectory of a point target in satellite videos may always be finished with a straight line, indicating a linear stationary time series. In order to prevent modeling instability and slow down the rate of convergence, we introduces a simplified but effective SES method [57], which performs motion estimation while assuming smoothness constraints.

Considering the current stage of development of the tracking field, our proposed approach is based on the DiMP tracker [45], which consists of two branches: target classification and target localization. The categorization branch is an online learning network capable of identifying rough places. These coarse positions are then sent into the target localization branch to estimate the precise target position. We suggest a number of enhancements that should help the model track uncertainty more effectively and increase its resilience. The architecture of our proposed tracker is shown as Fig. 1. The detailed process of the innovative proposed tracking method may be summed up as follows: 1) Feature Extractor; 2) Model Predictor; 3) Uncertainty Online Learning.

Below, we go over the architecture and training approach for our entire model, including all of our advancements. Since the Model Predictor module we utilized is exactly the same as DiMP tracker, it will not be described in detail in this article.

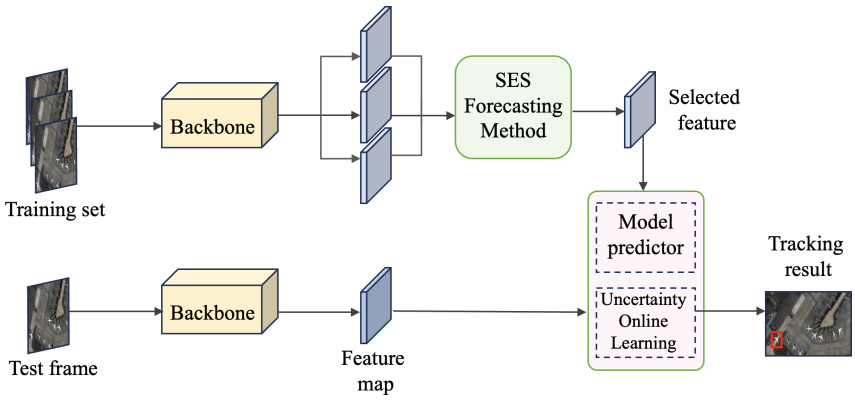

Fig. 1. An architecture of our tracking framework.

3.2 Feature Extractor

Similar to DiMP tracker, our final tracking architecture has two branches: a testing frame branch and a training set branch. Firstly, we extract deep features of testing frame and training set by a common backbone network. Then, we utilize SES Forecasting Mehod to optimize the potential for point target tracking. The determined position of the i frame is defined as $p_i, 0 < i < X$, where X is the total number of frames in the current video sequence. The translation vector δ_t denotes the translation of the target between $t-1$ frame and t frame. As a result, the translation vector δ_t could be calculated by

$$\delta_t = p_t - p_{t-1} \tag{1}$$

We define the $\hat{p}$ as the position that estimated by SES forecating method. And the estimated translation vector $\hat{\delta}_t$ could be calculated by

$$\hat{\delta}_t = \hat{p}_t - p_{t-1} = \alpha\delta_{t-1} + (1-\alpha)\hat{\delta}_{t-1}, \tag{2}$$

where α is a smoothing constant ranging from 0 to 1.

Since universal baseline trackers always employ the determined position of the previous frame to obtain the search region, they are susceptible to interference caused by SOs surrounding the target. However, in our suggested method, the coarse position determined by SES is used to place the tracked object in the middle of the search region to reduce background noise and the uncertainty of the object.

3.3 Uncertainty Online Learning

On top of the core online learning classification branch, our tracker includes a separate regression branch that assesses the shape of the target and is trained to calculate the target's Intersection Over Union (IOU) with any bounding box proposal. In order to augment the classification branch and further reduce the uncertainty of the target, we introduce uncertainty prediction and use this measure of uncertainty to determine which frames are sent to the online learning regression branch during testing.

Our regression branch takes in a proposal bounding box and returns a real number estimating the IOU between the target and the bbox proposal. We further extend the network to incorporate a measure of uncertainty γ. Therefore, the output is shown as following:

$$IOU_{\Theta}(B) = (y, \gamma) \tag{3}$$

where the Θ indicates the weights of the neural network. The γ means the aleatoric uncertainty associated with the IOU prediction y returned by the network IOU. Then we utilize the following loss function to train the network using the ground truth IOU determined by the labels:

$$L(\theta) = \sum_i [\frac{1}{2} exp(-\gamma_i)||y_i - \hat{y}_i||^2 + \frac{1}{2}\gamma_i] \tag{4}$$

The loss function directs γ to take a high value when the error $||y_i - \hat{y}_i||^2$ is substantial. Thus, learned simultaneously with the predictions y_i and our specific loss function, γ can estimate the noise of the input data, allowing us to filter away unreliable samples from the training set sent to the online learning branch.

4 Experiments

4.1 Implementation Details

Our proposed apporach is implemented in Python ustilizing PyTorch on a Nvidia GTX 1080ti GPU with 24GB memory. Our tracker was implemented based on the DiMP architecture by using ResNet50 as backbone.

4.2 Datasets and Evaluation Metrics

SV248S Dataset. The 248 video sequences in the SV248S dataset [58] have a duration of 20–30.12 s with a frame rate of 25 frames per second. The sequences range in length from 500 to 753 frames. Over 90% of the targets in this dataset are autos since the dataset's focus is on the tracking challenges posed by small targets in remote sensing satellite video tracking.

SatSOT Dataset. Jilin-1, Skybox, and Carbonite-2 are the three commercial satellites that provide spaceborne imagery of SatSOT Dataset [59]. The image frames in this dataset are cropped from the original photos, and it comprises 105 satellite video sequences totaling 27 664 frames.

Evaluation Metrics. In this work, the concepts of precision and success rate from one-pass evaluation (OPE) are applied to the quantitative assessment. The center localization error (CLE), which is the Euclidean distance between the target GT's center and its anticipated bounding box, is used to calculate the tracking precision.

4.3 Results Comparison

For comparison, the following 12 trackers are utilized in this experimental study: MOSSE, CSK, KCF, Staple, ECO, SiamFC, SiamRPN, SiamRPN++, SiamMask, DiMP, ToMP and TCTrack. As demonstrated in Table 1, we could find that the performance of our tracker is better than other state-of-the-art trackers. In the SV248S Dataset, our tracker achieves 44.6% in success rate and 2.2% higher than the best tracker SiamRPN++. In the SatSOT Dataset, our proposed method gets 1.9% higher than SiamRPN++. To sum up, we can draw the following conclusion: the tracker we proposed can effectively improve the tracking effect of targets in satellite videos.

Table 1. Comparison with state-of-the-art trackers on the SatSOT and SV248S in terms of precision and success rate.

Trackers	Source	SV248S		SatSOT	
		Prec	Succ	Prec	Succ
MOSSE	CVPR2010	16.6	7.8	24.2	26.9
CSK	ECCV2012	8.9	5.0	23.7	24.7
KCF	TPAMI2014	43.6	19.6	52.1	39.3
Staple	CVPR2016	34.3	14.7	46.2	38.2
ECO	ICCV2017	67.7	40.6	54.9	38.7
SiamFC	ECCV2016	63.4	39.4	49.8	41.3
SiamRPN	CVPR2018	34.0	14.5	50.0	38.5
SiamRPN++	CVPR2019	67.3	42.4	54.0	40.0
SiamMask	CVPR2019	56.5	22.1	55.2	39.8
DiMP	ICCV2019	59.6	36.0	51.8	42.0
ToMP	CVPR2022	38.8	16.5	49.3	38.9
TCTrack	CVPR2022	32.5	13.0	45.7	32.9
Ours	–	68.5	44.6	57.1	46.8

5 Conclusion

This paper proposes a novel DiMP-based tracking technique for performing object tracking tasks in satellite videos. To reduce the uncertainty of the target and improve tracking performance, two novel modules are introduced to the DiMP architecture. Particularly, in order to maximize the potential for point target tracking, we employ the SES Forecasting Method. And we propose an uncertainty online learning module to measure the uncertainty of tracking objects. A comprehensive set of experiments has shown that, in terms of tracking accuracy and success rate, the suggested strategy can outperform the most advanced techniques. To summarise, the accuracy, robustness, and efficiency of the suggested tracking method make it very ideal for tracking moving objects in satellite movies.

Acknowledgements. This work is supported in part by the National Key Research and Development Plan under Grant No. 2022YFB3104700, the National Science Foundation of China under Grant No. 61976158 and No. 62376198, the National Science Foundation of China under Grant No. 62076182. This paper is partially supported by the Jiangxi "Double Thousand Plan", and the National Natural Science Foundation of China (Serial No. 62163016), and the Jiangxi Provincial natural science fund (No. 20212ACB202001) and the National Natural Science Foundation of China No. 62006172.

References

1. Kugarajeevan, J., Kokul, T., Ramanan, A., Fernando, S.: Transformers in single object tracking: an experimental survey. IEEE Access (2023)
2. Fu, C., Lu, K., Zheng, G., et al.: Siamese object tracking for unmanned aerial vehicle: a review and comprehensive analysis. Artif. Intell. Rev. **56**(Suppl 1), 1417–1477 (2023)
3. Upadhyay, P., Gupta, S.: Introduction to satellite imaging technology and creating images using raw data obtained from landsat satellite. ICGTI-2012 **1**(1), C126–C134 (2012)
4. Danovaro, R., Fanelli, E., Aguzzi, J., et al.: Ecological variables for developing a global deep-ocean monitoring and conservation strategy. Nat. Ecol. Evolut. **4**(2), 181–192 (2020)
5. Jiang, D.: The construction of smart city information system based on the internet of things and cloud computing. Comput. Commun. **150**, 158–166 (2020)
6. Zhao, C., Liu, H., Su, N., Wang, L., Yan, Y.: Ranet: a reliability-guided aggregation network for hyperspectral and RGB fusion tracking. Remote Sensing **14**(12), 2765 (2022)
7. Klinger, T., Rottensteiner, F., Heipke, C.: Probabilistic multi-person localisation and tracking in image sequences. ISPRS J. Photogramm. Remote. Sens. **127**, 73–88 (2017)
8. Wilson, D., Alshaabi, T., Van Oort, C., Zhang, X., Nelson, J., Wshah, S.: Object tracking and geo-localization from street images. Remote Sensing **14**(11), 2575 (2022)
9. Du, S., Wang, S.: An overview of correlation-filter-based object tracking. IEEE Trans. Comput. Soc. Syst. **9**(1), 18–31 (2021)
10. Xing, X., Yongjie, Y., Huang, X.: Real-time object tracking based on optical flow. In: 2021 International Conference on Computer, Control and Robotics (ICCCR), IEEE, pp. 315–318 (2021)
11. Yu, H., Li, G., Su, L., Zhong, B., Yao, H., Huang, Q.: Conditional GAN based individual and global motion fusion for multiple object tracking in UAV videos. Pattern Recogn. Lett. **131**, 219–226 (2020)
12. Acharya, D., Ramezani, M., Khoshelham, K., Winter, S.: Bim-tracker: a model-based visual tracking approach for indoor localisation using a 3D building model. ISPRS J. Photogramm. Remote Sens. **150**, 157–171 (2019)
13. Lyu, Y., Yang, M.Y., Vosselman, G., Xia, G.-S.: Video object detection with a convolutional regression tracker. ISPRS J. Photogramm. Remote Sens. **176**, 139–150 (2021)
14. Held, D., Thrun, S., Savarese, S.: Learning to track at 100 FPS with deep regression networks. In: Leibe, B., Matas, J., Sebe, N., Welling, M. (eds.) ECCV 2016. LNCS, vol. 9905, pp. 749–765. Springer, Cham (2016). https://doi.org/10.1007/978-3-319-46448-0_45
15. Fernando, T., Denman, S., Sridharan, S., Fookes, C.: Tracking by prediction: a deep generative model for mutli-person localisation and tracking. In: IEEE Winter Conference on Applications of Computer Vision (WACV). IEEE 2018, pp. 1122–1132 (2018)
16. AlBasiouny, E.R., Attia, A.-F., Abdelmunim, H.E., Abbas, H.M.: Robust visual tracking using very deep generative model. J. Big Data **10**(1), 3 (2023)
17. Zhou, W., Miwa, S., Tsujimura, R., Nguyen, T.-B., Okawa, T., Okamoto, K.: Bubble feature extraction in subcooled flow boiling using AI-based object detection and tracking techniques. Int. J. Heat Mass Transf. **222**, 125 188 (2024)

18. Xu, Y., Wang, Z., Li, Z., Yuan, Y., Yu, G.: SiamFC++: towards robust and accurate visual tracking with target estimation guidelines. In: Proceedings of the AAAI Conference on Artificial Intelligence, vol. 34, pp. 12 549–12 556 (2020)
19. Bolme, D.S., Beveridge, J.R., Draper, B.A., Lui, Y.M.: Visual object tracking using adaptive correlation filters. In: IEEE Computer Society Conference on Computer Vision and Pattern Recognition. IEEE 2010, pp. 2544–2550 (2010)
20. Han, J., Ma, K.-K.: Fuzzy color histogram and its use in color image retrieval. IEEE Trans. Image Process. **11**(8), 944–952 (2002)
21. Van De Weijer, J., Schmid, C., Verbeek, J., Larlus, D.: Learning color names for real-world applications. IEEE Trans. Image Process. **18**(7), 1512–1523 (2009)
22. Parrish, C.H.: Color names and color notions. J. Negro Educ. **15**(1), 13–20 (1946)
23. Henriques, J.F., Caseiro, R., Martins, P., Batista, J.: Exploiting the circulant structure of tracking-by-detection with kernels. In: Fitzgibbon, A., Lazebnik, S., Perona, P., Sato, Y., Schmid, C. (eds.) ECCV 2012. LNCS, vol. 7575, pp. 702–715. Springer, Heidelberg (2012). https://doi.org/10.1007/978-3-642-33765-9_50
24. Dalal, N., Triggs, B.: Histograms of oriented gradients for human detection. In: IEEE Computer Society Conference on Computer Vision and Pattern Recognition (CVPR'05), vol. 1, no. 2005, pp. 886–893. IEEE (2005)
25. Bertinetto, L., Valmadre, J., Golodetz, S., Miksik, O., Torr, P.H.: Staple: complementary learners for real-time tracking. In: Proceedings of the IEEE Conference on Computer Vision and Pattern Recognition, pp. 1401–1409 (2016)
26. Li, Y., Zhu, J.: A scale adaptive kernel correlation filter tracker with feature integration. In: Agapito, L., Bronstein, M.M., Rother, C. (eds.) ECCV 2014. LNCS, vol. 8926, pp. 254–265. Springer, Cham (2015). https://doi.org/10.1007/978-3-319-16181-5_18
27. Danelljan, M., Bhat, G., Shahbaz Khan, F., Felsberg, M.: Eco: efficient convolution operators for tracking. In: Proceedings of the IEEE Conference on Computer Vision and Pattern Recognition, pp. 6638–6646 (2017)
28. Ma, C., Huang, J.-B., Yang, X., Yang, M.-H.: Hierarchical convolutional features for visual tracking. In: Proceedings of the IEEE International Conference on Computer Vision, pp. 3074–3082 (2015)
29. Bhat, G., Johnander, J., Danelljan, M., Khan, F.S., Felsberg, M.: Unveiling the power of deep tracking. In: Proceedings of the European Conference on Computer Vision (ECCV), pp. 483–498 (2018)
30. Wang, Z., Miao, D., Zhao, C., Luo, S., Wei, Z.: A robust long-term pedestrian tracking-by-detection algorithm based on three-way decision. In: Mihálydeák, T., et al. (eds.) IJCRS 2019. LNCS (LNAI), vol. 11499, pp. 522–533. Springer, Cham (2019). https://doi.org/10.1007/978-3-030-22815-6_40
31. He, K., Zhang, X., Ren, S., Sun, J.: Deep residual learning for image recognition. In Proceedings of the IEEE Conference on Computer Vision and Pattern Recognition, pp. 770–778 (2016)
32. Wang, L., Guo, S., Huang, W., Qiao, Y.: Places205-vggnet models for scene recognition, arXiv preprint arXiv:1508.01667 (2015)
33. Bertinetto, L., Valmadre, J., Henriques, J.F., Vedaldi, A., Torr, P.H.S.: Fully-convolutional Siamese networks for object tracking. In: Hua, G., Jégou, H. (eds.) ECCV 2016. LNCS, vol. 9914, pp. 850–865. Springer, Cham (2016). https://doi.org/10.1007/978-3-319-48881-3_56
34. Guo, D., Wang, J., Cui, Y., Wang, Z., Chen, S.: SiamCAR: siamese fully convolutional classification and regression for visual tracking. In: Proceedings of the IEEE/CVF Conference on Computer Vision and Pattern Recognition, pp. 6269–6277 (2020)

35. Chen, Z., Zhong, B., Li, G., et al.: SiamBAN: target-aware tracking with Siamese box adaptive network. IEEE Trans. Pattern Anal. Mach. Intell. **45**(4), 5158–5173 (2022)
36. Li, B., Wu, W., Wang, Q., Zhang, F., Xing, J., Yan, J.: Siamrpn++: evolution of Siamese visual tracking with very deep networks. In: Proceedings of the IEEE/CVF Conference on Computer Vision and Pattern Recognition, pp. 4282–4291 (2019)
37. Simonyan, K., Zisserman, A.: Very deep convolutional networks for large-scale image recognition, arXiv preprint arXiv:1409.1556 (2014)
38. Zhu, X.-F., Wu, X.-J., Xu, T., Feng, Z.-H., Kittler, J.: Complementary discriminative correlation filters based on collaborative representation for visual object tracking. IEEE Trans. Circuits Syst. Video Technol. **31**(2), 557–568 (2020)
39. Bai, S., He, Z., Dong, Y., Bai, H.: Multi-hierarchical independent correlation filters for visual tracking. In: IEEE International Conference on Multimedia and Expo (ICME). IEEE 2020, pp. 1–6 (2020)
40. Henriques, J.F., Caseiro, R., Martins, P., Batista, J.: High-speed tracking with kernelized correlation filters. IEEE Trans. Pattern Anal. Mach. Intell. **37**(3), 583–596 (2014)
41. Danelljan, M., Robinson, A., Shahbaz Khan, F., Felsberg, M.: Beyond correlation filters: learning continuous convolution operators for visual tracking. In: Leibe, B., Matas, J., Sebe, N., Welling, M. (eds.) ECCV 2016. LNCS, vol. 9909, pp. 472–488. Springer, Cham (2016). https://doi.org/10.1007/978-3-319-46454-1_29
42. Danelljan, M., Häger, G., Khan, F.S., Felsberg, M.: Discriminative scale space tracking. IEEE Trans. Pattern Anal. Mach. Intell. **39**(8), 1561–1575 (2016)
43. Danelljan, M., Hager, G., Shahbaz Khan, F., Felsberg, M.: Learning spatially regularized correlation filters for visual tracking. In: Proceedings of the IEEE International Conference on Computer Vision, pp. 4310–4318 (2015)
44. Danelljan, M., Bhat, G., Khan, F.S., Felsberg, M.: Atom: accurate tracking by overlap maximization. In: Proceedings of the IEEE/CVF Conference on Computer Vision and Pattern Recognition, pp. 4660–4669 (2019)
45. Bhat, G., Danelljan, M., Gool, L.V., Timofte, R.: Learning discriminative model prediction for tracking. In: Proceedings of the IEEE/CVF International Conference on Computer Vision, pp. 6182–6191 (2019)
46. Danelljan, M., Gool, L.V., Timofte, R.: Probabilistic regression for visual tracking. In: Proceedings of the IEEE/CVF Conference on Computer Vision and Pattern Recognition, pp. 7183–7192 (2020)
47. Du, B., Sun, Y., Cai, S., Wu, C., Du, Q.: Object tracking in satellite videos by fusing the kernel correlation filter and the three-frame-difference algorithm. IEEE Geosci. Remote Sens. Lett. **15**(2), 168–172 (2017)
48. Shao, J., Du, B., Wu, C., Zhang, L.: Can we track targets from space? A hybrid kernel correlation filter tracker for satellite video. IEEE Trans. Geosci. Remote Sens. **57**(11), 8719–8731 (2019)
49. Li, Y., Bian, C.: Object tracking in satellite videos: a spatial-temporal regularized correlation filter tracking method with interacting multiple model. IEEE Geosci. Remote Sens. Lett. **19**, 1–5 (2022)
50. Xuan, S., Li, S., Han, M., Wan, X., Xia, G.-S.: Object tracking in satellite videos by improved correlation filters with motion estimations. IEEE Trans. Geosci. Remote Sens. **58**(2), 1074–1086 (2019)
51. Li, Y., Bian, C., Chen, H.: Object tracking in satellite videos: correlation particle filter tracking method with motion estimation by Kalman filter. IEEE Trans. Geosci. Remote Sens. **60**, 1–12 (2022)

52. Guo, Y., Yang, D., Chen, Z.: Object tracking on satellite videos: a correlation filter-based tracking method with trajectory correction by Kalman filter. IEEE J. Sel. Top. Appl. Earth Obs. Remote Sens. **12**(9), 3538–3551 (2019)
53. Yang, J., Pan, Z., Wang, Z., Lei, B., Hu, Y.: Siammdm: an adaptive fusion network with dynamic template for real-time satellite video single object tracking. IEEE Trans. Geosci. Remote Sens. (2023)
54. Chen, Y., Tai, L., Sun, K., Li, M.: Monopair: monocular 3D object detection using pairwise spatial relationships. In: Proceedings of the IEEE/CVF Conference on Computer Vision and Pattern Recognition, pp. 12 093–12 102 (2020)
55. Feng, D., Rosenbaum, L., Dietmayer, K.: Towards safe autonomous driving: capture uncertainty in the deep neural network for lidar 3d vehicle detection. In: 21st International Conference on Intelligent Transportation Systems (ITSC). IEEE 2018, pp. 3266–3273 (2018)
56. Choi, J., Chun, D., Kim, H., Lee, H.-J.: Gaussian YOLOV3: an accurate and fast object detector using localization uncertainty for autonomous driving. In: Proceedings of the IEEE/CVF International Conference on Computer Vision, pp. 502–511 (2019)
57. Nazim, A., Afthanorhan, A.: A comparison between single exponential smoothing (SES), double exponential smoothing (DES), holt's (brown) and adaptive response rate exponential smoothing (arres) techniques in forecasting Malaysia population. Glob. J. Math. Anal. **2**(4), 276–280 (2014)
58. Li, Y., Jiao, L., Huang, Z., et al.: Deep learning-based object tracking in satellite videos: A comprehensive survey with a new dataset. IEEE Geosci. Remote Sens. Mag. **10**(4), 181–212 (2022)
59. Zhao, M., Li, S., Xuan, S., Kou, L., Gong, S., Zhou, Z.: Satsot: a benchmark dataset for satellite video single object tracking. IEEE Trans. Geosci. Remote Sens. **60**, 1–11 (2022)

Three-Way Hybrid Sampling Using Granular Balls for Imbalanced Classification

Qin Xie[1,2,3], Qinghua Zhang[1,2(✉)], Nanfang Luo[1,2,3], and Guoyin Wang[1,2]

[1] Chongqing Key Laboratory of Computational Intelligence, Chongqing University of Posts and Telecommunications, Chongqing 400065, China
zhangqh@cqupt.edu.cn

[2] Key Laboratory of Big Data Intelligent Computing, Chongqing University of Posts and Telecommunications, Chongqing 400065, China

[3] School of Computer Science and Technology, Chongqing University of Posts and Telecommunications, Chongqing 400065, China

Abstract. Imbalanced data is prevalent in various fields, including disease diagnosis. Effective imbalanced learning methods are crucial for improving supervised learning algorithms. Existing preprocessing methods of imbalanced learning still suffer from blurred class boundaries, weak robustness, and high time costs. In this paper, a three-way hybrid sampling method using granular balls (TWHGBS) for imbalanced binary classification is proposed. First, an overlap-based granular ball generation (OGBG) method is proposed using k-division. Second, undersampling and oversampling methods are concatenated to give a new hybrid sampling method. Specifically, based on the overlap relation between granular balls (GBs), an undersampling method is proposed to identify borderline samples. An oversampling method is proposed for synthesizing minority samples within GB based on overlap degrees adaptively. Experimental results demonstrate that the TWHGBS-based classifiers exhibit superior effectiveness and robustness in terms of $G-mean$ when compared with the existing GB-based undersampling method (GBU) and two conventional hybrid methods, namely, SMOTE-Tomek Links method (STomek) and SMOTE-ENN method (SENN).

Keywords: Imbalanced datasets · Hybrid sampling · Granular computing · Three-way decisions · Imbalanced classification

1 Introduction

Learning from an imbalanced dataset which is with skewed class distribution, referred to as imbalanced learning, is a challenge in the field of machine learning [10]. Various real-world datasets exhibit inherent skew, such as the patient dataset containing far more normal individuals than sick individuals. Directly training machine learning models on such an imbalanced dataset often leads to the overfitting of majority samples and underfitting of minority samples. After

M. Hu et al. (Eds.): IJCRS 2024, LNAI 14840, pp. 86–102, 2024.
https://doi.org/10.1007/978-3-031-65668-2_7

decades of development, diverse imbalanced learning methods have emerged, falling into three main categories: algorithm-level approaches, cost-sensitive learning, and preprocessing approaches.

Algorithm-level approaches balance the impact of skewed class distribution of datasets by proposing specific machine learning models, including ensemble learning [6,11]. Cost-sensitive learning balances the impact of class skew by giving different penalty weights to different misclassifications to increase the importance of minority samples, including the cost-based boosting models [8,13]. Besides, [21] proposes an evolutionary cost-sensitive deep belief network for imbalanced classification. However, the above-mentioned imbalanced learning methods are all coupled with machine learning models. The preprocessing approaches decouple the imbalanced learning mechanism from the machine learning models, which makes these approaches portable. They balance skewed class distribution by preprocessing datasets, including oversampling methods [7,9], undersampling methods [1,15], and hybrid sampling methods [2,3]. However, there are still some limitations that require further improvement, such as the existing undersampling methods may remove important borderline samples; the existing oversampling methods might blur class boundaries; the oversampling and undersampling both cannot handle highly imbalanced datasets; the existing hybrid sampling methods exhibit high time complexity and are unsatisfactory in processing label noise datasets.

Granular computing (GrC) [20] is a new computing paradigm that can greatly improve computing efficiency by granulating complex datasets and using information granules (IGs) instead of samples as the basic computing unit. After decades of development, GrC has been combined with various machine learning models to improve the performance of data mining [14,22]. For instance, a long-term prediction method based on the back-propagation neural network using IGs as input is given [14]. Notably, some studies have introduced GrC to imbalanced learning. For instance, a novel rough-granular computing method is proposed to synthesize new samples in specific regions of feature space [5]. Besides, [18] proposes the GBU, which uses IGs represented by balls to describe the original dataset. Thus, the distribution of the sampled dataset based on GBs remains consistent with the original dataset. The time complexity of GBU is linear. However, GBU, being an undersampling method, has limitations for highly imbalanced datasets. In addition, GBU implements uniform sampling across all GBs, leading to redundancy in the sampled dataset for classification.

Three-way decisions [19], a branch of GrC, advocates understanding and processing complex issues through three different and related parts, that is, conquering by three. The three-way decisions has been combined with numerous excellent machine learning models to improve the performance and efficiency of data mining. For instance, [12] proposes a novel image recognition algorithm based on sequential three-way decisions introduced to speed up the inference in a convolutional neural network. Therefore, a three-way hybrid sampling method using GBs for imbalanced binary classification is proposed in this paper to address the aforementioned limitations. The main contributions of this paper are as follows.

- The proposal of the undersampling method based on the overlap relation between GBs enables the identification of samples on class boundaries;
- The proposal of the oversampling method based on the overlap degree of heterogeneous GBs allows adaptively synthesis of new minority samples within GB to balance skewed class distribution while alleviating blurring class boundaries;
- The proposed TWHGBS is characterized by robustness, low time complexity, and the ability to handle highly imbalanced datasets.

The remainder of this paper is organized as follows. Section 2 reviews related works on the preprocessing approaches of imbalanced learning and the GB-based undersampling method. In Sect. 3, the TWHGBS is introduced in detail. The performance of the proposed method is demonstrated in Sect. 4. Finally, the conclusion and further work are presented in Sect. 5.

2 Related Work

2.1 Notations

Let $D(D = \{(\boldsymbol{x}_1, y_1), (\boldsymbol{x}_2, y_2), \cdots, (\boldsymbol{x}_N, y_N)\})$ be a binary dataset with N samples and p features, where $\boldsymbol{x}_i \in \chi \subseteq \mathcal{R}^p$ represents the feature vector, $y_i \in \mathcal{Y} = \{l_1, l_2\}$ denotes corresponding classes, and $i = 1, 2, \cdots, N$. The majority class of D is denoted as D', and the minority class is denoted as D''. The imbalance ratio IR is $IR = |D'|/|D''|$, where $|\bullet|$ represents the cardinality of set $\bullet$. And, G is a set of GBs generated on D, where $G = \{gb_1, gb_2, \cdots, gb_m\}$. The majority GB set in G is denoted as G', and the minority one is denoted as G''. Samples with the same label are called homogeneous samples; otherwise, they are called heterogeneous samples. The same goes for GBs.

2.2 Preprocessing Approaches

Undersampling Methods remove some majority samples so that the sample size of each class is close to balance. The representative methods include Tomek Links (Tomek) [1] and Edited Nearest Neighbor (ENN) [15]. The Tomek aims to balance the class distribution by removing majority or both majority and minority samples that form Tomek links. A Tomek link refers to a pair of samples formed by two different class samples, with each being the nearest neighbor of the other. Notably, the samples forming the Tomek link often are noisy samples or borderline samples. The ENN removes majority samples that exhibit significant differences from minority samples to balance the class distribution. Specifically, the ENN employs the kNN method to identify the k nearest neighbors for all majority samples. Subsequently, for each majority sample, it identifies the minority samples among its k nearest neighbors. If the number of minority samples exceeds $k/2$, the corresponding majority sample is removed.

Oversampling Methods eliminate skewed class distribution by increasing the size of the minority class. The representative method is the synthetic minority over-sampling technique (SMOTE) [7]. SMOTE oversamples by synthesizing new samples near minority samples. Specifically, given a binary dataset D and its imbalance ratio IR, the number SN of synthetic samples for each minority sample based on IR can be determined first. Second, for each minority sample, find its k nearest neighbor minority samples. Third, among these k samples, new minority samples are generated by random interpolation. Repeat SN times to obtain SN synthetic minority samples.

Hybrid Sampling Methods are a group of combination methods combining the oversampling and undersampling methods. Representative methods include STomek [3] and SENN [2]. SENN first applies the SMOTE to oversample the minority class. Subsequently, the ENN is employed to undersample the majority class in the oversampled dataset. STomek replaces the undersampling method of ENN with the Tomek Link. It is worth noting that the STomek only deletes the majority samples which form Tomek Links.

2.3 GB-Based Undersampling Method

The GB-based undersampling method is a two-stage learning method, which includes the granular ball generation (GBG) stage and the undersampling stage. The core idea of the GBG method is to cover a dataset with a set of balls, where a ball is called a GB which is indeed an IG. Additionally, the granulation process of the GBG method can be briefly described as follows. First, the whole training dataset is initialized as the initial GB. Second, k-means [17] or k-division [16] is employed to split the GB into k finer GBs whose centers and radii are determined using Definition 1. Notably, for a dataset with k classes, using k-division, there would be k clusters with randomly selected k heterogeneous samples as centers, and a sample in a cluster has a smaller distance to its center than that to the center of the other cluster. The quality of the GB is measured using the purity defined in Definition 2. The closer the purity is to 1.0, the closer the distribution characteristics of GBs are to the original dataset. Iteratively split each GB until the purity of all GB reaches the threshold.

Definition 1. *Given a dataset D, suppose G is a set of GBs generated on D. For $\forall gb_i \in G$, it is generated on $D_i (D_i \subseteq D)$, and the center $\boldsymbol{c}_i$ and radius r_i of gb_i are respectively defined as follows,*

$$\boldsymbol{c}_i = \frac{1}{|D_i|} \sum_{(\boldsymbol{x},y)\in D_i} \boldsymbol{x}, \tag{1}$$

$$r_i = \frac{1}{|D_i|} \sum_{(\boldsymbol{x},y)\in D_i} \triangle(\boldsymbol{x}, \boldsymbol{c}_i), \tag{2}$$

where $\triangle(\cdot, \star)$ denotes the distance function. And, without losing generality, all distances in this paper refer to Euclidean distances.

Definition 2. *Given a dataset D, suppose G is a set of GBs generated on D. For $\forall gb_i \in G$, it is generated on $D_i(D_i \subseteq D)$, its label and purity are defined respectively as follows,*

$$l_i = \arg\max_{l_j \in L_i} |\{(\boldsymbol{x}, y) \in D_i | y = l_j\}|, \tag{3}$$

$$p_i = \frac{|\{(\boldsymbol{x}, y) \in D_i | y = l_i\}|}{|D_i|}, \tag{4}$$

where L_i represents the class set of D_i.

The core idea of the GB-based undersampling method can be briefly described as follows. Given a binary dataset D, a GB set G can be obtained using any GBG method. First, for each $gb \in G$ that covers samples less than or equal to $2 * p$, all the covered samples are put into the sampled dataset. Second, for each minority $gb \in G$ that covers more than $2 * p$ samples, the covered minority samples are merged into the sampled dataset. Third, for each majority $gb \in G$ that covers more than $2 * p$ samples, $2 * p$ majority samples are put into the sampled dataset, where $2 * p$ samples are the nearest to the GB's surface in each feature dimension. Finally, if the class distribution is still skewed, more majority samples are randomly selected and merged into the sampled dataset.

3 Approach

3.1 Framework

In this section, the proposed TWHGBS will be introduced in detail. Its framework is shown in Fig. 1, including the OGBG method and a novel three-way hybrid sampling method.

As shown in Module 1 of Fig. 1, the proposed OGBG method first treats the entire training dataset as the initial cluster. It then iteratively performs k-division on every cluster that does not reach the purity threshold until the purity of all clusters reaches the given threshold.

As shown in Module 2 of Fig. 1, for the sampling stage, the TWHGBS includes two parts: undersampling based on GBs and oversampling based on these undersampled GBs. From the perspective of three-way decisions, considering the overlap relation between the majority GBs and the minority GBs, all the GBs are divided and conquered: unsampled GBs, undersampled GBs, and oversampled GBs. First, take the GB as the basic computing unit, and by judging the overlap relation between the GBs, any heterogeneous GB pair with an overlap relation is obtained as the undersampled result, representing the delayed decision region for oversampling later. The remaining GBs are put into the rejection region and will not be processed anymore. Second, determine the class distribution of samples covered by all the GBs in the delayed decision region, put the majority samples into the hybrid sampled dataset, and the majority GBs are regarded as objects belonging to the acceptance region correspondingly. Third, new samples are adaptively synthesized within each GB in the update delayed decision region. Finally, the GBs in the delayed decision region are all put into the accepted region; these samples covered are put into the hybrid sampled dataset.

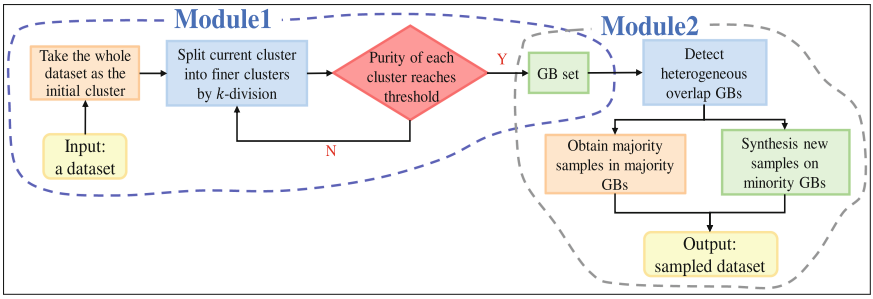

Fig. 1. Architecture of TWHGBS.

3.2 Generation of Granular Balls

For the sampling task to obtain borderline samples, it was hoped that there would be an overlap relation between the borderline GBs. Therefore, the criteria of GBG can be reduced to two basic ones: first, the samples covered by the GB set should be as consistent as possible with the original dataset; second, the samples belonging to any GB should be within or on the ball in terms of feature space. Thus, the GB is redefined as follows,

Definition 3. *Given a dataset D, suppose G is a set of GBs generated on D. For $\forall gb_i \in G$, it is defined as $gb_i = (\boldsymbol{c}_i, r_i, l_i, O_i)$ and generated on $O_i (O_i \subseteq D)$, and the radius r_i of gb_i is defined as follows,*

$$r_i = \max\{\triangle(\boldsymbol{x}, \boldsymbol{c}_i) \mid (\boldsymbol{x}, y) \in O_i\}, \tag{5}$$

where center $\boldsymbol{c}_i$ is defined as Definition 1, label l_i is defined as Definition 2.

In addition, inspired by the previous work [16], the k-division method can quickly divide a cluster into k smaller clusters, where k represents the number of classes in the cluster. Therefore, the OGBG method is proposed.

Given a dataset D, the working process of the OGBG method is as follows. As shown in Step 1 of Module 1 in Fig. 1, the whole dataset D is initialized as the initial cluster $O_i (O_i = D), i = 1$. Generally, the purity threshold should be greater than the purity of the initial cluster. As shown in Step 2, k-division is performed on any O_i to obtain a set of finer clusters $E = \bigcup_{j=1}^{k'} \{O_j\}$. Notably, if a cluster contains only one sample, the sample is an outlier and needs to be deleted; thus, $k' <= k$. As shown in Step 3, if $p_j < P$, then O_j returns to Step 2, where P is the given purity threshold and the purity p_j of O_j is obtained using the Eq. 4; otherwise, as shown in Step 4, a new GB will be put into the GB set, where the GB is generated on O_j using Definition 3. Repeat steps 2–4 above until all clusters reach the purity threshold. Finally, the GB set $G = \{gb_1, gb_2, \cdots, gb_m\}$ can be obtained. Algorithm 1 shows the complete process of the OGBG method. The time complexity of Algorithm 1 is $O((tk - t + 1)N)$, where t is the number of iterations, and $k = 2$ for the binary dataset. Compared with the GBG method

[16], Algorithm 1 has no global division, which can further accelerate the process of GBG.

Algorithm 1: OGBG Method.

Input : Dataset D, purity threshold P.
Output: The GB set G.

Treat the entire D as the initial cluster $O_i(i = 1)$;
$G \leftarrow \emptyset$ ▷ initialize GB set;
$E \leftarrow \{O_1\}$ ▷ initialize cluster set;
repeat
  for *each cluster* $O_i \in E$ **do**
    Calculate purity p_i by Eq. 4 ;
    if $p_i < P$ **then**
      split O_i into $E'(E' = \bigcup_{j=1}^{k'} O_j)$ using k-division ;
      if $|E'| == 1$ *and* $|O_i| == |O_j|$ **then**
        Construct GB $gb = (\boldsymbol{c}, r, l, O)$ on O_j by Definition 3;
        Delete samples in O_j that are inconsistent with l;
        $G \leftarrow G + \{gb\}$;
        $E \leftarrow E - \{O_i\}$;
      else
        $E \leftarrow E + E'$;
        $E \leftarrow E - \{O_i\}$;
    else
      Construct GB $gb = (\boldsymbol{c}, r, l, O)$ on O_i by Definition 3;
      $G \leftarrow G + \{gb\}$;
      $E \leftarrow E - \{O_i\}$;
until $E == \emptyset$;
Return G.

3.3 GB-Based Borderline Undersampling Method

For classification tasks, borderline samples are key samples, and the same applies when dealing with imbalanced datasets. The samples within each GB essentially form a cluster, and the overlap relation between GBs can reflect the distance and similarity of the corresponding clusters. If there is an overlap relation between any two heterogeneous GBs, the overlap region represents samples from different classes. That is, these GBs and the within samples lie on class boundaries. Therefore, by analyzing the overlap relation among GBs in the feature space to study data distribution, a GB-based undersampling method is proposed to obtain borderline GBs and the borderline samples approximately.

As shown in Step 1 of Module 2 in Fig. 1, according to Sect. 3.2, a GB set $G = G' + G''$ that covers the original dataset can be obtained. As shown in Step

2, detect heterogeneous GBs with the overlap relation. Specifically, for each $gb' \in G'$, calculate the distance between it and each $gb'' \in G''$ using Eq. 6.

$$d(gb', gb'') = \triangle(\boldsymbol{c'}, \boldsymbol{c''}) - (r' + r''). \tag{6}$$

Then, for $\forall gb \in G$, count the heterogeneous overlap number $ON(gb)$ by Eq. 7, where $ON(gb)$ represents the number of heterogeneous GBs that overlap with gb.

$$ON(gb) = \sum_{gb^\star \in G, l \neq l^\star} f(gb, gb^\star), \tag{7}$$

$$f(gb, gb^\star) = \begin{cases} 1 & \text{if } d(gb, gb^\star) < 0 \\ 0 & \text{if } d(gb, gb^\star) >= 0 \end{cases}, \tag{8}$$

where $gb = (\boldsymbol{c}, r, l, O), gb^\star = (\boldsymbol{c^\star}, r^\star, l^\star, O^\star)$. If $ON(gb) >= 1$, gb is considered as a borderline GB that needs to be put into the undersampled GB set $B = \bigcup_{i=1}^{m'} \{gb_i\}$, $m' <= m$. And, $S = \{(\boldsymbol{x}, y) \mid (\boldsymbol{x}, y) \in O, gb \in B\}$ is the corresponding undersampled dataset.

Given a binary dataset includes 57 majority samples marked blue points and 24 minority samples marked orange points. Using the OGBG method, several GBs are generated, including 4 majority GBs $\{gb_1, gb_2, gb_3, gb_4\}$ marked blue circles and 3 minority GBs $\{gb_5, gb_6, gb_7\}$ marked orange circles as shown in Fig. 2(a). Using Eq. 7, since $ON(gb_1) < 1$, it is not distributed on the class boundary, and $ON(gb_i) >= 1, i = 2, 3, \cdots, 7$, then the borderline GB set is $B = \{gb_i \mid i = 2, 3, \cdots, 7\}$, the undersampled dataset is $S = \{(\boldsymbol{x}, y) \mid (\boldsymbol{x}, y) \in O, gb \in B\}$ shown in Fig. 2(b).

Lines 3–7 of Algorithm 2 show the detailed steps of the proposed undersampling method. Assume that Algorithm 1 constructs m_1 majority GBs and m_2 minority GBs on the dataset D. Then, the time complexity of the GB-based undersampling method is $O(m_1 * m_2)$.

3.4 GB-Based Oversampling Method

For the imbalanced dataset, the problem caused by the severe shortage of minority samples can be alleviated by increasing the number of minority samples. As shown in Module 2 of Fig. 1, by undersampling on the original dataset, the number of majority samples will be reduced, and the imbalance ratio will be reduced to a certain extent, but oversampling may still be required.

In the feature space, the samples contained in the GB represent the typical characteristics of the class corresponding to the ball. Therefore, an oversampling method for synthesizing new samples in each minority GB is proposed. Considering that the borderline GBs are obtained from the proposed undersampling method in Sect. 3.3, the overlap area indicates that the majority samples are indistinguishable from minority samples. Therefore, the overlap information is considered to determine the number of synthetic samples within each GB and the synthesis rules for each new sample.

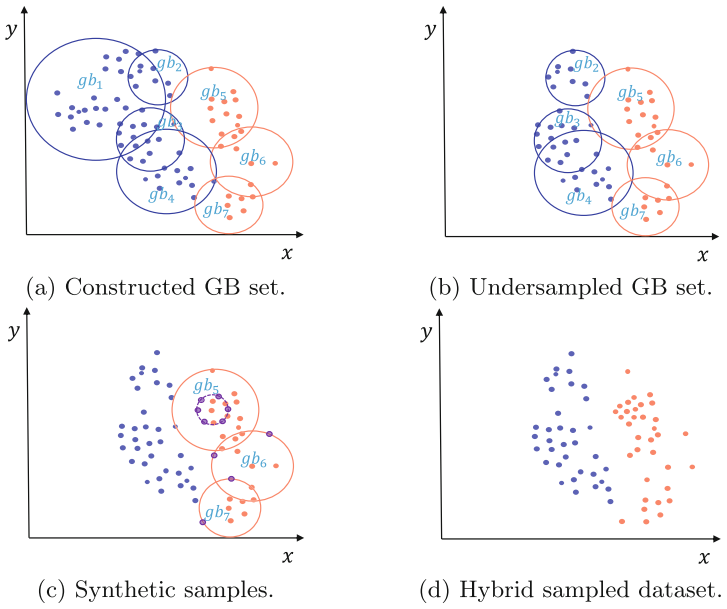

(a) Constructed GB set. (b) Undersampled GB set.

(c) Synthetic samples. (d) Hybrid sampled dataset.

Fig. 2. Sampling process using TWHGBS. (Color figure online)

According to Sect. 3.3, there is an undersampled dataset S, which includes N_1 majority samples and N_2 minority samples. And, $B = B' + B''$ is the corresponding undersampled GB set, including a set of majority GB B' and a set of minority GB B''. First, calculate the imbalance number $IN, IN = N_1 - N_2$, representing the difference in the number of majority and minority samples. Second, according to Eq. 9, for each $gb \in B''$, calculate the synthetic sample number $SN(gb)$. Third, synthesize new samples using Eq. 10 and put them into S.

$$SN(gb) = \left\lfloor \frac{ON(gb)}{\sum_{gb^\star \in B''} ON(gb^\star)} * IN \right\rfloor. \tag{9}$$

Any synthetic sample within $gb = (\boldsymbol{c}, r, l, O)$ can be expressed as follows,

$$(\boldsymbol{x}, y) = (\boldsymbol{c} + \boldsymbol{x'} * r * \frac{1}{ON(gb)}, l), \tag{10}$$

where $\boldsymbol{x'}$ represents a randomly generated p-dimensional unit vector.

According to Eq. 10, the larger the $ON(gb)$, the closer the new sample generated within gb is to the center of the GB, thereby maximizing the quality of the synthetic samples while reducing the possibility of blurring class boundaries. In summary, nearly $N_1 + N_2 + IN$ samples are sampled with the proposed oversampling method compared with the undersampled $N_1 + N_2$ samples; nearly $N_1 + N_2 + IN$ samples are sampled with the proposed hybrid sampling compared with the original N samples, and the imbalance ratio is close to 1.

According to the undersampled GB set B and the undersampled dataset S shown in Fig. 2(b), since the number of blue points is greater than in orange, that is $N_1 = 35$, $N_2 = 24$, then the imbalance number $IN = 11$, there are the majority GBs $B' = \{gb_2, gb_3, gb_4\}$ and the minority GBs $B'' = \{gb_5, gb_6, gb_7\}$. Since $ON(gb_5) = 3$, $ON(gb_6) = 1$, $ON(gb_7) = 1$, then $SN(gb_5) = 6$, $SN(gb_6) = 2$, $SN(gb_7) = 2$. Then, for gb_5, 6 new samples need to be synthesized. The new samples are distributed on the concentric hypersphere with gb_5, whose radius is $1/3 * r_5$. Similarly, gb_6 and gb_7 randomly generate two new samples, respectively, as shown in Fig. 2(c). Figure 2(d) shows the hybrid sampled dataset. As a result, the size of the majority class and minority class are 35 and 34, respectively.

Lines 8–13 of Algorithm 2 show the detailed steps of the proposed oversampling method. Assume that the undersampled dataset contains N_1 majority and N_2 minority samples. Then, the time complexity of the GB-based oversampling method is $O(N_1 - N_2)$. Thus, the time complexity of the proposed TWHGBS is $O((tk - t + 1)N + m_1 * m_2 + N_1 - N_2)$. In addition, the time complexity of STomek and SENN is $O(N_2 * N + \alpha * N_2 + (N_1 + (1 + \alpha)N_2)^2)$, where α is the sampling multiple of SMOTE. In summary, the time complexity of TWHGBS is linear, while STomek and SENN are both square.

Algorithm 2: TWHGBS method.

Input : Dataset D, purity threshold P.
Output: Sampled dataset S.

1 $B \leftarrow \emptyset$ ▷ initialize borderline GB set;
2 Generate a GB set $G = \{gb_1, gb_2, \cdots, gb_p\}$ on D by Algorithm 1;
3 **for** $gb \in G$ **do**
4 Obtain the heterogeneous overlap number $ON(gb)$ using Eq.7;
5 **if** $ON(gb) >= 1$ **then**
6 $B \leftarrow B + \{gb\}$;
7 $S \leftarrow S + O$ ▷ $gb = (\boldsymbol{c}, r, l, O)$;
8 Obtain the majority GB set B' and minority GB set B'' on B;
9 Obtain the imbalance number IN on all samples covered by B;
10 **for** $gb \in B''$ **do**
11 Obtain the synthetic sample number $SN(gb)$ based on Eq. 9;
12 Randomly synthesise a set of new samples $\bigcup_{i=1}^{SN(gb)}\{(\boldsymbol{x}_i, y)\}$ using Eq. 10 ▷ y is the minority class;
13 $S \leftarrow S + \bigcup_{i=1}^{SN(gb)}\{(\boldsymbol{x}_i, y)\}$;
14 Return S.

4 Experimental Results and Analysis

4.1 Experimental Settings

Ten benchmark imbalanced datasets are used in this section, with detailed information shown in Table 1. The smallest imbalance ratio of these datasets is 1.86,

and the largest is 53.07. For binary imbalanced classification, $G-mean$ [4] is a widely used metric that simultaneously measures the performance of classifiers for majority and minority examples. The $G-mean$ is defined as follows.

$$G-mean=\sqrt{sensitivity*specificity}, \tag{11}$$

where $sensitivity = TP/(TP+FN)$ represents the accuracy of majority samples, and $specificity = TN/(TN+FP)$ represents the accuracy of minority samples. The value range of $G-mean$ is $[0,1]$. The larger the value, the better the classification performance.

Table 1. Details of datasets.

Dataset	Samples	Minority	Features	IR
wisconsin	683	239	9	1.86
ecoli-0_vs_1 (ecoli)	220	77	7	1.86
yeast1	1484	429	8	2.46
newthyroid2	215	35	5	5.14
page-blocks-1-3_vs_4 (page-blocks)	472	28	10	15.86
dermatology-6	358	20	34	16.9
car-good	1728	69	6	24.04
yeast5	1484	44	8	32.73
winequality-white-3_vs_7 (winequality)	900	20	11	44
kr-vs-k-zero_vs_eight (kr-vs-k)	1460	27	6	53.07

The TWHGBS is validated with GBU, STomek, and SENN on two sample classifiers: Support Vector Machine (SVM) and Logistic Regression (LR). GBU is a representative GB-based undersampling method, and STomek and SENN are representative hybrid sampling methods. To reduce the risk of overfitting, a five-fold cross-validation method is employed. Considering the randomness of TWHGBS and GBU, the TWHGBS-based classifier and GBU-based classifier repeatedly performed ten times five-fold cross-validation. Additionally, for standard datasets, the purity thresholds of TWHGBS and GBU are set to 1.0. For label noise datasets, the purity thresholds of TWHGBS and GBU are traversed in steps of 0.01 in the $[\beta,1]$, where β represents the purity of the initial cluster for TWHGBS or the initial GB for GBU. In addition, the parameters of STomek and SENN are consistent with the default parameters in imblearn, and that of SVM and LR are consistent with the default parameters in scikit-learn. Both imblearn and scikit-learn are open-source Python libraries.

4.2 Effectiveness

In this section, the effectiveness of TWHGBS is demonstrated. Columns 2–6 of Table 2 respectively represent the average test $G-mean$ on TWHGBS-based

SVM, GBU-based SVM, STomek-based SVM, SENN-based SVM, and SVM on each dataset. Table 3 shows the results on LR. The best score is in bold in this paper.

As shown in Table 2, the TWHGBS-based SVM is better than the STomek-based SVM and SENN-based SVM on most datasets and is better than the GBU-based SVM on all datasets. The performance of SVM directly using the original dataset is worse than that of all the sampling-based SVM. Similar conclusions can also be obtained in Table 3.

There are three reasons why TWHGBS has such outstanding performance. First, compared to GBU, an undersampling method, TWHGBS is a hybrid sampling method focusing on borderline samples to avoid interference by non-borderline samples, so TWHGBS generally performs better than GBU, not only on highly imbalanced datasets. Second, the SMOTE exhibits shortcomings, such as blurring class boundaries, redundant synthetic samples, and an inability to handle datasets with an extremely high imbalance ratio. STomek and SENN first employ SMOTE for oversampling and then undersample based on the over-sampled dataset. Thus, they inherit the shortcomings of SMOTE. In addition, STomek and SENN do not focus on the class boundaries, which may remove necessary borderline samples. Therefore, TWHGBS outperforms STomek and SENN on most datasets. Third, for imbalanced datasets, directly training the classifier on the original dataset might result in underfitting for minority classes and overfitting for majority classes. Therefore, the performance of classifiers that consider imbalanced learning is better than those that do not.

Table 2. Comparison on test $G - mean$ of SVM.

Dataset	TWHGBS	GBU	STomek	SENN	Original
wisconsin	**0.9745**	0.9666	0.9707	0.9739	0.9666
ecoli	**0.9720**	0.9457	0.9624	0.9624	0.9463
yeast1	**0.7001**	0.2489	0.6990	0.6610	0.2453
newthyroid2	**0.9703**	0.6952	0.9490	0.9611	0.6952
page-blocks	**0.8277**	0.1428	0.7965	0.7953	0.0000
dermatology-6	**1.0000**	0.9119	**1.0000**	**1.0000**	0.8878
car-good	**0.9354**	0.0000	0.9303	0.9281	0.0000
yeast5	0.9597	0.0000	**0.9617**	0.9610	0.0000
winequality	0.5978	0.0000	0.6287	**0.6428**	0.0000
kr-vs-k	0.9719	0.0000	**0.9731**	0.9727	0.0000
Average	**0.8910**	0.3911	0.8871	0.8858	0.3741

4.3 Robustness

To verify the robustness of the TWHGBS, label noise datasets with sample proportions of 10% and 30% are randomly constructed manually on all datasets

Table 3. Comparison on test $G-mean$ of LR.

Dataset	TWHGBS	GBU	STomek	SENN	Original
wisconsin	**0.9732**	0.9613	0.9708	0.9729	0.9613
ecoli	**0.9636**	0.9504	0.9597	0.9560	0.9463
yeast1	**0.7038**	0.4685	0.7008	0.6807	0.4737
newthyroid2	**0.9726**	0.7568	0.9639	0.9639	0.6509
page-blocks	**0.8151**	0.4996	0.8125	0.8113	0.3778
dermatology-6	**1.0000**	0.9232	**1.0000**	**1.0000**	0.9146
car-good	0.8566	0.0105	0.8566	**0.8588**	0.0000
yeast5	0.9632	0.0141	**0.9661**	0.9625	0.0667
winequality	**0.6305**	0.0000	0.5800	0.5954	0.0000
kr-vs-k	**0.9318**	0.0476	0.9021	0.9007	0.0000
Average	**0.8810**	0.4632	0.8712	0.8702	0.4391

listed in Table 1. Specifically, samples are selected randomly on each dataset, and the labels of these samples are changed. Table 4 shows the results on the datasets with a label noise ratio of 10%. Expressly, columns 2–3 represent the average test $G-mean$ of TWHGBS-based SVM and GBU-based SVM with the optimal purity threshold on each dataset, and columns 7–8 respectively correspond to the optimal thresholds for TWHGBS and GBU simultaneously. Notably, $-$ means that the average test $G-mean$ of the GBU-based SVM is the same under any given purity threshold. Moreover, columns 4–6 represent the average test $G-mean$ of STomek-based SVM, SENN-based SVM, and SVM on each dataset, respectively. Table 5 shows the results on datasets with a label noise ratio of 30%.

According to Table 4 and Table 5, the classification results of TWHGBS-based SVM on most datasets are better than that of GBU-based SVM, STomek-based SVM, SENN-based SVM, and SVM. There are three reasons why the TWHGBS has such outstanding robustness. First, the GBG method is noise-tolerant, in which the majority of samples within GB determine the label of GB. Thus, GB-based sampling methods also inherit this property. Second, the GBG method of TWHGBS focuses on the borderline samples to avoid some noisy samples, which makes TWHGBS have better noise resistance than GBU, STomek, and SENN. Third, STomek and SENN employ SMOTE, so the synthesized new samples are highly affected by noisy samples, and even undersampling methods such as Tomek Links and ENN cannot eliminate the influence completely.

4.4 Parameter Sensitivity Analysis

The impact of the purity threshold on TWHGBS is verified in this section. Figure 3 shows the average test $G-mean$ of TWHGBS-based LR with the purity threshold traversed in steps of 0.01 within $[0.85, 1]$ on several standard datasets, such as page-blocks and ecoli.

Table 4. Comparison on test $G-mean$ of SVM(Noise rate:10%).

Dataset	TWHGBS	GBU	STomek	SENN	Original	Best purity	
						TWHGBS	GBU
wisconsin	**0.8630**	0.8612	0.8580	0.8620	0.8511	0.9	0.98
ecoli	**0.8586**	0.8415	0.8471	0.8403	0.8408	0.71	0.99
yeast1	**0.6556**	0.2874	0.6522	0.5567	0.1187	0.81	0.7
newthyroid2	0.7219	0.5006	0.6754	**0.7472**	0.4163	0.84	0.85
page-blocks	**0.4910**	0.0000	0.3200	0.4060	0.0000	0.91	–
dermatology-6	**0.6110**	0.4832	0.6013	0.4634	0.4100	0.96	0.87
car-good	0.6199	0.0000	**0.6264**	0.5765	0.0000	0.91	–
yeast5	**0.5299**	0.0000	0.5163	0.1425	0.0000	0.92	–
winequality	0.4902	0.0000	**0.4937**	0.0000	0.0000	0.9	–
kr-vs-k	**0.5194**	0.0000	0.5099	0.3989	0.0000	0.91	–
Average	**0.6361**	0.2974	0.6100	0.4993	0.2637	–	–

Table 5. Comparison on test $G-mean$ of SVM(Noise rate:30%).

Dataset	TWHGBS	GBU	STomek	SENN	Original	Best purity	
						TWHGBS	GBU
wisconsin	**0.6745**	0.6734	0.6706	0.6689	0.6719	0.8	0.77
ecoli	0.6605	0.6535	0.6613	**0.6753**	0.6498	0.7	0.78
yeast1	**0.5608**	0.0000	0.5177	0.2366	0.0000	0.62	–
newthyroid2	0.4835	0.3480	**0.5238**	0.0538	0.1000	0.64	0.68
page-blocks	**0.4378**	0.0000	0.4350	0.2056	0.0000	0.71	–
dermatology-6	**0.4777**	0.0000	0.4444	0.1364	0.0000	0.71	–
car-good	**0.5130**	0.0000	0.4927	0.1495	0.0000	0.76	–
yeast5	0.4863	0.0000	**0.5090**	0.0000	0.0000	0.7	–
winequality	**0.4630**	0.0000	0.4620	0.0000	0.0000	0.71	–
kr-vs-k	**0.4747**	0.0000	0.4718	0.0647	0.0000	0.77	–
Average	**0.5232**	0.1675	0.5188	0.2191	0.1422	–	–

From Fig. 3, it can be observed that as the purity threshold increases, the performance of TWHGBS-based LR is better. The reason is that as the purity of the GB increases, the constructed GBs using any GBG method describe the original dataset more accurately, similar to the GBG of GBU. Therefore, it is reasonable to set the threshold for GB-based sampling methods, namely TWHGBS and GBU, to 1.0 on the standard dataset.

Notably, for the page-blocks, it can be observed that when the purity threshold is between 0.94 and 0.95, the performance of TWHGBS-based LR is significantly improved. The reason is that the page-blocks contains 444 majority

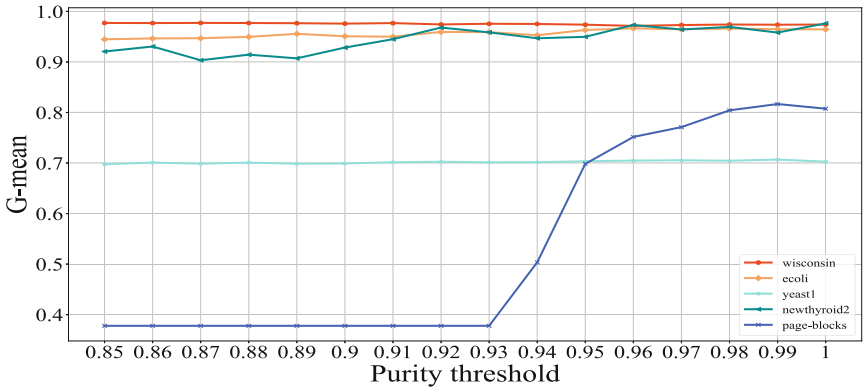

Fig. 3. Impact of purity threshold on test $G - mean$ of TWHGBS-based LR.

samples and 28 minority samples. According to the OGBG method, the purity of the initial cluster is 0.9407. Therefore, TWHGBS only takes effect when the purity threshold exceeds 0.9407.

5 Conclusion

Effective solutions to the class imbalanced problem are crucial for improving performance across applications like disease diagnosis. This paper proposes an alternative hybrid sampling method to tackle the prevalent challenge of learning from imbalanced binary datasets. The proposed TWHGBS integrates undersampling and oversampling methods using GBs generated by the proposed OGBG method. Extensive experiments on 10 public imbalanced binary datasets demonstrate that TWHGBS achieves superior performance and robustness compared to an existing GB-based undersampling method and conventional hybrid sampling methods like STomek. Notably, TWHGBS maintains effectiveness even on highly skewed datasets and exhibits strong robustness against label noise datasets. Moreover, a more general method to deal with imbalanced multi-class datasets will be studied for our future work.

Acknowledgements. This work was supported by the National Natural Science Foundation of China (No. 62221005, No. 62276038), the Joint Fund of Chongqing Natural Science Foundation for Innovation and Development (No. CSTB2023NS CQ-LZX0164), the Chongqing Talent Program (No. CQYC20210202215), the Graduate Scientific Research Innovation Project of Chongqing under Grant (NO. CYB22244), and the Doctoral Talent Training Program of Chongqing University of Posts and Telecommunications (No. BYJS202305).

References

1. Two modifications of CNN. IEEE Trans. Syst. Man Cybern. **SMC-6**(11), 769–772 (1976). https://doi.org/10.1109/TSMC.1976.4309452
2. Batista, G.E., Bazzan, A.L., Monard, M.C., et al.: Balancing training data for automated annotation of keywords: a case study. Wob **3**, 10–8 (2003)
3. Batista, G.E., Prati, R.C., Monard, M.C.: A study of the behavior of several methods for balancing machine learning training data. ACM SIGKDD Explor. Newsl. **6**(1), 20–29 (2004). https://doi.org/10.1145/1007730.1007735
4. Bekkar, M., Djemaa, H.K., Alitouche, T.A.: Evaluation measures for models assessment over imbalanced data sets. J. Inf. Eng. Appl. **3**(10), 27–38 (2013)
5. Borowska, K., Stepaniuk, J.: A rough-granular approach to the imbalanced data classification problem. Appl. Soft Comput. **83**, 105607 (2019). https://doi.org/10.1016/j.asoc.2019.105607
6. Breiman, L.: Random forests. Mach. Learn. **45**, 5–32 (2001). https://doi.org/10.1023/A:1010933404324
7. Chawla, N.V., Bowyer, K.W., Hall, L.O., Kegelmeyer, W.P.: SMOTE: synthetic minority over-sampling technique. J. Artif. Intell. Res. **16**, 321–357 (2002). https://doi.org/10.1613/jair.953
8. Chen, T., Guestrin, C.: XGBoost: a scalable tree boosting system. In: Proceedings of the 22nd ACM SIGKDD International Conference on Knowledge Discovery and Data Mining, pp. 785–794 (2016). https://doi.org/10.1145/2939672.2939785
9. Dablain, D., Krawczyk, B., Chawla, N.V.: DeepSMOTE: fusing deep learning and SMOTE for imbalanced data. IEEE Trans. Neural Netw. Learn. Syst. **34**(9), 6390–6404 (2023). https://doi.org/10.1109/TNNLS.2021.3136503
10. Kaur, H., Pannu, H.S., Malhi, A.K.: A systematic review on imbalanced data challenges in machine learning: applications and solutions. ACM Comput. Surv. (CSUR) **52**(4), 1–36 (2019). https://doi.org/10.1145/3343440
11. Liu, Z., Chen, C.L.P., Feng, S., Feng, Q., Zhang, T.: Stacked broad learning system: from incremental flatted structure to deep model. IEEE Trans. Syst. Man Cybern. Syst. **51**(1), 209–222 (2021). https://doi.org/10.1109/TSMC.2020.3043147
12. Savchenko, A.V.: Fast inference in convolutional neural networks based on sequential three-way decisions. Inf. Sci. **560**, 370–385 (2021). https://doi.org/10.1016/j.ins.2021.01.068
13. Sun, Y., Kamel, M.S., Wong, A.K., Wang, Y.: Cost-sensitive boosting for classification of imbalanced data. Pattern Recogn. **40**(12), 3358–3378 (2007). https://doi.org/10.1016/j.patcog.2007.04.009
14. Wang, W., Liu, W., Chen, H.: Information granules-based BP neural network for long-term prediction of time series. IEEE Trans. Fuzzy Syst. **29**(10), 2975–2987 (2021). https://doi.org/10.1109/TFUZZ.2020.3009764
15. Wilson, D.L.: Asymptotic properties of nearest neighbor rules using edited data. IEEE Trans. Syst. Man Cybern. **SMC-2**(3), 408–421 (1972). https://doi.org/10.1109/TSMC.1972.4309137
16. Xia, S., Dai, X., Wang, G., Gao, X., Giem, E.: An efficient and adaptive granular-ball generation method in classification problem. IEEE Trans. Neural Netw. Learn. Syst. **35**(4), 5319–5331 (2024). https://doi.org/10.1109/TNNLS.2022.3203381
17. Xia, S., Liu, Y., Ding, X., Wang, G., Yu, H., Luo, Y.: Granular ball computing classifiers for efficient, scalable and robust learning. Inf. Sci. **483**, 136–152 (2019). https://doi.org/10.1016/j.ins.2019.01.010

18. Xia, S., Zheng, S., Wang, G., Gao, X., Wang, B.: Granular ball sampling for noisy label classification or imbalanced classification. IEEE Trans. Neural Netw. Learn. Syst. **34**(4), 2144–2155 (2023). https://doi.org/10.1109/TNNLS.2021.3105984
19. Yao, Y.: Tri-level thinking: models of three-way decision. Int. J. Mach. Learn. Cybern. **11**(5), 947–959 (2020). https://doi.org/10.1007/s13042-019-01040-2
20. Zadeh, L.A.: Toward a theory of fuzzy information granulation and its centrality in human reasoning and fuzzy logic. Fuzzy Sets Syst. **90**(2), 111–127 (1997)
21. Zhang, C., Tan, K.C., Li, H., Hong, G.S.: A cost-sensitive deep belief network for imbalanced classification. IEEE Trans. Neural Netw. Learn. Syst. **30**(1), 109–122 (2019). https://doi.org/10.1109/TNNLS.2018.2832648
22. Zhang, X., Liu, T., Li, P., Jia, W., Zhao, H.: Robust neural relation extraction via multi-granularity noises reduction. IEEE Trans. Knowl. Data Eng. **33**(9), 3297–3310 (2021). https://doi.org/10.1109/TKDE.2020.2964747

Identifying Important Concepts in the Concept Lattice Based on Concept Indices

Kuo Pang[1], Zhen Wang[2(✉)], Li Zou[3], and Mingyu Lu[1]

[1] Information Science and Technology College, Dalian Maritime University, Dalian 116024, China
{pangkuo_p,lumingyu}@dlmu.edu.com

[2] Weihai Institute of Beijing Jiaotong University, Weihai 264401, China
zhenwangnwu@163.com

[3] School of Computer Science and Technology, Shandong Jianzhu University, Jinan 250102, China
zouli20@sdjzu.edu.cn

Abstract. The concept lattice plays a fundamental role in formal concept analysis (FCA) and finds widespread application across various fields. However, the presence of a large number of nodes in the concept lattice can pose challenges when it comes to comprehending the acquired conceptual knowledge. The size of the concept lattice is a significant concern in FCA, and obtaining an appropriately sized lattice is of utmost importance. To address this issue, this paper introduces a novel model for identifying important concepts in the concept lattice. The proposed model leverages concept indices and complex network analysis techniques to reduce the size of the lattice and enhance the understanding of conceptual knowledge. To derive the most valuable concepts, concept indices are first proposed by both node attribute information and structural information. Second, to fuse the attribute and structural information of concepts, an information system for concept indices is developed. In addition, the K-means method is employed to comprehensively evaluate all concept indices and obtain important concept identification results. Finally, an empirical study and comparative analyze demonstrate that the proposed model can effectively identify important concepts in the concept lattice.

Keywords: Formal concept analysis · Concept lattice · Concept stability

1 Introduction

Formal concept analysis (FCA) [14] is a theoretical framework for knowledge discovery that operates on formal contexts, utilizing the concept lattice as a fundamental mathematical theory to effectively unveil the hierarchical structure of concepts within the formal context. The concept lattice has found

M. Hu et al. (Eds.): IJCRS 2024, LNAI 14840, pp. 103–117, 2024.
https://doi.org/10.1007/978-3-031-65668-2_8

widespread applications in diverse fields, including concept-cognitive learning [16], autonomous learning [5], and linguistic information processing [4,13].

FCA acknowledges that in real-world scenarios, formal contexts can frequently be extensive, leading to the emergence of complex concept lattices. The number of nodes in the concept lattice increases exponentially as the size of the formal context expands. Consequently, this exponential growth poses challenges in effectively handling and analyzing the concept lattice. In response to this challenge, researchers have dedicated significant efforts to developing methods for simplifying concept lattices [2,10,18]. Among these studies, Mi *et al.* [10] utilized conceptual clustering for concept learning, aiming to enhance concept classification performance. Dias *et al.* [2] conducted an analysis of concept lattice reduction by leveraging appropriate implication sets to maintain both the original and simplified structures. While these methods have proven to be highly effective, they do not fully consider the inherent characteristics of the concept itself and the structural information within the concept lattice.

To address this issue, we can consider two aspects of information:

1. *Node attribute information of concept lattice*: Existing methods for concept lattice reduction often incorporate interest measures or concept indices to ensure the quality of the lattice [3,8,11]. Therefore, utilizing interest measures as node attribute information in the concept lattice can be beneficial.
2. *Structural information of concept lattice*: Complex network analysis offers a range of methods for analyzing the overall structure and node attributes of complex networks. Various research approaches have been developed to identify key nodes in complex networks [12,17]. Since a concept lattice can be viewed as a type of network, analyzing its topological structure and overall properties can provide insights into the relationships between concepts. Interestingly, complex network analysis has not been extensively applied to concept lattices. Hence, exploring attribute analysis techniques from complex networks can be a valuable approach for studying the structural information of concept lattices.

Building upon the previous discussion, this paper introduces a novel model for identifying important concepts in concept lattices by leveraging complex network analysis and concept indices. The proposed model takes into account both the structural information and node attribute information of the concept lattice. Through an empirical study and comparative analysis, the effectiveness of the proposed model in identifying important concepts within the concept lattice is demonstrated.

The key innovations of this research can be summarized as follows:

– *Integration of Complex Network Analysis*: The research introduces the application of complex network analysis techniques to concept lattices. By treating the concept lattice as a network, the study leverages the tools and methodologies from complex network analysis to gain insights into the structural properties and relationships between concepts.

- *Consideration of Node Attribute Information*: The research incorporates node attribute information, specifically concept indices, as an additional factor in identifying important concepts within the lattice. By considering both the structural information and node attribute information, a more comprehensive and accurate identification of significant concepts is achieved.
- *Synthesis of Node Attribute Features and Structural Features*: The research utilizes the K-means method to synthesize node attribute features and structural features. By combining these two types of features, the research automatically obtains important concepts in the concept lattice.

These innovations contribute to advancing the field of concept lattice by providing a novel model that integrates complex network analysis, considers node attribute information, and employs the K-means method to identify important concepts. This comprehensive model enhances the effectiveness and accuracy of concept identification in concept lattices, facilitating knowledge discovery and understanding within complex datasets.

The subsequent sections of this study are structured as follows. Section 2 revisits foundational concepts and notions of FCA. Section 3 provides concept indices from the perspective of attribute information and structural information. Section 4 constructs an important concept identification model and gives the corresponding algorithm. Section 5 provides an empirical study with comparative analysis. Finally, we wrap up the paper with a summarization and a glimpse into potential future research directions, as detailed in Sect. 6.

2 Preliminaries

This section reviews the fundamental concepts associated with FCA.

2.1 FCA

Definition 1 [14]. *A formal context is a triple* (G, M, I)*, where* $G = \{g_1, g_2, \cdots, g_m\}$ *is a set of objects,* $M = \{m_1, m_2, \cdots, m_n\}$ *is a set of attributes, and* $I \subseteq G \times M$ *is a binary relation between* G *and* M*. For* $g_i \in G$ *and* $m_j \in M$*,* $(g_i, m_j) \in I$ *means that the object* g_i *has the attribute* m_j*.*

Definition 2 [14]. *Let* (G, M, I) *be a formal context. For* $X \subseteq G$ *and* $B \subseteq M$*, two operators "*$\uparrow$*" and "*$\downarrow$*" can be defined as follows:*

$$(\bullet)^{\uparrow} : 2^G \to 2^M,$$

$$X^{\uparrow} = \{m | m \in M,\ \forall g \in X,\ (g, m) \in I\}, \tag{1}$$

$$(\bullet)^{\downarrow} : 2^M \to 2^G,$$

$$B^{\downarrow} = \{g | g \in G,\ \forall m \in B,\ (g, m) \in I\}. \tag{2}$$

Definition 3 [14]. *Let* (G, M, I) *be a formal context, for* $X \subseteq G$ *and* $B \subseteq M$*, if there exist* $X^{\uparrow} = B$ *and* $X = B^{\downarrow}$*, then a pair* (X, B) *is called a concept of* (G, M, I)*.* X *and* B *are called the extent and intent of the concept* (X, B)*, respectively.*

3 Concept Indices

This section presents an analysis of the concept indices from two perspectives: the attribute information and the topology of the concept.

3.1 Concept Attribute Features

The concept attribute features, which serve as indices for evaluating the quality of concepts, are described as follows.

Support. Support is a crucial index utilized in data mining for discovering frequent itemsets [1]. Within the concept lattice, the support of a concept signifies its frequency of occurrence.

Definition 4. *Let (G, M, I) be a formal context and $L(G, M, I)$ be the set of all concepts. For $C = (X, B) \in L(G, M, I)$, the support of (X, B) is defined as*

$$Sup(C) = \frac{|B|}{|M|}. \tag{3}$$

The quality of a concept is evaluated by the number of attributes in its intent, denoted as $Sup(C)$. Concepts are selected based on their $Sup(C)$ values, subject to a minimum support threshold, min$Sup(C)$.

Stability. The stability of a concept [7] can be examined from two perspectives: intensional stability and extensional stability.

Definition 5. *Let (G, M, I) be a formal context and $L(G, M, I)$ be the set of all concepts. For $C = (X, B) \in L(G, M, I)$, the intensional stability of (X, B) is defined as*

$$\sigma_i(X, B) = \frac{|\{Y \subseteq X | Y^{\uparrow} = B\}|}{2^{|X|}}, \tag{4}$$

and the extensional stability of (X, B) is defined in the dual way

$$\sigma_e(X, B) = \frac{|\{Z \subseteq B | Z^{\downarrow} = X\}|}{2^{|B|}}. \tag{5}$$

The concept of stability is robust against noise. It is necessary to extract concepts with high stability.

Separation. The Separation index [6] quantifies the significance of the distinction between the objects encompassed by a concept and other objects, as well as between its attributes and other attributes.

Definition 6. *Let (G, M, I) be a formal context and $L(G, M, I)$ be the set of all concepts. For $C = (X, B) \in L(G, M, I)$, the separation of (X, B) is defined as*

$$Sep(C) = \frac{|X||B|}{\sum_{g \in X} |g^{\uparrow}| + \sum_{m \in B} |m^{\downarrow}| - |X||B|}. \tag{6}$$

Shannon Entropy. The computation of concept weights can be accomplished using Shannon entropy [15]. The selection of an appropriate granularity facilitates the effective identification of important concepts.

Definition 7. *Let (G, M, I) be a formal context and $L(G, M, I)$ be the set of all concepts. For any $m_i \in A$, the weight of m_i is defined as*

$$w(m_i) = \frac{E(m_i)}{\sum_{i=1}^{n} E(m_i)}, \tag{7}$$

where $E(m_i)$ represents the information entropy of attribute m_i, i.e.

$$E(m_i) = -\frac{|m_i^{\downarrow}|}{|G|} log_2 \frac{|m_i^{\downarrow}|}{|G|}. \tag{8}$$

The concept weights can be obtained by calculating the information entropy of each attribute.

Definition 8. *Let (G, M, I) be a formal context and $L(G, M, I)$ be the set of all concepts. For any $(X, B) \in L(G, M, I)$ and $m_j \in B$, the weight of (X, B) is defined as*

$$w(X, B) = \frac{\sum_j w(m_j)}{|B|}. \tag{9}$$

3.2 Concept Structural Features

A concept lattice can be represented as $\mathcal{G} = (N, E)$, where $N = \{c_1, c_2, \cdots, c_o\}$ denotes a set of concepts, $E = \{e_1, e_2, \cdots, e_p\}$ represents a set of edges connecting concepts, and o and p indicate the number of concepts and edges in the concept lattice, respectively. The top and bottom elements of the concept lattice are not taken into consideration.

Drawing inspiration from complex network analysis, we introduce methods from degree centrality, closeness centrality, eigenvector centrality, and clustering coefficient to identify and determine significant nodes within complex networks within the framework of FCA. These methods capture the concept structural features of the concept lattice.

Degree Centrality. Concepts that possess a substantial degree hold greater significance within the concept lattice compared to other concepts, making them worthy of consideration as important concepts. Such concepts commonly exhibit stronger connections to other concepts.

Definition 9. *Let (G, M, I) be a formal context and $\mathcal{G} = (N, E)$ be a concept lattice. For any $c_i \in N$, the degree centrality of c_i is defined as*

$$DC(c_i) = \frac{\sum_j e_{ij}}{o - 1}, \tag{10}$$

where e_{ij} denotes the edge between concepts c_i and c_j, c_j denotes any concept other than c_i, and o denotes the total number of concepts in the concept lattice. The value of e_{ij} is "1" if an edge exists between c_i and c_j, otherwise, its value is "0".

Closeness Centrality. Closeness centrality leverages the structural characteristics of the complete concept lattice, specifically the positioning of a concept within the lattice.

Closeness centrality assesses the proximity of a concept to all other concepts. A concept's closeness centrality increases as the average shortest distance to reach other concepts in the lattice decreases.

Definition 10. *Let (G, M, I) be a formal context and $\mathcal{G} = (N, E)$ be a concept lattice. For any $c_i \in N$, the closeness centrality of c_i is defined as*

$$CC(c_i) = [D_a(c_i)]^{-1}, \tag{11}$$

where $D_a(c_i)$ denotes the average distance of c_i to all other concepts in the concept lattice, i.e.

$$D_a(c_i) = \frac{\sum_{j \neq i}^{o} d_{ij}}{o - 1}, \tag{12}$$

where o denotes the total number of concepts in the concept lattice, d_{ij} denotes the shortest path between c_i and c_j.

Eigenvector Centrality. The significance of a concept within a concept lattice can be inferred from the quantity and significance of the generalized and specialized concepts linked to it.

Definition 11. *Let (G, M, I) be a formal context and $\mathcal{G} = (N, E)$ be a concept lattice. For any $c_i \in N$, the eigenvector centrality of c_i is defined as*

$$EC(c_i) = x_i = t \sum_{j=1}^{o} a_{ij} x_j, \tag{13}$$

where x_i denotes the degree of concept c_i, t denotes a constant, and $\boldsymbol{A} = a_{ij}$ denotes the adjacency matrix of the concept lattice.

Betweenness Centrality. Betweenness centrality captures the significance of a concept by considering the number of shortest paths that pass through it. By calculating the shortest paths between any two concepts within the concept lattice, we can determine the betweenness centrality of a concept, which is high when it lies on a substantial number of these paths.

Definition 12. *Let (G, M, I) be a formal context and $\mathcal{G} = (N, E)$ be a concept lattice. For any $c_i, c_j, c_k \in N$, the betweenness centrality of c_i is defined as*

$$BC(c_i) = \sum_{c_j, c_k \neq c_i} \frac{\sigma_{jk}(c_i)}{\sigma_{jk}}, \tag{14}$$

where σ_{jk} denotes the total number of shortest paths from concept c_j to c_k, $\sigma_{jk}(c_i)$ denotes the total number of shortest paths from concept c_j to c_k via c_i.

4 Important Concept Identification Model Based on Concept Indices

In this section, we introduce our proposed Important Concept Identification (ICI) model based on concept indices, where the overall architecture is shown in Fig. 1. We first construct the concept lattice based on the formal context via the concept induction operator. For each concept in the concept lattice, we compute its concept attribute and structural features, respectively. To integrate concept attributes and structural features to form a concept indices information system, we use K-means to establish a multi-metrics evaluation representation.

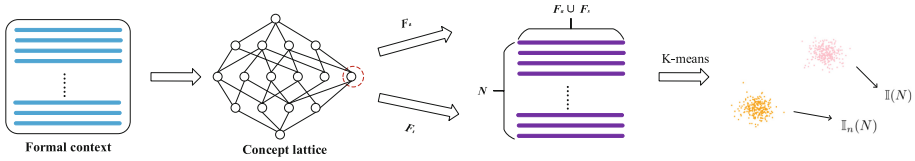

Fig. 1. The architecture of our proposed ICI. F_a and F_s are concept attribute features and concept structural features, respectively. $\mathbb{I}(N)$ and $\mathbb{I}_n(N)$ are important concepts and unimportant concepts, respectively. N is the set of remaining concepts excluding the top and bottom elements.

As we mentioned before, a concept metric can only reflect one feature of a concept, while the importance of a concept is the result of all features combined. In order to explicitly characterize all non-top and bottom element concepts, we give the following definition.

Definition 13. *A concept indices information system is a four-tuple* (N, P, V, f)*, where* N *is the set of remaining concepts excluding the top and bottom elements,* $P = F_a \cup F_s$ *is the set of concept indices,* V *is the range of concept indices, and* $f : N \times P \rightarrow V$ *is an information function that represents the corresponding mapping relationship between concepts and concept indices.*

The concept indices information system allows us to obtain the importance of concepts in different dimensions. In order to construct a comprehensive metric for identifying important concepts, we need to consider concept attribute and structural features. However, assigning weights to multiple metrics is difficult. We can use K-means clustering method to consider all concept indices. Based on the above discussion the complete clustering process is proposed (see Algorithm 1).

Algorithm 1 requires the remaining concepts with the top and bottom elements removed as input. Lines 1–11 calculate the attribute and structural features of each concept. Line 12 constructs the concept metrics information system, where each row represents a concept and each column represents a concept metric. Lines 13–19 cluster the concepts into two classes by the K-means algorithm. Line 20 identifies the important and unimportant concept classes by observing each class's attribute and structural features.

Algorithm 1. The clustering process of ICI

Require: The set of concepts $N\backslash(G,\emptyset),(\emptyset,M)$
Ensure: Important concepts $\mathbb{I}(N)$, unimportant concepts $\mathbb{I}_n(N)$
1: **for** each $c_i \in N\backslash(G,\emptyset),(\emptyset,M)$ **do**
2: Calculate $Sup(c_i)$ by Eq. 3
3: Calculate $\sigma_i(c_i)$ by Eq. 4
4: Calculate $\sigma_e(c_i)$ by Eq. 5
5: Calculate $Sep(c_i)$ by Eq. 6
6: Calculate $w(c_i)$ by Eqs. 7, 8 and 9
7: Calculate $DC(c_i)$ by Eq. 10
8: Calculate $CC(c_i)$ by Eqs. 11 and 12
9: Calculate $EC(c_i)$ by Eqs. 13
10: Calculate $C(c_i)$ by Eq. 14
11: **end for**
12: Construct (N, A, V, f)
13: Randomly use two concepts as the initial centroids r_1, r_2
14: **for** each $c_j \in N\backslash(G,\emptyset),(\emptyset,M), r_1, r_2$ **do**
15: $C_1 \Leftarrow \{c_j | d(c_j, r_1) \leq d(c_j, r_2)\}$
16: $C_2 \Leftarrow \{c_j | d(c_j, r_2) \leq d(c_j, r_1)\}$
17: **end for**
18: Recalculate the two centroids
19: Repeat Steps 14-18 until the two centroids no longer change.
20: Distinguish whether a concept is $\mathbb{I}(N)$ or $\mathbb{I}_n(N)$ in two clusters by concept metrics
21: Return $\mathbb{I}(N)$, $\mathbb{I}_n(N)$

5 Quantitative Analysis

This section is devoted to applying the proposed ICI model to an example and performing a comparative analysis.

5.1 An Empirical Study

As an illustrative example, we consider doctor consultations. The formal context (G, M, I) presented in Table 1 is examined, where $G = \{g_1, g_2, g_3, g_4, g_5\}$ represents five patients, and $M = \{m_1, m_2, m_3, m_4, m_5, m_6\}$ represents six distinct symptoms.

In accordance with Definitions 2 and 3, a total of sixteen concepts can be derived from (G, M, I), as presented in Table 2. The associated concept lattice is visualized in Fig. 2.

The ICI takes Table 1 as its input. In Fig. 2, we exclude the uppermost and lowermost elements of the concept lattice, as visualized in Fig. 3.

Table 1. Doctor consultation formal context (G, M, I)

G	m_1	m_2	m_3	m_4	m_5	m_6
g_1	1	1	0	0	1	1
g_2	1	0	1	1	0	1
g_3	1	0	1	0	0	0
g_4	0	1	1	0	1	1
g_5	0	0	1	1	1	0

Note: The attributes are: m_1: chills, m_2: runny nose, m_3: headache, m_4: cough, m_6: fever, m_6: fatigue.

Table 2. The set of all concepts

Index	Concept
c_1	$(\{g_1, g_2, g_3, g_4, g_5\}, \emptyset)$
c_2	$(\{g_1, g_2, g_4\}, \{m_6\})$
c_3	$(\{g_1, g_4, g_5\}, \{m_5\})$
c_4	$(\{g_2, g_3, g_4, g_5\}, \{m_3\})$
c_5	$(\{g_2, g_4\}, \{m_3, m_6\})$
c_6	$(\{g_4, g_5\}, \{m_3, m_5\})$
c_7	$(\{g_2, g_5\}, \{m_3, m_4\})$
c_8	$(\{g_5\}, \{m_3, m_4, m_5\})$
c_9	$(\{g_1, g_4\}, \{m_2, m_5, m_6\})$
c_{10}	$(\{g_4\}, \{m_2, m_3, m_5, m_6\})$
c_{11}	$(\{g_1, g_2, g_3\}, \{m_1\})$
c_{12}	$(\{g_1, g_2\}, \{m_1, m_6\})$
c_{13}	$(\{g_2, g_3\}, \{m_1, m_3\})$
c_{14}	$(\{g_2\}, \{m_1, m_3, m_4, m_6\})$
c_{15}	$(\{g_1\}, \{m_1, m_2, m_5, m_6\})$
c_{16}	$(\emptyset, \{m_1, m_2, m_3, m_4, m_5, m_6\})$

When calculating the structural features of concepts, the direction of edges in the concept lattice is not taken into account. The adjacency matrix corresponding to $L_o(G, M, I)$ is as follows:

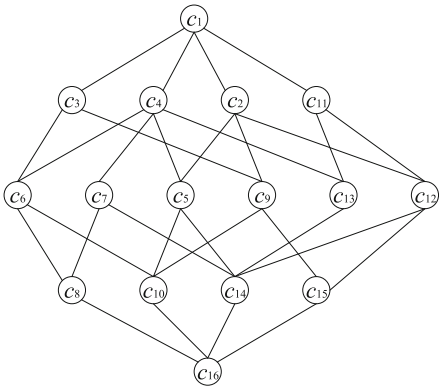

Fig. 2. Concept lattice $L(G, M, I)$

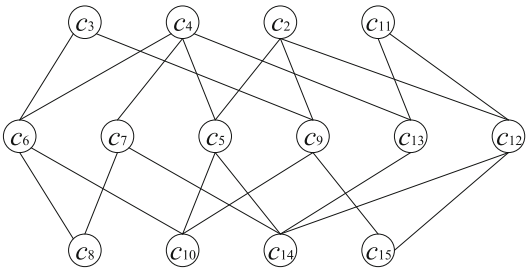

Fig. 3. Concept lattice $L_o(G, M, I)$ after remove the top and bottom elements

$$\boldsymbol{A}(c_i, c_j) = \begin{bmatrix} 1&0&0&1&0&0&0&1&0&0&1&0&0&0 \\ 0&1&0&0&1&0&0&1&0&0&0&0&0&0 \\ 0&0&1&1&1&1&0&0&0&0&0&1&0&0 \\ 1&0&1&1&0&0&0&0&1&0&0&0&1&0 \\ 0&1&1&0&1&0&1&0&1&0&0&0&0&0 \\ 0&0&1&0&0&1&1&0&0&0&0&0&1&0 \\ 0&0&0&0&1&1&1&0&0&0&0&0&0&0 \\ 1&0&0&0&0&0&0&1&1&0&0&0&0&1 \\ 0&0&0&1&1&0&0&1&1&0&0&0&0&0 \\ 0&0&0&0&0&0&0&0&0&1&1&1&0&0 \\ 1&0&0&0&0&0&0&0&0&1&1&0&1&1 \\ 0&0&1&0&0&0&0&0&0&1&0&1&1&0 \\ 0&0&0&1&0&1&0&0&0&0&1&1&1&0 \\ 0&0&0&0&0&0&0&1&0&0&1&0&0&1 \end{bmatrix}.$$

As outlined in Sect. 3, the attribute and structural features of all concepts can be computed to establish the concept indices information system, as presented in Table 3.

Table 3. Concept indices information system (N, P, V, f)

Concept	Sup	σ_i	σ_e	Sep	w	DC	CC	EC	BC
c_2	0.167	0.125	0.500	0.250	0.167	0.231	0.464	0.274	0.090
c_3	0.167	0.250	0.500	0.273	0.167	0.154	0.406	0.163	0.039
c_4	0.167	0.375	0.500	0.308	0.098	0.308	0.500	0.350	0.174
c_5	0.333	0.250	0.250	0.364	0.133	0.308	0.500	0.373	0.156
c_6	0.333	0.250	0.250	0.400	0.133	0.308	0.464	0.283	0.173
c_7	0.333	0.250	0.500	0.444	0.149	0.231	0.433	0.257	0.085
c_8	0.500	0.500	0.250	0.333	0.155	0.154	0.382	0.162	0.024
c_9	0.500	0.250	0.625	0.600	0.178	0.308	0.433	0.261	0.149
c_{10}	0.667	0.250	0.188	0.333	0.158	0.231	0.464	0.274	0.090
c_{11}	0.167	0.250	0.500	0.300	0.167	0.154	0.382	0.162	0.023
c_{12}	0.333	0.250	0.250	0.400	0.167	0.308	0.464	0.283	0.173
c_{13}	0.333	0.500	0.250	0.444	0.133	0.231	0.433	0.257	0.085
c_{14}	0.667	0.500	0.375	0.333	0.158	0.308	0.500	0.350	0.174
c_{15}	0.667	0.500	0.313	0.364	0.175	0.154	0.406	0.163	0.039

Note: Sup: support, σ_i: intensional stability, σ_e: extensional stability, Sep: separation, w: shannon entropy, DC: degree centrality, CC: closeness centrality, EC: eigenvector centrality, BC: betweenness centrality.

If the analysis is conducted using the original concept indices, it would emphasize the significance of higher-valued concept indices in the integrated analysis while diminishing the impact of lower-valued concept indices. To address this, we apply the Min-Max normalization method to the concept indices information system.

$$V'_{i,j} = \frac{V_{i,j} - min(V_j)}{max(V_j) - min(V_j)}, \tag{15}$$

where $V_{i,j}$ denotes the value of the data in row i and column j, $min(V_j)$ denotes the minimum value of the jth column, and $max(V_j)$ denotes the maximum value of the jth column.

The normalized concept indices information system (N, P, V', f) is obtained as shown in Table 4.

Based on the findings in Table 4, the K-means method is employed to classify the concepts within the normalized concept indices information system into two distinct categories. The resulting clusters are presented as follows.

$$C = \{\{c_2, c_4, c_5, c_6, c_7, c_9, c_{10}, c_{12}, c_{13}, c_{14}\}, \{c_3, c_8, c_{11}, c_{15}\}\}.$$

Through the observation and analysis of these two sets of clustering results, we can identify the sets of important and unimportant concepts, respectively.

$$\mathbb{I}(N) = \{c_2, c_4, c_5, c_6, c_7, c_9, c_{10}, c_{12}, c_{13}, c_{14}\},$$

Table 4. The normalized concept indices information system (N, P, V', f)

Concept	Sup	σ_i	σ_e	Sep	w	DC	CC	EC	BC
c_2	0.000	0.000	0.714	0.000	0.862	0.500	0.695	0.531	0.444
c_3	0.000	0.333	0.714	0.066	0.862	0.000	0.203	0.005	0.106
c_4	0.000	0.667	0.714	0.166	0.000	1.000	1.000	0.891	1.000
c_5	0.332	0.333	0.142	0.326	0.438	1.000	1.000	1.000	0.881
c_6	0.332	0.333	0.142	0.429	0.438	1.000	0.695	0.573	0.993
c_7	0.332	0.333	0.714	0.554	0.638	0.500	0.432	0.450	0.411
c_8	0.666	1.000	0.142	0.237	0.713	0.000	0.000	0.000	0.007
c_9	0.666	0.333	1.000	1.000	1.000	1.000	0.432	0.469	0.834
c_{10}	1.000	0.333	0.000	0.237	0.750	0.500	0.695	0.531	0.444
c_{11}	0.000	0.333	0.714	0.143	0.863	0.000	0.000	0.000	0.000
c_{12}	0.332	0.333	0.142	0.429	0.863	1.000	0.695	0.573	0.993
c_{13}	0.332	1.000	0.142	0.554	0.438	0.500	0.432	0.450	0.411
c_{14}	1.000	1.000	0.428	0.237	0.750	1.000	1.000	0.891	1.000
c_{15}	1.000	1.000	0.286	0.326	0.963	0.000	0.203	0.005	0.106

$$\mathbb{I}_n(N) = \{c_3, c_8, c_{11}, c_{15}\}.$$

We utilize t-SNE [9] to reduce the dimensionality of the normalized concept indices information system. This transformation converts the concept indices from an 8-dimensional space to a 3-dimensional representation, as illustrated in Fig. 4.

5.2 Comparative Analysis and Discussion

To validate the proposed model, attribute features and structural features of concepts are individually utilized to identify important concepts in the concept lattice depicted in Fig. 3. Two simplified versions of the proposed model, namely ICI-A and ICI-S, are introduced as follows:

- ICI-A: This variant removes the attribute features of concepts.
- ICI-S: This variant removes the structural features of concepts.

The important concept identification results for these different variants are presented in Table 5 and Fig. 5. Based on these results, the following observations can be made:

1. The important concept identification results of the ICI model and the ICI-S model differ, indicating that the structural information of the concept lattice has an impact on the identification of important concepts.
2. The attribute information of concepts has a greater influence on the identification results of important concepts compared to the structural information

of the concept lattice. Although the important concept identification results were the same for ICI and ICI-A, the distances between clusters and within important concepts differed. This suggests that attribute information plays a crucial role in determining the importance of concepts.

Table 5. The important concept identification results for two different variants

Model	Important concept identification results
ICI-A	$\{\{c_2, c_4, c_5, c_6, c_7, c_9, c_{10}, c_{12}, c_{13}, c_{14}\}, \{c_3, c_8, c_{11}, c_{15}\}\}$
ICI-S	$\{\{c_2, c_3, c_4, c_5, c_6, c_7, c_9, c_{11}, c_{12}\}, \{c_8, c_{10}, c_{13}, c_{14}, c_{15}\}\}$
ICI	$\{\{c_2, c_4, c_5, c_6, c_7, c_9, c_{10}, c_{12}, c_{13}, c_{14}\}, \{c_3, c_8, c_{11}, c_{15}\}\}$

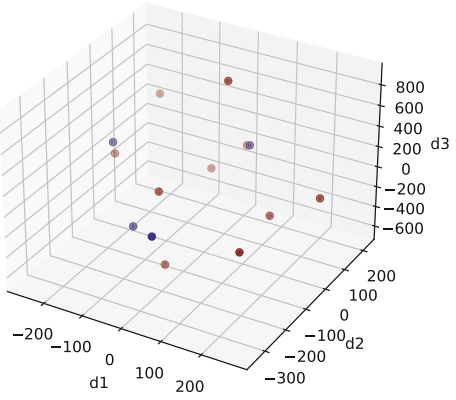

Fig. 4. t-SNE on the normalized concept indices information system after K-means

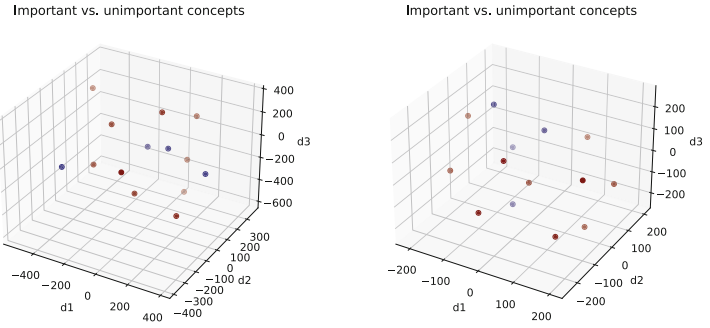

(a) Important concept identification results of ICI-A

(b) Important concept identification results of ICI-S

Fig. 5. Important concept identification results of ICI-A and ICI-S

6 Conclusions

This paper presents a novel model for identifying important concepts in concept lattices by leveraging complex network analysis and concept indices. The proposed model takes into account both the attribute information of the concept lattice nodes and the structural information of the concept lattice itself, resulting in a comprehensive and accurate identification of significant concepts. Through an empirical study and comparative analysis, the effectiveness of the proposed model in identifying important concepts within concept lattices has been demonstrated. In comparison to existing models for important concept identification, the following conclusions can be drawn:

1. Integration of complex network analysis techniques provides valuable insights into the structural properties and relationships between concepts, leading to a better understanding of the concept lattice as a network.
2. By considering node attribute information, the identification process is enhanced, resulting in more comprehensive results. The synthesis of attribute and structural features using the K-means method enables automatic identification of important concepts, thereby facilitating knowledge discovery within complex datasets.
3. The contributions of this research include the integration of complex network analysis, the consideration of node attribute information, and the synthesis of attribute and structural features for concept identification. These innovations advance the field of FCA and have potential applications in various domains.

Future research directions could explore the application of other complex network analysis techniques to concept lattices, investigate alternative methods for integrating attribute and structural information, and further evaluate the proposed model on different datasets and scenarios.

Acknowledgments. This work is supported by the National Natural Science Foundation of China (Nos. 61976124, 62176142) and the Talent Fund of Weihai Institute of Beijing Jiaotong University (No. 2024WHRC001).

Disclosure of Interests. The authors have no competing interests to declare that are relevant to the content of this article.

References

1. Agrawal, R., Imieliński, T., Swami, A.: Mining association rules between sets of items in large databases. In: Proceedings of the 1993 ACM SIGMOD International Conference on Management of Data, pp. 207–216 (1993)
2. Dias, S.M., Vieira, N.J.: A methodology for analysis of concept lattice reduction. Inf. Sci. **396**, 202–217 (2017)
3. Gao, J., Hao, F., Pei, Z., Min, G.: Learning concept interestingness for identifying key structures from social networks. IEEE Trans. Netw. Sci. Eng. **8**(4), 3220–3232 (2021)

4. Hao, F., Gao, J., Bisogni, C., Min, G., Loia, V., De Maio, C.: Stability of three-way concepts and its application to natural language generation. Pattern Recogn. Lett. **149**, 51–58 (2021)
5. Hao, F., Gong, Y., Yu, W., Loia, V.: Knowledge points navigation based on three-way concept lattice for autonomous learning. Pattern Recogn. Lett. **163**, 96–103 (2022)
6. Klimushkin, M., Obiedkov, S., Roth, C.: Approaches to the selection of relevant concepts in the case of noisy data. In: Kwuida, L., Sertkaya, B. (eds.) ICFCA 2010. LNCS (LNAI), vol. 5986, pp. 255–266. Springer, Heidelberg (2010). https://doi.org/10.1007/978-3-642-11928-6_18
7. Kuznetsov, S.O.: On stability of a formal concept. Ann. Math. Artif. Intell. **49**(1), 101–115 (2007)
8. Kuznetsov, S.O., Makhalova, T.: On interestingness measures of formal concepts. Inf. Sci. **442**, 202–219 (2018)
9. Van der Maaten, L., Hinton, G.: Visualizing data using t-SNE. J. Mach. Learn. Res. **9**(11), 2579–2605 (2008)
10. Mi, Y., Shi, Y., Li, J., Liu, W., Yan, M.: Fuzzy-based concept learning method: exploiting data with fuzzy conceptual clustering. IEEE Trans. Cybern. **52**(1), 582–593 (2020)
11. Mouakher, A., Yahia, S.B.: On the efficient stability computation for the selection of interesting formal concepts. Inf. Sci. **472**, 15–34 (2019)
12. Namtirtha, A., Dutta, A., Dutta, B.: Weighted kshell degree neighborhood: a new method for identifying the influential spreaders from a variety of complex network connectivity structures. Expert Syst. Appl. **139**, 112859 (2020)
13. Pang, K., Liu, P., Li, S., Zou, L., Lu, M., Martínez, L.: Concept lattice simplification with fuzzy linguistic information based on three-way clustering. Int. J. Approximate Reasoning **154**, 149–175 (2023)
14. Rudolf, W.: Restructuring lattice theory: an approach based on hierarchies of concept. In: Symposium on Ordered Sets 1982 (1982)
15. Singh, P.K., Kumar, C.A.: Concept lattice reduction using different subset of attributes as information granules. Granular Comput. **2**(3), 159–173 (2017)
16. Xu, W., Guo, D., Mi, J., Qian, Y., Zheng, K., Ding, W.: Two-way concept-cognitive learning via concept movement viewpoint. IEEE Trans. Neural Netw. Learn. Syst. **34**(10), 6798–6812 (2023)
17. Zhang, Y., Huang, G.: Identifying network structure characteristics and key factors for the co-evolution between high-quality industrial development and ecological environment. Environ. Dev. Sustain. **25**(7), 6591–6625 (2023)
18. Zhao, S., Qi, J., Li, J., Wei, L.: Concept reduction in formal concept analysis based on representative concept matrix. Int. J. Mach. Learn. Cybern. **14**(4), 1147–1160 (2023)

Result-Fusion-Based Temporal-Spatial Composite Sequential Three-Way Decisions

Yi Xu[1,2(✉)], QiSheng Zhu[1], ZhengYue Pan[1], ZiHeng Qiu[1], and XiaoJun Sun[1]

[1] School of Computer Science and Technology, Anhui University, Hefei 230601, Anhui, China
xuyi1023@126.com, E21201116@stu.ahu.edu.cn,
panzhengyue1018@163.com, 1584245419@qq.com, sunxj6@spdb.com.cn
[2] Key Laboratory of Intelligent Computing and Signal Processing, Ministry of Education, Anhui University, Hefei 230601, Anhui, China

Abstract. Temporal-spatial composite sequential three-way decisions can handle dynamic hybrid data from multiple levels effectively. However, the fusion method of dynamic hybrid data is based on composite binary relation, which is a feature level-based fusion method. In real applications, result-based fusion method is also very important for dynamic hybrid data. In this paper, result-fusion-based temporal-spatial composite sequential three-way decisions is proposed (TCSRF). Firstly, based on the optimistic, pessimistic, and mixed composite approximation, three kinds of result-fusion-based temporal-spatial composite sequential three-way decisions for dynamic hybrid data are proposed. Secondly, an algorithm of result-fusion-based temporal-spatial composite sequential three-way decisions is designed. Finally, experimental results demonstrate the effectiveness of our proposed model.

Keywords: Sequential three-way decisions · Dynamic hybrid data · Composite binary relation · Composite approximation

1 Introduction

In contrast to traditional two-way decisions that require an immediate choice, three-way decisions allow for a third option of non-commitment when there is insufficient information or weak evidence to support accepting or rejecting a decision at a specific level of detail. This approach, which is in line with human thinking, problem solving, and information processing, can significantly reduce decision-making costs from a granular computing perspective [1, 2]. Three-way decisions can be described and interpreted as a trisecting-acting-outcome (TAO) model [1], which contains three parts: trisecting, acting, and outcome. The trisecting is to divide a whole into three parts. The acting is to tackle three parts by three strategies. The outcome is to evaluate the effectiveness of the strategies and optimize the trisecting and acting to achieve desired results. In recent years, theory research on three-way decisions has rapidly increased, such as three-way clustering [3–6], three-way classification [7–12], three-way incremental learning [13,

Q. Zhu, Z. Pan, Z. Qiu and X. Sun—Contributing authors.

M. Hu et al. (Eds.): IJCRS 2024, LNAI 14840, pp. 118–132, 2024.
https://doi.org/10.1007/978-3-031-65668-2_9

14], and regret three-way decisions [15, 16]. Moreover, three-way decisions are also applied in many real-world applications, such as text processing [17], feature selection [18–20], frequent pattern discovery [21], data mining and knowledge acquisition [22–27].

The interdependence of temporality and spatiality is a crucial aspect of three-way decisions [28, 29]. Temporality pertains to multi-stage thinking, problem solving, and information processing using three-way decision systems that are subject to dynamic decision-making environments. On the other hand, spatiality relates to the comprehension, abstraction, and representation of data using multilevel and multiview perspectives based on information granularity and hierarchical granular structures. Yang and Li [30] investigated the combination of both aspects to handle dynamic hybrid data through sequential three-way decisions. A temporal-spatial composite sequential three-way decision based on composite binary relation (TSTWCR) is proposed. Composite binary relation is a feature level-based fusion method. In real applications, result-based fusion method is also very important for dynamic hybrid data. For example, patients usually visit different doctors for diagnosis in order to get more accurate diagnosis conclusions. Suppose there is a patient and several doctors. Each doctor gives the patient a diagnosis conclusion based on the examination results and their own diagnosis experience. In order to obtain more reasonable and accurate diagnosis results, it is necessary to integrate the diagnosis results of different doctors, that is, to fuse the decision results. Therefore, in this paper, result-fusion-based temporal-spatial composite sequential three-way decision is proposed. Firstly, based on the optimistic, pessimistic, and mixed composite approximation, three kinds of result-fusion-based temporal-spatial composite sequential three-way decisions for dynamic hybrid data are proposed. Secondly, an algorithm of result-fusion-based temporal-spatial composite sequential three-way decisions is designed. On each level of the proposed sequential three-way decisions, different decision attitudes can be achieved by different operations on composite approximation. Finally, experiments compared with TSTWCR are employed to demonstrate the effectiveness of the proposed model.

The rest of this paper is organized as follows. We present our proposed method in Sect. 2. Experiment results and discussions are shown in Sect. 3. The conclusion is in Sect. 4.

2 The Result-Fusion-Based Temporal-Spatial Composite Sequential Three-Way Decisions

Given a dynamic composite decision table $CDT^t = \left(U^t, AT^t = C^t \cup D^t, V^t, f^t\right)$, suppose at time t, $GGS^{(t,s)}$ is the multilevel composite granular structure and $GGS_j^{(t,s)}$ is the jth level of granular structure.

Firstly, we establish a framework for result-fusion-based temporal-spatial composite sequential three-way decisions using optimistic composite approximation. The term "optimistic" is used to describe the lower approximation (positive region) when multiple independent indiscernibility relations are considered, indicating that at least one relation must meet the inclusion criteria between the equivalence class and target concept. By leveraging the duality of positive and negative regions, we can define the negative region

of result-fusion-based temporal-spatial composite sequential three-way decisions based on optimistic composite approximation. This, in turn, enables the definition of optimistic result-fusion-based temporal-spatial composite sequential three-way decisions.

Definition 1. Given a dynamic composite decision table $CDT^t = (U^t, AT^t = C^t \cup D^t, V^t, f^t)$ at time t, $C^t = \bigcup_{i=1}^{m} C^{t_i}$, $C^{t_i} = \cup_{k=1}^{|C^{t_i}|} a_k^{t_i}$, $0 \le t_1 \le t_2 \le \ldots \le t_i \le \ldots \le t_m \le t$. Suppose $GGS^{(t,s)} = \left(GGS_1^{(t,s)}, GGS_2^{(t,s)}, \ldots, GGS_n^{(t,s)}\right)$ is a multilevel composite granular structure, $GGS_j^{(t,s)} = (U^{(t_i,s_j)}, C^{(t_i,s_j)}, [x]^{(t_i,s_j)}, Pr^{(t_i,s_j)}, \alpha^{(t_i,s_j)}, \beta^{(t_i,s_j)})$ is the jth level, $1 \le i \le m$, $1 \le j \le n$. Assume that $X^{(t_i,s_j)} \subseteq U^{(t_i,s_j)}$ is a target concept, $C^{(t_i,s_j)} = C^{t_1} \cup C^{t_2} \cup \ldots \cup C^{t_l}$ consists of l attribute types, $C^{t_k} \subseteq C^{(t_i,s_j)}$ is the kth type of attribute, $(\alpha^{(t_i,s_j)}, \beta^{(t_i,s_j)})$ is the pair of thresholds of the kth type of attribute, $1 \le k \le l$. On the jth level, the positive region, negative region and boundary region of optimistic result-fusion based temporal-spatial composite sequential three-way decisions can be calculated as follows:

$$
\begin{aligned}
POS^O(X^{(t_i,s_j)}) = \{&x \in U^{(t_i,s_j)} | Pr^{(t_i,s_j)}(X^{(t_i,s_j)} | [x]_{C^{t_1}}) \ge \alpha_1^{(t_i,s_j)} \vee Pr^{(t_i,s_j)} \\
&(X^{(t_i,s_j)} | [x]_{C^{t_2}}) \ge \alpha_2^{(t_i,s_j)} \vee \ldots \vee Pr^{(t_i,s_j)}(X^{(t_i,s_j)} | [x]_{C^{t_l}}) \ge \alpha_l^{(t_i,s_j)}\} \\
&= {}_{1 \le k \le l}^{\cup} POS_{C^{t_k}}(X^{(t_i,s_j)}) \\
NEG^O(X^{(t_i,s_j)}) = \{&x \in U^{(t_i,s_j)} | Pr^{(t_i,s_j)}(X^{(t_i,s_j)} | [x]_{C^{t_1}}) \le \beta_1^{(t_i,s_j)} \wedge Pr^{(t_i,s_j)} \\
&(X^{(t_i,s_j)} | [x]_{C^{t_2}}) \le \beta_2^{(t_i,s_j)} \wedge \ldots \wedge Pr^{(t_i,s_j)}(X^{(t_i,s_j)} | [x]_{C^{t_l}}) \le \beta_l^{(t_i,s_j)}\} \\
&= {}_{1 \le k \le l}^{\cap} NEG_{C^{t_k}}(X^{(t_i,s_j)}) \\
BND^O(X^{(t_i,s_j)}) &= U^{(t_i,s_j)} - POS^O(X^{(t_i,s_j)}) - NEG^O(X^{(t_i,s_j)})
\end{aligned}
\tag{1}
$$

where $Pr^{(t_i,s_j)}(X^{(t_i,s_j)} | [x]_{C^{t_k}}) = \frac{\left|(X^{(t_i,s_j)} \cap [x]_{C^{t_k}}\right|}{[x]_{C^{t_k}}}$ denotes the conditional probability,

$$
POS_{C^{t_k}}(X^{(t_i,s_j)}) = \{x \in U^{(t_i,s_j)} \left| Pr^{(t_i,s_j)}(X^{(t_i,s_j)}) \right| [x]_{C^{t_k}} \le \alpha_k^{(t_i,s_j)}\},
$$

$$
NEG_{C^{t_k}}(X^{(t_i,s_j)}) = \{x \in U^{(t_i,s_j)} \left| Pr^{(t_i,s_j)}(X^{(t_i,s_j)}) \right| [x]_{C^{t_k}} \le \beta_k^{(t_i,s_j)}\}.
$$

Secondly, by combining a family of lower approximations through intersection operation, we define the positive region of result-fusion-based temporal spatial composite sequential three-way decisions based on pessimistic composite approximation. The term "pessimistic" is used to describe the lower approximation (positive region) when multiple independent indiscernibility relations are considered, indicating that all relations must meet the inclusion criteria between the equivalence class and target concept. By taking advantage of the duality between positive and negative regions, we can define the negative region of result-fusion-based temporal-spatial composite sequential three-way decisions based on pessimistic composite approximation. This approach enables the definition of pessimistic result-fusion-based temporal-spatial composite sequential three-way decisions in the following manner.

Definition 2. Given a dynamic composite decision table $CDT^t = \left(U^t, AT^t = C^t \cup D^t, V^t, f^t\right)$ at time t, $C^t = \cup_{i=1}^{m} C^{t_i}$, $C^{t_i} = \cup_{k=1}^{|C^{t_i}|} a_k^{t_i}$, $0 \le t_1 \le t_2 \le \ldots \le$

$t_i \leq \ldots \leq t_m \leq$ t. Suppose $GGS^{(t,s)} = \left(GGS_1^{(t,s)}, GGS_2^{(t,s)}, ..., GGS_n^{(t,s)}\right)$ is a multilevel composite granular structure, $GGS_j^{(t,s)} = (U^{(t_i,s_j)}, C^{(t_i,s_j)}, [x]^{(t_i,s_j)}, Pr^{(t_i,s_j)}, \alpha^{(t_i,s_j)}, \beta^{(t_i,s_j)})$ is the jth level, $1 \leq i \leq m$, $1 \leq j \leq n$. Assume that $X^{(t_i,s_j)} \subseteq U^{(t_i,s_j)}$ is a target concept, $C^{(t_i,s_j)} = C^{t_1} \cup C^{t_2} \cup \ldots \cup C^{t_l}$ consists of l attribute types, $C^{t_k} \subseteq C^{(t_i,s_j)}$ is the kth type of attribute, $(\alpha^{(t_i,s_j)}, \beta^{(t_i,s_j)})$ is the pair of thresholds of the kth type of attribute, $1 \leq k \leq l$. On the jth level, the positive region, negative region and boundary region of pessimistic result-fusionbased temporal-spatial composite sequential three-way decisions can be calculated as follows:

$$\begin{aligned}
POS^P(X^{(t_i,s_j)}) &= \{x \in U^{(t_i,s_j)} | Pr^{(t_i,s_j)}(X^{(t_i,s_j)} | [x]_{C^{t_1}}) \geq \alpha_1^{(t_i,s_j)} \wedge Pr^{(t_i,s_j)} \\
&\quad (X^{(t_i,s_j)} | [x]_{C^{t_2}}) \geq \alpha_2^{(t_i,s_j)} \wedge \ldots \wedge Pr^{(t_i,s_j)}(X^{(t_i,s_j)} | [x]_{C^{t_l}}) \geq \alpha_l^{(t_i,s_j)}\} \\
&\quad = \underset{1 \leq k \leq l}{\cap} POS_{C^{t_k}}(X^{(t_i,s_j)}) \\
NEG^P(X^{(t_i,s_j)}) &= \{x \in U^{(t_i,s_j)} | Pr^{(t_i,s_j)}(X^{(t_i,s_j)} | [x]_{C^{t_1}}) \leq \beta_1^{(t_i,s_j)} \vee Pr^{(t_i,s_j)} \\
&\quad (X^{(t_i,s_j)} | [x]_{C^{t_2}}) \leq \beta_2^{(t_i,s_j)} \vee \ldots \vee Pr^{(t_i,s_j)}(X^{(t_i,s_j)} | [x]_{C^{t_l}}) \leq \beta_l^{(t_i,s_j)}\} \\
&\quad = \underset{1 \leq k \leq l}{\cup} NEG_{C^{t_k}}(X^{(t_i,s_j)}) \\
BND^P(X^{(t_i,s_j)}) &= U^{(t_i,s_j)} - POS^P(X^{(t_i,s_j)}) - NEG^P(X^{(t_i,s_j)})
\end{aligned} \tag{2}$$

where $POS_{C^{t_k}}(X^{(t_i,s_j)}) = \{x \in U^{(t_i,s_j)} \left| Pr^{(t_i,s_j)}(X^{(t_i,s_j)} \right| [x]_{C^{t_k}}) \geq \alpha_k^{(t_i,s_j)}\}$,

$NEG_{C^{t_k}}(X^{(t_i,s_j)}) = \{x \in U^{(t_i,s_j)} \left| Pr^{(t_i,s_j)}(X^{(t_i,s_j)} \right| [x]_{C^{t_k}}) \leq \beta_k^{(t_i,s_j)}\}$.

Additionally, the optimistic and pessimistic fusion strategies can result in two opposite ends of the spectrum. To be more precise, the optimistic fusion strategy is overly progressive, while the pessimistic fusion strategy is excessively conservative. In other words, these two strategies may construct too large or too small positive region. Hence, to obtain a modest decision results, we may adopt a mixed fusion strategy to define result-fusion-based temporal-spatial composite sequential three-way decisions as follows.

Definition 3. Given a dynamic composite decision table $CDT^t = \left(U^t, AT^t = C^t \cup D^t, V^t, f^t\right)$ at time t, $C^t = \cup_{i=1}^m C^{t_i}$, $C^{t_i} = \cup_{k=1}^{|C^{t_i}|} a_k^{t_i}$, $0 \leq t_1 \leq t_2 \leq \ldots \leq t_i \leq \ldots \leq t_m \leq$ t. Suppose $GGS^{(t,s)} = \left(GGS_1^{(t,s)}, GGS_2^{(t,s)}, \ldots, GGS_n^{(t,s)}\right)$ is a multilevel composite granular structure, $GGS_j^{(t,s)} = (U^{(t_i,s_j)}, C^{(t_i,s_j)}, [x]^{(t_i,s_j)}, Pr^{(t_i,s_j)}, \alpha^{(t_i,s_j)}, \beta^{(t_i,s_j)})$ is the jth level, $1 \leq i \leq m$, $1 \leq j \leq n$. Assume that $X^{(t_i,s_j)} \subseteq U^{(t_i,s_j)}$ is a target concept, $C^{(t_i,s_j)} = C^{t_1} \cup C^{t_2} \cup \ldots \cup C^{t_l}$ consists of l attribute types, $C^{t_k} \subseteq C^{(t_i,s_j)}$ is the kth type of attribute, $(\alpha^{(t_i,s_j)}, \beta^{(t_i,s_j)})$ is the pair of thresholds of the kth type of attribute, $1 \leq k \leq l$. On the jth level, the positive region, negative region and boundary region of mixed result-fusion-based temporal spatial composite sequential three-way decisions can be calculated as follows:

$$\begin{aligned}
POS^{\mathrm{M}} X^{(t_i,s_j)} &= \{x \in U^{(t_i,s_j)} \left\| C^{t_k} : Pr^{(t_i,s_j)}(X^{(t_i,s_j)} \right| [x]_{C^{t_k}}) \geq \alpha_k^{(t_i,s_j)}, 1 \leq k \leq l| \geq \lambda\} \\
&= \left\{x \in U^{(t_i,s_j)}\right\} \left\| POS_{C^{t_k}}(X^{(t_i,s_j)}) : x \in POS_{C^{t_k}}(X^{(t_i,s_j)}), 1 \leq k \leq l| \geq \lambda\right\}
\end{aligned}$$

$$NEG^{\mathrm{M}}X^{(t_i,s_j)} = x \in U^{(t_i,s_j)} \left\| C^{t_k} : Pr^{(t_i,s_j)}(X^{(t_i,s_j)} \left| [x]_{C^{t_k}} \le \beta_k^{(t_i,s_j)}, 1 \le k \le l| \ge \lambda \right.\right\}$$

$$= \left\{ x \in U^{(t_i,s_j)} \right\} \left\| NEG_{C^{t_k}}(X^{(t_i,s_j)}) : x \in NEG_{C^{t_k}}(X^{(t_i,s_j)}), 1 \le k \le l \ge |\lambda \right.\}$$

$$BND^{M}(X^{(t_i,s_j)}) = U^{(t_i,s_j)} - POS^{MP}(X^{(t_i,s_j)}) - NEG^{M}(X^{(t_i,s_j)}) \tag{3}$$

where $|*|$ denotes the cardinality of a set, $\lambda = 1, 2, \ldots, l$ is the control parameters of the result fusion, and l denotes the number of attribute types at the jth level of granular structure.

In Definition 3, we can select different result fusion strategies at each level by different λ. If $\lambda = 1$, the mixed result-fusion-based temporal-spatial composite sequential three-way decisions is degenerated to the optimistic result-fusion-based temporal-spatial composite sequential three-way decisions. If $\lambda = l$, the mixed result-fusion-based temporal-spatial composite sequential three-way decisions is degenerated to the pessimistic result-fusion-based temporal-spatial composite sequential three-way decisions. If $1 < \lambda < l$, the mixed result-fusion-based temporal-spatial composite sequential three-way decisions can obtain a neutral decision results between the optimistic and pessimistic result-fusion-based temporal-spatial composite sequential three-way decisions.

Theorem 1. *The positive regions of optimistic, pessimistic and mixed result-fusionbased temporal-spatial composite sequential three-way decisions satisfy the following formula:*

$$POS^{\mathrm{P}}X^{(t_i,s_j)} \subseteq POS^{\mathrm{M}}X^{(t_i,s_j)} \subseteq POS^{\mathrm{O}}X^{(t_i,s_j)} \tag{4}$$

Theorem 2. *The negative regions of optimistic, pessimistic and mixed result-fusionbased temporal-spatial composite sequential three-way decisions satisfy the following formula:*

$$NEG^{\mathrm{O}}X^{(t_i,s_j)} \subseteq NEG^{\mathrm{M}}X^{(t_i,s_j)} \subseteq NEG^{\mathrm{P}}X^{(t_i,s_j)} \tag{5}$$

The proofs of Theorem 1 and Theorem 2 are trivial, so we omit the proof details.

To better calculate the positive region and negative region of three resultfusion-based temporal-spatial composite sequential three-way decisions, we introduce two matrix-based approaches for the calculation of positive region and negative region.

Definition 4. Given a dynamic composite decision table $CDT^t = \left(U^t, AT^t = C^t \cup D^t, V^t, f^t\right)$ at time t, $C^t = \cup_{i=1}^{m} C^{t_i}$, $C^{t_i} = \cup_{k=1}^{|C^{t_i}|} a_k^{t_i}$, $0 \le t_1 \le t_2 \le \ldots \le t_i \le \ldots \le t_m \le$ t. Suppose $GGS^{(t,s)} = \left(GGS_1^{(t,s)}, GGS_2^{(t,s)}, \ldots, GGS_n^{(t,s)}\right)$ is a multilevel composite granular structure, $GGS_j^{(t,s)} = (U^{(t_i,s_j)}, C^{(t_i,s_j)}, [x]^{(t_i,s_j)}, Pr^{(t_i,s_j)}, \alpha^{(t_i,s_j)}, \beta^{(t_i,s_j)})$ is the jth level, $1 \le i \le m$, $1 \le j \le n$. Assume that $X^{(t_i,s_j)} \subseteq U^{(t_i,s_j)}$ is a target concept, $C^{(t_i,s_j)} = C^{t_1} \cup C^{t_2} \cup \ldots \cup C^{t_l}$ consists of l attribute types, $C^{t_k} \subseteq C^{(t_i,s_j)}$ is the kth type of attribute. The positive region matrix $\boldsymbol{POSM}_{C^{t_k}}$ of the kth type of attribute is defined as:

$$\boldsymbol{POSM}_{C^{t_k}} = [r_{C^{t_k}}(x_1), r_{C^{t_k}}(x_2), \ldots, r_{C^{t_k}}(x_n)]_{1\times \mathrm{n}} \tag{6}$$

where $r^{M}(x) = \begin{cases} 1, \left[r_{C^{t_1}}(x) + r_{C^{t_2}}(x) + \ldots + r_{C^{t_l}}(x)\right] \ge \lambda; \\ 0, \textit{else}. \end{cases}$

Definition 5. Given a dynamic composite decision table $CDT^t = \left(U^t, AT^t = C^t \cup D^t, V^t, f^t\right)$ at time t, $C^t = \cup_{i=1}^{m} C^{t_i}$, $C^{t_i} = \cup_{k=1}^{|C^{t_i}|} a_k^{t_i}$, $0 \le t_1 \le t_2 \le \ldots \le t_i \le \ldots \le t_m \le$ t. Suppose $GGS^{(t,s)} = \left(GGS_1^{(t,s)}, GGS_2^{(t,s)}, \ldots, GGS_n^{(t,s)}\right)$ is a multilevel composite granular structure, $GGS_j^{(t,s)} = \left(U^{(t_i,s_j)}, C^{(t_i,s_j)}, [x]^{(t_i,s_j)}, Pr^{(t_i,s_j)}, \alpha^{(t_i,s_j)}, \beta^{(t_i,s_j)}\right)$ is the jth level, $1 \le i \le m$, $1 \le j \le n$. Assume that $X^{(t_i,s_j)} \subseteq U^{(t_i,s_j)}$ is a target concept, $C^{(t_i,s_j)} = C^{t_1} \cup C^{t_2} \cup \ldots \cup C^{t_l}$ consists of l attribute types, $C^{t_k} \subseteq C^{(t_i,s_j)}$ is the kth type of attribute, $\boldsymbol{POSM}_{C^{t_k}}$ is the positive region matrix of the kth type of attribute. The positive region matrices of optimistic, pessimistic and mixed result-fusion-based temporal-spatial composite sequential three-way decisions are defined respectively as:

(1) Positive region matrix of optimistic result-fusion-based temporal-spatial composite sequential three-way decisions:

$$\boldsymbol{POS}^O X^{(t_i,s_j)} = [r^O(x_1), r^O(x_2), \ldots, r^O(x_n)]_{1 \times n} \tag{7}$$

where $r^O(x) = r_{C^{t_1}}(x) \wedge r_{C^{t_2}}(x) \wedge \ldots \wedge r_{C^{t_l}}(x)$.

(2) Positive region matrix of pessimistic result-fusion-based temporal-spatial composite sequential three-way decisions:

$$\boldsymbol{POS}^P X^{(t_i,s_j)} = [r^P(x_1), r^P(x_2), \ldots, r^P(x_n)]_{1 \times n} \tag{8}$$

where $r^P(x) = r_{C^{t_1}}(x) \wedge r_{C^{t_2}}(x) \wedge \ldots \wedge r_{C^{t_l}}(x)$.

(3) Positive region matrix of mixed result-fusion-based temporal-spatial composite sequential three-way decisions:

$$\boldsymbol{POS}^M X^{(t_i,s_j)} = [r^M(x_1), r^M(x_2), \ldots, r^M(x_n)]_{1 \times n} \tag{9}$$

where $r^M(x) = \begin{cases} 1, \left[r_{C^{t_1}}(x) + r_{C^{t_2}}(x) + \ldots + r_{C^{t_l}}(x)\right] \ge \lambda; \\ 0, \textit{else}. \end{cases}$

It is worth pointing out that, the mixed result fusion is a neutral strategy to fuse positive region matrices of different types of attributes. We can use the different combinations of intersection and union operations to obtain the different fusion results. For example, for three positive region matrices $\boldsymbol{POSM}_{C^{t_1}}$, $\boldsymbol{POSM}_{C^{t_2}}$ and $\boldsymbol{POSM}_{C^{t_3}}$, the mixed operation includes two different combinations, namely, $r^M(x) = r_{C^{t_1}}(x) \vee r_{C^{t_2}}(x) \wedge r_{C^{t_3}}(x)$. Similarly, for four positive region matrices $\boldsymbol{POSM}_{C^{t_1}}$, $\boldsymbol{POSM}_{C^{t_2}}$, $\boldsymbol{POSM}_{C^{t_3}}$, and $\boldsymbol{POSM}_{C^{t_4}}$, there are six cases for the mixed operation, namely, $r^M(x) = r_{C^{t_1}}(x) \vee r_{C^{t_2}}(x) \vee r_{C^{t_3}}(x) \wedge r_{C^{t_4}}(x)$, $r^M(x) = r_{C^{t_1}}(x) \vee r_{C^{t_2}}(x) \wedge r_{C^{t_3}}(x) \wedge r_{C^{t_4}}(x)$, $r^M(x) = r_{C^{t_1}}(x) \wedge r_{C^{t_2}}(x) \wedge r_{C^{t_3}}(x) \vee r_{C^{t_4}}(x)$, $r^M(x) = r_{C^{t_1}}(x) \wedge r_{C^{t_2}}(x) \vee r_{C^{t_3}}(x) \vee r_{C^{t_4}}(x)$, $r^M(x) = r_{C^{t_1}}(x) \vee r_{C^{t_2}}(x) \wedge r_{C^{t_3}}(x) \vee r_{C^{t_4}}(x) r^M(x) = r_{C^{t_1}}(x) \wedge r_{C^{t_2}}(x) \vee r_{C^{t_3}}(x) \wedge r_{C^{t_4}}(x)$. In reality, various combinations of the mixed operation may yield distinct fusion outcomes, and we can opt for the suitable one depending on the actual requirements. Next, we present the matrix-based computation approach for the negative region.

Definition 6. Given a dynamic composite decision table $CDT^t = \left(U^t, AT^t = C^t \cup D^t, V^t, f^t\right)$ at time t, $C^t = \cup_{i=1}^{m} C^{t_i}$, $C^{t_i} = \cup_{k=1}^{|C^{t_i}|} a_k^{t_i}$, $0 \le t_1 \le t_2 \le \ldots \le$

$t_i \le \ldots \le t_m \le$ t. Suppose $GGS^{(t,s)} = \left(GGS_1^{(t,s)}, GGS_2^{(t,s)}, \ldots, GGS_n^{(t,s)}\right)$ is a multilevel composite granular structure, $GGS_j^{(t,s)} = (U^{(t_i,s_j)}, C^{(t_i,s_j)}, [x]^{(t_i,s_j)}, Pr^{(t_i,s_j)}, \alpha^{(t_i,s_j)}, \beta^{(t_i,s_j)})$ is the jth level, $1 \le i \le m$, $1 \le j \le n$. Assume that $X^{(t_i,s_j)} \subseteq U^{(t_i,s_j)}$ is a target concept, $C^{(t_i,s_j)} = C^{t_1} \cup C^{t_2} \cup \ldots \cup C^{t_l}$ consists of l attribute types, $C^{t_k} \subseteq C^{(t_i,s_j)}$ is the kth type of attribute. The negative region matrix $\boldsymbol{NEGM}_{C^{t_k}}$ of the kth type of attribute is defined as:

$$\boldsymbol{NEGM}_{C^{t_k}} = [q_{C^{t_k}}(x_1), q_{C^{t_k}}(x_2), \ldots, q_{C^{t_k}}(x_n)]_{1\times n} \tag{10}$$

where.$q_{C^{t_k}}(x) = \begin{cases} 1, x \in NEG_{C^{t_k}}\left(X^{(t_i,s_j)}\right), x \in U; \\ 0, x \notin NEG_{C^{t_k}}\left(X^{(t_i,s_j)}\right), x \in U. \end{cases}$

Definition 7. Given a dynamic composite decision table $CDT^t = \left(U^t, AT^t = C^t \cup D^t, V^t, f^t\right)$ at time t, $C^t = \cup_{i=1}^m C^{t_i}$, $C^{t_i} = \cup_{k=1}^{|C^{t_i}|} a_k^{t_i}$, $0 \le t_1 \le t_2 \le \ldots \le t_i \le \ldots \le t_m \le$ t. Suppose $GGS^{(t,s)} = \left(GGS_1^{(t,s)}, GGS_2^{(t,s)}, \ldots, GGS_n^{(t,s)}\right)$ is a multilevel composite granular structure, $GGS_j^{(t,s)} = (U^{(t_i,s_j)}, C^{(t_i,s_j)}, [x]^{(t_i,s_j)}, Pr^{(t_i,s_j)}, \alpha^{(t_i,s_j)}, \beta^{(t_i,s_j)})$ is the jth level, $1 \le i \le m$, $1 \le j \le n$. Assume that $X^{(t_i,s_j)} \subseteq U^{(t_i,s_j)}$ is a target concept, $C^{(t_i,s_j)} = C^{t_1} \cup C^{t_2} \cup \ldots \cup C^{t_l}$ consists of l attribute types, $C^{t_k} \subseteq C^{(t_i,s_j)}$ is the kth type of attribute, $\boldsymbol{NEGM}_{C^{t_k}}$ is the negative region matrix of the kth type of attribute. The negative region matrices of optimistic, pessimistic and mixed result-fusion-based temporal-spatial composite sequential three-way decisions are defined respectively as:

(1) Negative region matrix of optimistic result-fusion-based temporal-spatial composite sequential three-way decisions:

$$\boldsymbol{NEG}^O X^{(t_i,s_j)} = [q^O(x_1), q^O(x_2), \ldots, q^O(x_n)]_{1\times n} \tag{11}$$

where $q^O(x) = q_{C^{t_1}}(x) \wedge q_{C^{t_2}}(x) \wedge \ldots \wedge q_{C^{t_l}}(x)$.

(2) Negative region matrix of pessimistic result-fusion-based temporal-spatial composite sequential three-way decisions:

$$\boldsymbol{NEG}^P X^{(t_i,s_j)} = [q^P(x_1), q^P(x_2), \ldots, q^P(x_n)]_{1\times n} \tag{12}$$

where.$q^P(x) = q_{C^{t_1}}(x) \wedge q_{C^{t_2}}(x) \wedge \ldots \wedge q_{C^{t_l}}(x)$.

(3) Negative region matrix of mixed result-fusion-based temporal-spatial composite sequential three-way decisions:

$$\boldsymbol{NEG}^M X^{(t_i,s_j)} = [q^M(x_1), q^M(x_2), \ldots, q^M(x_n)]_{1\times n} \tag{13}$$

where $q^M(x) = \begin{cases} 1, \left[q_{C^{t_1}}(x) + q_{C^{t_2}}(x) + \ldots + q_{C^{t_l}}(x)\right] \le \lambda; \\ 0, \textit{else}. \end{cases}$

In this subsection, we present an algorithm for result-fusion-based temporal-spatial composite sequential three-way decisions.

Algorithm 1. Result-fusion-based temporal-spatial composite sequential three-way decisions

Construct a multilevel composite granular structure $GGS^{(t,s)} = (GGS_1^{(t,s)}, GGS_2^{(t,s)}, \ldots, GGS_n^{(t,s)})$, where $GGS_j^{(t,s)} = (U^{(t_i,s_j)}, C^{(t_i,s_j)}, [x]^{(t_i,s_j)}, Pr^{(t_i,s_j)}, \alpha^{(t_i,s_j)}, \beta^{(t_i,s_j)})$ is the jth level of $GGS^{(t,s)}$, $C^{(t_1,s_1)} \subset \ldots \subset C^{(t_i,s_j)} \subset \ldots \subset C^{(t_m,s_n)} \subset AT^{(t,s)}$, $C^t = C^{t_1} \cup C^{t_2} \cup C^{t_3} \cup C^{t_4}$ consists of l attribute types, $C^{t_k} \subseteq C^{(t_i,s_j)}$ is the kth type of attribute.

Input: 1. A dynamic composite decision table $CDT^t = (U^t, AT^t = C^t \cup D^t, V^t, f^t)$ at time t, $C^t = \cup_{i=1}^{m} C^{t_i}$, $C^{t_i} = \cup_{k=1}^{|C^{t_i}|} a_k^{t_i}$, $0 \le t_1 \le t_2 \le \ldots \le t_i \le \ldots \le t_m \le$ t, where C^{t_i} arrived at time t_i is a subset of C^t with the same attribute type.

2. Decision classes: $\pi_D^{s_j} = \{D_1^{s_j}, D_2^{s_j}, \ldots, D_e^{s_j}\}$ denotes decision classes at time i and the jth level, which are a partition of U^t by decision attribute.

Output: The final three regions POS^t, BND^t, NEG^t. $POS^t = \emptyset$, $BND^t = \emptyset$, $NEG^t = \emptyset$;

1: **for** $1 \le j \le n$ **do**
2: **for** $1 \le k \le l$ **do**
3: **Compute** measure similarity functions for C^{t_k} ;
4: **Set** similarity thresholds for C^{t_k} ;
5: **Compute** relation matrices $\boldsymbol{R}_{C^{t_1}}$ for C^{t_k} ;
6: **Compute** $U^{(t_i,s_j)}/C^{t_k} = \{ [x]_{C^{t_k}} | \, x \in U^{(t_i,s_j)} \}$;
7: **Compute** the positive region matrix $\boldsymbol{POSM}_{C^{t_k}}$;
8: **Compute** the negative region matrix $\boldsymbol{NEGM}_{C^{t_k}}$;
9: **end for**
10: **Choose** optimistic, pessimistic or mixed result fusion strategy;
11: **Compute** $POS \bullet (\pi_D^{s_j})$, where $\bullet = O, P, M$;
12: **Compute** $NEG \bullet (\pi_D^{s_j})$, where $\bullet = O, P, M$;
13: **Compute** $BND \bullet (\pi_D^{s_j}) = U^{(t_i,s_j)} - POS \bullet (\pi_D^{s_j}) - NEG \bullet (\pi_D^{s_j})$, where $\bullet = O, P, M$;
14: $U^{(t_i,s_{j+1})} = BND \bullet (\pi_D^{s_j})$;
15: $\pi_D^{s_{j+1}} = \pi_D^{s_{j+1}} \cap U^{(t_i,s_{j+1})}$;
16: $POS^t = POS^t \cup POS \bullet (\pi_D^{s_j})$;
17: $NEG^t = NEG^t \cup NEG \bullet (\pi_D^{s_j})$;
18: $BND^t = U^t - POS^t - NEG^t$;
19: **if** $U^{(t_i,s_{j+1})} = \emptyset$ **then**
20: **return** POS^t, NEG^t;
21: **end if**
22: **end for**
23: **Output:** The final three regions POS^t, BND^t, NEG^t.

3 Experimental Analysis

In this section, we implement experiments to compare the proposed resultfusion-based temporal-spatial composite sequential three-way decisions with the temporal-spatial composite sequential three-way decisions based on composite binary relation (TST-WCR) [30]. Since we cannot obtain such dynamic hybrid datasets in existing public

database, we select six datasets from the UCI Machine Learning Database Repository (http://archive.ics.uci.edu/ml/). Firstly, the method in reference [31] is used to convert the numerical data into interval-value data. Than is, for numerical data, interval-value data is constructed as $[\mu - 2\sigma, \mu + 2\sigma]$, where μ is mean and σ is standard deviation. Secondly, we combine the single-value data from categorical data to generate some set-value data. Third, the decision classes of the datasets Dermatology, Annex, and Cylinder Bands are translated into binary decision classes. Finally, six dynamic hybrid datasets can be obtained outlined in Table 1 and each dataset has four different types of data: categorical data (*CA*), numerical data (*NA*), interval-valued data (*IA*), and set-valued data (*SA*), where (*) denotes the original number of attributes. All experiments are implemented on a PC with Microsoft Windows 7, Intel (R) Core (TM) i3–550 CPU @ 3.20 GHz and 8.0 GB memory. The programming language is Python 2.7.

We implement two groups of experiments. In the first group of experiments, we analysis the efficiency of three result fusion strategies. In the second group of experiments, we analysis the efficiency of composite sequential approach.

3.1 Analysis for Three Result Fusion Strategies

For simplicity, we randomly select 256 samples and three types of attributes (CA, NA, and IA) from each dataset to calculate the positive regions of result-fusion-based temporal-spatial composite sequential three-way decisions based on three result fusion strategies. Firstly, set similarity thresholds $\gamma^t = \delta^t = \eta^t = 0.7$ and thresholds $\alpha_1 = \alpha_2 = \alpha_3 = 0.4$, we calculate the positive region matrix of the three types of attributes. Then based on optimistic composite approximation, pessimistic composite approximation, and mixed composite approximation respectively to calculate the positive region matrix. Note that, the optimistic composite approximation is denoted as strategy $\vee\vee$. The pessimistic composite approximation is denoted as strategy $\wedge\wedge$. For the mixed composite approximation, we further consider two specific mixed operations denoted as strategy $\wedge\vee$ and strategy $\vee\wedge$. As the positive region matrix is 1×256, to display it easily, we reshape it as a 16×16 matrix.

Furthermore, to analyze the uncertainty of dynamic hybrid data under composite approximation and composite binary relation, we compare the approximation quality $\frac{|POS|}{|U|}$ of the proposed result-fusion-based temporal-spatial composite sequential three-way decisions with the temporal-spatial composite sequential three-way decisions based on composite binary relation (TSTWCR) [30]. To deal with hybrid data, the proposed model has three result fusion strategies: optimistic, pessimistic and mixed composite approximation, and TSTWCR also has three relation fusion strategies: optimistic, pessimistic and mixed composite binary relation. In what follows, the optimistic composite approximation and optimistic composite binary relation are uniformly denoted as strategy $\vee\vee$. The pessimistic composite approximation and pessimistic composite binary relation are uniformly denoted as strategy $\wedge\wedge$. For the mixed composite approximation and mixed composite binary relation, we further consider two specific mixed operations uniformly denoted as strategy $\wedge\vee$ and strategy $\vee\wedge$. For the calculation of approximation quality, we set the similarity thresholds $\gamma^t = \delta^t = \eta^t$ are changed from 0.5 to 0.95 with a step of 0.05 and $\alpha_1 = \alpha_2 = \alpha_3 = 0.4$.

Table 1. Description of datasets

Data	Objecti-ons	Classes	Attributes				
			C^{t_2}-*CA*	C^{t_2}-*NA*	C^{t_3}-*IA*	C^{t_4}-*SA*	Total
Credit	690	2	5(9)	3(6)	3(0)	2(0)	13(15)
Dermatology	366	2(6)	3(7)	3(6)	3(0)	2(0)	11(13)
Anneal	798	2(5)	15(30)	4(8)	3(0)	6(0)	28(38)
Cylinder_Bands	512	2(4)	3(7)	3(6)	3(0)	2(0)	11(13)
Horse	368	2	7(15)	4(7)	3(0)	4(0)	18(22)
Heart	270	2	3(7)	3(6)	3(0)	2(0)	11(13)

The approximation quality of the proposed result-fusion-based temporalspatial composite sequential three-way decisions and the temporal-spatial composite sequential three-way decisions based on composite binary relation are shown in Fig. 1. In Fig. 1, the x-coordinate pertains the similarity thresholds, and the y-coordinate pertains the approximate quality. Figure 1 shows that both for the proposed model and TSTWCR, the approximation quality based on strategy $\vee\vee$, strategy $\wedge\wedge$, strategy $\wedge\vee$ and strategy $\vee\wedge$ leads to the growth trend, namely, the uncertainty decreases with increasing similarity thresholds. However, the variation of approximation quality is non-monotonic. For the proposed model, generally speaking, the optimistic composite approximation (strategy $\vee\vee$) leads to a higher approximation quality. The pessimistic composite approximation (strategy $\wedge\wedge$) leads to a lower approximation quality. The mixed composite approximation (strategy $\wedge\vee$ and strategy $\vee\wedge$) leads to the medium approximation quality. For TSTWGC, on the contrary, generally speaking, the optimistic composite binary relation (strategy $\vee\vee$) leads to a lower approximation quality. The pessimistic composite binary relation (strategy $\wedge\wedge$) leads to a higher approximation quality. The mixed composite binary relation (strategy $\wedge\vee$ and strategy $\vee\wedge$) leads to the medium approximation quality. Therefore, to obtain the highest approximation quality, strategy $\vee\vee$ (blue ∇ polyline) is a good choice for the result-fusion-based temporal-spatial composite sequential

Table 2. The distribution of attributes under multilevel composite granular structure

Data	The number and types of attributes			
	Level-1	Level-2	Level-3	Distribution
Credit	{*CA*(3)}	{*CA*(3),*NA*(3)}	{*CA*(3),*NA*(3),*IA*(3),*SA*(2)}	(3;6;11)
Dermatology	{*CA*(1)}	{*CA*(1),*NA*(3)}	{*CA*(1),*NA*(3),*IA*(3),*SA*(2)}	(1;4;9)
Anneal	{*CA*(11)}	{*CA*(11),*NA*(4)}	{*CA*(11),*NA*(4),*IA*(3),*SA*(6)}	(11;15;24)
Cylinder_Bands	{*CA*(1)}	{*CA*(1),*NA*(3)}	{*CA*(1),*NA*(3),*IA*(3),*SA*(2)}	(1;4;9)
Horse	{*CA*(5)}	{*CA*(5),*NA*(4)}	{*CA*(1),*NA*(4),*IA*(3),*SA*(4)}	(5;9;16)
Heart	{*CA*(1)}	{*CA*(1),*NA*(3)}	{*CA*(3),*NA*(3),*IA*(3),*SA*(2)}	(1;4;9)

three-way decisions, but for the temporal-spatial composite sequential three-way decisions based on composite binary relation, strategy $\wedge\wedge$ (red $\times$ polyline) should be chosen. Moreover, note that the blue ∇ polyline is above the red $\times$ polyline in most situations, which shows that our model has higher approximation quality than that of TSTWCR.

3.2 Analysis for the Efficiency of Composite Sequential Approach

In this subsection, we analyze the efficiency of composite sequential three-way decision model. We construct a multilevel composite granular structure with three times and three levels, where level-1 contains categorical data at time t_1, level-2 contains categorical and numerical data at time t_2, and level-3 contains categorical, numerical, interval-valued, and set-valued data at time t_3. Table 2 shows the distribution of attributes at each level. Then, for the dynamic hybrid data, we can make a sequence of decisions from time t_1 to time t_3 and from level-1 to level-3 by the proposed result-fusion-based temporal-spatial composite sequential three-way decisions and the temporal-spatial composite sequential three-way decisions based on composite binary relation. The variation of three regions on each level of the proposed resultfusion-based temporal-spatial composite sequential three-way decisions and the temporal-spatial composite sequential three-way decisions based on composite binary relation are shown in Fig. 2. In Fig. 2, the x-coordinate pertains the level of composite granular structure, the left y-coordinate pertains the number of objects, and the right y-coordinate pertains four fusion strategies: strategy $\vee\vee$, strategy $\vee\wedge$, strategy $\wedge\vee$ and strategy $\wedge\wedge$.

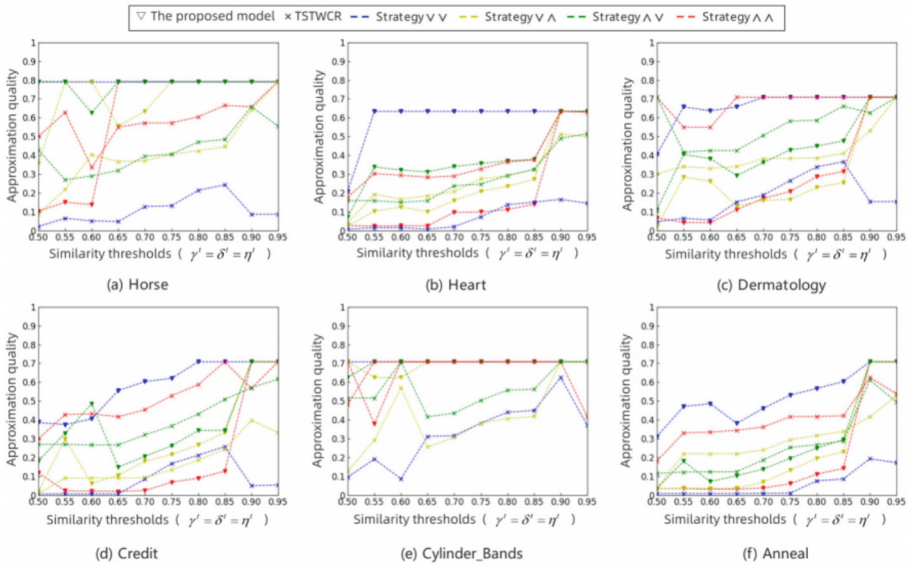

Fig. 1. Approximation quality of the proposed model and TSTWCR

Different colors denote different positive, boundary, and negative regions corresponding to four fusion strategies respectively. From level-1 to level-3, the boundary regions of the proposed model and TSTWCR both become smaller. Meanwhile, the positive and negative regions of the proposed model and TSTWCR both become bigger. Note that, for the proposed model with strategy $\vee\vee$, from level-1 to level-3, the increase of the positive and negative regions is the fastest and the decrease of the boundary region is the fastest. For TSTWCR with strategy $\wedge\wedge$, from level-1 to level-3, the increase of the positive and negative regions is the fastest and the decrease of the boundary region is the fastest.

Moreover, we compare the correct-acceptance rate $CAR = \frac{|POS \cap D|}{|POS|}$ to evaluate the accuracy on each level of the proposed result-fusion-based temporal-spatial composite sequential three-way decisions and the temporalspatial composite sequential three-way decisions based on composite binary relation. Figure 3 shows the variation of accuracy on each level of the proposed model and TSTWCR, where the x-coordinate pertains the level of composite granular structure, the y-coordinate pertains the correct-acceptance rate, (*1) represents the results of the proposed model and (*2) represents the results of TSTWGC. Figure 3 shows that, from level-1 to level-3, the correct-acceptance rates of the proposed model and TSTWCR both increase. Various datasets may lead to different accuracies at different levels. It is also possible to attain a reasonable and acceptable accuracy for each level through the adoption of distinct fusion strategies.

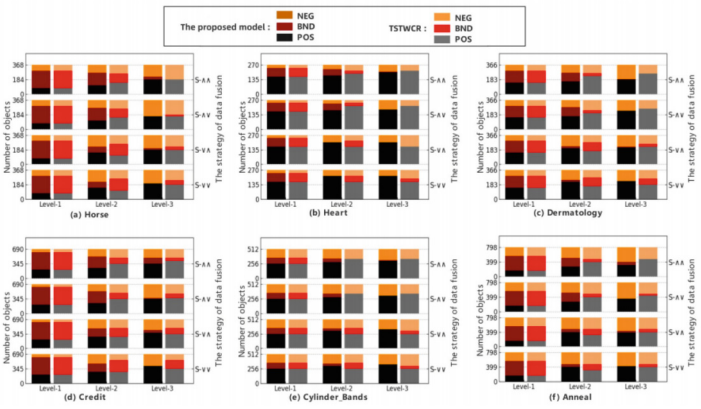

Fig. 2. Variation of three regions on each level of the proposed model and TSTWCR

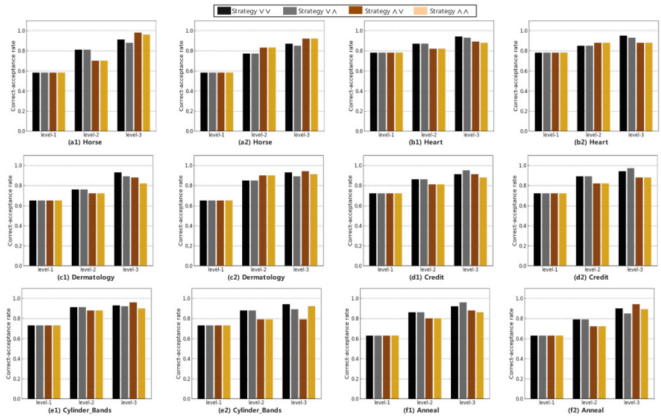

Fig. 3. Correct-acceptance rate on each level of the proposed model and TSTWCR

4 Conclusions

Temporal-spatial composite sequential three-way deci-sions is an effective method to handle dynamic hybrid da-ta from multiple levels. The fusion method of dynamic hybrid data is based on composite binary relation, which is a feature level-based fusion method. In this paper, con-sidering result-based fusion method is also very important for dynamic hybrid data in real applications, we propose result-fusion-based temporal-spatial composite sequential threeway decisions. Firstly, based on the optimistic, pes-simistic and mixed composite approximation, three kinds of result-fusion-based temporal-spatial composite sequen-tial three-way decisions for dynamic hybrid data are pro-posed. Secondly, an algorithm of result-fusion-based tem-poral-spatial composite sequential three-way decisions is designed. On each level of the proposed sequential three-way decisions, different decision attitudes can be achieved by different operations on composite approximation. Fi-nally, the feasibility and effectiveness of the proposed model are verified by comparing it with the existing model TSTWCR. Generally speaking, the approximation quality of the proposed model is higher than that of TSTWCR. The proposed model with optimistic composite approxi-mation often achieves the best performance, while TSTWCR with pessimistic composite binary relation of-ten achieves the best performance. In addition, the uncer-tainty of the proposed model with optimistic composite approximation is less and decrease faster than that of TSTWCR with pessimistic composite binary relation.

Acknowledgments. The author would like to thank the editors and the anonymous reviewers for their valuable comments and suggestions that improved the paper. This work was supported by the National Natural Science Foundation of China (No. 62076002) and the Natural Science Foundation of Anhui Province, China (No. 2008085MF194).

CRediT Authorship Contribution Statement. Yi Xu: Writing - original draft, Writing - review & editing, Conceptualization, Supervision. **Qisheng Zhu:** Writing - original draft, Writing

- review & editing. **Zhengyue Pan:** Writing - original draft, Writing - review & editing. **Ziheng Qiu:** Writing - review and editing, Software, Investigation, Data curation, Methodology. **Xiaojun Sun:** Writing - original draft, Contributed data and analysis tools.

Declaration of Competing Interest. The authors declare that they have no known competing financial interests or personal relationships that could have appeared to influence the work reported in this paper.

Data Availability Statement. Data will be made available on reasonable request.

References

1. Yao, Y.: Three-way decision and granular computing. Int. J. Approx. Reason. **103**, 107–123 (2018). https://doi.org/10.1016/j.ijar.2018.09.005
2. Yao, Y.: Three-way decisions and cognitive computing. Cogn. Comput. **8**(4), 543–554 (2016)
3. Wang, P., Shi, H., Yang, X., Mi, J.: Three-way k-means: integrating k-means and three-way decision. Int. J. Mach. Learn. Cybern. **10**(10), 2767–2777 (2019). https://doi.org/10.1007/s13042-018-0901-y
4. Afridi, M.K., Azam, N., Yao, J., Alanazi, E.: A three-way clustering approach for handling missing data using GTRS. Int. J. Approx. Reason. **98**, 11–24 (2018). https://doi.org/10.1016/j.ijar.2018.04.001
5. Wang, P., Yao, Y.: CE3: a three-way clustering method based on mathematical morphology. Knowl.-Based Syst. **155**, 54–65 (2018). https://doi.org/10.1016/j.knosys
6. Yu, H., Zhang, C., Wang, G.: A tree-based incremental overlapping clustering method using the three-way decision theory. Knowl.-Based Syst. **91**, 189–203 (2016). https://doi.org/10.1016/j.knosys.2015.05.028
7. Zhang, Q., Lv, G., Chen, Y., Wang, G.: A dynamic three-way decision model based on the updating of attribute values. Knowl.-Based Syst. **142**, 71–84 (2018). https://doi.org/10.1016/j.knosys.2017.11.026
8. Zhang, Q., Xia, D., Wang, G.: Three-way decision model with two types of classification errors. Inf. Sci. **420**, 431–453 (2017). https://doi.org/10.1016/j.ins.2017.08.066
9. Zhang, Y., Zhang, Z., Miao, D., Wang, J.: Three-way enhanced convolutional neural networks for sentence-level sentiment classification. Inf. Sci. **477**, 55–64 (2019). https://doi.org/10.1016/j.ins.2018.10.030
10. Zhang, Y., Miao, D., Zhang, Z., Xu, J., Luo, S.: A three-way selective ensemble model for multi-label classification. Int. J. Approx. Reason. **103**, 394–413 (2018). https://doi.org/10.1016/j.ijar.2018.10.009
11. Yao, Y., Hu, M., Deng, X.: Modes of sequential three-way classifications. In: International Conference on Information Processing and Management of Uncertainty in Knowledge-based Systems, pp. 724–735 (2018)
12. Wang, L., Yang, X., Chen, Y., Liu, L., An, S., Zhuo, P.: Dynamic composite decision-theoretic rough set under the change of attributes. Int. J. Comput. Intell. Syst. **11**(1), 355–370 (2018). https://doi.org/10.2991/ijcis.11.1.27
13. Luo, C., Li, T., Huang, Y., Fujita, H.: Updating three-way decisions in incomplete multi-scale information systems. Inf. Sci. **476**, 274–289 (2019). https://doi.org/10.1016/j.ins.2018.10.012
14. Yang, X., Li, T., Fujita, H., Liu, D.: A sequential three-way approach to multi-class decision. Int. J. Approx. Reason. **104**, 108–125 (2019). https://doi.org/10.1016/j.ijar.2018.11.001
15. Deng, J., Zhan, J., Xu, Z., Herrera-Viedma, E.: Regret-theoretic multiattribute decision-making model using three-way framework in multiscale information systems. IEEE Trans. Cybern. 1–14 (2022). https://doi.org/10.1109/TCYB.2022.3173374

16. Wang, W., Zhan, J., Zhang, C., Herrera-Viedma, E., Kou, G.: A regret-theory-based three-way decision method with a priori probability tolerance dominance relation in fuzzy incomplete information systems. Inf. Fusion **89**, 382–396 (2023). https://doi.org/10.1016/j.inffus.2022.08.027
17. Cheng, Y., Kai, R.: Text classification of minimal risk with three-way decisions. J. Inf. Optim. Sci. **39**(4), 973–987 (2018). https://doi.org/10.1080/02522667.2018.14620341
18. Zhang, X., Yang, J., Tang, L.: Three-way class-specific attribute reducts from the information viewpoint. Inf. Sci. **507**, 840–872 (2020). https://doi.org/10.1016/j.ins.2018.06.001
19. Ma, X.-A., Zhao, X.R.: Cost-sensitive three-way class-specific attribute reduction - sciencedirect. Int. J. Approx. Reason. **105**, 153–174 (2019). https://doi.org/10.1016/j.ijar.2018.11.014
20. Ren, M., Qu, Y., Deng, A.: Covering rough set-based three-way decision feature selection. In: 2018 Tenth International Conference on Advanced Computational Intelligence (ICACI), pp. 782–787 (2018). https://doi.org/10.1109/ICACI.2018.8377560
21. Min, F., Zhang, Z.-H., Zhai, W.-J., Shen, R.-P.: Frequent pattern discovery with tri-partition alphabets. Inf. Sci. **507**, 715–732 (2020). https://doi.org/10.1016/j.ins.2018.04.013
22. Zhan, J., Wang, J., Ding, W., Yao, Y.: Three-way behavioral decision making with hesitant fuzzy information systems: Survey and challenges. IEEE/CAA J. Autom. Sin. 1–21 (2022). https://doi.org/10.1109/JAS.2022.106061
23. Zhang, X., Yao, Y.: Tri-level attribute reduction in rough set theory. Expert Syst. Appl. **190**, 116187 (2022). https://doi.org/10.1016/j.eswa.2021.116187
24. Hao, C., Li, J., Fan, M., Liu, W., Tsang, E.C.C.: Optimal scale selection in dynamic multi-scale decision tables based on sequential three-way decisions. Inf. Sci. **415–416**, 213–232 (2017). https://doi.org/10.1016/j.ins.2017.06.03)
25. Wei, W., Liang, J.: Information fusion in rough set theory: an overview. Inf. Fusion **48**, 107–118 (2019). https://doi.org/10.1016/j.inffus.2018.08.007
26. Zheng, Y.: Methodologies for cross-domain data fusion: an overview. IEEE Trans. Big Data **1**(1), 16–34 (2015)
27. Huang, Y., Li, T., Luo, C., Fujita, H., Horng, S.J.: Dynamic fusion of multisource interval-valued data by fuzzy granulation. IEEE Trans. Fuzzy Syst. **26**(6), 3403–3417 (2018). https://doi.org/10.1109/TFUZZ.2018.2832608
28. Liu, D., Li, T., Liang, D., Yang, X.: The temporality and spatiality of three-way decisions. CAAI Trans. Intell. Syst. **14**(1), 141–149 (2019)
29. Yang, X., Li, T., Fujita, H., et al.: A unified model of sequential three-way decisions and multilevel incremental processing[J]. Knowl.-Based Syst. **134**, 172–188 (2017)
30. Yang, X., Li, T., Liu, D., Fujita, H.: A temporal-spatial composite sequential approach of three-way granular computing. Inf. Sci. **486**, 171–189 (2019)
31. Yang, X., Qi, Y., Yu, D.J., et al.: α-Dominance relation and rough sets in interval-valued information systems[J]. Inf. Sci. **294**, 334–347 (2015)

Three-Way Decision in Broad Senses

A Machine-People-Government Triangular Model of Smart Agriculture

Chuanlei Zhang[1,2] and Yiyu Yao[2(✉)]

[1] School of Artificial Intelligence Tianjin University of Science and Technology, Tianjin 300457, China
97313114@tust.edu.cn

[2] Department of Computer Science, University of Regina, Regina, SK S4S 0A2, Canada
Yiyu.Yao@uregina.ca

Abstract. Artificial intelligence (AI) is driving the transformation and upgrading of traditional agriculture towards digitization and intelligence, improving agricultural efficiency and structural optimization. The agricultural environment is dynamic, with numerous factors affecting the growth of crops and livestock, as well as their complex relationships. It is a grand challenge to understand and explain smart agriculture. There are numerous models and frameworks proposed for smart agriculture. Some of the problems with the existing studies include: (1) a lack of unified model or framework for smart agriculture, (2) an overlook of the involvement of the most important elements of any agriculture, namely, smart people, and (3) an insufficient consideration of the crucial role of smart government in modern agriculture. In this paper, we propose a Machine-People-Government triangular model for smart agriculture (MPG4SA), emphasizing the roles of machines, human contributors, and government. We introduce a conceptual three-level framework based on the Symbols-Meaning-Value (SMV) space for smart agriculture named SMV4SA. This framework delineates the nine critical roles of machine, people, and government across three layers: data acquisition, knowledge discovery, and decision-making. The framework may provide conceptual and theoretical support for end-to-end smart agriculture applications such as pre-production planning, in-season management, crop disease and pest recognition, post-production management, and government policy making.

Keywords: Smart agriculture · Three-way decision · Symbols-meaning-value space · Machine-people-government triad

1 Introduction

Smart agriculture, producing high yields with optimal use of various resources, is becoming imperatively important worldwide due to the increasing population

This work was partially supported by a Tianjin Scientific Research Plan Project (NO. 23YDTPJC00470, C.L. Zhang) and a Discovery Grant from NSERC, Canada (Y.Y. Yao). The authors appreciate the valuable comments from the reviewers.

M. Hu et al. (Eds.): IJCRS 2024, LNAI 14840, pp. 135–148, 2024.
https://doi.org/10.1007/978-3-031-65668-2_10

and scarcity and cost of resources such as water, fuel, and fertilizers. Recent studies indicate that the rapidly growing global population, projected to reach 9.7 billion by 2050, will necessitate a huge increase in crop production to meet food demands [1,2]. Smart agriculture serves as a pivotal tool to address and manage the threats, challenges, and risks posed by climate change, diseases, and pest attacks while ensuring sustainability [3,4]. Smart agriculture aids in mitigating the adverse effects of climate change, forecasts production and facilitates government long-term decision-making [5,6]. Smart agriculture involves real-time data collection related to soil and environmental factors, planting, knowledge management, harvesting, cost, pest management for predictive analysis, and decision-making.

There are various related concepts of smart agriculture which include precision agriculture, digital agriculture and smart agriculture. Precision agriculture integrates traditional agricultural practices with modern information technology, employing 3S technology (remote sensing, geographic information systems, and global positioning systems) as its core [7,8]. Digital agriculture focuses on digitizing agricultural production processes, driven by data, to establish digital-driven agricultural production management systems. This aims to achieve digitization, networking, and automation of agricultural production [7,8]. Smart agriculture, supported by Internet of Things (IoT) technology, represents a modern approach to agriculture, falling within the realm of agricultural informatization and evolving from the development of modern information technology. At its core, smart agriculture emphasizes information, knowledge and decision making, integrating modern technologies like the Internet, IoT, big data, cloud computing, and artificial intelligence into agriculture [9].

Smart agriculture intelligence entails the in-depth analysis of big data using artificial intelligence methods to uncover hidden patterns and rules. It transitions from big data to knowledge and further to decision-making, evolving with advancements in IoT, network technologies, and data analysis. Smart agriculture intelligence moves towards high-precision analysis, complex feature analysis, and intricate correlations among multiple factors and systems within the agricultural ecosystem [10].

There are many models and frameworks that have been proposed for smart agriculture. However, the primary issues with the current models or frameworks for smart agriculture are as follows: (1) The absence of a unified model or framework in smart agriculture. (2) Neglect of the crucial involvement of the most important elements of any agriculture, people. The advancement of smart agriculture necessitates cooperation among various experts from different domains, such as consultants, corporations, agriculture specialists, and government officials, yet they are not sufficiently considered in these frameworks. (3) Insufficient emphasis on the role of the government, which plays a pivotal role in modern agriculture by data standardization, research funding, and policy making across various smart agriculture related tasks.

Three-way decision (3WD) [11–14] is a decision-making approach that aligns with human cognitive processes and decision-making habits. Three-way decision is a fast, cost-effective, and fault-tolerant method for solving complex problems. Based on the principles of three-way decision, Yao [15] introduced the concept of Symbols-Meaning-Value (SMV) spaces from the perspectives of information science, management science, cognitive science, and computer science. Three-way decision and SMV space can serve as the foundation for describing, understanding, and constructing the content and manner of the perception of smart agriculture, what and how we know with smart agriculture, and what and how we do with smart agriculture. In this paper, we propose a Machine-People-Government triangular model for smart agriculture (MPG4SA), shown in Fig. 1, and a conceptual three-level framework for smart agriculture based on the Symbols-Meaning-Value (SMV) space (SMV4SA), shown in Fig. 2, for smart agriculture, with agricultural data acquisition, knowledge discovery and decision making as three layers.

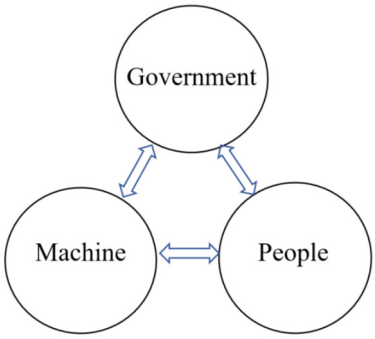

Fig. 1. Machine-People-Government Triangular model for smart agriculture (MPG4SA)

The main contributions of this paper are summarized as follows. (1) We introduce the concept of the three-way thinking and SMV space in the field of smart agriculture. (2) We propose a Machine-People-Government triangular model of smart agriculture (MPG4SA). (3) We propose a conceptual smart agriculture framework based on SMV, called SMV4SA, describing the nine roles played by machine, people and government in agricultural data acquisition, knowledge discovery and decision making three layers, respectively.

The rest of this paper is organized as follows. Section 2 investigates the related models and frameworks proposed in smart agriculture. Section 3 provides a brief theory on the three-way decision (3WD) and SMV spaces. Section 4 proposes the MPG4SA and SMV4SA in details. Section 5 concludes the study and outlines future work.

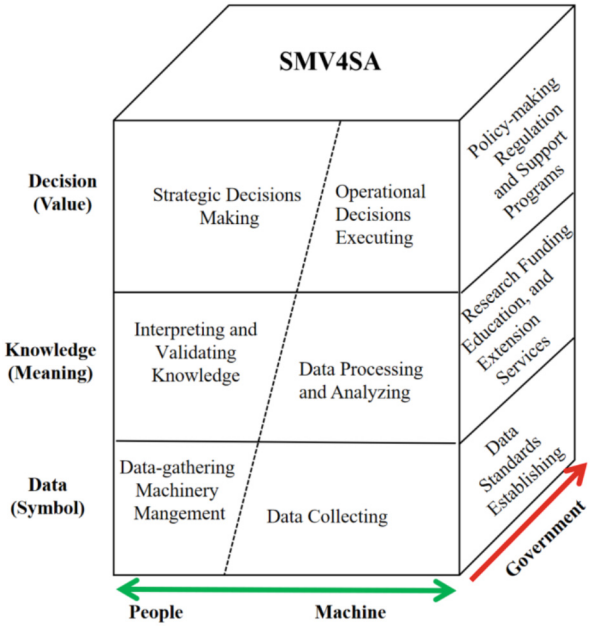

Fig. 2. SMV Space Based Framework for Smart Agriculture (SMV4SA)

2 A Brief Review of Studies on Smart Agriculture

Smart agriculture has emerged as a predominant trend in modern agriculture worldwide. Smart agriculture enables intelligent decision-making, partially or fully automating decision processes. This not only saves time and enhances security, but also reduces human errors, significantly improving the scientific and accurate nature of decision-making [16].

Researchers have contributed to the development of numerous agricultural digital models, cognitive computing models, and knowledge discovery models. For instance, the Newark Vertical Farm in New Jersey, USA, utilizes big data technology to analyze various parameters and achieves significant reductions in water and fertilizer usage while increasing yield. Similarly, Tuscia University in Italy employs big data and artificial intelligence to accelerate breeding research, potentially reshaping future farming practices. Big data-driven and knowledge-based decision-making is expected to replace manual experiential decision-making, with applications spanning the entire agricultural industry chain [9]. Mitra et al. [17] introduced a smart agriculture framework for automatic plant disease tracking, with applications such as the A-CPS system for apple leaf disease detection. This system, deployed in apple orchards, involves farmers, insurance providers, and scientists, with UAVs and smartphone cameras as key components. Angin et al. [2] proposed a low-cost farmland digital twin framework, called AgriLoRa, for smart agriculture. AgriLoRa utilizes

wireless sensor networks and cloud servers to detect plant diseases, weed clusters, and nutrient deficiencies. Qamar et al. [18] proposed a holistic framework, named Agri-PAD, which encompasses various aspects of agriculture, including crop and soil monitoring, precision farming, and market demand. The Agri-PAD framework integrates machine learning-based applications for precision, recommendation, and enterprise applications, aiming to enhance productivity through informed decision-making. Nazirul et al. [4] proposed a conceptual model for smart agriculture focusing on big data-driven sustainable agriculture. Ngo et al. [19] presented an agricultural data integration method using a constellation schema and knowledge extraction methods to improve crop yield and protect the environment. Kamilaris et al. [20] introduced AgriBigCAT, which utilizes geospatial big data analysis to estimate the environmental impact. This platform aids farmers' decision-making processes and administrative planning, aiming to increase food production while reducing environmental impact. Perera et al. [21] proposed a conceptual framework to provide a systematic classification of big data applications in smart farming from a socio-economic perspective.

Despite numerous frameworks proposed in agriculture, the lack of a universally unified model or theory in smart agriculture remains a fundamental issue. Agricultural data's diverse structures and lack of uniformity in collection, formats, and standards hinder effective data mining, while fragmented knowledge bases impede knowledge application. In addition, current frameworks often overlook the crucial role of machine, people and government.

Based on three-way decision we propose a Machine-People-Government triangular model for smart agriculture (MPG4SA) and propose a conceptual smart agriculture framework based on SMV, SMV4SA. They are used for discussions in data science, machines, smart people and governments in smart agriculture, which may have been overlooked in other models and frameworks. It offers an abstract, explainable and flexible approach, allowing for the incorporation of detailed optimizations as suitable theories, methods, and technologies become available.

3 An Overview of Three-Way Decision and SMV Spaces

The three-way decision (3WD), also known as the "threefold decision," is a concept developed through long-term research on rough set theory [11–14]. It has been used to summarize and categorize a decision-making approach that aligns with human cognitive processes and decision-making habits. In the context of probability rough set models, this approach involves two parameters, α and β, which divide the entire domain into three regions: the positive region, the boundary region, and the negative region. Based on this, the concept of three-way decision is introduced: rules generated from the positive region represent acceptance of something, rules generated from the negative region represent rejection, and rules from the boundary region represent the inability to make an acceptance or rejection judgment, termed deferred decision [11,22]. Three-way decision is a fast, cost-effective, high-yield, and fault-tolerant method for solving

complex problems. In 2012, a relatively complete theory and thought process related to three-way decision were introduced. Subsequently, in 2018, it was further improved into a more comprehensive divide-and-conquer model known as the TAO model [11]. Due to its straightforward thinking and practicality, three-way decision has found wide-ranging applications in various aspects of life. Its interpretability and feasibility in addressing problems involving uncertainty have made it a focal point in the field of knowledge discovery, guiding scientific research and practical problem-solving [23]. In 2021, a geometric representation structure of three-way decision was introduced, based on basic geometric concepts such as points, lines, triangles, circles, etc. Examples from different disciplines and domains were used to illustrate these structures and their physical interpretations [24]. Subsequently, in 2022, based on the principles of three-way decision, the concept model of data science and the Symbols-Meaning-Value (SMV) space were introduced. The SMV space is discussed from the perspectives of information science, management science, cognitive science, and computer science, focusing on its three dimensions [15]. In 2023, Yao re-formulated a TAO (Triading-Acting-Optimizing) framework of three-way decision, introduced and articulated the Dao, the way of three-way decision and the way of three-world thinking [25].

Shannon's information theory laid the foundation for modern data communication, significantly impacting numerous disciplines. To cast Shannon's work in a wide context of communications, Weaver [26] proposed a three-level classification of communication problems, which includes how accurately communication symbols are transmitted (the technical problem), how symbols effectively convey the desired meaning (the semantic problem), and how the received meaning effectively influences behavior in the expected manner (the effectiveness problem). Weaver's three-tiered concept is highly valuable because it can easily be applied to study and understand other types of human experiences. Based on Weaver's three-level classification of communication problems, Yao [15] introduced the concept of the Symbols-Meaning-Value (SMV) space. The SMV space serves as a foundational conceptual construct for describing, understanding, and constructing what we perceive, how we know, what we do, and how we do [16]. Specifically, he chose "symbol" and "meaning" from the first two levels of Weaver's issues and used "value" to describe the third level. The selection of "value" is based on the observation that information is valuable or effective only when it enables wise actions. These three elements, symbol, meaning, and value, constitute the SMV triplet. The three-tier SMV space can be understood as a relatively abstract concept that requires multiple interpretations. Generally, the terms "symbol", "meaning", and "value" are just labels for the many possible choices at these three levels. Choosing the correct terms may be an impossible task because any specific choice will highlight some aspects while pushing others into the background.

An practical approach to explaining the concept of the SMV space is to explore its various interpretations. In information science and management science, the SMV space corresponds to the data-knowledge-wisdom (DKW) hier-

archy, where data represents uninterpreted symbols, knowledge is about the meaning of data, and value is typically gained by wisely using knowledge (i.e., wisdom). In cognitive science, the SMV space corresponds to the three-level concept of human behavior: perception, cognition, and action. In a sense, perception focuses on signals (symbols), cognition focuses on understanding and knowledge (meaning), and action focuses on value. In simpler terms, the SMV space can also be seen as "seeing, knowing, and doing."

4 A Framework of Smart Agriculture

In this section, we propose a basic framework of smart agriculture based on two related models, namely, a Machine-People-Government triangular model for smart agriculture (MPG4SA) shown in Fig. 1 and a conceptual smart agriculture model based on SMV (SMV4SA) shown in Fig. 2.

4.1 MPG4SA: Machine-People-Government Triangular Model of Smart Agriculture

Smart agriculture does not mean information technology only. It requires the participation of machine, people and government. At the core of this relationship is division of labor, collaboration and communication. Machine collects data, but it is people who understand the nuances of farming and can apply this data effectively. Government set the stage for innovation and sustainability, ensuring that smart agriculture benefits farmers, the environment and society. Together, these three entities form a holistic ecosystem where data-driven decisions lead to improved productivity, efficiency, and sustainability in agriculture. This collaborative effort aims to shape the conceptualization, understanding, and planning of smart agriculture in a comprehensive manner. The three elements constitute a triad in 3WD demonstrated in Fig. 1. The relationship is a symbiotic one.

Smart agriculture is the most active agricultural productivity for the future, where technologies such as the Internet, agricultural artificial intelligence, agricultural big data, blockchain, and others will elevate the intelligence level of decision-making and management behavior among agricultural producers. Agricultural smart machines, such as agricultural sensors, agricultural robots, AI servers, and other machines, will achieve the transformation and upgrade traditional agricultural production tools. The research and application development of agricultural smart equipment in countries such as the United States, Germany, the United Kingdom, and Japan are progressing rapidly. Major agricultural production operations (including grafting, transplanting, spraying, harvesting of fruits and vegetables, feeding, cleaning, milking of livestock, poultry, online grading, labeling, packaging of agricultural products, etc.) have already realized or are in the process of realizing machine replacement or unmanned operation, significantly increasing labor productivity and agricultural resource utilization efficiency [27].

For smart agriculture to be truly effective, it must embody characteristics such as creativity, sustainability, and livability. The development of smart agriculture necessitates collaboration among various individuals, including farmers, consultants, corporations, agriculture specialists, and officials. Farmers and agricultural workers play important roles in the MPG4SA model. They are responsible for deploying, maintaining, and calibrating data-gathering machinery. Agricultural scientists, researchers, and agronomists contribute domain expertise and specialized knowledge to work alongside machines in interpreting and validating insights generated by AI models. Within the smart agriculture ecosystem, farmers and farm managers are crucial decision-makers. They utilize insights provided by AI models and data collected by machines to make informed and strategic decisions about their farming operations. Farmers rely on AI-generated recommendations for crop planting schedules, fertilizer applications, and pest control measures to optimize yields and reduce costs.

During the development of smart agriculture, the government coordinates various resources, strengthens government support, and breaks through some core technologies of smart agriculture. The government could initiate a number of major projects in smart agriculture, summarizing replicable and scalable models and experiences. At the same time, the government should formulate relevant subsidy policies, providing policy subsidies for the research and application of smart agricultural technology, exempting enterprises with smart agriculture as their core business from taxes, and reducing internet access and data transmission communication costs in rural areas. Furthermore, the government needs to establish smart agricultural technology standards and share data resources, especially focusing on the formulation of data standards, product standards, market access standards, and other standards. Additionally, government departments should open up agricultural data within a certain scope and establish a sharing mechanism.

4.2 SMV4SA: SMV Space Based Model for Smart Agriculture

One objective of this research is to develop a conceptual framework, named SMV4SA, which is a SMV based three-level framework for smart agriculture. The framework encompasses three layers which are data (Symbols), knowledge (Meaning) and decision (Value). In each layer, machine, people and government play different roles, which constitute a 3×3 matrix tasks. The nine tasks are 1) Data Collecting, 2) Data Processing and Analyzing, 3) Operational Decisions Executing, 4) Data-gathering Machinery Management, 5) Interpreting and Validating Knowledge, 6) Strategic Decisions Making, 7) Data Standards Establishing, 8) Research Funding, Education, and Extension Services, 9) Policy-making Regulation and Support Programs.

(1) Data Collecting
Machines play a crucial role in modern agriculture, providing efficiency, precision, and productivity enhancements across various tasks. In the data layer of SMV4SA, machines serve a pivotal role by collecting an extensive range of

agricultural data. Equipped with an array of sensors, drones, and IoT devices, these machines capture real-time information from the field. Sensors are strategically deployed in soil, on plants, and within machinery to monitor critical parameters such as soil moisture, temperature, nutrient levels, and crop health indicators. Drones, equipped with high-resolution cameras and multi-spectral sensors, provide aerial imaging and monitoring capabilities, capturing detailed pictures of fields to assess crop health, detect pest infestations, and identify areas of stress.The data amassed by these machines is both vast and continuous, offering farmers a comprehensive view of their fields. For instance, soil sensors can detect variations in moisture levels across different sections of a field, enabling farmers to implement precise irrigation strategies. Similarly, drones can identify areas that exhibit reduced vegetation vigor, signaling potential pest or disease outbreaks and prompting targeted interventions [8].

(2) Data Processing and Analyzing
In the knowledge layer of SMV4SA, machines are tasked with processing and analyzing the vast datasets collected in the data layer. Artificial Intelligence (AI) algorithms and machine learning models are employed to extract meaningful knowledge and patterns from the raw data. These algorithms can identify correlations between various data points, detect anomalies, and predict future trends in crop growth, pest outbreaks, or soil health. For instance, AI algorithms can analyze historical weather data, soil moisture levels, and crop yield data to create predictive models for optimal planting schedules. These models provide farmers with advice on the best planting windows to maximize yield potential based on historical trends and weather forecasts. Additionally, machine learning algorithms are utilized for image recognition in drone-captured images. They can discern subtle changes in plant color or texture indicative of pests or diseases. By analyzing these images, machines can alert farmers to potential issues before they escalate, enabling targeted interventions [9].

(3) Operational Decisions Executing
In the decision layer of SMV4SA, machines are responsible for executing operational decisions based on insights and recommendations generated in the knowledge layer. Automated systems and robotic machinery are deployed in the field to perform a range of tasks, from precise planting and fertilizing to targeted pest management. For example, automated irrigation systems, guided by AI models and real-time sensor data, adjust water flow rates and distribution patterns to ensure optimal soil moisture levels. Robotic weeders equipped with computer vision systems can identify and selectively remove weeds without the need for chemical herbicides, thus reducing environmental impact. Autonomous drones and unmanned ground vehicles (UGVs) are also integral to the decision layer, performing tasks such as crop scouting and monitoring. These machines patrol fields, identify areas of stress or disease, and relay this information back to farmers for timely intervention [10].

(4) Data-gathering Machinery Management
Farmers and agricultural workers are pivotal contributors in the data layer of SMV4SA. They are tasked with the deployment, maintenance, and calibration of data-gathering machinery. Before the planting season commences, farmers install sensors in the soil and configure drones for routine flyovers. They meticulously ensure that sensors are accurately calibrated to provide precise readings and that drones are programmed to capture specific areas of interest. Additionally, farmers actively participate in data collection through manual observations and input. They record field observations regarding crop growth stages, pest sightings, or weather conditions. Although this data isn't machine-collected, it holds immense value for validating the accuracy of sensor readings and refining predictive models. Farmers also serve as interpreters of the data generated by machines, leveraging their knowledge and experience to derive insights. They integrate data from various sources, such as soil moisture readings and weather forecasts, to make informed decisions about irrigation scheduling, pest management strategies, and crop rotation plans. Thus, farmers act as the vital link between the raw data collected by machines and the actionable insights crucial for optimizing agricultural practices [20].

(5) Interpreting and Validating Knowledge
Agricultural scientists, researchers, and agronomists play a crucial role in the knowledge layer of SMV4SA. They bring domain expertise and specialized knowledge to collaborate with machines in interpreting and validating the insights generated by AI models. These experts work closely with data scientists and engineers to develop and refine algorithms that can accurately predict crop behavior, disease patterns, and optimal management practices. Farmers actively engage with the knowledge layer by utilizing insights from AI models to make informed decisions. They rely on the expertise of agricultural scientists to comprehend the implications of the data and recommendations. For instance, a farmer may receive a recommendation from an AI model to adjust irrigation levels based on predicted weather patterns and soil moisture data. The farmer, with guidance from experts, decides whether to implement the recommendation based on their knowledge of local conditions and crop requirements. Moreover, farmers and agricultural experts contribute to the knowledge layer by validating and improving predictive models. They provide feedback on the accuracy of predictions and suggest adjustments to algorithms based on real-world observations. This iterative collaboration between humans and machines leads to more robust and reliable predictive models [28].

(6) Strategic Decisions Making
Farmers and farm managers serve as key decision-makers in the smart agriculture ecosystem. They leverage outputs provided by AI models and data collected by machines to make informed and strategic decisions about their farming operations. Farmers use AI-generated recommendations on crop planting schedules, fertilizer applications, and pest control measures to optimize yields and reduce costs. Human expertise is invaluable in interpreting and contextualizing recom-

mendations generated by machines. Farmers consider factors such as market demands, local weather conditions, and soil characteristics when implementing AI-driven decisions. For instance, a farmer may receive a recommendation from an AI model to adjust fertilizer application rates based on soil nutrient data. The farmer, drawing on their knowledge of the field's history and conditions, decides whether to follow the recommendation or make adjustments. Farmers also play a critical role in monitoring and evaluating the effectiveness of AI-driven decisions. They observe crop growth, pest levels, and overall field health, providing feedback on the outcomes of implemented strategies. This feedback loop allows farmers to refine their practices over time, continuously improving the decision-making process [28].

(7) Data Standards Establishing
Governments assume a supportive role in the data layer of SMV4SA, concentrating on standardization, data access, and infrastructure development. They establish standards for data collection and sharing, ensuring interoperability and data quality across diverse agricultural operations. For instance, governments may define protocols for sensor calibration or data transmission formats to facilitate seamless integration of data from varied sources. Moreover, government agencies contribute to data collection on a broader scale for monitoring and policy-making endeavors. They oversee networks of weather stations and environmental monitoring systems, amassing regional or national-level data on climate conditions, water availability, and environmental quality. This aggregated data is invaluable for evaluating the overall state of agriculture, identifying trends, and formulating informed policies. In terms of infrastructure, governments invest in the development of rural broadband networks and communication systems. These infrastructural advancements are indispensable for enabling the seamless transmission of data from remote agricultural locations to central databases. By enhancing connectivity, governments ensure that farmers have access to requisite technologies and data services essential for participating in smart agriculture initiatives [29].

(8) Research Funding, Education, and Extension Services
Governments contribute to the knowledge layer of SMV4SA through research funding, education, and extension services. They invest in research and development projects focused on advancing AI algorithms and machine learning techniques for agriculture. By funding research initiatives, governments support the development of innovative solutions to complex agricultural challenges. Agricultural extension services, often supported by government agencies, play a crucial role in translating research findings into practical knowledge for farmers. Extension agents work directly with farmers, providing training, workshops, and educational materials on the use of AI-driven technologies. They help farmers understand how to interpret the advice generated by AI models and apply them to their specific farming operations. Governments also facilitate knowledge sharing and collaboration within the agricultural community. They organize conferences, seminars, and workshop events where farmers, researchers, and industry profes-

sionals can exchange ideas and best practices. By fostering a culture of learning and knowledge sharing, governments enable the broader adoption of smart agriculture practices across the agricultural sectors [9,10].

(9) Policy-making, Regulation and Support Programs

Governments contribute to the decision layer of SMV4SA through policy-making, regulation, and support programs. They create policies that encourage the adoption of AI-driven technologies and sustainable farming practices. For example, governments may offer subsidies or tax incentives for farmers who invest in precision agriculture equipment or participate in data-sharing initiatives. Regulations related to data privacy, cybersecurity, and ethical AI use also fall within the government's purview. Governments establish guidelines to ensure that data collected by machines is securely stored, transmitted, and used. They set standards for data anonymization and protection to safeguard farmers' sensitive information. Government support programs provide financial assistance and technical expertise to farmers adopting smart agriculture practices. These programs may include funding for the purchase of AI-enabled machinery, training workshops on data interpretation, and access to agronomic experts for personalized advice. Moreover, governments monitor and evaluate the impact of smart agriculture on a broader scale. They assess the environmental, social, and economic outcomes of AI-driven practices to inform future policies and investments. By evaluating the effectiveness of smart agriculture initiatives, governments can ensure sustainable and equitable growth in the agricultural sector [9,10].

5 Conclusion

Smart agriculture is still in its early stages of development. There is currently no universally unified model or framework for the field. This paper presents a critical examination of existing models and frameworks for smart agriculture, highlighting several shortcomings such as the lack of a unified model, the oversight of the crucial role of smart people (including farmers and agriculture specialists), and the limited focus on government involvement. In response to these issues, the paper proposes a Machine-People-Government triangular model for smart agriculture (MPG4SA) and a conceptual three-level framework based on the Symbols-Meaning-Value (SMV) space (SMV4SA). The MPG4SA model takes into account the three essential components of smart agriculture: machines, smart people, and government. By integrating these elements, the model aims to provide a more comprehensive understanding of smart agriculture and its dynamics. Additionally, the SMV4SA framework describes the roles of machines, people, and government in agricultural data acquisition, knowledge discovery, and decision-making across three layers. The proposed model and framework offer a structured approach to addressing the complexities of modern agriculture, with implications for various stages of agricultural operations including pre-production planning, in-season management, harvest operations, post-production management, and government policy making. By emphasizing the roles and interactions of machines, smart people, and government, this research

provides a foundation for advancing the efficiency, sustainability, and effectiveness of smart agriculture practices.

The results of this paper have several practical implications for smart agriculture. The Machine-People-Government triangular model for smart agriculture (MPG4SA) and the Symbols-Meaning-Value (SMV) space-based framework (SMV4SA) can serve as a guide for future research and the development of end-to-end smart agriculture applications, ultimately facilitating the transformation and optimization of traditional agriculture through digitization and intelligence.

References

1. Hunter, M., Smith, R., Schipanski, M., Atwood, L., Mortensen, D.: Agriculture in 2050: recalibrating targets for sustainable intensification. Bioscience **67**(4), 386–391 (2017)
2. Angin, P., Anisi, M.H., Goksel, F., Gursoy, C.: Agrilora: a digital twin framework for smart agriculture. J. Wirel. Mobile Netw. Ubiq. Comput. Depend. Appl. **11**(4), 77–96 (2020)
3. Hirafuji, M.: A strategy to create agricultural big data. In: The 2014 Annual SRII Global Conference, pp. 249–250 (2014)
4. Nazirul, M., Sarker, I.: Big data driven smart agriculture: pathway for sustainable Development. In: The 2nd International Conference on Artificial Intelligence and Big Data, ICAIBD 2019, pp. 60–65 (2019)
5. Te, I.: Design of a platform for collecting and analyzing agricultural big data. J. Digital Contents Soc. **18**(1), 149–158 (2017)
6. Wu, Q., Liang, Y., Li, Y., Liang, Y.: Research on intelligent acquisition of smart agricultural big Data. In: The 25th International Conference on Geoinformatics, pp. 1–7 (2017)
7. Tang, S., Zhu, Q., Yan, G.: About basic conception of digital agriculture. Res. Agric. Modern. **23**(3), 183–187 (2002)
8. Li, D.: Internet of things and wisdom agriculture. Agric. Eng. **2**(1), 1–7 (2012)
9. Zhao, C.: Current situations and prospects of smart agriculture. J. South China Agric. Univ. **42**(6), 1–7 (2021)
10. Zhao, C.: Thoughts on the development of agricultural smart technology. Robot Ind. **4**, 36–40 (2020)
11. Yao, Y.Y.: Three-way decisions with probabilistic rough sets. Inf. Sci. **180**(3), 341–353 (2010)
12. Yao, Y.Y.: The superiority of three-way decision in probabilistic rough set models. Inf. Sci. **181**(6), 1080–1096 (2011)
13. Yao, Y.Y.: Tri-level thinking: models of three-way decision. Int. J. Mach. Learn. Cybern. **11**(5), 947–959 (2020)
14. Yao, Y.Y.: Three-way decisions and cognitive computing. Cogn. Comput. **8**(4), 543–554 (2016)
15. Yao, Y.Y.: Symbols-Meaning-Value (SMV) space as a basis for a conceptual model of data science. Int. J. Approx. Reason. **144**, 113–128 (2022)
16. Sun, J., Li, D., Xu, S.: Development strategy of agricultural big data and information infrastructure. Strat. Study CAE **23**(4), 10–18 (2021)

17. Mitra, A., Mohanty, S.P., Kougianos, E.: A smart agriculture framework to automatically track the spread of plant diseases using mask region-based convolutional neural network. I: Internet of Things, IoT through a Multi-disciplinary Perspective (IFIPIoT 2022), IFIP Advances in Information and Communication Technology, vol. 665, pp. 68–85 (2022)
18. Qamar, T., Bawany, N.Z.: Agri-PAD: a scalable framework for smart agriculture. Indon. J. Electr. Eng. Comput. Sci. **29**(3), 1597–1605 (2023)
19. Ngo, V.M., Kechadi, M.T.: Crop knowledge discovery based on agricultural big data integration. In: The 4th International Conference on Machine Learning and Soft Computing (ICMLSC 2020), pp. 46–50 (2020)
20. Kamilaris, A., Assumpcio, A., Blasi, A. B., Torrellas, M., Prenafeta-Boldú, F.X.: Estimating the environmental impact of agriculture by means of geospatial and big data analysis: the case of catalonia. In: From Science to Society, New Trends in Environmental Informatics, pp. 39–48 (2017)
21. Wolfert, S., Ge, L., Verdouw, C.: Big data in smart farming - a review. Agric. Syst. **153**, 69–80 (2017)
22. Yao, Y.Y.: Set-theoretic models of three-way decision. Granular Comput. **6**(1), 133–148 (2021)
23. Yao, Y.Y.: An outline of a theory of three-way decisions. In: Yao, J.T., et al. (eds.) RSCTC 2012. LNCS (LNAI), vol. 7413, pp. 1–17. Springer, Heidelberg (2012). https://doi.org/10.1007/978-3-642-32115-3_1
24. Yao, Y.Y.: The geometry of three-way decision. Appl. Intell. **51**(9), 6298–6325 (2021)
25. Yao, Y.Y.: The Dao of three-way decision and three-world thinking. Int. J. Approx. Reason. **162**, 109032 (2023)
26. Shannon, C.E.: A mathematical theory of communication. Bell Syst. Techn. J. **27**(3), 379–423 (1948)
27. Moysiadis, V., Sarigiannidis, P., Vitsas, V.: Smart farming in Europe. Comput. Sci. Rev. **39**, 100345 (2021)
28. Islam Sarker, M.N., Islam, M.S., Ali, M.A.: Promoting digital agriculture through big data for sustainable farm management. Int. J. Innov. Appl. Stud. **25**(4), 1235–1240 (2019)
29. Yadav, R., Rathod, J., Vaishnavi, N.: Big data meets small sensors in precision agriculture. In: National Conference Potential Research Avenues and Future Opportunities in Electrical and Instrumentation Engineering (ACEWRM 2015), pp. 1–4 (2015)

Three-Way Bibliometrics Analytics for Supporting Literature Review

Langwangqing Suo[1,2], Hai-Long Yang[1(✉)], and Yiyu Yao[2]

[1] School of Mathematics and Statistics, Shaanxi Normal University, Xi'an 710119, Shaanxi, China
Yanghailong@snnu.edu.cn

[2] Department of Computer Science, University of Regina, Regina, SK S4S 0A2, Canada
Yiyu.Yao@uregina.ca

Abstract. A theory of three-way decision concerns triadic thinking, triadic approaches to problem-solving, and triadic methods of computing. This paper applies the philosophy, principles, and methodology of three-way decision to the problem of conducting, constructing, and organizing a literature review in a field of study. First, we introduce the concept of a three-way literature review. Second, we consider the philosophy-theory-application triad for the literature review. We discuss three structures of the philosophy-theory-application triad from a geometric perspective that are useful for understanding the literature review. Third, we consider the who-what-when triad for the literature review. We apply a 3×3 method and propose a corresponding model of the literature review. The first 3 is the topic-author-time triad, which attempts to answer the fundamental question of "who did what when". The second 3 represents a three-level analysis of each of the first three: (1) categorizing topics into the three levels of the core topics, emerging topics, and to-be-explored topics, (2) classifying authors into the three levels of active authors, frequent authors, and occasional authors, and (3) dividing articles into the three levels of initial investigations, further developments, and most recent studies. Finally, we use the 3×3 model to analyze papers published on three-way conflict analysis. The 3×3 model may help researchers conduct a literature review systematically, as well as guide the design and implementation of intelligent systems for supporting literature review.

Keywords: Three-way decision · Triadic thinking · Three-way literature review · 3×3 method · Three-way bibliometrics analytics

1 Introduction

A theory of three-way decision, proposed by Yao [33,35,37–40], consists mainly of the philosophy of thinking in threes, the methodology of problem-solving in

This work was partially supported by a grant from the National Natural Science Foundation of China (No. 12171293), a grant from the China Scholarship Council (No. 202106870049), and a Discovery Grant from NSERC, Canada (Y.Y. Yao). The authors thank the reviewers for their valuable comments.

M. Hu et al. (Eds.): IJCRS 2024, LNAI 14840, pp. 149–164, 2024.
https://doi.org/10.1007/978-3-031-65668-2_11

threes, and the mechanism of computing in threes. It utilizes three elements, three parts, or three perspectives to explore, understand, and describe complex problems. From the cognitive, evolutionary, and cultural bases, Yao [40] explained the motivations, reasonable, and benefits of three-way decision. In recent years, three-way decision has been applied in various fields by virtue of its simplicity, practicality, and utility, for example, three-way classification [6,12,42], three-way clustering [1,24,41], three-way concept analysis [10,26,47], three-way conflict analysis [8,11,15,21,30], three-way approximations of fuzzy sets and shadowed sets [31,45], three-way recommendation systems [13,44], three-way attribute reduction [16,25,46], and so on. Motivated by these successful applications, in this paper, we explore a new application of three-way decision for organizing and structuring a literature review, opening up a new avenue of research for three-way decision.

A literature review plays an important role in any kind of scientific research [18,20]. More often than not, a good literature review increases the probability of success of any research programs and projects. By following the principles of three-way decision, we introduce the philosophy-theory-application triad and the who-what-when triad for understanding, organizing, and formulating a literature review, which is called a three-way literature review. For the philosophy-theory-application triad, we discuss three types of triadic structures: the trilevel hierarchy, triangular structure, and tripod structure. These three triadic structures provide not only a geometric structure for the philosophy-theory-application triad but also a useful understanding for the literature review. For the who-what-when triad, we propose a 3×3 model by applying the 3×3 method and the evaluation-based model. The key to the 3×3 model is how to construct and interpret two 3's. We construct and interpret the first 3 by using the topic-author-time triad. We use a three-level analysis for each part of the first 3 to construct the second 3. More specifically, we categorize topics into three levels: core topics, emerging topics, and to-be-explored topics. We classify authors into three levels: active authors, frequent authors, and occasional authors. We trisect articles into three levels: initial investigations, further developments, and most recent studies. The 3×3 model attempts to answer the fundamental question of who did what when characterized by the who-what-when triad. As a case study, we use the 3×3 model to analyze papers published on three-way conflict analysis. The results help us gain a deeper understanding of three-way conflict analysis.

The rest of the paper is organized as follows. Section 2 introduces the concept of a three-way literature review. Section 3 discusses three structures of the philosophy-theory-application triad used to construct the literature review (a trilevel hierarchy, triangular, and tripod). Section 4 explores the literature review with the who-what-when triad. We present a 3×3 model for bibliometrics analytics for supporting literature review. Section 5 conducts bibliometrics analytics of papers on three-way conflict analysis by using the 3×3 model. Section 6 summarizes the main results and comments on future research. The results of the paper have two applications, namely, helping a researcher in conducting literature review and building a system that supports literature review.

2 Three-Way Literature Review

A literature review is both a research task and a form of academic writing that systematically compiles, summarizes, and evaluates existing research, ideas, and results in a field of study [5,18,20,23,27]. It usually includes a review of relevant research, an analysis of the methodology and results of the research, and identification of shortcomings in existing research or recommendations for future research. A literature review is intended to provide readers with a comprehensive understanding of the research that has been done on a particular topic or field and to offer a foundation of theory and methodology for their own research. For example, Snyder [20] discussed literature reviews as a method of conducting research and outlined the different types of reviews, such as narrative, systematic, or integrative reviews. Palmatier et al. [18] explored the importance of literature reviews in terms of purpose, process, and structure. They pointed out that a review of existing research in a particular field can be useful for the scientific advancement of the field.

Three-way decision is a theory of triadic thinking, triadic methodology, and triadic computing [35,37,40]. A triad is an essential concept of three-way decision, which is a group of three things, items, or entities [40]. A triad offers a structural way of understanding and representing a whole by focusing on three main components or elements. There are multiple interpretations of a triad in different contexts and applications, such as three elements, three parts, three levels, three dimensions, three steps, three types, three sides, three granularities, and many others [37,38]. The triplet threeness-oneness-structuredness captures the three basic properties of a triad [40]. From the threeness, the triad is a conceptualization of the whole through three ingredients, which allows for solving more complex problems by considering the three basic components, parts, or elements. From the oneness, the triad is a unification and fusion of the three, which ensures that the three individual components, parts, or elements work together to describe and reflect the whole. From the structuredness, the three elements of a triad are usually linked to each other in a structured way to form a triadic structure, which combines the threeness and oneness of a triad. In other words, a triad is a set of three objects with a structure.

By collecting evidence from many disciplines and fields, Yao [35,37–40] has demonstrated that a tripartite theory, model, or explanation is normally simple-to-understand, easy-to-remember, and practical-to-use. It may be argued that a literature review based on a triadic structure shares the same advantages. In fact, many survey and review papers use various triadic schemes or organizations, for example, past-present-future, arts-science-application, results-perspectives-challenges, qualitative-quantitative-mixed, and others. We introduce the term "three-way literature review" to label and characterize the type of literature reviews that use triadic structures.

As examples of illustration, we take a look at several comprehensive literature reviews on three-way decision. Yang and Li [28] used complex networks to analyze articles on three-way decision and revealed the relationship between authors, papers, and keywords. Zhan et al. [43] reviewed the progress of three-

way behavioral decision-making with hesitant fuzzy information systems from the past, present, and future perspectives. Yang et al. [32] presented a unified framework for three-way multi-granularity learning by reviewing sequential three-way decision and multi-granularity learning. Wang et al. [24] reviewed the historical development of three-way clustering and noted some challenges and future research topics. The title of their paper explicitly contains the triad, foundations-survey-challenges. Ding et al. [2] reviewed the research progress of three-way decision methods in a generalized intuitionistic fuzzy environment and discussed challenges and future research directions. These review papers explore a triad of three relationships, namely, author-author, author-keyword, and keyword-keyword relation. They contribute greatly to the development of the field of three-way decision.

In the rest of the paper, we further explain the main ideas of three-way literature review by using the philosophy-theory-application triad and the who-what-when triad.

3 Literature Review with the Philosophy-Theory-Application Triad

We adopt the philosophy-theory-application triad, from a triarchic theory of granular computing [34] and the triangle of three-way decision [38], as a basic structure for understanding, organizing, and formulating a theory. We may interpret liberally the labels of the three components, for example, by using the philosophy/foundation-theory/methodology-application/practice triad. A literature review based on the philosophy-theory-application triad focuses on each of the three components and their interactions and relationships. Based on a study of many geometric structures, graphical representations, and semantics interpretations of a triad [38], we discuss three structures of the philosophy-theory-application triad for structuring a literature review.

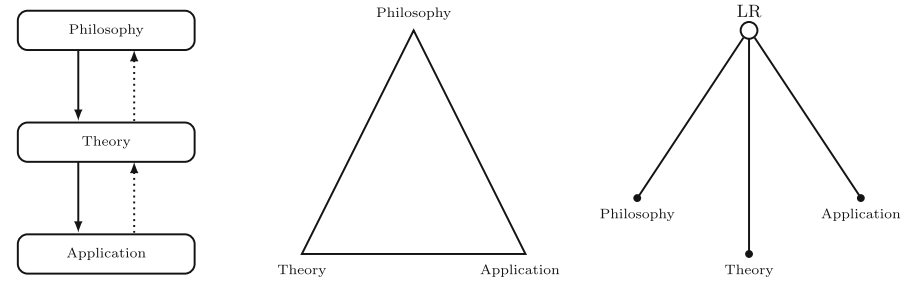

(a) Trilevel understanding (b) Triangle understanding (c) Tripod understanding

Fig. 1. Three triadic understandings of literature review

The first is a trilevel hierarchy of the literature review, which is shown in Fig. 1(a). A trilevel hierarchy is an important and useful mode for three-way

decision, which gives rise to trilevel thinking [37,38,40]. A trilevel approach deals with a complex whole from three comparatively simple and purposeful levels. As seen in Fig. 1(a), the application is at the bottom level, the theory is at the middle level, and the philosophy is at the top level. The top level is directly related to the middle level and indirectly related to the bottom level through the middle level. There is generally a control-support relationship between levels, i.e., top-down control and bottom-up support. Separation and integration are two important features of the trilevel hierarchy. With separation, each level focuses only on specific aspects of the whole, uses a different language for description and denotation, and provides an analysis and understanding of the whole. Separation allows us to concentrate on a particular level without the distraction or hindrance of others. With integration, a synthesis of the studies at three levels may offer a comprehensive analysis and understanding of the whole. Separating the whole into three levels simplifies the complexity of exploring the whole; integrating the outcomes from the three levels provides valuable insights into the whole.

The second is a triangular structure of the literature review, as shown in Fig. 1(b). The triangle suggests triangular thinking [38,40]. The triangle stands for a whole, the three vertices represent the three elements of a triad, and the three edges indicate the relationships between the three elements. In the triangular structure, each element is connected to the other two elements. The relationship between two elements may be interpreted in many different ways, such as dependencies, supports, associations, and others. In addition, implicit information about the relationship between elements can be seen by considering different edge numbers. One is that if we consider only one edge, we see the relationship between the two elements. The second is that if we consider any two edges simultaneously, we see the shared element in direct relation to two unshared elements, but not two unshared elements in direct relation to each other. The third is that if we consider all three edges, then each of the three corners occurs precisely twice. There are two types of relationship, a direct relationship given by an edge and an indirect relationship given by two edges through a third element.

The third is a tripod structure of the literature review (LR), which is shown in Fig. 1(c). The tripod has three supporting legs, which provides a great metaphor for model construction. It is well known for its stability, strength, balance, beauty, harmony, and completeness. In Fig. 1(c), the circle at the top represents the entire literature. The three solid circles at the bottom stand for philosophy, theory, and application. The three lines describe the relationship between whole and parts. From the top down, the whole is divided into three parts. From the bottom up, these three parts support the whole. The different parts are interconnected through their association with the whole. For example, philosophy and theory are related through the entire literature, while the tripod connects the three parts by the whole. A good argument is constructed and supported by using three pieces of evidence, three reasons, or three examples. Using the tripod metaphor, we may argue that a literature review is supported by three aspects of philosophy, theory, and application.

4 Literature Review with the Who-What-When Triad

Bibliometrics analytics is a statistical method for analyzing the distribution and characteristics of publications [17]. In this section, based on the who-what-when triad, we apply the 3×3 method and evaluation-based model to propose a 3×3 model for bibliometrics analytics for supporting literature review.

4.1 The 3×3 Method

Triadic thinking reflects the universal habits of human cognition and is a common way of thinking when we recognize, understand, and solve problems. However, when confronted with complex and multiple problems, a single triadic thinking style may be insufficient in terms of comprehension and in-depth. To solve this problem, Suo et al. [22] introduced the concept of double triadic thinking based on the idea of three-way decision. Double triadic thinking is a method or model that utilizes triadic thinking twice.

The notion of double triadic thinking uses different triadic structures, leading to a variety of 3×3 methods and structures. Suo et al. [22] proposed two particular 3×3 methods by combining trilevel hierarchical thinking and triangular thinking. One is the application of trilevel thinking at each of the three vertices of a triangle, which is called a (3-angle)×(3-level) method. The other is the application of triangular thinking at each of the three levels of a hierarchy, which is called a (3-level)×(3-angle) method.

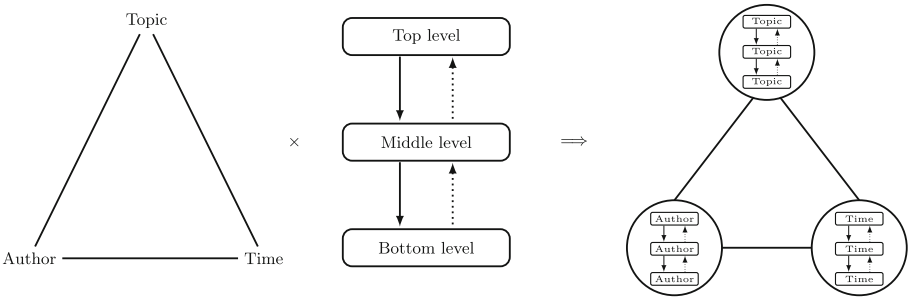

Fig. 2. A (3-angle)×(3-level) structure of literature review

The 3×3 method allows us to think, analyze, and solve problems from nine different perspectives or dimensions. For example, Yao [40] suggested a 3×3 structure framework for the explanation of explainable artificial intelligence based on the symbols-meaning-value space. Yang et al. [29] proposed a lattice-theoretic model of three-way conflict analysis by using the idea of the 3×3 method. We use the (3-angle)×(3-level) method to construct a 3×3 model of literature review, as shown in Fig. 2. The key to the 3×3 model is how to construct and interpret two 3's. For the literature review, we first construct

a topic-author-time triad to form the first 3. The first 3 is characterized by the what-who-when triad, which attempts to answer the basic question of who did what when. The topic-author-time triad is an important indicator when it comes to gaining insights into a field. Topics reflect the direction and focus of the research, authors generate scholarly contributions, and the time captures a history of development. Therefore, an insightful analysis of the topic-author-time triad can give a better understanding of a field. For the construction of the second 3, we draw results from an evaluation-based three-way decision model.

For trisecting a whole, Yao [33] proposed an evaluation-based model. Let U be a finite nonempty set of objects and $e : U \longrightarrow R$ be an evaluation function on U. For $x \in U$, $e(x)$ is evaluation value of x. Given a pair of low and high thresholds (l, h) with $l < h$, we trisect U into three parts based on the evaluation e as follows:

$$\begin{aligned} \mathrm{H}_{(l,h)}(e) &= \{x \in U \mid e(x) \geq h\}, \\ \mathrm{M}_{(l,h)}(e) &= \{x \in U \mid l < e(x) < h\}, \\ \mathrm{L}_{(l,h)}(e) &= \{x \in U \mid e(x) \leq l\}, \end{aligned} \tag{1}$$

where H, M, and L represent the set of objects with high, medium, and low evaluation values, respectively, and the subscripts (l, h) denote the construction of three parts based on a pair of thresholds (l, h).

4.2 A 3×3 Model of Literature Review

By following the principles of the (3-angle)×(3-level) method, we describe the first 3 by the topic-author-time triad and adopt the evaluation-based method to each part of the first 3 to form the second 3. There are two key points when applying the evaluation-based model. One is to construct an evaluation function. The other is to find a pair of appropriate thresholds. There are many ways to choose thresholds, including statistical analysis [4], expert opinion [14], empirical adjustment, and so on. In the 3×3 model, we choose a pair of thresholds based on the characteristics of the data set.

For topic-based analysis, we define an evaluation function on a set of topics T as follows:

$$f(t) = \text{the number of times that the topic } t \text{ appears in the database.} \tag{2}$$

For $t \in T$, $f(t)$ is frequency of t. Since the data set is constructed from a specific topic "X", the value of $f(t)$ is, in fact, a co-occurrence topic t with X. The next step is to set a pair of thresholds (r, c) with $r < c$. According to f and a pair of thresholds (r, c), we trisect the set of topics T into the core topics, emerging topics, and to-be-explored topics as follows:

$$\begin{aligned} \text{Core topics}_{(r,c)}(f) &= \{t \in T \mid f(t) \geq c\}, \\ \text{Emerging topics}_{(r,c)}(f) &= \{t \in T \mid r < f(t) < c\}, \\ \text{To-be-explored topics}_{(r,c)}(f) &= \{t \in T \mid f(t) \leq r\}. \end{aligned} \tag{3}$$

The core topics represent well-established research, which contributes to understanding the frontier problems and research highlights in the field. The emerging topics stand for rapidly growing research, which helps us to know the latest trends in the field. The to-be-explored topics denote possible new research, which provides us with possible future research directions in the field.

For author-based analysis, we define an evaluation function on a set of authors A as follows:

$$n(a) = \text{the number of articles by an author } a \text{ in the database.} \tag{4}$$

We set a pair of thresholds (o, i) with $o < i$. By the evaluation function n and a pair of thresholds (o, i), we trisect the set of authors A into the active authors, frequent authors, and occasional authors as follows:

$$\begin{aligned} \text{Active authors}_{(o,i)}(n) &= \{a \in A \mid n(a) \geq i\}, \\ \text{Frequent authors}_{(o,i)}(n) &= \{a \in A \mid o < n(a) < i\}, \\ \text{Occasional authors}_{(o,i)}(n) &= \{a \in A \mid n(a) \leq o\}. \end{aligned} \tag{5}$$

The active authors represent authors who published a large number of papers in a particular field. The frequent authors stand for authors who publish a large number of research papers in a relatively short period of time. The occasional authors denote occasional or new scholars involved in the field. By focusing on occasional authors we can get a more comprehensive view of researchers in the field, which prompts wider collaboration and communication.

For time-based analysis, we use the same idea to categorize articles into the initial investigations, further developments, and most recent studies. The initial investigations reflect the historical evolution of the particular field and offer the foundational knowledge for future research. The further developments help in understanding the latest discoveries and trends in a particular field. The most recent studies contribute to understanding the frontier issues in a specific field and provide robust clues for future research. The 3×3 model enables us to understand the evolution of a specific area and provides insights into emerging fields within the area.

5 A Literature Review of Three-Way Conflict Analysis Based on the 3×3 Model

In 1998, Pawlak [19] introduced a simple model of conflict analysis based on a three-valued rating by a set of agents on a set of issues. Three-way conflict analysis combines ideas of three-way decision and Pawlak conflict analysis. As a case study, this section conducts bibliometrics analytics of the field of three-way conflict analysis by using the 3×3 model. We use the Web of Science database to collect data related to three-way conflict analysis. By searching for the phrase "three-way decision" for the period from January 2009 to February 2024, we produce a dataset of $1,833$ papers. Out of these papers, we manually identify 43 papers on three-way conflict analysis.

For topics, we select 75 topics from 43 papers and denote the set of topics by T. By Eq.(2), we construct an evaluation function $f(t)$. Since our dataset is constructed by using the phrase "three-way conflict analysis", the value of $f(t)$ is, in fact, co-occurrence topic t with three-way conflict analysis. According to the characteristics of the dataset, we choose a pair of thresholds $(r, c) = (1, 5)$. After that, we obtain 7 core topics for 9.33%, 20 emerging topics for 26.67%, and 48 to-be-explored topics for 64% of three-way conflict analysis based on Eq.(3). To have an intuitive understanding of the results, we use the open-source software package Gephi to produce a visualization as shown in Fig. 3.

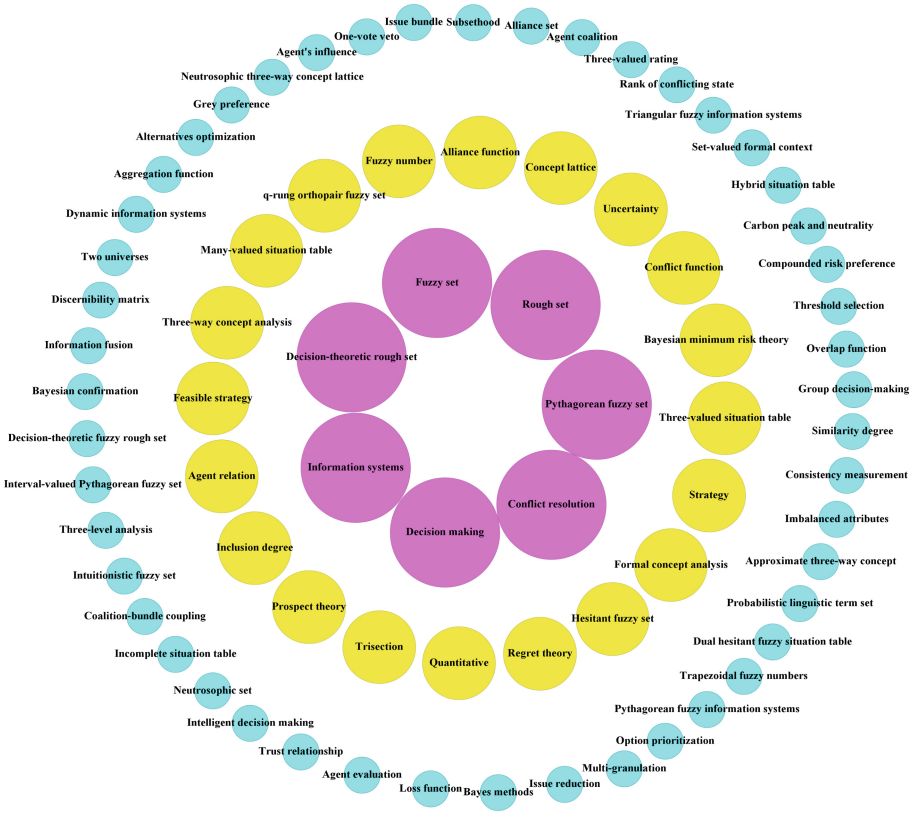

Fig. 3. Trilevel hierarchy of topics related to three-way conflict analysis

Figure 3 displays the trilevel hierarchy of topics by using concentric circles for representing the core topics, emerging topics, and to-be-explored topics. The figure consists of 75 nodes, and the node size represents the frequency of topics in three regions. In Fig. 3, the inner circle indicates the core topics, the middle circle signifies the emerging topics, and the outer circle represents the to-be-explored topics. From a hierarchical standpoint, Fig. 3 is a three-layer circle characterized

by an inner layer, a middle layer, and an outer layer. Such a hierarchy metaphorically suggests that the core topics support the emerging topics and the emerging topics support the to-be-explored topics. Conversely, the to-be-explored topics are established on the emerging topics, which in turn are established on the core topics. This structure helps us to gain insights into three-way conflict analysis. Taking the core topics as an example, there are topics such as decision-theoretic rough set, rough set, fuzzy set, conflict resolution, decision making, Pythagorean fuzzy set, and information systems. These topics constitute the cornerstone of three-way conflict analysis, providing a theoretical foundation and methodological guidance for in-depth research.

There are two possible routes for beginners who want to learn about the field of three-way conflict analysis. One is learning from the inside out and the other is learning from the outside in. More specifically, beginners should initially find a few articles within the core topics to grasp the core concepts and foundations. Then, it will turn to the emerging topics to understand the cutting-edge issues in three-way conflict analysis, which helps to determine the direction of research. Subsequently, attention turns to the to-be-explored topics, exploring potential new research in three-way conflict analysis. Once the direction of research is ascertained, it becomes necessary to learn from the outside in to acquire more details. The trilevel hierarchy of topics reveals the current status and trend of three-way conflict analysis research. This trend not only highlights the growing importance of three-way conflict analysis but also reflects the expanding interest and involvement of scholars in the field. Additionally, it provides useful hints for future research in three-way conflict analysis.

For authors, we select 86 authors from 43 papers and denote the set of authors by A. From Eq.(4), we construct an evaluation function $n(a)$. We set a pair of thresholds $(o, i) = (1, 3)$ based on the characteristics of the dataset. Subsequently, we obtain 9 active authors for 10.47%, 15 frequent authors for 17.44%, and 62 occasional authors for 72.09% of three-way conflict analysis based on Eq.(5). Likewise, we use the Gephi to visualize the results as depicted in Fig. 4.

Figure 4 shows the trilevel organization of authors by using concentric circles to indicate the active authors, frequent authors, and occasional authors. It consists of 86 nodes, and the node size stands for the number of articles published by authors in three regions. In Fig. 4, the inner circle represents the active authors, the middle circle indicates the frequent authors, and the outer circle signifies the occasional authors. This trilevel structure not only provides a distribution of authors but also serves as a framework for understanding trends in three-way conflict analysis. For example, the inner circle consists of nine authors, Lang Guangming, Yao Yiyu, Miao Duoqian, Li Xiaonan, Sun Bingzhen, Yang Hai-Long, Hu Mengjun, Yi Huangjian, and Wang Tianxing. They contribute to three-way conflict analysis by laying the groundwork for and motivating the study of three-way conflict analysis. For researchers and scholars, understanding this distribution can be essential for networking, collaboration, and literature review. By identifying the active authors, it is possible to gain insights into the core theories and methods that currently dominate three-way conflict analysis.

Fig. 4. Trilevel organization of authors related to three-way conflict analysis

Attention to the work of frequent authors offers an understanding into the ongoing development and a broader view of three-way conflict analysis. Meanwhile, exploring the work of occasional authors can reveal emerging trends and diverse perspectives.

Finally, we categorize the articles into the initial investigations, further developments, and most recent studies based on time. This one constitutes the three research periods of three-way conflict analysis, as illustrated in Fig. 5. Within each period, we construct networks showing author-topic and author-author relationships. Such a network not only answers the question of "who did what when", but also unveils a collaborative relationship between authors. By adopting this temporal categorization, we can gain a clearer picture of the research progress of three-way conflict analysis at different stages.

Figure 5(a) represents the initial investigations, covering the years 2017 to 2019. There are four articles in this group. Lang et al. [7,9] and Fan et al. [3]

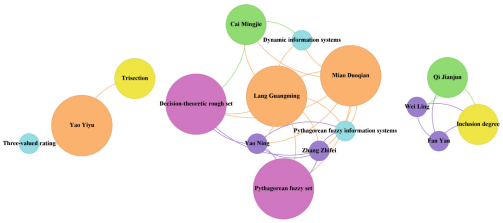

(a) Initial investigations 2017–2019

(b) Further developments 2020–2021

(c) Most recent studies 2022–2024

Fig. 5. Three periods of development of three-way conflict analysis

started a new research direction on combining three-way decision and Pawlak conflict analysis. They did not explicitly introduce the term "three-way conflict analysis". Yao [36] introduced the term for modeling three levels of strong conflict, weak conflict, and non-conflict. These four papers initiated the study

on three-way conflict analysis. As seen in Fig. 5(a), the initial investigations are composed of three research groups, one consisting of Yao Yiyu, the second comprising of Lang Guangming, Miao Duoqian, Cai Mingjie, Zhang Zhifei, and Yao Ning, and the third consisting of Qi Jianjun, Wei Ling, and Fan Yan. This network consists of a total of 16 nodes and 32 edges, where 9 nodes represent authors and 7 nodes stand for topics. It tells us information about what topics authors research and with whom they collaborate. For example, Lang Guangming, Miao Duoqian, and Cai Mingjie are connected to decision-theoretic rough set and dynamic information systems by edges, respectively, which suggests that these three authors investigated these two topics. Additionally, these three authors are connected by edges, which implies a collaborative relationship between them. Over time, three-way conflict analysis moved from the initial investigations to further developments. Figure 5(b) depicts the further developments, covering 15 articles published in the years 2020 to 2021. It consists of a total of 69 nodes and 189 edges, where 36 nodes indicate authors and 33 nodes denote topics. By comparing this period with the previous one, we find that this period not only joined new research groups but also merged some of the research groups from the previous period to form new research groups. For example, two new research groups have been joined, one consisting of Qi Jianjun, Zhi Huilai, Qin Keyun, Qian Ting, Ren Ruisi, and Yang Han, and the other consisting of Wang Tianxing, Li Huaxiong, Zhang Libo, and Hu Wenting. Figure 5(c) shows the most recent studies, covering 24 articles published in the years 2022 to 2024. It consists of a total of 110 nodes and 276 edges, where 59 nodes represent authors and 51 nodes indicate topics. As seen in Fig. 5(c), the three research groups have expanded to seven research groups, which illustrates that the three-way conflict analysis has attracted the interest of many scholars and achieved excellent results.

Through the above discussion, the 3×3 model helps us to gain insights into three-way conflict analysis. It reveals the current status of research, development trends, and cutting-edge issues in this field from the topic-author-time triad, which provides a valuable reference for researchers.

6 Conclusion

Guided by the philosophy, principles, and methodology of three-way decision, we have introduced the concept of a three-way literature review. We summarize the main contributions of the paper as follows. First, we have examined three structures of the philosophy-theory-application triad for the literature review, namely, a trilevel hierarchy, a triangular structure, and a tripod structure. These triadic structures provide a deep understanding of a framework for the literature review. Second, we have studied the who-what-when triad for organizing the literature review. In particular, we have proposed a 3×3 model by combining the 3×3 method and an evaluation-based model of three-way decision. In the 3×3 model, the first 3 represents the topic-author-time triad, and the second 3 signifies a three-level analysis of each of the first 3. The 3×3 model answers the basic question of who did what when characterized by the what-who-when triad.

Finally, we have used the 3×3 model to analyze papers on three-way conflict analysis, which results in a deeper understanding of three-way conflict analysis.

The paper provides a new framework for building a literature review by applying the principles, methodology, and tools of three-way decision theory to the organization and construction of the literature review. The 3×3 model offers a structured and comprehensive approach, enhancing the systematic analysis of existing research within a field. In future research, we will proceed in the following three directions: (1) the use of the number of citations and the impact factor for defining an evaluation function for trisection; (2) the study of the developmental changes in a field in terms of time; and (3) new methods that combine the 3×3 model with the existing bibliometrics analytics methods.

References

1. Ali, B., Azam, N., Yao, J.T.: A three-way clustering approach using image enhancement operations. Int. J. Approximate Reasoning **149**, 1–38 (2022)
2. Ding, J.J., Zhang, C., Li, D.Y., Zhan, J.M., Li, W.T., Yao, Y.Y.: Three-way decisions in generalized intuitionistic fuzzy environments: survey and challenges. Artif. Intell. Rev. **57**(2), 1–45 (2024)
3. Fan, Y., Qi, J., Wei, L.: A conflict analysis model based on three-way decisions. In: Nguyen, H.S., Ha, Q.-T., Li, T., Przybyła-Kasperek, M. (eds.) IJCRS 2018. LNCS (LNAI), vol. 11103, pp. 522–532. Springer, Cham (2018). https://doi.org/10.1007/978-3-319-99368-3_41
4. Gao, C., Yao, Y.: Determining thresholds in three-way decisions with chi-square statistic. In: Flores, V., et al. (eds.) IJCRS 2016. LNCS (LNAI), vol. 9920, pp. 272–281. Springer, Cham (2016). https://doi.org/10.1007/978-3-319-47160-0_25
5. Grant, M.J., Booth, A.: A typology of reviews: an analysis of 14 review types and associated methodologies. Health Inf. Libr. J. **26**(2), 91–108 (2009)
6. Hu, M.J.: Three-way Bayesian confirmation in classifications. Cogn. Comput. **14**(6), 2020–2039 (2022)
7. Lang, G.M., Miao, D.Q., Cai, M.J.: Three-way decision approaches to conflict analysis using decision-theoretic rough set theory. Inf. Sci. **406**, 185–207 (2017)
8. Lang, G.M., Miao, D.Q., Fujita, H.: Three-way group conflict analysis based on Pythagorean fuzzy set theory. IEEE Trans. Fuzzy Syst. **28**(3), 447–461 (2020)
9. Lang, G., Miao, D., Zhang, Z., Yao, N.: Conflict analysis for pythagorean fuzzy information systems. In: Polkowski, L., et al. (eds.) IJCRS 2017. LNCS (LNAI), vol. 10314, pp. 359–367. Springer, Cham (2017). https://doi.org/10.1007/978-3-319-60840-2_26
10. Li, J.H., Huang, C.C., Qi, J.J., Qian, Y.H., Liu, W.Q.: Three-way cognitive concept learning via multi-granularity. Inf. Sci. **378**, 244–263 (2017)
11. Li, X.N., Wang, X., Lang, G.M., Yi, H.J.: Conflict analysis based on three-way decision for triangular fuzzy information systems. Int. J. Approximate Reasoning **132**, 88–106 (2021)
12. Liu, D.: The effectiveness of three-way classification with interpretable perspective. Inf. Sci. **567**, 237–255 (2021)
13. Liu, D., Ye, X.Q.: A matrix factorization based dynamic granularity recommendation with three-way decisions. Knowl.-Based Syst. **191**, 105243 (2020)

14. Liu, J.B., Hu, S.L., Li, H.X., Liu, Y.J., Huang, B., Sun, Y.X.: Achieving threshold consistency in three-way group decision using optimization methodology and expert-weight-updating-strategy. Int. J. Approximate Reasoning **158**, 1–20 (2023)
15. Luo, J.F., Hu, M.J., Lang, G.M., Yang, X., Qin, K.Y.: Three-way conflict analysis based on alliance and conflict functions. Inf. Sci. **594**, 322–359 (2022)
16. Ma, X.A., Yao, Y.Y.: Three-way decision perspectives on class-specific attribute reducts. Inf. Sci. **450**, 227–245 (2018)
17. Merigó, J.M., Yang, J.B.: A bibliometric analysis of operations research and management science. Omega **73**, 37–48 (2017)
18. Palmatier, R.W., Houston, M.B., Hulland, J.: Review articles: purpose, process, and structure. J. Acad. Mark. Sci. **46**, 1–5 (2018)
19. Pawlak, Z.: An inquiry into anatomy of conflicts. Inf. Sci. **109**(1–4), 65–78 (1998)
20. Snyder, H.: Literature review as a research methodology: an overview and guidelines. J. Bus. Res. **104**, 333–339 (2019)
21. Suo, L.W.Q., Yang, H.L.: Three-way conflict analysis based on incomplete situation tables: a tentative study. Int. J. Approximate Reasoning **145**, 51–74 (2022)
22. Suo, L.W.Q., Yang, H.L., Yang, H., Yao, Y.Y.: Double triadic thinking and the 3×3 methods. J. Shaanxi Normal Univ. (Nat. Sci. Ed.) **52**(3), 1–10 (2024). (in Chinese)
23. Torraco, R.J.: Writing integrative literature reviews: guidelines and examples. Hum. Resour. Dev. Rev. **4**(3), 356–367 (2005)
24. Wang, P.X., Yang, X.B., Ding, W.P., Zhan, J.M., Yao, Y.Y.: Three-way clustering: foundations, survey and challenges. Appl. Soft Comput. **151**, 111131 (2024)
25. Wang, Z., Shi, C.J., Wei, L., Yao, Y.Y.: Tri-granularity attribute reduction of three-way concept lattices. Knowl.-Based Syst. **276**, 110762 (2023)
26. Wei, L., Liu, L., Qi, J.J., Qian, T.: Rules acquisition of formal decision contexts based on three-way concept lattices. Inf. Sci. **516**, 529–544 (2020)
27. Whittemore, R., Knafl, K.: The integrative review: updated methodology. J. Adv. Nurs. **52**(5), 546–553 (2005)
28. Yang, B., Li, J.H.: Complex network analysis of three-way decision researches. Int. J. Mach. Learn. Cybern. **11**, 973–987 (2020)
29. Yang, H., Yao, Y.Y., Qin, K.Y.: A lattice-theoretic model of three-way conflict analysis. Knowl.-Based Syst. **288**, 111470 (2024)
30. Yang, H.L., Wang, Y., Guo, Z.L.: Three-way conflict analysis based on hybrid situation tables. Inf. Sci. **628**, 522–541 (2023)
31. Yang, J.L., Yao, Y.Y.: A three-way decision based construction of shadowed sets from Atanassov intuitionistic fuzzy sets. Inf. Sci. **577**, 1–21 (2021)
32. Yang, X., Li, Y.H., Li, T.R.: A review of sequential three-way decision and multi-granularity learning. Int. J. Approximate Reasoning **152**, 414–433 (2023)
33. Yao, Y.: An outline of a theory of three-way decisions. In: Yao, J.T., et al. (eds.) RSCTC 2012. LNCS (LNAI), vol. 7413, pp. 1–17. Springer, Heidelberg (2012). https://doi.org/10.1007/978-3-642-32115-3_1
34. Yao, Y.Y.: A triarchic theory of granular computing. Granular Comput. **1**, 145–157 (2016)
35. Yao, Y.Y.: Three-way decisions and cognitive computing. Cogn. Comput. **8**(4), 543–554 (2016)
36. Yao, Y.Y.: Three-way conflict analysis: reformulations and extensions of the Pawlak model. Knowl.-Based Syst. **180**, 26–37 (2019)
37. Yao, Y.Y.: Tri-level thinking: models of three-way decision. Int. J. Mach. Learn. Cybern. **11**(5), 947–959 (2020)

38. Yao, Y.Y.: The geometry of three-way decision. Appl. Intell. **51**(9), 6298–6325 (2021)
39. Yao, Y.Y.: Symbols-Meaning-Value (SMV) space as a basis for a conceptual model of data science. Int. J. Approximate Reasoning **144**, 113–128 (2022)
40. Yao, Y.Y.: The Dao of three-way decision and three-world thinking. Int. J. Approximate Reasoning **162**, 109032 (2023)
41. Yu, H., Wang, X.C., Wang, G.Y., Zeng, X.H.: An active three-way clustering method via low-rank matrices for multi-view data. Inf. Sci. **507**, 823–839 (2020)
42. Yue, X.D., Chen, Y.F., Yuan, B., Lv, Y.: Three-way image classification with evidential deep convolutional neural networks. Cogn. Comput. **14**(6), 2074–2086 (2022)
43. Zhan, J.M., Wang, J.J., Ding, W.P., Yao, Y.Y.: Three-way behavioral decision making with hesitant fuzzy information systems: survey and challenges. IEEE-CAA J. Autom. Sin. **10**(2), 330–350 (2023)
44. Zhang, H.R., Min, F.: Three-way recommender systems based on random forests. Knowl.-Based Syst. **91**, 275–286 (2016)
45. Zhang, Q.H., Xia, D.Y., Liu, K.X., Wang, G.Y.: A general model of decision-theoretic three-way approximations of fuzzy sets based on a heuristic algorithm. Inf. Sci. **507**, 522–539 (2020)
46. Zhang, X.Y., Miao, D.Q.: Three-way attribute reducts. Int. J. Approximate Reasoning **88**, 401–434 (2017)
47. Zhi, H.L., Qi, J.J., Qian, T., Wei, L.: Three-way dual concept analysis. Int. J. Approximate Reasoning **114**, 151–165 (2019)

Approximate Criterion Reduction in Multi-criteria Trilevel Ranking Analysis

Chengjun Shi[1(✉)], Mengjun Hu[2], Qiaoyi Li[1], and Yiyu Yao[1]

[1] Department of Computer Science, University of Regina, Regina, SK S4S 0A2, Canada
csn838@uregina.ca

[2] Department of Mathematics and Computing Science, Saint Mary's University, Halifax, NS B3H 3C3, Canada

Abstract. This study explores the problem of criterion reduction in a specific class of multi-criteria decision-making problems known as trilevel rankings. A trilevel ranking trisects alternatives into three levels to represent the high, middle, and low, which can be viewed as a practice of three-way decision. By analyzing the trilevel structure, we present a formal definition of approximate criterion reduct. To construct an approximate criterion reduct, we introduce two measures for assessing the difference between trilevel rankings. The first one is a distance-based measure calculated by quantifying consistent, contradictory, and compatible pairs with respect to the two trilevel rankings. The second measure is built on a cost matrix that covers nine potential placements of alternatives, each with its associated cost. We design two heuristic algorithms for computing optimal approximate criterion reducts. These algorithms can be applied by using either of the proposed measures, offering flexibility and adaptability across a range of decision-making scenarios. Finally, we demonstrate the effectiveness of these algorithms through a series of experiments on real-world datasets.

Keywords: Three-way decision · criterion reduction · multi-criteria decision-making · trilevel ranking

1 Introduction

Attribute reduction is a fundamental topic in rough sets theory and has been extensively investigated across many domains [11,12,15,17,18,22–24,31,36]. Our previous work [20], presented at IJCRS 2022, generalized this concept to multi-criteria decision-making (MCDM) and introduced the concept of approximate criterion reduction. As commonly required in an attribute reduct, two critical

This work was partially supported by two Discovery Grants from NSERC, Canada (Y.Y. Yao and M.J. Hu) and grants from the National Natural Science Foundation of China (Nos. 62276217, 62076040, M.J. Hu). The authors thank the reviewers for their constructive comments.

M. Hu et al. (Eds.): IJCRS 2024, LNAI 14840, pp. 165–180, 2024.
https://doi.org/10.1007/978-3-031-65668-2_12

conditions should be satisfied by an approximate criterion reduct, namely, the sufficiency condition and the minimization condition. The sufficiency condition demands that the ranking produced by the reduct should be similar enough to the ranking produced by the entire criteria set. The minimization requires that no proper subset of the reduct satisfies the sufficiency condition. An approximate criterion reduct enables decision-makers to achieve close alternative rankings from a reduced set of criteria. This reduces the complexity and improves the efficiency of decision-making processes, while maintaining approximate effectiveness.

This work further investigates the approximate criterion reduction in a special but significant case of MCDM, where trilevel rankings of alternatives are considered. Trilevel ranking problems can be regarded as practical uses and applications of trilevel thinking [27], which follows the philosophy of three-way decision theory [28]. As the name suggests, a trilevel ranking assigns decision alternatives into three ordered levels. The usefulness of trilevel rankings is supported by a number of studies in the literature. Bradford's law [3] was proposed for the purpose of sorting references into three groups with a ratio of $1 : n : n^2$. Shenton and Hay-Gibson [19] visualized the distribution of Bradford's law by three distinct regions: a core zone, an intermediate area, and an outlying territory, with an implied ordering of core $\succ$ intermediate $\succ$ outlying, where $\succ$ means 'is preferred to'. In the field of inventory management, Flores and Whybark [9,10] proposed ABC analysis for categorizing items based on their significance and consumption value. 'A', 'B', and 'C' items are considered to be highly important, moderately important, and marginally important, respectively. This approach aligns with a trilevel ranking of A $\succ$ B $\succ$ C. Many research efforts have been made on the topic of multi-criteria ABC analysis [4,5,7,16,33]. Additionally, the theory of three-way decision has provided valuable insights into trilevel ranking problems [8,14,25,29,32,34,35].

A primary characteristic of trilevel rankings is that they do not necessitate the local preferences between alternatives at the same level, but rather the global preferences across levels. Therefore, the heuristic function used by Shi et al. [20] may not adequately reflect the difference between trilevel rankings. We develop two measures to address this issue. The first measure adopts the distance function between two orderings proposed by Kemeny and Snell [13] and used by Yao [26] in information retrieval systems. Pair-wise distances are summed up to define the distance between two rankings. The second measure is cost-based and inspired by decision-theoretic rough set (DTRS) models [30,31]. A cost matrix is used to represent the costs associated with the placement of alternatives in two trilevel rankings. These measures provide a more robust and fitting approach to quantifying the difference between trilevel rankings. They are integrated into heuristic algorithms that compute approximate criterion reducts.

The rest of the paper is organized as follows. Section 2 defines the notion of approximate criterion reduction in trilevel rankings. Section 3 presents a distance measure and a cost-sensitive measure to evaluate the difference between trilevel rankings. By utilizing these difference measures, we develop the deletion and

addition algorithms to generate approximate criterion reducts. Section 4 details the experimental validation, where the proposed algorithms are applied to five real-world datasets and the outcomes are visualized for comparison. Finally, Sect. 5 summarizes the main contributions of this research.

2 Approximate Criterion Reduction in Trilevel Rankings

A criterion reduct is defined on multi-criteria decision-making table, which contains all information about decision alternatives. This table is characterized as follows [21].

Definition 1. *A multi-criteria decision-making table* (MCDMT) *is a triplet* $\langle A, C, p\rangle$*, where* $A = \{a_1, \ldots, a_n\}$ *is a finite and non-empty set of* n *alternatives,* $C = \{c_1, \ldots, c_m\}$ *is a finite and non-empty set of* m *criteria, and* $p : A \times C \longrightarrow \Re$ *is a function that maps a decision alternative* a_i *and a criterion* c_j *into a value* $p(a_i, c_j)$ *in the set of real numbers* $\Re$*.*

Example 1. Table 1 takes nine cities and six criteria from an example on city ranking. The following ranking is generated by TOPSIS using all criteria:

$$a_9 \succ a_7 \succ a_2 \succ a_3 \succ a_8 \succ a_5 \succ a_6 \succ a_1 \succ a_4.$$

Table 1. An MCDMT

A	C					
	c_1	c_2	c_3	c_4	c_5	c_6
a_1	70.46	19.07	51.01	86.16	31.87	76.45
a_2	81.89	49.70	82.86	34.31	76.77	24.22
a_3	82.43	54.30	75.00	85.59	60.28	21.35
a_4	65.18	11.25	44.44	83.45	8.61	85.70
a_5	78.12	32.91	67.49	78.07	43.89	33.22
a_6	71.91	22.91	59.55	30.55	40.51	44.53
a_7	80.74	51.24	84.85	18.40	83.76	16.67
a_8	84.52	80.72	36.66	82.08	77.13	30.21
a_9	86.00	63.28	88.43	43.08	90.08	15.34

The ranking in Example 1 shows a complete ranking of individual alternatives. By considering sets of alternatives instead, we may derive multilevel rankings. Particularly, trilevel rankings consider three levels that are associated with high, middle, and low ranks. Accordingly, we present the following definition of a trilevel ranking.

Definition 2. *Suppose $C' \subseteq C$ is a set of criteria in an MCDMT. A trilevel ranking derived by C' is represented by a triplet as:*

$$T_{C'} = \langle H, M, L \rangle, \tag{1}$$

where H, M, and L are the sets of high-ranked, middle-ranked, and low-ranked alternatives, respectively.

In Definition 2, the triplet $T_{C'}$ is made up of three levels with inherent orders, namely, **H**igh-Rank level, **M**iddle-Rank level, and **L**ow-Rank level. Figure 1 describes a general structure of trilevel rankings. Specifically, the alternatives located at a higher level are considered to be ranked ahead of, or more preferred to, those positioned at a lower level.

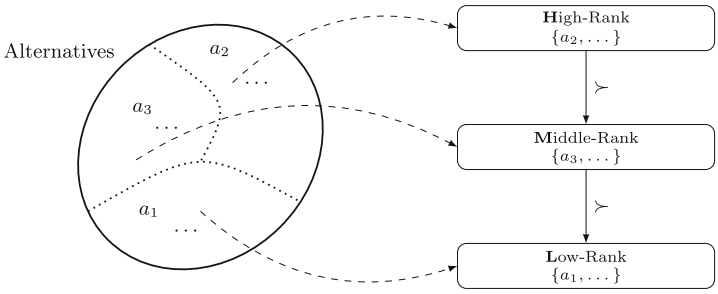

Fig. 1. The structure of a trilevel ranking

A trilevel ranking can be constructed from a complete ranking of individual alternatives computed by any classical MCDM model. Specifically, the alternatives are trisected into three ordered sets based on the complete ranking. The following Example 2 shows one of the many possible ways to trisect the alternatives.

Example 2. As an illustration, we adopt one of the most commonly used schemes of ABC analysis, where A, B, and C class respectively occupy 20%, 30%, and 50% of decision alternatives. Given the outcome ranking in Example 1, we can derive the following trilevel ranking T_C:

$$T_C = \langle H = \{a_7, a_9\}, M = \{a_2, a_3, a_8\}, L = \{a_1, a_4, a_5, a_6\} \rangle.$$

Intuitively, an approximate criterion reduction of C is a minimal subset of C that derives a trilevel ranking close to T_C.

Definition 3. *Given an* MCDMT*, suppose that $\mathbb{T}$ is the set of trilevel rankings of A. Let $Sim : \mathbb{T} \times \mathbb{T} \longrightarrow \Re$ be a similarity measure, where $\Re$ is the set of real numbers. A subset $R \subseteq C$ is called an α-approximate criterion reduct, if and only if, the following conditions are satisfied:*

1. Sufficiency*: $Sim(T_R, T_C) \geqslant \alpha$;*
2. Minimization*: $\forall R' \subsetneq R, Sim(T_{R'}, T_C) < \alpha$.*

Definition 3 modifies the notion of an approximate criterion reduct for rankings [20] to the special case of trilevel rankings. The *Sim* function can be achieved by using Spearman's Rank Correlation Coefficient (SRCC), which is robust to handle tied ranks. The modification retains the introduction of threshold α, which determines whether an outcome trilevel ranking is acceptable or not. There are two crucial conditions to identify a reduct R: sufficiency and minimization. The sufficiency condition requires that the trilevel ranking T_R must be acceptable for the decision-maker, that is, T_R must be sufficiently approximate to T_C. The minimization condition ensures that R is the minimal subset of criteria producing an acceptable trilevel ranking.

3 Constructing Approximate Criterion Reducts in Trilevel Rankings

This section explores methods to construct approximate criterion reducts in trilevel rankings. We introduce two specific measures to evaluate the difference between trilevel rankings. These measures are integrated into heuristic algorithms to construct an optimal approximate criterion reduct.

3.1 A Distance-Based Difference Measure

Kemeny and Snell [13] proposed a distance function to quantify the difference between two rankings. This function was used by Yao [26] in the field of information retrieval to evaluate system performance in ranking the results. We adopt the idea and define a distance-based measure.

The distance method is based on pair-wise comparisons. For an alternative pair $(a, a') \in A \times A$, there are three possibilities of the pair-wise comparison: (1) a is better than a', (2) a is equally good as a', and (3) a is worse than a'. Accordingly, we may define three binary relations on A to formulate these three cases.

Definition 4. *Given a trilevel ranking $T = \langle H, M, L\rangle$, we derive the following (strict)*[1] *preference relation $\succ_T$, indifference relation $\sim_T$, and dispreference relation $\prec_T$:*

$$\begin{aligned}
\succ_T &= \{(a,a') \in A \times A \mid (a \in H \wedge a' \in M) \vee (a \in H \wedge a' \in L) \vee (a \in M \wedge a' \in L)\} \\
&= (H \times M) \cup (H \times L) \cup (M \times L), \\
\sim_T &= \{(a,a') \in A \times A \mid (a \in H \wedge a' \in H) \vee (a \in M \wedge a' \in M) \vee (a \in L \wedge a' \in L)\} \\
&= (H \times H) \cup (M \times M) \cup (L \times L), \\
\prec_T &= \{(a,a') \in A \times A \mid (a \in M \wedge a' \in H) \vee (a \in L \wedge a' \in H) \vee (a \in L \wedge a' \in M)\} \\
&= (M \times H) \cup (L \times H) \cup (L \times M). \qquad (2)
\end{aligned}$$

[1] It should be noted that $\succ_T$ is a strict preference relation that does not include the indifference case. As weak preference relations are not considered in our work, we omit 'strict' in our discussions for simplicity.

Figure 2 illustrates the three relations. Reading along the arrow directions, the solid lines indicate that the starting alternatives at a higher level are preferred to the ending alternatives at a lower level; the dotted lines represent the indifference between alternatives at the same level; and the dashed lines mean that the starting alternatives at a lower level are dispreferred to the ending alternatives at a higher level.

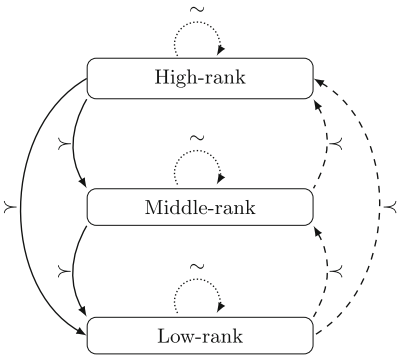

Fig. 2. An illustration of the preference, indifference, and dispreference relations

A few properties of the three relations can be easily verified.

Theorem 1. *The relations* $\succ_T$, $\sim_T$, *and* $\prec_T$ *satisfy the following properties:*

(P1) $\succ_T$ *and* $\prec_T$ *are weak orders.* $\sim_T$ *is an equivalence relation.*
(P2) $\succ_T$ *and* $\prec_T$ *are converse relations to each other, that is,* $\succ_T^c = \prec_T$ *and* $\succ_T = \prec_T^c$, *where* ^{c} *represents a converse relation. The converse of* $\sim_T$ *is itself, that is,* $\sim_T^c = \sim_T$.
(P3) *The three relations trisect* $A \times A$ *into three pair-wise disjoint parts, that is:*

$$\succ_T \cup \sim_T \cup \prec_T = A \times A;$$
$$\succ_T \cap \sim_T = \emptyset, \succ_T \cap \prec_T = \emptyset, \sim_T \cap \prec_T = \emptyset.$$

To measure the distance between two trilevel rankings, we compare them regarding every alternative pair. This is formally carried out by looking at the overlaps between the preference, indifference, and dispreference relations derived from them. Given two trilevel rankings T_1 and T_2, we have the following cases:

(1) consistent pairs: T_1 and T_2 are consistent on ranking the two alternatives.
(2) contradictory pairs: T_1 and T_2 prefer different alternatives.
(3) compatible pairs: one of T_1 and T_2 ranks the two alternatives as indifferent in the same level, while the other ranks them into different levels.

Definition 5. *Given two trilevel rankings T_1 and T_2, the sets of consistent Q^+, contradictory Q^-, and compatible Q^0 alternative pairs are defined as:*

$$\begin{aligned} Q^+ =&(\succ_{T_1} \cap \succ_{T_2}) \cup (\sim_{T_1} \cap \sim_{T_2}) \cup (\prec_{T_1} \cap \prec_{T_2}), \\ Q^- =&(\succ_{T_1} \cap \prec_{T_2}) \cup (\prec_{T_1} \cap \succ_{T_2}), \\ Q^0 =&(\sim_{T_1} \cap \succ_{T_2}) \cup (\sim_{T_1} \cap \prec_{T_2}) \cup (\prec_{T_1} \cap \sim_{T_2}) \cup (\succ_{T_1} \cap \sim_{T_2}). \end{aligned} \tag{3}$$

The three sets Q^+, Q^-, and Q^0 trisect the family of alternative pairs $A \times A$ into three pair-wise disjoint parts. By the property (P2) in Theorem 1, we have:

$$\begin{aligned} \prec_{T_1} \cap \prec_{T_2} &= (\prec^c_{T_1} \cap \prec^c_{T_2})^c = (\succ_{T_1} \cap \succ_{T_2})^c, \\ \prec_{T_1} \cap \succ_{T_2} &= (\prec^c_{T_1} \cap \succ^c_{T_2})^c = (\succ_{T_1} \cap \prec_{T_2})^c, \\ \sim_{T_1} \cap \prec_{T_2} &= (\sim^c_{T_1} \cap \prec^c_{T_2})^c = (\sim_{T_1} \cap \succ_{T_2})^c, \\ \prec_{T_1} \cap \sim_{T_2} &= (\prec^c_{T_1} \cap \sim^c_{T_2})^c = (\succ_{T_1} \cap \sim_{T_2})^c, \end{aligned}$$

where all superscripts ^{c} represent a converse relation.

Accordingly, we have the following theorem.

Theorem 2. *Given two trilevel ranking T_1 and T_2, the sets of consistent, contradictory, and compatible alternative pairs can be defined as:*

$$\begin{aligned} Q^+ =&(\succ_{T_1} \cap \succ_{T_2}) \cup (\sim_{T_1} \cap \sim_{T_2}) \cup (\succ_{T_1} \cap \succ_{T_2})^c, \\ Q^- =&(\succ_{T_1} \cap \prec_{T_2}) \cup (\succ_{T_1} \cap \prec_{T_2})^c, \\ Q^0 =&(\sim_{T_1} \cap \succ_{T_2}) \cup (\sim_{T_1} \cap \succ_{T_2})^c \cup (\prec_{T_1} \cap \sim_{T_2}) \cup (\prec_{T_1} \cap \sim_{T_2})^c. \end{aligned} \tag{4}$$

Adopting the ideas of Kemeny and Snell [13], we calculate the distance on consistent pairs as 0, compatible pairs as 1, and contradictory pairs as 2. Then we get the following distance measure between two trilevel rankings.

Definition 6. *Given two trilevel rankings T_1 and T_2, the distance-based measure is computed as:*

$$\begin{aligned} dis(T_1, T_2) &= 2|Q^-| + |Q^0| \\ &= 4|\succ_{T_1} \cap \prec_{T_2}| + 2|\sim_{T_1} \cap \succ_{T_2}| + 2|\prec_{T_1} \cap \sim_{T_2}|. \end{aligned} \tag{5}$$

This distance-based measure is symmetric, that is, we have $dis(T_1, T_2) = dis(T_2, T_1)$.

Example 3. Suppose we have the following two trilevel rankings:

$$\begin{aligned} T_1 =&\langle H_1 = \{a_1\}, M_1 = \{a_2, a_3\}, L_1 = \{a_4, a_5\}\rangle, \\ T_2 =&\langle H_2 = \{a_2\}, M_2 = \{a_1, a_4\}, L_2 = \{a_3, a_5\}\rangle. \end{aligned}$$

Their preference, indifference, and dispreference relations as:

$$\begin{aligned} \succ_{T_1} &= (H_1 \times M_1) \cup (H_1 \times L_1) \cup (M_1 \times L_1) \\ &= \{(a_1, a_2), (a_1, a_3), (a_1, a_4), (a_1, a_5), (a_2, a_4), (a_2, a_5), (a_3, a_4), (a_3, a_5)\}, \\ \sim_{T_1} &= (H_1 \times H_1) \cup (M_1 \times M_1) \cup (L_1 \times L_1) \\ &= \{(a_1, a_1), (a_2, a_2), (a_2, a_3), (a_3, a_2), (a_3, a_3), (a_4, a_4), (a_4, a_5), (a_5, a_4), (a_5, a_5)\}, \\ \prec_{T_1} &= (M_1 \times H_1) \cup (L_1 \times H_1) \cup (L_1 \times M_1) \\ &= \{(a_2, a_1), (a_3, a_1), (a_4, a_1), (a_5, a_1), (a_4, a_2), (a_4, a_3), (a_5, a_2), (a_5, a_3)\}; \end{aligned}$$

$$
\begin{aligned}
\succ_{T_2} &= (H_2 \times M_2) \cup (H_2 \times L_2) \cup (M_2 \times L_2) \\
&= \{(a_2, a_1), (a_2, a_4), (a_2, a_3), (a_2, a_5), (a_1, a_3), (a_1, a_5), (a_4, a_3), (a_4, a_5)\}, \\
\sim_{T_2} &= (H_2 \times H_2) \cup (M_2 \times M_2) \cup (L_2 \times L_2) \\
&= \{(a_2, a_2), (a_1, a_1), (a_1, a_4), (a_4, a_1), (a_4, a_4), (a_3, a_3), (a_3, a_5), (a_5, a_3), (a_5, a_5)\}, \\
\prec_{T_2} &= (M_2 \times H_2) \cup (L_2 \times H_2) \cup (L_2 \times M_2) \\
&= \{(a_1, a_2), (a_4, a_2), (a_3, a_2), (a_5, a_2), (a_3, a_1), (a_3, a_4), (a_5, a_1), (a_5, a_4)\}.
\end{aligned}
$$

Then, the three groups of pairs are calculated by Eq. (3) as:

$$
\begin{aligned}
Q^+ &= (\succ_{T_1} \cap \succ_{T_2}) \cup (\sim_{T_2} \cap \sim_{T_2}) \cup (\succ_{T_1} \cap \succ_{T_2})^c \\
&= \{(a_2, a_4), (a_2, a_5), (a_1, a_3), (a_1, a_5), (a_1, a_1), (a_2, a_2), (a_3, a_3), (a_4, a_4), \\
&\quad (a_5, a_5), (a_4, a_2), (a_5, a_2), (a_3, a_1), (a_5, a_1)\}, \\
Q^- &= (\succ_{T_1} \cap \prec_{T_2}) \cup (\succ_{T_1} \cap \prec_{T_2})^c \\
&= \{(a_1, a_2), (a_3, a_4), (a_2, a_1), (a_4, a_3)\}, \\
Q^0 &= (\sim_{T_1} \cap \succ_{T_2}) \cup (\sim_{T_1} \cap \succ_{T_2})^c \cup (\prec_{T_1} \cap \sim_{T_2}) \cup (\prec_{T_1} \cap \sim_{T_2})^c \\
&= \{(a_1, a_4), (a_3, a_5), (a_2, a_3), (a_4, a_5), (a_4, a_1), (a_5, a_3), (a_3, a_2), (a_5, a_4)\}.
\end{aligned}
$$

Therefore, the distance between T_1 and T_2 is:

$$dis(T_1, T_2) = 2|Q^-| + |Q^0| = 2 * 4 + 8 = 16.$$

3.2 A Cost-Sensitive Difference Measure

Another applicable measurement is motivated by DTRS models [30,31]. For a better understanding, we translate the terms of DTRS to fit the case of trilevel ranking. The costs in DTRS are induced by taking a particular action or making a decision, while the costs in trilevel rankings are produced by placements of alternatives. For example, given two trilevel rankings T_1 and T_2, we consider T_2 as a reorganization or rearrangement of T_1. Figure 3 and Table 2 jointly illustrate all of the nine cases in a rearrangement and the associated costs.

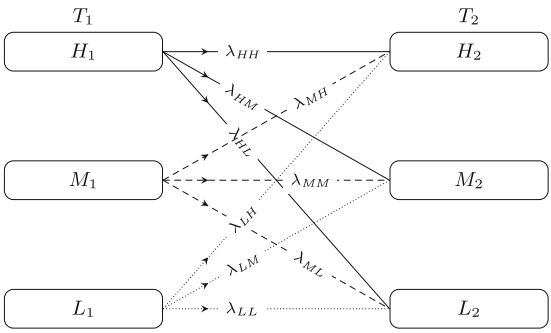

Fig. 3. The rearrangement of a trilevel ranking T_1 to T_2

The three solid arrow lines in Fig. 3 indicate that the alternatives in H_1 are placed to H_2, M_2, and L_2, respectively. Similarly, the dashed and dotted lines represent the corresponding placements. In Table 2, the rows denote the trilevel ranking T_1 and the columns represent the placements by T_2. For example, if an alternative a is placed in H_1 by T_1 and rearranged to M_2 by T_2, then it corresponds to the solid line from H_1 to M_2 in Fig. 3 and the relevant cost is λ_{HM} in Table 2.

Table 2. A cost matrix

T_1	T_2		
	H_2	M_2	L_2
H_1	λ_{HH}	λ_{HM}	λ_{HL}
M_1	λ_{MH}	λ_{MM}	λ_{ML}
L_1	λ_{LH}	λ_{LM}	λ_{LL}

With a given cost matrix, we define the cost-sensitive difference measure as the total cost of all the cases. The costs λ_{HH}, λ_{MM}, and λ_{LL} are assumed to 0, as they correspond to the scenarios where no difference exists. Thus, we define the cost-sensitive measure as follows.

Definition 7. *Given two trilevel rankings* $T_1 = \langle H_1, M_1, L_1\rangle$ *and* $T_2 = \langle H_2, M_2, L_2\rangle$*, the cost-sensitive measure is defined as:*

$$\begin{aligned} csm(T_1, T_2) =& \lambda_{HM}|H_1 \cap M_2| + \lambda_{HL}|H_1 \cap L_2| \\ &+ \lambda_{MH}|M_1 \cap H_2| + \lambda_{ML}|M_1 \cap L_2| \\ &+ \lambda_{LH}|L_1 \cap H_2| + \lambda_{LM}|L_1 \cap M_2|. \end{aligned} \tag{6}$$

The cost-sensitive measures involves directions in the rearrangement, as shown in Fig. 3. Thus, it is not symmetric, that is, we may not have $csm(T_1, T_2) = csm(T_2, T_1)$.

Example 4. We reuse the two trilevel rankings T_1 and T_2 given in Example 3. Suppose the cost matrix is given as:

$$cost = \begin{bmatrix} 0 & 5 & 9 \\ 3 & 0 & 3 \\ 7 & 4 & 0 \end{bmatrix}.$$

Then the cost-sensitive measure is computed as:

$$\begin{aligned} csm(T_1, T_2) =& 5|\{a_1\} \cap \{a_1, a_4\}| + 9|\{a_1\} \cap \{a_3, a_5\}| \\ &+ 3|\{a_2, a_3\} \cap \{a_2\}| + 3|\{a_2, a_3\} \cap \{a_3, a_5\}| \\ &+ 7|\{a_4, a_5\} \cap \{a_2\}| + 4|\{a_4, a_5\} \cap \{a_1, a_4\}| \\ =& 5 + 0 + 3 + 3 + 0 + 4 \\ =& 15. \end{aligned}$$

3.3 Heuristic Algorithms

We design two heuristic algorithms including a forward addition strategy and a backward deletion strategy. These algorithms can be operated by using either the distance-based measure or the cost-sensitive measure, depending on the specific requirements of the decision-maker. The step-by-step procedures of the two algorithms are described in Algorithms 1 and 2, respectively.

Algorithm 1. A deletion algorithm to compute approximate criterion reduct

Input: A multi-criteria decision-making table MCDMT $= \{A, C, p\}$;
A trilevel ranking T_C;
A threshold α.
Output: An approximate reduct R.
1: **let** $R = C$;
2: **while** True **do**
3: **for** $c \in R$ **do**
4: Calculate the difference between T_C and $T_{R-\{c\}}$;
5: Select a criterion c_{opt} that causes the minimum difference;
6: **end for**
7: **if** $Sim(T_{R-\{c_{\text{opt}}\}}, T_C) \geqslant \alpha$ **then**
8: **let** $R = R - \{c_{\text{opt}}\}$;
9: **else**
10: **break**;
11: **end if**
12: **end while**
13: **return** an approximate reduct R.

Algorithm 2. An addition algorithm to compute approximate criterion reduct

Input: A multi-criteria decision-making table MCDMT $= \{A, C, p\}$;
A trilevel ranking T_C;
A threshold α.
Output: An approximate reduct R.
1: **let** $R = \{\}$;
2: **while** $Sim(T_R, T_C) < \alpha$ **do**
3: **for** $c \in (C - R)$ **do**
4: Calculate the difference between T_C and $T_{R\cup\{c\}}$;
5: Select a criterion c_{opt} that attains the minimum difference;
6: **end for**
7: let $R = R \cup \{c_{\text{opt}}\}$;
8: **end while**
9: **return** an approximate reduct R.

In deletion algorithm, we start R with the criterion set C and delete criteria. During each pass of the loop, we look for an optimal criterion in R whose removal will cause minimum difference. We recursively find out and remove such

an optimal criterion c_{opt} from R until it cannot be reduced anymore, that is, further reduction of a single criterion will break the sufficiency condition. The addition algorithm is a reversed procedure, where R begins with an empty set. The algorithm continually adds an optimal criterion c_{opt}, whose addition into R attains the minimal difference from the ranking given by C. The process repeats until the reduct satisfies decision-maker's requirement.

4 Experimental Results

We examine the two algorithms with five practical datasets (taken from [1,2,6]). Table 3 summarises the features of the five datasets, including the name of dataset and the number of criteria and alternatives.

Table 3. The descriptions of datasets

Dataset ID	Name	Number of criteria	Number of alternatives
D1	Quake	4	2178
D2	City-Ranking	6	216
D3	Winequality-Red	11	1599
D4	Winequality-White	11	4898
D5	Pollution	16	60

Table 4 shows the final results obtained from the experiments of both the addition and deletion algorithms, utilizing both the distance-based measure and the cost-sensitive measure. For the cost-sensitive measure, we opt for the following three cost matrices:

$$cost_1 = \begin{bmatrix} 0 & 200 & 3500 \\ 1000 & 0 & 200 \\ 3000 & 200 & 0 \end{bmatrix}, cost_2 = \begin{bmatrix} 0 & 150 & 200 \\ 250 & 0 & 100 \\ 300 & 2000 & 0 \end{bmatrix}, cost_3 = \begin{bmatrix} 0 & 52 & 401 \\ 16 & 0 & 1737 \\ 13 & 25 & 0 \end{bmatrix}.$$

We choose 20%/30%/50% as the ratio of three levels and set a threshold of $\alpha = 0.85$ for these experiments. Table 4 records the size of each approximate criterion reduct, as well as its final SRCC. This coefficient is calculated by comparing T_R to T_C. These results provide a relatively comprehensive view of the performance and effectiveness of the proposed algorithms and measures under various conditions. The experiments of the two algorithms produce different reducts, indicating the distinct nature of each approach. For example, when employing the deletion strategy with the distance measure in Dataset D5, the final reduct contains 10 criteria. In contrast, the addition strategy with the same distance function leads to a reduct consisting of only 3 criteria. When applying the algorithms with cost-sensitive measure, different cost matrices produce different sizes of reducts, such as 11 and 10 for deletion and 3, 4, and 5 for addition.

Table 4. The performance of proposed algorithms ($\langle 2:3:5 \rangle$, $\alpha = 0.85$)

Dataset ID	Deletion Algorithm								Addition Algorithm							
	dis		csm 1		csm 2		csm 3		dis		csm 1		csm 2		csm 3	
	Size	SRCC	Size	SRCC	Size	SRCC	Size	SRCC	Size	SRCC	Size	SRCC	Size	SRCC	Size	SRCC
D1	3	0.8725	3	0.8725	3	0.8725	3	0.8725	3	0.8725	3	0.8725	3	0.8725	3	0.8725
D2	5	0.9247	5	0.9247	5	0.9247	5	0.9247	5	0.8578	5	0.8578	5	0.8532	5	0.8532
D3	8	0.8744	8	0.8715	8	0.8744	8	0.8744	6	0.8561	6	0.8561	9	0.8509	7	0.8801
D4	7	0.8805	7	0.8805	7	0.8805	7	0.8805	7	0.8805	7	0.8805	7	0.8805	7	0.8805
D5	10	0.8708	11	0.9238	10	0.8708	10	0.8708	3	0.8560	3	0.8560	4	0.8792	5	0.8560

To further show the performance of proposed methods, we visualize their applications on datasets D3 and D4. For both datasets, we execute the deletion and addition algorithms for five iterations. The intermediate results at each iteration step are illustrated in Fig. 4 for Dataset D3 and in Fig. 5 for Dataset D4.

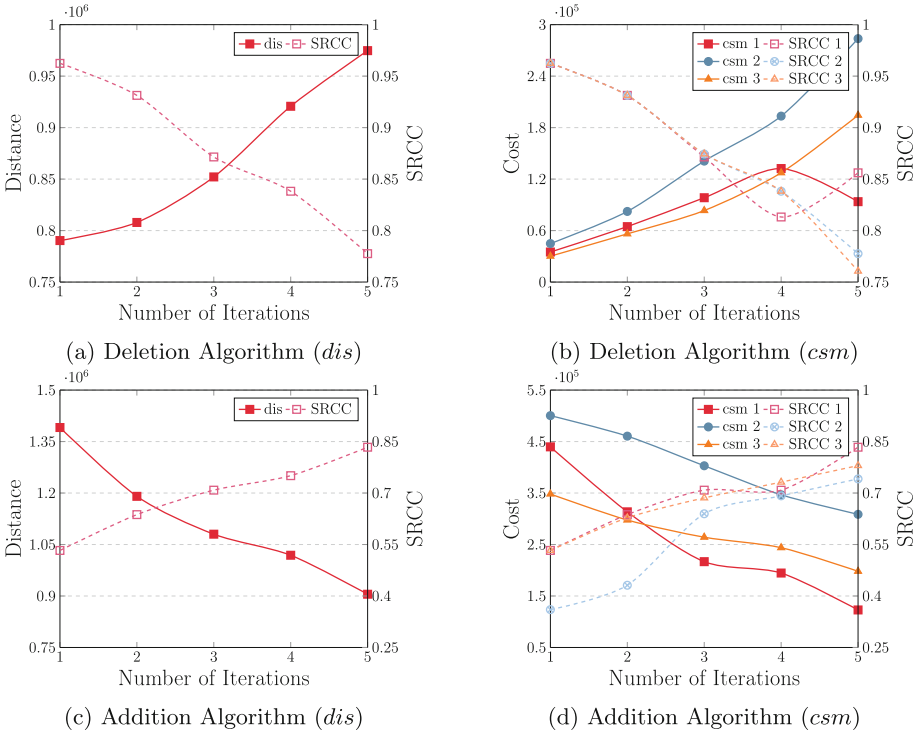

(a) Deletion Algorithm (*dis*)

(b) Deletion Algorithm (*csm*)

(c) Addition Algorithm (*dis*)

(d) Addition Algorithm (*csm*)

Fig. 4. Iterative process in Dataset D3

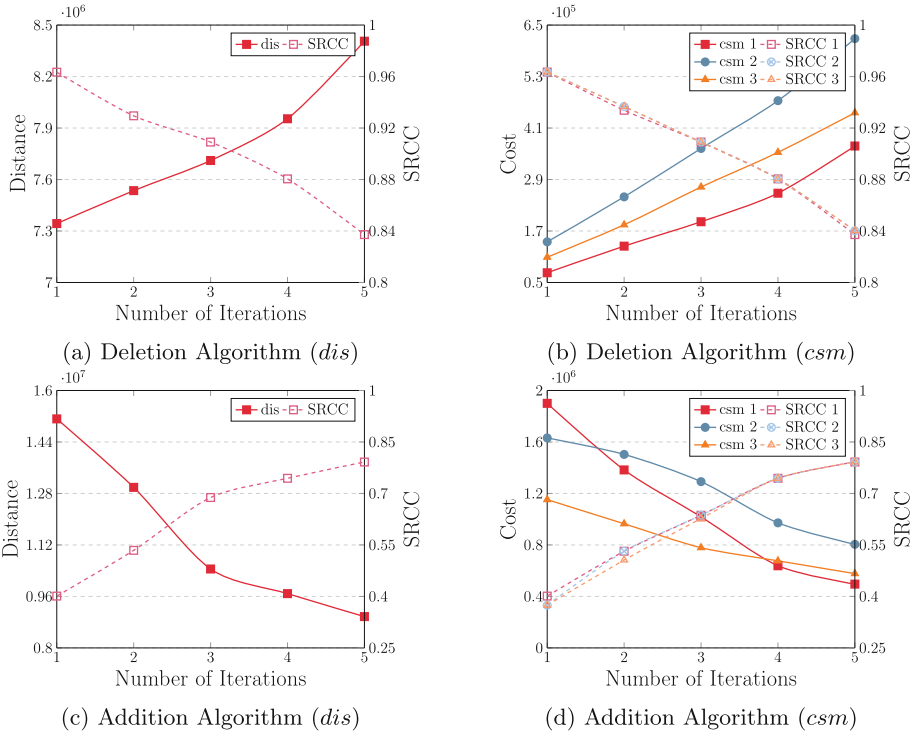

(a) Deletion Algorithm (*dis*)

(b) Deletion Algorithm (*csm*)

(c) Addition Algorithm (*dis*)

(d) Addition Algorithm (*csm*)

Fig. 5. Iterative process in Dataset D4

Figure 4 and 5 present insightful trends in both strategies. In the deletion strategy, we observe that as the distance or cost increases, there is a corresponding decrease in SRCC. On the other hand, an inverse trend is evident in the addition algorithm. These visualizations provide a clear view of the iterative progression and comparative effectiveness of the different measures and strategies utilized in our study.

In addition, we expand our analysis by appending three combinations of ratios for the three levels and thresholds. These combinations are designed to assess how different distributions of decision alternatives and threshold levels affect the performance and robustness of our models. As detailed in the following, Table 5 presents the results for a ratio of 2:3:5 with a threshold α of 0.75, Table 6 displays findings for a ratio of 1:2:7 and $\alpha = 0.80$, and Table 7 shows the results when the ratio is set to 2:2:6 and the threshold is 0.75. These additional experiments demonstrate the adaptability of our proposed methods under different trilevel rankings and thresholds.

Table 5. The performance of proposed algorithms ($\langle 2:3:5\rangle$, $\alpha = 0.75$)

Dataset ID	Deletion Algorithm								Addition Algorithm							
	dis		csm 1		csm 2		csm 3		dis		csm 1		csm 2		csm 3	
	Size	SRCC	Size	SRCC	Size	SRCC	Size	SRCC	Size	SRCC	Size	SRCC	Size	SRCC	Size	SRCC
D1	3	0.8725	3	0.8725	3	0.8725	3	0.8725	3	0.8725	3	0.8725	3	0.8725	3	0.8725
D2	3	0.8096	3	0.8096	3	0.8096	3	0.8096	3	0.7991	3	0.7678	3	0.7991	3	0.7991
D3	4	0.7506	5	0.8335	4	0.7506	5	0.7537	4	0.7506	5	0.8335	6	0.7827	5	0.7800
D4	5	0.7916	5	0.7916	5	0.7916	5	0.7916	5	0.7916	5	0.7916	5	0.7916	5	0.7916
D5	5	0.8476	3	0.7500	5	0.8476	9	0.8321	2	0.8024	2	0.7645	3	0.8411	2	0.8024

Table 6. The performance of proposed algorithms ($\langle 1:2:7\rangle$, $\alpha = 0.80$)

Dataset ID	Deletion Algorithm								Addition Algorithm							
	dis		csm 1		csm 2		csm 3		dis		csm 1		csm 2		csm 3	
	Size	SRCC	Size	SRCC	Size	SRCC	Size	SRCC	Size	SRCC	Size	SRCC	Size	SRCC	Size	SRCC
D1	3	0.8250	4	1.0000	3	0.8250	3	0.8250	3	0.8250	4	1.0000	4	1.0000	3	0.8250
D2	4	0.8021	4	0.8021	4	0.8021	4	0.8021	4	0.8192	4	0.8192	4	0.8114	4	0.8114
D3	8	0.8476	5	0.8086	7	0.8091	7	0.8091	5	0.8086	5	0.8086	7	0.8247	5	0.8086
D4	6	0.8337	6	0.8337	6	0.8370	6	0.8370	6	0.8337	6	0.8054	6	0.8337	6	0.8370
D5	8	0.9236	5	0.8056	8	0.9236	8	0.9236	4	0.8750	5	0.8056	5	0.8333	3	0.8056

Table 7. The performance of proposed algorithms ($\langle 2:2:6\rangle$, $\alpha = 0.75$)

Dataset ID	Deletion Algorithm								Addition Algorithm							
	dis		csm 1		csm 2		csm 3		dis		csm 1		csm 2		csm 3	
	Size	SRCC	Size	SRCC	Size	SRCC	Size	SRCC	Size	SRCC	Size	SRCC	Size	SRCC	Size	SRCC
D1	3	0.8603	3	0.8603	3	0.8603	3	0.8603	3	0.8603	3	0.8603	3	0.7576	3	0.8603
D2	4	0.8198	4	0.8198	4	0.8198	4	0.7933	3	0.7907	3	0.7907	4	0.8079	3	0.7907
D3	4	0.7816	4	0.7816	4	0.7816	5	0.7507	4	0.7816	4	0.7679	6	0.7972	6	0.7972
D4	4	0.7512	4	0.7512	4	0.7512	4	0.7512	4	0.7512	4	0.7512	5	0.7881	4	0.7512
D5	3	0.7500	3	0.7604	8	0.7917	9	0.8854	4	0.7500	3	0.7604	3	0.8021	3	0.7917

5 Conclusion

This paper studies the approximate criterion reduction in MCDM problems with trilevel rankings. Trilevel rankings ignore the preferences among alternatives at the same level and emphasize the orderings across levels. Taking this feature into consideration, we propose a formal definition of approximate criterion reducts in trilevel rankings. To concretize approximate criterion reducts, we present a distance-based measure and a cost-sensitive measure to evaluate the difference between two trilevel rankings. Subsequently, two heuristic algorithms of deletion and addition are developed by adopting either measure as the heuristic function. Finally, we conduct a series of experiments, including testing different combinations of strategies, heuristic functions, and cost matrices. The outcomes demonstrate that these measures effectively serve for finding the optimal approximate criterion reducts in trilevel rankings.

Future research will focus on exploring additional difference measures for trilevel rankings. There may be a potential in integrating our proposed measures with machine learning techniques. Such an integration may be developed as new approaches to deriving trilevel rankings.

References

1. Alcalá-Fdez, J., et al.: KEEL: a software tool to assess evolutionary algorithms for data mining problems. Soft. Comput. **13**, 307–318 (2009)
2. Alcalá-Fdez, J., et al.: KEEL data-mining software tool: data set repository, integration of algorithms and experimental analysis framework. J. Multiple-Valued Logic Soft Comput. **17**, 255–287 (2011)
3. Bradford, S.C.: Sources of information on specific subjects. Engineering **137**, 85–86 (1934)
4. Chen, Y., Li, K.W., Kilgour, D.M., Hipel, K.W.: A case-based distance model for multiple criteria ABC analysis. Comput. Oper. Res. **35**, 776–796 (2008)
5. Chen, Y., Li, K.W., Levy, J., Hipel, K.W., Kilgour, D.M.: A rough set approach to multiple criteria ABC analysis. In: Peters, J.F., Skowron, A. (eds.) Transactions on Rough Sets VIII. LNCS, vol. 5084, pp. 35–52. Springer, Heidelberg (2008). https://doi.org/10.1007/978-3-540-85064-9_3
6. Cortez, P., Cerdeira, A., Almeida F., Matos, T., Reis, J.: Wine quality. UCI Machine Learning Repository (2009)
7. Douissa, M.R., Jabeur, K.: A non-compensatory classification approach for multi-criteria ABC analysis. Soft. Comput. **24**, 9526–9556 (2020)
8. Du, J.L., Liu, S.F., Liu, Y.: A novel grey multi-criteria three-way decisions model and its application. Comput. Ind. Eng. **158**, Article 107405 (2021)
9. Flores, B.E., Whybark, D.C.: Multiple criteria ABC analysis. Int. J. Oper. Prod. Manag. **6**(3), 38–46 (1986)
10. Flores, B.E., Whybard, D.C.: Implementing multiple criteria ABC analysis. J. Oper. Manag. **7**, 79–85 (1987)
11. Gao, C., Wang, Z.C., Zhou, J.: Three-way approximate reduct based on information-theoretic measure. Int. J. Approximate Reasoning **142**, 324–337 (2022)
12. Jia, X.Y., Shang, L., Zhou, B., Yao, Y.Y.: Generalized attribute reduct in rough set theory. Knowl.-Based Syst. **91**, 204–218 (2016)
13. Kemeny, J.G., Snell, J.L.: Mathematical Models in the Social Sciences. Blaisdell, New York (1962)
14. Liang, D.C., Xu, Z.S., Liu, D., Wu, Y.: Method for three-way decisions using ideal TOPSIS solutions at Pythagorean fuzzy information. Inf. Sci. **435**, 282–295 (2018)
15. Liu, K.Y., Yang, X.B., Fujita, H., Liu, D., Yang, X., Qian, Y.H.: An efficient selector for multi-granularity attribute reduction. Inf. Sci. **505**, 457–472 (2019)
16. Ng, W.L.: A simple classifier for multiple criteria ABC analysis. Eur. J. Oper. Res. **177**, 344–353 (2007)
17. Pawlak, Z.: Rough sets. Int. J. Comput. Inform. Sci. **11**, 341–356 (1982)
18. Qian, Y.H., Liang, J.Y., Pedrycz, W., Dang, C.Y.: Positive approximation: an accelerator for attribute reduction in rough set theory. Artif. Intell. **174**, 597–618 (2010)
19. Shenton, A.K., Hay-Gibson, N.V.: Bradford's law and its relevance to researchers. Educ. Inf. **27**, 217–230 (2009)

20. Shi, C.J., Wang, Z., Wei, L., Yao, Y.Y.: Three-way approximate criterion reduction in multi-criteria decision analysis. In: Yao, J., Fujita, H., Yue, X., Miao, D., Grzymala-Busse, J., Li, F. (eds.) IJCRS 2022. LNCS, vol. 13633, pp. 289–303. Springer, Cham (2022). https://doi.org/10.1007/978-3-031-21244-4_22
21. Shi, C.J., Yao, Y.Y.: Trilevel multi-criteria decision analysis based on three-way decision. In: Intelligence Science III, IFIP Advances in Information and Communication Technology (IFIPAICT), vol. 623, pp. 115–124 (2021)
22. Wang, J., Miao, D.Q.: Analysis on attribute reduction strategies of rough set. J. Comput. Sci. Technol. **13**, 189–192 (1998)
23. Wang, Z., Shi, C.J., Wei, L., Yao, Y.Y.: Tri-granularity attribute reduction of three-way concept lattices. Knowl.-Based Syst. **276**, 110762 (2023)
24. Xu, W.H., Zhang, X.Y., Zhong, J.M., Zhang, W.X.: Attribute reduction in ordered information systems based on evidence theory. Knowl. Inf. Syst. **25**, 169–184 (2010)
25. Yan, K.Y., Yang, H.L., Guo, Z.L.: A novel three-way classification and ranking approach based on regret theory and TOPSIS. Inf. Sci. **666**, 120443 (2024)
26. Yao, Y.Y.: Measuring information retrieval effectiveness based on user preferences on documents. J. Am. Soc. Inf. Sci. **46**, 133–145 (1995)
27. Yao, Y.Y.: Tri-level thinking: models of three-way decision. Int. J. Mach. Learn. Cybern. **11**, 947–959 (2020)
28. Yao, Y.Y.: The Dao of three-way decision and three-world thinking. Int. J. Approximate Reasoning **162**, 109032 (2023)
29. Yao, Y., Shi, C.: 3RD: a multi-criteria decision-making method based on three-way rankings. In: Ramanna, S., Cornelis, C., Ciucci, D. (eds.) IJCRS 2021. LNCS (LNAI), vol. 12872, pp. 294–309. Springer, Cham (2021). https://doi.org/10.1007/978-3-030-87334-9_25
30. Yao, Y.Y., Wong, S.K.M.: A decision theoretic framework for approximating concepts. Int. J. Man Mach. Stud. **37**, 793–809 (1992)
31. Yao, Y.Y., Zhao, Y.: Attribute reduction in decision-theoretic rough set models. Inf. Sci. **178**, 3356–3373 (2008)
32. Ye, J., Zhan, J.M., Xu, Z.S.: A novel decision-making approach based on three-way decisions in fuzzy information systems. Inf. Sci. **541**, 362–390 (2020)
33. Yu, M.C.: Multi-criteria ABC analysis using artificial-intelligence-based classification techniques. Expert Syst. Appl. **38**, 3416–3421 (2011)
34. Zhan, J.M., Jiang, H.B., Yao, Y.Y.: Three-way multiattribute decision-making based on outranking relations. IEEE Trans. Fuzzy Syst. **29**, 2844–2858 (2021)
35. Zhang, K., Dai, J.H., Zhan, J.M.: A new classification and ranking decision method based on three-way decision theory and TOPSIS models. Inf. Sci. **568**, 54–85 (2021)
36. Zhang, X.Y., Yao, Y.Y.: Tri-level attribute reduction in rough set theory. Expert Syst. Appl. **190**, 116187 (2022)

New Models of Three-Way Conflict Analysis Based on Decision-Theoretic Rough Sets

Ping Liu, Qimei Xiao, Huiying Yu, and Guangming Lang(✉)

School of Mathematics and Statistics, Changsha University of Science and Technology, Changsha 410114, Hunan, People's Republic of China
langguangming1984@126.com

Abstract. Conflict is widespread in society, and trisecting an agent set is a crucial research direction in three-way conflict analysis. In practice, the varying risk preferences among decision-makers lead to diverse trisections of an agent set in similar circumstances. In this paper, we consider decision-makers' risk preferences and propose novel models of three-way conflict. Initially, we divide a set of issues into two disjoint subsets and utilize information entropy to compute issues' weights. Then, we design alliance measures regarding an individual issue through the transition probability function. Based on the issues' weights and alliance measures, we propose alliance probabilities between two agents. Additionally, we present risk-preferred, risk-averse, and risk-neutral decisions with the relative utility function. Finally, we design an algorithm to derive rules for three-way conflict analysis and demonstrate how to utilize the proposed model for decision-making through an example.

Keywords: Decision-theoretic rough sets · Three-way conflict analysis · Three-way decisions · Ranking

1 Introduction

Three-way decisions was introduced by Yao [1] in 2010. It divides a set into three mutually exclusive regions using certain strategies, and provides effective tools for addressing uncertainty problems. This theory has garnered increasing attention from scholars and has been widely investigated in both theoretical and applied aspects such as three-way clustering [2], sequential three-way decisions [3,4], three-way decisions with decision-theoretic rough sets (DTRSs) [5–10], three-way decisions with concept analysis [11,12]. Among them, three-way decisions with DTRSs is an important research direction, which calculates two thresholds by minimizing decision costs based on Bayesian theory, and partitions objects into positive regions, negative regions, and boundary regions. Recently, Xu et al. [13] provided the concepts of ranking and reference tuples for two-valued information table, and divided a set of objects into three disjoint parts based on matching functions regarding multiple attributes. Xu et al. [14] introduced a generalized three-way decisions model based on ranking and reference tuples.

Conflict is prevalent in society. How to study the nature of conflict and how to resolve conflicts are crucial topics in social life. Initially, Pawlak [15] established

M. Hu et al. (Eds.): IJCRS 2024, LNAI 14840, pp. 181–195, 2024.
https://doi.org/10.1007/978-3-031-65668-2_13

alliance, neutrality, and conflict relations between two agents with auxiliary functions, and investigated the conflict problems with rough set theory and graph theory. Subsequently, conflict analysis has attracted increasing attention from scholars. Some studies [16–24] have integrated conflict analysis with three-way decisions. For instance, Lang et al. [17] used decision-theoretic rough sets to calculate two thresholds for conflict analysis and discussed how to construct probabilistic conflict sets, neutral sets, and alliance sets in dynamic three-valued situation tables. Liu et al. [22] introduced alliance and conflict measures by considering weights of issues, and developed models of three-way conflict analysis with ideas of rankings and reference tuples.

In three-way conflict analysis, the loss function and conditional probability are two crucial topics to study conflict problems. The loss function is typically used to measure risk, and quantifies the losses incurred by agents assigned to alliance, neutral, or conflict sets. However, in some situations, decision-makers prioritize the utility derived from decision actions. Hence, some studies [25,26] used utility functions instead of loss functions. Recently, Zhan et al. [27] introduced the concept of relative utility function and provided a formula of calculating the relative utility value. The relative utility function can decrease errors during the decision-making process. Inspired by this point, we propose a new relative utility function that simultaneously takes into account the risk preferences of experts. In practical situations, decision-makers with different risk preferences may make different decisions in the same context, and a three-way conflict model must consider various risk preferences. There are several methods [28–30,32] for calculating the conditional probabilities. For example, Liang et al. [29] adopted the relative closenesses of the TOPSIS (Technique for Order Preference by Similarity to Ideal Solution) method to replace the conditional probabilities. Liang et al. [30] utilized measures of dual hesitant fuzzy entropy and cross-entropy to determine conditional probability. Based on the concept of ranking and reference tuples, we propose a novel approach to computing conditional probability. By utilizing the concepts of ranking and reference tuples, we aim to partition issues into two disjoint subsets based on their priorities. Subsequently, we calculate the conditional probability by the product of alliance measures regarding two issue subsets. This approach enables us to examine the relationship between two agents from two different perspectives. The contributions are briefly summarized as follows.

(1) We divide a set of issues into two disjoint subsets and introduce a novel method to compute issues' weights by employing information entropy. Then, we introduce alliance measures regarding an individual issue through a transition probability function. Based on the issues' weights and alliance measures, we propose alliance probabilities for three-way conflict analysis.
(2) We introduce a novel relative utility function, and determine two thresholds by maximizing the relative utility under decision-making behavior. Based on decision-makers with different risk preferences, we propose risk-preferred, risk-averse, and risk-neutral decisions for three-way conflict analysis.
(3) We design an algorithm to derive rules for three-way conflict analysis and demonstrate how to utilize the proposed model for decision-making through an example.

The rest of this paper is organized as follows: in Sect. 2, we review the fundamental concepts of three-way decisions with ranking and reference tuples, as well as the

concept of three-way decisions with decision-theoretic rough sets. Section 3 develops new three-way conflict models based on decision-theoretic rough sets. Section 4 demonstrates how to apply the proposed model to derive decision rules. Finally, Sect. 5 summarizes the work presented in this paper.

2 Preliminaries

In this section, we recall three-way decisions with ranking and references, and decision-theoretic rough sets.

2.1 Three-Way Decisions with Ranking and References

Definition 1. *(Pawlak [15], 1984) Let $S = (U, C, V, f)$ be an information table, where $U = \{x_1, x_2, \ldots, x_n\}$ is a non-empty finite set of objects, $C = \{c_1, c_2, \ldots, c_m\}$ is a non-empty finite set of attributes, $V = \bigcup\{V_c \mid c \in C\}$. Here, V_c represents the set of values of attribute c on all objects, and f is a function from $U \times C$ to V.*

We term information tables containing two attribute values as two-valued information tables, and most three-way decision models with ranking and reference tuples are typically designed for two-valued information tables.

Definition 2. *(Xu et al. [14], 2022) Let C represents a non-empty finite set of attributes. A ranking order $\prec_r$ over C divides C into two disjoint subsets C' and C'', where $C = \{C', C''\}$ and $C' \prec_r C''$. Here, C' and C'' denote the attribute sets in rank 1 and rank 2, respectively.*

We can partition a set of attributes into two disjoint subsets based on their ranking order, the ranking order is determined based on the importance of attributes or the preferences of decision-makers.

Definition 3. *(Xu et al. [14], 2022) Let $C = \{c_1, c_2, \ldots, c_m\}$ and $\prec_r$ be a ranking order of C. An m-tuple $\mathbf{x_r} = (f(x_r, c_1), f(x_r, c_2), \ldots, f(x_r, c_m))$ is a reference tuple and it satisfies*: (1) $f(x_r, c_k) \in \{0, 1\}$; (2) $f(x_r, c_i) = f(x_r, c_j)$ *when* $c_i \in C' \wedge c_j \in C'$ *or* $c_i \in C'' \wedge c_j \in C''$, *where* $k, i, j \in \{1, 2, \ldots, m\}$.

Definition 4. *(Xu et al. [14], 2022) Let $S = (U, C, V, f)$ be an information table, a ranking order $\prec_r$ divides the set C into two disjoint subsets C' and C'', a reference tuple $\mathbf{x_r} = (f(x_r, c_1), f(x_r, c_2), \ldots, f(x_r, c_m))$. Then the positive, negative and boundary regions with respect to $\prec_r$ and $\mathbf{x_r}$ are defined by:*

$$POS_{(\alpha,\beta)}(U) = \{x \in U \mid M_{C'}(x, x_r) \geq \alpha \wedge M_{C''}(x, x_r) > \beta\}, \tag{1}$$

$$NEG_{(\alpha,\beta)}(U) = \{x \in U \mid M_{C'}(x, x_r) < \alpha \wedge M_{C''}(x, x_r) \leq \beta\}, \tag{2}$$

$$\begin{aligned} BND_{(\alpha,\beta)}(U) = {} & \{x \in U \mid M_{C'}(x, x_r) \geq \alpha \wedge M_{C''}(x, x_r) \leq \beta\} \\ & \vee \{x \in U \mid M_{C'}(x, x_r) < \alpha \wedge M_{C''}(x, x_r) > \beta\}, \end{aligned} \tag{3}$$

where

$$M_{C'}(x, x_r) = \frac{\sum_{c_i \in C'} m_{c_i}(x, x_r)}{|C'|}, \tag{4}$$

$$M_{C''}(x, x_r) = \frac{\sum_{c_i \in C''} m_{c_i}(x, x_r)}{|C''|}, \tag{5}$$

$$m_{c_i}(x, x_r) = \begin{cases} 1, & \text{if } f(x, c_i) = f(x_r, c_i), \\ 0, & \text{if } f(x, c_i) \neq f(x_r, c_i). \end{cases} \tag{6}$$

The value of $M_{C'}(x, x_r)$ denotes a matching degree between $x \in U$ and x_r in rank 1, while the value of $M_{C''}(x, x_r)$ denotes a matching degree between x and x_r in rank 2.

2.2 Three-Way Decisions with Decision-Theoretic Rough Sets

Definition 5. *(Yao [31], 2008) Let $S = (U, A)$ be an information system, where $0 \leq \beta \leq \alpha \leq 1$. The probabilistic positive, boundary, and negative regions $POS_{(\alpha,\beta)}(X)$, $BND_{(\alpha,\beta)}(X)$, and $NEG_{(\alpha,\beta)}(X)$ of $X \subseteq U$ are defined by:*

$$\begin{aligned} POS_{(\alpha,\beta)}(X) &= \{x \in U \mid P(X \mid [x]) \geq \alpha\}, \\ BND_{(\alpha,\beta)}(X) &= \{x \in U \mid \beta < P(X \mid [x]) < \alpha\}, \\ NEG_{(\alpha,\beta)}(X) &= \{x \in U \mid P(X \mid [x]) \leq \beta\}. \end{aligned} \tag{7}$$

Hence, decision-theoretic rough set model was used to determine the thresholds α and β. This model involves two states $\Omega = \{X, \neg X\}$ and three actions $\mathscr{A} = \{a_P, a_B, a_N\}$, where X and $\neg X$ denote an object's presence and absence from set X, respectively. The actions a_P, a_B, and a_N classify an object x into the positive, boundary, and negative regions $\mathrm{POS}_{(\alpha,\beta)}(X)$, $BND_{(\alpha,\beta)}(X)$, and $NEG_{(\alpha,\beta)}(X)$ respectively. λ_{PP}, λ_{BP}, and λ_{NP} represent the losses incurred when taking actions a_P, a_B, and a_N, respectively, for an object belonging to X, while λ_{PN}, λ_{BN}, and λ_{NN} represent the losses when taking actions a_P, a_B, and a_N, respectively, for an object not belonging to X.

The expected losses $R(a_P \mid [x])$, $R(a_B \mid [x])$, and $R(a_N \mid [x])$ associated with each individual action for an object x are as follows:

$$\begin{aligned} R(a_P \mid [x]) &= \lambda_{PP} P(X \mid [x]) + \lambda_{PN} P(\neg X \mid [x]), \\ R(a_B \mid [x]) &= \lambda_{BP} P(X \mid [x]) + \lambda_{BN} P(\neg X \mid [x]), \\ R(a_N \mid [x]) &= \lambda_{NP} P(X \mid [x]) + \lambda_{NN} P(\neg X \mid [x]). \end{aligned} \tag{8}$$

The Bayesian decision procedure suggests the following minimum-cost decision rules:

Rule 1 : If $R(a_P \mid [x]) \leq R(a_B \mid [x])$ and $R(a_P \mid [x]) \leq R(a_N \mid [x])$, then $x \in POS_{(\alpha,\beta)}(X)$,

Rule 2 : If $R(a_B \mid [x]) \leq R(a_P \mid [x])$ and $R(a_B \mid [x]) \leq R(a_N \mid [x])$, then $x \in BND_{(\alpha,\beta)}(X)$,

Rule 3 : If $R(a_N \mid [x]) \leq R(a_P \mid [x])$ and $R(a_N \mid [x]) \leq R(a_B \mid [x])$, then $x \in NEG_{(\alpha,\beta)}(X)$.

Assuming $\lambda_{PP} \leq \lambda_{BP} \leq \lambda_{NP}$ and $\lambda_{NN} \leq \lambda_{BN} \leq \lambda_{PN}$, and considering the fact that $P(X \mid [x]) + P(\neg X \mid [x]) = 1$, the *Rule* 1, *Rule* 2, and *Rule* 3 can be simplified as follows:

Rule 1 : If $P(X \mid [x]) \geq \alpha$ and $P(X \mid [x]) \geq \gamma$, then $x \in \mathrm{POS}_{(\alpha,\beta)}(X)$,

Rule 2 : If $P(X \mid [x]) < \alpha$ and $P(X \mid [x]) > \beta$, then $x \in BND_{(\alpha,\beta)}(X)$,

Rule 3 : If $P(X \mid [x]) \leq \beta$ and $P(X \mid [x]) \leq \gamma$, then $x \in NEG_{(\alpha,\beta)}(X)$, where

$$\begin{aligned} \alpha &= \frac{\lambda_{PN} - \lambda_{BN}}{\lambda_{PN} - \lambda_{BN} + \lambda_{BP} - \lambda_{PP}}, \\ \beta &= \frac{\lambda_{BN} - \lambda_{NN}}{\lambda_{BN} - \lambda_{NN} + \lambda_{NP} - \lambda_{BP}}, \\ \gamma &= \frac{\lambda_{PN} - \lambda_{NN}}{\lambda_{PN} - \lambda_{NN} + \lambda_{NP} - \lambda_{PP}}. \end{aligned} \tag{9}$$

3 New Models of Three-Way Conflict Analysis Based on Decision-Theoretic Rough Sets

In this section, we provide three-way conflict analysis models based on decision-theoretic rough sets.

Definition 6. *(Pawlak [33], 1988) Let $S = (A, I, r)$ be a three-valued situation table, where $A = \{a_1, a_2, \ldots, a_n\}$ is a non-empty finite set of agents, $I = \{i_1, i_2, \ldots, i_m\}$ is a non-empty finite set of issues, the function $r : A \times I \longrightarrow \{-1, 0, +1\}$, where $r(a, i) = +1$ means that the agent a is positive on the issue i, $r(a, i) = -1$ means that the agent a is negative on the issue i, $r(a, i) = 0$ means that the agent a is neutral on the issue i.*

Definition 7. *Let $S = (A, I, r)$ be a three-valued situation table, a ranking order $\prec_r$ over I divides I into two disjoint subsets I' and I'' such that $I = I' \cup I''$, and $\omega_i^{\#}$ represents the weight of issue i such that $\sum_{i \in I^{\#}} \omega_i^{\#} = 1$ and $0 \leq \omega_i^{\#} \leq 1$ for $I^{\#} \in \{I', I''\}$. The weight $\omega_i^{\#}$ is defined as follows:*

$$\omega_i^{\#} = \frac{H(i)}{\sum_{i \in I^{\#}} H(i)}, \tag{10}$$

where

$$H(i) = -\sum_{h \in \{+1, 0, -1\}} [P(r(a, i) = h) \cdot \log_2 P(r(a, i) = h)]. \tag{11}$$

The value $P(r(a, i) = +1)$ represents the probability of an agent a that takes the positive attitude $+1$ on issue i, while the value $P(r(a, i) = 0)$ represents the probability of an agent a that takes the neutral attitude 0 on issue i, and the value $P(r(a, i) = -1)$ represents the probability of an agent a that takes the negative attitude -1 on issue i. Here, $H(i)$ denotes the entropy of issue i, which measures the uncertainty of agents' attitudes on issue i.

Definition 8. *Let $S = (A, I, r)$ be a three-valued situation table, where a ranking order $\prec_r$ over I divides I into two disjoint subsets I' and I'' such that $I = I' \cup I''$. For any*

$a_i, a_j \in A$, the alliance measure $M^{'}(a_i, a_j)$ between agents a_i and a_j in rank 1 and the alliance measure $M^{''}(a_i, a_j)$ in rank 2 are defined as follows:

$$M^{'}(a_i, a_j) = \sum_{i \in I^{'}} [\omega_i^{'} \cdot m(a_i, a_j)], \tag{12}$$

$$M^{''}(a_i, a_j) = \sum_{i \in I^{''}} [\omega_i^{''} \cdot m(a_i, a_j)], \tag{13}$$

where

$$m(a_i, a_j) = 1 - \frac{\left| r(a_i, i) - r(a_j, i) \right|}{2}. \tag{14}$$

The values of $M^{'}(a_i, a_j)$ and $M^{''}(a_i, a_j)$ fall within the range of $[0, 1]$. We define $M(a_i, a_j) = M^{'}(a_i, a_j) \cdot M^{''}(a_i, a_j)$, which represents the likelihood of agents a_i and a_j. That is, a larger value of $M(a_i, a_j)$ implies a higher alliance probability between a_i and a_j, while a smaller value suggests a lower alliance probability between them.

Definition 9. *Let $S = (A, I, r)$ be a three-valued situation table. For any $a_i, a_j \in A$, the alliance probability $P(a_i, a_j)$ between a_i and a_j is defined as follows:*

$$P(a_i, a_j) = \frac{\ln (R \cdot M(a_i, a_j) + 1)}{\ln (R + 1)}, \tag{15}$$

where the values of $M(a_i, a_j)$ fall within the range of $[0, 1]$, the values of $P(a_i, a_j)$ ranges from 0 to 1. The parameter R is adjustable, and appropriate probability levels can be explored by varying $R \in [1, \infty)$ in different scenarios, thereby avoiding situations where $M(a_i, a_j)$ values are too small and ensuring meaningful probability values.

Definition 10. *Suppose $S = (A, I, r)$ is a three-valued situation table, the relative utility functions $\tilde{u}_{AA}$, $\tilde{u}_{NA}$, $\tilde{u}_{CA}$, $\tilde{u}_{CC}$, $\tilde{u}_{NC}$,and $\tilde{u}_{AC}$ are defined by:*

$$\tilde{u}_{AA} = u_{AA} - u_{CA}, \tag{16}$$

$$\tilde{u}_{NA} = u_{NA} - u_{CA}, \tag{17}$$

$$\tilde{u}_{CA} = u_{CA} - u_{CA} = 0, \tag{18}$$

$$\tilde{u}_{AC} = u_{AC} - u_{AC} = 0, \tag{19}$$

$$\tilde{u}_{NC} = u_{NC} - u_{AC}, \tag{20}$$

$$\tilde{u}_{CC} = u_{CC} - u_{AC}. \tag{21}$$

Assume $\tilde{u}_{NA} = k\tilde{u}_{AA}$, $\tilde{u}_{NC} = k\tilde{u}_{CC}$, *and* $k \in [0, 1]$, *then* $\tilde{\alpha}$, $\tilde{\beta}$, *and* $\tilde{\gamma}$ *can be represented as:*

$$\begin{aligned}\tilde{\alpha} &= \frac{k\tilde{u}_{CC}}{k\tilde{u}_{CC} + \tilde{u}_{AA} - k\tilde{u}_{AA}} \\ &= \frac{k\tilde{u}_{CC}}{k\tilde{u}_{CC} + (1-k)\tilde{u}_{AA}}, \end{aligned} \tag{22}$$

$$\begin{aligned}\tilde{\beta} &= \frac{\tilde{u}_{CC} - k\tilde{u}_{CC}}{\tilde{u}_{CC} - k\tilde{u}_{CC} + k\tilde{u}_{AA}} \\ &= \frac{(1-k)\tilde{u}_{CC}}{(1-k)\tilde{u}_{CC} + k\tilde{u}_{AA}}, \end{aligned} \tag{23}$$

$$\tilde{\gamma} = \frac{\tilde{u}_{CC}}{\tilde{u}_{CC} + \tilde{u}_{AA}}, \tag{24}$$

where $k \in [0, 1]$ serves as a utility pursuit coefficient, and indicates decision-makers' preference for non-deterministic choices. Based on the study [27], it can be inferred that $\tilde{\alpha}$, $\tilde{\beta}$, and $\tilde{\gamma}$ satisfy $\tilde{\alpha} > \tilde{\gamma} > \tilde{\beta}$ when $k \in (0.5, 1]$. Furthermore, the thresholds derived from the relative utility functions in Table 2 are equivalent to those obtained from the utility functions in Table 1. In Table 1, b_C, b_N, and b_A denote three actions in classifying agent a_j into $CO(a_i)$, $NE(a_i)$, and $AL(a_i)$, respectively; u_{CC}, u_{NC}, and u_{AC} represent the utility of taking actions b_C, b_N, and b_A, respectively, when the agent a_j belongs to $CO(a_i)(\neg\mathrm{T(C)})$; u_{CA}, u_{NA}, and u_{AA} represent the utility of taking actions b_C, b_N, and b_A, respectively, when the agent a_j belongs to $AL(a_i)(\mathrm{T(A)})$.

Table 1. Utility Functions

	T(A)	¬T(C)
b_A	u_{AA}	u_{AC}
b_N	u_{NA}	u_{NC}
b_C	u_{CA}	u_{CC}

Table 2. Relative Utility Functions

	T(A)	¬T(C)
b_A	$\tilde{u}_{AA}$	0
b_N	$\tilde{u}_{NA}$	$\tilde{u}_{NC}$
b_C	0	$\tilde{u}_{CC}$

Definition 11. *Let* $S = (A, I, r)$ *be a three-valued situation table. The formulas for the relative utility function* $\tilde{u}_{AA}$ *associated with adopting behavior* b_A *in the state* $T(A)$*, and the relative utility function* $\tilde{u}_{CC}$ *linked to the adoption of behavior* b_C *in the state* $\neg T(C)$*, can be formulated as follows:*

$$\tilde{u}_{AA} = \frac{1 - e^{-\theta\delta_{AA}}}{\theta}, \tag{25}$$

$$\tilde{u}_{CC} = \frac{1 - e^{-\theta\delta_{CC}}}{\theta}, \tag{26}$$

where $\theta \in (0, 1)$ stands for a risk aversion coefficient, the variable δ_{AA} and δ_{CC} represent the evaluation values of adopting behaviors b_A and b_C in the state $T(A)$ and $\neg T(C)$, respectively.

The values of $\tilde{\alpha}, \tilde{\beta}$, and $\tilde{\gamma}$ are determined solely by $k, \tilde{u}_{AA}$, and $\tilde{u}_{CC}$. Due to the inverse relationship between the risk aversion coefficient θ and the utility pursuit coefficient k, we set $k = 1 - \frac{\theta}{2}$, where $k \in (0.5, 1)$. By substituting Formulas (25)-(26), along with $k = 1 - \frac{\theta}{2}$, into Formulas (22)-(23), we obtain:

$$\tilde{\alpha} = \frac{1}{1 + \frac{\theta}{2-\theta} \cdot \frac{1-e^{-\theta\delta_{AA}}}{1-e^{-\theta\delta_{CC}}}}, \tag{27}$$

$$\tilde{\beta} = \frac{1}{1 + \frac{2-\theta}{\theta} \cdot \frac{1-e^{-\theta\delta_{AA}}}{1-e^{-\theta\delta_{CC}}}}. \tag{28}$$

From Formulas (27)-(28), it's apparent that the values of $\tilde{\alpha}$ and $\tilde{\beta}$ are linked to θ, along with the given constants δ_{AA} and δ_{CC}. Thus, they can be regarded as dependent solely on θ. Experts exhibit different types of risk preferences, which can be categorized into risk preference, risk aversion, and risk neutrality. Different types of experts with varying risk aversion coefficients result in different thresholds, and lead to the following three decision types.

(1) For risk-preferred decision, the risk aversion coefficient θ_p is relatively small, risk-averse decision rules are listed as follows:

$$\begin{aligned}
&\text{If } P(a_i, a_j) \geq \tilde{\alpha}_p, \text{ then } a_j \in AL_\beta^\alpha(a_i),\\
&\text{If } \tilde{\beta}_p < P(a_i, a_j) < \tilde{\alpha}_p, \text{ then } a_j \in NE_\beta^\alpha(a_i),\\
&\text{If } P(a_i, a_j) \leq \tilde{\beta}_p, \text{ then } a_j \in CO_\beta^\alpha(a_i).
\end{aligned}$$

(2) For risk-averse decision, the risk aversion coefficient θ_a is relatively large, risk-averse decision rules are listed as follows:

$$\begin{aligned}
&\text{If } P(a_i, a_j) \geq \tilde{\alpha}_a, \text{ then } a_j \in AL_\beta^\alpha(a_i),\\
&\text{If } \tilde{\beta}_a < P(a_i, a_j) < \tilde{\alpha}_a, \text{ then } a_j \in NE_\beta^\alpha(a_i),\\
&\text{If } P(a_i, a_j) \leq \tilde{\beta}_a, \text{ then } a_j \in CO_\beta^\alpha(a_i).
\end{aligned}$$

(3) For risk-neutral decision, the risk aversion coefficient θ_n is relatively medium, risk-averse decision rules are listed as follows:

$$\begin{aligned}
&\text{If } P(a_i, a_j) \geq \tilde{\alpha}_n, \text{ then } a_j \in AL_\beta^\alpha(a_i),\\
&\text{If } \tilde{\beta}_n < P(a_i, a_j) < \tilde{\alpha}_n, \text{ then } a_j \in NE_\beta^\alpha(a_i),\\
&\text{If } P(a_i, a_j) \leq \tilde{\beta}_n, \text{ then } a_j \in CO_\beta^\alpha(a_i).
\end{aligned}$$

The set $AL_\beta^\alpha(a_i)$ contains the agents allied with a_i, the set $NE_\beta^\alpha(a_i)$ contains agents being neutral with a_i, and the set $\mathrm{CO}_\beta^\alpha(a_i)$ includes agents that are in conflict with a_i.

Then, we explore the size relationship between $\tilde{\alpha}_*$ and $\tilde{\beta}_*(* \in \{a, p, n\})$ in different risk preference decisions. The relationship of $\tilde{\alpha}_*$, $\tilde{\beta}_*$, and θ_* is depicted in Fig 1, where $\delta_{AA} = 1$, $\delta_{CC} = 2$, x-axis, and y-axis are $\tilde{\alpha}_*$ ($\tilde{\beta}_*$), and θ_* respectively. In Fig 1, it shows that the threshold α_* decreases and the threshold $\tilde{\beta}_*$ increases with the increase of θ_*. Because $\theta_p < \theta_n < \theta_a$, it follows that $\tilde{\alpha}_p > \tilde{\alpha}_n > \tilde{\alpha}_a$, and $\tilde{\beta}_p < \tilde{\beta}_n < \tilde{\beta}_a$.

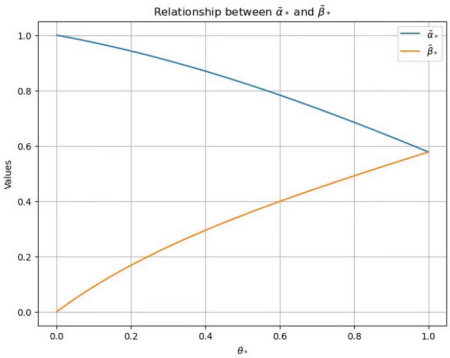

Fig. 1. Curved line of $\tilde{\alpha}_*$ and $\tilde{\beta}_*$ with regard to θ_*

Based on Definition 9 for $P(a_i, a_j)$ and Definition 11 for relative utility functions, we calculate the expected utility values $U\left(b_\bullet \mid a_j\right), \bullet \in \{A, N, C\}$ as follows:

$$U\left(b_A \mid a_j\right) = \tilde{u}_{AA}P(a_i, a_j) + \tilde{u}_{AC}(1 - P(a_i, a_j)), \tag{29}$$

$$U\left(b_N \mid a_j\right) = \tilde{u}_{NA}P(a_i, a_j) + \tilde{u}_{NC}(1 - P(a_i, a_j)), \tag{30}$$

$$U\left(b_C \mid a_j\right) = \tilde{u}_{CA}P(a_i, a_j) + \tilde{u}_{CC}(1 - P(a_i, a_j)). \tag{31}$$

In accordance with the Bayesian procedure, the action with the maximum expected utility value should be chosen. Therefore, for each agent a_j, we can derive the following three decision rules:

(1) *Rule* 1 : $if\ U\left(b_A|a_j\right) > U\left(b_N|a_j\right)\ and\ U\left(b_A|a_j\right) > U\left(b_C|a_j\right), then\ a_j \in AL_\beta^\alpha(a_i)$,
(2) *Rule* 2 : $if\ U\left(b_N|a_j\right) > U\left(b_A|a_j\right)\ and\ U\left(b_N|a_j\right) > U\left(b_C|a_j\right), then\ a_j \in NE_\beta^\alpha(a_i)$,
(3) *Rule* 3 : $if\ U\left(b_C|a_j\right) > U\left(b_A|a_j\right)\ and\ U\left(b_C|a_j\right) > U\left(b_N|a_j\right), then\ a_j \in CO_\beta^\alpha(a_i)$.

Assuming $\tilde{u}_{AA} > \tilde{u}_{NA} > \tilde{u}_{CA}$ and $\tilde{u}_{CC} > \tilde{u}_{NC} > \tilde{u}_{AC}$, and considering the fact that $P(a_i, a_j) + (1 - P(a_i, a_j)) = 1$, then the *Rule* 1, *Rule* 2, and *Rule* 3 can be equivalently expressed as the following rules:

(1) *Rule* 1 : $if\ P(a_i, a_j) \geq \tilde{\alpha}\ and\ P(a_i, a_j) \geq \tilde{\gamma}, then\ a_j \in AL_\beta^\alpha(a_i)$,
(2) *Rule* 2 : $if\ P(a_i, a_j) \leq \tilde{\alpha}\ and\ P(a_i, a_j) \geq \tilde{\beta}, then\ a_j \in NE_\beta^\alpha(a_i)$,
(3) *Rule* 3 : $if\ P(a_i, a_j) \leq \tilde{\gamma}\ and\ P(a_i, a_j) \leq \tilde{\beta}, then\ a_j \in CO_\beta^\alpha(a_i)$.

When $k \in (0.5, 1]$, $\tilde{u}_{AA},\ \tilde{u}_{CC} > 0$, $\tilde{\alpha}$, $\tilde{\beta}$, and $\tilde{\gamma}$ satisfy $\tilde{\alpha} > \tilde{\gamma} > \tilde{\beta}$, then *Rule* 1, *Rule* 2, and *Rule* 3 can be simplified as follows:

(1) *Rule* $1'$: $if\ P(a_i, a_j) \geq \tilde{\alpha}, then\ a_j \in AL_\beta^\alpha(a_i)$,
(2) *Rule* $2'$: $if\ \tilde{\beta} < P(a_i, a_j) < \tilde{\alpha}, then\ a_j \in NE_\beta^\alpha(a_i)$,
(3) *Rule* $3'$: $if P(a_i, a_j) \leq \tilde{\beta}, then\ a_j \in CO_\beta^\alpha(a_i)$.

Next, we provide Algorithm 1 for obtaining decision rules. The time complexity of Step 4 is $O(m^2n)$, where $|A| = m$ and $|I| = n$, and the time complexity of Step 7 is $O(n^2)$. Therefore, the time complexity of Algorithm 1 is $O(m^2n + n^2)$.

Algorithm 1. The algorithm of constructing decision rules for three-valued situation tables.

Input: $S = (A, I, r)$, R, δ_{AA}, δ_{CC}, θ;
Output: $AL_{\beta}^{\alpha}(a_i)$, $NE_{\beta}^{\alpha}(a_i)$, $CO_{\beta}^{\alpha}(a_i)$;
1: Input a three-valued situation table $S = (A, I, r)$;
2: Divide I into two disjoint subsets I' and I'';
3: Calculate weights ω_i for $i \in I$ according to Definition 7;
4: Compute alliance measure $M^{'}(a_i, a_j)$ of agents a_i and a_j in rank 1 and the alliance measure $M^{''}(a_i, a_j)$ in rank 2 according to Definition 8;
5: Compute the alliance probability $P(a_i, a_j)$ according to Definitions 8 and 9;
6: Calculate $\tilde{\alpha}$ and $\tilde{\beta}$ using Formulas (27)-(28);
7: Construct $AL_{\beta}^{\alpha}(a_i)$, $NE_{\beta}^{\alpha}(a_i)$, and $CO_{\beta}^{\alpha}(a_i)$;
8: Output $AL_{\beta}^{\alpha}(a_i)$, $NE_{\beta}^{\alpha}(a_i)$, and $CO_{\beta}^{\alpha}(a_i)$;

4 An Illustrative Example

We employ an example to illustrate that how to use the model of three-way conflict analysis based on decision-theoretic rough sets. The example pertains to the development plan for Gansu Province [34]. In Gansu Province, there are fourteen main cities, namely, Lanzhou–a_1, Jinchang–a_2, Baiyin–a_3, Tianshui–a_4, Jiayuguan–a_5, Wuwei-a_6, Zhangye–a_7, Pingliang–a_8, Jiuquan–a_9, Qingyang–a_{10}, Dingxi–a_{11}, Longnan–a_{12}, Linxia–a_{13}, and Gannan–a_{14}. When the government of Gansu Province makes a development plan for the next year, eleven issues, namely, Construction of Roads–i_1, Factories–i_2, Entertainment–i_3, Educational Institutions–i_4, Total Population of Residence–i_5, Ecology Environment–i_6, Number of Senior Intellectuals–i_7, Traffic Capacity–i_8, Mineral Resources–i_9, Sustainable Development Capacity–i_{10}, and Water Resource Carrying Capacity–i_{11}, are involved among the fourteen cities. Due to variations in economic situations, environmental conditions, and development needs among the fourteen cities, they exhibit varying attitudes toward various development issues. The attitudes of the fourteen cities on the eleven issues are shown in Table 3, where +1 means that the city supports this issue, 0 means that the city is neutral on this issue, and -1 means that the city is against this issue.

First, by Definition 7, we obtain the weight for each issue i of Table 3 as follows:

$$\omega_{i_1} = 0.212, \quad \omega_{i_2} = 0.217, \quad \omega_{i_3} = 0.133, \quad \omega_{i_4} = 0.221, \quad \omega_{i_5} = 0.217,$$
$$\omega_{i_6} = 0.149, \quad \omega_{i_7} = 0.160, \quad \omega_{i_8} = 0.160, \quad \omega_{i_9} = 0.184, \quad \omega_{i_{10}} = 0.189,$$
$$\omega_{i_{11}} = 0.158.$$

By Definitions 8 and 9, we obtain the alliance probability between agents as shown in Table 4. According to Formulas (27)–(28), we obtain thresholds for three types of

Table 3. The attitudes of fourteen cities on eleven issues

A	i_1	i_2	i_3	i_4	i_5	i_6	i_7	i_8	i_9	i_{10}	i_{11}
a_1	+1	−1	0	−1	+1	−1	0	−1	+1	−1	+1
a_2	0	+1	−1	0	0	+1	−1	0	0	+1	−1
a_3	−1	0	−1	−1	−1	+1	+1	−1	−1	0	0
a_4	0	0	−1	+1	+1	−1	−1	+1	0	−1	−1
a_5	−1	+1	−1	0	−1	+1	0	0	−1	+1	+1
a_6	0	+1	0	−1	−1	−1	−1	−1	0	+1	−1
a_7	+1	+1	0	+1	0	+1	0	+1	+1	+1	0
a_8	−1	0	−1	+1	−1	0	+1	+1	−1	0	+1
a_9	+1	+1	0	−1	+1	+1	−1	−1	+1	+1	−1
a_{10}	−1	−1	−1	0	+1	−1	+1	0	−1	−1	+1
a_{11}	−1	0	−1	−1	−1	−1	−1	−1	−1	0	−1
a_{12}	0	+1	0	−1	+1	+1	+1	−1	0	+1	0
a_{13}	−1	0	−1	+1	0	0	0	+1	−1	0	+1
a_{14}	−1	−1	−1	0	−1	−1	−1	0	−1	−1	−1

Table 4. Alliance probabilities between two agents

	a_1	a_2	a_3	a_4	a_5	a_6	a_7	a_8	a_9	a_{10}	a_{11}	a_{12}	a_{13}	a_{14}
a_1	1	0.26	0.38	0.50	0.20	0.46	0.42	0.21	0.59	0.65	0.47	0.53	0.34	0.43
a_2	0.26	1	0.54	0.65	0.75	0.77	0.72	0.43	0.74	0.35	0.64	0.72	0.54	0.58
a_3	0.38	0.54	1	0.31	0.75	0.56	0.34	0.76	0.42	0.60	0.75	0.66	0.66	0.60
a_4	0.50	0.65	0.31	1	0.30	0.50	0.50	0.54	0.44	0.60	0.60	0.37	0.65	0.63
a_5	0.20	0.75	0.75	0.30	1	0.57	0.59	0.75	0.43	0.59	0.52	0.59	0.74	0.59
a_6	0.46	0.77	0.56	0.50	0.57	1	0.50	0.32	0.74	0.25	0.83	0.72	0.33	0.58
a_7	0.42	0.72	0.34	0.50	0.59	0.50	1	0.50	0.70	0.20	0.26	0.63	0.61	0.20
a_8	0.21	0.43	0.76	0.54	0.75	0.32	0.50	1	0.10	0.67	0.53	0.34	0.92	0.60
a_9	0.59	0.74	0.42	0.44	0.43	0.74	0.70	0.10	1	0.10	0.52	0.80	0.20	0.20
a_{10}	0.65	0.35	0.60	0.60	0.59	0.25	0.20	0.67	0.10	1	0.48	0.44	0.70	0.76
a_{11}	0.47	0.64	0.75	0.60	0.52	0.83	0.26	0.53	0.52	0.48	1	0.51	0.55	0.78
a_{12}	0.53	0.72	0.66	0.37	0.59	0.72	0.63	0.34	0.80	0.44	0.51	1	0.38	0.20
a_{13}	0.34	0.54	0.66	0.65	0.74	0.33	0.61	0.92	0.20	0.70	0.55	0.38	1	0.60
a_{14}	0.43	0.58	0.60	0.63	0.59	0.58	0.20	0.60	0.20	0.76	0.78	0.20	0.60	1

decisions. We assume risk aversion coefficients of $\theta_a = 0.9$, $\theta_n = 0.6$, and $\theta_p = 0.2$. According to Formulas (25)–(26), we obtain $\tilde{\alpha}_a = 0.54$, $\tilde{\beta}_a = 0.44$, $\tilde{\alpha}_n = 0.69$, $\tilde{\beta}_n = 0.29$, $\tilde{\alpha}_p = 0.89$, and $\tilde{\beta}_p = 0.09$ with $\delta_{AA} = 6$ and $\delta_{CC} = 5$. Based on the decision rules for risk-averse, risk-neutral, and risk-preferred decisions, we derive the alliance, neutral, and conflict sets for each agent, as depicted in Tables 5, 6, and 7, respectively.

Table 5. Alliance, Neutral, and Conflict Sets for Risk-Averse Decision Maker

A	$AL_\beta^\alpha(a_i)$	$NE_\beta^\alpha(a_i)$	$CO_\beta^\alpha(a_i)$
a_1	$\{a_1, a_9, a_{10}\}$	$\{a_4, a_6, a_{11}, a_{12}\}$	$\{a_2, a_3, a_5, a_7, a_8, a_{13}, a_{14}\}$
a_2	$\{a_2, a_4, a_5, a_6, a_7, a_9, a_{11}\}$	$\{a_3, a_{12}, a_{13}, a_{14}\}$	$\{a_1, a_8, a_{10}\}$
a_3	$\{a_3, a_5, a_6, a_8, a_{10}, a_{11}, a_{12}, a_{13}, a_{14}\}$	$\{a_2\}$	$\{a_1, a_4, a_7, a_9\}$
a_4	$\{a_2, a_4, a_{10}, a_{11}, a_{13}, a_{14}\}$	$\{a_1, a_6, a_7, a_8, a_9\}$	$\{a_3, a_5, a_{12}\}$
a_5	$\{a_2, a_3, a_5, a_6, a_7, a_8, a_{10}, a_{12}, a_{13}, a_{14}\}$	$\{a_{11}\}$	$\{a_1, a_4, a_9\}$
a_6	$\{a_2, a_3, a_5, a_6, a_9, a_{11}, a_{12}, a_{14}\}$	$\{a_1, a_4, a_7\}$	$\{a_8, a_{10}, a_{13}\}$
a_7	$\{a_2, a_5, a_7, a_9, a_{12}, a_{13}\}$	$\{a_4, a_6, a_8\}$	$\{a_1, a_3, a_{10}, a_{11}, a_{14}\}$
a_8	$\{a_3, a_5, a_8, a_{10}, a_{13}\}$	$\{a_4, a_7, a_{11}, a_{14}\}$	$\{a_1, a_2, a_6, a_9, a_{12}\}$
a_9	$\{a_1, a_2, a_6, a_7, a_9, a_{12}\}$	$\{a_4, a_{11}\}$	$\{a_3, a_5, a_8, a_{10}, a_{13}, a_{14}\}$
a_{10}	$\{a_1, a_3, a_4, a_5, a_8, a_{10}, a_{13}, a_{14}\}$	$\{a_{11}, a_{12}\}$	$\{a_2, a_6, a_7, a_9\}$
a_{11}	$\{a_2, a_3, a_4, a_6, a_{11}, a_{13}, a_{14}\}$	$\{a_1, a_5, a_8, a_9, a_{10}, a_{12}\}$	$\{a_7\}$
a_{12}	$\{a_2, a_3, a_5, a_6, a_7, a_9, a_{12}\}$	$\{a_1, a_{10}, a_{11}\}$	$\{a_4, a_8, a_{13}, a_{14}\}$
a_{13}	$\{a_3, a_4, a_5, a_7, a_8, a_{10}, a_{11}, a_{13}, a_{14}\}$	$\{a_2\}$	$\{a_1, a_6, a_9, a_{12}\}$
a_{14}	$\{a_2, a_3, a_4, a_5, a_6, a_8, a_{10}, a_{11}, a_{13}, a_{14}\}$	$\{\phi\}$	$\{a_1, a_7, a_9, a_{12}\}$

Table 6. Alliance, Neutral, and Conflict Sets for Risk-Neutral Decision Maker

A	$AL_\beta^\alpha(a_i)$	$NE_\beta^\alpha(a_i)$	$CO_\beta^\alpha(a_i)$
a_1	$\{a_1\}$	$\{a_2, a_5, a_8\}$	$\{a_3, a_4, a_6, a_7, a_9, a_{10}, a_{11}, a_{12}, a_{13}, a_{14}\}$
a_2	$\{a_2, a_5, a_8, a_9, a_{12}\}$	$\{a_1\}$	$\{a_3, a_4, a_6, a_7, a_{10}, a_{11}, a_{13}, a_{14}\}$
a_3	$\{a_3, a_5, a_8, a_{11}\}$	$\{\phi\}$	$\{a_1, a_2, a_4, a_6, a_7, a_9, a_{10}, a_{12}, a_{13}, a_{14}\}$
a_4	$\{a_4\}$	$\{\phi\}$	$\{a_1, a_2, a_3, a_5, a_6, a_7, a_8, a_9, a_{10}, a_{11}, a_{12}, a_{13}, a_{14}\}$
a_5	$\{a_2, a_3, a_5, a_8, a_{13}\}$	$\{a_1\}$	$\{a_4, a_6, a_7, a_9, a_{10}, a_{11}, a_{12}, a_{14}\}$
a_6	$\{a_2, a_6, a_9, a_{11}, a_{12}\}$	$\{a_{10}\}$	$\{a_1, a_3, a_4, a_5, a_7, a_8, a_{13}, a_{14}\}$
a_7	$\{a_2, a_7, a_9\}$	$\{a_{10}, a_{11}, a_{14}\}$	$\{a_1, a_3, a_4, a_5, a_6, a_8, a_{12}, a_{13}\}$
a_8	$\{a_3, a_5, a_8, a_{13}\}$	$\{a_1, a_9\}$	$\{a_2, a_4, a_6, a_7, a_{10}, a_{11}, a_{12}, a_{14}\}$
a_9	$\{a_2, a_6, a_7, a_9, a_{12}\}$	$\{a_8, a_{10}, a_{13}, a_{14}\}$	$\{a_1, a_3, a_4, a_5, a_8, a_{11}\}$
a_{10}	$\{a_{10}, a_{13}, a_{14}\}$	$\{a_6, a_7, a_9\}$	$\{a_1, a_2, a_3, a_4, a_5, a_8, a_{11}, a_{12}\}$
a_{11}	$\{a_3, a_6, a_{11}, a_{14}\}$	$\{a_7\}$	$\{a_1, a_2, a_4, a_5, a_8, a_9, a_{10}, a_{12}, a_{13}\}$
a_{12}	$\{a_2, a_6, a_9, a_{12}\}$	$\{a_{14}\}$	$\{a_1, a_3, a_4, a_5, a_7, a_8, a_{10}, a_{11}, a_{13}\}$
a_{13}	$\{a_5, a_8, a_{10}, a_{13}\}$	$\{a_9\}$	$\{a_1, a_2, a_3, a_4, a_6, a_7, a_{11}, a_{12}, a_{14}\}$
a_{14}	$\{a_{10}, a_{11}, a_{14}\}$	$\{a_7, a_9, a_{12}\}$	$\{a_1, a_2, a_3, a_4, a_5, a_6, a_8, a_{13}\}$

By analyzing the alliance set, neutral set, and conflict set of each city in Gansu Province, we can gain a better understanding of the interests and trade-offs involved in formulating urban development plans. Simultaneously, the three types of decision rules based on different risk preferences provide a comprehensive description of decision-making diversity, rather than merely a singular types of decision rules. This comprehensive analysis helps deepen our understanding of the potential impacts that the development plan for Gansu Province may have on each city, and provides valuable insights for policy makers and stakeholders.

Table 7. Alliance, Neutral, and Conflict Sets for Risk-Preferred Decision Maker

A	$AL^{\alpha}_{\beta}(a_i)$	$NE^{\alpha}_{\beta}(a_i)$	$CO^{\alpha}_{\beta}(a_i)$
a_1	$\{a_1\}$	$\{a_2, a_3, a_4, a_5, a_6, a_7, a_8, a_9, a_{10}, a_{11}, a_{12}, a_{13}, a_{14}\}$	$\{\phi\}$
a_2	$\{a_2\}$	$\{a_1, a_3, a_4, a_5, a_6, a_7, a_8, a_9, a_{10}, a_{11}, a_{12}, a_{13}, a_{14}\}$	$\{\phi\}$
a_3	$\{a_3\}$	$\{a_1, a_2, a_4, a_5, a_6, a_7, a_8, a_9, a_{10}, a_{11}, a_{12}, a_{13}, a_{14}\}$	$\{\phi\}$
a_4	$\{a_4\}$	$\{a_1, a_2, a_3, a_5, a_6, a_7, a_8, a_9, a_{10}, a_{11}, a_{12}, a_{13}, a_{14}\}$	$\{\phi\}$
a_5	$\{a_5\}$	$\{a_1, a_2, a_3, a_4, a_6, a_7, a_8, a_9, a_{10}, a_{11}, a_{12}, a_{13}, a_{14}\}$	$\{\phi\}$
a_6	$\{a_6\}$	$\{a_1, a_2, a_3, a_4, a_5, a_7, a_8, a_9, a_{10}, a_{11}, a_{12}, a_{13}, a_{14}\}$	$\{\phi\}$
a_7	$\{a_7\}$	$\{a_1, a_2, a_3, a_4, a_5, a_6, a_8, a_9, a_{10}, a_{11}, a_{12}, a_{13}, a_{14}\}$	$\{\phi\}$
a_8	$\{a_8, a_{13}\}$	$\{a_1, a_2, a_3, a_4, a_5, a_6, a_7, a_9, a_{10}, a_{11}, a_{12}, a_{14}\}$	$\{\phi\}$
a_9	$\{a_9\}$	$\{a_1, a_2, a_3, a_4, a_5, a_6, a_7, a_8, a_{10}, a_{11}, a_{12}, a_{13}, a_{14}\}$	$\{\phi\}$
a_{10}	$\{a_{10}\}$	$\{a_1, a_2, a_3, a_4, a_5, a_6, a_7, a_8, a_9, a_{11}, a_{12}, a_{13}, a_{14}\}$	$\{\phi\}$
a_{11}	$\{a_{11}\}$	$\{a_1, a_2, a_3, a_4, a_5, a_6, a_7, a_8, a_9, a_{10}, a_{12}, a_{13}, a_{14}\}$	$\{\phi\}$
a_{12}	$\{a_{12}\}$	$\{a_1, a_2, a_3, a_4, a_5, a_6, a_7, a_8, a_9, a_{10}, a_{11}, a_{13}, a_{14}\}$	$\{\phi\}$
a_{13}	$\{a_8, a_{13}\}$	$\{a_1, a_2, a_3, a_4, a_5, a_6, a_7, a_9, a_{10}, a_{11}, a_{12}, a_{14}\}$	$\{\phi\}$
a_{14}	$\{a_{14}\}$	$\{a_1, a_2, a_3, a_4, a_5, a_6, a_7, a_8, a_9, a_{10}, a_{11}, a_{12}, a_{13}\}$	$\{\phi\}$

5 Conclusion

In this paper, we introduced novel three-way conflict analysis models based on decision-theoretic rough sets. First, we employed a ranking approach to partition a set of issues into two distinct subsets. Subsequently, we introduced alliance measures for individual issue using a transition probability function. By leveraging the computed issue weights and alliance measures, we derived alliance probabilities. Additionally, we presented risk-preferred, risk-averse, and risk-neutral decision rules using the relative utility function. The proposed decision model realistically reflects the diversity of decisions under different risk preferences and provides a practical explanation and illustration of decision-making for various risk preferences. However, there are still some limitations to consider. This model involves manually assigned parameters when calculating alliance probabilities and utility functions based on evaluation values, and have a certain level of subjectivity.

In the future, we plan to explore complex information systems related to conflicts, such as incomplete information systems and fuzzy information systems. Moreover, we intend to develop effective algorithms to compute conflict, neutral, and alliance sets in these complex information systems, and aim to enhance the relationships among agents.

Acknowledgements. This work is supported by the National Natural Science Foundation of China (No. 62076040), the Scientific Research Fund of Hunan Provincial Education Department (No. 22A0233), the Scientific Research Fund of Chongqing Key Laboratory of Computational Intelligence (No. 2020FF04), the Postgraduate Scientific Research Innovation Project of Changsha University of Science and Technology (No. CSLGCX23106).

References

1. Yao, Y.Y.: Three-way decision with probabilistic rough sets. Inf. Sci. **180**, 341–353 (2010)
2. Khan, G.A., Hu, J., Li, T., Diallo, B., Zhao, Y.: Multi-view low rank sparse representation method for three-way clustering. Int. J. Mach. Learn. Cybern. **13**, 233–253 (2021)
3. Li, H.X., Zhang, L.B., Huang, B., Zhou, X.Z.: Sequential three-way decision and granulation for cost-sensitive face recognition. Knowl.-Based Syst. **91**, 241–251 (2016)
4. Li, H.X., Zhang, L.B., Zhou, X.Z., Huang, B.: Cost-sensitive sequential three-way decision modeling using a deep neural network. Int. J. Approximate Reasoning **85**, 68–78 (2017)
5. Liang, D.C., Pedrycz, W., Liu, D., Hu, P.: Three-way decisions based on decision-theoretic rough sets under linguistic assessment with the aid of group decision making. Appl. Soft Comput. J. **29**, 256–269 (2015)
6. Li, J.H., Huang, C.C., Qi, J.J., Qian, Y.H., Liu, W.Q.: Three-way concept learning via multi-granularity. Inf. Sci. **378**, 244–263 (2017)
7. Li, H.X., Zhou, X.Z.: Risk decision making based on decision-theoretic rough set: a three-way view decision model. Int. J. Comput. Intell. Syst. **4**, 1–11 (2011)
8. Liu, D., Liang, D.C., Wang, C.C.: A novel three-way decision model based on incomplete information system. Knowl.-Based Syst. **91**, 32–45 (2016)
9. Yang, X.P., Yao, J.T.: Modelling multi-agent three-way decisions with decision-theoretic rough sets. Fund. Inform. **115**(2–3), 157–171 (2012)
10. Zhou, B., Yao, Y.Y., Luo, J.G.: Cost-sensitive three-way email spam filtering. J. Intell. Syst. **42**(1), 19–45 (2014)
11. Yao, Y.Y.: Interval sets and three-way concept analysis in incomplete context. Int. J. Mach. Learn. Cybern. **8**(1), 3–20 (2017)
12. Deng, T., Long, B., Xu, W., Yao, Y.: Adjunctive three-way concepts from positive and negative concepts in lattice-valued formal contexts. Int. J. Approximate Reasoning **161**, 108989 (2023)
13. Xu, W.Y., Jia, B., Li, X.N.: A two-universe model of three-way decision with ranking and reference tuple. Inf. Sci. **581**, 808–839 (2021)
14. Xu, W.Y., Jia, B., Li, X.N.: A generalized model of three-way decision with ranking and reference tuple. Int. J. Approximate Reasoning **144**, 51–68 (2022)
15. Pawlak, Z.: On conflicts. Int. J. Man Mach. Stud. **21**, 127–134 (1984)
16. Li, X.N., Yan, Y.C.: A dynamic three-way conflict analysis model with adaptive thresholds. Inf. Sci. **657**, 119999 (2024)
17. Lang, G.M., Mao, D.Q., Cai, M.G.: Three-way decision approaches to conflict analysis using decision-theoretic rough set theory. Inf. Sci. **406–407**, 185–207 (2017)
18. Lang, G.M.: A general conflict analysis model based on three-way decision. Int. J. Mach. Learn. Cybern. **11**, 1083–1094 (2020)
19. Lang, G.M., Mao, D.Q., Fujita, H.: Three-way group conflict analysis based on Pythagorean fuzzy set theory. IEEE Trans. Fuzzy Syst. **28**, 447–461 (2020)
20. Lang, G.M., Yao, Y.Y.: New measures of alliance and conflict for three-way conflict analysis. Int. J. Approximate Reasoning **132**, 49–69 (2021)
21. Lang, G.M., Yao, Y.Y.: Formal concept analysis perspectives on three-way conflict analysis. Int. J. Approximate Reasoning **152**, 160–182 (2023)
22. Liu, S., Hu, M., Zhang, Z., Lang, G.: Three-way conflict analysis for three-valued situation tables with rankings and reference tuples. In: International Joint Conference on Rough Sets, pp. 231–245. Springer, Cham (2023). https://doi.org/10.1007/978-3-031-50959-9_16
23. Lin, C., Xiao, Q., Yu, H., Lang, G.: New models of three-way conflict analysis for incomplete situation tables. In: International Joint Conference on Rough Sets, vol. 14481, pp. 270–282. Springer, Cham (2023). https://doi.org/10.1007/978-3-031-50959-9_19

24. Zhi, H.L., Li, J.H.: Component similarity based conflict analysis: an information fusion viewpoint. Inf. Fusion **104**, 102157 (2024)
25. Wang, T.X., Li, H.X., Qian, Y.H., Huang, B., Zhou, X.Z.: A regret-based three-way decision model under interval type-2 fuzzy environment. IEEE Trans. Fuzzy Syst. **30**(1), 175–189 (2020)
26. Zhang, Q.H., Xie, Q., Wang, G.Y.: A novel three-way decision model with decision-theoretic rough sets using utility theory. Knowl.-Based Syst. **159**, 321–335 (2018)
27. Zhan, J.M., Ye, J., Ding, W.P., Liu, P.D.: A novel three-way decision model based on utility theory in incomplete fuzzy decision systems. IEEE Trans. Fuzzy Syst. **30**(7), 2210–2226 (2022)
28. Jia, F., Liu, P.D.: A novel three-way decision model under multiple-criteria environment. Inf. Sci. **471**, 29–51 (2019)
29. Liang, D.C., Xu, Z.S., Liu, D., Wu, Y.: Method for three-way decisions using ideal TOPSIS solutions at Pythagorean fuzzy information. Inf. Sci. **435**, 282–295 (2018)
30. Liang, D.C., Wang, M.W., Xu, Z.S., Liu, D.: Risk appetite dual hesitant fuzzy three-way decisions with TODIM. Inf. Sci. **507**, 585–605 (2020)
31. Yao, Y.Y.: Probabilistic rough set approximations. Int. J. Approximate Reasoning **49**, 255–271 (2008)
32. Liu, P.D., Wang, Y.M., Jia, F., Fujita, H.: A multiple attribute decision making three-way model for intuitionistic fuzzy numbers. Int. J. Approximate Reasoning **119**, 177–203 (2020)
33. Pawlak, Z.: An inquiry into anatomy of conflicts. Inf. Sci. **109**, 65–78 (1998)
34. Sun, B.Z., Chen, X.T., Zhang, L.Y., Ma, W.M.: Three-way decision making approach to conflict analysis and resolution using probabilistic rough set over two universes. Inf. Sci. **507**, 809–822 (2020)

Three-Way Conflict Analysis with Negative Feedback

Yucong Yan(✉) and Xiaonan Li

School of Mathematics and Statistics, Xidian University, Xi'an 710071, China
ycyan18@163.com

Abstract. Conflict often arises when individuals have different opinions. Owing to the ubiquity of conflict, conflict analysis is always widely discussed. Recently, the three-way conflict analysis proposed by Yao has attracted much attention. In Yao's framework, each three-way conflict model consists of the whole, trisections, and final results. However, the final results are induced once a trisection is given. In other words, the model cannot correct the final results. Therefore, we provide a new conflict analysis framework with negative feedback. This way, we can deliver better results, even when we are not given proper thresholds in advance. In addition, we provide three algorithms for three-way conflict models with negative feedback in this paper after showing the new framework. In the third algorithm, we focus on coalitions instead of trisections while improving thresholds, which distinguishes greatly from previous models.

Keywords: Conflict analysis · Three-way decision · Thresholds selection · Negative feedback

1 Introduction

Since conflict is everywhere in real life, conflict analysis is always a widely discussed topic. Many conflict analysis models have been proposed, among which Pawlak's model has recently attracted a lot of attention. Pawlak firstly considers conflict analysis from a viewpoint of rough set theory in [1,2].

The models of Pawlak are based on information systems $S = (U, A)$, where those sets U are sets of agents and A are sets of issues (attributes). In the system, each pair of agent $x \in U$ and issue $a \in A$ is mapped to one of the three values -1, 0, 1 which are usually written as $+$, 0 and $-$ for convenience. The values $+$, 0 and $-$ denote the agent x having a positive, neutral and negative attitude to issue a respectively. With the information system, Pawlak focuses on the relation between agents in single and multiple issues. Based on given sets of issues, relations between agents are trisected into allied, neutral and conflict relations. Finally, the models output groups of coalitions, and each coalition is

This work was supported by the Natural Science Basic Research Program of Shaanxi Province (Nos. 2023-JC-YB-005).

M. Hu et al. (Eds.): IJCRS 2024, LNAI 14840, pp. 196–209, 2024.
https://doi.org/10.1007/978-3-031-65668-2_14

a set of agents in allied relation. Based on Pawlak's models, a series of improved models are presented using many math tools, such as lattice concept [4], game theory [5], fuzzy set theory [6,7] and fuzzy numbers ranking [8]. And there also are some works done with application [9,10]. Among these improved models, three-way conflict models are in a vital position.

Considering three-way decision [11,12] is also about trisection, Yao proposed three-way conflict analysis [13,14] which added a decision-making part after getting the trisections. In the three-way conflict analysis, there are several kinds of trisection models, and the dominant ones are models of agents and models of pairs of agents. In Yao's framework, Pawlak's models belong to models of pairs of agents. For now, much work has been done with three-way conflict analysis. Some authors focus on improving models of agents by changing measures [15], some consider models of pairs of agents [16], some improve the thresholds [17,18] and some changing the information systems [19,20]. To summarize, Yao defined new trisection models and, most importantly, offered a new framework of conflict analysis concerning trisecting and decision-making.

However, there is a problem in the existing framework. The problem is that the trisection is induced without negative feedback, which means that the model would deliver wrong results once the inputs, especially the thresholds, are not proper at the beginning. Therefore, to obtain more proper results, we provide a new framework of conflict analysis with negative feedback in this paper. Besides a new framework, there are other two contributions of this study. First, we give a new algorithm for models of agents to obtain final trisections and do not need to know the thresholds in advance. Second, in the models of pairs with negative feedback, the coalitions instead of the trisection results are considered to be the feedback, which can be seen in Fig. 2.

2 Classical Three-Way Conflict Analysis

The classical three-way conflict analysis is proposed by Yao in [13]. In the study, there are two main kinds of three-way conflict models involved: the models of agents and the models of pairs of agents.

A classical three-way conflict model consists of three components: Information tables as inputs, trisections induced and outcomes computed with the trisections, which is shown in Fig. 1. It should be noticed that we add the trisection model as a component in Fig. 1. This is for better display in Fig. 2.

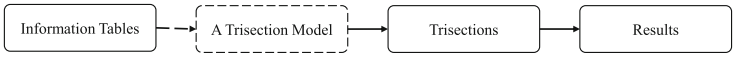

Fig. 1. A Classical Three-way Conflict Model

The difference between three-way conflict models of agents and three-way conflict models of pairs of agents exists in their trisection models. In Sects. 2.1 and 2.2, we show their trisection models respectively.

2.1 Trisection Models of Agents

The classical three-way conflict analysis is on the basis of information tables defined in Definition 1.

Definition 1. *[13] An information table is a triplet $S = (U, A, r)$, where U is a finite nonempty set of agents, A is a finite nonempty set of issues, and $r : U \times A \to V$ is a function that maps a pair of an agent and an issue to a value in a value set V.*

If V equals to $\{-1, 0, +1\}$, then the table is called a three-valued (information) table. In detail, $+1$, 0 and -1 denote positive, neutral and negative attitude respectively. And if V equals to $[-1, +1]$, then the table is called a many-valued (information) table. Information tables are equivalent to information systems most of the time. In this paper, we do not distinguish them from each other as that doesn't affect much.

In [13], there are several three-way conflict models of agents. However, we there only consider the most general and popular one of them which is shown in Definition 2.

Definition 2. *[13] For an information table $S = (U, A, r)$, an aggregated rating of an agent $x \in U$ on non-empty subset of issues $J \subseteq A$ is given by $\boldsymbol{r}(x, J) = \frac{1}{|J|} \sum_{i \in J} r(x, i)$. With a pair of thresholds (α, β), $-1 \leq \beta < 0 < \alpha \leq +1$, a trisection of the set of agents is given by:*

$$
\begin{aligned}
U_J^{[\alpha,1]} &= \{x \in U \mid \boldsymbol{r}(x, J) \geq \alpha\}, \\
U_J^{(\beta,\alpha)} &= \{x \in U \mid \beta < \boldsymbol{r}(x, J) < \alpha\}, \\
U_J^{[-1,\beta]} &= \{x \in U \mid \boldsymbol{r}(x, J) \leq \beta\}.
\end{aligned}
$$

The three sets $U_J^{[\alpha,1]}$, $U_J^{(\beta,\alpha)}$ and $U_J^{[-1,0]}$ are explained as sets of agents who have positive, neutral and negative attitude respectively.

Since the original paper [13] was proposed, a lot of improvements have been done with the aggregation operator, i.e. $\mathbf{r}$ in Definition 2. Considering all these models that only vary in aggregation operators, we define the classical trisection model of agents in Definition 3.

Definition 3. *For an information table $S = (U, A, r)$, $f : x \times J \mapsto [-1, 1]$ is an aggregation operator of an agent $x \in U$ on a non-empty subset of issues $J \subseteq A$. With a pair of thresholds (α, β), $-1 \leq \beta < 0 < \alpha \leq +1$, a trisection of the set of agents is given by:*

$$
\begin{aligned}
U_J^{[\alpha,1]} &= \{x \in U \mid f(x, J) \geq \alpha\}, \\
U_J^{(\beta,\alpha)} &= \{x \in U \mid \beta < f(x, J) < \alpha\}, \\
U_J^{[-1,\beta]} &= \{x \in U \mid f(x, J) \leq \beta\}.
\end{aligned}
$$

2.2 Trisection Models of Pairs of Agents

As is the case with the models of agents, the paper [13] also contains several models of pairs of agents. Still, only the most general and popular one is presented in Definition 4.

Definition 4. *[13] For an information table $S = (U, A, r)$, $c_a : U \times U \to [0, 1]$ is a function defined on the set of agents concerning an issue $a \in A$. For a subset of issues $J \subseteq A$, we define a conflict function $\boldsymbol{c}_J : U \times U \to [0, 1]$ as follows: for $x, y \in U$, $\boldsymbol{c}_J(x, y) = \frac{1}{|J|} \sum_{a \in J} c_a(x, y)$. With a pair of thresholds (α, β), $-1 \leq \beta < 0 < \alpha \leq +1$, a trisection of the set of all pairs of agents is given by:*

$$
\begin{aligned}
R_J^{[\alpha,1]} &= \{(x, y) \in U \times U \mid \boldsymbol{c}_J(x, y) \geq \alpha\}, \\
R_J^{(\beta,\alpha)} &= \{(x, y) \in U \times U \mid \beta < \boldsymbol{c}_J(x, y) < \alpha\}, \\
R_J^{[0,\beta]} &= \{(x, y) \in U \times U \mid \boldsymbol{c}_J(x, y) \leq \beta\}.
\end{aligned}
$$

In the models of pairs, the Cartesian product $U \times U$ is trisected, while the model of agents trisects the agent set U. The elements in $U \times U$ are called pairs of agents. And the pairs in $R_J^{[\alpha,1]}$, $R_J^{(\beta,\alpha)}$ and $R_J^{[0,\beta]}$ are considered to be in allied, neutral and conflict relation respectively. In contrast with the model of agents where agents in $U_J^{[\alpha,1]}$ take positive attitude, allied pairs are in $R_J^{[0,\beta]}$.

Then we give the definition of the classical trisection model of pairs of agents in Definition 5. The model in Definition 5 does not only contain the original model in [13] but also consists of many other trisection models that only differ from the original one in the conflict functions. (e.g. [17])

Definition 5. *For an information table $S = (U, A, r)$, $g : x \times y \times J \mapsto [0, 1]$ is a conflict operator of for $x, y \in U$ on a non-empty subset of issues $J \subseteq A$. With a pair of thresholds (α, β), $0 \leq \beta < 0.5 < \alpha \leq 1$, a trisection of the set of all pairs of agents is given by:*

$$
\begin{aligned}
R_J^{[\alpha,1]} &= \{(x, y) \in U \times U \mid g(x, y, J) \geq \alpha\}, \\
R_J^{(\beta,\alpha)} &= \{(x, y) \in U \times U \mid \beta < g(x, y, J) < \alpha\}, \\
R_J^{[0,\beta]} &= \{(x, y) \in U \times U \mid g(x, y, J) \leq \beta\}.
\end{aligned}
$$

Remark 1. Suppose that $S = (U, A, r)$ is an information table and J is a subset of A. In the existing works of conflict analysis, final results can be obtained immediately once the thresholds are given. However, owing to the lack of negative feedback, the thresholds are usually computed subjectively and experimentally. This also makes it impossible for these models to get correct outcomes once the thresholds are not given properly at the beginning. Hence in Sect. 3, we attempt to give a methodology for three-way conflict models adding negative feedback, and thus the trisection models could be constantly improved by analyzing the results they delivered and finally achieving ideal outcomes rather than completely relying on getting proper thresholds at the very beginning.

3 Three-Way Conflict Models of Agents with Negative Feedback

A comparison of the classical three-way conflict model and the one with negative feedback can be seen in Fig. 2.

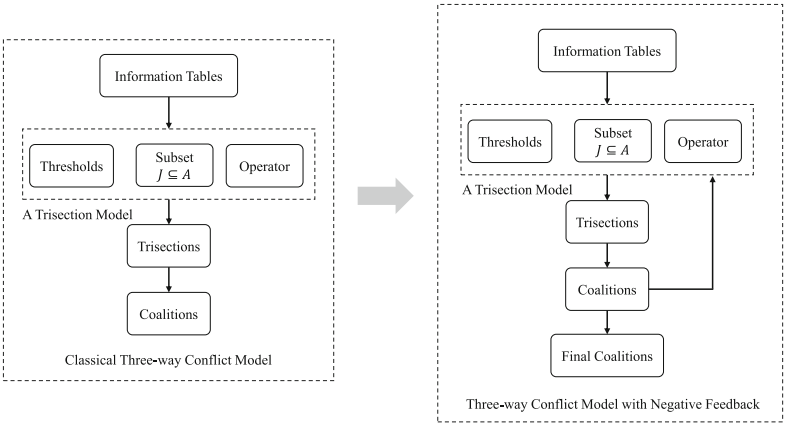

Fig. 2. A comparison between classical conflict model and the one with feedback.

As stated in Remark 1, to get more ideal outcomes, we attempt to add negative feedback in three-way conflict analysis. Since the outcomes of three-way conflict models are coalitions, we take the evaluation of coalitions to be the feedback. And in this study, the evaluation of a coalition refers to two parts: the sum of distance for any two agents in the coalition, and the sum of distance for two agents one of which is in the coalition and the other not. An illustrative figure is shown in Fig. 3. Then we consider a coalition to be superior when it has a lower value in the first part and a higher sum in the second part. In addition, we should notice that the trisection is the group of coalitions for the models of agents. Then we have to define the two parts of evaluation for each coalition in Definitions 6, 7 and 8.

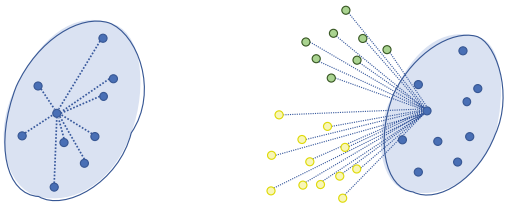

Fig. 3. Two parts concerns the coalition evaluation.

For an information table $S = (U, A, r)$, $f : x \times J \mapsto [-1, 1]$ is an aggregation operator of an agent $x \in U$ on a non-empty subset of issues $J \subseteq A$. Let $\mathbf{x} = f(x, J)$, $\mathbf{y} = f(y, J)$ and distance function $F : [-1, 1] \times [-1, 1] \to [0, 1]$, where for all $\mathbf{x}, \mathbf{y} \in [-1, 1]$, $F(\mathbf{x}, \mathbf{y}) = F(\mathbf{y}, \mathbf{x})$.

Definition 6. *$h_{11} : (0, 1] \to [0, \infty)$, $h_{12} : (0, 1] \to [0, \infty)$.*

$$h_{11}(\alpha) := \sum_{x,y \in U_J^{[\alpha,1]}}^{x \neq y} F(\boldsymbol{x}, \boldsymbol{y}), \quad h_{12}(\alpha) := \sum_{y \notin U_J^{[\alpha,1]}}^{x \in U_J^{[\alpha,1]}} F(\boldsymbol{x}, \boldsymbol{y}),$$

Definition 7. *$h_{21} : [-1, 0) \times (0, +1] \to [0, \infty)$, $h_{22} : [-1, 0) \times (0, +1] \to [0, \infty)$.*

$$h_{21}(\alpha, \beta) := \sum_{x,y \in U_J^{(\beta,\alpha)}}^{x \neq y} F(\boldsymbol{x}, \boldsymbol{y}), \quad h_{22}(\alpha, \beta) := \sum_{y \notin U_J^{(\beta,\alpha)}}^{x \in U_J^{(\beta,\alpha)}} F(\boldsymbol{x}, \boldsymbol{y}),$$

Definition 8. *$h_{31} : [-1, 0) \to [0, \infty)$, $h_{32} : [-1, 0) \to [0, \infty)$.*

$$h_{31}(\beta) := \sum_{x,y \in U_J^{[-1,\beta]}}^{x \neq y} F(\boldsymbol{x}, \boldsymbol{y}), \quad h_{32}(\beta) := \sum_{y \notin U_J^{[-1,\beta]}}^{x \in U_J^{[-1,\beta]}} F(\boldsymbol{x}, \boldsymbol{y}).$$

Then the thresholds can be obtained by solving a multi-objective programming problem in the following.

$$(P_1) \quad \begin{cases} \min \ \mathbf{f}(\alpha, \beta) = (f_1(\alpha, \beta), -f_2(\alpha, \beta)) \\ s.t. \ \ 0 < \alpha \leq 1 \\ \qquad 0 > \beta \geq -1 \end{cases}$$

where

$$f_1(\alpha, \beta) := h_{11}(\alpha) + h_{31}(\beta), + h_{21}(\alpha, \beta)$$
$$f_2(\alpha, \beta) := h_{12}(\alpha) + h_{32}(\beta) + h_{22}(\alpha, \beta),$$

and h_{11}, h_{12}, h_{21}, h_{22}, h_{31}, h_{32} are defined in Definitions 6, 7 and 8.

To solve (P_1), we transform (P_1) to (P_1')

$$(P_1') \quad \begin{cases} \min \ \lambda_1 f_1(\alpha, \beta) - \lambda_2 f_2(\alpha, \beta) \\ s.t. \ \ \lambda_1 + \lambda_2 = 1 \\ \qquad 0 < \alpha \leq 1, 0 > \beta \geq -1 \\ \qquad \lambda_1 \geq 0, \lambda_2 \geq \text{`}0 \end{cases}$$

Proposition 1. *Let $0 < \alpha \leq 1$ and $0 > \beta \geq -1$. Then*

$$f_1(\alpha, \beta) + \frac{1}{2} f_2(\alpha, \beta) = \sum_{x,y \in U}^{x \neq y} F(\boldsymbol{x}, \boldsymbol{y})$$

Then we define (P_1'') and (P_1''), and (P_1'), (P_1'') and (P_1''') are equivalent to each other.

$$(P_1'') \quad \begin{cases} \min \ f_1(\alpha, \beta) \\ s.t. \ \ 0 < \alpha \leq 1 \\ \quad\ \ 0 > \beta \geq -1 \end{cases} \qquad (P_1''') \quad \begin{cases} \min \ -f_2(\alpha, \beta) \\ s.t. \ \ 0 < \alpha \leq 1 \\ \quad\ \ 0 > \beta \geq -1 \end{cases}$$

Although (P_1'') and (P_1''') are equivalent, we only give an algorithm for the models of agents with negative feedback based on (P_1'') in Algorithm 1.

Algorithm 1: An algorithm of models of agents

Input: Information system $S = (U, A, r)$, a set $J \subseteq A$, operators $f : U \times 2^A \to [-1, 1]$ and $F : [-1, 1] \times [-1, 1] \to [0, 1]$

Step 1 Build a matrix $Q \in R^{n\times 1}$ that stores the values of all $f(x_i, J)$, $x_i \in U$ in descending order, and the original position i is stored in the corresponding row of matrix $K \in R^{n\times 1}$;

Step 2 Create a matrix $P \in R^{n\times n}$, $n = |U|$. Let $x_i, x_j \in U$, $\mathbf{x}_i = f(x_i, J)$, $\mathbf{x}_j = f(x_j, J)$. If $i = j$, then $P(i, j) = 0$; otherwise, $P(i, j) = F\left(\mathbf{x}_{K(i)}, \mathbf{x}_{K(j)}\right)$;

Step 3 Trisection and improving with negative feedback;

$min = \sum_{u=1}^{n} \sum_{v=1}^{n} P(u, v)$, $\alpha = 1$, $\beta = 0$;

for $i = 1 : |Q|$ **do**

  If i is not the largest j such that $Q(j) == Q(i)$, $j = 1, 2, \cdots |Q|$, then we skip to the next iteration of the loop;

  for $j = i + 1 : |Q|$ **do**

    If i is not the smallest j such that $Q(j) == Q(i)$, $j = 1, 2, \cdots |Q|$, then we skip to the next iteration of the loop;

    if $Q(i) > 0 \wedge Q(j) < 0 \vee$ **then**

      Compute $h_{i1}(Q(i))$, $i = 1, 2, 3$;

      Compute $f_1(Q(i), Q(j)) = h_{11}(Q(i)) + h_{31}(Q(j)) + h_{21}(Q(i), Q(j))$;

      if $f_1(Q(i), Q(j)) < min$ **then**

        $min = f_1(Q(i), Q(j))$, $\alpha = Q(i)$, $\beta = Q(j)$;

      end

    end

  end

end

Step 4 Compute the final trisection with obtained α and β;

Output: The final trisection

4 Three-Way Conflict Models of Pairs with Negative Feedback

In three-way models of agents, the final results are trisection results. And if we consider the trisection of pairs to be the final results, then we can get an algorithm for similarly trisecting the pairs of agents by changing Algorithm 1 slightly. This algorithm is given in Algorithm 2.

Algorithm 2: An algorithm of models of pairs

Input: Information system $S = (U, A, r)$, a set $J \subseteq A$, operators $g : U \times U \times 2^A \to [0,1]$ and $F : [0,1] \times [0,1] \to [0,1]$

Step 1 Build a matrix $Q \in R^{m\times 1}$, $m = n^2$, $n = |U|^2$ which stores all the values of $g(x_p, x_q, J)$, $x_i \in U$, $x_j \in U$ in descending order, and the original position $i = n(p-1)+q$ is stored in the corresponding row of matrix $K \in R^{m\times 1}$;

Step 2 Create a matrix $P \in R^{m\times m}$. Let $x_p, x_q \in U$, and $r_i = g(x_p, x_q, J)$, where $i = n(p-1)+q$. If $i = j$ or $i = n(p-1)+p$ or $j = n(p-1)+p$, $p = 1, \cdots, n$, then $P(i,j) = 0$; otherwise, $P(i,j) = F\left(r_{K(i)}, r_{K(j)}\right)$;

Step 3 Except for $min = \sum_{u=1}^{m}\sum_{v=1}^{m} P(u,v)$, others are the same with the Step 3 in Algorithm 1;

Step 4 Compute the final trisection with obtained α and β, and thus get final coalitions;

Output: The final coalitions

In the following, we consider groups of coalitions that are not trisections, and we discuss the algorithm with coalition evaluation being negative feedback for models of pairs. First, we give a definition of coalitions in our study.

Definition 9. *For an information table $S = (U, A, r)$, if sets V_i, $i = 1, \cdots, m$ are coalitions of agents, then*

1. $\bigcup_{i=1}^{m} V_s = U$;
2. *for all $i \neq j$, $V_i \cap V_j = \emptyset$;*
3. $V_i \neq \emptyset$, $i = 1, \cdots, m$.

In the following, we give the definition of the two parts of evaluation for all coalitions in Definition 10. For an information table $S = (U, A, r)$, $f : x \times J \mapsto [-1, 1]$ is an aggregation operator of an agent $x \in U$ on a non-empty subset of issues $J \subseteq A$. Let $\mathbf{x} = f(x, J)$, $\mathbf{y} = f(y, J)$ and distance function $F : [-1,1] \times [-1,1] \to [0,1]$, where for all $\mathbf{x}, \mathbf{y} \in [-1,1]$, $F(\mathbf{x}, \mathbf{y}) = F(\mathbf{y}, \mathbf{x})$.

Definition 10. $h_{i,j} : (0.5, 1] \times [0, 0.5) \to [0, \infty)$, $i = 1, \cdots, m$, $j = 1, 2$.

$$h_{i,1}(\alpha, \beta) = \sum_{x,y\in V_i}^{x\neq y} F(\boldsymbol{x}, \boldsymbol{y}),\ h_{i,2}(\alpha, \beta) = \sum_{x\in V_i}^{y\notin V_i} F(\boldsymbol{x}, \boldsymbol{y}),$$

$$h_{i,3}(\alpha, \beta) = |U| - |V_i|,$$

where $h_{i,3}$ is a penalty function. For a coalition V_i, $i = 1, \cdots, m$, $|V_i|$ is inversely proportional to $h_{i,3}$, which reveals a preference for coalitions with more agents.

Then the thresholds are obtained by solving a multi-objective programming problem in the following.

$$(P_2) \quad \begin{cases} \min \ \mathbf{f}(\alpha,\beta) = (f_1(\alpha,\beta), -f_2(\alpha,\beta), f_3(\alpha,\beta)) \\ s.t. \ \ 0 < \alpha \leq 1 \\ \qquad 0 > \beta \geq -1 \end{cases}$$

where

$$f_j(\alpha,\beta) := \sum_{i=1}^{m} h_{i,j}(\alpha,\beta),$$

where $j = 1, 2, 3$.

To solve (P_2), we transform (P_2) to (P_2'), and (P_1'), (P_1'') and (P_1''') are equivalent to each other.

$$(P_2') \quad \begin{cases} \min \ \lambda_1 f_1(\alpha,\beta) - \lambda_2 f_2(\alpha,\beta) + \lambda_3 f_3(\alpha,\beta) \\ s.t. \ \ \lambda_1 + \lambda_2 + \lambda_3 = 1, \\ \qquad 0.5 < \alpha \leq 1, 0.5 > \beta \geq 0, \\ \qquad \lambda_1 \geq 0, \lambda_2 \geq 0, \lambda_3 \geq 0, \\ \qquad \lambda_3 < 1. \end{cases}$$

Proposition 2. *Let* $0.5 < \alpha \leq 1$ *and* $0.5 > \beta \geq 0$. *Then*

$$f_1(\alpha,\beta) + \frac{1}{2} f_2(\alpha,\beta) = \sum_{x,y \in U}^{x \neq y} F(\boldsymbol{x}, \boldsymbol{y})$$

Then we define (P_2'') and (P_2'').

$$(P_2'') \quad \begin{cases} \min \ f_1(\alpha,\beta) + \lambda f_3(\alpha,\beta) \\ s.t. \ \ 0.5 < \alpha \leq 1, \\ \qquad 0.5 > \beta \geq 0, \\ \qquad \lambda > 0. \end{cases} \qquad (P_2''') \quad \begin{cases} \min \ -f_2(\alpha,\beta) + \lambda f_3(\alpha,\beta) \\ s.t. \ \ 0.5 < \alpha \leq 1, \\ \qquad 0.5 > \beta \geq 0, \\ \qquad \lambda > 0. \end{cases}$$

Still, we only give an algorithm for the models of agents with negative feedback based on (P_2'') in Algorithm 3.

5 An Illustrative Example

In this section, we give an example to illustrate the three algorithms with an information table $S = (U, A, r)$ for the Middle East conflict in Table 1. This is a classical information system from Pawlak [1].

The agent set U consists of six agents which are six countries. In detail, the six countries are: Israel, Egypt, Palestinians, Jordan, Syria and Saudi Arabia. And there are five issues in the issue set A, such as "Israeli military outpost along the Jordan River", "Israeli retains East Jerusalem" and "Israeli military outposts on the Golan Heights". In addition, the function r maps agents and issues to values of attitude, and the attitude values are in corresponding entries in Table 1. As

Algorithm 3: An algorithm of models of pairs with coalition evaluation being negative feedback

Input: Information system $S = (U, A, r)$, a set $J \subseteq A$, operator $g : U \times U \times 2^A \to [0, 1]$ and a preference parameter λ.

Step 1 Create a matrix $P \in R^{n \times n}$, $n = |U|$. Let $x_i, x_j \in U$. If $i = j$, then $P(i, i) = 0$; otherwise, $P(i, j) = g(x_i, x_j, J)$;

Step 2 Build a matrix $Q \in R^{n^2 \times 1}$ that stores the values of all $g(x_i.x_j, J)$, $x_i, x_j \in U$ in descending order;

Step 3 Trisection and improving with negative feedback;

$min = \sum_{u=1}^{n} \sum_{v=1}^{n} P(u, v) + n * \lambda(n-1)$, $\alpha = 1$, $\beta = 0$;

for $i = 1 : |Q|$ **do**

  If i is not the largest j such that $Q(j) == Q(i)$, $j = 1, 2, \cdots |Q|$, then we skip to the next iteration of the loop;

  for $j = i + 1 : |Q|$ **do**

    If i is not the smallest j such that $Q(j) == Q(i)$, $j = 1, 2, \cdots |Q|$, then we skip to the next iteration of the loop;

    if $Q(i) > 0.5 \wedge Q(j) < 0.5$ **then**

      Create coalitions V_s, $s = 1, \cdots, m$;

      $h_{s1}(Q(i), Q(j)) = \sum_{x_u, x_v \in V_s} P(u, v)$, $s = 1, \cdots, m$;

      $h_{s3}(Q(i), Q(j)) = n - |V_i|$, $s = 1, \cdots, m$;

      Compute $f_\ell(Q(i), Q(j)) = \sum_{s=1}^{m} h_{s\ell}(Q(i), Q(j))$, $\ell = 1, 3$;

      eval $= f_1(Q(i), Q(j)) + \lambda f_3(Q(i), Q(j))$;

      if $eval < min$ **then**

        $min = f_1(Q(i), Q(j))$, $\alpha = Q(i)$, $\beta = Q(j)$, ;

      end

    end

  end

end

Step 4 Compute the final coalitions with obtained α and β;

Output: The final coalitions

given the definition of information table in Definition 1, the attitude values $+$, $-$, 0 present positive, negative and neutral attitude respectively. For instance, the $(1, 1)$th entry of Table Table 1 reveals that Israel x_1 is opposed to a_1, i.e., "autonomous Palestinian state on the West Bank and Gaza".

Table 1. An information system for the Middle East conflict.

U	a_1	a_2	a_3	a_4	a_5
x_1	$-$	$+$	$+$	$+$	$+$
x_2	$+$	0	$-$	$-$	$-$
x_3	$+$	$-$	$-$	$-$	0
x_4	0	$-$	$-$	0	$-$
x_5	$+$	$-$	$-$	$+$	$-$
x_6	0	$+$	$-$	0	$+$

5.1 The Algorithm for Models of Agents

Input Information system $S = (U, A, r)$ in Table 1, a set $J = A \subseteq A$, operators $f : x \times J \mapsto \frac{1}{5} r(x, i)$, $x \in U$ and $F(\mathbf{x}, \mathbf{y}) = \frac{1}{2} |\mathbf{x} - \mathbf{y}|$, $\mathbf{x}, \mathbf{y} \in [-1, 1]$.
Step 1 Build $Q = [0.6, 0.2, -0.2, -0.4, -0.4, -0.6]^\top$ and $K = [1, 6, 5, 2, 3, 4]^\top$
Step 2 Create a matrix $P \in R^{n \times n}$, $n = |U| = 6$. Let $x_i, x_j \in U$, $\mathbf{x}_i = f(x_i, J)$, $\mathbf{x}_j = f(x_j, J)$. If $i = j$, then $P(i, j) = 0$; otherwise, $P(i, j) = F\left(\mathbf{x}_{K(i)}, \mathbf{x}_{K(j)}\right)$

$$P = \begin{bmatrix} 0.0 & 0.2 & 0.4 & 0.5 & 0.5 & 0.6 \\ 0.2 & 0.0 & 0.2 & 0.3 & 0.3 & 0.4 \\ 0.4 & 0.2 & 0.0 & 0.1 & 0.1 & 0.2 \\ 0.5 & 0.3 & 0.1 & 0.0 & 0.0 & 0.1 \\ 0.5 & 0.3 & 0.1 & 0.0 & 0.0 & 0.1 \\ 0.6 & 0.4 & 0.2 & 0.1 & 0.1 & 0.0 \end{bmatrix}$$

Step 3 Trisection and improving with negative feedback
$min = \sum_{u=1}^{n} \sum_{v=1}^{n} P(u, v) = 9$, $\alpha = 1$, $\beta = 0$
Round 1 $i = 1$, $i < |Q| = 6$, $Q(i) \neq Q(i + 1)$.
$j = 2$: Since $Q(j) > 0$, nothing is performed.
$j = 3$: With $Q(i) = 0.6 > 0$, $Q(j) = -0.2 < 0$, we have that

$$h_{11}(0.6) = \sum_{k=1}^{1} \sum_{\ell=1}^{1} P(k, \ell) = 0, \quad h_{31}(-0.2) = \sum_{k=3}^{6} \sum_{\ell=3}^{6} P(k, \ell) = 1.2,$$

$$h_{21}(0.6, -0.2) = \sum_{k=2}^{2} \sum_{\ell=2}^{2} P(k, \ell) = 0.$$

Then, $f_1(0.6, -0.2) = 1.2$ such that $f_1(0.6, -0.2) < min = 9$. Now, $min = 1.2$, $\alpha = 0.6$, $\beta = -0.2$.

$j = 4$: $f_1(0.6, -0.4) = 0 + 0.4 + 0.4 = 0.8 < min = 1.2$. Now, $min = 0.8$, $\alpha = 0.6$, $\beta = -0.4$.

$j = 5$: $Q(j) = Q(5) = -0.4 = Q(4) = Q(j - 1)$, then nothing is performed.

$j = 6$: $f_1(0.6, -0.6) = 0 + 2 + 0 = 2.6 > min = 1.2$.

Round 2 i=2 $\cdots$

$\vdots$

Round 6 i=6 $\cdots$

All the possible values of f_1 are shown in Table 2 where the $*$ means nothing there is performed.

Therefore, $(Q(1), Q(4)) = (0.6, -0.4)$ and $(Q(2), Q(4)) = (0.2, -0.4)$, $(Q(2), Q(6)) = (0.2, -0.6)$ are the best thresholds.

In Step 1 and Step 2, we get an adjacency matrix P whose (i, j)th entry stores the difference degree between the two corresponding agents. And the two agents' scores there, computed by f for computing the (i, j)th entry, are the ith and jth highest respectively. Algorithm 1 finally gives three groups of coalitions as final outputs, and the three ones are shown in Table 3 with their corresponding thresholds.

Table 2. Corresponding values of f_1.

$i\backslash j$	1	2	3	4	5	6
1	*	*	1.2	0.8	*	2.6
2	*	*	1.6	0.8	*	0.8
3	*	*	*	*	*	*
⋮	⋮	⋮	⋮	⋮	⋮	⋮
6	*	*	*	*	*	*

Table 3. Best thresholds and the trisections induced for models of agents.

α	β	$U_A^{[\alpha,1]}$	$U_A^{[-1,\beta]}$	$U_A^{(\beta,\alpha)}$
0.6	−0.4	$\{x_1\}$	$\{x_4, x_6\}$	$\{x_2, x_3, , x_5\}$
0.2	−0.4	$\{x_1, x_6\}$	$\{x_4\}$	$\{x_2, x_3, , x_5\}$
0.2	−0.6	$\{x_1, x_6\}$	$\{x_2, x_3, x_4\}$	$\{x_5\}$

5.2 The Algorithm for Models of Pairs

Since Algorithm 2 is similar to 1, we only discuss Algorithm 3 here.
Input. Information system $S = (U, A, r)$ in Table 1, a set $J = A \subseteq A$, operator $g : x \times y \times J \mapsto \frac{1}{2|J|} \sum_{a \in J} |r(x, a) - r(y, a)|$ and a preference parameter $\lambda = 0.5$.
Step 1. Create a matrix $P \in R^{n \times n}$, $n = |U|$. Let $x_i, x_j \in U$. If $i = j$, then $P(i, j) = 0$; otherwise, $P(i, j) = g\,(x_i, x_j, J)$.

$$P = \begin{bmatrix} 0 & 0.9 & 0.9 & 0.8 & 0.8 & 0.4 \\ 0.9 & 0 & 0.2 & 0.3 & 0.3 & 0.5 \\ 0.9 & 0.2 & 0 & 0.3 & 0.3 & 0.5 \\ 0.8 & 0.3 & 0.3 & 0 & 0.2 & 0.4 \\ 0.8 & 0.3 & 0.3 & 0.2 & 0 & 0.6 \\ 0.4 & 0.5 & 0.5 & 0.4 & 0.6 & 0 \end{bmatrix}$$

Step 2. Build a matrix $Q \in R^{n^2 \times 1}$ that stores the values of all $g(x_i.x_j, J)$, $x_i, x_j \in U$ in descending order.

$$Q = [0.9, 0.9, 0.9, 0.9, 0.8, 0.8, 0.8, 0.8, 0.6, 0.6, 0.5, 0.5, 0.5, 0.5, 0.4, 0.4, 0.4,$$
$$0.4, 0.3, 0.3, 0.3, 0.3, 0.3, 0.3, 0.3, 0.3, 0.2, 0.2, 0.2, 0.2, 1, 1, 1, 1, 1, 1]^\top$$

Step 3. Trisection and improving with negative feedback.
$min = \sum_{u=1}^{n} \sum_{v=1}^{n} P(u, v) + n * \lambda(n-1) = 14.8 + 15 = 29.8$, $\alpha = 1$, $\beta = 0$
Round 1 to 3 $i = 1, \cdots, 3$: Since $Q(i) = Q(i+1)$, nothing is performed
Round 4 $i = 4$: When $j = 5, \cdots, 14$, $Q(j) \geq 0.5$.

$j = 15$: $\alpha = 0.9$, $\beta = 0.4$. Then $V_1 = \{x_1, x_6\}$, V_2=$\{x_2, x_3, x_4, x_5\}$.

$$\left[\begin{array}{c|cccccc} & x_1 & x_2 & x_3 & x_4 & x_5 & x_6 \\ \hline x_1 & & & & & & \\ x_2 & 0.9 & & & & & \\ x_3 & 0.9 & \mathbf{0.2} & & & & \\ x_4 & 0.8 & \mathbf{0.3} & \mathbf{0.3} & & & \\ x_5 & 0.8 & \mathbf{0.3} & \mathbf{0.3} & \mathbf{0.2} & & \\ x_6 & \mathbf{0.4} & 0.5 & 0.5 & \mathbf{0.4} & 0.6 & \end{array}\right] \rightarrow \left[\begin{array}{c|cc} & x_1 & \{x_1, x_6\} \quad \{x_2, x_3, x_4, x_5\} \\ \hline \{x_1, x_6\} & 0.4 & \\ \{x_2, x_3, x_4, x_5\} & 0.675 & 0.267 \end{array}\right]$$

In this case, $f_1(0.8, 0.4) = 0.8 + 3.2 = 4$, $f_3 = \lambda(6-2) + \lambda(6-4) = 3$, we have eval $= 7 < min = 29.8$. Then $min = 4$, $\alpha = 0.8$, $\beta = 0.4$ (Tables 4 and 5).

Table 4. Corresponding values of eval.

$i(\alpha)\backslash j(\beta)$	15(0.4)	19(0.3)	27(0.2)	31(0)
4(0.9)	7	9.2	9.8	15
8(0.8)	7	9.2	9.8	15
10(0.6)	7	9.2	9.8	15

Table 5. Evaluation of coalitions and corresponding β.

β	eval	coalitions
0.4	7	$\{x_1, x_6\}, \{x_2, x_3, x_4, x_5\}$
0.3	9.2	$\{x_1\}, \{x_6\}, \{x_2, x_3, x_4, x_5\}$
0.2	9.8	$\{x_1\}, \{x_6\}, \{x_2, x_3\}, \{x_4, x_5\}$
0	15	$\{x_1\}, \{x_2\}, \{x_3\}, \{x_4\}, \{x_5\}, \{x_6\}$

Therefore, the final coalition is $\{x_1, x_6\}, \{x_2, x_3, x_4, x_5\}$. For the third algorithm, it should be mentioned that the final coalitions only concern β, as the coalition creation approach we use there only refer to allied relations.

6 Conclusion

In this study, we propose a new framework of three-way conflict analysis by adding negative feedback which is the evaluation of coalitions. For the models of agents, the coalitions are the sets in trisections, while the coalitions in the models of pairs are agent sets computed by relations, and they are not sets in trisections. In conclusion, three-way conflict analysis with negative feedback is significant and has much prospect. And the three-way conflict analysis corresponding to other decisions is waiting for further discussion.

References

1. Pawlak, Z.: An inquiry into anatomy of conflicts. J. Inform. Sci. **109**, 65–78 (1998)
2. Pawlak, Z., Skowron, A.: Rough sets: some extensions. Inf. Sci. **177**(1), 28–40 (2007)
3. Sun, B.Z., Ma, W.M., Zhao, H.Y.: Rough set-based conflict analysis model and method over two universes. Inf. Sci. **372**, 111–125 (2016)
4. Zhi, H.L., Li, J.H.: Component similarity based conflict analysis: an information fusion viewpoint. Inf. Fusion **104**, 102157 (2024)
5. Yu, J., Hipel, K.W.: Graph model under unknown and fuzzy preferences. IEEE Trans. Fuzzy Syst. **28**(2), 1063–6706 (2020)
6. Li, X.N., Wang, X., Lang, G.M., Yi, H.J.: Conflict analysis based on three-way decision for triangular fuzzy information systems. Int. J. Approximate Reasoning **132**, 88–106 (2021)
7. Yi, H.J., Zhang, H.M., Li, X.N., Yang, Y.P.: Three-way conflict analysis based on hesitant fuzzy information systems. Int. J. Approximate Reasoning **139**, 12–27 (2021)
8. Li, X.N., Wei, X.L., Qian, Z.H.: A probability-measure-based approach to ranking fuzzy numbers via three-way decision and its application to conflict analysis. Fuzzy Sets Syst. **465**, 108539 (2023)
9. Przybyła-Kasperek, M., Wakulicz-Deja, A.: The strength of coalition in a dispersed decision support system with negotiations. Eur. J. Oper. Res. **252**, 947–968 (2016)
10. Przybyła-Kasperek, M.: Practically motivated adaptive fusion method with tie analysis for multilabel dispersed data. Expert Syst. Appl. **219**, 119601 (2023)
11. Yao, Y.Y.: Three-way decisions with probabilistic rough sets. Inf. Sci. **180**(3), 341–353 (2010)
12. Yao, Y.Y.: Three-way decision and granular computing. Int. J. Approximate Reasoning **103**, 107–123 (2018)
13. Yao, Y.Y.: Three-way conflict analysis: reformulations and extensions of the Pawlak model. Knowl.-Based Syst. **180**, 26–37 (2019)
14. Lang, G.M., Luo, J.F., Yao, Y.Y.: Three-way conflict analysis: a unification of models based on roug sets and formal concept analysis. Knowl.-Based Syst. **194**, 105556 (2020)
15. Lang, G.M., Yao, Y.Y.: New measures of alliance and conflict for three-way conflict analysis. Int. J. Approximate Reasoning **132**, 49–69 (2021)
16. Hu, M.J.: Modeling relationships in three-way conflict analysis with subsethood measures. Knowl.-Based Syst. **260**, 110131 (2023)
17. Xu, W.Y., Jia, B.: Three-way conflict analysis with similarity degree on an issue set. Int. J. Mach. Learn. Cybern. **15**(2), 405–427 (2024)
18. Li, X.N., Yan, Y.C.: A dynamic three-way conflict analysis model with adaptive thresholds. Inf. Sci. **657**, 119999 (2024)
19. Du, J.L., Liu, S.F., Liu, Y., Yi, J.H.: A novel approach to three-way conflict analysis and resolution with Pythagorean fuzzy information. Inf. Sci. **584**, 65–88 (2022)
20. Lin, T.T., Yang, B.: The resolution of q-rung orthopair fuzzy set based three-way group conflict analysis. J. Intell. Fuzzy Syst. **44**(6), 10565–10580 (2023)

Rental Market Data Mining

Estate 360: AI-Driven Centralized Real Estate Platform

Neeyati Mehta, Sameer Patel(✉), Zaid Shaikh, Jerry Caleb, and Kritika Koirala

Saint Mary's University, Halifax, NS B3H 3C3, Canada
{neeyati.mehta,sameer.patel,zaidmohammedsiddique.shaikh, jerry.jebasingh}@smu.ca

Abstract. Halifax's rental sector faces significant challenges, including affordability issues and regulatory inefficiencies. The lack of a centralized, data-driven platform further complicates strategic decision-making for property managers and policymakers. Our paper introduces Estate 360°, a comprehensive digital solution designed to transform the Halifax rental market by integrating advanced data analytics, automated data collection, and user-friendly interfaces. This platform enhances stakeholder decision-making by providing real-time insights and predictive analytics, enabling swift, informed responses to market dynamics. Our solution not only promises to streamline operations and reduce reliance on outdated data collection methods but also equips users with the tools necessary to stay competitive and strategically aligned with evolving market conditions.

Keywords: Real Estate · Machine Learning · Data Analysis · Web Scraping · Automation · XGBoost · Tableau

1 Introduction

1.1 Background

Halifax's rental market is currently facing significant challenges driven by a lack of affordable housing options and sufficient regulatory measures to stabilize rising costs. Despite government interventions, including a 2% rent cap and measures to restrict "renovictions," the rental landscape remains troubled, with many residents expressing financial distress and dissatisfaction through public protests and social media [7,10]. This situation is compounded by demographic changes and economic shifts that influence housing demand and rental rates, making the need for effective responsiveness more critical than ever [3]. Additionally, manual data collection leads to inefficiencies, as property managers often depend on outdated methods that slow down their responses. The lack of a centralized platform for accessing and analyzing real-time market rental rates results in infrequent dashboard updates, which do not reflect current market conditions. This reliance

M. Hu et al. (Eds.): IJCRS 2024, LNAI 14840, pp. 213–229, 2024.
https://doi.org/10.1007/978-3-031-65668-2_15

on human labor not only increases the risk of errors but also hinders effective decision-making [14].

The absence of a unified platform for analyzing market rental rates severely undermines decision-making and competitiveness in Halifax's rental market. Without a comprehensive system to manage crucial data such as vacancy rates and average rents provided by entities like the Canadian Mortgage and Housing Corporation (CMHC) [8,17], stakeholders lack the tools necessary for strategic planning. This deficiency prevents property managers and policymakers from aligning rental prices with market conditions and enhancing property value assessments systematically [21]. Industry survey emphasizes the need for integrated data analysis tools and technology that can support informed decisions and adapt to market changes. These studies show that accurately assessing rental rates requires an understanding of various factors, including property features, market demand, and comparable property rents [13,19,24].

1.2 Research Objective

The objective of this research is to design and implement a comprehensive centralized data analysis platform specifically tailored for the Halifax rental market. This platform will facilitate the aggregation, analysis, and visualization of up-to-date rental data, including vacancy rates, average rents, and market trends. By integrating diverse data sources, the system aims to give property managers and policymakers real-time insights and predictive analytics for strategic decision-making. The goals of the research are listed below.

Data Integration. Develop a robust system that consolidates data from multiple sources, including local government databases and private rental listings, to create a comprehensive overview of the market landscape.

Analytical Tools Development. Create advanced analytical tools within the platform that allow users to identify patterns, predict market trends, and assess the impact of economic and demographic changes on rental prices and availability.

User-Friendly Interface. Design an intuitive, user-friendly interface that enables easy access to complex data analyses, making it practical for stakeholders with varying levels of technical expertise.

Market Responsiveness. Enhance the ability of property managers to respond to market changes effectively by providing them with tools to adjust rental prices accurately and swiftly, thereby increasing market competitiveness.

1.3 Scope of Study

The scope of this study centers on the development of a centralized data analysis platform for the Halifax Regional Municipality rental market, with a strong focus on leveraging data collected from multiple online sources. The aim is to enhance decision-making capabilities through advanced data integration and real-time analytics.

Data Collection and Integration: The platform aggregated data from approximately 20 rental websites *(Refer to Table 1)* to ensure a broad and comprehensive dataset. The websites targeted for data scraping include:

Table 1. Targeted Rental Websites

Hotpads	RentFaster	Zumper	Kijiji	Rentals
Happipad	Rent Seeker	444 Rent	Dexel	JDE
Werkliv	West22	Killam	Westwood	Capriet
Templeton	NorthPoint	HappyPlace	Ansell Prop	Olympus

2 Literature Review

The research conducted on the rental market has consistently highlighted the critical role of factors such as location, property characteristics, and market dynamics in influencing rental prices and property valuations. For example, studies show that proximity to amenities such as shops and schools, along with attributes like property size and condition, significantly impact rental rates [2,13]. This understanding underscores the need for advanced data analytics in real estate to capture and analyze these influences accurately [22].

Building on the foundational knowledge of market influences, web scraping emerges as a pivotal technology in real estate, enhancing the depth and accuracy of data collection. Studies suggest that by automating the extraction of property details from various online sources, web scraping strengthens market analysis and predictive analytics [5,6,15,16,20,27]. This method ensures the real-time accuracy of listings, which is crucial for strategic decision-making and optimizing property management [12,25]. It provides a comprehensive database that includes off-market properties and new listings, thus effectively identifying market trends and opportunities [11,26]. Through its ability to maintain updated and detailed property information, web scraping has become an indispensable tool in modern real estate analytics.

Additionally, integrating machine learning techniques in real estate valuation marks a significant shift, improving property market analysis through advanced

technology [4,23]. Research has demonstrated that ML models such as Random Forest, Decision Trees, and Support Vector Machines are highly effective for predicting property prices and rents by examining complex interactions among the various factors that influence real estate values [1,9,24]. These models facilitate the integration of a vast array of data points-from physical property attributes to economic indicators-thereby improving the accuracy and reliability of property appraisals.

This seamless transition from the analysis of market dynamics to the application of web scraping and machine learning illustrates how technological advancements are intricately linked to enhancing the efficacy and efficiency of real estate market analyses.

There are several platforms in the market that offer similar data analysis capabilities for the real estate sector. Our application, while conceptually similar to others, incorporates a unique combination of features not commonly found in the current market. Following is the group of top applications in this domain being compared with our application on certain parameters in Table 2.

Table 2. Estate 360 vs Current Market Solutions

Features	Estate360	Attom Slns	DealPath	CBRE
Data Coverage	Halifax	US	US	Global
Customization	High	Moderate	Limited	No
Predictive Analytics	Advanced	Basic	Advanced	Advanced
Real-Time Data	Yes	No	No	No
User Interface	User-Friendly	Complex	Complex	Complex

3 Proposed System

To address the current challenges in real estate, this paper proposes "Estate 360°", a comprehensive digital solution aimed at transforming the property rental market. This system dynamically accesses market data through advanced data analytics and user-friendly dashboards, designed to simplify data aggregation, streamline processing, and enhance decision-making with predictive analytics and real-time insights. It automates data collection via web scraping from various property management and rental websites, displaying the data on dashboards that provide insights into market trends, competitive positioning, and pricing strategies. Furthermore, this data is used to train a machine-learning model that predicts rental prices, thereby improving the platform's responsiveness to market changes.

Our solution is built on an automated data collection system that uses advanced web scraping and API integration technologies to continuously gather the latest rental data. This ensures the accuracy of our market analyses. At the heart of the platform is a sophisticated machine-learning model powered by finely tuned XGBoost Model, which process large datasets to predict rental prices and market trends in real-time. This approach not only enhances the precision of predictions but also minimizes manual data analysis, boosting operational efficiency significantly.

3.1 Automated Data Collection

The proposed solution automates data collection by using advanced web scraping and API integration to gather important property data from various real estate websites. This includes details such as the number of bedrooms and bathrooms, property size, utilities, amenities, and parking availability. The system reduces the need for manual labor and minimizes errors by ensuring that data collection scripts run daily.

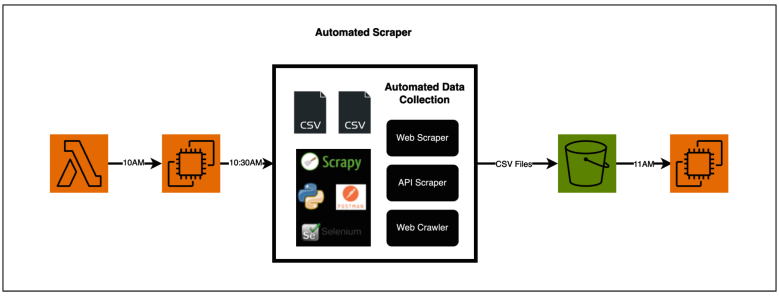

Fig. 1. Automated Data Collection Process

Figure 1 illustrates the automated data collection process utilized in our solution. A Lambda function triggers an EC2 instance at 10 AM daily for data collection. Tools like Scrapy, Selenium, and Postman are used to gather data, which is then saved in CSV format and stored in an S3 bucket. At 10:30 AM, another EC2 instance merges these CSV files to create a unified dataset ready for analysis. This setup enhances data handling efficiency and ensures our database consistently reflects up-to-date market conditions.

3.2 Real-Time Dashboards

The platform provides multiple user-friendly, interactive dashboards that display processed data in a visually intuitive format.

Overview Dashboard. The dashboard *(Refer to Fig 2)* offers insights into the rental market within the HRM area. A heat map indicates the density of rent prices per square foot, with warmer colors showing higher prices. A rent distribution graph provides a visual representation of the number of listings across different rent ranges within major regions like Dartmouth, Bedford, and the Halifax Peninsula. The sidebar allows filtering by minor regions, adjusting the display of listings on the map and charts. Lastly, a bar chart compares the average rent per bedroom size, showing a progressive increase in rent as the number of bedrooms increases.

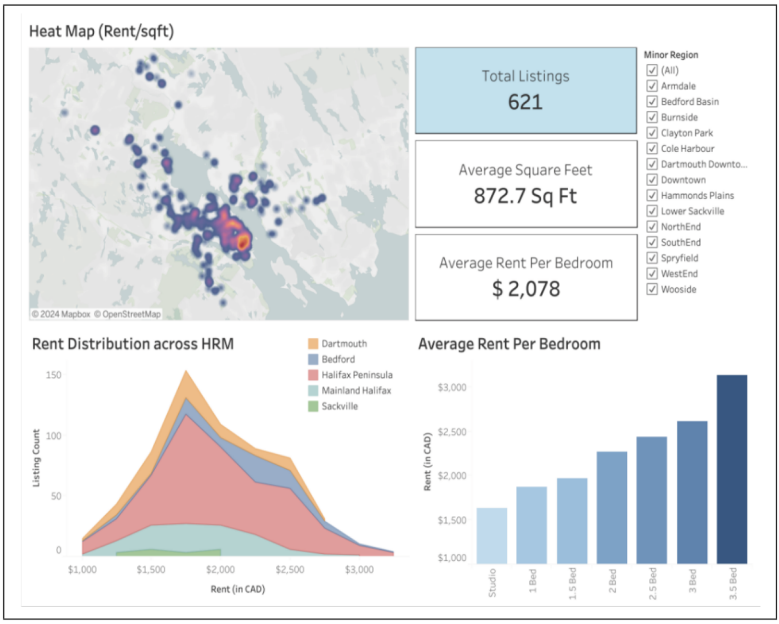

Fig. 2. Snapshot of the Overview Dashboard

Parking Dashboard. This dashboard *(Refer to Fig. 3)* offers provides a detailed layout of parking costs within the HRM area. It includes a map that spatially represents the distribution of free and paid parking spots, depicted by colored dots. Key figures presented are the counts of free parking (208) and paid parking (413), alongside the average parking cost calculated. The table offers a granular view of average parking costs by major and minor regions. At the bottom, a legend classifies the parking types, including free parking and paid parking, both with and without cost associated.

Available Listings Dashboard. This dashboard *(Refer to Fig. 4)* displays data on available real estate listings. It features a map that illustrates the location of listings within the area. Additional filters allow viewers to sort listings

by the number of bedrooms and bathrooms, as well as the availability of water, heat, and electricity. Parking types are also categorized, including free parking and both paid parking options.

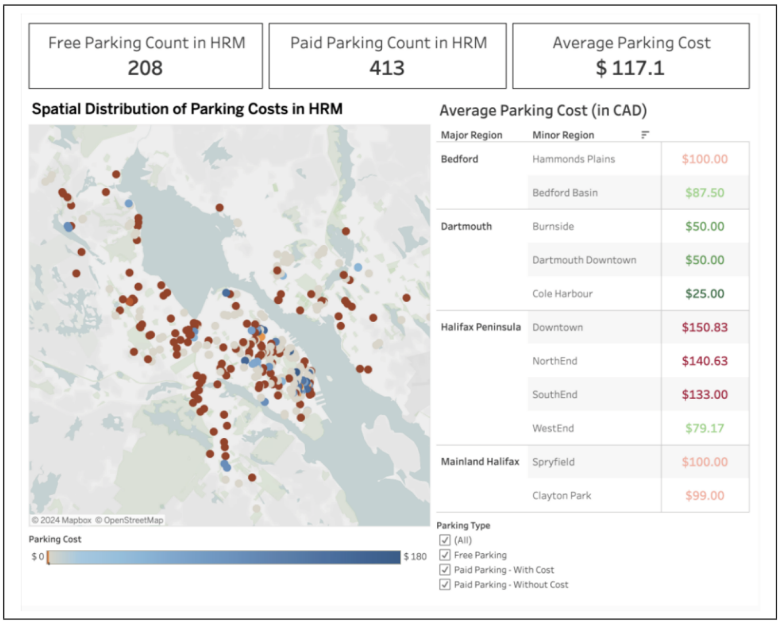

Fig. 3. Snapshot of the Parking Dashboard

Competitor Analysis Dashboard. The dashboard *(Refer to Fig. 6)* features several distinct sections that outline property management data. Firstly, there is a map visualization that graphically displays the geographical layout of properties with color-coded dots, indicating their distribution. Additionally, the dashboard presents an overview of rental increments over the years, specifically detailing the annual increases. Another component is the detailed breakdown of rental increments by region, which lists both major and minor regions such as Bedford Basin and Clayton Park, among others. Lastly, the dashboard includes a comparative bar chart of yearly rental increments, comparing the performance of Southwest Properties against that of Universal Groups and Northpoint Properties.

Upcoming Projects Dashboard. The Upcoming Projects Dashboard *(Refer to Fig. 7)* showcases the locations on a map, along with the number of builders involved. The bar chart on the dashboard illustrates the status of the properties,

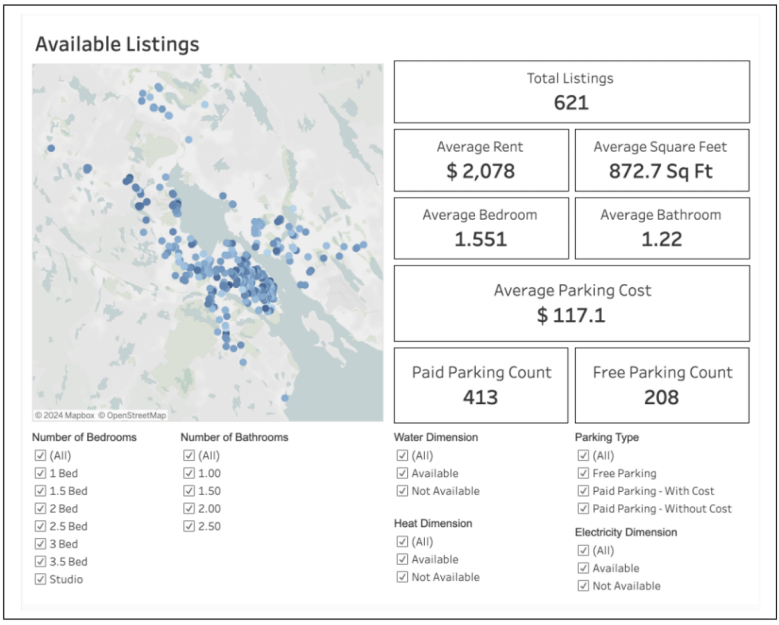

Fig. 4. Snapshot of the Available Listings Dashboard

categorizing them as completed, upcoming projects, or under construction. Additionally, there's an option to filter the displayed data by specific builders. The color-coded dots on the map correspond to different statuses of the properties for an at-a-glance spatial analysis.

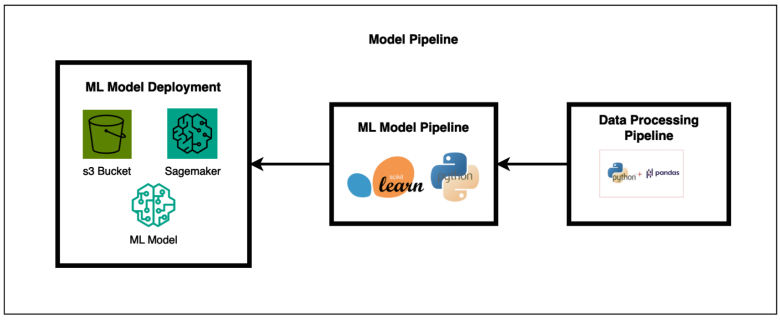

Fig. 5. Model Pipeline

3.3 Insightful Rental Forecast

A key feature of the platform is its advanced predictive analytics, which enables accurate forecasting of rent prices based on geographical data. This capability allows users to make informed decisions on setting competitive rental prices. This foresight enhances property management strategies, enabling more dynamic market responsiveness and improved operational decisions.

Based on Fig. 5, we have setup a Model pipeline, which fetches data from the database, and processes data for it to feed it into the ML Model. The ML Model is then trained on the data, once the model is trained, it is then deployed on sagemaker reference.

3.4 In-House Developed APIs

By using custom-built APIs designed for this platform, we eliminate reliance on unreliable third-party APIs. This improves the platform's reliability and security, ensuring that proprietary data and functions are securely managed by platform administrators and users. This approach protects sensitive information and enhances system performance. All our APIs are developed InHouse, ensuring that our system does not have any dependencies on any external platforms.

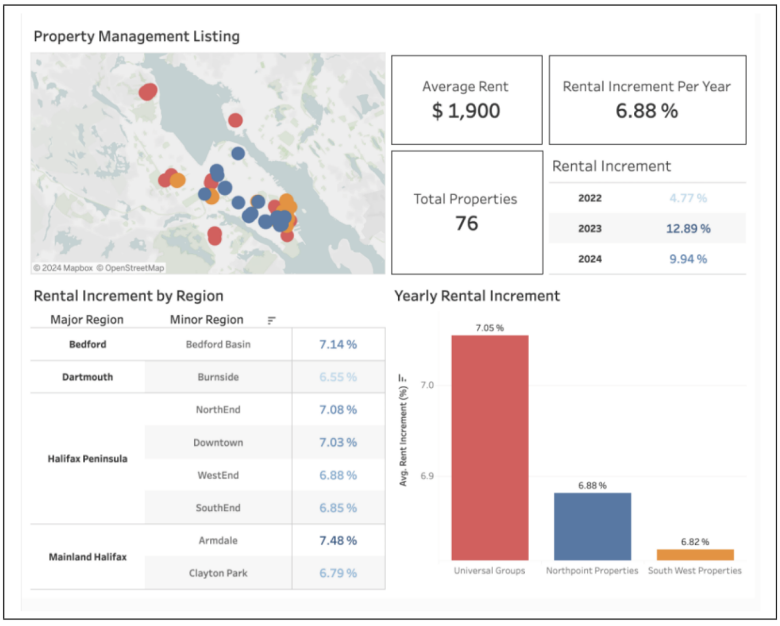

Fig. 6. Snapshot of the Competitor Analysis Dashboard

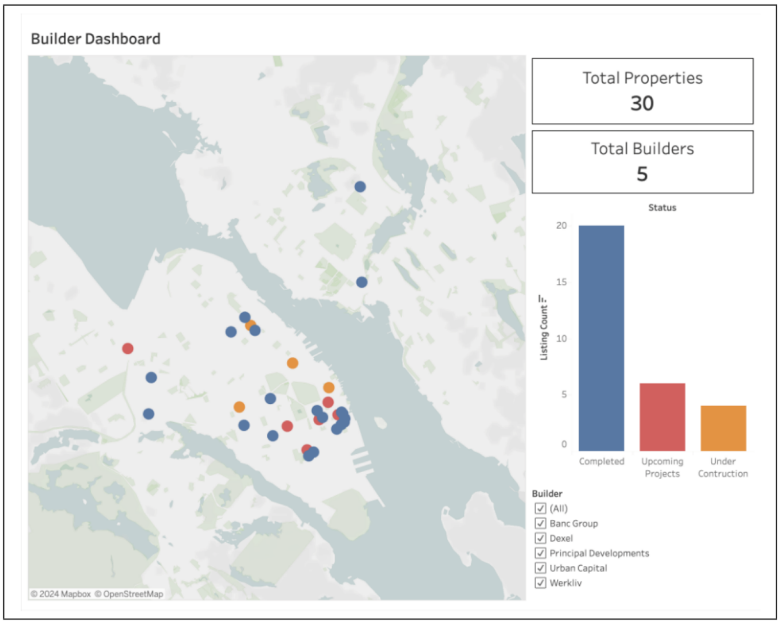

Fig. 7. Snapshot of the Upcoming Projects Dashboard

Walk Score API. The Walk Score API calculates scores based on the proximity of necessary amenities within walking distance of a given location. By inputting latitude and longitude coordinates, users receive a score reflecting how easy it is to complete daily errands on foot. This API enhances user understanding of a property's location desirability based on walkability.

Bike Score API. This API provides scores based on the number of essential services within biking distance from a specific location. Users input geographical coordinates to receive a bike score, which helps assess the bike-friendliness of that area.

Transit Score API. The Transit Score API evaluates the accessibility of public transport from a particular location, using the number of bus stops within walking distance as a parameter. By submitting latitude and longitude, the API returns a score indicating the convenience of public transit.

Upcoming Project Alerts API. The system features automated alerts that notify users about new project developments promptly. These alerts keep users informed in real-time, enabling them to respond quickly to market changes and opportunities.

4 Methodology

4.1 Data Processing and Augmentation

Before diving into the specifics of model training, it is crucial to outline the state of our dataset and the preprocessing steps undertaken. The original dataset consisted of 1403 data rows, each with 30 features. Upon processing, the shape of the dataset was altered to 1032 entries with an expanded feature set due to one-hot encoding, resulting in 52 features. The processed dataset was then split into two subsets at an 80%-20% ratio to facilitate model training and testing. The training set consisted of 825 data rows, while the testing set consisted of 207 data rows. Table 3 depicts all the necessary features that have been used for Model Training.

To further enhance the model's learning capacity, data augmentation techniques were employed, doubling the dataset size to 2064 entries. This expanded dataset underwent a similar division, allocating 1651 entries for training and 413 for testing.

Table 3. Model Features

Address	MajorRegion	MinorRegion	Latitude	Longitude
Type	PropertyType	Size	Bedrooms	Bathrooms
Heat	Water	Hydro	Furnished	Pet
Smoking	Gym	Parking	AC	Appliance
Storage	Transit	Walk	Bike	Crime
Grocery	Recreation	Education	Emergency	Listing Rent

Model Selection and Training. Now, based on our train, test split, various ML Algorithms such as Ridge Regression, Random Forest, Decision Tree, LightGBM, ElasticNet, XGBoost. Etc were trained. Table 4 depicts the various model results on the test set. Despite an MAE of 207.90 by the Random Forest Regressor, The XGBoost Model was selected for further fine-tuning due to a better R2 of 0.73 and a balanced combination of MAE and RMSE i.e. 217.07 and 304.32.

4.2 Model Parameter Tuning

The optimization of our XGBoost model's hyperparameters was a critical step towards enhancing its predictive performance. A range of hyperparameters was meticulously selected for tuning, Table 6 shows the hyperparameters that were used to fine-tune the XGBoost Model. Further fine-tuning of the XGBoost model, helped the results increase drastically, getting a MAE Score of 132.62 and R2 of 0.88. Table 5 shows the fine-tuned model results on the test set.

Table 4. Baseline Model Results

Model Name	MAE	RMSE	R2
Ridge Regression	261.68	362.83	0.62
Random Forest	207.90	316.44	0.71
SVR	438.58	597.59	–0.04
LightGBM	223.60	315.61	0.71
ElasticNet	273.31	386.45	0.57
K-NN	279.23	404.88	0.52
Decision Tree	317.24	483.76	0.32
XgBoost	217.07	304.32	0.73

Table 5. Fine-tuned ML Model Results

Model Name	MAE	RMSE	R2
Fine-Tuned XGBoost	132.62	195.91	0.88

Table 6. XGBoost Hyperparameters

Parameters	Values
N Estimators	200
Max Depth	5
Learning Rate	0.01
Subsample	0.7
Colsample Bytree	0.9
Min Child Weight	2
Gamma	0.1
Reg Alpha	0.1
Reg Lambda	0.01

4.3 Model Validation

On applying 5-Fold Cross Validation on the fine-tuned XGBoost Model, the results were quite robust. The model achieved a low average Mean Absolute Error (MAE) of 140.85, indicating the proximity of the predictions to the actual values. Consistency in model performance is evident with a low standard deviation in MAE (±4.97). A high average R-squared value of 0.83 suggests that the model explains 83% of the variance in the data, providing a strong fit. The Root Mean Squared Error (RMSE), another key metric reflecting average error magnitudes, stands at an average of 222.59 with low variability (±20.63) (Table 7).

Table 7. Summary of Model Evaluation Metrics Across Folds

Metrics	Fold1	Fold2	Fold3	Fold4	Fold5	Average
MAE	139.3	138.4	136.8	150.6	138.9	140.85 ± 4.97
RSME	203.1	207.2	217.5	261.1	223.7	222.59 ± 20.63
R2	0.86	0.84	0.85	0.81	0.78	0.83 ± 0.03

4.4 Model Visualization

In order to interpret the model, and understand the importance of various features on the Model, a SHAPELY graph was plotted. In Fig 8, it clearly shows that features like bedroomCount, listingSizeSquareFeet and bathroomCount have the highest impact on the model whereas features like listingType and listingMinorRegion seem to have less impact on the model, with most SHAPY values clustered around zero.

4.5 Architecture

Figure 9 outlines the architecture of our solution. For our Automated Scraping Solution, we have a Lambda Function setup which gets triggered daily to initiate our EC2 Instance where all our scraping scripts gets executed, these scripts are based on Selenium, Scrapy, and Python. Once all the data is scraped, all the data gets stored in our s3 bucket, and all the processed and structured data is then sent to our AWS RDS Database.

Once we have structured data in our Database, this data is then used for our real-time dashboards using Tableau and ML Model Training. We have setup a ML Model Training pipeline, which will fetch data from the database, apply feature engineering on it, train our models, and finally deploy the model to AWS Sagemaker Inference. These Dashboards and Models are then integrated with our application where the application's back-end is based on Flask and the front-end is based on ReactJS. An SMTP server is also setup on our EC2 Instance, which focuses on sending automated alerts to business basis on any new and significant developments.

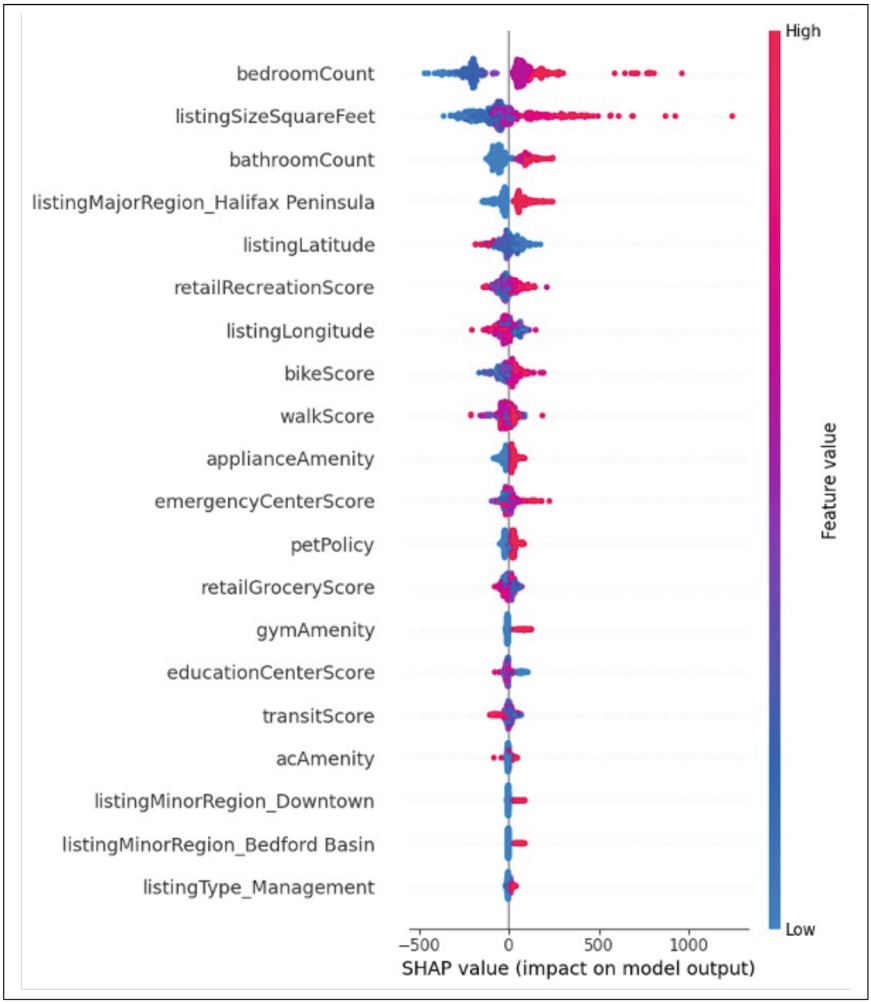

Fig. 8. SHAPELY Visualization

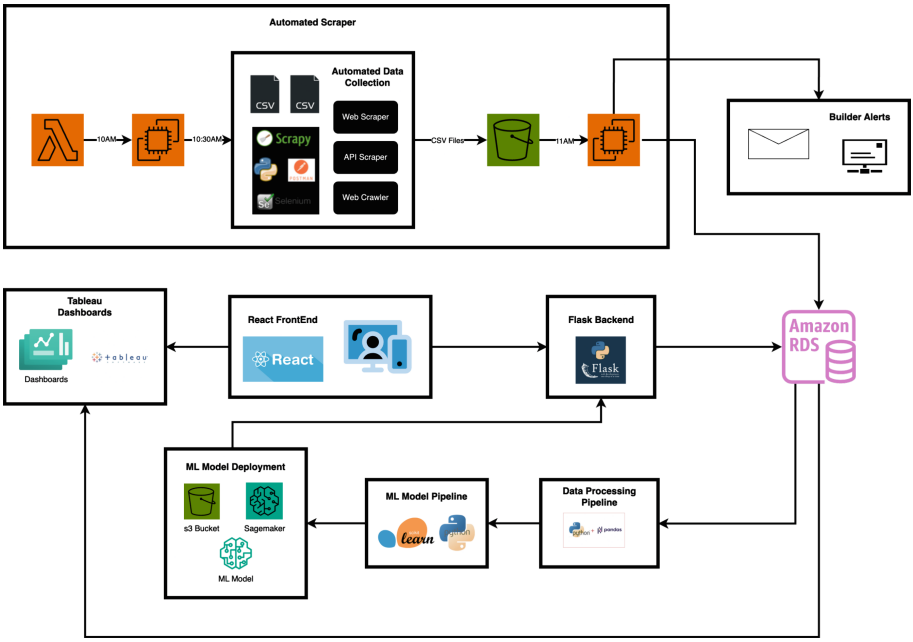

Fig. 9. Architecture Diagram

5 Conclusion and Future Scope

The proposed platform, Estate 360°, offers a transformative solution to the challenges in the Halifax rental market. With its advanced data analytics, automated data collection, and user-friendly interfaces, Estate 360° enhances decision making for property managers and policymakers. By integrating real-time data with predictive analytics, the platform allows stakeholders to quickly and accurately respond to market dynamics, ensuring competitiveness and strategic alignment. The implementation of Estate 360° aims to streamline operations, reduce manual data collection, minimize errors, and boost operational efficiency. Its ability to provide insights into market trends, competitor analysis, and rent predictions gives users a competitive advantage, effectively positioning them to seize market opportunities. The future development of the solution will focus on several key areas to further enhance its capabilities and reach within the market.

Expansion to Additional Markets. While currently focused on Halifax, there is potential to adapt and expand the platform to other regions, accommodating different market dynamics and regulatory environments. This scalability could make our platform a valuable tool for a broader range of users across various geographical locations.

Enhanced Machine Learning Models. As the platform collects more data over time, there will be opportunities to refine the predictive analytics capabilities. Implementing more sophisticated machine learning models could improve the accuracy of predictions regarding rent prices and market trends.

Acknowledgments. We would like to acknowledge with much appreciation the crucial role of Dr. Pawan Lingras and Mr. Shameer Iqbal who helped us along the way with their insightful feedback, and practical advice which helped us in coordinating the overall project.

References

1. Abdul Salam, M.H., Mohd, T., Masrom, S., Johari, N., Mohamad Saraf, M.H.: Machine learning algorithms on price and rent predictions in real estate: a systematic literature review. In: Rethinking Built Environment: Towards a Sustainable Future, pp. 260–270 (2022)
2. Asaftei, G.M., Sanghvi, A., Doshi, S., Means, J.: The Potential in Real Estate Analytics, McKinsey, New York (2018)
3. Balakrishnan, D.M., Ramprasath, J.: Prediction of data analysis using machine learning techniques. Int. J. Aquat. Sci. **12**(3), 2755–2762 (2021)
4. Baur, K., Rosenfelder, M., Lutz, B.: Automated real estate valuation with machine learning models using property descriptions. Expert Syst. Appl. **213**, 119147 (2023). https://doi.org/10.1016/j.eswa.2022.119147
5. Bergadano, F., Bertilone, R., Paolotti, D., Ruffo, G.: Learning real estate automated valuation models from heterogeneous data sources. Int. J. Real Estate Stud. **15**(1), 72–85 (2021). https://doi.org/10.11113/intrest.v15n1.10
6. Berry, N.: Modern web scraping and data analysis tools to discover historic real estate development opportunities (2022)
7. Bricongne, J.C., Meunier, B., Pouget, S.: Web-scraping housing prices in real-time: the covid-19 crisis in the UK. J. Hous. Econ. **59**, 101906 (2023). https://doi.org/10.1016/j.jhe.2022.101906
8. CMHC: Rental market report data tables
9. Conway, J.J.E.: Artificial intelligence and machine learning : current applications in real estate (2018)
10. Hebert, N.: An overview of Halifax. Nova Scotia's rental housing market. Saint Mary's University, Halifax, N.S. (2022)
11. Jach, T.: Web scraping methods used in predicting real estate prices. In: Wojtkiewicz, K., Treur, J., Pimenidis, E., Maleszka, M. (eds.) ICCCI 2021. CCIS, vol. 1463, pp. 375–387. Springer, Cham (2021). https://doi.org/10.1007/978-3-030-88113-9_30
12. Joshi, S.: How MLS APIs & web scraping techniques enhance real estate listings
13. Khountham, A.: Rental market analysis. (RMA), A complete guide for investors (2023)
14. Kok, N., Koponen, E.L., Martínez-Barbosa, C.A.: Big data in real estate? From manual appraisal to automated valuation. J. Portfolio Manage. **43**(6), 202–211 (2017). https://doi.org/10.3905/jpm.2017.43.6.202
15. Munceanu, R.: The complete guide to web scraping real estate data - WebScrapingAPI (2021)

16. Nehal: Mastering the market: Real estate data scraping & trend analysis (2023)
17. Ngoc, N.M., Tien, N.H., Anh, D.B.H.: Opportunities and challenges for real estate brokers in post covid-19 period. J. Sci. Technol. **170**(10), 203–208 (2020)
18. OpenAI: Chatgpt: Optimizing language models for dialogue. Software available from OpenAI (2023)
19. Ortscheid, T.: Understanding rental rate trends: a comprehensive analysis of the property management industry (2023)
20. Park, S.J.P.: Data science strategies for real estate development (2020)
21. Pérez-Rave, J.I., Correa-Morales, J.C., González-Echavarría, F.: A machine learning approach to big data regression analysis of real estate prices for inferential and predictive purposes. J. Prop. Res. **36**(1), 59–96 (2019). https://doi.org/10.1080/09599916.2019.1587489
22. Rafiei, M.H., Adeli, H.: A novel machine learning model for estimation of sale prices of real estate units. J. Constr. Eng. Manag. **142**(2), 04015066 (2016). https://doi.org/10.1061/(ASCE)CO.1943-7862.0001047
23. Samadani, S., Costa, C.J.: Forecasting real estate prices in Portugal : a data science approach. In: 2021 16th Iberian Conference on Information Systems and Technologies (CISTI), pp. 1–6 (2021). https://doi.org/10.23919/CISTI52073.2021.9476447
24. Su, T., Li, H., An, Y.: A BIM and machine learning integration framework for automated property valuation. J. Build. Eng. **44**, 102636 (2021). https://doi.org/10.1016/j.jobe.2021.102636
25. Vinciguerra, P.: Web scraping in real estate: Techniques and insights, web scraping club (2023)
26. Viriato, J.C.: AI and machine learning in real estate investment. J. Portf. Manag. **45**(7), 43–54 (2019). https://doi.org/10.3905/jpm.2019.45.7.043
27. Williams, O.: Identifying real estate development opportunities: web-scraping, regex patterns & string-searching algorithms (2021)

Housing Rental Information Management and Prediction System Based on CatBoost Algorithm - a Case Study of Halifax Region

Shuangrun Shao[1], Bingxi Zhao[2], Xiangen Cui[1(✉)], Yihong Dai[1], and Beining Bao[1]

[1] School of Economics and Management, Beijing Jiaotong University, Beijing 100044, China
{21711106,22711042,22725048,20723041}@bjtu.edu.cn
[2] School of Electronic and Information Engineering, Beijing Jiaotong University, Beijing 100044, China
23721035@bjtu.edu.cn

Abstract. Considering the growing demands for efficient information retrieval from house rental markets by non-professional users, we develop a comprehensive framework for house information management, visualization, and prediction based on the CatBoost algorithm. We aim to promote the digital transformation of house rental market management and drive innovation in management methods. The conception and ideas of the Housing Rental Information Management and Prediction System are initially proposed, with subsequent application in Halifax, Canada. Integrating the Tableau server, database, and prediction model, we build a seamless web system to harmonize management, visualization, and prediction functionalities for rental house data. The details and effects of the application of the CatBoost algorithm within this system are emphasized, highlighting its precision, adaptability, and business viability in forecasting the house rental market.

Keywords: CatBoost Algorithm · House Price Prediction · Information Management and Prediction System

1 Introduction

Price prediction of rental houses is crucial for effective housing administration [1]. Despite market fluctuations, house prices are mainly influenced by factors such as location, amenities, and convenience [2]. Reliable house price forecasts based on these parameters can enhance housing market management, maximizing total surplus. Various models have been developed for forecasting house prices. Park and Bae [3] developed a housing price prediction model based on machine learning algorithms such as C4.5, RIPPER, Naive Bayesian and AdaBoost, and compared their classification accuracy performance. Sharma et al. [4] employed the XGBoost algorithm for house price prediction, while Zhang et al. [5] used regression methods and algorithms based on textual description data.

Given the instability of rental house data, the choice of prediction model is critical. Among popular algorithms, CatBoost stands out as a Gradient Boosting Decision Trees

M. Hu et al. (Eds.): IJCRS 2024, LNAI 14840, pp. 230–246, 2024.
https://doi.org/10.1007/978-3-031-65668-2_16

(GBDT) framework based on oblivious trees, offering strong support for categorical features and requiring less data [6]. Jabeur et al. [7] demonstrated the adaptability of CatBoost in corporate failure prediction and house price prediction. Similar tree boosting methods have been applied to house price prediction [8], with Sharma et al. [4] reporting the development of an optimal house price prediction model based on XGBoost.

Different from previous work, this paper explores the potential of the CatBoost algorithm for real estate price prediction. We develop a new system integrating management, visualization, and prediction functions for data of rental houses, with the prediction module based on CatBoost. We specifically apply our system to Halifax (Nova Scotia, Canada), addressing the demands of potential users by providing a platform to gather relevant information, train and deploy the CatBoost prediction model, and offer easy interaction with both the prediction and visualization modules. Our platform provides a pragmatic approach for house management in Halifax and demonstrates the significant competence of the CatBoost algorithm in pricing analysis of rental houses.

In Sect. 2, we introduce the CatBoost algorithm and the Housing Rental Information Management and Prediction System (HRMPS). Section 3 explains how we apply the CatBoost model to our case. Section 4 demonstrates the final effects of HRMPS applied in Halifax, based on current housing market data. Finally, in Sect. 5, we discuss the conclusion and evaluation of our work.

2 Principles of HRMPS Based on CatBoost Algorithm

2.1 Principle of the CatBoost Model

The concept of ensemble modeling involves combining several weak learners using a specific strategy to collectively accomplish a task. A specific combination strategy can help the ensemble model reduce prediction bias or variance. Common strategies for ensemble modeling include bagging, stacking, and boosting. Gradient Boosting Decision Trees (GBDT) stands out as a remarkable method in boosting models, where the Kth tree is used to fit the residuals left by the previous K-1 trees, continuously reducing the overall model error [9].

CatBoost, along with LightGBM and XGBoost, are collectively known as the three major methods under GBDT. They are all improvements implemented under the GBDT algorithm. Initially designed to handle categorical features more effectively, CatBoost also introduces better solutions for gradient bias and prediction shift issues, enhancing the algorithm's accuracy and generalization ability [10].

In supervised learning, the loss function is usually as follows:

$$L(f(x), y) = \sum_i \omega \cdot l(f(x_i), y_i) + J(f) \tag{1}$$

where,

- $l(f(x), y)$ is the value of the loss function at the point (x, y),
- ω_i is the weight of the i-th object,
- $J(f)$ is the regularization term.

CatBoost use multiple decision trees f^t to build the model F^T, with trees constructed sequentially, each aimed at fitting the negative gradient g_i of the loss function L in the current model [11].

$$F^T = \sum_{t=1}^{T} f^t \tag{2}$$

$$g_i = -\left.\frac{\partial i(a, y_i)}{\partial a}\right|_{a=F^{T-1}(x_i)} \tag{3}$$

The quality of fitting the negative gradient g_i of the loss function by each decision tree is measured by a score function.

CatBoost's default score function is Cosine, but it allows users to choose other score functions, including L2, Newton, Cosine, and NewtonL2, which means users can choose first-order or second-order gradient calculations. It's important to note that when training on CPU, only Cosine and L2 scoring functions are supported [9].

$$Cosine = \frac{\sum \omega_i \cdot a_i \cdot g_i}{\sqrt{\sum \omega_i a_i^2} \cdot \sqrt{\sum \omega_i g_i^2}} \tag{4}$$

where,

- a_i is the prediction of candidate tree f^t for the i-th object x_i,
- ω_i is the weight of the i-th object.

Efficient handling of categorical features is a key feature of CatBoost. For low-cardinality features, CatBoost typically uses the one-hot encoding method to convert features into numerical values. Unlike many models, CatBoost performs one-hot encoding not during data preprocessing but during model training, which is a more efficient method. However, for high-cardinality categorical features, one-hot encoding may lead to the curse of dimensionality. In such cases, CatBoost uses the Target Statistics method to convert categorical features into numerical values. An effective approach is the Greedy TS with prior distribution added [12].

$$\hat{x}_k^i = \frac{\sum_{j=1}^{n} \mathbb{I}\left\{x_j^i = x_k^i\right\} \cdot y_j + \alpha p}{\sum_{j=1}^{n} \mathbb{I}\left\{x_j^i = x_k^i\right\} + \alpha} \tag{5}$$

where,

- i indicates category i,
- k indicates sample k,
- $\mathbb{I}\left\{x_j^i = x_k^i\right\}$ is to determine whether the current sample j belongs to the same category i as sample k, with 1 indicating a match and 0 indicating otherwise,
- p is the prior probability, which is the average of all target values in the dataset,
- α is the weight controlling the involvement of the prior in encoding.

Algorithm1. Building a tree in CatBoost

input : M, $\{(\mathbf{x}_i, y_i)\}_{i=1}^{n}$, α, L, $\{\sigma_i\}_{i=1}^{s}$, $Mode$

$grad \leftarrow CalcGradient(L, M, y)$;
$r \leftarrow random(1, s)$;
if $Mode = Plain$ **then**
  $G \leftarrow (grad_r(i)$ for $i = 1..n)$;
if $Mode = Ordered$ **then**
  $G \leftarrow (grad_{r,\sigma_r(i)-1}(i)$ for $i = 1..n)$;
$T \leftarrow$ empty tree;
foreach *step of top-down procedure* **do**
  foreach *candidate split* c **do**
    $T_c \leftarrow$ add split c to T;
    if $Mode = Plain$ **then**
      $\Delta(i) \leftarrow \text{avg}(grad_r(p)$ for $p : leaf_r(p) = leaf_r(i))$ for $i = 1..n$;
    if $Mode = Ordered$ **then**
      $\Delta(i) \leftarrow \text{avg}(grad_{r,\sigma_r(i)-1}(p)$ for $p : leaf_r(p) = leaf_r(i), \sigma_r(p) < \sigma_r(i))$ for $i = 1..n$;
    $loss(T_c) \leftarrow \cos(\Delta, G)$
  $T \leftarrow \arg\min_{T_c}(loss(T_c))$
if $Mode = Plain$ **then**
  $M_{r'}(i) \leftarrow M_{r'}(i) - \alpha\,\text{avg}(grad_{r'}(p)$ for $p : leaf_{r'}(p) = leaf_{r'}(i))$ for $r' = 1..s$, $i = 1..n$;
if $Mode = Ordered$ **then**
  $M_{r',j}(i) \leftarrow M_{r',j}(i) - \alpha\,\text{avg}(grad_{r',j}(p)$ for $p : leaf_{r'}(p) = leaf_{r'}(i), \sigma_{r'}(p) \leq j)$ for $r' = 1..s$, $i = 1..n$, $j \geq \sigma_{r'}(i) - 1$;
return T, M

In addition, by utilizing Ordered Boosting, CatBoost overcomes gradient bias and prediction shift issues [13]. Traditional GBDT methods use all dataset information when calculating the residuals for each data point, which can lead to overfitting. To prevent target leakage, CatBoost uses a strategy where each sample is estimated with a separate model trained on other samples to calculate its gradient. This change from biased to unbiased estimation helps CatBoost better address gradient bias issues. The description of building a tree in CatBoost can be found in Algorithm 1.

Another significant difference between CatBoost and other models is its use of oblivious trees as basic predictors [12]. In each step, the leaves of the previous tree are split using the same conditions, selecting the feature split with the lowest loss and applying it to all levels of nodes. This balanced tree structure aids in efficient CPU implementation, reducing prediction time, and serves as regularization to prevent overfitting. Also, this allows the model use histogram-based methods to search for the best split, distinguishing it from XGBoost and LightGBM, which rely on atomic operations and are more efficient for GPU calculations.

2.2 System Constructure and Data Connection

Our system achieves the five major functions of data mining, analysis, prediction, visualization, and web integration through the collaborative coordination of multiple modules. We will introduce the principles and contents of these modules. Specific applications will be demonstrated in the second part (Fig. 1).

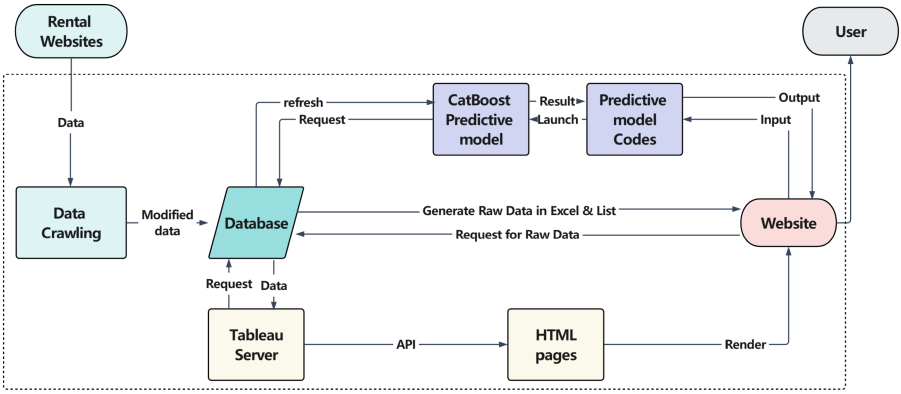

Fig. 1. Data Flow Chart of HRMPS

In general, our system integrates five major modules, including data crawling, data analysis, data prediction, data visualization and web integration, to comprehensively and efficiently connect data from rental websites to the user end [14].

Data Crawling. Based on Python, we crawl data from several rental websites and filter relevant house rental information, transforming it into usable data types.

Data Analysis. Employing the MySQL database, we establish a connection between the crawled data and the database, storing the data within [15]. Additionally, by setting up further patterns, the database is programmed to drive the corresponding data crawling process at regular intervals, ensuring updates to existing data.

Data Prediction. Leveraging the CatBoost decision model based on Python, we process the database data into feature data of the corresponding format and train multiple generations to obtain a predictive model. If necessary, the predictive model can be updated as the data in the database is updated.

Data Visualization. Utilizing Tableau's cloud service feature, we connect it with our MySQL database to import and visualize the data, incorporating various functions such as data filtering. Furthermore, employing Tableau's data refreshing feature ensures that the visualized images are updated as the database data changes [16].

Web Integration. We deploy our predictive model and data visualization modules in the server, which is connected to web, enabling users from any region to access our system via URL and operate as needed [17].

3 CatBoost Prediction Model Based on Halifax House Rental Dataset

3.1 Data Preparation and Pre-processing

The data set used in this paper is the data of house for rent in Halifax, Nova Scotia from March 24, 2024 to May 9, 2024 that crawled from the online house rental website. The raw dataset in Table 1 includes the house rent price and the property characteristics of the rental house.

Database Connection Configuration and Data Acquisition. First, we configure the database connection for the dataset, including parameters such as host address, port number, username, password, and database name. By creating the database connection string db_url, we connect to the MySQL database and execute the SQL query SELECT * FROM rental_data_analysis to load the query results into the "dataframe" form [18].

Data Cleaning and Processing. In the data preprocessing phase, we address the numeric substitution of "Studio" and "5 + " in the "Bedroom" feature, converting them to float64. Additionally, we standardize the "Type" feature by replacing "Apartments" with "Apartment". The "Bathroom", "Parking Included", and "Size_sqft" features are also converted to float64. For the feature "Move_In_Date", we first convert it to datetime format. Then, we calculate the number of days from today until the house is available to

move in. For entries where the date is "Not Available," the number of days is positive, indicating availability in the future. For entries with available dates, the number of days is negative, representing the days since the availability date.

To ensure data accuracy and completeness, we remove rows where the "Price" feature is listed as "Please Contact" and the "Size_sqft" feature is marked as "Not Available". Furthermore, we convert the data type of "Price", "Bedroom", "Bathroom", "Parking Included", and "Size_sqft" features to float64 for numerical calculations and analysis.

Table 1. Halifax House Rent Dataset Features

Features	Detailed introduction	Variable type
Price	The price of the house (USD)	Float
Bedroom	The number of bedrooms	Float
Bathroom	The number of bathrooms	Float
Size_sqft	The size of the house (sqft)	Float
Type	The type of the house is apartment, condo, house, townhouse, duplex/triplex or basement	String
Latitude	The latitude of the house	Float
Longitude	The longitude of the house	Float
Utilities_Included	Whether hydro, heat and water are provided	String
Wi_Fi_and_More	Whether Wi-Fi and TV cable are included	String
Parking_Included	The number of parking	Float
Agreement_Type	Whether the agreement type is 1 year or month-to-month	String
Move_In_Date	The day when the house is available	String
Pet_Friendly	Whether pets can be kept in the house	String
Furnished	Whether the house contains furniture	String
Appliances	Whether laundry and Dishwasher is provided	String
Air_Conditioning	Whether air conditioning is included	String
Personal_Outdoor_Space	Whether yard and balcony are included	String
Smoking_Permitted	Whether smoking is permitted in the house	String

By calculating the mean (2129.75) and standard deviation (28.30) of the "Price" feature, we determine the outlier threshold using a 3σ approach. Subsequently, we generate a histogram of the "Price" variable for visual inspection. Outliers are identified and excluded based on the criterion of retaining data within the range of the mean plus or minus 3 times the standard deviation ($2044.85 \leq \text{Price} \leq 2214.65$) (Fig. 2).

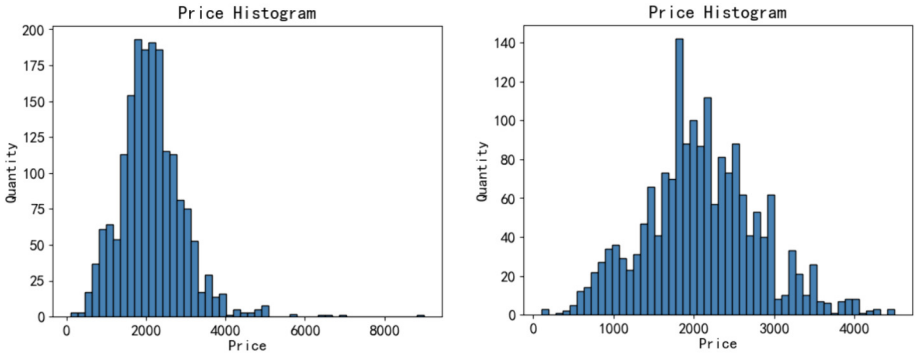

Fig. 2. Price Histogram before and after Removing Outliers

3.2 Exploratory Data Analysis

Descriptive Statistical Analysis. While performing the data analysis, we analyze the basic statistics of the dataset, including mean, standard deviation, minimum, maximum, etc., in order to gain insight into the distribution and characteristics of the data. At the same time, the distribution of each feature is described, which helps us to understand the overall characteristics and rules of the data (Table 2).

Table 2. Descriptive Statistical of Halifax House Rental Dataset

Feature	Latitude	Longitude	Bedroom	Bathroom	Parking Included	Move-In Date	Size_sqft
Count	1,776	1,776	1,776	1,776	1,776	1,684	1,776
Mean	44.67	−63.62	1.85	1.36	0.76	−3.55	1,020.99
Std	0.06	0.30	0.99	0.60	0.82	60.37	1,151.99
Min	44.48	−75.48	0.00	1.00	0.00	−1,286.00	1.00
25%	44.64	−63.64	1.00	1.00	0.00	−25.00	611.50
50%	44.65	−63.59	2.00	1.00	1.00	−9.00	900.00
75%	44.68	−63.58	2.50	2.00	1.00	22.00	1,209.25
Max	45.36	−63.01	5.00	4.00	3.00	144.00	41,252.00

Longitude and Latitude Distribution. The latitude mean in the dataset is 44.67 with a standard deviation of 0.06, and the longitude mean is -63.62 with a standard deviation of 0.30. This indicates that the data points are mainly concentrated around these mean values with a small range of variation.

Number of Bedrooms and Bathrooms. Bedroom has a mean of 1.85 with a standard deviation of 0.99, and Bathroom has a mean of 1.36 with a standard deviation of 0.60. Most listings have 1 to 2 bedrooms and 1 to 2 bathrooms.

Parking Included. Parking included has a mean of 0.76 and a standard deviation of 0.82. Most listings provide parking, but some do not.

Move-In Date. The mean of move-in date is − 3.55 with a standard deviation of 60.37. This means that more than half of the homes are now ready for occupancy.

House Size. The average value of house size (Size_sqft) is 1020.99, and the standard deviation is 1151.99. Listings with sizes between 611.50 and 1209.25 are more common, but larger listings also exist, with a maximum value of 41252.00.

Based on the above analysis, the listings in the dataset are mainly concentrated in a certain range, and most of the listings have 1 to 2 bedrooms and 1 to 2 bathrooms, provide parking Spaces, and the house size is at a medium level. In addition, we observe that there are some missing values in the "Move-In Date" feature, but the CatBoost model can handle this effectively.

Distribution of Specific Categorical Variables. To understand the housing rental situation in the Halifax market, we also examine the distribution of different types of rental houses (Fig. 3).

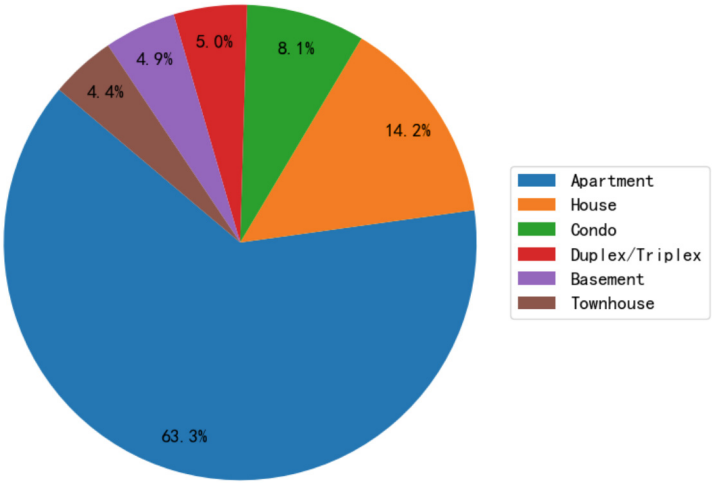

Fig. 3. Percentage of Feature - Type

Apartments dominate the housing rental market in Halifax, with houses and condos following as the next popular choices. Other housing types, including duplexes/triplexes, basements, and townhouses, have smaller market shares, indicating relatively lower demand.

Correlation Analysis for Numerical Variables. In the correlation analysis, we carefully investigate the relationships between each feature to identify strong correlations with the target variable. This analysis provides valuable insights into how different features, such as house size and price, interact and contribute to the target variable.

In Fig. 4, We observe that the number of bedrooms and bathrooms has a relatively strong correlation with the price, while the correlation between parking included and price is relatively low. Surprisingly, the correlation between size_sqft and price is the lowest, presenting a departure from established paradigms. This incongruity implies that purchasers assign greater value to meticulously designed and functionally optimized spatial arrangements, even within more compact real estate holdings, thereby augmenting their perceived worth and consequentially elevating transaction prices.

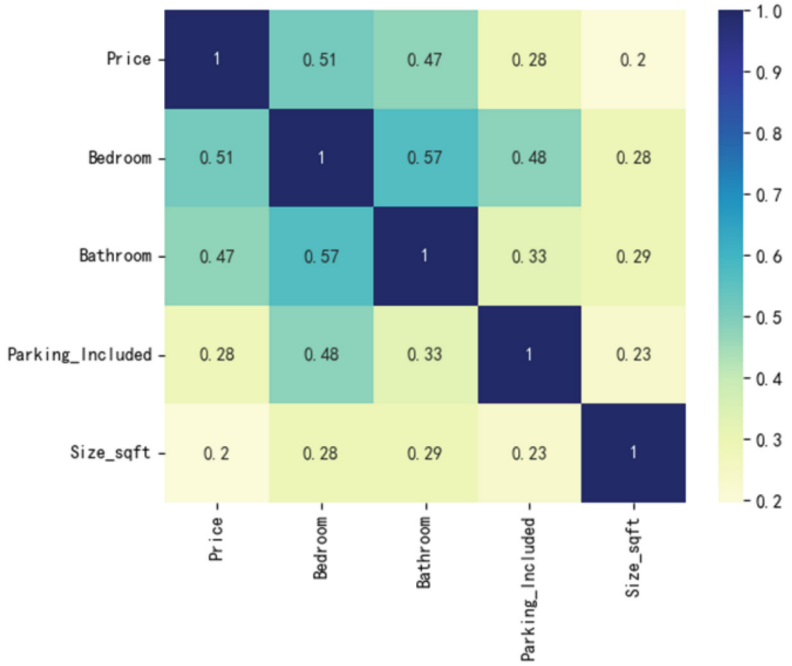

Fig. 4. Heat Map for Numerical Variables

3.3 Model Training

Dataset Splitting. During model training, the dataset is split into a training set and a test set, where the training set is 80% and the test set is 20%. This means that 80% of the data is used to train the model while 20% of the data is used to evaluate the performance of the model. By splitting in this way, it can be helpful to use the test set to tune the hyperparameters of the model to improve the performance of the model.

Model Parameter Settings. The parameters selected for the model, such as the number of iterations, learning rate, tree depth, loss function, evaluation metric, random seed, and overfitting detection settings, are crucial for enhancing prediction accuracy and generalization capabilities.

By setting the number of iterations to 500, the model can learn dataset patterns and features more effectively. A learning rate of 0.13 balances training speed and accuracy, while a tree depth of 11 allows for learning complex patterns without risking overfitting. The RMSE loss function optimizes model training by reducing errors between predicted and true values. Consistency between the RMSE loss function and evaluation metric ensures accurate model assessment. A random seed of 99 aids results reproducibility, while overfitting detection settings prevent model overfitting.

K-fold Cross-Validation Process and Results ($\mathbf{K = 5}$). We adopted a k-fold (5-fold) cross-validation approach, where the dataset is divided into 5 subsets, and training and validation are performed alternately on each subset to evaluate the generalization ability and stability of the model. By analyzing the cross-validation results, we select the optimal model parameters and performance metrics to ensure that the model performs stably and has good generalization ability on different datasets.

3.4 Model Evaluation and Performance

Feature Importance Calculation and Visualization. Feature Weights: During training, the model assigns a weight to each feature based on information gain and Gini coefficient. These weights indicate the importance the model places on each feature. Higher weights suggest that the feature has a greater impact on the model's predictions, making them a key component of feature importance analysis.

Through the analysis of feature importance, we can discover that the number of bedrooms, the size of the house, and other intrinsic attributes of the house has higher importance, while additional features such as "furnished" and "air conditioning" have relatively lower importance (Fig. 5).

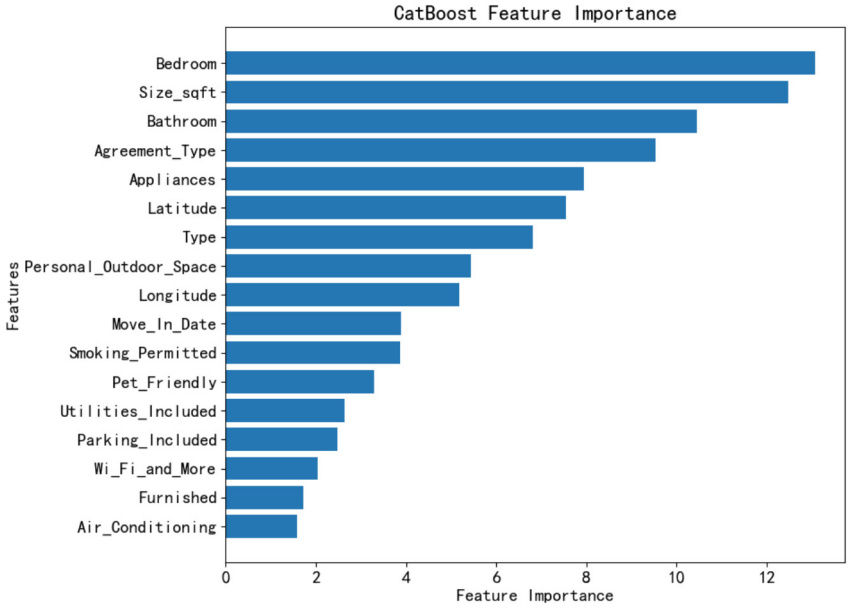

Fig. 5. Feature Importance

Model Performance Analysis. Interpretable R-squared of 0.77, taking into account the number of independent variables used in the model, provides a more accurate measure of model fit, indicating that the model can explain approximately 77% of the variance in the dependent variable. A mean absolute error (MAE) of 196.03 reflects the average absolute difference between predicted and actual values, with a lower MAE indicating more accurate predictions. The mean squared error (MSE) of 100072.66, representing the average squared difference between predicted and actual values, also suggests more accurate predictions by the model (Table 3).

Table 3. Model Performance Metrics

Interpretable R^2	mean absolute error (MAE)	mean square error (MSE)
0.77	196.03	100072.66

These data demonstrate that our use of the CatBoost model for house price prediction in Halifax is relatively accurate and can provide effective assistance to house rental professionals (Fig. 6).

The model is accurate for most of the price predictions, but has relatively poor prediction accuracy for values that are far from the mean. We look forward to proposing new methods to produce better performance in future study.

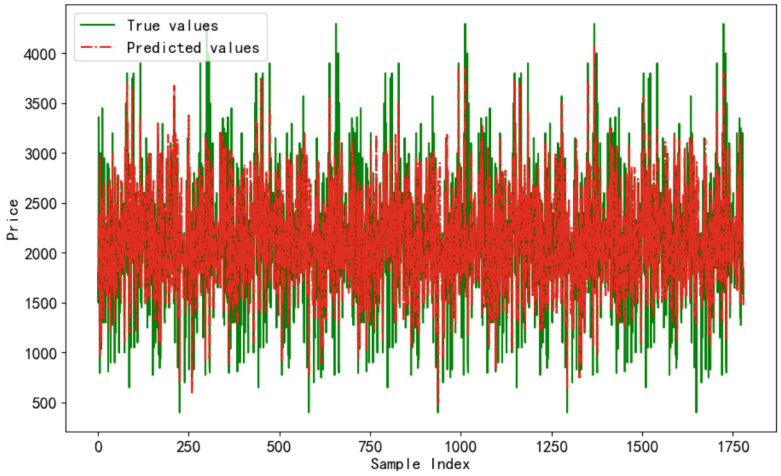

Fig. 6. Comparison of True and Predicted Values

4 Application of HRMPS in Halifax Region

In the case of Halifax, HRMPS is presented on the webpage in HTML language. Through the integrated connection of the webpage, server, and data source by Axios [19] and Node [20], we can easily ensure that the information on the webpage remains up-to-date [21]. Our webpage consists of two main subpages: the visualization page and the prediction page.

Within the visualization page, users can utilize sliders above the tableau module [22] to filter the desired property types based on price and area [23]. Additional filters and

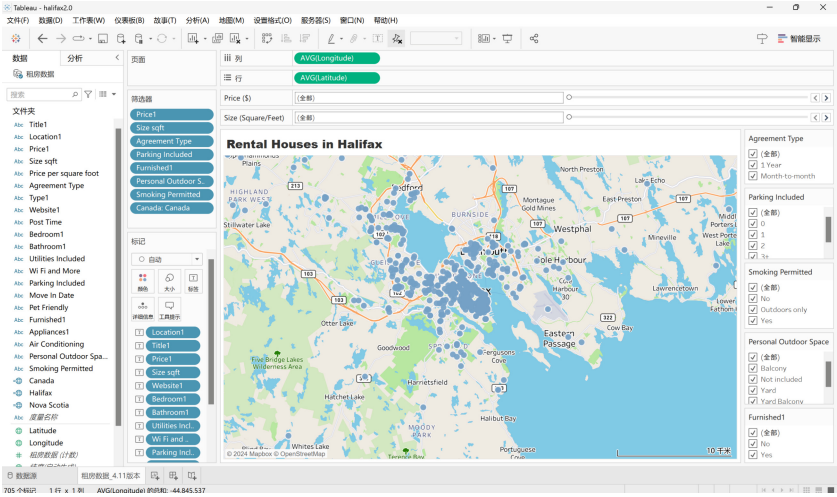

Fig. 7. Visualization of the Halifax dataset on Tableau

options can be selected from specific perspectives on the right sidebar. Detailed information about each specific location, including a link to the official website of the house, is provided. The housing listings and search modules are located on the right side of the visualization page, allowing users to access house information by entering keywords in the search box or scrolling through the list. The download buttons for downloading house data and the prediction module are located at the top of the visualization page (Figs. 7 and 8).

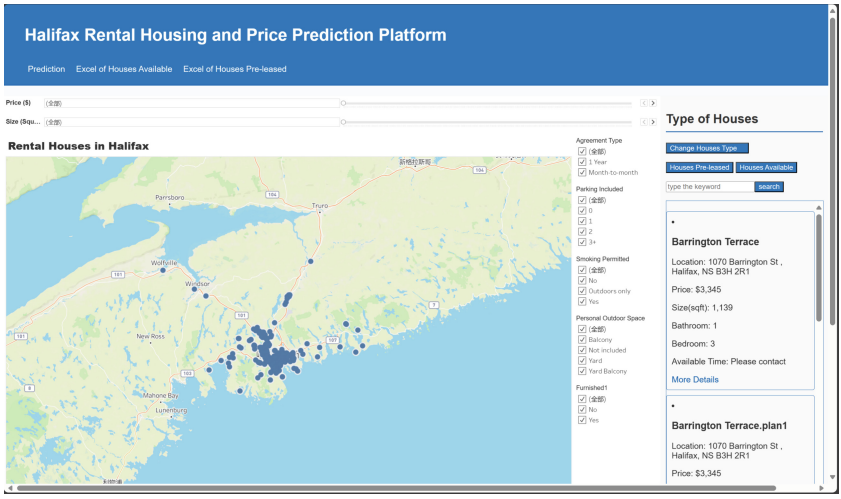

Fig. 8. Visualization of the Halifax dataset on Web Site

Users can navigate to the prediction page by clicking on the "prediction" button. In this page, users can interactively input or select specific information to make predictions according to their requirements. Notably, for latitude and longitude input, we have integrated the Google Maps API, enabling users to select a point on the map instead of manually entering coordinates [24]. The server-side program will automatically use the latitude and longitude of the selected point as input for price prediction. Upon completion of the form and clicking the "Submit" button, the predicted price will be returned (Fig. 9).

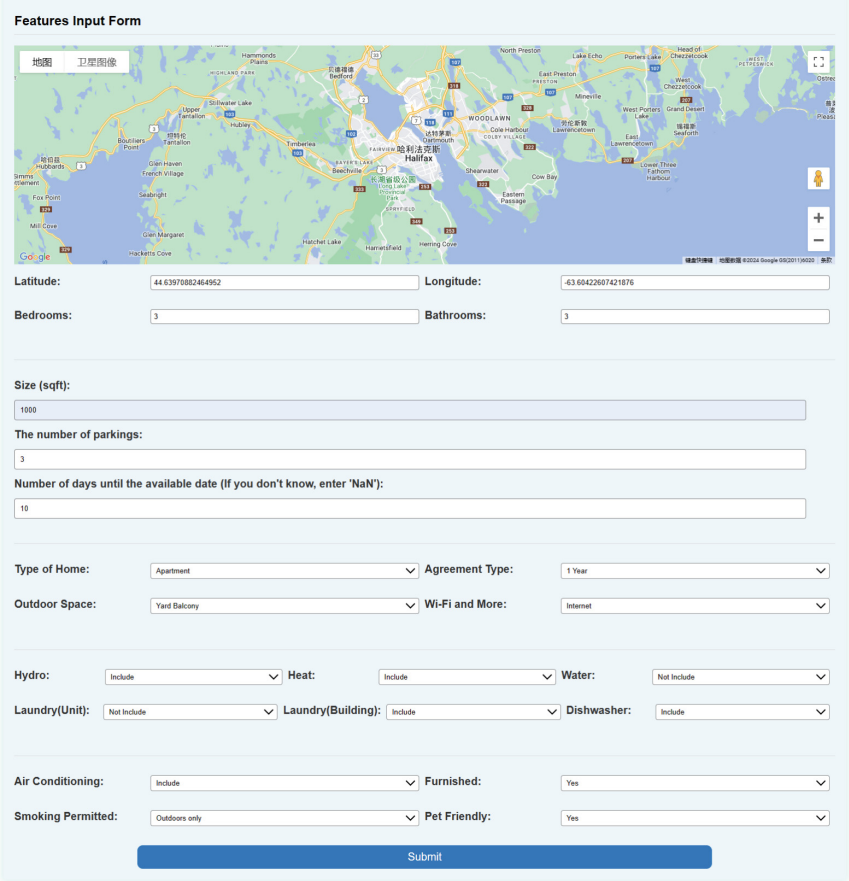

Fig. 9. Prediction Features Input Form on Web Site

5 Conclusions

In conclusion, the Housing Rental Information Management and Prediction System based on CatBoost Algorithm (HRMPS) not only features a comprehensive structure, extensive functionality, and strong practicality but also possesses significant adaptability and commercial prospects, bringing new perspectives and opportunities to the house rental information management field.

The system exhibits a comprehensive structure and functionality, providing a holistic solution for house rental information management. By integrating five major functions including data mining, analysis, prediction, visualization, and web integration, users are able to complete the entire process from data processing to decision support within a single platform. This comprehensiveness not only enhances the practical value of the system but also improves user experience, enabling more effective responses to the complexities of the house rental market environment. Additionally, the system's data

refreshing feature based on databases and Tableau enables automatic updates, significantly reducing the workload for data maintenance and enhancing the timeliness and accuracy of information.

The system's practicality is demonstrated by its ability to address real-world problems. Using the application in the Halifax region as an example, the system not only conducts data analysis and prediction for specific issues but, more importantly, its models are built based on actual demands, ensuring high authenticity and reliability. In contrast, many theoretical models often struggle to be directly applicable in practical contexts, whereas our system can directly confront and solve real-world problems, ensuring its feasibility and effectiveness in practice.

Finally, the adaptability and commercial prospects of the system add long-term value. The system can easily adapt to various regional house rental information management needs, and based on its fundamental model approach, with appropriate upgrades and adjustments, can achieve initial commercial development. For instance, by enhancing data security, optimizing user interfaces, and providing customized services, our system can attract more commercial clients and generate broader applications and value in the house rental industry and related fields. This commercial prospect not only enhances the system's sustainability but also brings broader development opportunities and returns for users and investors.

Acknowledgement. The authors thank Dr. Zhen Wang for providing valuable comments and suggestions on Halifax Housing Rental Information Management and Prediction System. The authors would also like to thank anonymous reviewers for their constructive comments.

References

1. Shen, H., Li, L., Zhu, H., Liu, Y., Luo, Z.: Exploring a pricing model for urban rental houses from a geographical perspective. Land **11**(1), 4 (2022). https://doi.org/10.3390/land11010004
2. Goodhart, C., Hofmann, B.: House Prices and the Macroeconomy: Implications for Banking and Price Stability. Oxford University Press eBooks, Oxford (2006). https://doi.org/10.1093/oso/9780199204595.001.0001
3. Park, B., Bae, J.K.: Using machine learning algorithms for housing price prediction: the case of Fairfax county, Virginia housing data. Expert Syst. Appl. **42**, 2928–2934 (2015). https://doi.org/10.1016/j.eswa.2014.11.040
4. Sharma, H., Harsora, H., Ogunleye, B.: An optimal house price prediction algorithm: XGBoost. Analytics. **3**, 30–45 (2024). https://doi.org/10.3390/analytics3010003
5. Zhang, H., Li, Y., Branco, P.: Describe the house and i will tell Tou the price: house price prediction with textual description data. Nat. Lang. Eng. **29**, 1–35 (2023). https://doi.org/10.1017/s1351324923000360
6. Hancock, J.T., Khoshgoftaar, T.M.: CatBoost for big data: an interdisciplinary review. J. Big Data. **7**, 94 (2020). https://doi.org/10.1186/s40537-020-00369-8
7. Jabeur, S.B., Gharib, C., Mefteh-Wali, S., Arfi, W.B.: CatBoost model and artificial intelligence techniques for corporate failure prediction. Technol. Forecast. Soc. Chang. **166**, 120658 (2021). https://doi.org/10.1016/j.techfore.2021.120658
8. Hjort, A., Scheel, I., Sommervoll, D.E., Pensar, J.: Locally interpretable tree boosting: an application to house price prediction. Decis. Support. Syst. **178**, 114106 (2024). https://doi.org/10.1016/j.dss.2023.114106

9. Friedman, J.H.: Greedy function approximation: a gradient boosting machine. Ann. Stat. **29**, 189–232 (2001)
10. Prokhorenkova, L., Gusev, G., Vorobev, A., Dorogush, A.V., Gulin, A.: CatBoost: Unbiased Boosting with Categorical Features. Curran Associates Inc. 32, 6639–6649 (2018)
11. Score functions - algorithm details. https://catboost.ai/en/docs/concepts/algorithm-score-functions, Accessed 10 May 2024
12. Samat, A., Li, E., Du, P., Liu, S., Miao, Z., Zhang, W.: CatBoost for RS image classification with pseudo label support from neighbor patches-based clustering. IEEE Geosci. Remote Sens. Lett. **19**, 1–5 (2022). https://doi.org/10.1109/lgrs.2020.3038771
13. Adler, A.I., Painsky, A.: Feature importance in gradient boosting trees with cross-validation feature selection. Entropy **24**(5), 687 (2022). https://doi.org/10.3390/e24050687
14. Sayyad, S., Saraf, A., Kale, D., Pardeshi, N.: House price and rent prediction using machine learning. IRJMETS **3**(5), 1098–1103 (2021). https://doi.org/10.56726/IRIMETS40466
15. Raj, A., Meghana, D'Souza, P., Rodrigues, R.: Implementation of MySQL in Python. Int. J. Res. Anal. Rev. **7**(1), 447–451 (2020)
16. Khedikar, K.A.: Data analytics for business using Tableau. In: Proceedings of the International Conference on Innovative Computing & Communication (2021).https://doi.org/10.2139/ssrn.3835030
17. Lu, L., Cen, G., Gao, W., Wang, Q., Zhao, J., Du, J.: A research of information management system solution base on centos & Oracle, IEEE pp. 309–312 (2010)
18. Satoto, K.I., Isnanto, R.R., Kridalukmana, R., Martono, K.T.: Optimizing MySQL database system on information systems research, publications and community service, IEEE, pp. 1–5 (2016). https://doi.org/10.1109/ICITACEE.2016.7892476
19. Kholmatov, A.: Widely used libraries in the JavaScript programming language and their capabilities. Int. Res. Sci. J. **2**(10), 18–25 (2023)
20. Bangare, S. L., Gupta, S., Dalal, M., Inamdar, A: Using Node.Js to build high speed and scalable backend database server. NCPCI **19**, 61–64 (2016)
21. Taneja, S., Gupta, P.R.: Python as a tool for web server application development. Int. J. Inf. Commun. Comput. Technol. **2**(1), 77–83 (2014)
22. Batt, S., Grealis, T., Harmon, O., Tomolonis, P.: Learning Tableau: a data visualization tool. J. Econ. Educ. **51**(3), 317–328 (2020). https://doi.org/10.1080/00220485.2020.1804503
23. Balaji, N., Pai, B.H.K., Bhat, B., Praveen, B.: Data visualization in Splunk and Tableau: a case study demonstration. J. Phys. Conf. Ser. **1767**, 012008 (2021). 1767 012008. https://doi.org/10.1088/1742-6596/1767/1/012008
24. Hu, S., Dai, T.: Online map application development using Google Maps API, SQL database, and ASP.NET. Int. J. Inf. Commun. Technol. Res. **3**(3), 102–110 (2013)

A Novel Approach to Rental Market Analysis for Property Management Firms Using Large Language Models and Machine Learning

Raoof Naushad(✉), Rakshit Gupta(✉), Tejasvi Bhutiyal, and Vrushali Prajapati

Department of Mathematics and Computing Science, Saint Mary's University, Halifax, NS B3H3C3, Canada
{raoof.naushad,rakshit.gupta,tejasvi.bhutiyal, vrushalisavankumar.prajapati}@smu.ca

Abstract. This research paper presents a novel approach to Rental Market Analysis for Property Management Firms using Large Language Models (LLMs) and Machine Learning techniques. The proposed system leverages LLM-based web scraping to extract data from dynamic websites, enabling the automated collection of relevant market information. By employing LLMs, the system generates insightful comparisons between property management firms and their listed properties, providing a comprehensive understanding of the competitive landscape. Additionally, an ensembled machine learning approach, utilizing multiple models, is developed to accurately predict rental prices. The integration of these cutting-edge technologies empowers property management firms with a dashboard that offers insightful analytics, predictive capabilities, and generated insights for data-driven decision-making. The system's architecture combines Python, ReactJS, AWS, PowerBI, PostgreSQL and OpenAI APIs to create a user-friendly interface that facilitates seamless data interaction and enhances insight generation. By automating data collection, analysis, and insight generation, this novel approach revolutionizes traditional rental market analysis processes, enabling property management firms to stay competitive and optimize their business strategies in dynamic rental markets.

Keywords: Rental Market Analysis · Property Management · Large Language Models · Machine Learning · Web Scraping · Predictive Analytics · Ensembled Models · Automated Data Collection

1 Introduction

1.1 Background

Rental Market Analysis is essential for the success of Property Management Firms, enabling them to optimize pricing strategies and maintain a competitive edge. Traditional methods, however, are manual and time-consuming, hindering the firms' ability to adapt

M. Hu et al. (Eds.): IJCRS 2024, LNAI 14840, pp. 247–261, 2024.
https://doi.org/10.1007/978-3-031-65668-2_17

quickly to market dynamics [1]. The emergence of Large Language Models (LLMs) and Machine Learning techniques offers a transformative potential for Rental Market Analysis [2].

Property Management Firms often struggle with the manual collection and processing of data, leading to outdated or incomplete information, which complicates decision-making. Moreover, the lack of automated tools and real-time analytics further limits their capability to derive actionable insights from the data [3].

To address these challenges, we propose NS-Rentals, a novel system utilizing LLMs and machine learning to automate data collection, cleaning, analysis, and insight generation. NS-Rentals integrates technologies such as LLM-based web scraping, ensembled machine learning, and dynamic user interfaces, offering a comprehensive solution that provides real-time insights into the rental market [4]. This system is designed to enhance predictive analytics, automate data management, and enable quick responses to market changes, significantly reducing the time and resources required for effective market analysis.

The primary objective of this research is to evaluate the efficacy of NS-Rentals in revolutionizing Rental Market Analysis, empowering Property Management Firms with the ability to make informed, data-driven decisions [5]. The significance of this research lies in its potential to streamline processes, enhance strategic decision-making, and provide firms with a competitive advantage in a rapidly evolving market.

2 Related Works

Recent advancements in machine learning (ML) and large language models (LLMs) have provided significant insights into various analytical domains, including rental market analysis. Several researchers have contributed to this field by integrating these technologies for data collection, analysis, and prediction.

Liu et al. (2023) explore the use of pre-trained language models for various datasets, highlighting the versatility of LLMs in data-driven scenarios, including property management and rental predictions. This work demonstrates the effectiveness of reinforcement learning models combined with LLMs for enhancing prediction accuracy in dynamic markets like real estate [6]. Biderman et al. (2023) provide a comprehensive analysis of large language models across different scales. They emphasize the correlation between model size and performance, suggesting that larger models exhibit enhanced capabilities in capturing market nuances, crucial for rental market predictions [7]. Ziems et al. (2024) discuss the potential of LLMs in computational social science, which can be applied to analyze real estate markets by understanding market trends and consumer behavior through language processing tools [8]. Rae et al. (2021) investigates the use of ensembled ML models in prediction tasks, demonstrating that combining multiple models often results in improved accuracy and robustness against varying data qualities. This approach is beneficial for predicting rental prices where market conditions fluctuate frequently [9]. Gao et al. (2023) introduce Program-aided Language models (PAL) that leverage the capabilities of LLMs to read and interpret market data, providing a novel approach for comparative analysis in the property sector [10].

Teubner et al. (2023) discuss the increasing prominence of LLMs in generating actionable insights from large data sets. Their study emphasizes how LLMs streamline

web scraping processes, making them more efficient and less prone to errors typically associated with traditional scraping techniques. This application directly supports use cases in competitive market analyses such as the rental sector [11]. Fellman, Tyo, and Lipton (2024) present advances in web data mining, highlighting the integration of multimodal data extraction methods enhanced by LLMs. Their research outlines the potential for these models to offer deeper insights by analyzing diverse data types, crucial for understanding nuanced market dynamics [12]. Lei, Docherty, and Cooper (2024) explore how LLMs can generate significant insights through automated web scraping, specifically focusing on their application in materials science. While their domain focus is different, the techniques discussed are applicable to rental market analysis, where diverse data sources are prevalent [13].

These studies collectively underscore the transformative impact of LLMs and ML techniques in rental market analysis. They offer a roadmap for property management firms to leverage cutting-edge technologies for data-driven decision-making and strategic planning. By automating the collection, analysis, and prediction processes, these approaches significantly enhance operational efficiency and market responsiveness for property management firms.

3 Methodology

3.1 System Architecture

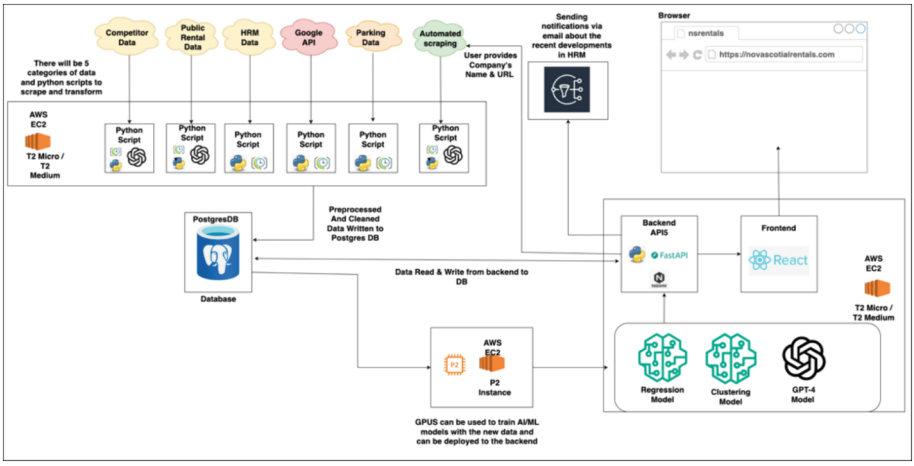

Fig. 1. Architecture

The proposed system (Fig. 1), NS-Rentals, employs a modular architecture designed to optimize the rental market analysis process through advanced technologies and frameworks. This system is hosted on Amazon Web Services (AWS) to leverage its scalability and reliability, ensuring efficient deployment and operation.

- Data Acquisition: Utilizes Python scripts on AWS EC2 instances, scheduled to run as cron jobs twice daily. These scripts scrape data from multiple sources including competitor data, public rental listings, and regional data from Halifax Regional Municipality (HRM).
- Data Processing and Storage: Scraped data undergoes cleaning and processing to ensure quality before storage in a PostgreSQL database. An incremental load strategy minimizes redundancy, focusing only on new or updated listings.
- Backend Server: Powered by FastAPI, this layer facilitates robust and efficient API management, connecting the data backend with the frontend application.
- Frontend Application: Developed using ReactJS, the frontend provides a dynamic and interactive user interface, enabling users to seamlessly explore and analyze data.

3.2 Dataset

The research utilizes a comprehensive dataset comprising various data streams (Fig. 2) to offer a holistic view of the rental market:

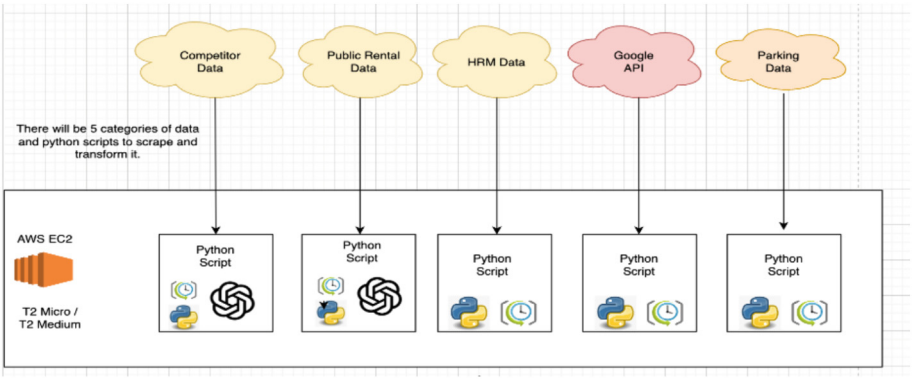

Fig. 2. Data Collection and Preparation

Competitor (Builders) Data
Extracted using advanced LLM-based web scraping techniques, capturing essential market offerings.

Public Rental Listings
Includes data from online platforms specific to the Halifax region.

Commercial Parking Data
Details parking facilities' data, impacting rental property desirability.

Halifax Regional Municipality (HRM) Data
Includes building permits and zoning changes to forecast market supply.

Location and Proximity Data via Google API
Uses Google API for accurate property geolocation and proximity to essential services.

3.3 Feature Engineering/Selection

In this study, feature engineering plays a pivotal role in transforming raw data into a structured and analyzable format, specifically for predicting the monthly rent of apartments and houses. Unstructured text from real estate listings is converted into structured data using Large Language Models (LLMs), which systematically process and organize textual descriptions into JSON formats suitable for database storage and analysis, as demonstrated by Radford et al. (2019) [15]. Additionally, categorical data such as property types and zoning classifications are numerically encoded through label encoding to avoid the high dimensionality associated with one-hot encoding, a technique highlighted for its effectiveness by Harris et al. (2020) [16].

Numerical attributes like rates and square footage undergo logarithmic transformations to normalize distributions and reduce skewness, enhancing model accuracy and stability, a method supported by Osborne (2010) [17]. Furthermore, continuous data such as apartment sizes are categorized into distinct bins ('unit_size_buckets'), which simplifies analysis by highlighting non-linear relationships, as discussed by Liu et al. (2018) [18]. The integration of geographic data using the Google API enriches the dataset by providing distances to essential services, thereby influencing rental desirability and pricing, a technique validated by Zhang et al. (2021). These engineered features are essential for the subsequent machine learning analysis, ensuring that the models are fed data that accurately reflects the complexities of the rental market.

Engineered Features
We engineered several attributes to provide a clearer picture of what each rental property offers. These attributes are directly derived from textual descriptions using Large Language Models (LLMs) which parse and organize data into structured formats:

- Utility Inclusions: Attributes such as utility_water, utility_heat, utility_electricity, and wifi_included clarify what utilities and services are included in the rental price, a crucial consideration for renters.
- Furnishings: The is_furnished attribute specifies the furnishing status of the property, which significantly impacts rental desirability and pricing.
- Parking: The parking_availability attribute details the specifics of parking facilities, another important factor for potential renters.
- Pet Policy: The pet_friendly attribute indicates whether pets are allowed, affecting the suitability of the property for pet owners.
- Location Coordinates: Attributes add_lat and add_long provide precise geographical coordinates of the properties, derived from the address.

Derived Features via Google API
Utilizing the Google API, we enriched the dataset with geographical distances from each property to key locations, which can significantly influence rental decisions:

- Proximity Features: Attributes like dist_school, dist_restaurant, dist_downtown, dist_busstop, and distances to notable areas such as Rockingham, Clayton Park, Larry Uteck area, and central Halifax provide insights into the property's accessibility and neighborhood desirability.

Final Feature Set
After thorough exploratory data analysis and feature engineering, the final set of features used for modeling includes:

- Basic Information: building_name, apartment_number, address, add_lat, add_long, company_name, property_type.
- Unit Specifications: bedroom_count, bathroom_count, is_furnished.
- Utility and Amenities: utility_water, utility_heat, utility_electricity, wifi_included.
- Parking Details: parking_availability, parking_slots, parking_rates, parking_distance, parking_address.
- Pet Policy: pet_friendly.
- Additional Attributes: unit_size, included_appliances, lease_duration, availability_status.
- Proximity Measures: dist_hospital, dist_school, dist_restaurant, dist_downtown, dist_busstop, dist_rockingham, dist_clayton_park, dist_larry_uteck_area, dist_central_halifax.

3.4 AI and ML Methodology

Ensemble ML Model for Prediction

In our analysis of the Halifax rental market, we employed a systematic approach to predict rental prices, beginning with an extensive data cleaning and preparation phase. The initial dataset comprised 2,275 records with 47 features, which were refined through geographic enrichment using Google API for precise location data and parking data integration to enhance listings. Outliers with unrealistically low rents were removed to maintain data integrity, and non-essential attributes such as building names were excluded to focus on variables directly impacting rental prices. Missing values were meticulously handled by imputing with median or mode values based on the feature type.

Following data preparation, exploratory data analysis (EDA) was conducted to uncover key insights and correlations between property features and rental prices. This phase included correlation analysis to identify strong predictors and outlier management to normalize distributions of key variables like monthly rent and apartment size. New categorical features based on proximity to essential amenities were created and encoded to refine the predictive model's accuracy. Feature engineering also played a crucial role in transforming raw data into structured formats that are more amenable to modeling.

The final modeling phase (Fig. 3) employed an ensemble learning approach, integrating several machine learning models to leverage their collective strengths and mitigate individual weaknesses. Models such as Random Forest [25], Gradient Boosting [26], XGBoost [27], CatBoost [28], and Lasso [29] to leverage their collective strengths and mitigate individual weaknesses. These models were selected after exploring 9 different ML models including Artificial Neural Networks, with hyperparameter tuning facilitated by the Optuna framework [30] and k-fold cross-validation. The ensemble model was weighted according to performance metrics from the validation dataset, focusing on minimizing the root mean square error (RMSE) and maximizing the R-square value. This comprehensive methodology ensured the development of a robust predictive model that

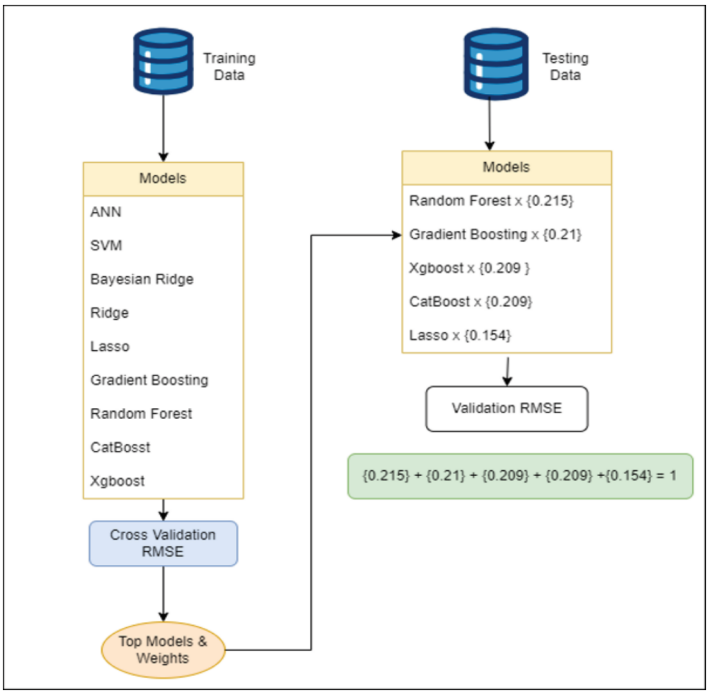

Fig. 3. Ensemble Learning

effectively captures the dynamics of the rental market, providing accurate and actionable insights for property management and investment strategies.

Nearest Neighbors (NN) for Competitive Analysis

The Nearest Neighbors (NN) algorithm plays a pivotal role in our strategy to position property management firms competitively in the real estate market. By employing the NN algorithm, specifically optimized with the 'ball_tree' method, we effectively identify the top five listings that most closely match each competitor's property.

The training of the Nearest Neighbors model was meticulously carried out on pre-processed data, focusing on features that define competitive attributes of properties. We fine-tuned the model by adjusting the number of neighbors and distance metrics to ensure that the model does not overly restrict or dilute the recommendations. After various experiments, the model was set to identify ten nearest neighbors, striking a balance that provides diverse and relevant comparisons across the competitive landscape. The choice of the 'ball_tree' algorithm was crucial for managing the high-dimensional data efficiently, significantly speeding up the query times for nearest neighbors searches compared to brute-force methods [20, 21].

This analytical capability equips property management firms with the intelligence to refine their marketing and pricing strategies effectively. By understanding the finer

nuances of how their properties compare to competitors, they can make informed decisions that help their offerings stand out in a dynamic market.

LLM-Based Web Scrapping

In this study, we employ advanced web scraping techniques powered by Large Language Models (LLMs) to collect data from dynamic websites. The scraping process utilizes Python scripts that leverage tools such as BeautifulSoup, Selenium, and Scrapy to extract HTML content from targeted websites. The extracted content undergoes post-processing to retain only the relevant information. To enhance the accuracy and efficiency of the data extraction process, the system employs a technique called Chain of Thoughts (CoT) in conjunction with the OpenAI GPT-4-Turbo model. CoT is an iterative approach that guides the LLM to extract listings based on a predefined database schema. By providing the model with a one-shot prompting technique, where an example input and output are used as a reference, the system ensures consistent and valid data extraction from the websites. Chain-of-thought prompting is a powerful method that enhances the performance of LLMs by encouraging them to mimic human reasoning processes. By incorporating instructions into the input prompt, the model is directed to explain its reasoning step by step, providing not only the final answer but also the intermediate steps leading to that conclusion. This technique has proven effective in improving model performance on complex tasks that require logical thinking, calculations, and decision-making [22, 23].

LLM Generated Insights

Our system generates two types of LLM-powered insights to aid in the comparative analysis of property management offerings. The first type of insight involves comparing two property management firms. When a comparison is initiated, relevant data about the selected properties is retrieved and passed to the GPT-4-Turbo model using a one-shot prompting technique. This method allows the model to understand the specifics of the required insights, enabling it to generate detailed comparisons that highlight the strengths and weaknesses of each firm. Similarly, the second type of insight focuses on comparing individual properties. Utilizing the same one-shot prompting technique, the GPT-4 model processes the provided data to produce insights that evaluate factors like location, amenities, and pricing, thereby aiding potential renters or investors in making informed decisions.

The one-shot prompting approach is crucial in both scenarios, as it equips the LLM to quickly adapt to the specific analysis task, ensuring that the insights generated are not only relevant and informative but also directly applicable to the user's needs. This technique underscores the potential of LLMs to transform data into actionable intelligence, thus providing NS-Rentals with a significant advantage in the competitive real estate market [15, 24].

4 Results and Validation

4.1 Ensemble-Based ML Rent Prediction Model Results

For a comprehensive understanding of the model's predictive capability, two primary metrics were employed:

- RMSE (Root Mean Square Error): This quantifies the average deviation between the model's predictions and the actual rental values, providing a measure of prediction error.
- R-Square (Coefficient of Determination): This reflects the proportion of the variance in rental prices that is predictable from the model's features.

The RMSE for various regression models are below (Fig. 4).

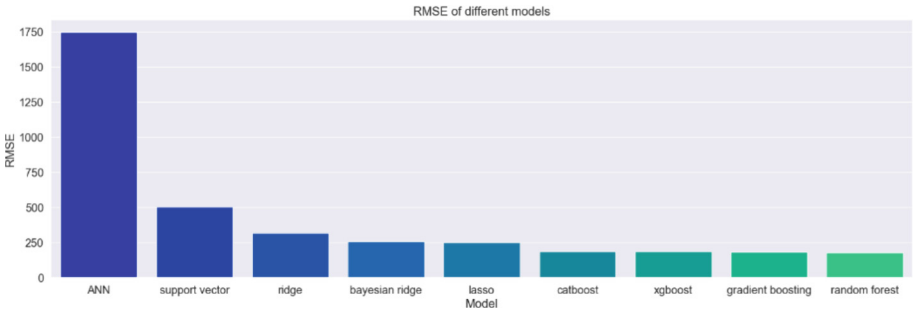

Fig. 4. Root Mean Square Error (RMSE) for various regression models

After exporting various predictive models using training data. The selection criteria hinged on:

- The strengths of each algorithm and its suitability for the dataset were considered based on their RMSE.
- Priority was given to models like XGBoost, CatBoost, Random Forest for their ensemble techniques which have proven beneficial in reducing overfitting and enhancing generalization in structured datasets [14] (Table 1).

Table 1. Various Model used for Ensemble Learning

Model	Interpretation	RMSE	Ensemble	Model
ANN	ANN model has the highest RMSE, suggesting that it might be overfitting to the training data	1746.375	N/A	N/A
SVM	The SVM's RMSE is lower than the ANN, indicating better performance. This may be due to its ability to find a hyperplane that best separates the data points	504.122	N/A	N/A

(*continued*)

Table 1. (*continued*)

Model	Interpretation	RMSE	Ensemble	Model
Bayesian Ridge	This model introduces Bayesian inference to the ridge regression, which could explain the lower RMSE due to its probabilistic approach that can handle uncertainty and prevent overfitting	257.869	N/A	N/A
Lasso Regression	Lasso introduces L1 regularization, which can zero out less important features, leading to simpler and more interpretable models that performed relatively well in validation	252.184	1/252.184	0.1540.154
Gradient Boosting	Shows a significant improvement and lower RMSE. Its iterative approach to minimizing errors can be attributed to its strong performance	185.215	1/185.215	0.21
Random Forest	As an ensemble of decision trees, it naturally handles non-linear data well. Its good performance might stem from its ability to average out biases and reduce variance	181.253	1/181.253	0.215
CatBoost	Tailored to handle categorical variables effectively, its lower RMSE could be due to its ability to prevent overfitting on the training dataset, which can be quite common with gradient boosting methods	186.419	1 / 186.419	0.209
XGBoost	It generally performs well on structured data and its low RMSE here suggests that it effectively captured the patterns in the dataset, possibly due to its sophisticated regularization which improves model generalizability	186.289	1/186.289	0.209

Final Model Predictive Performance: The culmination of the model training process was an ensemble approach, wherein individual model predictions were weighted and normalized. The key performance indicators were:

- RMSE: Achieved a value of 182.02, suggesting the predictions are within a reasonable margin of error.
- R-Square: An impressive 0.85, denoting that the model accounts for 85% of the variability in rental prices (Fig. 5).

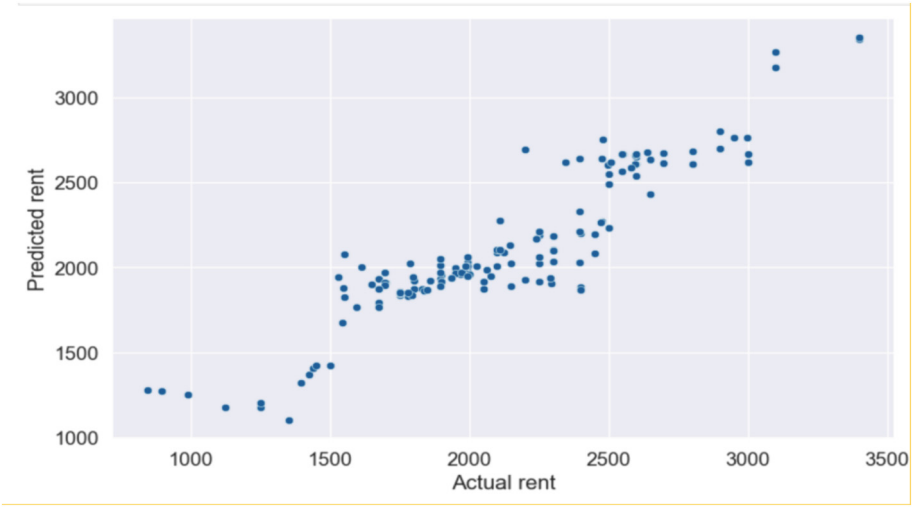

Fig. 5. A scatter plot of actual vs. predicted rents

The scatter plot analysis of actual versus predicted rents demonstrates strong model accuracy, particularly within the median price range, indicating reliable predictions where data is densest. However, there is noticeable variability at the pricing extremes, pointing to less precision for properties with very low or high rents. Isolated data points, especially at higher rental values, suggest potential outliers or unique property features that are not fully captured by the model. Overall, the ensemble model effectively reflects Halifax's rental market dynamics and supports pricing strategies.

4.2 Nearest Neighbor Results

To validate the model's effectiveness, the silhouette score was computed for the cluster formed by the target property and its nearest neighbors against the rest of the properties. For a given set of properties, we treated the target southwest property and its nearest neighbors (competitor property) as a "cluster" and computed the silhouette score with respect to this and other properties. A silhouette score of 0.4103441791255 was achieved, indicating a moderate to good level of separation between the target property's cluster and other properties. This score suggests that the nearest neighbors identified share more similarity with the target southwest property than with properties outside of this cluster, validating the model's capability in generating relevant property recommendations.

4.3 Validation and Evaluation of LLM BASED Insights Generation

In the results and validation section of our study, we utilized the GPT-4 Preview model to assess the quality of insights generated by the Language Learning Model (LLM). To facilitate this evaluation, the GPT-4 Preview was prompted to act in the capacity of a property management expert, tasked with assessing the insights based on parameters such as Consistency, Insight Utility, and Correctness (Figs. 6 and 7).

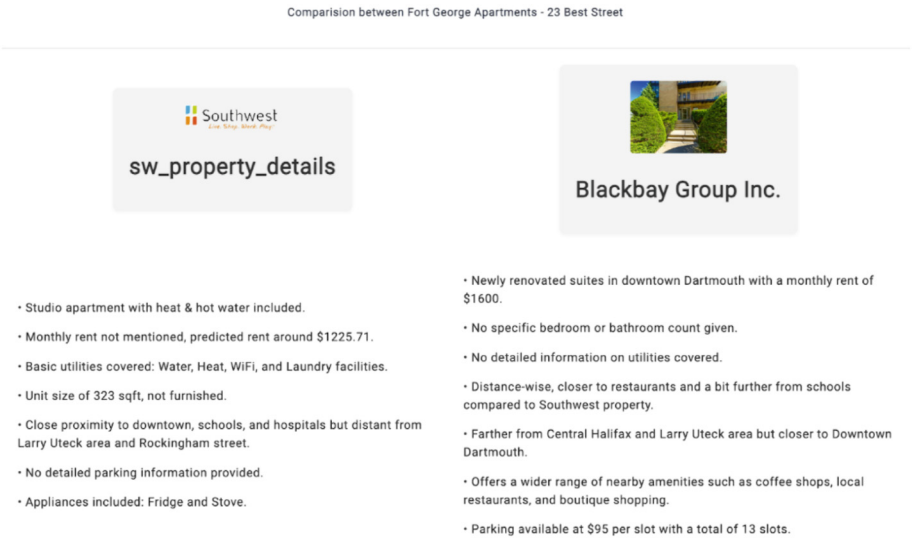

Fig. 6. LLM Based Insights Generated by GPT-4

Metric	Score (out of 100)	Comments
Consistency Rate	80	Consistent format in descriptions but varying detail level in utility information.
Insight Utility	85	Useful insights into location, amenities, and pricing that aid in decision-making.
Correctness	90	Accurate depiction of property features and offerings based on the screenshot.

Fig. 7. Validation of LLM Based Insights by GPT-4-Preview

To conduct this evaluation, detailed descriptions and relevant information about each property were provided to the GPT-4 Preview model. Following this, the model was asked to generate comparative insights, mimicking the real-world decision-making process of property management professionals. The comparison results from the GPT-4 Preview were then used as a benchmark to evaluate the insights generated by the LLM.

The insights generated by the LLM were scored based on how well they aligned with the benchmark insights from the GPT-4 Preview model. This comparative analysis yielded scores for each evaluation parameter, which demonstrated the LLM's capability in providing accurate and useful insights for property management (Table 2).

Table 2. LLM Evaluation Results

Metrices	Score percentage
Consistency Rate	89
Insight Utility	87
Correctness	85

This method of validation not only confirms the efficacy of the LLM in generating actionable insights but also highlights the advanced capabilities of GPT-4 Preview in performing as an expert evaluator within this domain.

5 Conclusion

This research presents NS-Rentals, a novel system leveraging Large Language Models (LLMs) and machine learning to revolutionize rental market analysis for property management firms. By automating data collection from dynamic websites using LLM-based web scraping, NS-Rentals provides a comprehensive and up-to-date view of the competitive landscape. The system's ensembled machine learning approach offers accurate rental price predictions, empowering firms to optimize pricing strategies. Furthermore, the integration of LLMs enables the generation of insightful comparisons between both property management firms and individual properties, offering a deeper understanding of market dynamics.

NS-Rentals, through its user-friendly dashboard, facilitates seamless data interaction and empowers data-driven decision-making. The system's architecture, built upon a combination of Python, ReactJS, AWS, PowerBI, PostgreSQL, and OpenAI APIs, ensures scalability, reliability, and efficient deployment. This research demonstrates the significant potential of LLMs and machine learning to transform traditional rental market analysis, providing property management firms with the tools and insights necessary to thrive in a dynamic market. Future work will explore incorporating additional data sources, refining LLM-generated insights, and developing personalized recommendations based on user preferences and market trends.

References

1. Preweda, E. Current problems of valuation and real estate management by value. https://www.researchgate.net/profile/Edward-Preweda/publication/266683482_Current_problems_of_valuation_and_real_estate_management_by_value/links/569a8b3b08aeeea9859ee5d8/Current-problems-of-valuation-and-real-estate-management-by-value.pdf

2. Large language models for automated data science: introducing CAAFE for context-aware automated feature engineering. In: Proceedings of NeurIPS (2023). https://proceedings.neurips.cc/paper_files/paper/2023/file/8c2df4c35cdbee764ebb9e9d0acd5197-Paper-Conference.pdf
3. Big data: the management revolution. https://tarjomefa.com/wp-content/uploads/2017/04/6539-English-TarjomeFa-1.pdf
4. Sheth, A., et al.: Chatgpt needs spade (sustainability, privacy, digital divide, and ethics) evaluation: a review. Cogn. Syst. Res. **74** (2024). https://link.springer.com/article/10.1007/s12559-024-10285-1
5. Donner, H. Digital Cities: Real Estate Development Driven by Big Data. https://www.researchgate.net/profile/Herman-Donner/publication/325253311_Digital_Cities_Real_Estate_Development_Driven_by_Big_Data/links/5cdbac94458515712eac2286/Digital-Cities-Real-Estate-Development-Driven-by-Big-Data.pdf
6. Liu, Y., et al.: Summary of chatgpt-related research and perspective towards the future of large language models. Meta-Radiol. (2023)
7. Biderman, S., et al.: Pythia: A suite for analyzing large language models across training and scaling. In: Proceedings of Machine Learning Research (2023)
8. Ziems, C., et al.: Can large language models transform computational social science?. Comput. Linguist. (2024)
9. Rae et al. 2021, "Scaling language models: Methods, analysis & insights from training gopher," arXiv preprint, 2021
10. Gao, L., et al.: Pal: Program-aided language models. In: Proceedings of Machine Learning Research (2023)
11. Teubner, T., et al.: Welcome to the era of chatgpt et al. the prospects of large language models. Bus. Inf. Syst. Eng. **65**, 95–101 (2023)
12. Fellman, E., Tyo, L., Lipton, Z.C.: The future of web data mining: Insights from multimodal and code-based extraction methods. In: Proceedings of the 7th Workshop on CASE (2024)
13. Lei, G., Docherty, R., Cooper, S.J.: Materials science in the era of large language models: a perspective arXiv preprint, 2024 (2024)
14. Acharya, S.: Comparative analysis of classification accuracy for XGBoost, LightGBM, CatBoost, H2O, and Classifium (2022). https://hiof.brage.unit.no/hiof-xmlui/bitstream/handle/11250/3053129/Acharya_Shubodha.PDF?sequence=1
15. Radford, A., et al.: Language Models are Unsupervised Multitask Learners. OpenAI Blog (2019)
16. Harris, Z., et al.: Effective encoding of categorical data. Mach. Learn. Res. (2020)
17. Osborne, J.: Improving your data transformations: applying the box-cox transformation. Pract. Assess. Res. Eval. **15**(12), 1–9 (2010)
18. Liu, B., et al.: Enhancing the handling of continuous attributes in decision tree learning. IEEE Trans. Knowl. Data Eng. (2018)
19. Zhang, P., et al.: Geographic data integration in real estate analysis. J. Real Estate Res.
20. Altman, N.S.: An introduction to kernel and nearest-neighbor nonparametric regression. Am. Stat. **46**(3), 175–185 (1992)
21. Muja, M., Lowe, D.G.: Fast Approximate nearest neighbors with automatic algorithm configuration. In: International Conference on Computer Vision Theory and Applications (VISAPP'09), INSTICC Press (2009)
22. Brown, T.B., et al.: Language Models are Few-Shot Learners. arXiv preprint arXiv:2005.14165(2020)
23. Wei, J., et al.: Chain of Thought Prompting Elicits Reasoning in Large Language Models. arXiv preprint arXiv:2201.11903(2022)
24. Devlin, J., Chang, M.W., Lee, K., Toutanova, K.: BERT: Pre-training of Deep Bidirectional Transformers for Language Understanding. arXiv preprint arXiv:1810.04805 (2018)

25. Breiman, L.: Random forests. Mach. Learn. **45**(1), 5–32 (2001)
26. Friedman, J.H.: Greedy function approximation: a gradient boosting machine. Ann. Stat. (2001)
27. Chen, T., Guestrin, C.: XGBoost: a scalable tree boosting system. In: Proceedings of the 22nd ACM SIGKDD International Conference on Knowledge Discovery and Data Mining (2016)
28. Prokhorenkova, L., Gusev, G., Vorobev, A., Dorogush, A., Gulin, A.: CatBoost: unbiased boosting with categorical features. NeurIPS (2018)
29. Tibshirani, R.: Regression shrinkage and selection via the lasso. J. R. Stat. Soc. Ser. B (Methodological) (1996)
30. Akiba, T., Sano, S., Yanase, T., Ohta, T., Koyama, M.: Optuna: A Next-generation Hyperparameter Optimization Framework. KDD, 2019 (2019)

Applications of Deep Learning and Soft Computing

Clinical Medical Test Decision-Making of Liver Disease Using Granular-Ball Rough Set

Fanxin Xu[1,2], Zuqiang Su[1,2], and Guoyin Wang[1,2(✉)]

[1] Chongqing Key Laboratory of Computational Intelligence, Chongqing University of Posts and Telecommunications, Chongqing 400065, People's Republic of China
{suzq,wanggy}@cqupt.edu.cn
[2] Key Laboratory of Cyberspace Big Data Intelligent Security, Ministry of Education, Chongqing 400065, People's Republic of China
xufanxin@stu.swun.edu.cn

Abstract. Liver disease accounts for 4% of all deaths worldwide. Existing research on liver disease with rough set mostly studied from the perspective of clinical diagnosis, but has not yet been studied from the perspective of clinical medical test decision-making. To address the problem, this paper first converts the clinical diagnosis problem of liver disease into the clinical medical test decision-making problem of liver disease. Then the rough set variant of granular-ball rough set can be used to reduce the attributes of clinical medical test decision-making tasks of liver disease. Next, the clinical medical test decision-making problem is simplified to a classification task. Finally, the proposed method is experimentally verified on the processed liver disease dataset.

Keywords: rough set · granular-ball · clinical medical test · decision-making

1 Introduction

Liver disease accounts for over two million deaths annually and accounts for 4% of all deaths worldwide (1 out of every 25 deaths) [4]. The WHO has called on countries to eliminate viral hepatitis, which is one of the liver disease, as a public health threat by 2030 [15,24]. In the clinical diagnosis process of liver disease, doctors comprehensively analyze the patient's physical signs and marker test results to determine whether the patient has liver disease. Before determining that the patient has a certain liver disease, doctors will comprehensively consider the patient's clinical physical signs, and then decide which clinical medical tests the patient should undergo [5]. The issue of clinical medical test decision-making can be abstracted from clinical diagnosis decision-making for liver disease, see Fig. 1. This issue can be specifically formulated as: without prior knowledge, from

This work was supported by the National Key R&D Program of China under grant number 2021YFF0704100.

M. Hu et al. (Eds.): IJCRS 2024, LNAI 14840, pp. 265–279, 2024.
https://doi.org/10.1007/978-3-031-65668-2_18

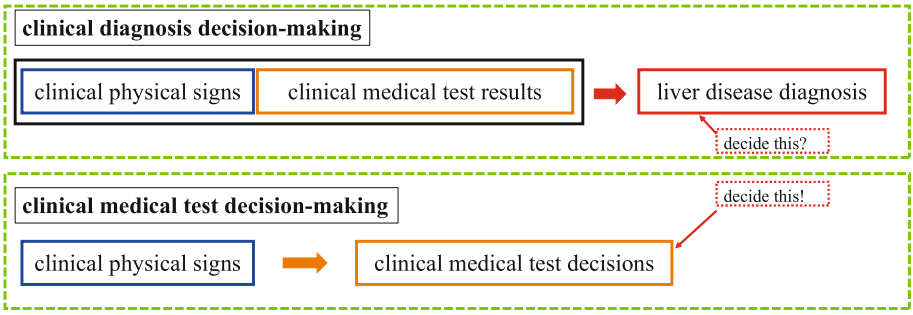

Fig. 1. Clinical diagnosis decision-making vs. Clinical medical test decision-making.

a data-driven perspective, assuming that doctors have determined the specific clinical physical signs of patients with liver disease, what test decisions should doctors make about clinical medical tests?

Rough set is a typical data analysis method, and it has had many applications in liver disease diagnosis. Rough set is initially introduced by Pawlak [17]. Yahia *et al.* merged the rough set with neural networks to do medical diagnosis task [25]. Kaya and Uyar proposed a hybrid medical decision support system based on rough set and extreme learning machine to do the diagnosis of hepatitis disease [13]. Acharjya and Ahmed using the bat algorithm to select attributes and using rough set to generate decision rules [2]. Kumari and Acharjya proposed a decision support system based on the rough set and the artificial fish swarm algorithm for diagnosis of hepatitis disease [14]. The targets of all these methods are all clinical diagnostic problems of liver disease. Then a natural problem can be raised, since rough set can be used for clinical diagnosis of liver diseases, can rough set also be used for clinical medical test decision-making of liver disease?

The classic rough set proposed by Pawlak is only applicable to discrete data [23]. In the attributes of clinical physical signs of liver disease, there is a mixture of discrete and continuous data. Neighborhood rough set [21] is a common rough set variant used for continuous data, but it loses the ability to represent knowledge with equivalence classes [23]. Combining the advantages of classical rough set in discrete data and neighborhood rough set in continuous data, and inspired by granular cognitive computing proposed by Wang [9], Xia *et al.* proposed granular-ball rough set, which can process both discrete data and continuous data. Compared with the classical rough set, is granular-ball rough set more suitable for clinical medical test decision-making that mix discrete data and continuous data? The main contributions of this paper are as follows:

1) Converting the clinical diagnosis decision-making problem of liver disease into the clinical medical test decision-making problem of liver disease.

2) Taking advantage of that granular-ball rough set can handle both discrete data and continuous data simultaneously, granular-ball rough set is better to do attribute reduction on clinical physical attributes than classical rough set.

3) After attribute reduction, the selected attributes are used to do experimental verification by the classifier to prove the effectiveness of granular-ball rough set for clinical medical test decision-making problem.

2 What Is the Clinical Medical Test Decision-Making in Liver Disease?

Figure 1 shows the comparison between the clinical medical test decision-making problem and the clinical diagnosis decision-making problem. To elaborate what is the clinical medical test decision-making in liver disease, this paper extract several real samples from the datasets of [28,29] as example table, then using this example table to explain how to transform the clinical diagnosis decision-making problem of liver disease into a clinical medical test decision-making problem.

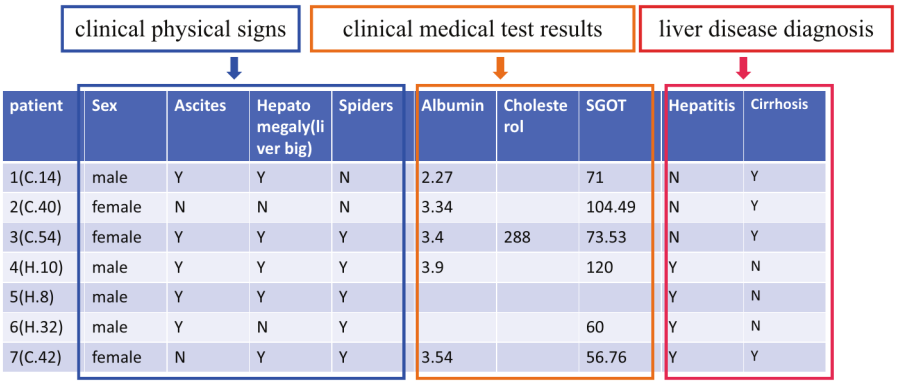

patient	Sex	Ascites	Hepato megaly(liver big)	Spiders	Albumin	Cholesterol	SGOT	Hepatitis	Cirrhosis
1(C.14)	male	Y	Y	N	2.27		71	N	Y
2(C.40)	female	N	N	N	3.34		104.49	N	Y
3(C.54)	female	Y	Y	Y	3.4	288	73.53	N	Y
4(H.10)	male	Y	Y	Y	3.9		120	Y	N
5(H.8)	male	Y	Y	Y				Y	N
6(H.32)	male	Y	N	Y			60	Y	N
7(C.42)	female	N	Y	Y	3.54		56.76	Y	Y

Fig. 2. Clinical diagnosis decision-making in liver disease.

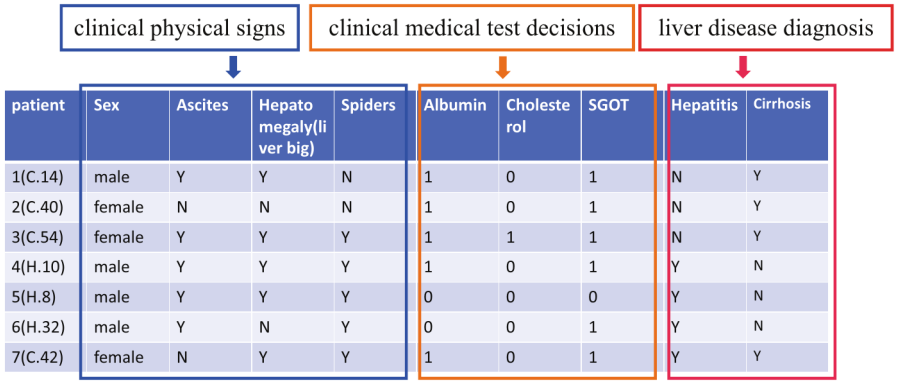

patient	Sex	Ascites	Hepato megaly(liver big)	Spiders	Albumin	Cholesterol	SGOT	Hepatitis	Cirrhosis
1(C.14)	male	Y	Y	N	1	0	1	N	Y
2(C.40)	female	N	N	N	1	0	1	N	Y
3(C.54)	female	Y	Y	Y	1	1	1	N	Y
4(H.10)	male	Y	Y	Y	1	0	1	Y	N
5(H.8)	male	Y	Y	Y	0	0	0	Y	N
6(H.32)	male	Y	N	Y	0	0	1	Y	N
7(C.42)	female	N	Y	Y	1	0	1	Y	Y

Fig. 3. Clinical medical test results convert to clinical medical test decisions.

Figure 2 shows the example table. The first column represents the patient sample that selected from [28,29]. Taking the representation of '1(C.14)' as an

example. '1' represents the ID of the patient sample in this example table, 'C' represents the dataset of [29], '14' represents the corresponding sample ID in the corresponding dataset. 7 samples have been selected in this example table, 4 samples from [29], 3 samples from [28]. The 'clinical physical signs' in Fig. 2 represent the patient's clinical physical signs before clinical medical test. In the clinical physical signs, 'Y' indicates that this phenomenon of the attribute exists, 'N' indicates the opposite. The 'clinical medical test results' in Fig. 2 represent the patient's clinical medical test results which doctor choose to do. Items with value indicate that the patient has undergone the corresponding clinical medical test, and items without value indicate the opposite. The 'liver disease diagnosis' in Fig. 2 represent the patient's clinical diagnosis of liver disease. 'Y' indicates that this patient has the corresponding liver disease, and 'N' indicates the opposite.

clinical physical signs | clinical medical test decisions

patient	Sex	Ascites	Hepato megaly(liver big)	Spiders	Albumin	Cholesterol	SGOT
1(C.14)	male	Y	Y	N	1	0	1
2(C.40)	female	N	N	N	1	0	1
3(C.54)	female	Y	Y	Y	1	1	1
4(H.10)	male	Y	Y	Y	1	0	1
5(H.8)	male	Y	Y	Y	0	0	0
6(H.32)	male	Y	N	Y	0	0	1
7(C.42)	female	N	Y	Y	1	0	1

Fig. 4. Clinical medical test decision-making in liver disease.

In the clinical medical test results in Fig. 2, some items have values and some items have no values. Assuming that the item without value means that doctors think this clinical medical test is not necessary. Then the clinical medical test results in Fig. 2 can be converted into the clinical medical test decisions in Fig. 3. '1-0' means that the doctor thinks this medical test should be done or not.

Because the problem of this paper is to decide which clinical medical test items to do based on the clinical physical signs in patients, the final diagnosis of liver disease is not within the scope of discussion. Therefore, the final clinical medical test decision-making in liver disease can be seen in Fig. 4.

3 Rough Set Theory and Granular-Ball Rough Set

3.1 Rough Set Theory

Rough Set Theory(RS) [17] was proposed by Professor Pawlak in 1982, it has been widely used in many fields such as machine learning, data mining, and artificial neural networks [1,8,12]. RS mainly use an information system as the research object to study the dependencies between attributes [11]. Formally, the information system can be expressed as the 4-tuple [18]: $S = \langle U, A, V, f \rangle$. The detailed definition of information system refer to Definition 1.

Definition 1. *Let $S = \langle U, A, V, f \rangle, A = C \cup D$, represent an information system. U represents a finite nonempty set of objects. U is also called the universe. R represents a finite nonempty set of attributes, the subsets C and D are called condition attribute set and decision attribute set, respectively. $V = \cup_{a \in A} V_a$ denotes the set of all attribute values, where V_a denotes the set of values of attribute a. $f : U \times A \rightarrow V$ denotes a mapping function: $\forall x_i \in U, a \in A, f(x_i, a) \in V_a$.*

When the set of attributes in the information system satisfies $A = C \cup D, C \cap D = \emptyset, D \neq \emptyset$, the information system is called a decision system $\langle U, C, D \rangle$, where C is the condition attribute set and D is the decision attribute set.

Definition 2. *Let $S = \langle U, A, V, f \rangle, A = C \cup D$, be an information system. $\forall x, y \in U$ and $B \subseteq A$, the indiscernible relation $\mathrm{IND}(B)$ of the attribute subset B is defined as:*

$$\mathrm{IND}(B) = \{(x, y) \in U \times U | f(x, a) = f(y, a), \forall a \in B\}. \tag{1}$$

In RS, $f(x, a)$ represents the attribute value of a in the sample x. $f(x, a) = f(y, a)$ represents that the sample x and the sample y have the same value in attribute a. If the sample x and the sample y both have the same value under the attribute subset B, the sample x and the sample y are indiscernible. The partition according to the indiscernible relation $\mathrm{IND}(B)$ can be formed in Definition 3.

Definition 3. *Let $S = \langle U, A, V, f \rangle, A = C \cup D$, be an information system. $\forall B \subseteq A$, $\mathrm{IND}(B)$ is an equivalence relation on U. $\mathrm{IND}(B)$ creates a partition of U, denoted as $U/\mathrm{IND}(B)$, abbreviated as U/B. Suppose that $U/B = \{X_1, X_2, \cdots, X_k\}$, if $X_i, X_j \subseteq U, X_i \cap X_j = \emptyset (i \neq j), \cup_{i=1}^{k} X_i = U$, the equivalence class of an sample x can be defined as:*

$$[x]_{\mathrm{IND}(B)} = \{y \in U | (x, y) \in \mathrm{IND}(B)\}. \tag{2}$$

$[x]_{\mathrm{IND}(B)}$ can be simply as $[x]_B$ or $[x]$, if no confusion arises.

When the partition formed by indiscernible relation is used to describe a subset of universe, two sets can naturally be used to describe the relationship between the partition formed by indiscernible relation and the subset of universe. See Definition 4 and Definition 5 for details. Definition 4 describe one subset of universe, Definition 5 describe multiple subsets of universe.

Definition 4. *Let $S = \langle U, A, V, f\rangle, A = C \cup D$, be an information system. $\forall B \subseteq A$, there is a corresponding indiscernible relation R_B on U. For a subset $X \subseteq U$, its lower and upper approximation sets with respect to B are defined as follows:*

$$\overline{R_B}(X) = \{x \in U | [x]_B \cap X \neq \emptyset\}, \tag{3}$$

$$\underline{R_B}(X) = \{x \in U | [x]_B \subseteq X\}, \tag{4}$$

where $[x]_B$ denotes the equivalence class of x.

Definition 5. *Let $S = \langle U, C, D\rangle$ be a decision system. Denoting the partition of the universe U by the decision attribute set D into k equivalence class by $U/D = \{X_1, X_2, \cdots, X_k\}$. $\forall B \subseteq C$, there is a corresponding indiscernible relation R_B on U. The upper and the lower approximations of D with respect to B are defined as follows:*

$$\overline{R_B}(D) = \cup_{i=1}^{k} \overline{R_B}(X_i), \tag{5}$$

$$\underline{R_B}(D) = \cup_{i=1}^{k} \underline{R_B}(X_i). \tag{6}$$

According to the upper and the lower approximation sets, the universe can be divided into three disjoint regions, namely, the positive, boundary and negative regions. See Definition 6 for details.

Definition 6. *Let $S = \langle U, C, D\rangle$ be a decision system. $\forall B \subseteq C$, the positive region, the boundary region and the negative region of D with respect to B are defined as follows:*

$$\mathrm{POS}_B(D) = \underline{R_B}(D), \tag{7}$$

$$\mathrm{BND}_B(D) = \overline{R_B}(D) - \underline{R_B}(D), \tag{8}$$

$$\mathrm{NEG}_B(D) = U - \overline{R_B}(D). \tag{9}$$

3.2 Granular-Ball Rough Set

Granular-ball rough set(GBRS) is based on granular-ball computing(GBC) [23]. The core idea of granular-ball computing is to use granular balls(GB) to fully or partially cover the sample space [22]. GBC is used to adaptively generate many GBs with different radii, and propose replacing the input points with the granular ball to do the classifier task. The quality of a granular ball is measured by the *purity* of the ball, which is defined as the majority of samples with unified labels in one granular ball. In GBRS, the purity threshold is setting as 1.

In a rough set, all samples in the universe must be covered. Thus, the objective function of GBRS can be described as covering all samples with the minimum number of stable granular balls [23]. The objective function also need to meet two constraint conditions: 1) $purity(GB_j) = 1$ and 2) no overlap between the granular balls. See [23] for details.

Definition 7. *Let* $S = \langle U, A, V, f\rangle, A = C \cup D$, *be an information system.* $\forall x, y \in U$ *and* $B \subseteq A$, *the indiscernible granular-ball relation* $\mathrm{INDGB}(B)$ *of the attribute subset* B *is defined as:*

$$\mathrm{INDGB}(B) = \{(x, y) \in U \times U | f(x, a) = f(y, a) = GB, \forall a \in B\}. \tag{10}$$

In the GBRS, $f(x, a) = GB$ represents that x belong to the granular ball GB. $f(x, a) = f(y, a) = GB$ represents that x and y belong to the same granular ball under the attribute set a. The partition according to the indiscernible granular-ball relation $\mathrm{INDGB}(B)$ can be formed in Definition 8.

Definition 8. *Let* $S = \langle U, A, V, f\rangle, A = C \cup D$, *be an information system.* $\forall B \subseteq A$, $\mathrm{INDGB}(B)$ *is an equivalence relation on* U, $\mathrm{INDGB}(B)$ *can create a partition of* U, *denoted as* $U/\mathrm{INDGB}(B)$. *The equivalence class in* $U/\mathrm{INDGB}(B)$ *is defined as:*

$$[x]_{\mathrm{INDGB}(B)} = \{y \in U | (x, y) \in \mathrm{INDGB}(B)\}. \tag{11}$$

The partition formed by indiscernible granular-ball relation is used to describe a subset of universe. Definition 9 for one subset of universe, Definition 10 for multiple subsets of universe. Definition 11 for three disjoint regions.

Definition 9. *Let* $S = \langle U, A, V, f\rangle, A = C \cup D$, *be an information system.* $\forall B \subseteq A$, *there is a corresponding indiscernible relation* $\mathrm{INDGB}(B)$ *on* U, *this equivalence relation is abbreviated as* GBR_B. *For a subset* $X \subseteq U$, *its lower and upper approximation sets with respect to* B *are defined as follows:*

$$\overline{\mathrm{GBR}_B}(X) = \{x \in U | [x]_{\mathrm{INDGB}(B)} \cap X \neq \emptyset\}, \tag{12}$$

$$\underline{\mathrm{GBR}_B}(X) = \{x \in U | [x]_{\mathrm{INDGB}(B)} \subseteq X\}. \tag{13}$$

Definition 10. *Let* $S = \langle U, C, D\rangle$ *be a decision system. Denoting the partition of the universe* U *by the decision attribute set* D *into* k *equivalence class by* $U/D = \{X_1, X_2, \cdots, X_k\}$. $\forall B \subseteq C$, *there is a corresponding indiscernible relation* GBR_B *on* U. *The upper and the lower approximations of* D *with respect to* B *are defined as follows:*

$$\overline{\mathrm{GBR}_B}(D) = \cup_{i=1}^{k} \overline{\mathrm{GBR}_B}(X_i), \tag{14}$$

$$\underline{\mathrm{GBR}_B}(D) = \cup_{i=1}^{k} \underline{\mathrm{GBR}_B}(X_i). \tag{15}$$

Definition 11. *Let* $S = \langle U, C, D\rangle$ *be a decision system.* $\forall B \subseteq C$, *there is a corresponding indiscernible relation* GBR_B *on* U. *The positive region, the boundary region and the negative region of* D *with respect to* B *are defined as follows:*

$$\mathrm{POS}_B(D) = \underline{\mathrm{GBR}_B}(D), \tag{16}$$

$$\mathrm{BND}_B(D) = \overline{\mathrm{GBR}_B}(D) - \underline{\mathrm{GBR}_B}(D), \tag{17}$$

$$\mathrm{NEG}_B(D) = U - \overline{\mathrm{GBR}_B}(D). \tag{18}$$

4 Methodology

The difference between GBRS and RS mainly lies in the generation method of the positive region. GBRS can simultaneously generate equivalence classes on mixed attributes, and thus have advantages in the generation of the positive region. This paper use GBRS to select the clinical physical sign attributes. The attribute reduction of GBRS is mainly divided into two parts, one is the generation of granular balls, the other is the selection method of attribute reduction [23].

Algorithm 1. Generation of Granular Balls in the GBRS

Input: A dataset $\langle U, A\rangle$, N samples: $U = \{x_1, x_2, \cdots, x_n\}$, with K attributes: $A = \{a_1, a_2, \cdots, a_k\}$; the lower bound of the size of the granular-ball LBS;
Output: the granular balls with a purity equal to 1 belong to the positive region $NOLGBs$;

the current granular-ball set: $CGBs \leftarrow U$;
the granular-ball set in the next iteration: $NGBs \leftarrow \emptyset$;
// If the granular-ball does not produce a new split, it will stop.
repeat
  for each $GB_i \in CGBs$ **do**
    if $purity(GB_i) < 1$ and $|GB_i| > LBS$ **then**
      Split GB_i into m sub-granular-balls $\{GB_j^{'}, j = 1, ..., m\}$, where m denotes the number of different labels in GB_i;
      $NGBs = NGBs + \{GB_j^{'}\}$;
    else
      $NGBs = NGBs + \{GB_i\}$;
    end if
  end for
  $CGBs = NGBs$;
  $NGBs = \emptyset$;
until $|NGBs| == |CGBs|$;

the overlap granular-balls set: $OLGBs = \emptyset$;
the no overlap granular-balls set: $NOLGBs = \emptyset$;
//Remove the overlap between heterogeneous granular-balls.
repeat
  for each $GB_i \in CGBs$ **do**
    if there is overlap between GB_i and GB_j, $GB_j \in CGBs$ which has a different label **then**
      Split the larger granular-ball and add the sub-granular-balls into $OLGBs$;
    else
      $NOLGBs = NOLGBs + \{GB_i\}$;
    end if
  end for
  $CGBs = OLGBs$
until $|OLGBs| == 0$

Algorithm 1 is the generation method of granular balls [23]. This algorithm consists of two parts. The first part is to generate granular balls that meet the conditions until the granular balls cannot be split. The second part is to eliminate the overlapping granular balls so that there is no overlap between each granular ball. Through the above algorithm, the effect of the granular balls covering all samples is achieved.

Algorithm 2. attribute reduction in the GBRS

Input: A dataset $U = \{x_1, x_2, \cdots, x_n\}$;
Output: Attribute set $C^{''}$;

The dimension of each sample: d;
the i-th attribute of the sample: a_i;
for $l \in \{a_1, a_2, ..., a_d\}$ **do**
  The minimum number of samples in the ball is $min\_sample = 2 * (d - l)$;
  $pos\_num = 0$;
  $C^{''} = \emptyset$;
  $C^{'} = \{a_1, a_2, ..., a_d\}$;
  repeat
    for $a_i \in C^{'}$ **do**
      The data set U based on the current attribute set $T = C^{''} \cup \{a_i\}$ is input to the algorithm 1 for granular-balls splitting; the number of samples in the positive region balls is $ball\_num_i$, calculated by Eq.(13);
    end for
    The largest $max\_num = \max(ball\_num_i)$ and its corresponding attribute a^* are selected;
    if $max\_num > pos\_num$ **then**
      $pos\_num = max\_num$;
      $C^{''} = C^{''} + \{a^*\}$;
      $C^{'} = C^{'} - \{a^*\}$;
    end if
  until $C^{'} = \emptyset$ or $max\_num \leq pos\_num$
end for

Algorithm 2 is the attribute reduction method in [23]. This algorithm selects attributes based on the growth of the number of positive region samples. If the positive region samples increase after adding attributes, the attribute with the largest increase will be selected as the final attribute in the current round.

5 Descriptions of Datasets for Experiments

The research problem is to determine which clinical medical tests should be performed based on the clinical physical signs of patients with liver disease. Based on the goal of this problem, two eligible UCI public datasets are used for experiments, both are Hepatitis dataset [28] and Cirrhosis Patient Survival Prediction dataset [29].

5.1 Hepatitis Dataset

Hepatitis dataset contains 155 samples with 20 attributes [28]. Based on the meaning of the attributes, 13 condition attributes including Sex, Steroid, Antivirals, Fatigue, Malaise, Anorexia, Liver Big, Liver Firm, Spleen Palpable, Spiders, Ascites, Varices, and Histology attributes are used as clinical physical signs. 5 condition attributes including Bilirubin, Alk Phosphate, Sgot, Albumin, and Protime attributes are used as clinical medical test decision-making attributes.

Preprocessing method for the clinical physical sign attributes in Hepatitis dataset. 10 clinical physical sign attributes including Steroid, Fatigue, Malaise, Anorexia, Liver Big, Liver Firm, Spleen Palpable, Spiders, Ascites, and Varices attributes contain missing values. Assuming that these clinical signs are normal, which resulted in the doctor not recording them. According to the above principles, the missing values of the attribute Liver Firm are filled with '2' as 'yes', the other attributes are filled with '1' as 'no'.

Preprocessing method for the clinical medical test decision-making attributes in Hepatitis dataset. 5 clinical medical test decision-making attributes including Bilirubin, Alk Phosphate, Sgot, Albumin, and Protime contain missing values. Assuming that the missing value part means that the doctor think the patient does not require medical test of the corresponding attributes while others are the opposite, the items with values is converted into '1' as 'done'; the items with missing values is converted into '0' as 'not done'.

5.2 Cirrhosis Patient Survival Prediction Dataset

Cirrhosis Patient Survival Prediction dataset contains 418 samples with 20 attributes [29]. Based on the meaning of the attributes, 9 condition attributes including Drug, Sex, Ascites, Hepatomegaly, Spiders, Edema, Stage, Bilirubin, and Albumin attributes are used as clinical physical signs. 7 condition attributes including Cholesterol, Copper, Alk_Phos, SGOT, Tryglicerides, Platelets, and Prothrombin attributes are used as clinical medical test decision-making attributes.

Preprocessing method for the clinical physical sign attributes in Cirrhosis Patient Survival Prediction dataset. 3 clinical physical sign attributes including Ascites, Hepatomegaly, and Spiders attributes contain missing values. Assuming that these clinical signs are normal, which resulted in the doctor not recording them. According to the above principles, the missing values are filled with '0' as 'no'. Preprocessing the value of the attribute Drugs as: D-penicillamine as '1', placebo as '2', NA as '0'. Preprocessing the value of all attributes as: 'N' as '0', 'Y' as '1', 'S' as '2'.

Preprocessing method for the clinical medical test decision-making attributes in Cirrhosis Patient Survival Prediction dataset. 7 clinical medical test decision-making attributes including Cholesterol, Copper, Alk_Phos, SGOT, Tryglicerides, Platelets, and Prothrombin attributes contain missing values. The missing values are preprocessed same in Hepatitis dataset. According to the meaning of Stage attribute, the 6 samples which contain the missing value in Stage attribute should be deleted, the total samples number changes from 418 to 412.

6 Experimental Results

There is currently no independent study on clinical medical test decision-making for liver disease in the rough set field, in order to demonstrate the effectiveness of GBRS in the clinical medical test decision-making problem for liver disease, this paper followed the original experimental setup in [23]. Using GBRS to perform attribute reduction on clinical physical signs, and then use the dataset after attribute reduction to do the classification task of clinical medical medical test decision-making. In order to be consistent with the classifier adopted in GBRS, kNN is adopted as the classifier. RS uses an attribute reduction algorithm based on the degree of significance, which proposed by Pawlak [19].

This paper randomly divide the training set and test set of the dataset into ratios of 9:1, 8:2, 7:3, 6:4, 5:5, the results can be seen in Table 1 and Table 3.

6.1 Comparison in Cirrhosis Dataset

In the cirrhosis dataset, 9 clinical physical signs are used as condition attributes and 7 clinical medical test attributes are used as decision attributes. The 7 decision attributes are combined together as the result for classification. The comparison results can be seen in Table 1. In Table 1, *train acc* represents the accuracy of the model in the training set, and *test acc* represents the accuracy of the model in the test set.

Table 1. Comparison results in cirrhosis dataset.

ratios	evaluation	original data+classifier	RS+classifier	GBRS+classifier
9:1	train acc	89.5	88.4	**90.5**
	test acc	85.7	90.5	**95.2**
8:2	train acc	90.9	89.4	**91.2**
	test acc	88.0	85.5	**90.4**
7:3	train acc	91.0	89.2	**91.7**
	test acc	85.5	85.5	**89.5**
6:4	train acc	89.5	89.5	**91.1**
	test acc	85.5	86.7	**90.9**
5:5	train acc	89.3	71.8	**92.2**
	test acc	**86.9**	64.1	60.7

According to the comparison results in cirrhosis dataset in Table 1, the accuracy results on the training set and test set by GBRS are better than RS and original data in different ratios except 5:5. When the ratio of training set to test set is 5:5, the accuracy result on the training set in original data and the test set in original data remain stable, while the accuracy of the data after attribute reduction by RS drops greatly, and the accuracy of the data after attribute reduction by GBRS has over-fitting phenomenon. The accuracy result on the test set is much lower than the training set.

Table 2. Comparison attributes reduction in cirrhosis dataset.

attribute name	ratios	9:1		8:2		7:3		6:4		5:5	
	original	RS	GBRS	RS	GBRS	RS	GBRS	RS	GBRS	RS	GBRS
Drug	√	√	√	√	√	√	√	√	√	×	√
Sex	√	×	×	×	×	×	×	×	√	×	×
Ascites	√	×	×	×	×	×	×	×	√	×	×
Hepatomegaly	√	×	×	×	×	×	×	×	×	×	×
Spiders	√	×	×	×	×	×	×	×	×	×	×
Edema	√	×	×	×	×	×	×	×	√	×	√
Stage	√	√	√	√	√	√	√	×	×	×	×
Bilirubin	√	√	×	√	×	√	×	√	×	√	×
Albumin	√	√	×	√	×	√	×	√	√	√	√

According to the attribute reduction results in Table 2, in the data ratios of 9:1, 8:2 and 7:3, the attributes selected by RS and GBRS remain stable. GBRS selected the attributes by the algorithm 2. The attributes selected by GBRS are a subset of the attributes selected by RS. In the data ratios of 6:4 and 5:5, the number of attributes selected by GBRS is higher than RS.

6.2 Comparison in Hepatitis Dataset

Table 3. Comparison results in hepatitis dataset.

ratios	evaluation	original data+classifier	RS+classifier	GBRS+classifier
9:1	train acc	58.3	58.3	58.3
	test acc	37.5	37.5	**56.3**
8:2	train acc	58.9	58.9	55.6
	test acc	38.7	38.7	38.7
7:3	train acc	54.6	**56.5**	45.4
	test acc	51.1	46.8	**57.4**
6:4	train acc	59.1	59.1	**66.7**
	test acc	32.3	32.3	**41.9**
5:5	train acc	61.0	**62.3**	61.0
	test acc	32.1	30.8	**37.2**

According to the comparison results in hepatitis dataset in Table 3, when the data ratios are in 9:1, 8:2 and 6:4, there is little difference in accuracy among the original dataset, the dataset after RS attribute reduction, and the dataset after GBRS attribute reduction. The accuracy result on the training set and the

test set after GBRS attribute reduction are better than the accuracy result on the training set and the test set in the original dataset. When the data ratios are in 7:3 and 5:5, the accuracy result on the training set after RS attribute reduction is higher than the original dataset, the accuracy result on the test set after GBRS attribute reduction is higher than the original dataset.

Table 4. Comparison attributes reduction in hepatitis dataset.

attribute name	ratios	9:1		8:2		7:3		6:4		5:5	
	original	RS	GBRS	RS	GBRS	RS	GBRS	RS	GBRS	RS	GBRS
Sex	√	√	√	√	√	√	√	√	√	√	√
Steroid	√	√	√	√	√	√	×	√	√	√	√
Antivirals	√	√	√	√	√	√	√	√	√	√	×
Fatigue	√	√	×	√	×	√	×	√	×	√	√
Malaise	√	√	√	√	√	√	√	√	√	√	×
Anorexia	√	√	×	√	×	√	√	√	√	√	×
Liver Big	√	√	√	√	√	√	×	√	×	√	×
Liver Firm	√	√	√	√	√	√	√	√	√	√	√
Spleen Palpable	√	√	×	√	×	√	√	√	√	√	√
Spiders	√	√	√	√	√	√	×	√	×	√	×
Ascites	√	√	×	√	×	√	√	√	×	×	√
Varices	√	√	×	√	×	×	√	√	×	√	√
Histology	√	√	√	√	√	√	×	√	√	√	√

According to the attribute reduction results in Table 4, in all different dataset partition ratios, the number of attributes selected by GBRS is much smaller than the number of attributes selected by RS. The number of selected attributes in RS is either the same as the original dataset or one less than the original dataset.

7 Discussion

Already in 1983, [16] has already raised the issue of patients' clinical medical test decision-making. From the perspective of doctors, the author showed that because clinician's professional practice habits tend to be more conservative, clinicians often arrange more tests for patients than patients actually needed. In subsequent studies, from a medical perspective, studies on changing doctors' behavior to solve patients' clinical medical test decision-makings were also proposed in [3,7]. In [27], the authors used medical records and clinical guideline information to support the orders of medical tests. In [10], the authors used a decision-tree-based Bayesian approach to do medical test rationing.

Clinical medical tests are of importance to doctors in diagnosing diseases. This paper starts from the necessity of clinical medical test decision-making and

applies rough set to this problem for the first time. Rough set uses the attribute reduction method on this problem to prove that some clinical physician signs can also make clinical medical test decisions comparable to all clinical physician signs in liver disease. This paper currently only making preliminary attempts, and it is worth looking forward to expect more variants of rough set [6,20,26] to be applied to this problem in the future.

8 Conclusion

It is an interesting attempt to abstract the clinical medical test decision-making problem of liver disease from the clinical diagnosis of liver disease. Through this attempt, doctors can get the necessary attributes to make clinical medical test decisions from the answer to this problem. Granular-ball rough set is a representative rough set algorithm, through its attribute reduction, doctors can obtain necessary clinical physical sign attributes from liver disease dataset to help determine the necessity of clinical medical tests. After experimental verification on the liver disease dataset, granular-ball rough set can obtain more better classification performance comparable to all clinical physician attributes while using fewer attributes. Granular-ball rough set has shown advantages in the small dataset of this paper, but whether it can maintain its advantages in larger datasets is still a problem. It is worth looking forward to more rough set attempts on this problem.

References

1. Abu-Gdairi, R., El-Atik, A.A., El-Bably, M.K.: Topological visualization and graph analysis of rough sets via neighborhoods: a medical application using human heart data. AIMS Math. **8**(11), 26945–26967 (2023)
2. Acharjya, D.P., Ahmed, P.K.: A hybridized rough set and bat-inspired algorithm for knowledge inferencing in the diagnosis of chronic liver disease. Multimedia Tools Appl. **81**(10), 13489–13512 (2022)
3. Davis, D.A., Thomson, M.A., Oxman, A.D., Haynes, R.B.: Changing physician performance: a systematic review of the effect of continuing medical education strategies. Jama **274**(9), 700–705 (1995)
4. Devarbhavi, H., Asrani Sumeet, S.K., Arab, J.P., Nartey, Y.A., Pose, E., Kamath, P.S.: Global burden of liver disease: 2023 update. J. Hepatol. **14**(18), 516–537 (2023)
5. Fuguang, S., Jin, R.: Advances in the diagnosis of nonalcoholic fatty liver disease. Chinese Bull. Life Sci. **35**(10), 1348–1357 (2023)
6. Ji, X., Peng, J., Zhao, P., Yao, S.: Extended rough sets model based on fuzzy granular ball and its attribute reduction. Inf. Sci. **640**(12), 119071 (2023)
7. Glasziou, P., Hilden, J.: Test selection measures. Med. Decis. Making **9**(2), 133–141 (1989)
8. Guoyin, W., Xiao, H.: A self-learning model under uncertain condition. J. Softw. **14**(6), 1096–1102 (2003)
9. Guoyin, W.: DGCC: data-driven granular cognitive computing. Granular Comput. **2**(4), 343–355 (2017)

10. Herazo-Padilla, N., Augusto, V., Dalmas, B., Xiaolan, X., Bongue, B.: A decision-tree-based Bayesian approach for chance-constrained health prevention budget rationing. IEEE Trans. Autom. Sci. Eng. **19**(3), 2322–2338 (2021)
11. Hong, Y., Guoyin, W., Yiyu, Y.: Current research and future perspectives on decision-theoretic rough sets. Chinese J. Comput. **38**(8) (2015)
12. Jothi, G., Inbarani, H.H., Azar, A.T., Devi, K.R.: Rough set theory with Jaya optimization for acute lymphoblastic leukemia classification. Neural Comput. Appl. **31**(9), 5175–5194 (2019)
13. Kaya, Y., Uyar, M.: A hybrid decision support system based on rough set and extreme learning machine for diagnosis of hepatitis disease. Appl. Soft Comput. **13**(8), 3429–3438 (2013)
14. Kumari, N., Acharjya, D.P.: A decision support system for diagnosis of hepatitis disease using an integrated rough set and fish swarm algorithm. Concurrency Comput. Pract. Experience **34**(21), e7107 (2022)
15. Laffey, J.G., et al.: Potentially modifiable factors contributing to outcome from acute respiratory distress syndrome: the LUNG SAFE study. Intensive Care Medicine **42**(12), 1865–1876 (2016)
16. Lundberg, G.D.: Perseveration of laboratory test ordering: a syndrome affecting clinicians. JAMA **249**(5), 639–639 (1983)
17. Pawlak, Z.: Rough sets. Int. J Comput. Inf. Sci. **11**(5), 341–356 (1982)
18. Pawlak, Z.: Rough sets and intelligent data analysis. Inf. Sci. **147**(1–4), 1–12 (2002)
19. Pawlak, Z., Skowron, A.: Rough sets and Boolean reasoning. Inf. Sci. **177**(1), 41–73 (2007)
20. Qian, W., Xu, F., Huang, J., Qian, J.: A novel granular ball computing-based fuzzy rough set for feature selection in label distribution learning. Knowl.-Based Syst. **278**(10), 110898 (2023)
21. Qinghua, H., Daren, Y., Zongxia, X.: Numerical attribute reduction based on neighborhood granulation and rough approximation. J. Softw. **19**(3), 640–649 (2008)
22. Shuyin, X., Yunsheng, L., Xin, D., Guoyin, W., Hong, Y., Yuoguo, L.: Granular ball computing classifiers for efficient, scalable and robust learning. Inf. Sci. **483**, 136–152 (2019)
23. Shuyin, X., et al.: GBRS: a unified granular-ball learning model of pawlak rough set and neighborhood rough set. IEEE Trans. Neural Netw. Learn. Syst. (2023)
24. Sidhu, S.S., Sharma, B.C., Goyal, O., Kishore, H., Kaur, N.: L-ornithine L-aspartate in bouts of overt hepatic encephalopathy. Hepatology **67**(2), 700–710 (2018)
25. Yahia, M.E., Mahmod, R., Sulaiman, N., Ahmad, F.: Rough neural expert systems. Expert Syst. Appl. **18**(2), 87–99 (2000)
26. Yuan, K., Xu, W., Miao, D.: A local rough set method for feature selection by variable precision composite measure. Appl. Soft Comput. **155**(4), 111450 (2024)
27. Zhuang, Z.Y., Wilkin, C.L., Ceglowski, A.: A framework for an intelligent decision support system: a case in pathology test ordering. Decis. Support Syst. **55**(2), 476–487 (2013)
28. Hepatitis. UCI Machine Learning Repository (1998). https://doi.org/10.24432/C5Q59J. Accessed 20 Jan 2024
29. Dickson, E., Grambsch, P., Fleming, T., Fisher, L., Langworthy, A.: Cirrhosis patient survival prediction. UCI Mach. Learn. Repository (2023). https://doi.org/10.24432/C5R02G. Accessed 20 Jan 2024

Lung Cancer Risk Prediction Model Trained with Multi-source Data

Shijie Sun, Hanyue Liu, Ye Wang, and Hong Yu(✉)

Chongqing Key Laboratory of Computational Intelligence,
Chongqing University of Posts and Telecommunications, Chongqing 400065, China
yuhong@cqupt.edu.cn

Abstract. Recent research about lung cancer risk prediction model require the data for predicting as same as the data for training whether based on single-source data or multi-source data. Both of them either cannot fully use collected multi-source data to train model or need higher data cost to predict. If the model is trained by gathered multi-source data, but still make prediction by single-source data, the cost of the patients will be avoid increasing. In this work, the cross-modal knowledge distillation technique is introduced to train the lung cancer risk prediction model for the purpose. However, present cross-modal knowledge distillation techniques are incapable of dealing with different biases in data sources. To solve this problem, the model performs features extraction on a sample from multiple perspectives. For validating the efficacy, the proposed model is evaluated with eight baselines on the NLST dataset, which includes CT image data as well as questionnaire data. In terms of AUC, the results demonstrate that the proposed model outperforms the vanilla MLP by 10.88% and the best baseline by 2.71%. The proposed model may effectively exploit history data, ensuring not only the accuracy of prediction but also lowering the user's expenditure for data.

Keywords: lung cancer · risk prediction · multi-source data · cross-modal knowledge distillation

1 Introduction

Lung cancer is one of the most burdensome malignancies in the world. According to the GLOBOCAN 2020 database, in all cases of malignancy, the global cases of lung cancer are 11.4% and the mortality rate is 18.0% [25]. It is the leading cause of cancer death worldwide. Early prediction of lung cancer can effectively reduce the burden from lung cancer. Risk prediction models can calculate the probability that an individual will develop lung cancer over a period of time in the future, thereby identifying people at high risk for lung cancer. The higher accuracy of prediction model, the better early detection of lung cancer.

To identify the high-risk groups of lung cancer, the risk prediction model are used to calculate the probability of developing lung cancer in the future. As the result, medical intervention could be made earlier. For the input of trained prediction model, it is costly or difficult to obtain medical data which is generated at

M. Hu et al. (Eds.): IJCRS 2024, LNAI 14840, pp. 280–294, 2024.
https://doi.org/10.1007/978-3-031-65668-2_19

the diagnosis stage, because risk predictions are often made before patients enter medical institutions. Another fact is that the risk prediction model is trained by the collected data, such as historical lung cancer data and the data collected from lung screening projects. Those data have the diversity of big data, such as abundant data sources, various data modes and views, and the multi-stage nature of medical data. The stages of lung cancer data include: screening, diagnosis, treatment, re-examination, follow-up, etc.

The existing algorithms could be classified according to the data used by the model. They could be divided into the following two categories: based on single-source data, such as questionnaire data [5,11,26], imaging data [3,31], metabolic data [12], genomic data [17], and based on multi-sources data [20]. Analysing from a perspective about practice, more studies focus on questionnaire data and image data, such as prediction [11], prognosis [8], diagnosis [19,24], etc. Existing techniques with single-source data for risk prediction are based on single classifiers, such as logistic regression [5,26], decision tree [23], or based on ensemble learning techniques [11]. There are also studies on the application of computer vision techniques based on deep learning for image data [3,31]. The multi-modal techniques with multi-source data based on deep learning uses more kinds of data for risk prediction [6,11,20].

From the perspective of the way for improving the accuracy of the model, the above methods could be divided into two categories. One is to design a new classifier, the other way is to increase the training data. The first measure is increasing training samples. It is the most direct and effective way, which can make the classifier has more comprehensive learning during the training process, but samples cannot be increased unlimitedly. First, it is expensive to conduct questionnaire surveys over and over again for an unlimitedly increasing data requirement. Second, the population of a region is limited, so it is difficult to obtain unlimited samples. There are also methods to increase data by appending features or views to improve the classifier performance. The representative method is multi-modal and multi-view method. By using more features for training, the classifier can learn more comprehensively, too. However, for current algorithms, these additional features also need to be input into the trained model when the model is used to make prediction. From the above risk prediction description, these data are either expensive to collect, such as CT images, or cannot be collected during prediction, such as pathology images. It conduct to increases the cost of using the model.

In this work, we try to design a training method on image data and questionnaire data for achieve the goal – using multi-source data training model whose input is single-source data. About this method, the model uses only questionnaire data for predicting. The purpose is improving the efficiency utilizing of existing data for enhancing model while avoid increasing the cost of using the model.

One possible way to achieve this goal is to use a model pre-trained with CT image data to assist in the training of the model which trained with questionnaire. Similar work has been studied in other fields, and the technique is called

cross-modal knowledge distillation [22,30]. Therefore, we consider adopting the cross-modal knowledge distillation to achieve the goal.

This work contributions are mainly as follows:

- A lung cancer risk prediction model which can make full use of existing collected multi-source data while avoid increasing the cost of using the model.
- The effect about data utilizing of the method is verified. Compared with eight models which are derived from single-source data technique—only trained with questionnaire, our model could effectively utilize existing collected data. As the result our model outperforms the vanilla MLP by 10.88% and outperforms the best baseline model by 2.71%, in terms of AUC.
- In order to alleviate impact from the differences and noise between different data sources, knowledge distillation is applied to a part of the network, and then the different extracted features are used to make prediction.

2 Background

2.1 Risk Prediction and Early Diagnosis of Lung Cancer

For lung cancer risk prediction, existing models can be divided into two categories: models with single-source data and models with multi-source data.

Models with Single-Source Data: Classifying by data source, commonly used data include the questionnaires data that consist of demographic, smoking history, disease history, and other data from questionnaires, the CT image data from CT examinations, and the metabolic data from blood tests, etc. These data show the relevant feature of the patients from different views. The data from the questionnaire include basic information of the patient, such as education, race, ethnicity, and common risk factors for lung cancer, such as age, family history, and disease history. CT image data show the shape of the patient's lungs. Metabolic data can be used to obtain tumour information by detecting tumour biomarkers in the blood.

Existing methods for questionnaire data include logistic regression, decision trees, and ensemble Learning (XGBoost). Logistic regression is a typical risk prediction modelling method, such as the PLCO model [26] which AUC was 0.8. These models which are based on logistic regression have been confirmed to be able to avoid more lung cancer deaths than the USPSTF standard [28]. The ensemble learning technique represented by XGBoost [7] has shown better performance in lung cancer risk prediction. Mamun et al. used the 10-fold cross-validation method to verify the performance of ensemble learning algorithms on the Kaggle lung cancer dataset, and the AUC and ACC of XGBoost, LightGBM, Bagging and AdaBoost all reached above 0.9 [18].

For neural network models, CNN, 3DCNN and other architectures have emerged, hence computer vision technique has a better application in the medical. In terms of CT image data, Ardila et al. [3] applied the I3D model to CT image data, and the AUC of the one-year risk prediction for all samples by CT

image data in the NLST dataset was 0.94. Zhang et al. [31] proposed a new pre-training method to reduce the model's dependence on ROI labelling and achieve the performance in lung nodule detection that AUC was 0.88.

Ensemble learning algorithms are also applied in the work of predicting lung cancer through metabolomics data. Guan et al. used the detected lung cancer markers to predict lung cancer by XGBoost algorithm. For both the training group and the test group, the AUC was 0.81 [12].

Models with Multi-source Data: Because of development of machine learning, using multi-source data for lung cancer prediction could provide superior prediction performance compared to using only a single-source data. Lung cancer is a complex disease, and the integration of multi-source data could provide more comprehensive information. Park et al. developed a prediction model and a multi-omics data affinity artificial intelligence algorithm based on graph convolutional network, which integrated mRNA expression, DNA methylation and DNA sequencing data, achieving AUC of 0.994 [20]. Barrett and Viana used intermediate and intermodal relationships between CT scans and clinical data to provide a more accurate lung cancer classification task performance, achieving AUC of 0.843 [6]. Gould et al. used XGBoost to predict lung cancer risk based on questionnaire data and laboratory test data, achieving AUC of 0.85 in a 3 to 6 month window for all screening participants [11].

In above cases, multi-source data could build better model than single-source data. However, it requires the data for predicting as same as the data for training when making prediction. Thus, the cost of obtaining input data for prediction becomes higher by this limitation.

2.2 Cross-Modal Knowledge Distillation

Potential gaps between cross-modal data could lead to difficulties in learning for student model, which in turn limits the performance of knowledge distillation [22]. A common solution is to pass annotation or label information through paired samples, shown in Fig. 1 [10]. Zhao et al. carried out cross-modal distillation through synchronous radio signals and camera images to distil knowledge from radio-based model of human posture recognition to image-based models, so as to complete the task of human posture estimation through walls or obscured images [32]. To improve action recognition performance using only RGB images, Thoker, Fida and Gall obtained paired samples from two modalities: RGB video and human action skeleton sequences. These pairings are used to distil the knowledge generated from RGB video into a skeleton-based model of human action recognition [29].

There are other measures to pair samples for knowledge distillation. Ren et al. trained a teacher model based on two modalities of sound and silent video, and distilled knowledge from the teacher model to the student model using only silent video [22]. Hoffman et al. proposed a modality hallucination architecture to implement cross-modal distillation [13]. Passalis et al. proposed probability knowledge distillation [21] and proof the reasonability of this method by quadratic mutual information.

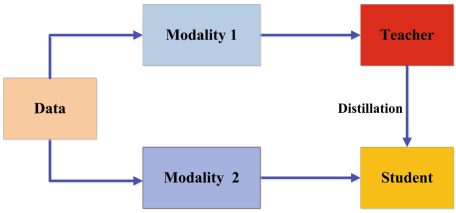

Fig. 1. Cross-modal knowledge distillation [10]

Because of bias among data from different sources [16], the cross-modal knowledge distillation cannot directly applicated.

3 Proposal Method

Considering that different biases between different data sources may lead to noise, in the first stage of model training, only part of the network will accept knowledge distillation (Fig. 2). In the second stage, features extracted by different feature extraction modules will be integrated and the rest network will be trained (Fig. 3 left). Finally, the trained model (Fig. 3 right) will be used for risk prediction.

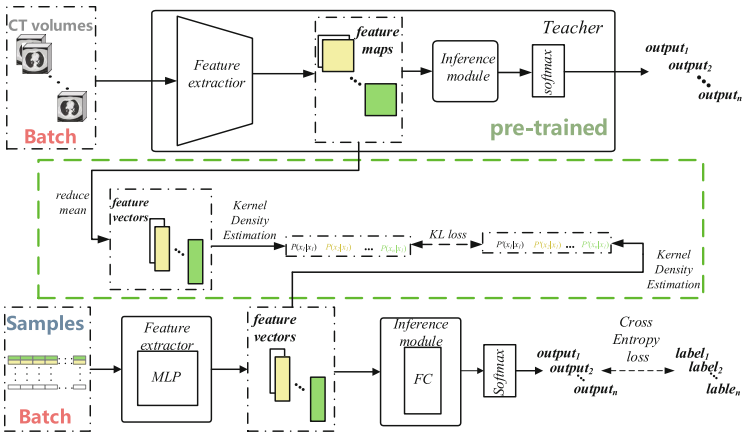

Fig. 2. Feature extraction part training with CT

3.1 Knowledge Distillation

In the existing studies [29,32], the distillation of knowledge from a fine-grained level could achieve ideal performance, but only when crossed modalities are similar, such as: RGB image to infrared image such image to image type, or

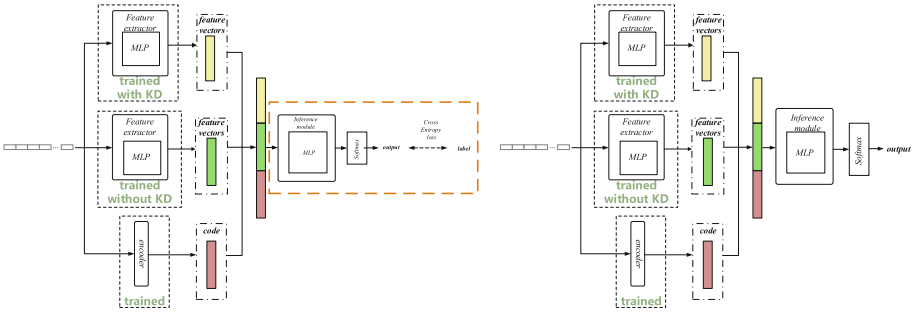

Fig. 3. In left image, where is framed by orange dotted lines is the rest part of the model training, and the right image is the trained model when the model makes predictions (Color figure online)

similar to video to audio such sequence to sequence type. But, in the case of unstructured image data paired with structured tabular data, there is a greater gap between two modalities. The different information contained in these data further increases the complexity and challenge of model training for students. Taking it into consideration, the knowledge is distilled at the coarse-grained level by align the conditional probability distribution of the feature space between the student model and the teacher model thought KL divergence [21].

As shown in the green dotted line in Fig. 2, First, the $n * m$ dimensional $featuremap$ extracted from the teacher's model is transformed into the $n * 1$ dimensional feature vector $\boldsymbol{v}$. Here, the row by line averaging method is used:

$$\boldsymbol{featuremap} = Feature\_extractor_{teacher}(CT\_volume), \tag{1}$$

$$\boldsymbol{v} = mean(\boldsymbol{featuremap}, 1). \tag{2}$$

The function $mean(\boldsymbol{x}, y)$ represents averaging the tensor $\boldsymbol{x}$ in the order $y(y = 0, 1, 2, ..., n)$ dimension. The conditional probability density of samples in a batch $p(x_i|x_j)$ is then estimated by kernel density estimation (KDE):

$$p(x_i|x_j) = \frac{K(x_i, x_j)}{\sum_{j=1, j\neq i}^{N} K(x_i, x_j)}, \tag{3}$$

where x_i, x_j are samples in a batch. For a batch$X$, $x_i, x_j \in X$, $K(\cdot)$ is the kernel function, and $p(x_i|x_j)$ represents the conditional probability density of sample x with respect to x_i in a batch. The cosine function as the kernel function is recommended to use in [21]:

$$K(x_i, x_j) = \frac{1}{2}\left(\frac{\boldsymbol{v}_i \cdot \boldsymbol{v}_j^T}{\|\boldsymbol{v}_i\| \left\|\boldsymbol{v}_j^T\right\|}\right). \tag{4}$$

In Eq. 4, $\boldsymbol{v}_i, \boldsymbol{v}_j^T$ respectively represent the feature vector. Let $p(x_i|x_j)$ be the probability density of the sample in the feature space of the student model,

$q(x_i|x_j)$ be the probability density of the sample in the feature space of the teacher model, then the loss of feature distillation is obtained:

$$loss_{KD} = \frac{1}{n}\sum_{k=1}^{n} KL(q(x_i|x_j)||p(x_i|x_j)). \tag{5}$$

3.2 Features Extraction

Through knowledge distillation, the prediction model could be improved accuracy in imitating the intermediate representation of the model which makes prediction by CT image data. However, since questionnaire data and CT image data come from two different data sources, both have different bias [16]. As a result, bias from CT image data could be introduced as noise during the training of the prediction model.

The ensemble learning model is robust to noise by multiple models, so the inspiration drawn from it. Different feature extractors are used to extract different features for prediction to alleviate noise originating from CT images. And these extractors are trained independently in first training stage. Feature extractors are performed on the questionnaire data in the model, as shown in Fig. 3 right. Three feature extraction steps for the questionnaire data are the feature extraction processes of two classifiers, and the coding process of a linear encoder. One of the two classifiers is trained under knowledge distillation and the other is trained without knowledge distillation. The encoder is from trained linear autoencoder.

Through the feature extraction of these three parts, the model obtains three representations related to the sample. The representation of these three parts are the feature vector $\boldsymbol{v}_1$ generated with the knowledge of CT image data, the feature vector $\boldsymbol{v}_2$ generated without the knowledge of CT image data, and the sample encoding result ***code*** through the linear encoder, and then the features in the form of concatenation as the input is sent to the inference module.

3.3 Optimizing

The model is based on multilayer perceptron (MLP), and the back propagation algorithm is used to train the model in two stage. The first stage is for training the feature extraction part of the model, which consists of three parts: the feature extraction part of the classifier which is trained with both CT image data and questionnaire data, the feature extraction part of the classifier which is trained only with questionnaire data, and the encoder part of the auto-encoder which is trained on questionnaire data. In the second stage of model training, the parameters of the above three feature extraction modules are fixed. Then the feature vectors output by these three modules will be concatenated as the input of the inference module for the inference module training or online prediction.

When training with CT image data and questionnaire data, the loss function consists of two parts, one is the loss $loss_{KD}$ for knowledge distillation, and the

other is the cross-entropy $loss_{CE}$ with correct labels of samples. Finally, the loss function is obtained by the weighted combination of two loss:

$$loss_{module_1} = \alpha loss_{CE} + (1-\alpha) loss_{KD}. \tag{6}$$

In model training practice, we found that at the beginning of model training, the gradient provided by distillation loss is much smaller than provided by cross entropy (about 20000 to 30000 times). The direction of gradient descent is important in gradient descent algorithm. The loss that provides the larger gradient could plays a leading role in model training, as the result of large gradient difference between two losses. It affects the performance of knowledge distillation. Although the gradient gap between the two will be narrow at the progress of training, the model has been overfitting. So the loss in Eq. 6 is corrected by follow:

$$loss_{module_1} = \alpha loss_{CE} + (1-\alpha) loss_{KD} * grad\_ratio, \tag{7}$$

$$grad1\_norm = \left\| \frac{\partial loss_{CE}}{\partial \boldsymbol{\Theta}} \right\|_2, \tag{8}$$

$$grad2\_norm = \left\| \frac{\partial loss_{KD}}{\partial \boldsymbol{\Theta}} \right\|_2, \tag{9}$$

$$grad\_ratio = \frac{grad1\_norm}{grad2\_norm}. \tag{10}$$

In the above equation, $\boldsymbol{\Theta}$ represents the parameters of the model, $grad1\_norm$ is the 2-norm (modulus length) of the gradient provided by the cross-entropy loss, and $grad2\_norm$ is the 2-norm of the gradient provided by the distillation loss. Through this way, the gap of gradient provided by the two losses would be narrow, which could be conducive to promoting the distillation performance.

For the classifier which is trained only with questionnaire data, the loss function is cross entropy loss:

$$loss_{CE} = y_{lable} * log(y_{predict}) + (1 - y_{label}) * log(1 - y_{predit}). \tag{11}$$

The reconstruction loss of linear autoencoder:

$$reconstruct_{AE} = (y_{sample} - y_{reconstruct\_sample})^2. \tag{12}$$

In the first stage of model training, modules are trained independently. The loss for inference module in the second stage of model training, in Fig. 3 left, is also cross-entropy loss, which is the same as Eq. 11. Different from the training in the first stage, the model parameters of the model feature extractors are fixed and do not participate in the training. At last, in order to make each module more suitable for each other, the whole model is fine tuned at a lower learning rate.

4 Experiment Data

4.1 NLST

In this work, United States National Lung Screening Trail [27] was used data. The National Lung Screening Trial is a randomized controlled clinical trial of screening tests for lung cancer. The participants were randomly assigned to the two study arms in equal proportions. One arm received low-dose helical computed tomography (CT), while other received a single-view chest X-ray. The selected feature included information of the study, questionnaire data, smoking history, working history, disease history, personal cancer history and family lung cancer history.

We selected 4820 samples of the dataset, among which 2222 samples had available CT image data, and it would be used as the training set. Another 2598 samples without available CT image data would be sampled to generate the verification set and the testing set. The selected time window is one year.

4.2 Dataset Split

Participants in the NLST screening trial were randomly assigned to two study groups, one using CT and the other using X-rays. As a result, some samples in the dataset have corresponding CT image, while other samples without CT image. Thus, samples with CT image were taken as training sets. 1:1 sampling was performed on samples without CT image, and two datasets were verification sets and test sets respectively.

4.3 Data Prepossessing

For tabular data, according to the data dictionary, the samples whose first diagnosis of lung cancer is less than 365 days was selected as positive samples, and those whose first diagnosis is greater than 365 days or whose value is null was selected as negative samples. For the missing values, the samples with missing attributes is deleted. However, for some cases where the missing values has a special meaning in the data dictionary, such as the age at which the participant stopped smoking (age_quit), the missing value are filled with -1 to indicate that the participant do not provide relevant information. For CT image data, the processing process is referred to kaggle scientific data bowl [1], resampling, segmentation and normalization image, and transformed image files into the form of third-order tensors which could be used by deep learning models.

5 Experiment and Result

5.1 Setup

Teacher Model: The teacher model is trained on the CT dataset, which can complete the lung cancer risk prediction through CT images with good performance. This work [3], completed the prediction of lung cancer with a time

window of one year. The Inflated 3D ConvNet architecture is used to complete the analysis of the whole lung. In this work, this model architecture is used as a teacher network for pre-training to assist student model training.

Metric: Area under receiver curve (AUC) is used to evaluate the overall performance of the model on the dataset. Specificity is used to evaluate the ability of the screening model to exclude negative samples. False Positive Rate (FPR) is the metric associated with it, it means that percentage of participants who were actually disease-free but were judged to be sick. Sensitivity is used to evaluate the ability of the model to detect positive samples. To comprehensively evaluate performance, G-Mean is used, and finally we include ACC as a commonly used evaluation metric into the experiment:

$$Sensitivity = \frac{TP}{TP + FN}, \tag{13}$$

$$Specificity = \frac{TN}{TN + FP}, \tag{14}$$

$$ACC = \frac{TN + TP}{TN + PN + FP + TP}, \tag{15}$$

$$FPR = \frac{FN}{TN + FP} = 1 - Specificity, \tag{16}$$

$$G\text{-}Mean = \sqrt{Sensitivity * Specify}. \tag{17}$$

Hyperparameter Optimization and Setting: For the baseline model, the optuna tool-kit [2] is used to conduct hyperparameter optimization (HPO) for models. For the Epoch, several value are selected as the search space according to the characteristics of the model. For other discrete parameters, feasible values for each parameter that do not conflict with other parameters are included in the search scope. For continuous parameters with a range, such as 0 to 1, their range will be used as the search space. For other continuous parameters which are without certain range, a suitable range that cannot make models overfitting are selected as the search space. After the search, baseline models is retrained by the selected parameters in order to prevent overfitting, and the models with top N performance on the verification set ware tested on the test set, and best performance of baseline models is selected. For the proposed model, the architecture of MLP for both feature extractors is $[127-50-34-15]$, the dropout for each layer are $[0, 0.7, 0.6, 0.5]$. The architecture of linear auto-encoder is $[127 - 50 - 127]$, the dropout is 0.5. The architecture of the head of the proposed model is $[15-2]$, the dropout is 0.5. The optimizator for proposed model is Adam optimizer.

Threshold Chosen: Due to data imbalance, the probability of risk prediction of the model trends to be low, so the probability threshold of risk prediction is determined according to the Youden index. The maximum probability threshold corresponding to the Youden index is selected as the threshold of binary classification.

5.2 Comparison

Baseline: To verify effectiveness of our model about data leverage, our model is compared with eight existing representative algorithms, including three traditional ML algorithms (logistic regression, KNN, and decision trees), two ensemble learning algorithms (XGBoost, CatBoost), and three DL models (MLP, TabNet [4], GANDALF [15]). Among them, XGBoost [11], logistic regression [5,26] and decision tree [23] are the commonly used models of tabular data for risk prediction. XGBoost and CatBoost are two representative algorithms in ensemble learning. For deep learning models, MLP and TebNet are representative method of DNN and tabular learning respectively. The TebNet and GANDALF are implemented by Pytrochtabular tool-kit [14]. All of baseline models are only trained with questionnaire.

In order to evaluate the model more comprehensively, the experiment recorded metric results of each method from two perspectives. Table 1 records performance of each method after threshold chosen, Table 2 records performance of each method in different FPR.

Table 1. Comparison Result – Threshold Chosen

	AUC	Sensitivity	Specificity	G-Mean	ACC
XGBoost [7]	77.19	79.41	67.04	72.96	77.19
CatBoost [9]	73.98	50.00	87.91	66.29	86.91
LR	68.54	64.71	70.20	67.40	69.98
DT	65.96	82.35	47.91	62.81	51.88
KNN	73.04	52.94	84.51	66.89	89.99
MLP	71.50	67.64	75.81	71.31	75.51
TabNet [4]	73.48	82.35	55.97	67.89	56.66
GANDALF [15]	68.15	73.53	59.76	66.28	60.12
Ours	79.28	70.58	79.13	74.74	78.90

According to Table 1, XGBoost, decision tree and TabNet have high sensitivity in prediction, they tend to classify patients into high risk groups. However, low specificity could result in high false positive rate, which could lead to unnecessary detection and extra cost in practice. CatBoost, KNN and our model have high specificity. They are conservative in classifying patients into high-risk groups, thus detection cost could be saved. However, poor sensitivity of CatBoost and KNN show that they are difficult to detect lung cancer patients. From balanced performance of specificity and sensitivity by the G-mean, our model is better than other models, and from overall performance as measured by the AUC, our model is better than other models.

According to Table 2, in different FPR, almost all cases, the sensitivity of our method is higher than that of other models, except in case of 40% FPR. Our method could more easily detect high-risk patients in most cases.

Table 2. Comparison Result – Threshold Not Chosen

	Sensitivity						AUC
	10%FPR	20%FPR	30%FPR	40%FPR	50%FPR	60%FPR	
XGBoost [7]	32.35	58.82	64.71	**79.41**	85.29	**91.18**	77.19
CatBoost [9]	38.24	55.88	64.71	70.59	79.41	82.35	73.98
LR	29.41	50	64.71	64.71	73.53	82.35	68.54
DT	17.65	38.24	55.88	70.59	70.59	85.29	65.96
KNN	41.18	52.94	52.94	73.53	73.53	85.29	73.04
MLP	35.29	50	67.65	73.53	82.35	85.29	71.5
TabNet [4]	35.29	44.12	61.76	73.53	85.29	88.24	73.48
GANDALF [15]	29.41	38.24	52.94	70.59	76.47	79.41	68.15
Ours	**41.18**	**64.71**	**73.53**	76.47	**91.18**	**91.18**	**79.28**

To sum up, on the one hand, due to the full use of multi-source data our model is better than baseline models. On the other hand, because the data for prediction is only questionnaire, proposed model could keep the characteristic of low data cost for prediction.

5.3 Ablation

In order to verify the effectiveness of two parts of our model—cross-modal knowledge distillation and the features extraction—for multi-source data training, we respectively test the performance of the vanilla MLP (MLP^1), cross-modal knowledge distillation (MLP^2) and features extraction (MLP^3) according to the *Setup*, and compare and analyze the test results.

Table 3. Ablation Result – Threshold Chosen

	AUC	Sensitivity	Specifity	G-Mean	ACC
MLP^1	71.50	67.64	75.81	71.61	75.51
MLP^2	77.27	**73.52**	73.75	73.64	73.67
MLP^3	**79.28**	70.58	**79.13**	**74.74**	**78.90**

Table 4. Ablation Result – Threshold Not Chosen

	Sensitivity						AUC
	10%FPR	20%FPR	30%FPR	40%FPR	50%FPR	60%FPR	
MLP^1	35.29	50	67.65	73.53	82.35	85.29	71.5
MLP^2	38.24	61.76	**73.53**	**79.41**	88.24	**91.18**	77.27
MLP^3	**41.18**	**64.71**	**73.53**	76.47	**91.18**	**91.18**	**79.28**

As the results shown in Tables 3 and 4, the performance of the MLP^3 is the best, and the performance of only using cross-modal knowledge distillation is second, both are better than the vanilla MLP performance. It demonstrates that two parts of proposed model is effective for collected multi-source data utilizing.

6 Conclusion

In this article, multi-source data training method for lung cancer prediction model is proposed after three methods for improving the performance of lung cancer prediction model is compared. This method utilizes the diversity of medical data to expand the training data of the model to improve the performance of the prediction model, while avoid increasing the cost of using the model. Considering the differences between data, the model has three feature extraction modules, which are the feature extraction module after cross-modal knowledge distillation, the feature extraction module without distillation, and the linear encoder. The model is trained in two steps, and finally the model performance was improved again.

7 Future Work

Of course, the comprehensive exploration of this method is not performed, for example: 1) Whether multi-source training is suitable for tasks corresponding to medical data at different stages, such as: diagnosis, re-examination, and so on. 2) The current work is only discussed under the two data sources. In the future, it is interesting to discuss whether this method can be extended to more data sources. 3) The current work of this method requires matching of two data of training samples during model training, which increases the constraints on training data and reduces the utilization rate of data or samples in a form. It needs to be solved in the follow-up research. 4) The knowledge distillation method in this work uses off-line distillation. It is interesting to explore other method to perform multi-source data training. 5) The current work has not dealt with the feature fusion problem of multiple feature extractors.

Acknowledgement. The authors thank the National Cancer Institute for access to NCI's data collected by the National Lung Screening Trial (NLST). This work was jointly supported by the National Key R&D Program of China under grant number 2021YFF0704103, and the National Natural Science Foundation of China under grant number 62136002 and 62221005.

References

1. Buckeye, A.J., Kirby, J., et al.: Data science bowl 2017 (2017). https://kaggle.com/competitions/data-science-bowl-2017
2. Akiba, T., Sano, S., Yanase, T., Ohta, T., Koyama, M.: Optuna: a next-generation hyperparameter optimization framework. In: Proceedings of the 25th ACM SIGKDD International Conference on Knowledge Discovery & Data Mining, pp. 2623–2631 (2019)
3. Ardila, D., et al.: End-to-end lung cancer screening with three-dimensional deep learning on low-dose chest computed tomography. Nat. Med. **25**(6), 954–961 (2019)
4. Arik, S.Ö., Pfister, T.: TabNet: attentive interpretable tabular learning. In: Proceedings of the AAAI Conference on Artificial Intelligence, vol. 35, pp. 6679–6687 (2021)
5. Bach, P.B., et al.: Variations in lung cancer risk among smokers. J. Natl Cancer Inst. **95**(6), 470–478 (2003)
6. Barrett, J., Viana, T.: EMM-LC fusion: enhanced multimodal fusion for lung cancer classification. AI **3**(3), 659–682 (2022)
7. Chen, T., et al.: XGBoost: extreme gradient boosting. R package version 0.4-2 **1**(4), 1–4 (2015)
8. Daza, L., Castillo, A., Escobar, M., Valencia, S., Pinzón, B., Arbeláez, P.: LUCAS: LUng CAncer screening with multimodal biomarkers. In: Syeda-Mahmood, T., et al. (eds.) CLIP/ML-CDS -2020. LNCS, vol. 12445, pp. 115–124. Springer, Cham (2020). https://doi.org/10.1007/978-3-030-60946-7_12
9. Dorogush, A.V., Ershov, V., Gulin, A.: CatBoost: gradient boosting with categorical features support. arXiv preprint arXiv:1810.11363 (2018)
10. Gou, J., Yu, B., Maybank, S.J., Tao, D.: Knowledge distillation: a survey. Int. J. Comput. Vision **129**, 1789–1819 (2021)
11. Gould, M.K., Huang, B.Z., Tammemagi, M.C., Kinar, Y., Shiff, R.: Machine learning for early lung cancer identification using routine clinical and laboratory data. Am. J. Respir. Crit. Care Med. **204**(4), 445–453 (2021)
12. Guan, X., et al.: Construction of the XGBoost model for early lung cancer prediction based on metabolic indices. BMC Med. Inform. Decis. Mak. **23**(1), 1–16 (2023)
13. Hoffman, J., Gupta, S., Darrell, T.: Learning with side information through modality hallucination. In: Proceedings of the IEEE Conference on Computer Vision and Pattern Recognition, pp. 826–834 (2016)
14. Joseph, M.: Pytorch tabular: a framework for deep learning with tabular data. arXiv preprint arXiv:2104.13638 (2021)
15. Joseph, M., Raj, H.: GANDALF: gated adaptive network for deep automated learning of features (2023)
16. Lee, C.H., Yoon, H.J.: Medical big data: promise and challenges. Kidney Res. Clin. Pract. **36**(1), 3 (2017)
17. Liu, S., Yao, W.: Prediction of lung cancer using gene expression and deep learning with KL divergence gene selection. BMC Bioinform. **23**(1), 175 (2022)
18. Mamun, M., Farjana, A., Al Mamun, M., Ahammed, M.S.: Lung cancer prediction model using ensemble learning techniques and a systematic review analysis. In: 2022 IEEE World AI IoT Congress (AIIoT), pp. 187–193. IEEE (2022)
19. Mukherjee, S., Bohra, S.: Lung cancer disease diagnosis using machine learning approach. In: 2020 3rd International Conference on Intelligent Sustainable Systems (ICISS), pp. 207–211. IEEE (2020)

20. Park, M.K., et al.: Deep-learning algorithm and concomitant biomarker identification for NSCLC prediction using multi-omics data integration. Biomolecules **12**(12), 1839 (2022)
21. Passalis, N., Tefas, A.: Learning deep representations with probabilistic knowledge transfer. In: Ferrari, V., Hebert, M., Sminchisescu, C., Weiss, Y. (eds.) ECCV 2018. LNCS, vol. 11215, pp. 283–299. Springer, Cham (2018). https://doi.org/10.1007/978-3-030-01252-6_17
22. Ren, S., Du, Y., Lv, J., Han, G., He, S.: Learning from the master: distilling cross-modal advanced knowledge for lip reading. In: Proceedings of the IEEE/CVF Conference on Computer Vision and Pattern Recognition, pp. 13325–13333 (2021)
23. Spitz, M.R., et al.: A risk model for prediction of lung cancer. J. Natl. Cancer Inst. **99**(9), 715–726 (2007)
24. Sun, W., Zheng, B., Qian, W.: Computer aided lung cancer diagnosis with deep learning algorithms. In: Medical Imaging 2016: Computer-Aided Diagnosis, vol. 9785, pp. 241–248. SPIE (2016)
25. Sung, H., et al.: Global cancer statistics 2020: GLOBOCAN estimates of incidence and mortality worldwide for 36 cancers in 185 countries. CA Cancer J. Clin. **71**(3), 209–249 (2021)
26. Tammemagi, C.M., et al.: Lung cancer risk prediction: prostate, lung, colorectal and ovarian cancer screening trial models and validation. J. Natl. Cancer Inst. **103**(13), 1058–1068 (2011)
27. National Lung Screening Trial Research Team: The national lung screening trial: overview and study design. Radiology **258**(1), 243–253 (2011)
28. Ten Haaf, K., et al.: A comparative modeling analysis of risk-based lung cancer screening strategies. JNCI J. Natl. Cancer Inst. **112**(5), 466–479 (2020)
29. Thoker, F.M., Gall, J.: Cross-modal knowledge distillation for action recognition. In: 2019 IEEE International Conference on Image Processing (ICIP), pp. 6–10. IEEE (2019)
30. Wang, D., et al.: End-to-end voice conversion via cross-modal knowledge distillation for dysarthric speech reconstruction. In: 2020 IEEE International Conference on Acoustics, Speech and Signal Processing (ICASSP), ICASSP 2020, pp. 7744–7748. IEEE (2020)
31. Zhang, S., Li, Z., Zhou, H.Y., Ma, J., Yu, Y.: Advancing 3D medical image analysis with variable dimension transform based supervised 3D pre-training. Neurocomputing **529**, 11–22 (2023)
32. Zhao, M., et al.: Through-wall human pose estimation using radio signals. In: Proceedings of the IEEE Conference on Computer Vision and Pattern Recognition, pp. 7356–7365 (2018)

Advancing ITS Applications with LLMs: A Survey on Traffic Management, Transportation Safety, and Autonomous Driving

Dingkai Zhang[1(✉)], Huanran Zheng[2], Wenjing Yue[2], and Xiaoling Wang[2]

[1] The Key Laboratory of Road and Traffic Engineering, Ministry of Education, Tongji University, Shanghai 200092, China
dkzhang@tongji.edu.cn

[2] School of Computer Science and Technology, East China Normal University, Shanghai 200062, China
{hrzheng,wjyue}@stu.ecnu.edu.cn, xlwang@cs.ecnu.edu.cn

Abstract. In the past two years, large language models (LLMs) have shown extensive attention in the applications of intelligent transportation systems (ITS). Despite the huge potential, there is still a lack of comprehensive understanding of the advantages, challenges, and future efforts of LLMs in the transportation field. In this paper, we present a systematic investigation in this field, underlining their approaches and performance in improving forecasting accuracy, decision-making capability, and sim-to-real tasks. We first explore the current applications of LLMs in traffic management, transportation safety, and autonomous driving, as well as analyze their advantages and limitations. Then we also list some typical datasets employed within this domain. Challenges and prospects of the development of LLMs for ITS applications are discussed, encompassing technological, security, and policy aspects. We aim to offer a holistic overview of the transformative impact of LLMs in the transportation field, highlight their significance, and provide some possible views for future research and development.

Keywords: Large Language Model · Intelligent Transportation Systems · Autonomous Driving

1 Introduction

LLMs have rapidly emerged as significant approaches across various domains, demonstrating their capability to emulate human-like intelligence with high precision [16]. LLMs, such as GPT-4 [1], PaLM-2 [2], and LLaMA-2 [33], have been investigated for their potential to enhance the prediction and decision-making performance of ITS applications, particularly in traffic management,

M. Hu et al. (Eds.): IJCRS 2024, LNAI 14840, pp. 295–309, 2024.
https://doi.org/10.1007/978-3-031-65668-2_20

transportation safety, and autonomous driving tasks. Although these are still at an exploratory stage, LLMs have demonstrated the possibility of improving mobility and management paradigms in ITS [30].

Recent advancements in LLMs have enabled them to address complex tasks, ranging from semantic analysis [15] to contextual response generation [23]. These capabilities are significant for ITS, where prediction and decision-making processes rely on high-performance of data processing and understanding. For example, the application of LLMs in traffic management systems can improve the way traffic flow is monitored. It processes dynamic data to predict traffic congestion and suggest optimal routing strategies [50]. The powerful processing capability of LLMs can also help researchers analyze data from different sources to understand accident reports and identify potential risks, thus enhancing the safety of transportation [47]. Moreover, LLMs have shown great possibilities in simulating human-like intelligence, while their applications in autonomous driving have received much attention. These research studies mainly focus on perception algorithms enhancement [48], motion planning improvement [6], and control mechanisms improvement [8], thereby improving the response speed, decision-making accuracy, and operation reliability of autonomous driving.

However, there are challenges when applying LLMs to improve ITS applications, including data privacy issues, system fault tolerance requirements, and ethical implications [30,51]. Therefore, the application of LLMs in realistic traffic scenarios is still being explored, and their reliability and effectiveness are to be verified.

The main contributions of this paper are summarized as follows:

(1) A comprehensive overview of research on LLMs for ITS applications is outlined, focusing on traffic management, transportation safety, and autonomous driving, discussing their potential to increase forecasting accuracy, improve safety, and enhance decision-making processes.
(2) Existing relevant datasets are systematically summarized, including those for single tasks and complex scenarios.
(3) The potential challenges in LLMs for ITS applications are discussed, including data privacy, system robustness, and ethical considerations. In addition, some possible future research directions are listed.

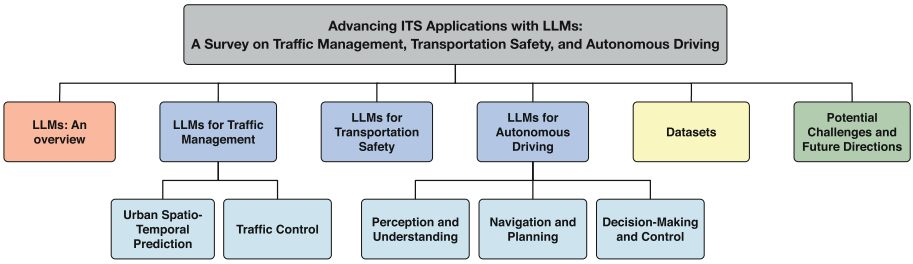

Fig. 1. The structure of this paper

As shown in Fig. 1, our survey paper aims to provide a comprehensive overview of LLMs for ITS applications. The following section provides a brief overview of LLMs. Sections 3 to 5 present current published works about LLMs related to traffic management, transportation safety, and autonomous driving. Section 6 lists recent datasets that can be used as benchmarks to evaluate LLM-based models for ITS tasks. In the last two sections, we discuss the potential challenges that LLMs for ITS applications may face and some possible directions for future research.

2 LLMs: An Overview

LLMs, such as GPT-3 [3], LLaMA [33], and GPT-4 [1] implement language functions primarily through advanced text generation. These models achieve semantic understanding and cognitive capabilities comparable to human processing levels by being trained on large amounts of Internet data [16]. LLMs also have several emerging capabilities, including in-context learning, instruction following, and chain of thought reasoning. These capabilities extend LLMs to autonomous domains and then build systems that can implement decision-making and problem-solving. Furthermore, the combination of LLMs with other models constitutes a significant advancement in cross-modal learning.

The integration of vision, language, video, and audio modalities has been a primary objective in AI research for decades. With the rising need for multimodal interaction, LLMs have progressed from processing solely text to handling multiple modalities, leading to the development of Multimodal Large Language Models (MLLMs). MLLMs enhance LLMs' capabilities to evolve from large-scale pre-training to task-specific fine-tuning. BLIP-2 [19] combines convolutional neural networks with text representations to produce images from textual inputs. DALL-E [26], which is built on the GPT-3 [3] framework, generates images from text descriptions thereby demonstrating multimodal models' applicability in diverse fields. GPT-4V[1] demonstrates notable capabilities in enhancing understanding of traffic scenarios, thus supporting flow control, accident analysis, and driving decision applications. In the above MLLMs research, instruction tuning is a central method to enable models to follow instructions across various modalities [13,19]. This approach allows models to integrate visual cues with textual commands, such as identifying objects in images based on text descriptions and instructions.

In addition to cross-modal learning, some studies combine real-world sensor data with LLMs. They link verbal instructions to perceptual inputs to enhance the model's understanding of the physical environment, and they are able to interpret those understandings through languages [31,35]. Voyager [35] demonstrates AI's lifelong learning. It mimics human learning patterns by interacting with the environment in an improved way and acquiring knowledge continuously. Voxposer [17] further extends the usefulness of LLMs for ITS applications by applying these models to create robot trajectories for a variety of manipulation tasks.

[1] https://openai.com/research/gpt-4v-system-card.

3 LLMs for Traffic Management

The challenges of handling complex and dynamic traffic data, as well as the need for adaptive traffic management solutions, show the critical importance of LLMs for the current traffic management research [30]. Their advanced language and data processing capabilities enable the integration of heterogeneous information sources, such as traffic reports [51], sensor data [48], and map data [8], into coherent insights. In this way, highly accurate traffic flow predictions and sophisticated traffic management strategies are achieved. Table 1 summarizes LLM-based research for traffic management in prediction and traffic control tasks with their advantages and limitations.

Table 1. Summary of recent research on LLMs for traffic management.

Model	Year	Backbone	Task	Advantages	Limitations
ChatGPT for GTFS [11]	2023	GPT-3.5 GPT-4	Prediction	Demonstrate a reasonable understanding of GTFS by ChatGPT	Rely on the support of program synthesis
TFM [40]	2023	GPT-3	Prediction	Understand dynamic traffic flow through LLMs	Hard to balance joint probabilities and granularity
UniST [46]	2024	GPT-3	Prediction	Mimick the key features of LLMs for spatio-temporal prediction	Have difficulties in variations in data distributions across different scenarios
TrafficGPT [50]	2023	GPT-3.5	Traffic Control	Integrates ChatGPT with traffic foundation models effectively	Hard to handle extensive numerical data and interact with simulations
Mixed Traffic Control via RL [34]	2023	GPT-4	Traffic Control	Solve mixed traffic control problems without expert knowledge	Get inconsistent outcomes across different traffic scenarios
LLMLight [18]	2024	GPT-4	TSC	Have capabilities for interpretable and human-like decision- making in TSC	Require specialized training and fine-tuning
PromptGAT [10]	2024	GPT-4	TSC	Reduce the sim-to-real performance gap in TSC significantly	Have difficulties in unobserved states and lead to significant prediction errors under specific scenarios

3.1 Urban Spatio-Temporal Prediction

Urban spatio-temporal forecasting predicts the dynamic patterns of urban activities in both space and time. Figure 2 includes an example of applying a prompt to predict traffic flow based on spatio-temporal data. It begins with extracting features from abundant spatio-temporal data, then proceeds to pre-training with tasks like spatial association learning and pattern recognition. Then, structured prompts are applied to guide the LLM in predicting traffic flow for specified periods at given locations.

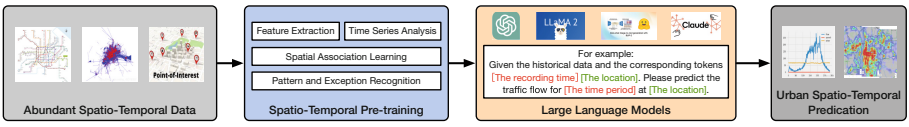

Fig. 2. An general pipeline of using LLMs to enhance urban spatio-temporal prediction.

ChatGPT for GTFS [11] benchmarks OpenAI's GPT-3.5-Turbo and GPT-4 to investigate the performance of using natural language prompts to retrieve urban-related information, such as the number of trains visiting a station in a period, from the General Transit Feed Specification (GTFS) dataset. The study demonstrates that using prompts to interpret complex GTFS data is effective, with results showing that ChatGPT correctly answered 59.7% and 73.3% of multiple-choice questions, respectively. However, ChatGPT was hard to process complex queries. Its accuracy drops significantly without the program synthesis support, which indicates a lack of deep understanding of the GTFS schema and data relationships.

For forecasting road traffic flows, some studies investigate the effectiveness of applying LLMs [40,46]. TFM [40] captures the participatory behavior and interaction of transportation system actors using graph structures and dynamic graph generation algorithms, which provides an adaptive and flexible way to model complex transportation problems. However, it faces challenges in balancing the complexity of solving joint probabilities and managing the granularity of traffic prediction, which may affect the precision in simulating real-world traffic behaviors. UniST [46] is the first general spatio-temporal prediction model that takes advantage of using prompts through LLMs. To create a unified sequence format that is compatible with the Transformer architecture, it processes diverse city and domain data by using spatio-temporal tokenizers. UniST captures complex spatio-temporal correlations through a masking strategies-based pre-training model. Through spatio-temporal knowledge-guided prompts, it can generate prompts that share attributes across datasets according to domain knowledge. It was tested through datasets across 15 cities and 6 domains, which significantly verified LLMs' capabilities in few-shot and zero-shot prediction. However, the variation in data distribution may affect its adaptability and accuracy in different scenarios.

LLMs show promise in spatio-temporal forecasting by effectively interpreting complex datasets with structured prompts and capturing intricate data correlations. However, they have difficulties in complex queries and exhibit variable accuracy across different data distributions, which reveal a limited deep understanding of domain-specific schemas and relationships.

3.2 Traffic Control

Another traffic management application that has been attempted to be optimized using LLMs is traffic control, including Traffic Flow Control (TFC) and Traffic Signal Control (TSC). Since the real traffic environment is very complex, how to avoid lane congestion is a main purpose of traffic control [29]. Figure 3 illustrates that factors such as vehicles, road conditions, and signal lights in the scene are observed through a prompt. Then LLM agents generate responses that inform traffic control actions, such as adjusting signal switches to alleviate traffic congestion. Research on TFC includes combining LLMs with traffic base models [50] and reinforcement learning (RL) techniques [34]. LLMs for TFC effectively augment data analysis and decision-making in complex scenarios, even helping

non-experts to make successful decisions [34]. However, they face challenges with extensive numerical data and exhibit variable performance across different traffic conditions.

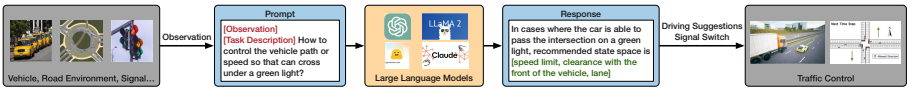

Fig. 3. An general workflow of using LLMs to give suggestions for traffic control.

LLMLight [18] first guides LLMs to optimize traffic signal configuration using commonsense enhanced hints. The process begins by transforming dynamic traffic conditions into human-readable texts that serve as inputs for the LLM. Then LightGPT is designed as a specialized LLM fine-tuned for the TSC task. It is trained through imitation fine-tuning and learned from high-quality control actions and rationales derived from GPT-4. Policy refinement is then applied using a critical model to enhance the decision-making capability of the LLM. Experiments on nine real-world and synthetic datasets showed that LLMLight with LightGPT achieved competitive results, while it answered 73.3% of multiple-choice questions correctly and achieved up to 93% accuracy for simple queries in an information extraction task using GTFS data. The results showed significant improvements over traditional traffic-based models and reinforcement learning methods. However, it requires specialized training and fine-tuning to align with specific TSC tasks, which present challenges in initial setup and adaptation. PromptGAT [10] enhances the reasoning ability of the model. It optimizes the performance in the TSC task by asking LLMs for dynamic traffic information, as well as it enhances action transformation by incorporating human knowledge with LLMs, thus significantly reducing the sim-to-real performance gap in TSC. PromptGAT may have difficulties in unobserved states and rare conditions in the real world, which can lead to significant prediction errors under those specific scenarios. Therefore, although LLMs have made some achievements in dealing with decision-making problems in complex scenes, the research on them is still under exploration due to the changeable traffic environment.

4 LLMs for Transportation Safety

In the field of traffic safety research, accident analysis is a necessary task [32], such as static environment analysis [49], dynamic collision detection [20], and accident cause analysis [32], etc. LLMs's powerful text analysis capabilities and their integration with perceptual models are expected to help researchers gain a deeper understanding of traffic safety-related information. Table 2 summarizes LLM-based research for transportation safety in accident text analysis and multisensory safety analysis tasks with their advantages and limitations.

Table 2. Summary of recent research on LLMs for transportation safety.

Model	Year	Backbone	Task	Advantages	Limitations
ChatGPT is on the Horizon [51]	2023	GPT-3.5	Accident Text Analysis	Explore ChatGPT in accident report analysis and traffic data augmentation	Discuss several challenges which could hinder practical deployment
Large Language Models in Analyzing Crash Narratives [24]	2023	ARD GPT-4	Accident Text Analysis	Extract information from crash narratives efficiently	Exhibit variable performance depending on the complexity of information
GPT-4V as Traffic Assistant [53]	2024	GPT-4	Multisensory Safety Analysis	Explore GPT-4V in recognizing and analyzing complex traffic events	Requires additional modalities beyond texts and images
AccidentGPT [36]	2023	GPT-4	Multisensory Safety Analysis	Offer comprehensive accident analysis and prevention through multi-modal and multi-sensor framework	Depend on the integration of additional modalities and accurate multi-sensor data

ChatGPT is on the Horizon [51] demonstrated the potential of LLMs for automating accident reporting. The experimental results show that ChatGPT achieved a 90% true positive rate for accident information extraction, 80% for accident classification, and 75% for accident data imputation, matching the performance of models specifically fine-tuned for each task. Moreover, ChatGPT is also able to augment long-tail data based on prompts. However, it encounters challenges such as model bias, data privacy, model vulnerability, and hallucination, which could hinder its practical deployment in traffic safety applications. Mumtarn et al. [24] investigated the ability of three LLMs, ChatGPT, BARD, and GPT-4, to understand accident narratives. By comparing their responses to queries, it was found that the results were more accurate for the binary answer questions, but relatively poor for the complex questions. And their answers in the task of determining the responsible party had obvious bias.

It is a more direct way to recognize and understand traffic accidents through pictures and videos at the accident scene. Zhou and Knoll [53] explored the capabilities of the GPT-4V model through a representative set of traffic accident videos. It showed that GPT-4V can successfully identify accidents in the vast majority of tasks without any specific prompting strategies or fine-tuning methods, which demonstrated its powerful zero-shot capability. In addition, it was found that GPT-4V can formulate reasonable emergency measures and perform severity analysis by combining accident features and relevant contextual information extracted from images. Figure 4 shows examples of GPT-4V's understanding capabilities in traffic accident scenarios and potentially risky urban road scenarios. Traffic scenario A(top) is a picture containing a traffic accident, and traffic scenario B(bottom) is a series of screenshots from a video [36]. AccidentGPT [36] is the first large-scale model to integrate comprehensive scenario understanding into traffic safety research for accident analysis and prevention. However, its effectiveness is dependent on the integration of additional modalities and accurate multi-sensor data, which may limit its application in environments where such data integration is challenging or incomplete.

LLMs demonstrate high accuracy and zero-shot capabilities in traffic accident identification and analysis, offering detailed extraction and classification of accident data. However, they face challenges such as model bias and dependency on complex data integration, limiting their practical deployment in traffic flow control.

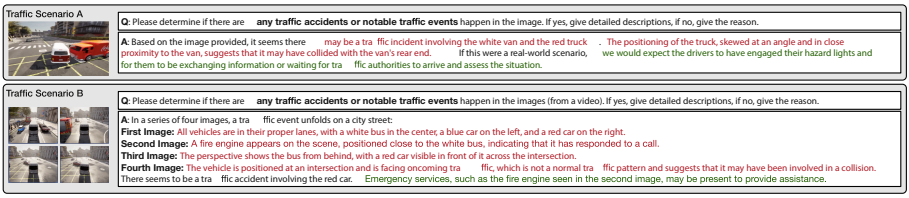

Fig. 4. GPT-4V evaluation of interpretability and inference of traffic anomaly scenarios.

5 LLMs for Autonomous Driving

With the development of LLMs, they bring innovation to the research in the autonomous driving domain. [13,22]. These aspects collectively advance the development of vehicles that operate without human intervention, thus contributing to the evolution of mobility. Figure 5 shows a general workflow of autonomous driving including inputs, models, and tasks. Sensor inputs and text tokens are processed through models. Models are trained in simulations for real-world application. Prompts are utilized as structured queries or instructions to guide the models in performing specific tasks such as perception, planning and control, answering questions, or content generation. Table 3 summarizes LLM-based research for autonomous driving in perception, planning, decision-making, and control tasks with their advantages and limitations.

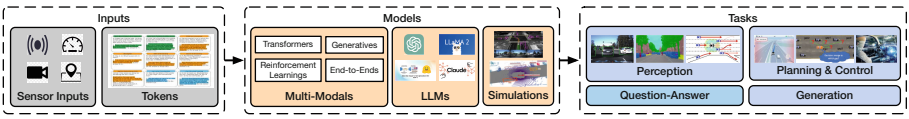

Fig. 5. A general pipeline of LLMs for autonomous driving.

5.1 Perception and Understanding

The core of autonomous driving technology is perception and understanding, where vehicles must accurately interpret their surroundings to navigate the driving. LLMs play a foundational role in processing vast amounts of sensory data

Table 3. Summary of recent research on LLMs for autonomous driving.

Model	Year	Backbone	Task	Advantages	Limitations
HiLM-D [13]	2023	BLIP-2	Perception	Incorporate high-resolution information effectively	Be limited by datasets and may not capture extreme weather conditions
Talk2BEV [12]	2023	BLIP-2 MiniGPT-4 InstructBLIP-2	Perception Planning	Allow to use language-enhanced maps for visual and spatial reasoning without task-specific training	Require human-verified annotations and heavily dependent on the quality of BEV prediction models
VisionLLM [38]	2024	LLaMA	Perception Planning Decision-making	Handle open-ended vision-centric tasks through unified language prompts	Require significant alignment between vision and language modalities, and depend on the specific prompts
LiDAR-LLM [43]	2023	GPT-4	Perception	Comprehend and reason about 3D scenes	Face challenges with sparsity and complexity in outdoor LiDAR data and relies on the quality and availability of 3D LiDAR-text pairing data
Dolphins [21]	2023	LLaMA	Perception Planning Decision-making	Implement vision-language model to process multimodal inputs and generate informed outputs corresponding to the provided instructions	Depend on the quality and scope of its training datasets highly
OccWorld [52]	2023	GPT-3	Perception	Forecast future scene evolution and ego movements without needing instance and map supervision	Hard to forecast new vehicles
LM-Nav [27]	2023	GPT-3	Planning Control	Execute complex, long-horizon navigation tasks from natural language prompts without language-annotated robot data	Rely on landmarks heavily
Drive as You Say [7]	2023	GPT-4	Planning Decision-making	Enable communication between drivers and vehicles	Lack of LLM's direct environmental perception
Dilu [41]	2023	GPT-3.5 GPT-4	Decision-making	Show strong generalization abilities and effective use of the memory module	Experience decision-making latency of 5–10 s and may generate hallucinations
ReAct [44]	2023	GPT-3	Decision-making	Enhance model interpretability and trustworthiness	Depend heavily on the quality of the prompting setup
DriveLLM [9]	2024	GPT-3.5	Decision-making	Process edge cases effectively	Faces challenges with real-time performance
LLM-Assist [28]	2023	GPT-3 GPT-4	Planning Decision-making	Enhance decision-making under uncertainty	Require high computational resources
DriveMLM [39]	2023	GPT-3.5	Planning Decision-making Control	Achieve high flexibility and interpretability	Depend highly on the quality and breadth of its training dataset

from cameras, LiDAR, radar, and other sensors, to create a comprehensive understanding of the environment. Thus they can identify objects, assess distances, and understand complex scenarios such as pedestrian movements, traffic flow, and road conditions [12].

The cross-modal analysis capability of MLLMs enhances their popularity for addressing both object detection and semantic segmentation. HiLM-D [13] has investigated the use of MLLMs to detect single objects. To focus on potential risks, it processes low-resolution videos through a reasoning branch while incorporating high-resolution images in a perception branch to enhance object detection. Integrated seamlessly with existing LLMs, HiLM-D demonstrated notable improvements on this benchmark with a 4.8% increase in BLEU-4 for captioning accuracy and a 17.2% rise in mIoU for object detection. The results show its capability to provide a more nuanced understanding of driving scenes. After exploring the ability of MLLMs to detect a single object, Talk2BEV [12] dived into the

understanding of the whole scene and tried to perceive human-car and car-to-car interactions. It processes multi-view images and LiDAR data to generate BEV maps. It operates without the need for task-specific models or fine-tuning. However, the performance of these models relies heavily on the integration quality of multimodal data and may require sophisticated processing of different resolutions to focus effectively on relevant objects and interactions within complex scenes.

Describing images by text is another improvement in applying LLMs to 3D object detection. VisionLLM [38] employs a language-guided image tokenizer and an LLM-based decoder to interpret and execute a wide range of vision-centric tasks as defined by the prompts. This approach facilitates a seamless blend of vision and language tasks, allowing for flexible task definitions and management using language instructions. It achieved over 60% mean average precision on the COCO dataset, which is comparable to detection-specific models. However, it requires significant alignment between vision and language modalities and is dependent on the specific prompts. The open-vocabulary approach allows the capability to self-update and learn new labels when encountering new objects or scenes. Thus, it can better adapt and deal with various unknown objects and scenes. LiDAR-LLM [43] applied LLMs for a comprehensive outdoor 3D scene understanding through tasks like 3D captioning and question answering. It achieved a 40.9 BLEU-1 score in 3D captioning and 63.1% classification accuracy in question answering. However, it faces challenges with sparsity and complexity in outdoor LiDAR data and relies on the quality and availability of 3D LiDAR-text pairing data for training, which may limit its application in scenarios not covered by the data.

It is also a focus and difficulty of research to construct a world model that tends to be more extensive real scene through LLMs. OccWorld [52] uses a GPT-like spatio-temporal generative transformer to predict future scene and ego car tokens, thus decoding both future occupancy and self-trajectories. Performance evaluations on the nuScenes benchmark reveal its competency in modeling dynamic driving scenes and planning. It achieved an average intersection over union of 26.63 and a mean of 17.13 for 3-second futures given 2-second histories. Moreover, it produced planning trajectories with an L2 error of 1.16 without relying on instance and map annotations. However, It's difficult to forecast new vehicles entering the view, because of the limitation arising from their absence in input data. Dolphins [21] is also highly dependent on the quality and scope of its training datasets. Therefore, the sim-to-real task is still the difficulty of research. Due to the variability of real world scenarios, how to reduce the dependence of models on datasets is still being explored.

5.2 Navigation and Planning

LLMs help incorporate human-like reasoning into the navigation process, enabling vehicles to make safer and more effective choices by learning about subtleties and potential hazards in the environment. LM-Nav [27] is a robotic navigation system built entirely from pre-trained navigation models, CLIP and

GPT-3, without requiring any fine-tuning or language-annotated robot data. Its performance is bounded by the landmark detection capabilities of the vision-language model. Cui et al. [7] processes prompts as spoken instructions from drivers, employing these for real-time contextual analysis and driving execution. However, it is constrained by the LLMs' limited direct perception capabilities. It achieved a 4.8% increase in BLEU-4 for captioning accuracy and a 17.2% rise in mIoU for object detection which improved driving decisions with personalization through real-time feedback.

5.3 Decision-Making and Control

In the domain of autonomous driving, the decision-making processes and control are increasingly being augmented by LLMs. Several studies [41,44] explored the implementation of basic decision-making through LLMs. They show that LLMs may experience decision-making latency and hallucinations that affect real-time responsiveness. Their effectiveness can be constrained by limited support for complex behaviors and heavy dependence on the quality of prompt setup, requiring extensive fine-tuning to optimize performance.

In addition to achieving basic decision-making, the researchers also worked on enabling more advanced and complex human-vehicle interactions. DriveLLM's [9] process begins with an LLM-AD Bridge that aligns the decision-making criteria of autonomous driving with the interpretive functions of LLMs. In this way, common sense reasoning and decision-making are enabled based on a comprehensive array of inputs, including real-time information about vehicle states, map data, and passenger requests. LLM-Assist [28] controls autonomous driving in closed-loop by LLMs, and a memory module is introduced to record important driving information such as driving scene and driving experience. DriveMLM [39] can perform closed-loop autonomous driving in a real-world simulator. The model uses driving rules, user prompts, and various sensors' data as inputs, and enables the driver to make decisions with explanations. However, LLMs face significant challenges in real-time applications in these research studies due to high computational demands, decision-making latency, hallucinations, extensive and high-quality training dataset dependency, and robust multimodal input requirements. These limitations can restrict LLMs' practical deployment and performance in dynamic and complex scenarios.

6 Datasets

In this section, we enumerated some typical benchmark datasets that could be used for LLMs for ITS applications (a summary is shown in Table 4). These datasets range from individual tasks, such as traffic flow prediction and object detection, to synthetic scenes, such as scenario understanding.

Table 4. Summary of ITS domain datasets for LLMs' evaluation.

Datasets	Main Tasks	URLs
GTFS_LLM [11]	GTFS Data Understanding	https://github.com/UTEL-UIUC/GTFS_LLM
PeMS[a]	Traffic Flow Predication	https://dot.ca.gov/programs/traffic-operations/mpr/pems-source
nuScenes [4]	Object Detection	https://www.nuscenes.org/nuscenes
DeepAccident [37]	Scenario Understanding	https://deepaccident.github.io/
Waymo [14]	Scenario Understanding	https://github.com/waymo-research/waymo-open-dataset
MAPLM [5]	Scenario Understanding	https://github.com/LLVM-AD/MAPLM
NuScenes-QA [25]	VQA	https://github.com/qiantianwen/NuScenes-QA
DAIR-V2X [45]	V2X	https://github.com/AIR-THU/DAIR-V2X

[a]https://dot.ca.gov/programs/traffic-operations/mpr/pems-source

7 Potential Challenges and Future Directions

Applying LLMs to ITS applications comes with challenges related to model bias, safety, reliability, artificial hallucination, computational demands, and integration with existing infrastructure.

Model bias stems from skewed training data which can lead to unfair or sub-optimal decision-making processes, thus affecting traffic routing and safety measures [30]. Safety and reliability concerns are amplified by the unpredictable nature of LLM outputs, which could compromise the operational integrity of ITS and endanger user safety [42]. Furthermore, artificial hallucination poses a threat to the accurate interpretation of traffic scenarios, which potentially leads to erroneous decision-making [9]. Computational requirements for fine-turning LLMs are substantial and would limit their deployment in ITS applications due to the high processing power needed. This issue often strains system efficiency and escalates costs, particularly in real-time applications [8]. Additionally, integration challenges arise from attempting to seamlessly incorporate LLMs with existing models.

Addressing these challenges necessitates a multifaceted approach. Future research should focus on enhancing the dynamic adaptation of LLMs to real-time conditions. This involves not only overcoming computational limitations through model and hardware optimizations but also ensuring that safety measures derived from LLMs are effective and equitable across different user demographics. In terms of model bias, a concerted effort is needed to diversify training datasets and apply fairness-aware algorithms to mitigate output skew. For safety and reliability, rigorous testing and robust data governance are required to manage LLMs' unpredictable outputs effectively. Tackling artificial hallucination requires methods that improve model understanding and prevent false extrapolations.

Additionally, efforts to standardize LLMs in ITS applications are essential for broader adoption. This includes developing adaptable LLM solutions and creating interoperability standards within ITS applications. A multidisciplinary, collaborative approach is vital for the responsible development of LLMs, prioritizing societal values and regulatory compliance.

8 Conclusion

This paper comprehensively discussed the performance of LLMs in advancing ITS applications, focusing on traffic management, transportation safety, and autonomous driving tasks. We provided an extensive review of relevant research and datasets, as well as discussed the main challenges and future directions in the field.

References

1. Achiam, J., et al.: GPT-4 technical report. arXiv preprint arXiv:2303.08774 (2023)
2. Anil, R., et al.: PaLM 2 technical report. arXiv preprint arXiv:2305.10403 (2023)
3. Brown, T., et al.: Language models are few-shot learners. In: Advances in Neural Information Processing Systems, vol. 33, pp. 1877–1901 (2020)
4. Caesar, H., et al.: nuScenes: a multimodal dataset for autonomous driving. In: CVPR (2020)
5. Cao, X., et al.: MAPLM: a real-world large-scale vision-language dataset for map and traffic scene understanding (2023). https://github.com/LLVM-AD/MAPLM
6. Cui, C., Ma, Y., Cao, X., Ye, W., Wang, Z.: Drive as you speak: enabling human-like interaction with large language models in autonomous vehicles. In: Proceedings of the IEEE/CVF Winter Conference on Applications of Computer Vision, pp. 902–909 (2024)
7. Cui, C., Ma, Y., Cao, X., Ye, W., Wang, Z.: Receive, reason, and react: drive as you say, with large language models in autonomous vehicles. IEEE Intell. Transp. Syst. Mag. (2024)
8. Cui, C., et al.: A survey on multimodal large language models for autonomous driving. In: Proceedings of the IEEE/CVF Winter Conference on Applications of Computer Vision, pp. 958–979 (2024)
9. Cui, Y., et al.: DriveLLM: charting the path toward full autonomous driving with large language models. IEEE Trans. Intell. Veh. **9**, 1450–1464 (2024)
10. Da, L., Gao, M., Mei, H., Wei, H.: Prompt to transfer: sim-to-real transfer for traffic signal control with prompt learning. In: Proceedings of the AAAI Conference on Artificial Intelligence, vol. 38, pp. 82–90 (2024)
11. Devunuri, S., Qiam, S., Lehe, L.: ChatGPT for GTFS: benchmarking LLMs on GTFS understanding and retrieval
12. Dewangan, V., et al.: Talk2BEV: language-enhanced bird's-eye view maps for autonomous driving. arXiv preprint arXiv:2310.02251 (2023)
13. Ding, X., Han, J., Xu, H., Zhang, W., Li, X.: HiLM-D: towards high-resolution understanding in multimodal large language models for autonomous driving. arXiv preprint arXiv:2309.05186 (2023)
14. Ettinger, S., et al.: Large scale interactive motion forecasting for autonomous driving: the Waymo open motion dataset. In: Proceedings of the IEEE/CVF International Conference on Computer Vision (ICCV), pp. 9710–9719, October 2021
15. Gokul, A.: LLMS and AI: understanding its reach and impact (2023)
16. Hardy, M., Sucholutsky, I., Thompson, B., Griffiths, T.: Large language models meet cognitive science: LLMS as tools, models, and participants. In: Proceedings of the Annual Meeting of the Cognitive Science Society, vol. 45 (2023)

17. Huang, W., Wang, C., Zhang, R., Li, Y., Wu, J., Fei-Fei, L.: VoxPoser: composable 3d value maps for robotic manipulation with language models. arXiv preprint arXiv:2307.05973 (2023)
18. Lai, S., Xu, Z., Zhang, W., Liu, H., Xiong, H.: Large language models as traffic signal control agents: capacity and opportunity (2023)
19. Li, J., Li, D., Savarese, S., Hoi, S.: BLIP-2: bootstrapping language-image pre-training with frozen image encoders and large language models. arXiv preprint arXiv:2301.12597 (2023)
20. Liu, R.W., Liang, M., Nie, J., Lim, W.Y.B., Zhang, Y., Guizani, M.: Deep learning-powered vessel trajectory prediction for improving smart traffic services in maritime internet of things. IEEE Trans. Netw. Sci. Eng. **9**, 3080–3094 (2022)
21. Ma, Y., Cao, Y., Sun, J., Pavone, M., Xiao, C.: Dolphins: multimodal language model for driving. arXiv preprint arXiv:2312.00438 (2023)
22. Mao, J., Qian, Y., Zhao, H., Wang, Y.: GPT-driver: Learning to drive with GPT. arXiv preprint arXiv:2310.01415 (2023)
23. Martino, A., Iannelli, M., Truong, C.: Knowledge injection to counter large language model (LLM) hallucination. In: Pesquita, C., et al. (eds.) ESWC 2023. LNCS, vol. 13998, pp. 182–185. Springer, Cham (2023). https://doi.org/10.1007/978-3-031-43458-7_34
24. Mumtarin, M., Chowdhury, M.S., Wood, J.: Large language models in analyzing crash narratives – a comparative study of ChatGPT, BARD and GPT-4. arXiv preprint arXiv:2308.13563 (2023)
25. Qian, T., Chen, J., Zhuo, L., Jiao, Y., Jiang, Y.G.: NuScenes-QA: a multi-modal visual question answering benchmark for autonomous driving scenario. arXiv preprint arXiv:2305.14836 (2023)
26. Ramesh, A., et al.: Zero-shot text-to-image generation. In: International Conference on Machine Learning, pp. 8821–8831. PMLR (2021)
27. Shah, D., Osinski, B., Ichter, B., Levine, S.: LM-Nav: robotic navigation with large pre-trained models of language, vision, and action. In: Conference on Robot Learning (2022)
28. Sharan, S., Pittaluga, F., Chandraker, M., et al.: LLM-assist: enhancing closed-loop planning with language-based reasoning. arXiv preprint arXiv:2401.00125 (2023)
29. Sheikh, M.S., Peng, Y., et al.: A comprehensive review on traffic control modeling for obtaining sustainable objectives in a freeway traffic environment. J. Adv. Transp. **2022**, 1012206 (2022)
30. Shoaib, M.R., Emara, H.M., Zhao, J.: A survey on the applications of frontier AI, foundation models, and large language models to intelligent transportation systems. In: 2023 International Conference on Computer and Applications (ICCA), pp. 1–7. IEEE (2023)
31. Song, C.H., Wu, J., Washington, C., Sadler, B.M., Chao, W.L., Su, Y.: LLM-planner: few-shot grounded planning for embodied agents with large language models. In: Proceedings of the IEEE/CVF International Conference on Computer Vision, pp. 2998–3009 (2023)
32. Sun, W., Abdullah, L.N., Khalid, F., binti Sulaiman, P.S.: Intelligent analysis of vehicle accidents to detect road safety: a systematic literature review. Int. J. Acad. Res. Bus. Soc. Sci. **13**, 1–17 (2023)
33. Touvron, H., et al.: Llama 2: open foundation and fine-tuned chat models. arXiv preprint arXiv:2307.09288 (2023)
34. Villarreal, M., Poudel, B., Li, W.: Can ChatGPT enable its? The case of mixed traffic control via reinforcement learning. In: ITSC, pp. 3749–3755. IEEE (2023)

35. Wang, G., et al.: Voyager: an open-ended embodied agent with large language models. arXiv preprint arXiv:2305.16291 (2023)
36. Wang, L., et al.: AccidentGPT: accident analysis and prevention from V2X environmental perception with multi-modal large model. arXiv preprint arXiv:2312.13156 (2023)
37. Wang, T., et al.: DeepAccident: a motion and accident prediction benchmark for V2X autonomous driving. arXiv preprint arXiv:2304.01168 (2023)
38. Wang, W., et al.: VisionLLM: large language model is also an open-ended decoder for vision-centric tasks. In: Advances in Neural Information Processing Systems 36 (2024)
39. Wang, W., et al.: DriveMLM: aligning multi-modal large language models with behavioral planning states for autonomous driving. arXiv preprint arXiv:2312.09245 (2023)
40. Wang, X., Wang, D., Chen, L., Wang, F.Y., Lin, Y.: Building transportation foundation model via generative graph transformer. In: 2023 IEEE 26th International Conference on Intelligent Transportation Systems (ITSC), pp. 6042–6047. IEEE (2023)
41. Wen, L., et al.: DiLu: a knowledge-driven approach to autonomous driving with large language models. arXiv preprint arXiv:2309.16292 (2023)
42. Xu, Z., et al.: DriveGPT4: interpretable end-to-end autonomous driving via large language model. arXiv preprint arXiv:2310.01412 (2023)
43. Yang, S., et al.: Lidar-LLM: exploring the potential of large language models for 3d lidar understanding. arXiv preprint arXiv:2312.14074 (2023)
44. Yao, S., et al.: React: synergizing reasoning and acting in language models. In: International Conference on Learning Representations (2023)
45. Yu, H., et al.: DAIR-V2X: a large-scale dataset for vehicle-infrastructure cooperative 3d object detection. In: Proceedings of the IEEE/CVF Conference on Computer Vision and Pattern Recognition (CVPR), pp. 21361–21370, June 2022
46. Yuan, Y., Ding, J., Feng, J., Jin, D., Li, Y.: UniST: a prompt-empowered universal model for urban spatio-temporal prediction. arXiv preprint arXiv:2402.11838 (2024)
47. de Zarzà, I., de Curtò, J., Roig, G., Calafate, C.T.: LLM multimodal traffic accident forecasting. Sensors **23**(22), 9225 (2023)
48. Zhang, K., Zhou, F., Wu, L., Xie, N., He, Z.: Semantic understanding and prompt engineering for large-scale traffic data imputation. Inf. Fusion **102**, 102038 (2024)
49. Zhang, L., et al.: Analysis of traffic accident based on knowledge graph. J. Adv. Transp. (2022)
50. Zhang, S., Fu, D., Zhang, Z., Yu, B., Cai, P.: TrafficGPT: viewing, processing and interacting with traffic foundation models. arXiv preprint arXiv:2309.06719 (2023)
51. Zheng, O., Abdel-Aty, M., Wang, D., Wang, Z., Ding, S.: ChatGPT is on the horizon: could a large language model be all we need for intelligent transportation? arXiv preprint arXiv:2303.05382 (2023)
52. Zheng, W., Chen, W., Huang, Y., Zhang, B., Duan, Y., Lu, J.: OccWorld: learning a 3d occupancy world model for autonomous driving. arXiv preprint arXiv:2311.16038 (2023)
53. Zhou, X., Knoll, A.C.: GPT-4v as traffic assistant: an in-depth look at vision language model on complex traffic events. arXiv preprint arXiv:2402.02205 (2024)

Automated Brain Tumor Classification with Deep Learning

Venkata Sai Krishna Chaitanya Kandula and Yan Zhang(✉)

California State University San Bernardino, 5500 University Parkway, San Bernardino, CA 92407, USA
008133327@coyote.csusb.edu, Yan.Zhang@csusb.edu

Abstract. Brain Tumors are the abnormal growth of cells within the brain that can be categorized as benign (non-cancerous) or malignant (cancerous). Accurate and timely classification of brain tumors is crucial for effective treatment planning and patient care. Medical imaging techniques like Magnetic Resonance Imaging (MRI) provide detailed visualizations of brain structures, aiding in diagnosis and tumor classification. In this paper, we propose a brain tumor classifier applying deep learning methodologies to automatically classify brain tumor images without any manual intervention. The classifier uses deep learning architectures to extract features and classify brain MRI images. Specifically, Convolutional Neural Networks (CNNs) are trained on a diverse dataset of brain tumor images. The CNN learns intricate patterns and features within the images, enabling it to classify various tumor types. Transfer learning, utilizing pre-trained models such as Visual Geometry Group and EfficientNet, enhances the CNN model's ability to generalize across different datasets. The performance of the Visual Geometry Group and EfficientNet models are evaluated and compared. The metrics like accuracy, precision, recall and F1 score are used to evaluate the efficacy of each model in brain tumor classification. This project contributes to the advancement of automated brain tumors diagnosis, potentially improving patient outcomes through more efficient diagnosis strategies.

Keywords: Brain Tumor Classification · Deep Learning · Convolutional Neural Network · Visual Geometry Group · EfficientNet

1 Introduction

Effective treatment of brain tumors requires early stage detection and classification of tumors. The diagnostic process for brain tumors relies on the analysis of brain images acquired through Magnetic Resonance Imaging (MRI) [20]. The initial step in assessing a patient's condition with a brain tumor involves the precise interpretation of the images. The task of identifying brain tumors becomes challenging in the absence of an automated detection system. Diagnoses related to the brain demand careful attention as even the slightest error

M. Hu et al. (Eds.): IJCRS 2024, LNAI 14840, pp. 310–324, 2024.
https://doi.org/10.1007/978-3-031-65668-2_21

can lead to adverse consequences. The formation of tumor cells in the human brain increases the risk of significant mortality. Brain tumors exhibit instability for approximately twenty-five days due to the complexity of the tissues involved. The average survival rate for individuals is typically less than 14 months [12]. More accurate computer-based automated tumor detection/diagnosis methods are needed to understand and intervene in this real situation.

The construction of an automated classifier necessitates the use of effective deep learning model Convolutional Neural Network (CNN) to achieve optimal classification performance. The concept behind an automated classifier is to expand CNN's capabilities through tasks such as cropping, rotating, labeling, flattening, and converting input images to grayscale. A significant challenge lies in supplying a well-preprocessed input image that enables the classifier to determine the type of tumor present. Furthermore, achieving the highest accuracy with minimal computational resources presents additional challenges.

The objective of this study is to categorize the type of tumor present in a patient's brain MRI image. In addition to this primary goal, our research aims to highlight the advantages and disadvantages of the models employed for brain tumor classification. The Automated Brain Tumor Classifier developed in this project is a sophisticated system that is designed to automatically classify brain tumor images and provide the likelihood of the classified tumor without the manual intervention. This study conducts a comparative analysis of the performance of three models: Visual Geometry Group 16-layer (VGG-16), Visual Geometry Group 19-layer (VGG-19), and EfficientNet (B2, B3) in the context of brain tumor classification. VGG-16 and VGG-19, two deep convolutional neural networks, differ in the number of weight layers: VGG-16 has 16 layers, while VGG-19 has 19 [18]. EfficientNet is based on compound scaling technique, which balances model depth, width, and resolution [15]. EfficientNet features variable input shapes based on the scaling factor and utilizes depth-wise separable convolutions in its convolutional layers.

This study conducts a thorough assessment and juxtaposition of the capabilities of VGG-16, VGG-19, and EfficientNet. The primary metrics for this evaluation are their efficiency and accuracy, particularly in the realm of brain tumor classification tasks. We will delve into aspects such as the models' performance, computation time, inherent complexity, and their precision in classification.

2 Related Work

This study builds upon foundational work in deep learning for image recognition, such as Zisserman and Karen's exploration of very deep convolutional networks [19] and Bhatt et al.'s comprehensive review of CNN variants for computer vision [2]. To encompass a range of approaches to brain tumor detection utilizing deep learning techniques, Naseer et al. evaluated the performance of a deep learner CNN using augmented brain MRI for diagnosis, highlighting the efficacy of convolutional neural networks in this domain [9]. The proposed CNN model achieved 92%–98% accuracy on the chosen datasets. Additionally, Zulfiqar et

al. proposed the use of EfficientNets for multi-class classification of brain tumor types [20]. Khan et al. present a deep convolutional neural network for accurate brain tumor detection [6]. Transfer learning was leveraged, as demonstrated by Samee et al. [12] and Srikanth [13], with the former employing a hybrid transfer learning model and the latter utilizing VGG-16 for classification tasks attaining the accuracy of 95% with computational time of 26 ms. These studies collectively contribute to the advancement of image classification by integrating deep learning methodologies, indicating the growing interest and effectiveness of such approaches in medical imaging analysis.

3 Data Collection and Preprocessing

The dataset used in this experiment is published on Kaggle and the dataset consists of 7023 images of human brain MRI images which are classified into 4 categories: glioma, meningioma, pituitary, and healthy brain [10]. Inputs are provided in the form of images. Output is expected to be a class label that falls into one of the four categories. The dataset is balanced with inputs in all kinds of categories. For classification at the model level, we represented classes as follows: No Tumor (0), Glioma (1), Meningioma (2), and pituitary(3). After inputting an image, we apply 224×224 dimension preprocessing. Preprocessing w.r.t image data includes cropping (height $\times$ width), rotating, resizing, gray scaling etc. For example: we do not consider image borders, names, and labels. These input features are not able to predict the output. So, cleaning these kind of features from actual images is required beforehand. The image data between these pixels is considered as an input feature. Output is dependent on the image data fed in the NumPy array. The dataset is split into a training set and a test set. There are 5140 images in the training set, 572 images in the validation set, and 1311 images in the test set.

4 Methodologies

4.1 Convolutional Neural Networks (CNNs)

A Convolutional Neural Network (CNN), also known as a ConvNet, is a specialized neural network architecture tailored for tasks in image recognition and computer vision [6,16]. It employs convolutional and pooling layers to process data. Figure 1 provides the simplified diagram of CNN from input to output layer [11] The key components of a CNN are as follows [2,8]:

– Convolutional layers serve as the building blocks of CNNs. Convolution operations are performed between the input images and a filter or kernel and involve sliding the kernel over the input data and computing the element-wise multiplication followed by summation, enabling the network to capture patterns and features in the images. Convolutional layers are where features of input images are extracted.

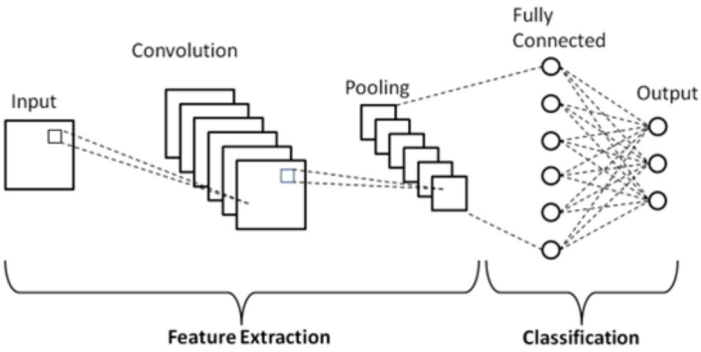

Fig. 1. Schematic Diagram of CNN

- Activation functions enable CNN models to capture complex patterns in the data by introducing nonlinearity into the network. Rectified Linear Unit (ReLU) function is used in this project.
- Pooling layers often are implemented as max pooling, these layers play a role in downsampling the dimensions of feature maps, reducing load and parameter count while preserving information.
- Connected layers appear at the end of the network for classification purposes. They take high-level features extracted by convolutional and pooling layers and map them to class scores.
- Flattening layers help to convert the data into a one-dimensional vector. Flattening is a common practice before feeding the results of pooling layers into connected layers.
- Dropout is a regularization technique used to prevent overfitting during training by randomly disconnecting a fraction of connections.
- When dealing with classification tasks, the SoftMax activation function is frequently employed in the output layer to transform the network scores into probability distributions across classes.

CNNs have demonstrated state-of-the-art performance in various computer vision challenges [6]. Due to its ability to autonomously learn features from input data, CNNs are highly effective in tasks such as image classification, object detection, and image segmentation [16].

4.2 Visual Geometry Group - 16 Layers (VGG-16)

The Visual Geometry Group - 16 layers (VGG-16) model is a type of deep CNN architecture developed by the Visual Graphics Group (VGG) at the University of Oxford [12]. VGG-16 has gained popularity for its performance in tasks related to image classification, and it is well known for its consistent structure [18]. It comprises a total of 16 layers, including both fully connected layers, as shown in Fig. 2. The architecture follows a pattern consisting of repeated layers with

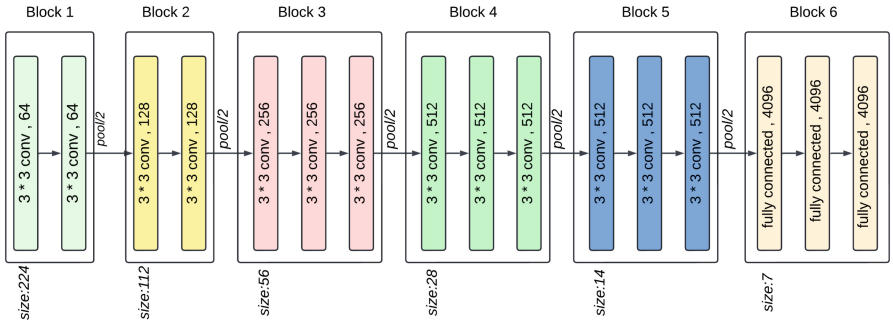

Fig. 2. VGG-16 Architecture

small 3×3 filters, followed by max-pooling layers; three connected layers are placed after the layers [13]. In VGG-16, all convolutional layers utilize filters with dimensions of 3×3. The stride (the amount by which the filter moves) for these layers is set to 1 pixel. After each set of layers, a max pooling is applied. The max pooling involves using filters sized at 2×2 and moving them with a stride of 2 pixels. The final stages of VGG-16 consist entirely of layers that possess respective neuron counts of 4096. The last layer contains precisely 1000 neurons corresponding to the output classes.

The pre-trained weights of VGG-16 have proven to be quite useful as a starting point for transfer learning in computer vision tasks [17]. In applications, VGG-16 can be widely employed for tasks like image classification, object detection, and feature extraction [14].

4.3 Visual Geometry Group - 19 Layers (VGG-19)

Visual Geometry Group - 19 layers (VGG-19), introduced by Andrew Zissermanis and Karen Simonyan, is a deep convolutional neural network architecture that gained prominence for its simplicity and effectiveness in image classification tasks [19]. The key characteristics of VGG networks are their uniform architecture with small 3×3 convolutional filters and the stacking of multiple convolutional layers. Amin, et al. explored the impact of increasing network depth on image classification performance, demonstrating that deeper models tend to perform better on large-scale visual recognition tasks [1].

Figure 3 illustrates the architecture of VGG-19. Feature extraction functionality consists of 16 convolutional layers which are divided into 5 blocks. The first two blocks are identical compared to VGG-16. 3 more layers are added from block 3 to block 5. During the training process, our ConvNets receive a fixed size 224×224 RGB image as input. We simply adjust the RGB value calculated from the training set by subtracting it from each pixel. The image then goes through a series of convolutional layers that utilize filters with a receptive field size of 3×3 to capture left/right, up/down, and center concepts. Additionally, we

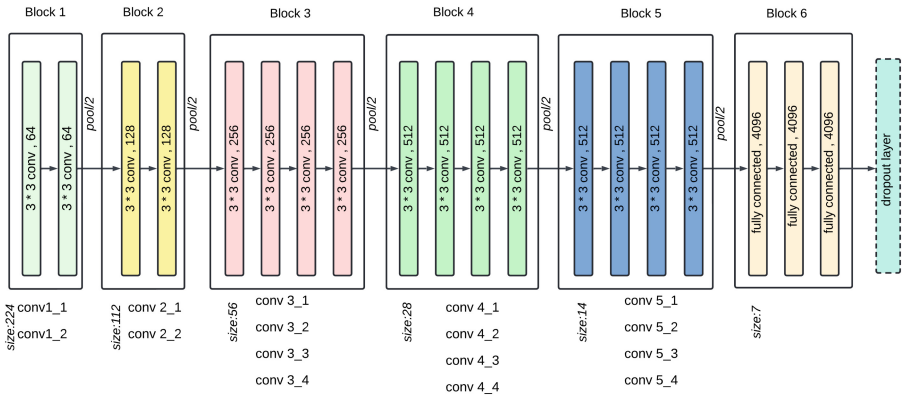

Fig. 3. VGG-19 Architecture

incorporate 1×1 convolution filters, in one configuration to perform transformations on input channels followed by non-linearity. The convolution stride remains at 1 pixel and spatial padding ensures that the spatial resolution is maintained post convolution with a padding of 1 pixel, for every 3×3 convolutional layer. A series of layers precedes three connected layers in various architectures; the initial two consist of 4096 channels each while the final convolutional layer with 1000 channels corresponds to the 1000 classes in the ImageNet dataset, which is commonly used as a benchmark dataset for the ImageNet Large Scale Visual Recognition Challenge (ILSVRC) [6]. The ultimate layer is the dropout layer and is optional. The setup of the connected layers remains consistent, across all networks. For the experimental purpose, we have implemented it in a sequential manner of layers instead of making use of the existing Keras inline function.

4.4 EfficientNet

EfficientNet is a group of CNN architectures created to strike a balance between accuracy, efficiency, and model size [7]. It aims to optimize resources while maintaining performance levels. EfficientNet introduces a method called compound scaling that uniformly scales the network's width, depth, and resolution [15]. This scaling factor is determined by a user-defined compound coefficient (ϕ) which considers the resources [15].

EfficientNet utilizes depth convolutions to reduce parameters and computational requirements. These convolutions consist of two steps; depth convolution followed by point convolution [15]. The depth-wise convolution operation is a key component of the EfficientNet architecture, where each input channel is convolved separately with its corresponding filter. After the depth-wise convolution, a point-wise convolution is applied, where a 1×1 convolution is performed

to combine the output channels of the depth-wise convolution. To effectively capture low-level features, the model employs inverted residuals in its architecture [4]. Linear bottlenecks are also introduced to enhance information flow throughout the network [4]. The fundamental building block of EfficientNet is a block that incorporates wise separable convolutions and linear bottlenecks. EfficientNet adjusts the input resolution, in conjunction with the network architecture to capture spatial information [2]. This means that using resolution images leads to the extraction of features.

EfficientNet offers multiple model variants (B0 to B7) with different scaling coefficients [7]. These variants are designed to accommodate varying resource limitations catering to both devices and larger cloud-based models. By adjusting ϕ based on the target resolution, EfficientNet can achieve a balance between model accuracy and computational efficiency across different resource constraints. This allows EfficientNet models to be efficiently scaled up or down to meet specific requirements while maintaining performance. EfficientNet has proven its excellence in image classification tasks by delivering top-notch performance while maintaining efficiency in terms of model size and computational requirements [15]. It has gained adoption across computer vision applications and serves as a benchmark architecture for tasks like image recognition and object detection, through transfer learning and fine-tuning [7].

5 Experiments

5.1 Hardware Resources

The experiment setup in this paper is geared towards showcasing the performance of the selected models. In the implementation phase, our initial focus lies in identifying the hardware prerequisites.

VGG models, known for their deep architecture and large parameter count, are featured prominently. Our focus lies on the implementation intricacies of the 16 and 19 layer versions. For effective execution, a dual-core processor coupled with a minimum RAM capacity of 4 GB is warranted. The inference and training stages necessitate a GPU equipped with at least 4 GB of VRAM, exemplified by models such as the NVIDIA GTX 1060 or superior variants. VGG is widely acknowledged for its computational intensity, particularly in CNN settings.

EfficientNet, on the other hand, seeks to achieve peak accuracy while judiciously managing computational resources. To effectively run EfficientNet models, a dual-core processor complemented by a RAM capacity of 2 GB or more is indispensable. Additionally, a GPU boasting a minimum of 2 GB of VRAM, exemplified by models like the NVIDIA GTX 1050 or higher, is deemed necessary.

5.2 Evaluation Metrics

Evaluation metrics serve as quantitative measures employed to gauge the efficacy of a machine learning model. These metrics furnish valuable insights into the model's performance across a spectrum of parameters, including accuracy, precision, recall, and the F1-score, among others.

Confusion Matrix. In the realm of machine learning, a confusion matrix stands as a pivotal tool, encapsulated within a tabular structure, offering a detailed breakdown of real labels or ground truth vs predicted labels [5]. Beyond a mere assessment of the model's performance, this matrix extends a holistic analysis of its generalization capabilities across diverse classes [5]. True labels adorn the y-axis, while the predicted class labels adorn the x-axis within the confusion matrix. Such matrices prove instrumental in evaluating both binary and multi-class classification tasks.

Classification Report. The classification report emerges as a succinct synopsis, amalgamating a plethora of performance metrics gleaned from the confusion matrix, including accuracy, precision, recall, and the F1-score, alongside support statistics [3]. Collectively, these metrics furnish a comprehensive overview of the model's efficacy in tackling classification challenges [3]. The classification report serves as a beacon, illuminating the model's performance for each individual class and discerning any potential biases towards specific classes.

Accuracy. Accuracy measures the proportion of correctly classified instances among all instances. It is calculated as the ratio of the number of correctly predicted instances to the total number of instances. It gives the percentage of how accurate the proposed model will be on testing [3].

$$Accuracy = \frac{\text{Number of Correct Predictions}}{\text{Total Number of Predictions}} \tag{1}$$

Precision. Precision for a particular class c is calculated as the ratio of the number of true positives (correctly predicted instances of class c) to the sum of true positives and false positives (instances incorrectly predicted as class c) [3].

$$Precision_c = \frac{\text{True Positives}_c}{\text{True Positives}_c + \text{False Positives}_c} \tag{2}$$

Recall (Sensitivity or True Positive Rate). Recall for a particular class c measures the proportion of correctly predicted positive instances of class c among all actual positive instances of class c. It focuses on the ability of the classifier to find all positive instances of class c [3].

$$Recall_c = \frac{\text{True Positives}_c}{\text{True Positives}_c + \text{False Negatives}_c} \tag{3}$$

F1-Score. F1-Score is the harmonic mean of precision and recall. It provides a single metric that balances both precision and recall, making it useful for imbalanced datasets [3].

$$F1Score_c = 2 \times \frac{\text{Precision}_c \times \text{Recall}_c}{\text{Precision}_c + \text{Recall}_c} \tag{4}$$

5.3 Module Evaluations

The performance of deep learning models hinges on the chosen model architecture and its parameters. Total parameters can be categorized into two types: trainable and non-trainable. Trainable parameters undergo learning and updating throughout the training process. These parameters wield a direct influence on the model's performance and are fine-tuned using optimization algorithms, such as gradient descent, to minimize the loss function. Conversely, non-trainable parameters remain fixed and untouched during training. In scenarios involving pre-trained models, like pre-trained neural networks for image recognition, it may be desirable to freeze certain layers' weights to preserve their learned features. These layers serve as feature extractors and maintain their constancy during subsequent fine-tuning stages.

An epoch concludes when the model has traversed the entire training dataset once. The number of epochs serves as a hyperparameter that necessitates configuration before commencing model training. Determining the appropriate number of epochs relies on several factors, including the task's complexity, the dataset's size, and the convergence behavior of the model. Finding the optimal balance among these considerations is paramount for achieving optimal model performance.

VGG-16. We have applied each input image to the VGG-16 model. VGG-16 is implemented from Keras package which consists of trainable and non-trainable parameters. In total, the model comprises 16,816,452 parameters, with 2,101,764 parameters are trainable and 14,714,688 as non-trainable. Table 1 represents the classification report of VGG-16 model. Healthy brain category achieves 100% precision, recall and f1-score for all images. While meningioma category faces the least precision. Support represents the number of actual occurrences of each class in the dataset, that is, it is the number of true instances for each class. The support row of the classification report illustrates that 2 out of 1311 images are unclassified. Table 2 represents the confusion matrix of VGG-16 model which demonstrates that the highest number of misclassifications happens with glioma test images.

Continuing with the computation time of model compilation, each epoch takes approximately 100 ms per step, resulting in a total of 16 s per epoch. Running 20 epochs requires a total time of $16 \times 20 = 320$ s (or approximately 5.3 min).

Table 1. Classification Report of VGG-16

	Precision	Recall	f1-score	support
Healthy	1.00	1.00	1.00	405
Glioma	0.95	0.92	0.93	309
Meningioma	0.90	0.95	0.92	288
Pituitary	1.00	0.97	0.99	307
			Total	1309

Table 2. Confusion matrix of VGG-16

	No Tumor	Glioma	Meningioma	Pituitary
No Tumor	403	1	2	0
Glioma	0	284	24	0
Meningioma	0	14	273	1
Pituitary	1	1	6	299

VGG-19. Unlike VGG-16 implementation from Keras package, VGG-19 implementation is done in a sequential layers manner as per architecture. The convenience of this approach is to balance the computation resources usage with the execution time. Few of the output layers are optional to implement like Dropout. We can achieve a decent accuracy of 96%. Due to model complexity, VGG-19 holds a large number of parameters. As a custom model, the trainable parameters of the VGG-19 model are 139,586,628 and non-trainable parameters are 0. These are very high compared to VGG-16. These numbers represent the training of the model from scratch with no pretrained features or knowledge. The advantage of building a custom model is that it can learn from scratch or fine-tune effectively. Table 3 represents the classification report of VGG-19 model on the test set. Compared with the classification report of VGG-16 shown in Table 1, glioma category faces the least precision of 0.93, which means 93% of instances predicted as glioma are correct. While a recall score of 0.97 for glioma category means that 97% of the actual glioma image instances are correctly identified.

Table 3. Classification Report of VGG-19

	Precision	Recall	f1-score	support
Healthy	1.00	0.98	0.99	411
Glioma	0.93	0.97	0.95	285
Meningioma	0.95	0.91	0.93	319
Pituitary	0.97	0.99	0.98	294
			Total	1309

An F1-score of 0.99 for healthy category indicates that the model achieves a high balance between precision and recall for that class. Table 4 represents the confusion matrix of VGG19 model on the test set. Unlike VGG-16, the highest number of misclassifications 30 happened with meningioma category images. While pituitary category images achieve the least number of misclassifications 2.

Table 4. Confusion matrix of VGG-19

	No Tumor	Glioma	Meningioma	Pituitary
No Tumor	403	0	8	0
Glioma	0	277	7	1
Meningioma	2	21	289	7
Pituitary	0	1	1	292

As for the computation time of VGG-19 model, per epoch, is approximately 306 ms per step, totaling around 50 s. Running 20 epochs requires a total time of $50 \times 20 = 1000$ s (or approximately 16.6 min).

EfficientNet (B2,B3). In our experimental setup, we leveraged built-in functionalities provided by the Keras library to implement and evaluate two variants of EfficientNet, namely B2 and B3. While EfficientNet boasts a powerful architecture, it is not as intricately structured as VGG, resulting in a comparatively lower parameter count. Specifically, the parameter count for EfficientNet B2 is below 50% of that of VGG-16, underscoring its efficiency in resource utilization.

However, as we move up the EfficientNet variants, such as to B3, the parameter count increases, necessitating additional computation time and resources. This increment in parameters enhances the model's capacity to capture more intricate patterns and nuances within the data, albeit at the cost of increased computational overhead. Table 5 provides a detailed breakdown of the parameter counts for both EfficientNet B2 and B3, elucidating their respective computational requirements.

Table 5. Parameter Count for EfficientNet B2 and B3

Model	Total Paras	Trainable Paras	Non-trainable Paras
EfficientNet B2	8,135,933	8,065,542	70,391
EfficientNet B3	11,184,179	11,093,804	90,375

For EfficientNet B2, each epoch is executed in approximately 52 s. Over the course of 20 epochs, the total execution time amounts to 1040 s (or 17.3 min). In contrast, EfficientNet B3 exhibits a longer execution time, with each epoch

taking around 65 s. Consequently, the total time required to complete 20 epochs sums up to 1300 s (or 21.3 min). The computational demands associated with the B3 variant are notably higher compared to B2, rendering it less cost-effective in terms of execution time [10]. Considering the results, it is advised to opt B2 for the dataset.

Upon meticulous analysis, both the B2 and B3 variants achieved an impressive accuracy of 99.5% and 99.8%. Notably, the B2 variant reached this accuracy level by the 4th iteration, while the B3 variant accomplished the same feat by the 3rd iteration. In Table 6, the classification report of the EfficientNet B2 model represents the highest precision, recall, and f1-score of the Healthy category. Overall EfficientNet (B2) model achieves a decent balance between precision and recall for every class. Table 7 represents the confusion matrix derived from the EfficientNet B2 model. Only 7 out of 1308 images (total support) test data are misclassified and 3 out of 1311 images are not predicted.

Table 6. Classification Report of EfficientNet (B2)

	Precision	Recall	f1-score	support
Healthy	1.00	1.00	1.00	404
Glioma	0.99	1.00	0.99	295
Meningioma	0.99	0.98	0.99	308
Pituitary	1.00	0.99	1.00	301
			Total	1308

Table 7. Confusion matrix of EfficientNet (B2)

	No Tumor	Glioma	Meningioma	Pituitary
No Tumor	404	0	0	0
Glioma	0	295	0	0
Meningioma	0	4	303	1
Pituitary	0	0	2	299

5.4 Performance Comparison

Table 8 shows the accuracy of three models VGG-16, VGG-19 and EfficientNet(B2). The EfficientNet (B2) variant achieved high accuracy with a smaller number of epochs and the trade-off is computation time. VGG-16 performs less accuracy at initial epochs and improves over iterations. Increase in variations of VGG and EfficientNet models like (VGG-19, VGG21, B0, B3, B5, B7) will result in higher accuracy at initial epochs due to the convolutional layers processing. Table 9 displays the execution time (in seconds) for each epoch across three models: VGG-16, VGG-19, and EfficientNet (B2). VGG-16 completes execution in

Table 8. Accuracy comparison

	VGG-16	VGG-19	EfficientNet(B2)
Accuracy	96%	96%	99%

1/3 of the time consumed by EfficientNet. Figure 4 (a) represents accuracy plots of three selected models. EfficientNet(B2) achieved the highest accuracy within a few iterations and maintains this accuracy consistently across 20 epochs. In contrast, VGG-16 and VGG-19 exhibit inconsistent declines in accuracy throughout the 20 epochs. Figure 4 (b) represents loss plots that converge after certain epochs which illustrate that all models perform equally after iterations.

Table 9. Execution time comparison

	VGG-16	VGG-19	EfficientNet(B2)
Seconds per epoch	16	50	52
Seconds for 20 epochs	320	1000	1040

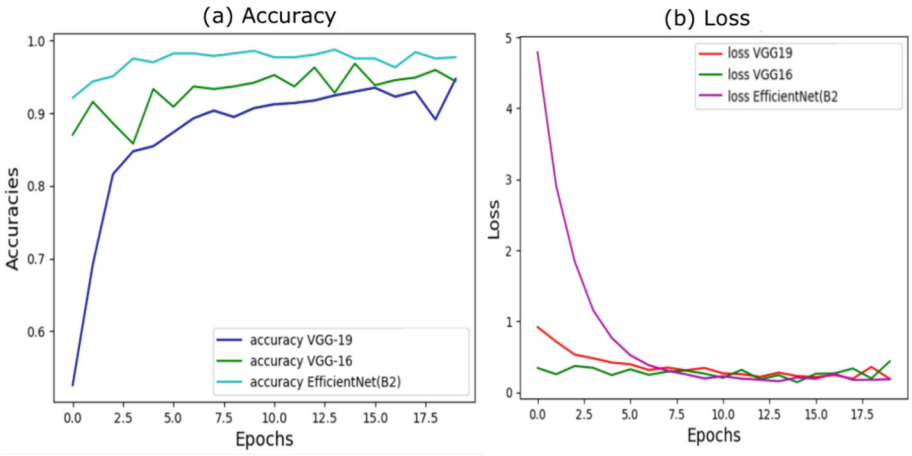

Fig. 4. Comparison of accuracy and loss of three models

6 Conclusion

In conclusion, this paper aims to develop and evaluate automated classifiers for MRI brain images to accurately identify the presence of brain tumors. Leveraging convolutional neural networks (CNNs), specifically VGG-16, VGG-19, and EfficientNet, our objective is to achieve high classification accuracy while prioritizing computational efficiency. This experiment meticulously addresses hardware

considerations essential for model implementation. VGG models, renowned for their deep architectures, necessitate substantial computational resources, especially GPUs with significant VRAM, while EfficientNet variants demonstrate efficiency by achieving high accuracy with relatively modest hardware specifications.

Each model's performance is rigorously evaluated and compared based on various metrics, including confusion matrices and classification reports, which offer comprehensive insights into model performance across different classes of brain tumors. Experimental results underscore the effectiveness of CNNs in accurately classifying brain tumor images, with EfficientNet exhibiting promising results in achieving high accuracy with relatively fewer parameters, while VGG models demonstrate competitive performance albeit with higher computational demands.

The automated brain tumor classifier's performance depends on the quality of trained data. Unseen/unrecognized patterns in test data might lead to classification errors. There are over 120 sub-categories of Glioma, Meningioma, and Pituitary Tumors. Brain tumors exhibit a wide range of morphological and biological variability, making accurate classification challenging. Factors such as tumor size, location, and histological subtype can introduce complexities that may not be adequately captured by the classifier. Complex models like VGG-19 might suffer with overfitting. Models trained on one dataset from one institution or population may not generalize well to data from other sources due to differences in imaging protocols, patient demographics, and tumor characteristics.

The findings of this research lay a robust foundation for future investigations in the domain of automated brain tumor classification. Future explorations may involve refining model architectures, exploring additional CNN variants, optimizing hyperparameters, and integrating advanced techniques such as transfer learning to further enhance classification accuracy and efficiency.

References

1. Amin, J., Anjum, M.A., Sharif, M., Kadry, S., Crespo, R.G.: Visual geometry group based on u-shaped model for liver/liver tumor segmentation. IEEE Lat. Am. Trans. **21**(4), 557–564 (2023)
2. Bhatt, D., Patel, C., Talsania, H., et al.: CNN variants for computer vision: history, architecture, application, challenges, and future scope. Electronics **20** (2021). https://doi.org/10.3390/electronics10202470
3. Grandini, M., Bagli, E., Visani, G.: Metrics for multi-class classification: an overview. arXiv preprint arXiv:2008.05756 (2020)
4. Hoang, V.T., Jo, K.H.: Practical analysis on architecture of efficientnet. In: 2021 14th International Conference on Human System Interaction (HSI), pp. 1–4. IEEE (2021)
5. Hossin, M., Sulaiman, M.N.: A review on evaluation metrics for data classification evaluations. Int. J. Data Min. Knowl. Manag. Process **5**(2), 1 (2015)
6. Khan, M.S.I., Rahman, A., et al.: Accurate brain tumor detection using deep convolutional neural network. Comput. Struct. Biotechnol. J. **20**, 4733–4745 (2022). https://doi.org/10.1016/j.csbj.2022.08.039

7. Koonce, B., Koonce, B.: Efficientnet. Convolutional neural networks with swift for Tensorflow: image recognition and dataset categorization, pp. 109–123 (2021)
8. Li, Z., Liu, F., Yang, W., Peng, S., Zhou, J.: A survey of convolutional neural networks: analysis, applications, and prospects. IEEE Trans. Neural Netw. Learn. Syst. **33**(12), 6999–7019 (2021)
9. Naseer, A., Yasir, T., Azhar, A., et al.: Computer-aided brain tumor diagnosis: performance evaluation of deep learner CNN using augmented brain MRI. Int. J. Biomed. Imaging 1–11 (2021). https://doi.org/10.1155/2021/5513500
10. Nickparvar, M.: Brain tumor MRI dataset (2021). Accessed 20 Feb 2024
11. Phung, V., Joo, R.E.: A high-accuracy model average ensemble of convolutional neural networks for classification of cloud image patches on small datasets. Appl. Sci. **9**(21), 4500 (2019). https://doi.org/10.3390/app9214500
12. Samee, N., Mahmoud, N., Atteia, G., et al.: Classification framework for medical diagnosis of brain tumor with an effective hybrid transfer learning model. Diagnostics (Basel) **12**(10) (2022). https://doi.org/10.3390/diagnostics12102541
13. Srikanth, T.: Transfer learning using VGG-16 with deep convolutional neural network for classifying images. Int. J. Sci. Res. Publ. (IJSRP) **9**(10), 143–150 (2019). https://doi.org/10.29322/IJSRP.9.10.2019.p9420
14. Tammina, S.: Transfer learning using VGG-16 with deep convolutional neural network for classifying images. Int. J. Sci. Res. Publ. (IJSRP) **9**(10), 143–150 (2019)
15. Tan, M., Le, Q.: Efficientnet: rethinking model scaling for convolutional neural networks. In: International Conference on Machine Learning, pp. 6105–6114. PMLR (2019)
16. Yamashita, R., Nishio, M., Do, R.K.G., Togashi, K.: Convolutional neural networks: an overview and application in radiology. Insights Imaging **9**, 611–629 (2018)
17. Zakaria, N., Hassim, Y.M.M.: Improved image classification task using enhanced visual geometry group of convolution neural networks. JOIV: Int. J. Inform. Vis. **7**(4), 2498–2505 (2023)
18. Zakaria, N., Hassim, Y.M.M.: A review study of the visual geometry group approaches for image classification. J. Appl. Sci. Technol. Comput. **1**(1), 14–28 (2024)
19. Zisserman, A., Karen, S.: Very deep convolutional networks for large-scale image recognition. arXiv preprint (2014)
20. Zulfiqar, F., Bajwa, U.I., Mehmood, Y.: Multi-class classification of brain tumor types from MR images using efficientnets. Biomed. Signal Process. Control **84** (2023). https://doi.org/10.1016/j.bspc.2023.104777

Author Index

M. Hu et al. (Eds.): IJCRS 2024, LNAI 14840, pp. 325–326, 2024.
https://doi.org/10.1007/978-3-031-65668-2